Field Guide to Geologic Processes in Cascadia

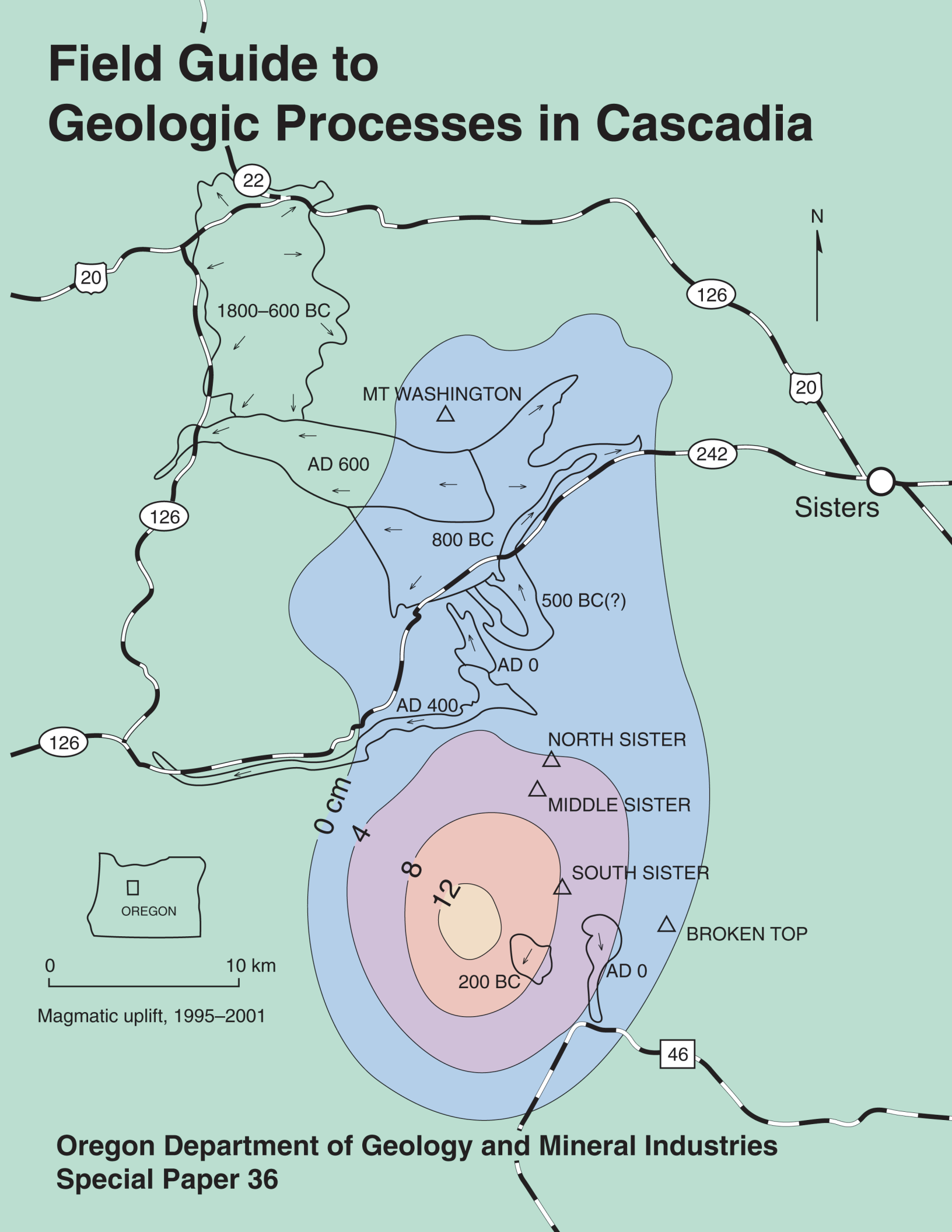

Oregon Department of Geology and Mineral Industries
Special Paper 36

Field Guide to Geologic Processes in Cascadia

Field Trips to Accompany the 98th Annual Meeting of the Cordilleran Section of the Geological Society of America May 13–15, 2002, Corvallis, Oregon

Edited by
George W. Moore
Oregon State University

2002

Oregon Department of Geology and Mineral Industries
Special Paper 36

FRONT COVER. Map of the Three Sisters area showing dated lava flows and magmatic uplift in centimeters between 1995 and 2001 (from Charles W. Wicks and Edward M. Taylor)
BACK COVER (clockwise from upper left). Olympic Mountains landsat image; Multnomah Falls; Dant Debris Flow; Deschutes River Canyon; Dune Paleosols

Local Committee of the 98th Annual Meeting Cordilleran Section of the Geological Society of America Corvallis, Oregon, May 13–15, 2002

Local committee chair	**Robert S. Yeats**
Technical program chair	**Andrew J. Meigs**
Field trip chair	**George W. Moore**
Workshop chair	**Robert J. Lillie**
Student paper judging chair	**Anita L. Grunder**
Exhibits chair	**Cyrus W. Field**
Poster and special events chair	**Roy D. Haggerty**
Operations chair	**John H. Dilles**
Finance chair	**Edward M. Taylor**
Treasurer	**Karen L. Logan**
Transportation chair	**Brennan T. Jordan**
Registration chair	**Jeffery H. Templeton**
Audiovisual chair	**Julia A. Jones**
Housing coordinator	**Roger L. Nielsen**
Catering chair	**Ellen J. Moore**
Student workers coordinator	**Randall L. Milstein**
Webmaster	**Stephen L. Young**

Coordinators for Affiliated Societies

Northwest Energy Association, AAPG	**H. Jack Meyer**
Association of Engineering Geologists	**Scott F. Burns**
National Association of Geology Teachers	**Larry G. Enochs**
Paleontological Society	**Ellen J. Moore**
Association of Woman Geoscientists	**Dawn J. Wright**

Oregon Department of Geology and Mineral Industries Special Papers, ISSN 0278-3703
Published in conformance with Oregon Revised Statutes 516.030

The Oregon Department of Geology and Mineral Industries is publishing this report because the information furthers the mission of the department. To facilitate timely distribution of the information, the report is published as received from its editor

For copies of this publication, please contact
Nature of the Northwest Information Center, 800 NE Oregon Street, #5, Portland, OR 97232-2162
(503) 872-2750, http://www.naturenw.org

CONTENTS

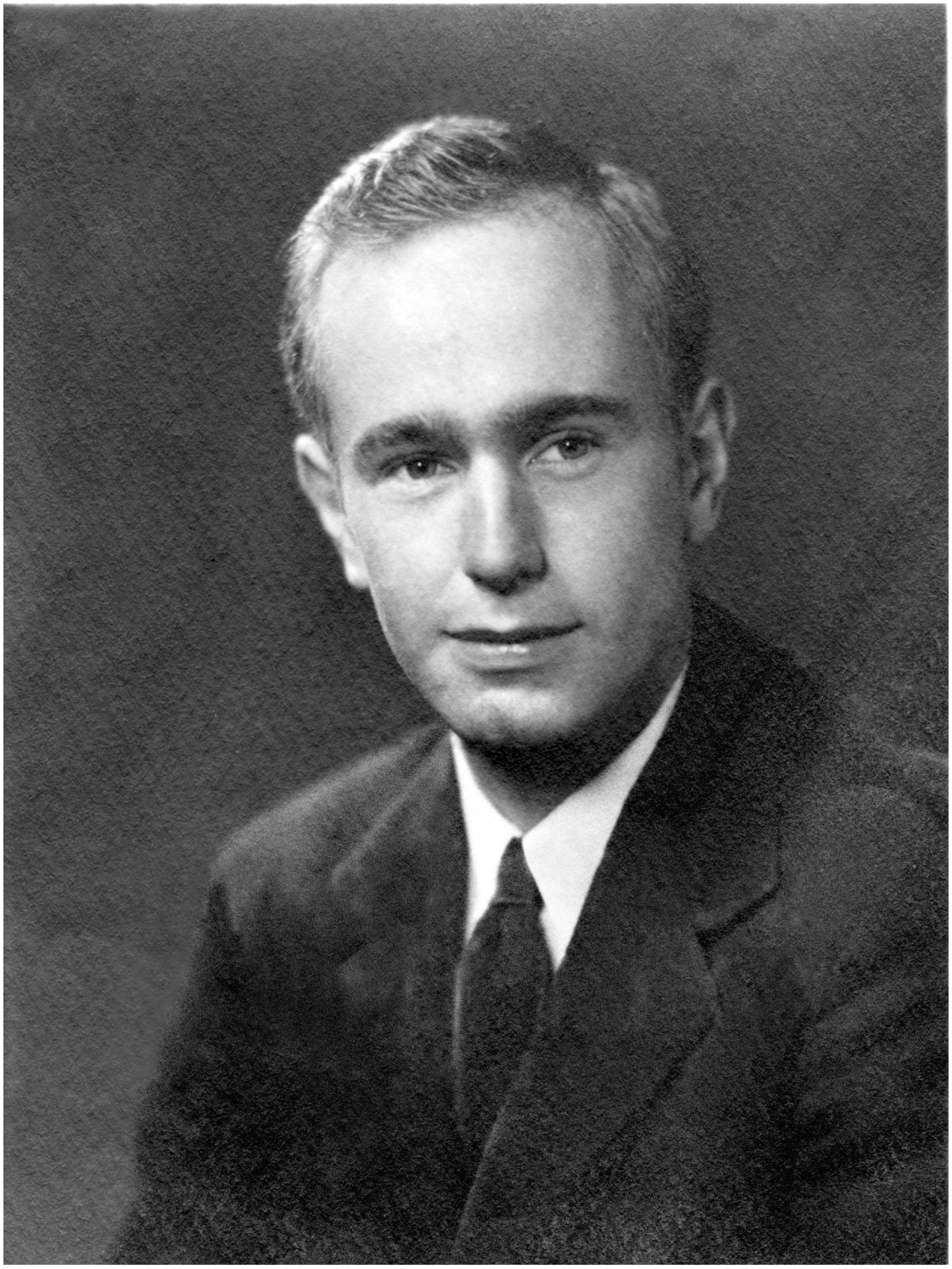

GEORGE W. WALKER

DEDICATION

The story is told about George Walker discussing Eastern Oregon sites with a pair of widely traveled law-enforcement officers from Oregon's Department of Fish and Wildlife. Although not a game of one-upsmanship, the conversation moved to comparing "who'd been where." Walker skunked the other two; not only had he seen most of the places they described, but he'd been to a gazillion other sites as well.

George Walker's mapping was from an era of rapid reconnaissance, known jokingly as mile-a-minute mapping. It was common for him to complete a 15-minute quadrangle in a week, an entire 1-degree by 2-degree quadrangle in one or two field seasons. In field vehicles he bounced through a region traversed only by sparse jeep trails. Roads now paved were only dusty ruts through sagebrush and sand.

Walker's maps remain important despite, in some cases, nearly 50 years of progress. Subsequent detailed mapping has improved our knowledge but has not changed the broad understanding first imparted by George's work. No finer testimony exists than to see the culmination of his statewide knowledge displayed proudly today as the Geologic Map of Oregon. With this in mind we humbly add our contributions.

The field-trip authors

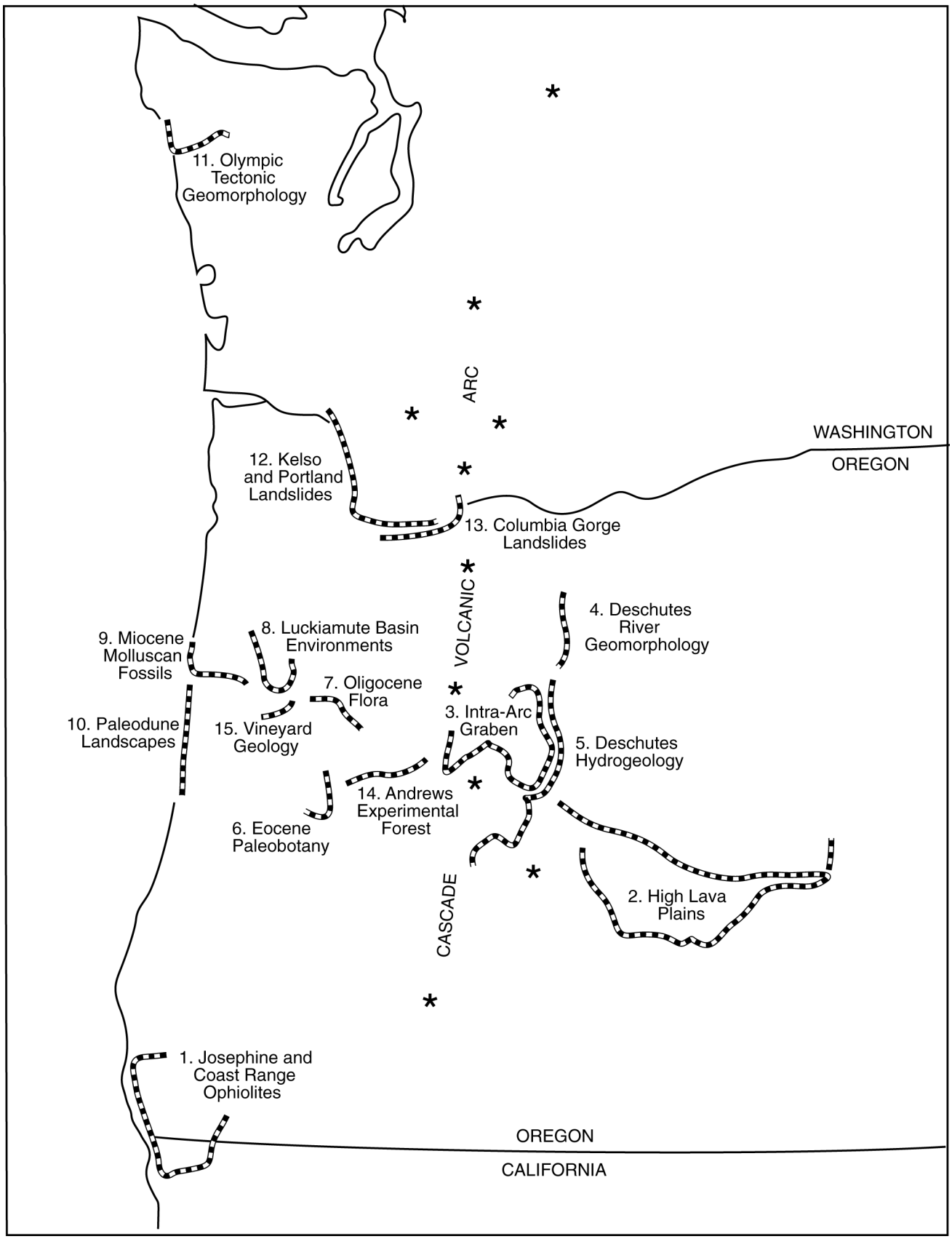

Frontispiece. Routes of the field trips covered in this book.

Josephine and Coast Range Ophiolites, Oregon and California

Gregory D. Harper, Department of Earth and Atmospheric Sciences, State University of New York, Albany, New York 12222; gdh@csc.albany.edu

Mario J. Giaramita, Department of Physics and Geology, California State University, Stanislaus, Turlock, California 95382; marty@geology.csustan.edu

Stefan B. Kosanke, Department of Earth and Atmospheric Sciences, State University of New York, Albany, New York 12222; cohent@concentric.net

INTRODUCTION

Ophiolites are generally regarded as fragments of ocean crust and upper mantle formed by seafloor spreading. As such they play a key role in the interpretation of the tectonic evolution of mountain belts. Modern tectonic environments of seafloor spreading include midocean ridges and suprasubduction zone settings. Spreading in the latter occurs where magmatic arcs are under extension and is the end product of a period of arc rifting. Seafloor spreading in back-arc basins has been known for some time, but it is now well established that rifting and even initial spreading can actually begin in either the fore-arc or back-arc (Hawkins, 1995). Many, if not most, ophiolites show petrologic characteristics or overlying sequences suggesting formation in suprasubduction zone settings (Pearce and others, 1984). This is the case for the two ophiolites viewed on this trip: The Josephine and Coast Range Ophiolites.

The Josephine and Coast Range Ophiolites, which are similar in age (about 165 Ma), can be viewed as comprising two ophiolite belts that extend from California into Oregon (Fig. 1). The more western Coast Range Ophiolite belt in California consists of many remnants that are mostly dismembered and incomplete. The eastern belt includes the Josephine Ophiolite in the Klamath Mountains and the Smartville Ophiolite in the Sierra Nevada foothills, although some workers suggest the Smartville and Josephine are unre-

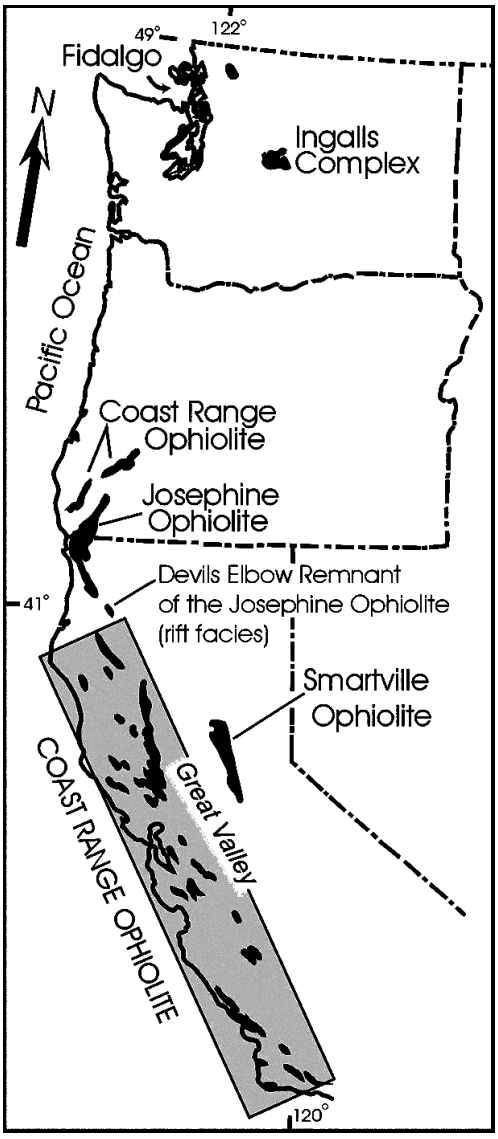

Figure 1. Distribution of Middle Jurassic ophiolites in the western United States. In California and Oregon, these occur as two belts: the Coast Range Ophiolite (western ophiolite belt), and the Josephine and related Smartville Ophiolites (map courtesy of R. Miller).

Field Guide to Geologic Processes in Cascadia: Oregon Department of Geology and Mineral Industries Special Paper 36, 2002.

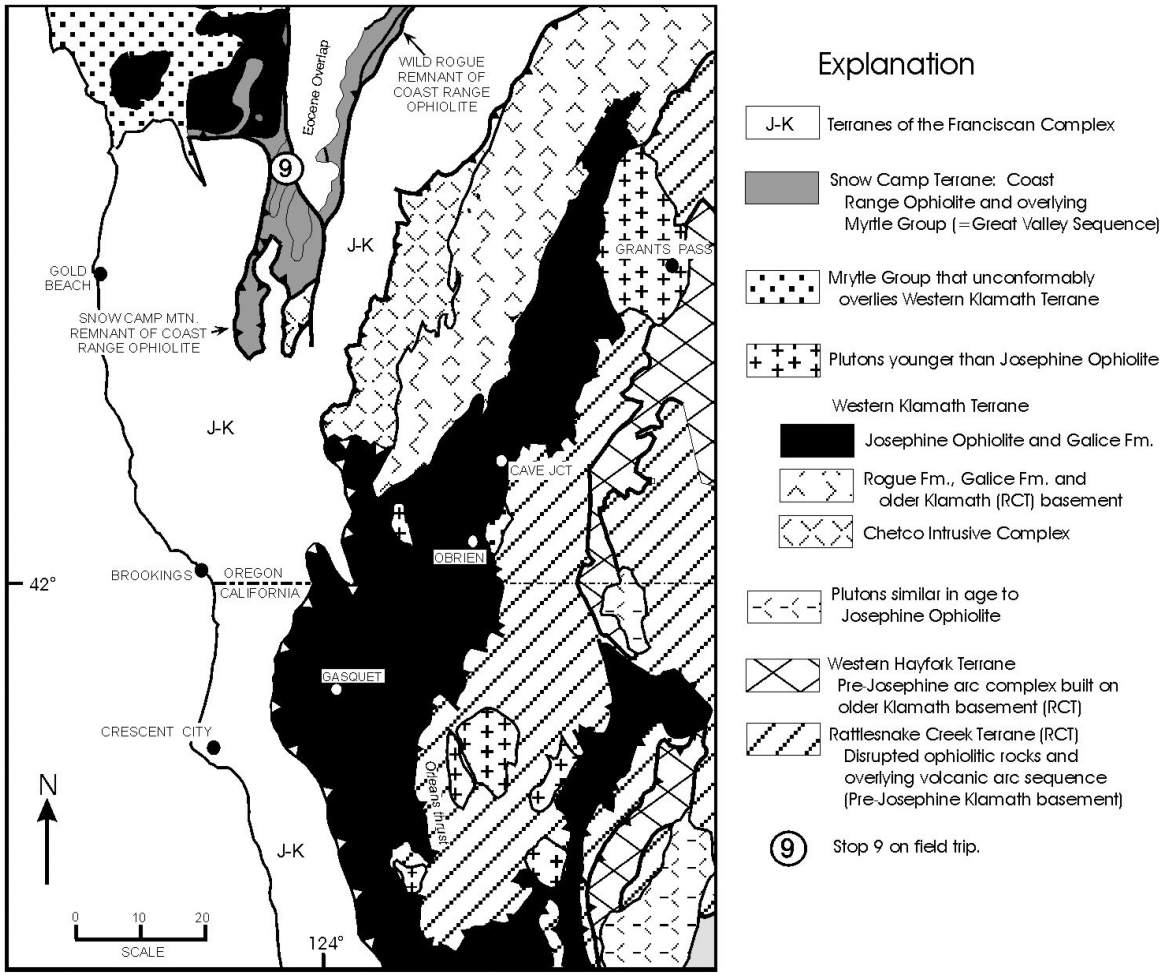

Figure 2. Terrane map of the west-central Klamath Mountains.

lated (Godfrey and Dilek, 2000). Volcanic-arc rock and flysch in the Western Klamath Terrane, which includes the Josephine Ophiolite, have equivalents in the Sierra Nevada foothills, for example, the Logtown Ridge and Mariposa Formations (Burchfiel and Davis, 1981; Saleeby, 1992).

The relationship between the Coast Range Ophiolite belt and the eastern Josephine–Smartville Ophiolite belt is obscured in California by a great thickness of sediment underlying the Great Valley (see Godfrey and Dilek, 2000, for interpretations of basement underlying the Great Valley based on geophysical data). In southwest Oregon, however, the two ophiolites occur as close together as 20 km (Fig. 2).

The Josephine and Coast Range Ophiolites are of simillar age, but whether they are related is uncertain. The Josephine is a classic complete ophiolite that is well constrained (and generally accepted) to have formed by rifting of a west-facing magmatic arc built on the margin of North America (Harper and Wright, 1984; Wyld and Wright, 1988; Dickinson and others, 1996).

By contrast, the origin of the Coast Range Ophiolite is controversial, in particular as to whether it is exotic to North America (Dickinson and others, 1996). Many workers are not aware that remnants of the Coast Range Ophiolite crop out in southwestern Oregon (Fig. 1), although their presence has been recognized for some time (Blake and others, 1985). On this field trip we will visit one ot the recently well-studied occurrences of a probable remnant of the Coast Range Ophiolite in Oregon exposed in the Wild Rogue River Wilderness (Kosanke, 2000).

WESTERN KLAMATH TERRANE AND JOSEPHINE OPHIOLITE

The Klamath Mountains comprise a series of east dipping thrust sheets that become

progressively younger to the west (Burchfiel and Davis, 1981) A terrane map of the west-central Klamath Mountains is shown in Figure 2, and the tectonostratigraphy of some of these terranes is shown in Figure 3. Note that the Western Klamath Terrane (formerly the "Western Jurassic Belt") is divided into three subterranes (Blake and others, 1985).

Josephine Ophiolite and Galice Formation

The southern subterrane (Smith River Subterrane) includes the Josephine Ophiolite and a conformably overlying sedimentary sequence (Figs. 3, 4).

The Josephine Ophiolite is a complete ophiolite that is exposed on the flanks of large open folds and is repeated by thrust faulting (NE part of Fig. 4). The ophiolite consists, from base to top, of harzburgite (a peridotite) and lesser dunite tectonite of upper mantle origin, plutonic igneous rocks of cumulate origin, high-level varitextured gabbro, a sheeted-dike complex, and pillow lava (Fig. 5). The dipping sheeted dikes and igneous layering shown in Figure 5 may seem unusual; these are due to on-axis tilting completed prior to eruption of the uppermost pillow lavas (Alexander and Harper, 1992).

Sediment interbedded with, and interstitial to, pillow lava include chert and radiolarian argillite, some having elevated Fe and Mn contents, and are thus similar to the sediments directly overlying the ophiolite (Pinto-Auso and Harper, 1985; Harper and others, 1988). A pebbly graywacke bed 10 cm thick discovered beneath the uppermost flow of the Josephine Ophiolite is very similar in clast composition to basal graywackes of the Galice Formation described below.

The Josephine Ophiolite is conformably overlain by a sequence of chert and siliceous (radiolarian) argillite, previously called the "hemipelagic sequence" or "volcanopelagic sequence" (Pessagno and Blome, 1990; Dickinson and others, 1996). Pure chert beds are not abundant; rather, black argillaceous chert (or radiolarian argillite) and green tuffaceous chert are interbedded. Elevated iron and manganese contents occur 8 to 21 meters above the ophiolite, apparently representing material precipitated from "off-axis" hydrothermal hot springs (Pinto-Auso and Harper, 1985). Metalliferous sediment typically lies directly above the pillow lava of modern ocean crust and ophiolites, and it is locally interbedded with the Josephine lavas. Such rocks, sometimes called umbers, are formed by precipitation from low- or high-T hot springs on the ridge axis. The metal component of these "off-axis" metallifeous sediments may be from off-axis low-T hot springs (Pinto-Auso and Harper, 1985) or distal deposits from hot springs situated on another (possibly propagating) spreading axis in the Josephine Basin (G. Harper, in review).

The pelagic-hemipelagic sequence grades upward into a flysch sequence (deep-ocean

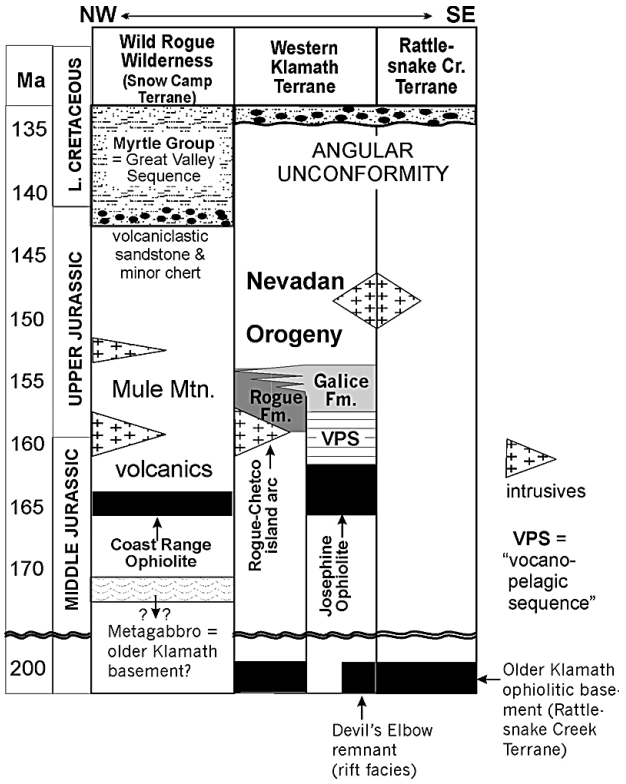

Figure 3. Tectonostratigraphy of some of the terranes in Figure 2, showing the Coast Range and Josephine Ophiolites. The Rogue Formation is volcanic (part of an island arc), whereas the Galice Formation consists of graywacke and slate (flysch), locally with members of Rogue-like volcanic rocks. In California, sedimentary rock overlying the Coast Range Ophiolite ranges from predominantly volcaniclastic rocks, to tuffaceous chert, to ophiolitic breccia (Hopson and others, 1981; Robertson, 1990).

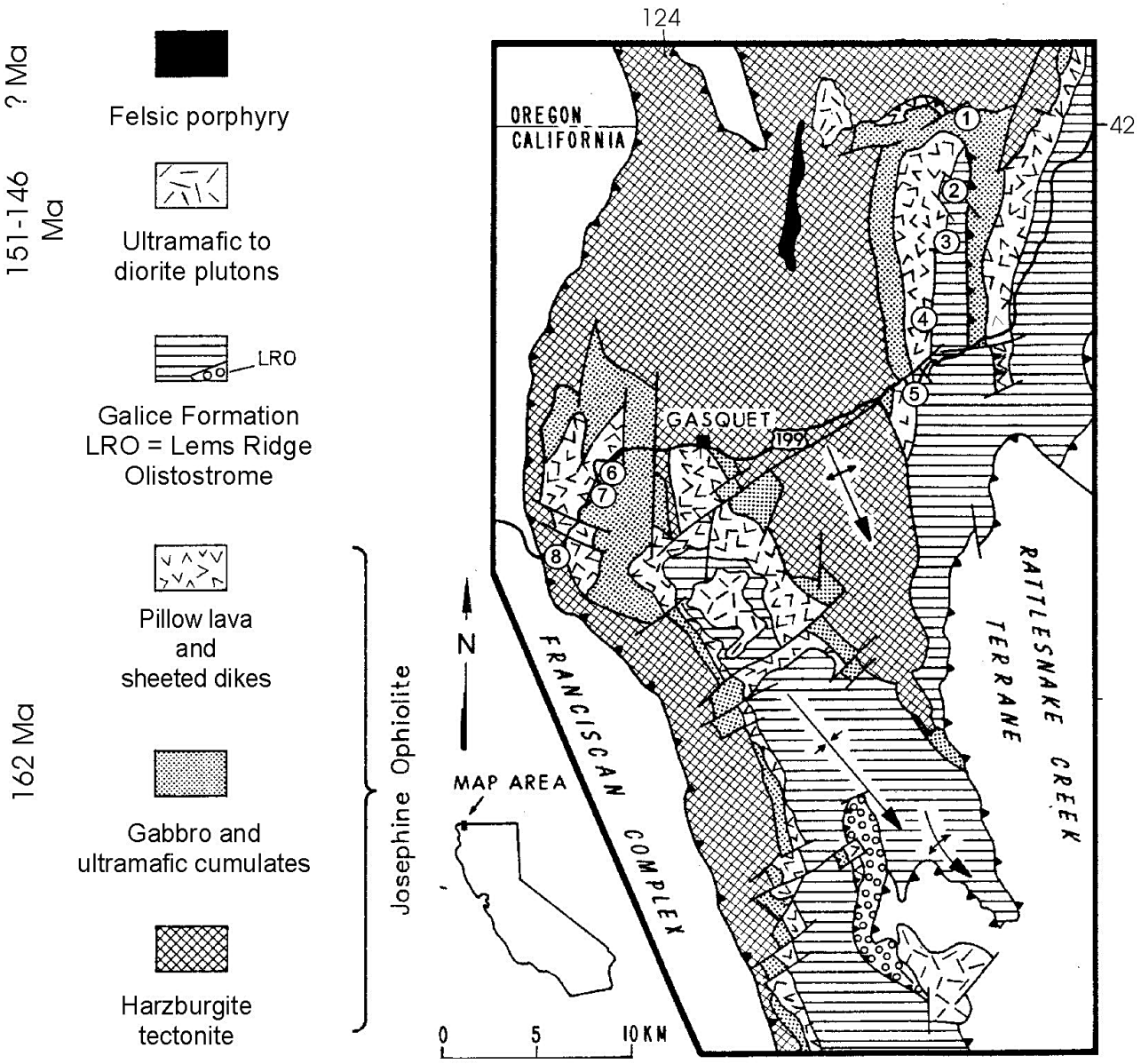

Figure 4. Simplified geologic map of the central part of the Josephine Ophiolite showing circled stops for the field trip.

graywacke, slate, and rare conglomerate) of the Galice Formation. The graywackes consist largely of volcanic rock fragments and plagioclase (especially near the base of the Galice Formation), but also contain chert, argillite, and metamorphic rock fragments and well-rounded (recycled) zircon grains. The source area for the graywackes, as well as the graywacke interbedded with the pillow lava, was most likely a magmatic arc built on older rocks of the Klamath Mountains (Snoke, 1977;Harper, 1984).

The Josephine Ophiolite and overlying Galice Formation are intruded by numerous 146-151 Ma calc-alkaline dikes and sills, most of which are hornblende basaltic andesite, but include andesite and dacite (Stop 3). Plutons related to these dikes also intrude the (Orleans) roof thrust at the top of the Josephine–Galice thrust sheet.

Age data for the Josephine and its overlying sedimentary rocks are summarized in Figure 3. The ophiolite has yielded Pb/U zircon ages of 162 $\pm$ 1 and 164 $\pm$ 1 Ma from plagiogranite (Wyld and Wright, 1988; Harper and others, 1994) and a late Middle Jurassic biostratigraphic age based on radiolarians from

chert within the pillow lavas (Pessagno and Blome, 1990). The pelagic-hemipelagic sequence is well dated by radiolarians, and deposition of the Galice flysch is constrained to have started at about 157 Ma and ended by 150 Ma (Pessagno and Blome, 1990; Harper and others, 1994).

The Galice Formation is overlain with great unconformity by Lower Cretaceous nonmarine and marine sedimentary rocks near Obrien, just north of the Oregon border (Fig. 2; Harper and others, 1994, and references therein). These sediments are correlative to the Great Valley Group that overlies Klamath Mountain basement at the north end of the Great Valley and which once extended across the Klamath Mountains.

Rogue–Chetco Island Arc Complex

Much of the Western Klamath Terrane consists of an island-arc complex (Harper and others, 1994; Yule, 1996) consisting of (1) the Late Jurassic Rogue Formation (a thick sequence of tuff, volcanic breccia, volcaniclastic sandstone, and minor lava flows, and (2) the Chetco Complex, consisting of the 161-157 Ma Illinois River Batholith and its ultramafic and mafic wall rocks (Dick, 1977; Yule, 1996).

The Rogue Formation overlies an older disrupted ophiolitic basement, probably correlative with the Rattlesnake Creek Terrane (Fig. 3; Yule, 1996). The Rogue Formation, like the Josephine Ophiolite, is conformably overlain by flysch of the Galice Formation (Fig. 3). The Chetco Complex underlies these rocks and the Josephine Ophiolite along a regional thrust fault (Madstone Cabin Thrust) that was active at the same time as the "roof" thrust of the Western Klamath Terrane (Harper and others, 1994).

"Rift facies" of the Josephine Ophiolite

One of the important aspects of the Western Klamath Terrane is the presence of several "rift facies" related to the Josephine Ophiolite. These consist of older Klamath basement, specifically the approximately 200 Ma ophiolitic Rattlesnake Creek Terrane (RCT), intruded and overlain by approximately 165 Ma (Josephine age) mafic dike complexes, ophiolite breccia, pillow lava, and ophiolite breccia (Saleeby and others, 1982; Wyld and Wright, 1988; Yule, 1996).

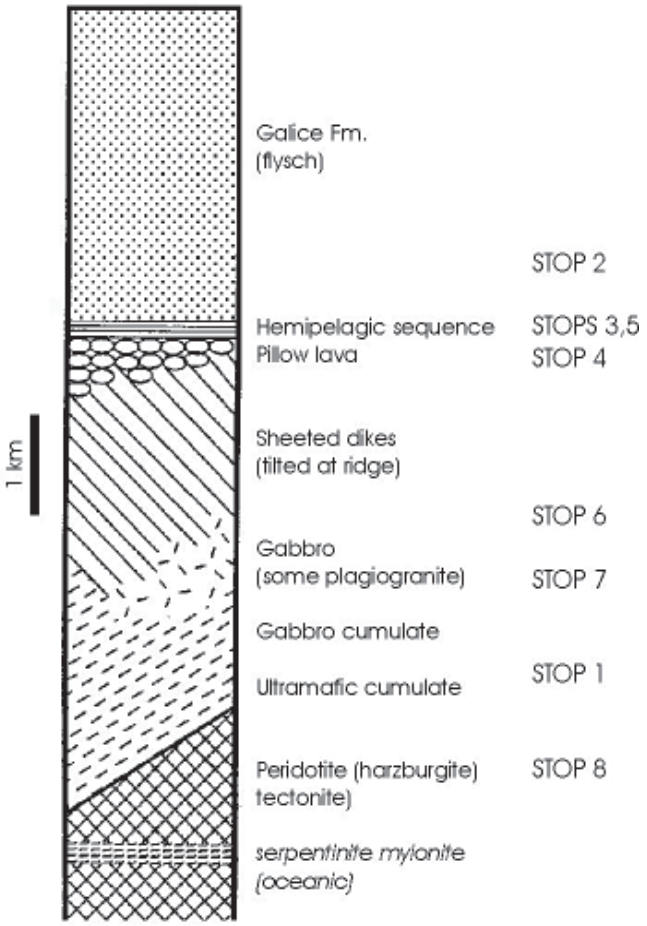

Figure 5. The Josephine Ophiolite and conformably overlying sedimentary rocks. The location of stops within the section are indicated at the right.

These occur in the Rattlesnake Creek Terrane itself, structurally above the Josephine Ophiolite in the area of Figure 2 (Preston Peak Complex; Snoke, 1977; Saleeby and others, 1982), and flanking the main Josephine Ophiolite body to the north, where it forms the basement for the Rogue Formation (Yule, 1996). In addition, Rattlesnake Creek-like ophiolitic basement lies beneath the Devils Elbow Remnant of the Josephine Ophiolite in the southern Klamath Mountains (Fig. 1, 3; Wyld and Wright, 1988), apparently having formed during an advanced stage of rifting just prior to the onset of seafloor spreading. These rift facies are consistent with other evidence suggesting that the Josephine Ophiolite formed by rifting of a magmatic arc built on older terranes of the Klamath Mountains (Saleeby and others, 1982; Wyld and Wright, 1988; Saleeby, 1992; Yule, 1996).

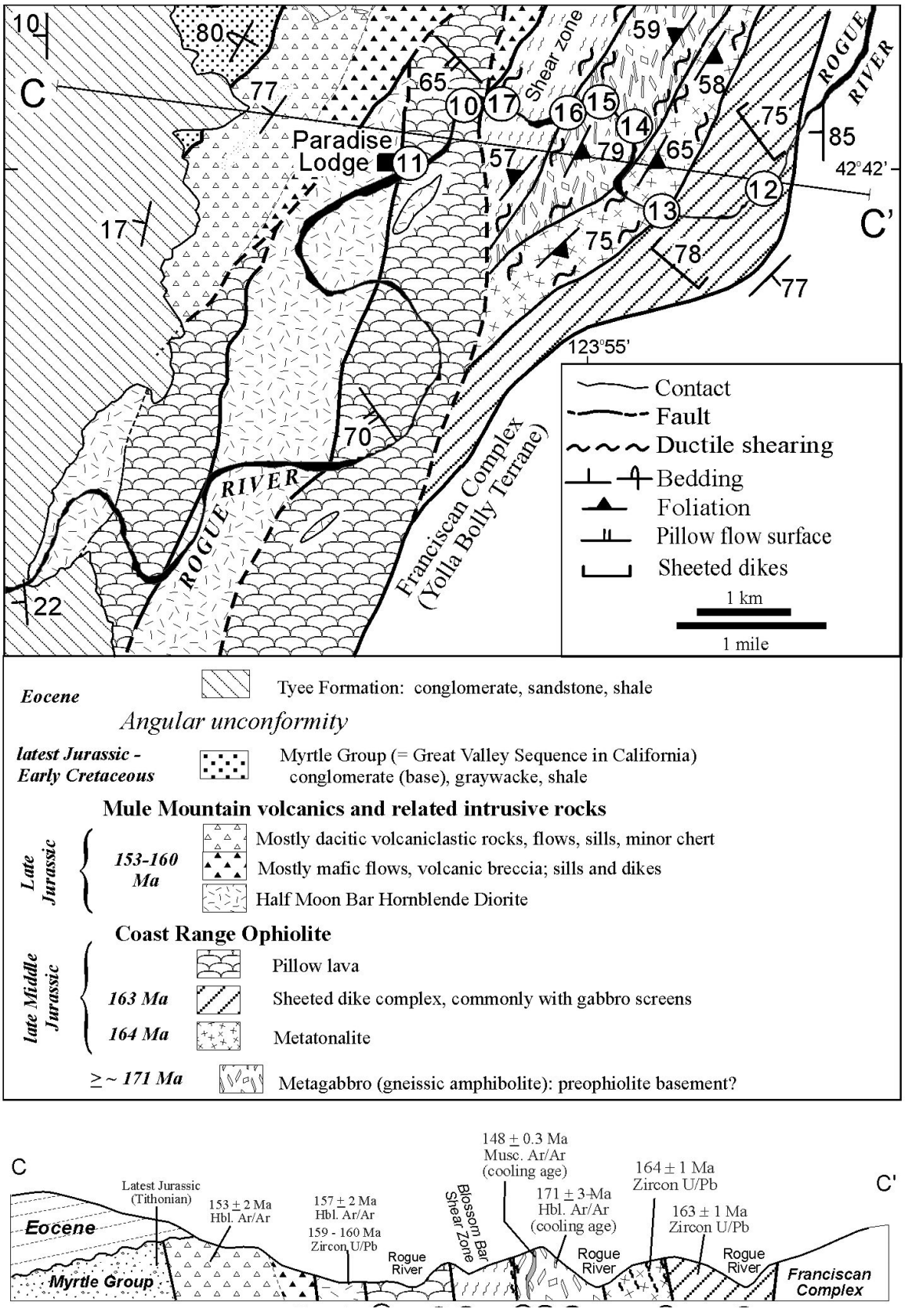

Figure 6. Geologic map and cross section of the geology along the Rogue River within the Wild Rogue Wilderness showing stops made on the field trip (modified from Kosanke, 2000).

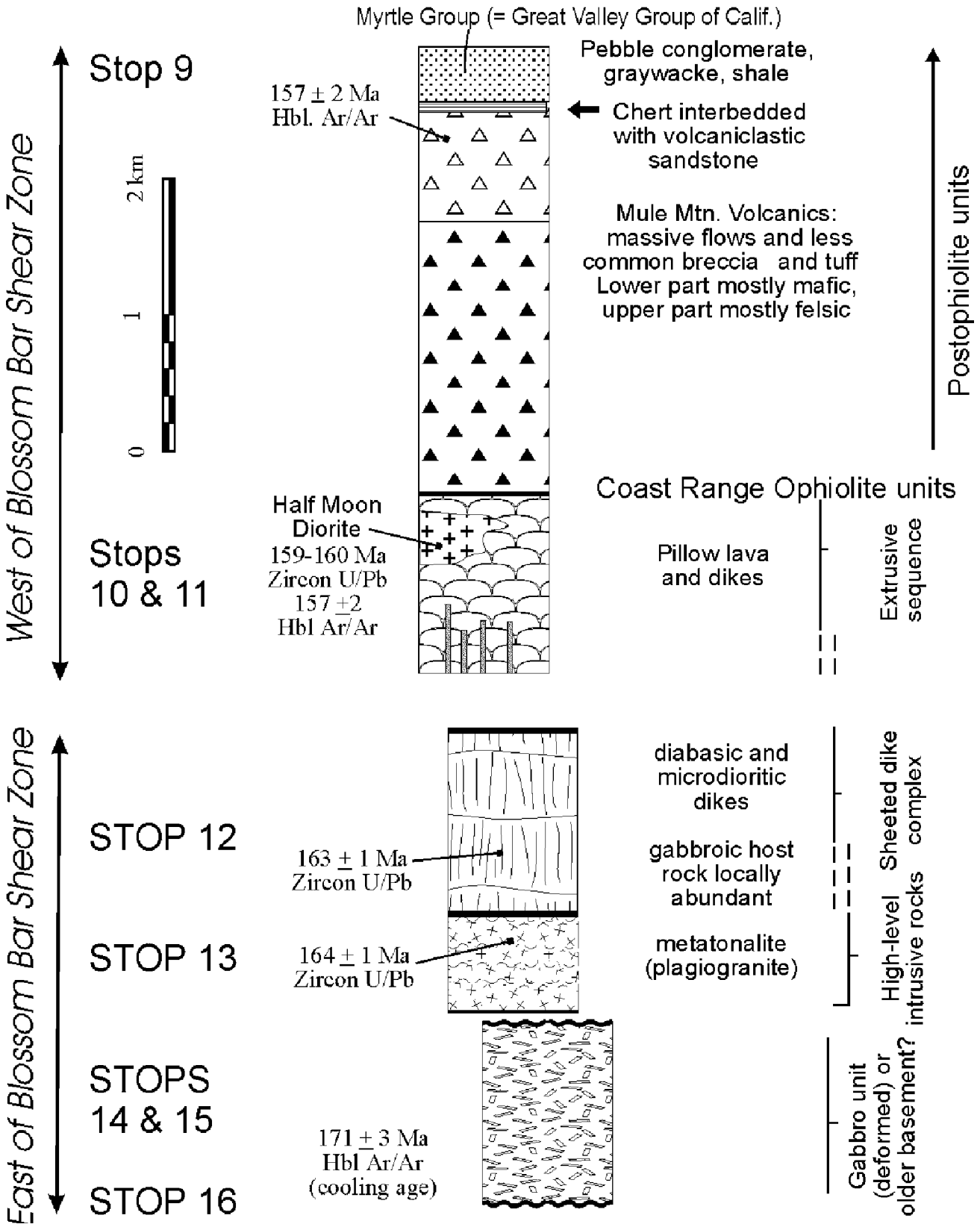

Figure 7. Tectonostratigraphy of the Coast Range Ophiolite and overlying rocks of the Snow Camp Terrane in the Wild Rogue Wilderness area visited on the field trip. The location of stops within the section are indicated on the left (modified from Kosanke, 2000).

Outliers of the Western Klamath Terrane

Figure 2 shows outliers of the Western Klamath Terrane both east and northwest of the Coast Range Ophiolite (part of the Snow Camp Terrane; Fig. 2). The eastern outlier, along the east side of the southern part of the Snow Camp Terrane, is clearly a klippe of the Chetco Complex that is in fault contact with the Coast Range Ophiolite (Blake and others, 1985; A. Schoonmaker and G. Harper, unpublished field data). This is an important locality, because the Coast Range Ophiolite and Western Klamath Terrane are in contact, whereas an analogous contact in California lies hidden beneath the Great Valley.

The northwest outliers consist predominantly of the Galice Formation. Recently, ophiolitic rocks including sheeted dikes, most likely of the Josephine Ophiolite, have been mapped in the westernmost outlier (Giaramita and Harper, 2001). As in the main part of the Western Klamath Terrane near Obrien, Oregon (Fig. 2), the Galice Formation in these outliers is unconformably overlain by Lower Cretaceous strata (Blake and others, 1985).

Nevadan Orogeny

One of the differences between the Josephine and Coast Range Ophiolites is that only the former has been affected by the Late Jurassic Nevadan Orogeny (see data and discussion in Harper and others, 1994). This includes thrusting of the Josephine Ophiolite and overlying Galice Formation more than 40 km beneath older terranes of the Klamath Mountains (Orleans Thrust, Fig. 2); thrusting of the Chetco Complex beneath the Josephine Ophiolite; tight-to-isoclinal folding of the Galice Formation; formation of slaty cleavage; and prehnite-pumpellyite to lower-greenschist facies regional metamorphism. Deposition of the Galice Formation (flysch), which began at about 157 Ma, likely records the onset of the Nevadan Orogeny in the Klamath Mountains. Thrusting was essentially completed by about 150 Ma, but regional metamorphism and possibly deformation of the Galice Formation continued until about 135 Ma (Harper and others, 1994).

Metamorphic grade and deformation in the Galice Formation increases toward the south in the area of Figure 4 (Harper and others, 1988); this is evident from sedimentary rocks at Stops 2 and 3, which have no slaty cleavage, to Stop 5 where a slaty cleavage is well developed, and grains in graywacke are strongly flattened.

SNOW CAMP TERRANE AND COAST RANGE OPHIOLITE

The Coast Range Ophiolite in California is typically faulted and to a large extent dismembered. It forms the basement for the latest Jurassic to Cretaceous Great Valley Group (deep-water fore-arc basin deposits). In California, deposits above the Coast Range Ophiolite and beneath the Great Valley Group, representing the time interval of approximately 165 to 145 Ma, range from predominantly tuffaceous chert, to volcaniclastic rocks, to ophiolitic breccia (Hopson and others, 1981; Robertson, 1990; Dickinson and others, 1996).

The Coast Range Ophiolite was recognized in southwestern Oregon by Blake and others (1985), who included it and the overlying Myrtle Group (correlative with Great Valley Group in California) in the Snow Camp Terrane (Figs. 2, 3). The Coast Range Ophiolite has recently been studied in detail in two areas within the Snow Camp Terrane: the Snow Camp Mountain area in the south (Harper and others, 2000, and in preparation) and the Wild Rogue River Wilderness area in the northeast (Kosanke, 2000). The southern part of the terrane, in the area of Snow Camp Mountain, has all the components of a complete ophiolite sequence, including upper mantle peridotite, ultramafic cumulates, cumulate gabbro, sheeted dikes (mostly having gabbro screens), and pillow lava. Like the California remnants, it is faulted and largely dismembered. Basal sediments in the Snow Camp Mountain area include chert, minor ophiolitic breccia, and at least some volcaniclastic sandstone (G. Harper, unpublished field data). This is overlain, apparently conformably, by the latest Jurassic to Cretaceous equivalent of the Great Valley Group (Myrtle Group) consisting of pebble conglomerate (near base), graywacke, and mudstone (we will visit the latter at Stop 9). These rocks occur at structurally, and locally topographically, high levels. Unfortunately this area is usually inaccessible until early June, and thus will not be visited on this field trip.

Wild Rogue Ophiolite Remnant of the Coast Range Ophiolite

We will visit the Wild Rogue Ophiolite (WRO) remnant of the Coast Range Ophiolite (Fig. 2) where it is exposed along the Rogue River in the Wild Rogue Wilderness area (Fig. 6). All units of the Wild Rogue Ophiolite and the overlying Myrtle Group in this area are subvertical, and, in the west, are unconformably overlain by gently dipping Eocene strata. The rock units in the Wild Rogue Ophiolite (Fig. 6, 7) are divided into those east and west of a 0.5- to 0.9 km-wide ductile shear zone, mapped and named the Blossom Bar Shear Zone by Kosanke (2000).

The ophiolitic rocks (Fig. 6, 7) in the Wild Rogue Ophiolite are in some ways distinctive compared to the Coast Range Ophiolite remnant in the Snow Camp Mountain area and to California Coast Range Ophiolite remnants in general. In particular, ductily deformed rocks are present, including a major ductile shear zone, and postophiolite intrusions are common. Possibly this section represents a transition from the Josephine to the Coast Range Ophiolite, assuming they were formed in the same basin. Alternatively, volcanic rocks and the Myrtle Group west of the Blossom Bar Shear Zone may belong to the Snow Camp Terrane (pillow lava would be the only part belonging to the Coast Range Ophiolite) and those units east of the shear zone might comprise an outlier of the Josephine Ophiolite.

Rocks West of the Blossom Bar Shear Zone

West of the shear zone is a sequence of pillow lava of the Coast Range Ophiolite overlain by the Mule Mountain Volcanics that in turn is overlain, apparently conformably, by the Myrtle Group (Great Valley Group equivalent). Perhaps as much as a kilometer or more of pillow lava is exposed in this area, but the total thickness is unknown because the base is faulted (Fig. 6). Hydrothermal metamorphism is evident from patchy epidosites common in the pillows as well as from low-grade metamorphic mineral assemblages (Kosanke, 2000). Some of the pillows are hematitic. Interpillow red chert and rare discontinuous beds of chert occur within the pillow lava but did not yield any datable radiolarians (E. Pessagno, personal communication). Trace and rare-earth element geochemistry shows that the pillow lava has affinities to island-arc tholeiites, but some is transitional to midocean ridge basalt (Kosanke, 2000).

The pillow lava, which is considered the upper part of the Coast Range Ophiolite, is overlain by a thick sequence of volcanic rocks informally called the Mule Mountain Volcanics (Kosanke, 2000). The lower part consists primarily of mafic flows and minor volcanic breccia estimated to be approximately 2 km thick. These are overlain by intermediate to silicic volcaniclastic sandstone, tuff, breccia, and minor chert. The only age data from the Mule Mountain Volcanics is an Ar/Ar hornblende (igneous) age of 153 $\pm$ 2 Ma on a dacite flow or sill from the upper part of the unit (Fig. 6, 7). Radiolarians in the chert are too poorly preserved for dating (E. Pessagno, personal communication).

Intrusive rocks informally named the Half Moon Diorite have been mapped in this area. For the most part, they occur in fault slices adjacent to the pillow lava unit, but preserved intrusive contacts with the pillow lava have been mapped around small intrusives related to this diorite (Fig. 6). The predominant rock type is hornblende diorite, but a range of rock types includes hornblende quartz gabbro and hornblende tonalite. One Ar/Ar hornblende age and two Pb/U zircon ages fall in the range of 157 to 160 Ma (Fig. 6, 7). These intrusive rocks are petrogenetically unrelated to the pillow lava, having petrographic and geochemical characteristics of calc-alkaline rocks of magmatic arcs.

Rocks East of the Blossom Bar Shear Zone

East of the Blossom Bar shear zone is what seems to be an east-facing sequence of ophiolite units, including metagabbro, metatonalite (plagiogranite), and a sheeted dike complex (first recognized by Ramp and Gray, 1980). The sheeted dike complex consists of well-defined dikes averaging approximately 1 meter in width. Many of the dikes have been intruded and "split" by other dikes, and screens of layered gabbro (sheets of wall rock) are locally abundant. A plagiogranite within a gabbro screen yielded a Pb/U zircon age of 163 $\pm$ 1 Ma (Fig. 6, 7; Kosanke and others, manuscript in preparation). The sheeted dikes are in general

mafic, but intermediate-composition dikes (microdiorite and micro-quartz diorite) are common and are often porphyritic (Kosanke, 2000). Many of these intermediate dikes seem to have been intruded relatively late into the sheeted-dike complex based on relative ages worked out using chilled margins. These late dikes have calc-alkaline magmatic affinities, compared to the predominantly island-arc tholeiite affinities of most of the sheeted dikes (Kosanke, 2000). These late dikes are not dated but may be related to the adjacent metatonalite or possibly to the postophiolite Half Moon Bar Diorite and Mule Mountain Volcanics.

West of the sheeted-dike complex is the metatonalite unit. This unit yielded a Pb/U zircon age of 164 ± 1 Ma (Fig. 6, 7). It is foliated and lineated, much of it strongly, but the intensity of the deformation is variable and is locally nearly absent. Gray dikes and enclaves are locally present. The deformation is especially strong along contacts with the sheeted dike complex and metagabbro; this and mylonitic fabrics indicate that the deformation is due to ductile shearing, perhaps coeval with deformation in the Blossom Bar Shear Zone. Microstructures and mineral assemblages indicate deformation at approximately 300 to 500·C (Kosanke, 2000).

The metagabbro unit is for the most part a gneissic amphibolite; fine-grained amphibolites also occur and seem to have been dikes originally. As in the metatonalite, deformation in the metagabbro is heterogeneous, and some outcrops show relict igneous textures with little deformation (Stop 14). Much of the metagabbro has relict magmatic foliation (aligned hornblende + plagioclase) overprinted by solid-state deformation and recrystallization under amphibolite facies. Temperature during amphibolite metamorphism is estimated from plagioclase-hornblende geothermometry to be between 636 and 670·C (Kosanke, 2000). The amphibolite facies assemblage is variably overprinted by the lower greenschist facies assemblage (retrograde metamorphism). The origin of the metagabbro is uncertain; it may simply be the gabbroic unit of the ophiolite that underwent considerable ductile deformation and amphibolite facies metamorphism at the ridge axis, similar to that observed in some gabbros in modern ocean crust. On the other hand, the following suggests the metagabbro had a distinct geologic history from the other ophiolitic units, at least until the onset of the retrograde greenschist facies metamorphism that affected the metatonalite and sheeted dike complex (Kosanke, 2000): (1) a hornblende Ar/Ar cooling age of 171 ± 3 Ma is significantly older than the 164 Ma zircon ages for the sheeted dike complex and metatonalite unit; because this age represents the time the metagabbro cooled below approximately 500·C, it is a minimum igneous age for this unit; (2) trace and rare-earth element geochemistry of the metagabbro indicates that it is petrogenetically unrelated to the pillow lava, metatonalite, and sheeted-dike units; (3) the textures and geochemistry of the metagabbro are unlike those of the gabbro screens in the sheeted dike complex. These distinctions suggest that the metagabbro unit may be a fragment of older basement that was rifted during ophiolite formation. If so, this remnant of the Coast Range Ophiolite might be a "rift facies" much like those associated with the Josephine Ophiolite. Obtaining an igneous age for the metagabbro unit will be necessary to fully evaluate this hypothesis.

Rare muscovite-garnet tonalite dikes locally occur in the metagabbro unit (Stop 15) and cut foliation in the metagabbro. These dikes, however, have been ductily deformed to some extent. Microstructures and textures in these dikes are the same as those in the metatonalite unit and the Blossom Bar Shear Zone, thus suggesting deformation at temperatures of approximately 300 to 500·C. Two Ar/Ar ages on muscovite from two of these dikes yielded similar ages of 148.5 ± 0.2 and 148.0 ± 0.5 Ma (Kosanke and others, manuscript in preparation). These ages represent the time of cooling of muscovite below its closure temperature of approximately 350·C, and as such represent minimum igneous ages. This temperature provides a minimum age on deformation, not only in these dikes but also in the adjacent metatonalite and the Blossom Bar Shear Zone.

Blossom Bar Shear Zone and Age of Ductile Deformation

The Blossom Bar Shear Zone is 0.4 to 0.9 km wide and consists of mafic to silicic

ultramylonites and mylonites variably overprinted by cataclasis and cut by syntectonic to posttectonic veins (Kosanke, 2000). Lineations plunge steeply, and sense-of-shear indicators (asymmetric porphyroclasts; S-C and C-C′ composite foliations) indicate west side up. Many of these rocks are very fine grained, and the mafic mylonites are chlorite rich. Microstructures and mineral assemblages indicate deformation under similar conditions as the metatonalite, approximately 300 to 500·C. The eastern contact with the metagabbro and (younger?) quartz diorite is gradational and defined by an increase in strain.

The age of the shear zone, as well as ductile deformation in the metatonalite unit and muscovite garnet dikes, is considered by Kosanke (2000) to postdate the ophiolite. North of the Rogue River, foliated outcrops of volcanic breccia along the western margin of the shear zone suggest that the ductile deformation occurred after deposition of at least some of the Mule Mountain volcanic rocks, but this relationship is not well constrained due to limited outcrop. The muscovite cooling age in deformed tonalite dikes in the metagabbro unit suggests that temperatures remained sufficiently high for deformation of silicic rocks until about 148 Ma. An alternative explanation is that the ductile deformation in the shear zone and metatonalite occurred at or near the ridge axis when the ophiolite was forming in response to structural extension. In any case, the amphibolite facies deformation in the metagabbro is relatively old, based on its 171 Ma cooling age that should essentially date the end of amphibolite-facies metamorphism, as the closure temperature for hornblende is approximately 500·C.

Restoration of the Coast Range Ophiolite in this area to the time that the overlying latest Jurassic Myrtle Group was deposited brings the units back to subhorizontal. This results in the Franciscan Complex structurally beneath the Coast Range Ophiolite, as is the case in California. The metagabbro, metatonalite, and sheeted dike units, however, are in reverse order compared to typical ophiolite pseudostratigraphy. The contacts between these units are faulted, and sense-of-shear indicators indicate the metagabbro and metatonalite were thrust north over the sheeted-dike complex, which can account for the reverse order. When restored, the Blossom Bar Shear Zone is subhorizontal, and sense-of-shear indicators indicate rocks of the shear zone are thrust northwest over the metagabbro and metatonalite units.

The inferred age of ductile deformation in the Blossom Bar Shear Zone as well as the inferred contractional deformation falls within the age range of the Nevadan Orogeny that affects the Josephine Ophiolite and other units of the Western Klamath Terrane. Such deformation has not, to our knowledge, been reported in the California Coast Range Ophiolite, and it is absent in the ophiolitic rocks of the Snow Camp Mountain area farther south in the Snow Camp Terrane (Blake and others, 1985; G. Harper, unpublished field data).

Is the Wild Rogue Ophiolite Remnant Actually the Coast Range Ophiolite?

Several features of the Wild Rogue Wilderness ophiolitic rocks are unusual compared to California occurrences of the Coast Range Ophiolite, and different from the ophiolitic rocks of the southern Snow Camp Terrane (Snow Camp Mountain area). Because of this, we are somewhat uncertain whether the ophiolitic rocks we visit on the Rogue River are part of the Coast Range Ophiolite or an outlier of the Josephine Ophiolite.

One of the primary differences between the California Coast Range Ophiolite remnants and the Josephine Ophiolite is the overlying stratigraphy, in particular, the timing of the onset of flysch deposition. On the Josephine Ophiolite, the Galice flysch deposition began at approximately 157 Ma and ended by 150 Ma. In contrast, flysch deposition did not begin until the latest Jurassic (about 145 Ma) on the Coast Range Ophiolite and its overlying volcano-pelagic sequence. In addition, the Josephine Ophiolite and overlying Galice Formation underwent regional low-grade metamorphism and associated deformation during the main phase of the Nevadan Orogeny (about 155–145 Ma). In contrast, the Coast Range Ophiolite was covered conformably during this time interval with "volcano-pelagic" sediment and locally thick sequences of volcaniclastic rocks (Del Puerto and Llanada Remnants of the Coast Range Ophiolite; Hopson and others, 1981; Robertson, 1990;

Dickinson and others, 1996). These differences are perhaps best indicated by the relationship of the Great Valley Group to these ophiolites: the Josephine Ophiolite and the Galice Formation are overlain with great unconformity, whereas the Coast Range Ophiolite and overlying sequences are overlain conformably (Fig. 3).

As noted above, the sequence of pillow lava and overlying volcanic rocks and Myrtle Group have stratigraphic relationships most consistent with the Coast Range Ophiolite and overlying sequences in California, especially those with thick volcaniclastic sequences. These rocks do not seem to be regionally metamorphosed as do the Josephine and overlying Galice Formation, and there is no evidence of an unconformable contact with the overlying Myrtle Group. An unusual aspect of these rocks, however, is the presence of calc-alkaline intrusions (Half Moon Diorite) as old as 160 Ma, older than those in the Josephine Ophiolite (151–146 Ma; Harper and others, 1994) or those cutting the Coast Range Ophiolite in some remnants (Dickinson and others, 1996).

Rocks east of the Blossom Bar Shear Zone are less readily correlated with the Coast Range Ophiolite, although their position structurally beneath the pillow-lava unit and above the Franciscan Complex is consistent with their being part of the same terrane. The presence of a sheeted-dike complex is unusual in the Coast Range Ophiolite (Hopson and others, 1981), but it is typical of the Josephine Ophiolite (Harper, 1984). The metagabbro, metatonalite, and Blossom Bar Shear Zone do not have similar equivalents in either the Coast Range or Josephine Ophiolites. The significance of this deformation is uncertain, but if the inferred age of the shear-zone deformation is correct it may well have occurred during Nevadan-age thrusting (about 155–150 Ma; Harper and others, 1994). What might be the source of heat for the Blossom Bar Shear Zone? Kosanke (2000) notes that ductile deformation overlapped with epidote and prehnite veining, and suggests that hydrothermal circulation, possibly associated with magmatism related to the Half Moon Diorite and Mule Mountain Volcanics, was the heat source. This interpretation is consistent with the retrograde nature of veins in the shear zone, with the youngest veins including the zeolite laumontite.

In summary, the Wild Rogue Ophiolite Remnant is interpreted to be part of the Coast Range Ophiolite. We cannot rule out, however, that it is an outlier of the Josephine Ophiolite. One possibility is that the Coast Range Ophiolite and Josephine Ophiolite were originally continuous, or at least formed by spreading in the same basin, and that the Wild Rogue Remnant represents a transition between them. Furthermore, the presence of a possible old metagabbro unit suggests that this remnant might represent a rift facies similar to those associated with the Josephine Ophiolite (Saleeby and others, 1982; Wyld and Wright, 1988; Harper and others, 1994; Yule, 1996).

ROAD LOG

Mileage is given below both as cumulative miles from the starting point of Day 1 in Cave Junction as well as miles between stops or geographic features. In addition, longitude and latitude are given so that stops can be accurately located with a GPS unit.

For those using this field guide on their own, the U.S. Forest Service map of the Six Rivers National Forest is a useful aid for location of stops in the Josephine Ophiolite and can be purchased at the U.S. Forest Service Ranger Station in Gasquet, California (Fig. 2). The Wild Rogue Ophiolite Remnant is in a wilderness area. Access from the coast is restricted to jet boat from Gold Beach, Oregon, or Foster Bar near Agness, Oregon (companies that provide this service are based in Gold Beach). The Rogue River Trail can also be taken from Foster Bar. The Wild Rogue Ophiolite Remnant is accessible by road, albeit a time consuming drive, from either Grants Pass or Gold Beach, Oregon. The contact between the sheeted dike complex and Franciscan Complex on Figure 6 is located less than 1 kilometer downstream from Marial Lodge on the Rogue River (north side of river). The road to Marial Lodge and nearby Tucker Flat Campground and Rogue River Ranch Historical Site are shown on U. S. Forest Service maps for the Wild Rogue Wilderness and for the Siskiyou National Forest. The trail following the north bank of the Rogue River can be accessed at the end of this road. Access by raft from upriver is by permit only and takes 2 days.

Day 1

The field trip leaves at 8 a.m. from the Junction Inn in Cave Junction, Oregon. Drive south on US 199 to Obrien, Oregon. We are driving over graywacke and slate (flysch) of the Galice Formation that overlies the Josephine Ophiolite, although most is covered by Quaternary alluvium. As we drive south, orange-weathering peridotite (basal unit of Josephine Ophiolite) is evident in the poorly vegetated mountains to the west; in this area, the entire crustal sequence of the ophiolite has been cut out by a large north-striking normal fault. As we near Obrien, the hill to the east of US 199 consists of Lower Cretaceous (Hauterivian) nonmarine conglomerate (red at base) and shallow-marine sandstone that overlie the Western Klamath Terrane with great unconformity. These strata are correlative to the Great Valley Group that unconformably overlies the Klamath Mountain accreted terranes at the north end of the Great Valley.

Drive south on US 199 to Obrien, Oregon.

7.3 7.3 Turn right (west) at main intersection onto paved road (Lone Mt Road).

8.2 0.9 Turn left (south) at intersection (stay on Lone Mt Rd, which becomes USFS. Road 4402).

13.4 5.2 Cross bridge over Whiskey Creek.

17.9 4.5 Pass intersection with Del Norte County Road 316 (bear right). Continue on same road (still USFS Road 4402, now called Wimer Road).

18.9 1.0 Turn left at intersection with USFS. Road 19N01 and park vehicles (41·59.000′, 123·48.199′). Walk back along road (east) 0.1 mile to intersection with small road on left (north; USFS road 085). Walk up this road approximately 0.1 mile and look at outcrops in grassy areas to the right (east) of the road.

STOP 1. (approx. 41·59. 948′, 123·48.147′) These outcrops are ultramafic cumulates at the base of the plutonic sequence of the Josephine Ophiolite, not far above the basal mantle peridotite (to north). The cumulates consist of clinopyroxenite (cpxite), dunite, and wehrlite (cpx + olivine). Note igneous layering, strong alignment of cpx in cpxites, and poikilitic cpx in some wehrlites. Cpx is fresh, but olivine is partially serpentinized and appears dull black in hand sample.

Reverse direction, back-tracking (east) down USFS 4402 (Wimer Road) to intersection with County Road 316.

19.9 1.0 Turn right at the intersection onto Del Norte 316 and drive south; this road follows Shelly Creek.

22.5 2.6 Massive outcrop on right (west) side of road just past an intersection with U.S.F.S. road 18N17 on the left (east), just beyond bridge over a small creek (milepost 9.08 marker).

STOP 2. (41·58.002′, 123·48.447′) Observe massive graywacke of the Galice Formation. Stratigraphically, this outcrop is part of a predominantly massive graywacke unit at the base of the Galice flysch that conformably overlies the pelagic-hemipelagic sequence we will see at the next stop. The bivalve *Buchia concentrica* collected from beneath the bridge indicates a Late Jurassic (late Oxfordian to early Kimmeridgian) age. Clasts in these basal wackes are predominantly andesite rock fragments and plagioclase with up to 5% detrital cpx and altered glass fragments; these clasts suggest derivation from an active magmatic arc. The wackes also have clasts probably derived from older rocks of the Klamath Mountains, including chert (some Triassic), metamorphic rock fragments and minerals, and well-rounded (recycled) zircon (Snoke, 1977; Harper, 1984).

These graywackes have been regionally metamorphosed to prehnite-pumpellyite facies, but are essentially undeformed here; to the south and east they are semischist interbedded with slate. This regional metamorphism and associated deformation occurred during the

Late Jurassic Nevadan Orogeny (Harper and others, 1994, and references therein).

Continue south on Del Norte 316.

23.5 1.0 Quarry at tight right bend in road.

STOP 3a. (41·57.351′, 123·49.043′) This quarry and road cut expose the pelagic-hemipelagic sequence ("volcano-pelagic" of Dickinson and others, 1996) stratigraphically below the graywacke seen at the last stop and which conformably overlies the Josephine Ophiolite. The contact with pillow lava is poorly exposed in the south side of the quarry. The rocks exposed here include radiolarian chert, radiolarian mudstone, tuffaceous chert, and metalliferous (Fe-rich) sediment. The age range for this hemipelagic-pelagic sequence is about 162 to 157 Ma, based on both radiometric and biostratigraphic data (Harper and others, 1994, and references therein).

Light colored rocks are dacite sills belonging to the syntectonic 151-146 Ma calc-alkaline dikes, sills, and small plutons that cut the ophiolite, the Galice Formation, and the roof (Orleans) thrust (Fig. 2; Harper, 1984; Harper and others, 1994, and references therein). One of the sills increases thickness considerably from the road outcrop into the quarry, having a "minilaccolith" shape.

The lower and upper parts of the sequence at this locality are thin bedded, but the middle of the sequence, in the main part of the road cut, consists mostly of unusual massive to irregularly bedded black (Mn stained) rock. This part of the section, which occurs 8 to 21 meters above the base of the sequence, consists of iron- and manganese-rich sediment, but also contains a significant amount of siliceous (radiolarian) and terrestrial mud components (Pinto-Auso and Harper, 1985).

Green tuffaceous chert lies above the metalliferous horizon. Sand-size grains of volcanic quartz and plagioclase are in places visible with a hand lens; in thin section, radiolarians and altered glass fragments are also visible (Pinto-Auso and Harper, 1985).

Continue south on Del Norte 316.

23.7 0.2 High road cut on right side of road beneath power lines, just beyond county road milepost 7.86.

STOP 3b. (41·56.686′, 123·49.231′) Road cut in upper pillow lava of Josephine Ophiolite. Careful observation is needed to pick out the chilled margins on the pillows and the interstitial dark green chert between the pillows. The green color of the pillow lava is due to low-grade metamorphic minerals including chlorite, albite, and pumpellyite (Harper and others, 1988); relict igneous cpx is typically present. Most upper pillow lavas of the Josephine Ophiolite are geochemically distinct (midocean ridge basalt, or MORB) from the lower pillow lavas and sheeted-dike complex (predominantly transitional island-arc tholeiite to MORB).

Continue south on Del Norte 316.

29.5 5.8 Small road intersection on left. Stay on main road.

29.8 0.3 Major intersection. Turn left (south) to stay on Del Norte 316, which follows Patrick Creek south toward U.S. 199.

30.5 0.7 Cross bridge over mouth of Shelly Creek; a primitive USFS campground lies on the west side of road north of the creek.

31.7 1.2 Intersection with USFS 18N16. Turn left (east) onto this road, which will take us up to the top of Shelly Creek Ridge.

34.4 2.7 Intersection. Bear to left (north).

35.0 ~0.6 Quarry on right (east) side of road on Shelly Creek Ridge.

STOP 4. (approx. 41·53.85′, 123·49.83′) This quarry exposes lower pillow lava of the Josephine Ophiolite, which is typically strongly altered by hydrothermal metamorphism (especially evident from patchy epidote-rich and hematitic alteration; Harper and others, 1988). Pillows do not weather out here, but rather pillow outlines are visible on surfaces of huge blocks on the quarry floor. Volcanic breccia is

exposed at the far south end of the quarry. In thin section, some of the pillows have pseudomorphs of olivine microphenocrysts containing inclusions of Cr-spinel. Chemically, they are high-Mg, high-Cr, and low-Ti basalt having affinities to depleted island-arc tholeiite or high-Ca boninite. Such lavas only occur in the lower pillow lava of the Josephine Ophiolite; they are chemically and petrographically distinct from the rest of the ophiolite pillow lavas (G. Harper, unpublished data and manuscript in review), including commonly being highly vesicular, and they constitute perhaps 10-20% of the lower pillow lava by volume.

Turn around and drive back to main road along Patrick Creek (Del Norte 316)

38.3 3.3 Intersection with Patrick's Creek Rd. Turn left (south).

39.2 0.9 Intersection with US 199. Turn left (east).

40.1 0.9 Pull off into parking area on right side of road, jusr after narrow stretch with vertical road cuts on highway.

STOP 5. (41·52.158, 123·49.839') This is an ptional stop (Stop 2 of Harper, 1989; may be covered by high river water). This is the type section of the pillow lava unit of the Josephine Ophiolite and overlying pelagic-hemipelagic sequence that grades upward into the overlying flysch (Harper, 1984; Pessagno and Blome, 1990). Biostratigraphic and radiometric age data indicate that the sequence exposed at this locality ranges from approximately 162 Ma (pillow lavas) to 157 Ma. As at Stop 3, light-gray sills and dikes cut this section, belonging to the 146 to 151 Ma suite of syntectonic calc-alkaline intrusives (Harper and others, 1994).

Leave vehicles and walk back (south) along highway to near the beginning of the guardrail. Continue walking south along the highway (careful of traffic!) for approximately 120 meters and descend down steep embankment of loose rock to the river; the place to descend is upriver from the mouth of a creek that is visible on the other side of the river. Walk downstream to outcrops across from the mouth of this creek. Exposed here are cross sections of pillows in walls of large pothole (more evident if rock wetted) overlain by a thick massive lava flow. The lava dips approximately 65· upriver; careful observation of the massive flow reveals columnar joints plunging about 35· downstream. Proceed upriver (upsection) where the top of the massive flow is exposed. It can be seen to grade into a spectacular "isolated-pillow breccia" (with chilled minipillows). This breccia is overlain by meter-size pillows with paleomagnetic drill holes, which are in turn overlain by large lobate (mattress-shaped) pillows evident as cross sections on a vertical wall. Epidosites are well developed here and represent pathways of discharging mineralizing fluids (Harper et al., 1988). These lava flows are all highly fractionated Fe- and Ti-rich basalts (Fe-Ti basalts) of MORB affinity that comprise the upper pillow lava unit (Harper, in review). A modern tectonic setting where such basalts occur is at propagating tips of spreading ridges.

Climb back up to the highway and walk back (north) toward the parking area. Near the end of the guardrail, drop down to the river to an exposure of the contact between the pillow lava unit and the overlying hemipelagic-pelagic sequence (Harper, 1984); on the opposite side of the river, the contact is a few meters to the right (downstream) of limonite-stained thin-bedded sediment. The details of the contact, as well as chilled margins in the pillows, are much easier to see if the rocks are wetted. The pillows below the contact are lobate; chilled margins are difficult to see, but look for dark chilled margins and triangular shaped junctions filled with light-green chert and dark elongate glass fragments. These pillows are also highly fractionated Fe-Ti basalt and have abundant microphenocrysts of plagioclase and clinopyroxene.

The sedimentary sequence exposed above the depositional contact is the same as at Stop 3, except that the entire pelagic-hemipelagic sequence and its transition into the Galice Formation flysch is exposed. The basal 45 m of sediment overlying the ophiolite consist of chert, tuffaceous chert, and siliceous argillite (black). Nodules of limestone occur in some layers. A metalliferous horizon such as that

seen at Stop 3 lies about 5 meters stratigraphically above (upstream) from the depositional contact (Pinto-Auso and Harper, 1985) and is evident from abundant limonite staining. At approximately 35 to 40 meters stratigraphically above the contact, bedding in the hemipelagic sequence is disrupted; this seems to have been during soft-sediment deformation and predates dike intrusion. Careful observation shows a volcanic pebbly mudstone bed in this zone. At about 45 meters above the contact with the pillow lava, two thick graywacke beds mark the beginning of flysch deposition. These are overlain by about 40 meters of silty radiolarian argillite exposed continuously to a sharp bend in the river (100 m stratigraphically above the ophiolite). Slate with abundant limestone nodules and a hornblende andesite sill occur at the bend in the river where the outcrops end at a pool. Massive graywacke and some pebble conglomerate, correlative with the graywacke at Stop 2, are exposed farther up section (upstream).

Nevadan structures evident in this section include a bedding-parallel slaty cleavage, boudinage of sills, fibrous extension veins, and flattened pebbles in graywacke. At stops 2 and 3, this deformation is not evident; this difference reflects an overall southward increase in Nevadan deformation that is related to regional low-grade metamorphism (Harper and others, 1988).

Return to vehicles and drive back (south and west) along US 199.

Between Patrick Creek Lodge and the village of Gasquet, we will be driving across the basal peridotite unit of the Josephine Ophiolite exposed in the core of a large anticline (Fig. 4). Most of what is exposed is sheared and serpentinized along a northeast-striking fault zone. Many landslides are evident, some of which are active.

48.3	8.2	Store–Post Office in village of Gasquet (pronounced Gas-Key).
48.9	0.6	Bridge over Hardscrabble Creek.
52.0	3.1	Large open area along US 199 with few trees and a clear view of Smith River and outcrops along river. Pull off onto wide paved shoulder along the left (river) side of the highway.

STOP 6. (41·60.257′, 124·02.095′) This north-trending stretch of the river exposes transitions from mostly gabbro to nearly 100% sheeted dikes, with the contact crossing the upper and lower parts of the north-trending section (this is Stop 4 of Harper, 1989). This outcrop has been the topic of considerable study, including the nature of the dike-gabbro transition, dike intrusion, hydrothermal metamorphism, and oceanic faulting (Alexander and Harper, 1993). The 162±1 Ma U/Pb zircon age on the Josephine Ophiolite is from a plagiogranite (cut by sheeted dikes) in this outcrop (Harper and others, 1994).

First we will walk back up the road (north) to where trees begin and descend to prominent outcrops along the river. These outcrops consist of sheeted dikes dipping downriver about 40· with screens (wall rock between dikes) of variably textured gabbro and other coarse-grained plutonic rocks (including some ultramafic cumulates!).

Walk back up to the highway shoulder and walk along the highway (downriver) to just past the end of the rock retaining wall. Look across at sheeted dikes dipping to the right (south) approximately 40·. Because we are in the core of a syncline, this is the actual dip of the sheeted dikes in the Josephine Ophiolite—the tilting of the sheeted dikes occurred at the ridge axis, probably as a result of normal faulting (Alexander and Harper, 1992). Note the thick, "soft" looking, steeply dipping dike across the river. This late dike is a Fe-Ti basalt related to the upper pillow lava. The upper pillow lava, this dike, and late ophiolite dikes cutting serpentinized peridotite are inferred to have propagated along strike from another ridge segment (Coulton and others, 1995; Harper, in review).

53.4	1.4	Turn left into a small unpaved parking area and park. A road descends to a gravel bar on the river (do not drive this road!). Walk down this road to the gravel bar.

STOP 7 (41·49.29′, 124·02.00′) This is an optional stop, depending on river level and time (Stop 5 of Harper, 1989). Walk a short distance downriver along the gravel bar to some very large slide boulders of plagiogranite. These boulders show excellent intrusive relationships, including intrusive breccia, a "pillowed dike" in plagiogranite, and in the farthest boulder, intrusive breccia cut by a mafic dike, in turn cut by a thin plagiogranite dike. This is the largest mass of plagiogranite found in the Josephine Ophiolite, having slid down from near the sheeted dike–gabbro contact, which is the level in the ophiolite in which all plagiogranites have been found.

Layered gabbro and ultramafic cumulate are exposed a few hundred feet up the river from the gravel bar, but these will probably not be accessible due to high river level.

		Return to vehicles. Turn left and continue down (south and west) US 199.
55.3	1.9	Large intersection (turn for Stout Grove). Turn left and cross bridge over the Middle Fork of the Smith River.
55.4	0.1	Turn right into parking lot and park (if you cross a second bridge you went too far). Leave cars and follow trail downriver past bathrooms (southwest) to a large outcrop high above the confluence of the Middle and South Forks of the Smith River.

STOP 8 (41·47.782′, 124·03.320′) Orange-weathering outcrops of the basal peridotite (harzburgite tectonite) unit of the Josephine Ophiolite. Fresh samples are greenish to black in hand sample; olivine may appear dull black due to partial serpentinization. In thin section only about 20% of the olivine is replaced by serpentine, and the orthopyroxene is fresh.

Although little, if any, evidence for foliation can be seen in these rocks, the rocks are actually highly deformed as indicated by microstructures and preferred orientation of olivine and pyroxene crystals. They are also highly depleted in alkalis and aluminum. They represent the residue (left over rock) after removal of a basaltic melt (Dick, 1977). In terms of seafloor spreading, these rocks flowed upward (in the solid state) beneath a spreading ridge, partially melted to produce mafic magma (which rose to the crust), and as a residue continued to flow upwards and move laterally to finally form the basement for the igneous rocks of the crustal section of the ophiolite.

This is the end of the field trip through the Josephine Ophiolite and its overlying sedimentary sequence. We will now drive to Brookings, Oregon.

55.7	0.3	Return to intersection with US 199.
57.3	1.6	Enter Redwood National Park and Jedadiah Smith State Park.
58.3	1.0	Intersection with Calif 197 (just before US 199 crosses Smith River). Turn right onto Calif 197.
65	6.7	Intersection with US 101. Turn right onto US 101 North.
81.8	16.8	Downtown Brookings, Oregon.

DAY 2

Day 2 starts with a 30-mile drive on US 101 from Brookings to Gold Beach, Oregon. The road log starts at the U.S. Forest Service Station on US 199, which is at the south end of Gold Beach.

		Leave U.S. Forest Service Station and drive to the north end of town.
1.6	1.6	Turn right (toward Motel 6) onto road just before crossing the large bridge over the Rogue River. This road follows the south bank of the Rogue River.
24.6	24.6	Park on left (north) side of road, just before crossing the bridge over the mouth of Illinois River.

STOP 9 (41·32.99′, 124·03.91′) In this outcrop (see Fig. 2 for location) are exposed graywacke and mudstone of the Myrtle Group (= Great Valley Group of California) that overlie the Coast Range Ophiolite south of this stop. A packet of medium- to thick-bedded graywacke occurs at the east end of the outcrop (probably submarine fan channel fill), whereas thin-bedded graywacke and shale (probably submarine fan overbank deposits) occur in the rest of the outcrop. Note folding.

This part of the Myrtle Group is Early Cretaceous in age; south of this outcrop it overlies a basal, uppermost Jurassic (Tithonian) pebble conglomerate unit, which in turn overlies the Coast Range Ophiolite. The Myrtle Group and its correlative Great Valley Group are interpreted to represent forearc basin sediment deposited west of the Cretaceous Andean-type arc built along western North America. Deposition started approximately 20 million years after formation of the Coast Range Ophiolite basement (Dickinson and others, 1996).

		Return to vehicles and continue driving on the road (upriver).
140.7	3.5	Cross bridge over Rogue River.
143.4	2.7	Turn right onto road to Foster Bar. Note steeply dipping Eocene sandstone and mudstone in road cuts; these strata are also exposed at the boat ramp at Foster Bar.
144.2	0.8	Foster Bar (42·37.94′, 124·02.90′). Park in large lot (near brick building with restrooms).

Board jet boats for 12-mile trip to Paradise Lodge. Gently east-dipping Eocene sedimentary strata are well exposed for several miles along the river. These give way to underlying conglomerate, some of which is red. The Eocene section overlies the Coast Range Ophiolite and overlying Myrtle Group with great unconformity. This unconformity is evident in a structural window through the Eocene strata 5 miles up river from Foster Bar, at Clay Hill Lodge (42·40.12′N, 123·58.69′W). The unconformity itself is not well exposed, but gently dipping Eocene conglomerate is exposed on the north side of the river just below the lodge, and steeply dipping strata of the Myrtle Group are evident on the south side of the river directly upstream. Eocene strata are again exposed upstream as we cross a normal fault. The angular unconformity between the steeply dipping Myrtle Group (and the underlying Coast Range Ophiolite) and gently dipping Eocene strata indicates substantial deformation sometime during the Cretaceous or early Tertiary.

After another 0.9 miles we cross into the area of the map shown in Figure 6. We will pass out of the Eocene strata and into the Snow Camp Mountain Terrane, which includes the Coast Range Ophiolite. Pillow lava is evident in some of the excellent exposures of greenstone along the river, including on the left (north and west) side of the river as we enter Huggins Canyon (42·40.81′N, 123·56.13′W), approximately 1.3 miles south of Paradise Lodge (Fig. 6).

Stop at Paradise Bar Lodge to unload gear.

Continue upstream in jet boat to Stop 10.

Pillow lava is exposed on both sides of the river upstream from Paradise Lodge. We will proceed up to a beach on the north side of the river where we will exit the jet boats. The beach is at the contact between the pillow lava unit and the Blossom Bar Shear Zone (Fig. 6). If possible with the jet boat, we will first stop and view pillows on the south side of the river at the base of a rockslide approximately 300 feet downstream from this beach.

STOP 10 (42·42.237′N, 123·55.393′W). Walk to second knob of greenstone downstream from the beach and look for pillow lava. There are many vague pillow forms. The pillow lava is strongly hydrothermally altered as evident from the abundant patchy epidote. As we continue walking downstream along the bedrock terrace, careful observation may reveal discontinuous chert layers up to about 20 cm thick interbedded with mafic lava. Approximately 300 feet downstream from Stop 10,

elongate pillows are evident, especially with binoculars, in large blocks in a rockslide across the river.

Continue walking downstream along the bedrock terrace, and eventually move uphill to intersect the Rogue River Trail. Follow the trail downriver (west and south).

STOP 11 Optional (approximately 42·42.290N, 123·55.536'W). This stop is below the Rogue River Trail on the bedrock terrace; the place to drop off the trail is near the end of the bedrock terrace and before the trail crosses a stream. We are still in the pillow lava unit of the Coast Range Ophiolite. An approximately 2 m-wide porphyritic andesite dike crops out along the side of an elongate notch (old channel?), trending roughly parallel to the trail. The dike is relatively light colored and cuts the pillow lava. This dike is probably related to the Half Moon Bar Diorite, just downstream (Fig. 6). Vague pillow shapes are visible here, but are not as clear as along the polished river outcrops.

Return to Rogue River Trail and continue downriver to Paradise Lodge.

DAY 3

The remainder of the field trip will consist of an approximately 5 mile round-trip hike from Paradise Lodge upstream along the Rogue River Trail. We will hike to the farthest stop, and then make the following stops on the way back. See Figures 6 and 7 for locations and context of these stops.

Hike up the Rogue River Trail 2.1 miles to Inspiration Point, which is clearly evident on the trail, as it is a high point and on a bend in the trail.

Inspiration Point lies in the sheeted dike unit, but it is not easy to see dikes here.

Continue on the trail upstream 0.23 miles, and stop on the trail just upstream from the mouth of Staircase Falls Creek, which is on the opposite side of the river (waterfalls visible in creek).

Steeply dipping sheeted dikes can be seen on the vertical wall left (east) of the creek mouth; gabbro screens are also evident from their lighter color.

Continue upstream along the trail for 0.21 mile until passing out of a wooded area along the trail. Follow a faint trail to the right, down to the bedrock terrace next to the river and near the Coffee Pot, a place where the river is extremely narrow and flows into a single whirlpool. Please be very careful around the river, especially the Coffee Pot, which has a strong downward suction.

STOP 12 (42·41.930'N, 123·54.869'W) Observe water-polished outcrops of sheeted dikes near the river, first upstream and then downstream from the Coffee Pot. Many subparallel diabase dikes are evident and have well-defined chilled margins. Gabbro screens (slivers of country rock between dikes) are common; they are cumulates with igneous layering oriented at a high angle to the dike margins. Plagiogranite within one of these screens yielded a 164 Ma U/Pb zircon age (J. Saleeby personal communication, and Kosanke and others, manuscript in preparation). Some of the late, thick dikes having two chilled margins are andesitic in composition (micro-diorites and micro-quartz diorites) and are often porphyritic.

Return to the Rogue River Trail and walk back downstream to approximately 800 feet past Inspiration Point. We will hike down a moderately steep embankment and work our way down to a bench at the top of a cliff that faces upriver.

STOP 13 (N 42·41.807'N, 123·54.511'W) The cliff face is a fault contact between the sheeted-dike complex (upstream) and a metatonalite ("plagiogranite") unit. The fault can also be seen as a cliff face on the other side of the river

and is oriented approximately N40E, 63E. We are standing on the metatonalite (downstream side of fault). Note that the metatonalite here is both strongly foliated (steep east dip) and lineated (steep plunge). Strained quartz grains can easily be observed with a hand lens. The deformed metatonalite has a mylonitic fabric that was developed under greenschist facies conditions. Darker dikes, also deformed, cut the lighter metatonalite. The metatonalite farther downstream has yielded a Pb/U zircon age of 163 ± 1 Ma and is thus essentially the same age as the adjacent sheeted-dike complex.

Approximately 350 feet downstream (42·42.826W, 123·54.591N), just past a sulfide-rich (brown weathering) fault zone, the metatonalite is well exposed in a water-polished outcrop near the river. As we continue walking downstream near the river edge, we will cross a high-strain zone where a large epidosite "porphyroclast" with tails can be seen. Continue walking downstream and observe mafic enclaves in an essentially undeformed tonalite.

Climb up to the Rogue River Trail and follow it downstream for approximately 0.4 miles.

The north-trending segment of the river and trail follows a mylonitic fault contact between the metatonalite and metagabbro units (Fig. 6; we won't see it). As the trail bends back to the left toward the northwest, metagabbro (mostly gneissic amphibolite) will become visible in float along the trail after we cross this shear zone.

STOP 14 (42º42.151'N, 123º54.674'W). Descend from the trail to a notch in the bedrock. Notice on the way down outcrops of foliated metagabbro, leucocratic layers of rock, fine-grained dike-like bodies, and epidosites.

Pegmatitic hornblende gabbro is first exposed along the upper part of the notch. Follow the notch down to a bench that lies approximately 15 to 30 feet above river level (in June) where finer grained and essentially undeformed metagabbro is exposed. The origin of this unit is uncertain. It is geochemically unrelated to the sheeted-dike complex, pillow lava unit, or the metatonalite (Kosanke, 2000), and has yielded a relatively old cooling age (below approximately 500·C) of 171 ± 3 Ma. It might represent preophiolite basement, in which case this ophiolite section is actually a rift facies similar to those related to the Josephine Ophiolite discussed in the text.

STOP 15 (42º42.204'N, 123º54.734W). Continue walking approximately 400 feet downstream to an outcrop on the bedrock terrace where two leucocratic muscovite-garnet metatonalite dikes are exposed, approximately 150 ft from the river's edge.

These dikes cut the metagabbro, yet were ductily deformed at lower temperatures; they may be related to the metatonalite unit upstream or to the postophiolite Half Moon Bar Diorite and Mule MountainVolcanics exposed to the west. A *minimum* age is given by two Ar/Ar muscovite ages of 148.0 and 148.5 Ma, which represent the time of cooling below approximately 300-350ºC (Kosanke, 2000). The cooling ages indicate that ductile deformation was ongoing until about 148 Ma, which overlaps with deformation related to the Nevadan Orogeny that affected the Western Klamath Terrane. Thus the ophiolitic rocks we have seen so far possibly represent an outlier of the Josephine Ophiolite. If they indeed belong to the Coast Range Ophiolite instead, this is the first reported occurrence of ductile deformation in the Coast Range Ophiolite that may be attributable to the Nevadan Orogeny.

STOP 16. Optional. Return to Rogue River Trail and continue hiking downstream for approximately 700 feet (42º42.289'N, 123º54.853W). We are near the western contact of the metagabbro unit with the Blossom Bar Shear Zone. Near the trail, notice deformed diorite with abundant enclaves or schlieren, and as we descend to the river notice the heterogeneity and deformation of the intrusive rocks. Descend to the prominent high outcrop, about 150 feet from the trail, along edge of the river overlooking the Blossom Bar Rapids just downriver. Rocks in this outcrop, unlike those we just passed, appear undeformed except for small, dark (greenschist facies) shear zones; this is a quartz diorite approximately 30 m wide that occurs along the western boundary of the Blossom Bar Shear Zone. Zircon from this rock

yielded a discordant age, even after reanalysis following abrasion of the zircon; the age is probably 157 Ma with a small inherited component of about 170 Ma (possibly from the metagabbro unit; J. Saleeby, personal communication; Kosanke, 2000; Kosanke and others, manuscript in preparation). Thus this intrusive may be related to the postophiolite Half Moon Bar Diorite and Mule Mountain Volcanics.

Return to trail and cross two wooden bridges as we continue downstream. We have crossed into the Blossom Bar Shear Zone, which is not well exposed here. This is a greenschist-facies ductile shear zone up to 0.9 km wide, consisting of highly strained mafic and silicic ultramylonites and mylonites. Before the next stop we will pass a small vertical cut in the cliff (42·42.222'N, 123· 55.412'W) where very fine-grained green phyllitic rocks are exposed. These are ultramylonites and mylonites, but this is not apparent except in thin section (Kosanke, 2000).

STOP 17 Continue about 50 feet to a high point on the trail and carefully descend to a promontory overlooking the river (42·42.233'N, 123·55.341'E), just upstream from a small beach. This outcrop is near the western boundary of the Blossom Bar Shear Zone, and the pillow basalt unit is exposed directly downriver. The rocks are strongly foliated and deformed, some with individual grains visible with a hand lens.

Return to Paradise Lodge and board the jet boat. The Half Moon Bar Diorite is poorly exposed along the trail down to the boat dock.

Return by Jet Boat to Foster Bar, return to Gold Beach, and drive to Corvallis.

REFERENCES

Alexander, R.J., and Harper, G.D, 1992, The Josephine Ophiolite: An ancient analogue for slow- to intermediate-spreading oceanic ridges, *in* Parson, L.M., Murton, B.J., and Browning, P., eds. Ophiolites and their modern oceanic analogues: Geological Society of London Special Publication 60, p. 3-38.

Alexander, R.J., Harper, G. D., and Bowman, J. R., 1993, Oceanic faulting and fault-controlled subseafloor hydrothermal alteration in the sheeted dike complex of the Josephine Ophiolite: Journal of Geophysical. Research. v. 98, p. 9731-9759.

Blake, M.C., Jr., Engebretson, D.C., Jayko, A.S., and Jones, D.L., 1985, Tectonostratigraphic terranes in southwest Oregon, *in* Howell, D.G., ed., Tectonostratigraphic terranes of the Circum Pacific Region: Circum-Pacific Council for Energy and Mineral Resources Earth Science Series, v. 1, p. 147-157.

Burchfiel, B.C., and Davis, G.A., 1981 Triassic and Jurassic tectonic evolution of the Klamath Mountains–Sierra Nevada geologic terrane, *in*, Ernst, W.G., ed., The Geotectonic Development of California: Englewood Cliffs, New Jersey, Prentice-Hall, p. 50-70.

Coulton, A.J., Harper, G.D., and O'Hanley, D.S., 1995, Oceanic vs. emplacement-age serpentinization in the Josephine Ophiolite: Implications for the nature of the moho at intermediate and slow spreading ridges: Journal of Geophysical Research, v. 100, p. 22,245-22,260.

Dick, H. J. B., 1977, Partial melting in the Josephine peridotite, I, The effect on mineral composition and its consequences for geobarometry and geothermometry: American Journal of Science, v. 277, p. 801-832.

Dickinson, W.R., Hopson, C.A., and Saleeby, J.B., 1996, Alternate origins of the Coast Range Ophiolite (California): Introduction and implications: GSA Today, v. 6, no. 2., p. 2-10.

Godfrey, N.J., and Dilek, Y., 2000, Mesozoic assimilation of oceanic crust and island arc into the North American continental margin in California and Nevada: Insights from geophysical data, *in* Dilek, Y., Moores, E.M., Elthon, D., and Nicolas, A., eds., Ophiolites and ocean crust: New insights from field studies and the ocean drilling program: Geological Society of America Special Paper 349, p. 365-382.

Harper, G.D., 1984, The Josephine Ophiolite, northwestern California: Geological Society of America Bulletin, v. 95, p. 1,009-1,026.

Harper, G.D., 1989, Field guide to the Josephine Ophiolite and coeval island arc complex, Oregon-California, *in* Geologic evolution of the northernmost Coast Ranges and western Klamath Mountains, California: Washington, D.C., 28th International Geologic Congress Field Trip Guidebook T308, American Geophysical Union, p. 2-20.

Harper, G.D., in review, Fe-Ti basalt and propagating rift tectonics in the Josephine Ophiolite.

Harper, G.D., Bowman, J.R., and Kuhns R., 1988, A field, chemical, and stable isotope study of submarine hydrothermal metamorphism of the Josephine Ophiolite, California-Oregon: Journal of Geophysical Research, v. 93, p. 4,625-4,656.

Harper, G.D., Saleeby, J.B., and Heizler, M., 1994, Formation and emplacement of the Josephine Ophiolite and the age of the Nevadan Orogeny in the Klamath Mountains, California-Oregon: U/Pb zircon and $^{40}Ar/^{39}Ar$ geochronology: Journal of Geophysical Research, v. 99, p. 4293-4321.

Harper G.D., and Wright, J.E., 1984, Middle to Late Jurassic tectonic evolution of the Klamath Mountains, California-Oregon: Tectonics v. 3, p. 759-772.

Hawkins, J. W., 1995, The geology of the Lau Basin, *in* Taylor, B., ed., Back-arc basins: tectonics and magmatism: New York, Plenum Press, p. 63-138.

Hopson, C.A., Mattinson, J.M., and Pessagno, E.A., Jr., 1981, Coast Range Ophiolite, western California, *in* Ernst, W.G., ed., The geotectonic development of California: Englewood Cliffs, New Jersey, Prentice-Hall, p. 418-510.

Kosanke, S.B., 2000, The geology, geochronology, structure, and geochemistry of the Rogue Wilderness Ophiolite, SW Oregon: Implications for the magmatic and tectonic evolution of the Coast Range Ophiolite: State University of New York, Albany, PhD Dissertation, 755 p.

Kosanke, S. B., Harper, G.D., and Heizler, M., 1999,Younger extrusive and intrusive volcanic arc rocks and Nevadan-age ductile deformation in the 164 Ma Coast Range Ophiolite: Geological Society of America Abstracts with Programs, v. 31, p. A61.

Pearce, J.A., Lippard, S.J., and Roberts, S., 1984, Characteristics and tectonic significance of supra-subduction zone ophiolites, *in* Kokelaar, B.P., and Howells, M.F., eds., Geology of marginal basins: Geological Society of London, Special Publication 16, p. 77-94.

Pessagno, E.A., and Blome, C.D., 1990, Implications of new Jurassic stratigraphic, geochronometric, and paleolatitudinal data from the Western Klamath Terrane (Smith River and Rogue Valley Subterranes): Geology, v. 18, p. 665-668.

Pinto-Auso, M., and Harper, G. D., 1985, Sedimentation, metallogenesis, and tectonic origin of the basal Galice Formation overlying the Josephine Ophiolite, northwestern California: Journal of Geology, v. 93, p. 713-725.

Ramp, L., and Gray, F., 1980, Sheeted dikes of the Rogue Wilderness, Oregon: Oregon Geology, v. 42, p. 119-124.

Robertson, A.H.F., 1990, Sedimentology and tectonic implications of ophiolite-derived clastics overlying the Jurassic Coast Range Ophiolite, northern California: American Journal of Science, v. 290, p. 109-163.

Saleeby, J.B., 1992, Petrotectonic and paleogeographic settings of U.S. Cordilleran ophiolites, *in* Burchfiel, B.C., Lipman, P.W., and Zoback, M.L., eds., The Cordilleran Orogen: Conterminous U.S.: Geological Society of America Geology of North America, v. G-3, p. 107-168.

Saleeby, J.B., Harper, G.D., Snoke, A.W., and Sharp, W.D., 1982, Time relations and structural-stratigraphic patterns in ophiolite accretion, west central Klamath Mountains, California: Journal of Geophysical Research, v. 87, p. 3831-3848.

Snoke, A.W., 1977, A thrust plate of ophiolitic rocks in the Preston Peak area, Klamath Mountains, California: Geological Society of America Bulletin, v. 88, p. 1641-1659.

Wyld, S.J., and Wright, J.E., 1988, The Devils Elbow ophiolite remnant and overlying Galice Formation: New constraints on the Middle to Late Jurassic evolution of the Klamath Mountains, California: Geological Society of America Bulletin, v. 100, p. 29-44.

Yule, J.D., 1996, Geologic and tectonic evolution of the Jurassic marginal basin lithosphere, Klamath Mountains, Oregon: California Institute of Technology, PhD Dissertation, 308 p.

Bimodal Volcanism and Tectonism of the High Lava Plains, Oregon

Brennan T. Jordan, Department of Geosciences, Oregon State University, Corvallis, Oregon 97331; jordanb@geo.orst.edu

Martin J. Streck, Department of Geology, Portland State University, Portland, Oregon 97201; streckm@pdx.edu

Anita L. Grunder, Department of Geosciences, Oregon State University, Corvallis, Oregon 97331; grundera@geo.orst.edu

INTRODUCTION

Overview and Tectonic Setting of the High Lava Plains

The High Lava Plains Province (HLP) is a volcanic upland east of the Cascade Range in central and southeastern Oregon. It is a bimodal volcanic field, composed primarily of late Tertiary and Quaternary basaltic lavas, rhyolite domes, and silicic tuffs, with intercalated volcaniclastic sediments. The HLP is the western part of a belt of volcanism at or near the northern margin of the Basin and Range Province that extends from the Cascades across the HLP, the Owyhee Plateau, and the Snake River Plain to the Yellowstone Plateau (Fig. 1). Interpreting magmatism of the HLP is complicated because the region has been affected by a multitude of tectonic processes (subduction, continental extension, a mantle plume).

The most enigmatic characteristic of the High Lava Plains Province is the systematic decrease in age of rhyolite domes toward the west (Fig. 2; MacLeod and others, 1975; Jordan, 2002; Jordan and others, in prep). This pattern of migrating silicic volcanism is most clearly illustrated as a series of west-younging isochrons (Fig. 2). These isochrons can be extended 50-100 km south of the HLP into the Basin and Range Province. The rate of propagation of silicic volcanism was ~35 km/m.y. from 10.5 to 5 Ma, slowing to 15-30 km/m.y. after that, with the rate depending on whether the end point is selected to be near Newberry Volcano or in the Cascade Range. Migrating silicic volcanism of the HLP mirrors the northeast-propagating trend across the Snake River Plain to the Yellowstone Plateau (Armstrong and others, 1976). The High Lava Plains trend is cited as evidence against a mantle plume origin for the Yellowstone trend (Hamilton, 1989), although models have been proposed to explain both in a mantle plume context (Draper, 1991). Other models explaining the tectonic origin of HLP magmatism invoke lithospheric deformation (Christiansen and McKee, 1978; Christiansen, 1993) or arc-related processes (Carlson and Hart, 1987).

We find the evidence compelling for a mantle plume origin of the Yellowstone–Snake

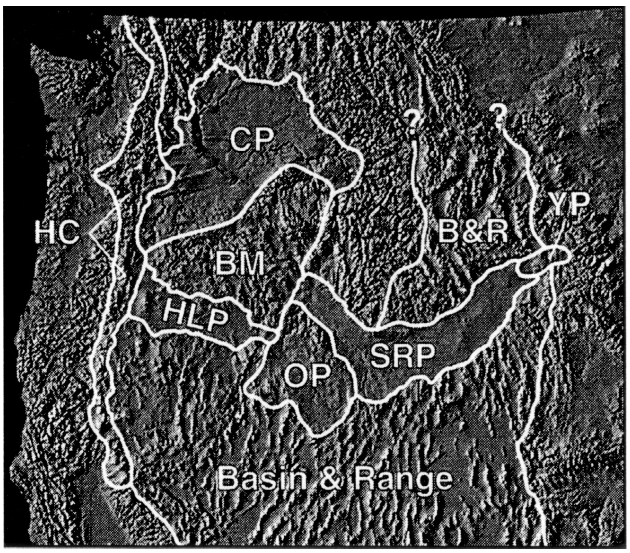

Figure 1. Map of the Pacific Northwest showing the High Lava Plains and adjacent provinces on the digital topographic base of Thelin and Pike (1991). HLP = High Lava Plains, HC = High Cascades, CP = Columbia Plateau, BM = Blue Mountains, OP = Owyhee Plateau, SRP = Snake River Plain, B&R = Basin and Range, and YP = Yellowstone Plateau.

Field Guide to Geologic Processes in Cascadia: Oregon Department of Geology and Mineral Industries Special Paper 36, 2002.

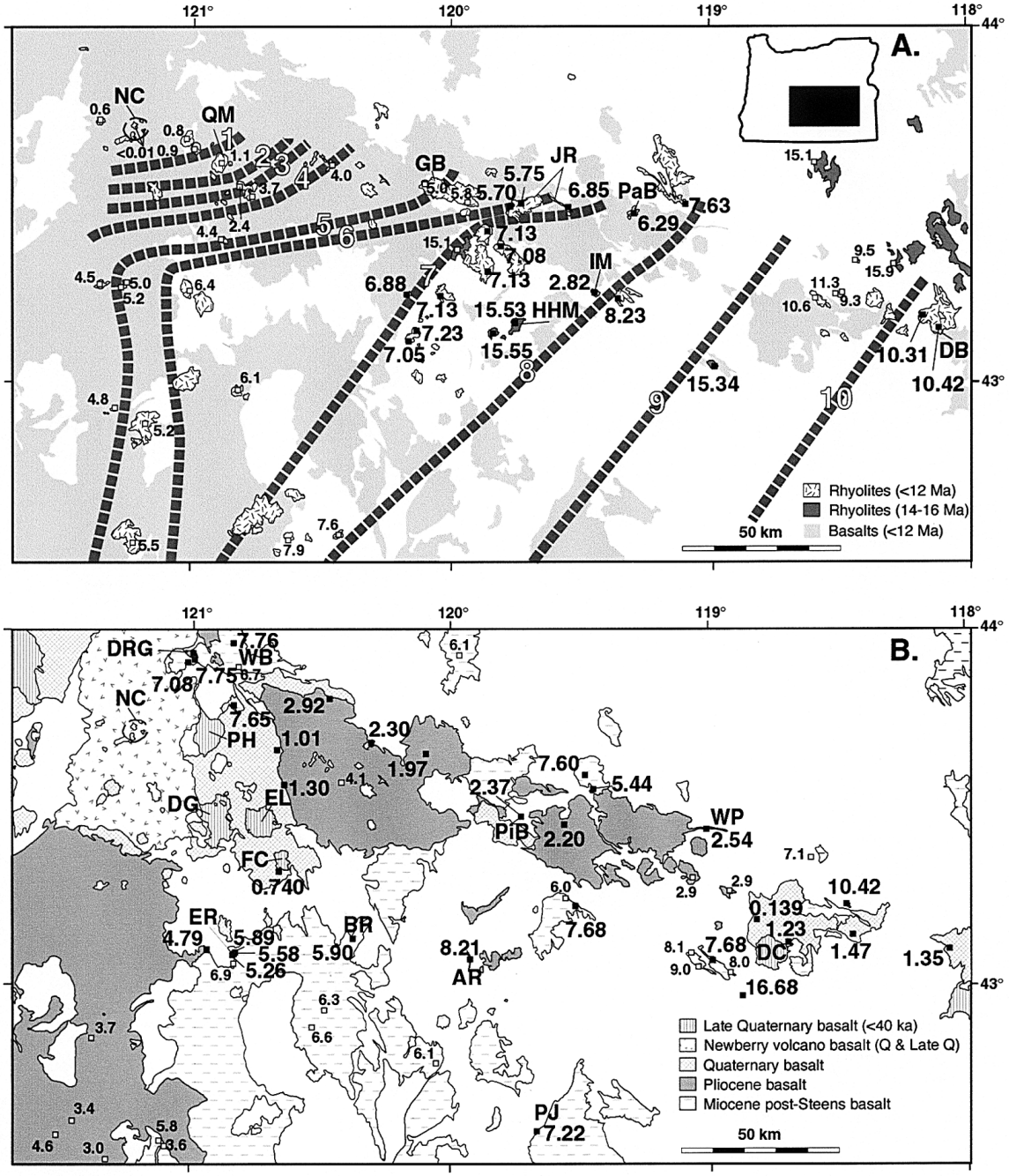

Figure 2. Maps of the High Lava Plains showing the distribution of (A) rhyolites and (B) basalts, with distribution of units modified from Walker and Reppening (1965), Walker and others (1967), Greene and others (1972), Walker (1991), and MacLeod and Sherrod (1992). Both maps show the locations of $^{40}Ar^{39}Ar$ ages of Jordan (2002), as well as previous age determinations, where not superceded by new ages, from Parker and Armstrong (1972), Walker (1974), McKee and others (1976), Fiebelkorn and others (1983), Hart and others (1984), Diggles and others (1990), Pickthorn and Sherrod (1990), and Johnson (1998). Ages reported prior to 1983 are shown as corrected by Fiebelkorn (1983) for a change in the ^{40}Ar decay constant. The15.9 Ma age is a weighted mean of two ages reported by Fiebelkorn and others (1983) for a rhyolite dome near Venator. Isochrons on the rhyolite age map are in 1 Ma increments, and are in part constrained by points off the map to the south. Abbreviations are: NC=Newberry Caldera, QM=Quartz Mountain, GB=Glass Butte, JR=Juniper Ridge, IM=Iron Mountain, PaB=Palomino Butte, DB=Duck Butte, DRG=Dry River Gorge, WB=West Butte, PH=Pot Holes lava, DG=Devil's Garden lava, ER=Egli Rim, EL=East lava, FC=Four Craters lava, BR=Burma Rim, AR=Abert Rim, PiB=Paiute Butte, PJ=Poker Jim Ridge, WP=Wright's Point, DC=Diamond Craters.

River Plain System (Pierce and Morgan, 1992; Smith and Braile, 1994). Inconsistencies with a plume model (track length too long, and off-axis position of eruptive centers of the Columbia River Basalt Group), can be accounted for by plume dynamics (Thompson and Gibson, 1991; Camp, 1995; Jordan, 2001).

Several lines of evidence suggest a link between the High Lava Plains and the Yellowstone–Snake River Plain system: (1) both trends of migrating silicic magmatism originate at the Owyhee Plateau on the axis of middle Miocene flood-basalt volcanism; (2) the two provinces with the intervening Owyhee Plateau constitute a nearly continuous belt of Pliocene and younger basaltic volcanism across the northern Basin and Range; and (3) a narrow, continuous, low-velocity seismic zone lies in the upper mantle across these provinces (Dueker and Humphreys, 1990; Hearn and others, 1991). That the provinces be linked does not require that they formed by the same exact process but suggests that the processes that formed them may be linked. We favor a model in which High Lava Plains magmatism is governed regionally by plume-related processes such as plume-head emplacement and sublithospheric flow of plume material (Jordan, 2001), with local control on the development of crustal magma chambers and the distribution of vents by preexisting lithospheric structure and deformation.

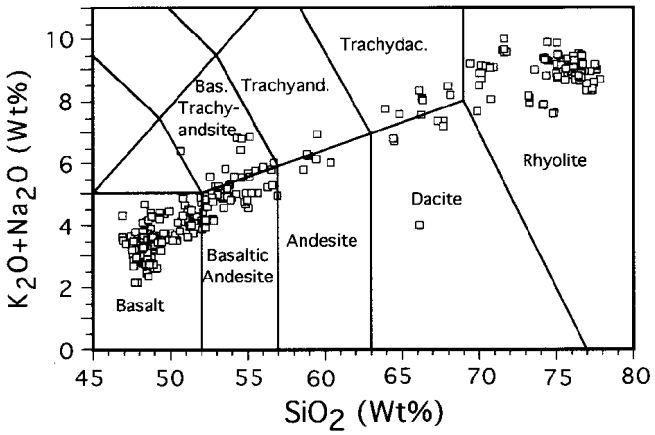

Figure 3. Classification (after LaBas and others, 1986) of 286 High Lava Plains lavas (late Miocene and younger). Note the strongly bimodal distribution (only 7% andesites and dacites). Intermediate rocks may have been disproportionately *oversampled* because of their petrologic significance, so the bimodal distribution is real. Data from MacLean (1994), Johnson (1995), Johnson (1998), Streck and Grunder (1999), Johnson and Grunder (2000), Jordan (2002), and unpublished data of A.L. Grunder and M.J. Streck.

Bimodal Volcanism of the High Lava Plains

Late Miocene and younger volcanism of the High Lava Plains was strongly bimodal (Fig. 3). Rhyolite was erupted in more than 60 domes or dome complexes, three major ash-flow tuffs (Prater Creek Tuff, Devine Canyon Tuff, and Rattlesnake Tuff), and several minor tuffs (tuff of Hampton and tuff of Buckaroo Lake). Most rhyolite domes of the HLP fit the pattern of age progression (Fig. 2). A notable exception is Iron Mountain, a 2.8 Ma dome located among 7-8 Ma domes. The vent locations for the tuffs are poorly constrained except for the Rattlesnake Tuff (Streck and Grunder, 1995; Stimac, 1996).

Silicic rocks are mainly high-silica rhyolites (>75 wt% SiO_2) and are metaluminous to mildly peralkaline (Table 1). Rhyolite lavas and tuffs are aphyric to moderately porphyritic, with varying combinations of plagioclase, quartz, sanidine, biotite, hornblende, and clinopyroxene phenocrysts (MacLean,1994; Streck and Grunder, 1995; Johnson and Grunder, 2000). All low-silica rhyolites and some high-silica rhyolites are interpreted to be the product of 5-30% partial melting of the middle or lower crust, while most high-silica rhyolites are interpreted as products of fractional crystallization of low-silica rhyolites (Grunder, 1992, MacLean, 1994; Streck and others, 1999; Johnson and Grunder, 2000; Streck, 2002).

Basalt of the High Lava Plains is not age-progressive like the rhyolite. Miocene and Pliocene basalt lavas (generally exposed in fault scarps and erosional valleys) are typically 2-5 m thick, and are commonly emplaced in compound lava sequences. Quaternary basalt of the HLP generally occurs in lava fields covering 20 to 100 km^2. Most lava fields were erupted from central vents or vent complexes, and others (for example, the Four Craters Lava Field) were fed by multiple vents, commonly aligned along fissures. Many lavas have pahoehoe surfaces and were inflated during emplacement

Table 1. Major and Trace Element Composition of High Lava Plains Rhyolites

Unit	Western High Lava Plains			Western Harney Basin (central High Lava Plains)								
	Quartz Mt. aphyric	Quartz Mt. porphyritic	Squaw Mountain	Horse Mountain	Palomino Butte	Juniper Ridge West	Juniper Ridge East	Rattlesnake Tuff Type-A	Rattlesnake Tuff Type-E	Prater Cr. Tuff	Devine Can. Tuff	Tuff of Hampton
XRF Wt%												
SiO_2	75.11	76.70	76.63	76.23	73.30	76.84	72.35	77.27	75.47	75.51	76.05	72.74
TiO_2	0.10	0.06	0.14	0.20	0.21	0.08	0.32	0.11	0.16	0.15	0.21	0.25
Al_2O_3	13.54	12.87	12.99	10.40	13.93	12.11	14.25	12.02	12.26	11.94	11.44	13.32
FeO*	1.49	1.06	1.69	3.59	1.88	1.32	2.13	0.86	2.18	2.47	2.53	3.20
MnO	0.04	0.02	0.05	0.10	0.05	0.03	0.04	0.08	0.10	0.05	0.04	0.10
MgO	-	-	0.05	-	0.52	-	0.56	-	0.01	-	0.25	0.20
CaO	0.88	0.58	0.76	0.18	1.95	0.68	1.75	0.30	0.50	0.26	0.30	1.61
Na_2O	4.66	4.15	4.58	4.81	3.35	4.12	3.73	3.87	4.61	3.68	2.82	3.86
K_2O	4.12	4.59	4.08	4.48	4.74	4.67	4.46	5.04	4.69	5.73	6.35	4.45
P_2O_5	0.02	0.02	0.03	0.02	0.06	0.01	0.07	0.02	0.01	0.01	0.02	0.25
(K+Na)/Al	0.89	0.92	0.90	1.23	0.76	0.98	0.77	0.89	1.03	1.03	1.01	0.84
XRF ppm												
Rb	131	142	112	122.6	110.9	96.6	114.2	122.7	63.5	100.4	89.8	70.1
Ba	919	906	1054	58	1215	709	1224	24.6	1835	78	45	1183
Sr	61	28	50	0.5	202	15.5	122	3.4	23.4	14.3	11.2	105
Zr	161	120	197	733	162	256	251	175	457	542	698	433
Nb	8	9	11.9	40.7	14.6	21.5	12.2	40.3	26.4	48.5	52.1	17.5
Y	42	46	54	108	23.7	91.2	26	100.5	76.2	79.9	86.7	70.8
Zn	53	52	70	191	36	109	36	88	113	105.8	138	92.9
Ga	21	20	20	22.6	14.5	19	14	17.8	18.6	20.2	24.7	19.1
Cr	-	-	2	1.5	3.4	-	-	1.6	0.3	-	-	3.2
INAA ppm												
Cs				5.8	3.8	3.1	5.5	4.5	2.4	2.6	2.1	2.5
Th				11.7	8.3	8.3	10.9	9.9	5.7	8.9	8.2	6.5
Hf				17.1	4.6	8.7	6.5	7.2	11.1	13.5	14.3	11
Ta				2.3	1.2	1.26	0.94	2.28	1.35	2.64	2.67	1.05
Sc				0.76	3.6	0.78	4.77	4.05	4.32	1.67	0.52	9.68
Co				0.23	2.8		2.93	0.05	0.13	0.45	0.5	0.51
La				61.9	26.6	33.1	22.5	21	51.7	59	118	31.4
Ce				139	47.4	76.5	46.8	54	112	129	207	69
Nd				68.4	19.3	36	19.9	32	58	53	89	34
Sm				16.16	3.77	12.41	3.67	9.06	13.39	10.69	18.6	8.35
Eu				1.37	0.63	0.87	0.71	0.65	2.48	0.29	0.8	2.07
Tb				2.86	0.63	2.13	0.62	2.17	2.13	1.86	2.52	1.9
Yb				11	2.97	9.2	2.98	10.22	7.91	8.27	8.8	7.16
Lu				1.58	0.44	1.23	0.49	1.54	1.23	1.23	1.31	1.07
Eu/Eu*				0.25	0.5	0.21	0.58	0.19	0.56	0.08	0.14	0.67
La_N/Yb_N				3.8	6.1	2.4	5.1	1.4	4.6	4.8	9.1	3
Ba/Rb	7	6.4	9.4	9.9	11	7.3	10.7	0.2	28.9	0.8	0.5	16.7

Note: XRF analyses aquired at Washington State Univeristy Geoanalytical Laboratory; INAA analyses aquired at Oregon State University
FeO*-all iron expressed as FeO
Eu/Eu*-Europium anomaly, actual Eu divided by Eu projected from adjacent rare earth elements
La_N/Yb_N-abundances normalized to chrondritic abundance before taking ratio

(Chitwood, 1994). Some Quaternary eruptive centers constructed small shield volcanoes. Cinder cones are abundant, especially in the western HLP and on the flanks of Newberry Volcano.

Most basaltic rocks of the High Lava Plains have a diktytaxitic texture with varying degrees of development of subophitic texture. They are generally aphyric to sparsely porphyritic, with olivine and plagioclase being the predominant phenocrysts; clinopyroxene phenocrysts are rare. High Lava Plains basaltic rocks (Table 2) are mostly high-alumina olivine tholeiites (HAOT of Hart and others, 1984), but

Table 1. Major and Trace Element Composition of High Lava Plains Rhyolites (cont)

	Western High Lava Plains							Western Harney Basin (central High Lava Plains)						
Sample#[1]	2-97	6-98	8-97	21-97	25-98	85-98	92-98	HP33	93.1ba	HBA6	HBA16	HBA3	SqBu-12	HBA13.1
XRF Wt%														
SiO_2	53.91	56.32	49.37	49.16	51.53	51.02	48.26	47.76	48.47	50.68	52.79	54.61	55.16	53.43
TiO_2	1.24	2.10	1.63	1.26	1.08	1.62	1.04	0.77	0.99	2.39	1.43	2.23	1.67	1.26
Al_2O_3	17.04	14.89	15.81	17.25	17.07	17.22	17.61	17.78	16.69	15.14	17.16	15.19	14.79	17.31
FeO*	9.16	9.76	9.22	9.41	8.29	8.78	9.26	9.38	10.21	13.22	9.08	10.32	12.43	8.67
MnO	0.17	0.19	0.16	0.17	0.15	0.16	0.18	0.21	0.20	0.33	0.17	0.21	0.40	0.15
MgO	4.84	3.43	8.22	8.74	8.00	6.82	9.21	10.43	8.88	3.21	5.41	3.10	2.15	5.30
CaO	7.61	7.19	10.60	10.10	9.91	9.38	11.57	11.44	11.75	6.92	8.64	6.44	5.60	8.57
Na_2O	3.82	3.94	2.67	3.05	3.06	3.69	2.67	1.95	2.45	4.39	3.65	3.96	4.72	3.59
K_2O	1.51	1.28	1.72	0.52	0.66	0.95	0.09	0.20	0.23	2.02	1.12	2.48	2.12	1.28
P_2O_5	0.69	0.90	0.60	0.34	0.23	0.38	0.12	0.09	0.11	1.70	0.55	1.46	0.96	0.44
Mg#	54	44	67	68	69	64	69	71	66	35	57	40	28	58
XRF ppm														
Rb	15	25	27	7	12	13	1	2	1.6	27	14	63	34	17
Ba	637	574	1449	370	232	268	64	65	156	1381	677	1021	1684	681
Sr	536	337	1199	468	394	427	181	197	383	258	446	210	256	466
Zr	169	152	195	95	101	165	59	47	51	550	157	337	873	159
Nb	12.2	9.3	7.1	5.1	6.7	16.7	2.5	2.1	1.2	52	10.6	29.1	56.3	10.3
Y	26	50	27	29	20	27	24	22	24	116	29	71	129	27
Zn	96	103	81	87	69	70	61	55	73	191	90	133	205	90
Ga	21	17	19	17	18	17	16	14	17	26	16	22	27.9	20
V	177	210	257	253	187	213	230	238	262	63	174	171	12.6	211
Cu	43	35	35	99	54	58	78	120	120	14	63	10	16.1	57
Ni	47	12	126	127	113	91	146	196	143	0.1	45	0.1	16.8	51
Cr	75	33	332	210	237	176	225	233	237	0.1	83	4	5.2	86
ICP-MS ppm								*INAA ppm*						
Cs								0.43	0.4	0.63	0.28	1.54	0.74	0.31
Th	1.13	2.93	2.11	0.94	1.34	1.59	0.1	0.44		3.04	1.13	5.63	3.55	1.1
Hf	3.91	4.17	4.93	2.41	2.32	3.84	1.47	1.13	1.41	14.2	3.75	8.72	17.45	3.78
Ta								0.07	0.08	2.71	0.57	1.62	2.69	0.53
Sc	23.9	32.3	32.5	29.5	29.7	29.9	40.1	40.4	47.5	37	26.7	23.3	41.33	25.6
Co	36.4	28.6	70.4	51.6	51.7	53.6	54.4	43.4	49.7	21.3	33.3	22.6	7.46	31.5
Pb	6.51	6.11	10.62	2.34	3.31	3.35	0.88							
Th	1.13	2.93	2.11	0.94	1.34	1.59	0.09							
La	25.6	20.6	28.6	10.2	9.82	15.6	2.65	2.07	3.36	67.6	19.2	39.9	62.1	19.6
Ce	57.5	47.3	71.3	23.3	23.8	37	8.04	5.7	8	160	39.7	87.6	138	38.4
Pr	7.59	6.82	10.48	3.42	3.19	4.90	1.316							
Nd	31.8	32.7	45.2	15.1	13.8	21.3	6.66	5.6	8.6	83	23.2	48.1	70	19.6
Sm	6.58	8.33	8.21	3.71	3.16	4.91	2.22	1.76	2.42	20.00	5.22	11.80	21.90	4.99
Eu	1.84	2.57	2.49	1.24	1.11	1.66	0.98	0.75	0.98	5.83	1.72	3.37	6.01	1.63
Gd	6.01	8.24	6.91	3.94	3.58	5.08	2.89							
Tb	0.90	1.36	0.94	0.68	0.59	0.83	0.56	0.45	0.62	3.57	0.84	1.99	3.51	0.80
Dy	5.15	8.05	5.15	4.10	3.80	5.08	3.57							
Yb	2.69	4.54	2.35	2.46	2.19	2.75	2.33	2.26	2.77	12.20	2.31	6.80	13.30	2.61
Lu	0.42	0.70	0.36	0.36	0.36	0.40	0.36	0.34	0.40	1.69	0.32	1.06	1.88	0.37
Eu/Eu*	0.91	0.93	0.98	0.98	1.00	1.00	1.17	1.11	1.05	0.85	1.00	0.85	0.83	0.99

Note: XRF analyses aquired at Washington State Univeristy Geoanalytical Laboratory; ICP-MS and INAA analyses aquired at Oregon State University

[1]WHLP removed from middle of XX-97 or XX-98 sample numbers

FeO*-all iron expressed as FeO

Eu/Eu*-Europium anomaly, actual Eu divided by Eu projected from adjacent rare earth elements

other basalt types, calc-alkaline and alkalic, occur as well (Table 2). They are generally primitive (60% have Mg# > 60), but 25% are basaltic andesites (Jordan, 2002). Major element variation trends (Fig. 4) show relatively tight clusters at MgO > 7 wt%, and considerably more scatter at lower MgO. Major element variations are consistent with fractional crystallization of plagioclase, olivine, and clinopyroxene, with variable degrees of assimilation (Streck and Grunder, 1999; Jordan, 2002). Some extreme compositions reflect protracted histories of fractionation, recharge, and assimilation (MacLean, 1994; Streck and Grunder, 1999).

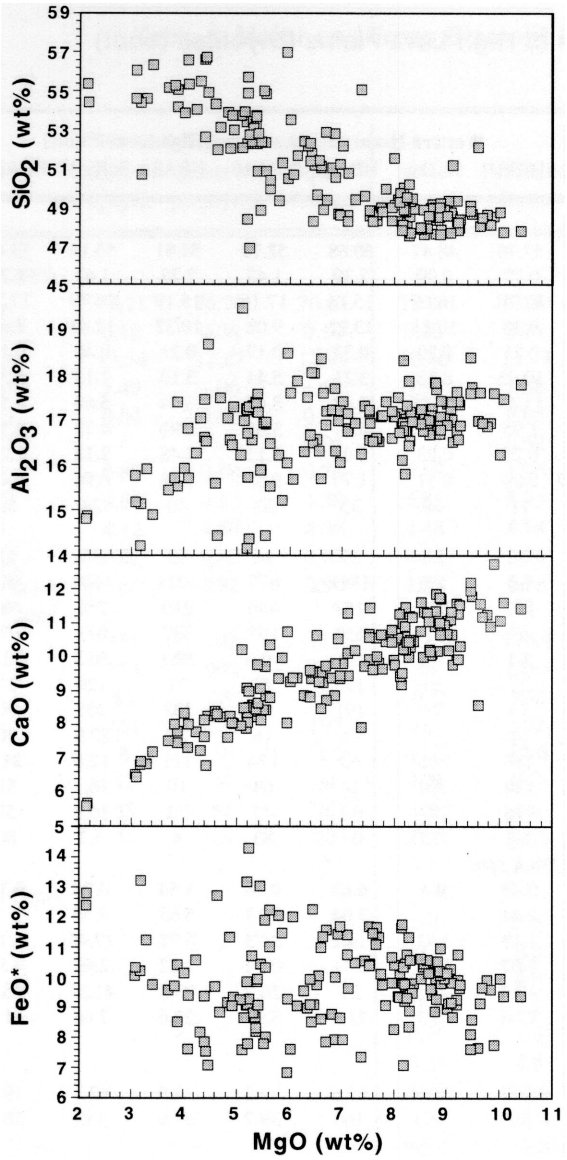

Figure 4. Selected variation plots of 170 High Lava Plains basaltic lavas.

Whereas compositionally intermediate rocks are volumetrically insignificant, they are ubiquitous and petrologically important. Most intermediate magmas of the High Lava Plains were derived by mixing between mafic and silicic melts (MacLean, 1994; Streck and Grunder, 1999; Johnson and Grunder, 2000), but some (for example, eastern Juniper Ridge) were derived from basalt by fractional crystallization and assimilation (MacLean, 1994).

Structural Setting of the High Lava Plains

The High Lava Plains Province lies between the extended Basin and Range Province and the Blue Mountains Province, which has undergone little to no Miocene and younger extension. The transition from the Basin and Range Province northward into the High Lava Plains is manifested by northward decrease in relief on Basin and Range fault-bounded range fronts and a wide zone of northwest-striking faults of modest normal offset (<100 m) within and south of the High Lava Plains. The Brothers Fault Zone (Lawrence, 1976) is a concentration of such northwest-striking faults that obliquely cuts the HLP (Fig. 5). The Brothers Fault Zone is often interpreted as a right-lateral strike-slip zone that accommodates the northward termination of Basin and Range extension (Lawrence, 1976), although with its steep faults of modest offset, the fault zone can account for little regional deformation.

Johnson (1995) documented that both the Basin and Range and Brothers Fault Zone faults were active in the eastern High Lava Plains by around 10 Ma. Hart and others (1984) suggested that faulting in the Basin and Range south of the central HLP (Poker Jim Rim and Abert Rim) occurred between 7 and 6 Ma. Holocene faulting has occurred on Basin and Range faults south of the HLP and on NW-trending faults in the southwestern HLP (Pezzopane and Weldon, 1993).

Brief Overview of Itinerary

Day 1: The formal road log begins in Bend, at the intersection of US 97 and US 20 (Fig. 6). The trip makes a southward transect of the High Lava Plains Province in the west and proceeds east along the southern edge of the HLP, at the border with the Basin and Range Province. Stops include basalt ranging from about 8 to 0 Ma, rhyolite domes, and faults of the Brothers Fault Zone as well as the Basin and Range. We will close the day with a section through ignimbrites and basalt in the central High Lava Plains where Basin and Range structure impinges, and a northward traverse of the central High Lava Plains. The day ends in Burns.

Day 2: The trip proceeds mainly west along the northern edge of the High Lava Plains, with consideration of the ignimbrites that are typical of the central High Lava Plains, followed by domes and mafic volcanic rocks, and Brothers Fault Zone faults. The last stop is at an ignimbrite of the western plains, and the trip ends in Bend.

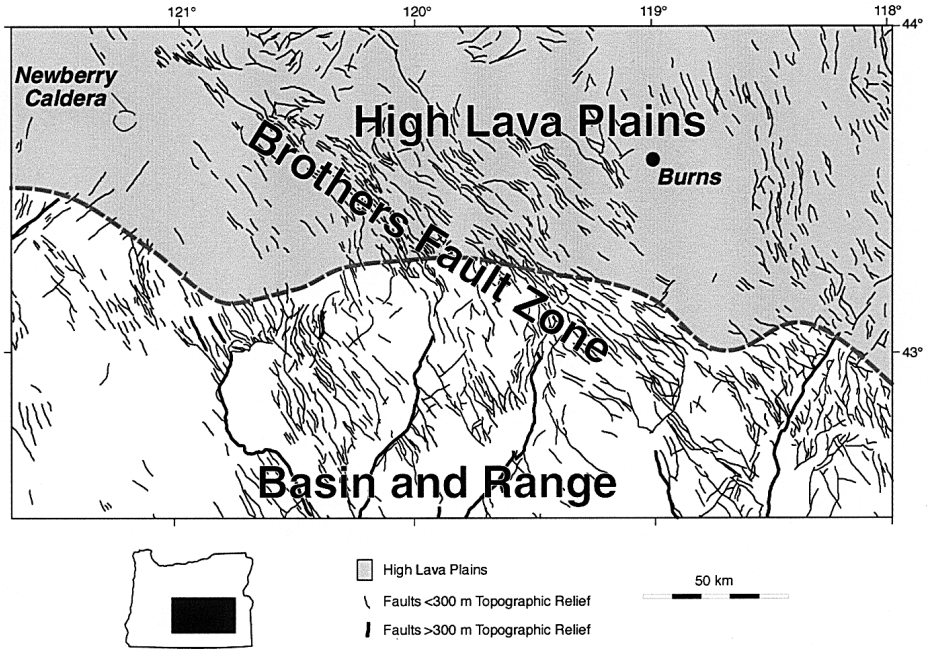

Figure 5. Map showing distribution of faults in the High Lava Plains and northern Basin and Range Province.

ROAD LOG

0.0 Start at the intersection of Highways 20 and 97 in Bend. Drive east on US 20.

0.7 Turn left at Pilot Butte.

1.9 Top of Pilot Butte. STOP 1. Scenic overview of Newberry Volcano, the Cascade Range, and other volcanic landforms at the northwestern margin of the High Lava Plains.

Stop 1. Pilot Butte: Overview

Pilot Butte affords a panoramic view. To the south lies Newberry Volcano, dotted with many cinder cones on its flanks. There is a sweeping view of the Oregon Cascades to the west, from Mt Thielsen in the southwest near Crater Lake, to Bachelor Butte (large scoria cone and ski area), Broken Top, South, Middle, and North Sisters, and sweeping northward, Mt Washington (with a prominent central plug), Three Finger Jack, Mt Jefferson, Olallie Butte, and Mt Hood. Black Butte, the large scoria cone in front of the Cascades to the northwest, lies at the south end of Green Ridge, a piece of a major down-to-the-west normal fault that bounds the eastern side of the High Cascades Graben. To the north lie Round Butte (4 Ma, alkali basalt), Smith Rocks and Gray Butte (John Day Formation age), and Powell Buttes (John Day). To the east lies West Butte, a 7.8 Ma basaltic andesite shield, with Horse Ridge, a fault-dissected hill of 7-8 Ma basalt to the right. Pine Mountain (also John Day) closes the panoramic circle back to Newberry Volcano.

Newberry Volcano

Newberry Volcano is a massive shield volcano at the western end of the High Lava Plains (MacLeod and others, 1995). It has a central caldera that hosts several Holocene rhyolite flows. The gently sloping flanks of Newberry are dotted with cinder cones, many of which are aligned to regional fault patterns. Holocene basaltic eruptions have occurred on the flanks of the volcano. Like the High Lava Plains, it is a bimodal volcanic center (MacLeod and Sherrod, 1988; Linneman and Meyers, 1991; MacLeod and others, 1995). As a site of Holocene rhyolitic volcanism, Newberry Volcano has been envisaged by some investigators as the current focus of the migrating silicic volcanism of the High Lava Plains (MacLeod and others, 1975), although others consider the HLP trend to project into the Cascade Range (Hill and Taylor, 1989).

Many workers consider Newberry Volcano to be a Cascade volcano. We take the

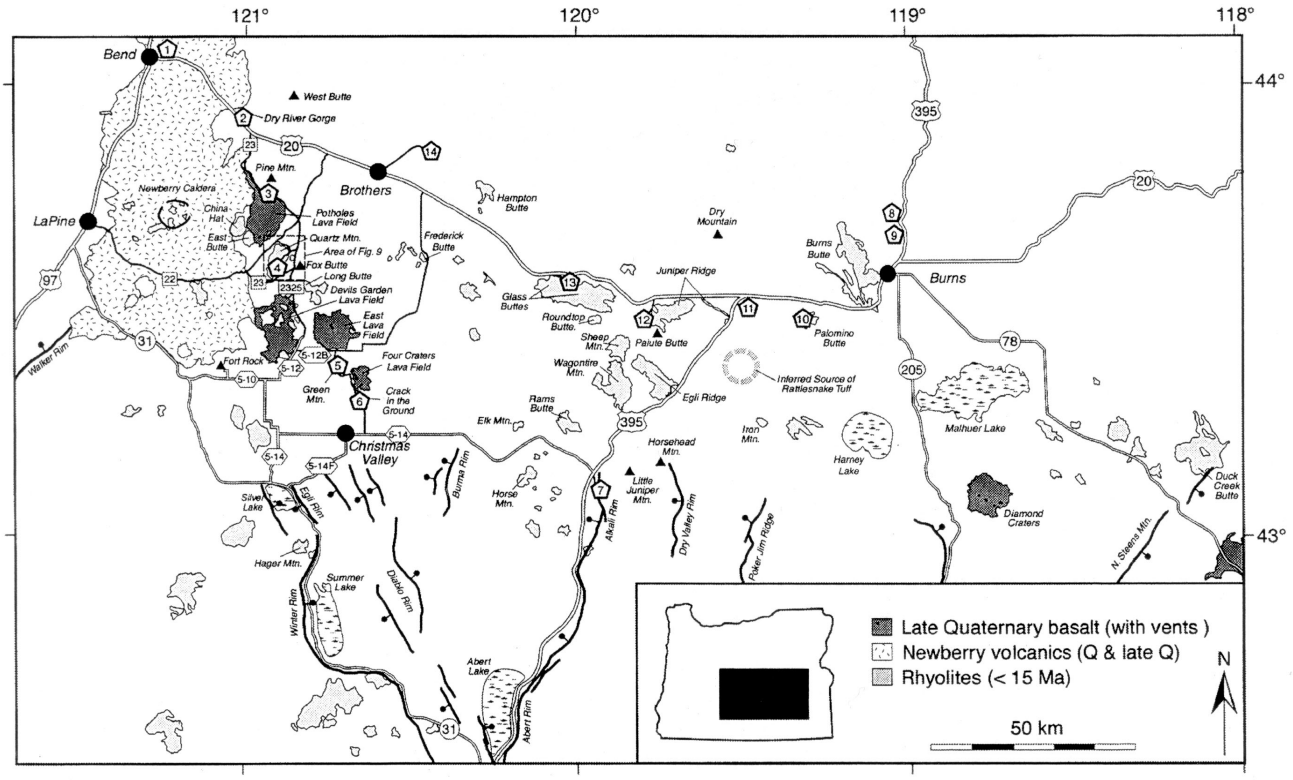

Figure 6. Map showing the route and stop locations described in this field guide. Also shown are rhyolite domes, late Quaternary basaltic lava fields (with vents), and major Basin and Range faults.

view that Newberry is probably neither a true Cascade Arc volcano nor a High Lava Plains volcano but is more likely a result of the complex interplay of processes related to both provinces. The Three Sisters area is where the HLP trend intersects the north-trending Cascade Arc and has been the volumetrically most productive part of the Cascade Range during the Quaternary (Sherrod and Smith, 1990). This in turn may be another manifestation of the interplay between the processes of both provinces.

Return to US 20

3.1 Continue west on US 20, crossing the "badlands", a plain underlain by basalt lavas with sources on the flanks of Newberry Volcano. Many cinder cones and lava tubes distinguish the area.

20.9 The road begins to ascend Horse Ridge and cuts into late Miocene mafic lava.

21.7 STOP 2. Overlook of Dry River Canyon. Oregon Geology Heritage Site. Walk about 350 m to promontory to the north. Distal view of Mt Washington, Black Butte, and Mt Jefferson.

Stop 2. Dry River Canyon

Draining of a Pleistocene lake has cut through a section of High Lava Plains basalts. Figure 7 shows the view from directly across the canyon (NE) to the lower end of the canyon (due N). Directly across the canyon, the continuous cliffs comprise a compound sequence of basaltic andesite lava and flow breccias erupted during a short period of time at about 7.75 Ma (Jordan, 2002). The sequence is systematically more chemically evolved up-section (Ni from 47 to 69 ppm; Ba from 637 to 567 ppm), suggesting withdrawal from a compositionally zoned magma chamber (2WHLP97 is basal flow; Table 2). Based on the gentle westward dip of this lava, it may have been erupted from a volcanic center to the east, perhaps West Butte. A thin unit of tuffaceous sediment occurs at the first break in slope, beginning a sequence of intercalated basalt and basaltic andesite lavas and tuffaceous sediment. This sequence thick-

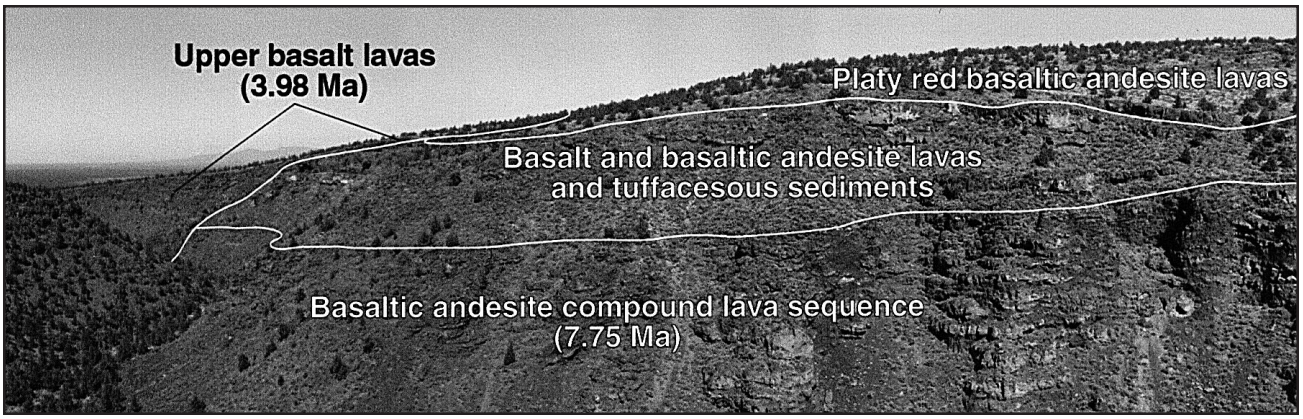

Figure 7. Photo looking north and northeast across the Dry River Canyon at Stop 2. Ages and contacts of units described in text are shown.

ens to the west (including the lavas that underlie our vantage point), suggesting that some lavas of this sequence may have been erupted from vents in the Horse Ridge area to the southwest. A sample Horse Ridge basalt, collected about 2 km south of our overlook, yielded an age of 7.08 Ma. At the rim on the on the opposite wall of the canyon, lava appears to drape an irregular paleotopographic surface. This lava (6WHLP98; Table 2) is the first of a sequence of red platy basaltic andesite lavas that continue to the ridge summit to the northeast. Overlying these lavas on the slope to the north is a series of basalt lava flows that was emplaced on a steep west-dipping paleotopographic surface at 3.98 Ma. These lavas are mineralogically and compositionally distinctive (8WHLP97; Table 2), with relatively coarse phenocrysts of olivine, plagioclase, and clinopyroxene, and very high K_2O (1.72 wt%) and Ba (1449 ppm) at high MgO (8.22 wt%).

The basalt sequence exposed in the Dry River Canyon demonstrates that basaltic volcanism was ongoing millions of years before High Lava Plains silicic volcanism arrived in the area at around 1 Ma. The lower basaltic andesite sequence coincides, within 2 standard deviations with five other basaltic lavas from across the HLP that cluster around 7.65 Ma, including nearby basaltic andesites from the summit of West Butte (7.76 Ma) and the southeast ridge of Pine Mountain (7.51 Ma). The basaltic episode at about 7.6 Ma represents the clearest widespread magmatic episode in the development of the HLP.

Across the canyon to the southeast (right of the area shown in Fig. 7) a northwest-trending fault of the Brothers Fault Zone has dropped the lower compound lava sequence about 40 m down to the southwest. Several slip surfaces with less than 1 m displacement are exposed in the tuffs directly across the canyon. Measurements made on one such surface with slickensides indicate nearly dip-slip normal displacement on a N50°W surface that dips 68° to the southwest.

Continue east on US 20.

23.4 USFS Rd 23-25 Turn right. To the east (back and left) you see Brothers Fault Zone faults. Look for these on the way back, forward and left (south) is Pine Mountain (a John Day age rhyolite dome complex) and China Hat, a rhyolite dome that is part of the westward-younging silicic trend of the High Lava Plains. The low-lying basaltic lavas were erupted from the flanks of Newberry Volcano, looming to the southwest.

29.5 Take the dirt road to the left, leaving USFS 25 to the right. This is USFS 23. Pine Mountain ahead and left, Potholes Lava Field to the right. On right skyline, China Hat is the western of three buttes. Left of China Hat lie East Butte and Quartz Mountain, also rhyolites, all about 1 Ma in age.

Figure 8. Photo of inflated lava at the northern margin of the Potholes Lava Field at Stop 3. Flow front consists of pahoehoe crust, which formed at near the horizontal and was tilted up to 40° during inflation.

34.1 Turn right on an unimproved dirt road that leads to a campsite under pines at the edge of the Potholes Lava Field. STOP 3. Walk along flow margin to the west about 300 m to marvel at the steep flow front.

Stop 3. Potholes Lava Field

The Potholes is a 65 km^2 late Quaternary basaltic lava field with an estimated age of 50 ka (Chitwood, 1994). The Potholes Lava Field is one of several Quaternary lava fields in central and southeastern Oregon cited by Chitwood (1994) as examples of inflated lavas. Inflation features are wonderfully exposed at this site (Fig. 8), including steep flow margins, tilted pahoehoe surfaces, breakouts, tumuli, and inflation clefts. Inflation of basalt lava flows occurs as follows: (1) the advancing flow front slows; (2) the strength and viscosity of the crust increases, restricting forward advance; (3) continued magma supply causes vertical inflation behind the stalled flow front; and (4) fracturing of the flow front during inflation may allow breakouts of lava and continued advance, possibly leaving deflation features in the flow behind. At this location, the flow front, which was initially probably less than 1 m high, is now about 10 m high, and pahoehoe surfaces that developed near the horizontal are now tilted to 40°.

The Potholes lava is diktytaxitic basalt with 10% phenocrysts, olivine much more abundant than plagioclase, generally 0.5-1.5 mm. The basalt (21WHLP97; Table 2) is somewhat primitive (MgO = 8.74 wt%, Ni = 157 ppm) but has moderately high K_2O (0.52 wt%). The Potholes lava is compositionally quite similar to the Devils Garden lava to the south (Fig. 6), and both stand out from other primitive High Lava Plains basalts because of their high La/Sm ratio (~2.6). The compositional similarity suggests that the two lavas may be closely related, and their vents are aligned on a northwest trend consistent with fault trends and other vent alignments. Based on these arguments, we consider it possible that the Potholes and Devils Garden lavas were erupted in a single event. However, Chitwood (1994) suggests that the Devils Garden lava may be

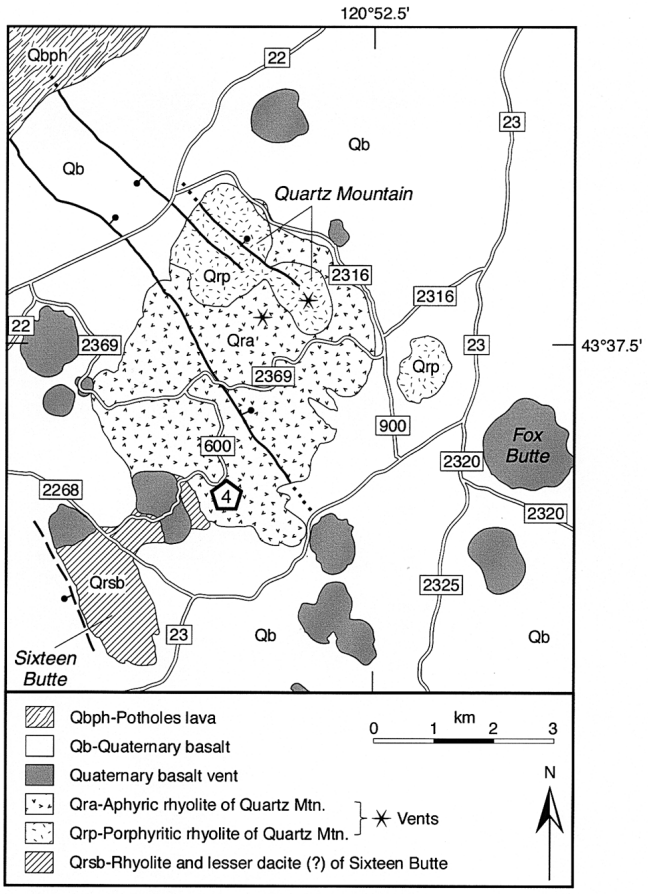

Figure 9. Geologic sketch map of Quartz Mountain. Location shown on Figure 6.

younger (estimated age of 20 ka) based on weathering characteristics. Carbon dating or surface-exposure dating may be required to resolve this issue.

As you walk along the flow front, also examine the pumice and ash below your feet. This is the Newberry Pumice, erupted between 1,300 and 1,600 years ago in association with emplacement of the Big Obsidian Flow in the caldera of Newberry Volcano (MacLeod and others, 1995). The current location is just within the 25 cm isopach of this deposit. The distribution pattern of the Newberry Pumice is elongate, oriented N80°E, with an aspect ratio of 8:1 (MacLeod and others, 1995).

Return to USFS 23 and continue right, south.

37.9 As we come around the south flank of Pine Mountain, the southeast ridge is visible on the skyline. The southeast ridge of Pine Mountian is made of 7.51 Ma basaltic andesite. This age is within 2 standard deviations of the ages of West Butte and the lower basaltic andesite at the Dry River Canyon and represents evidence in support of a postulated province-wide magmatic event at this time.

42.7 Go straight. Road on the right heads for LaPine.

47.4 Crossing a primitive basalt lava (0.19 wt% K_2O).

Turn right on USFS 2316, red cinder improved road.

Go left at T intersection with USFS 2269.

Stay right where USFS 900 comes in from left.

The road crosses a NW-striking normal fault that displaced the rhyolite lavas of Quartz Mountain about 30 m. The same fault offsets Quaternary basalt lavas to the northwest (Fig. 9), but to a lesser extent (~10 m).

Go left on USFS 600 (unimproved). The road crosses the pumiceous carapace atop the aphanitic rhyolite that is one of two main rhyolite lithologies at Quartz Mountain; the other is porphyritic rhyolite

STOP 4. Drop below the road to the south, working around a west-facing cliff that consists of the aphanitic rhyolite of Quartz Mountain.

Stop 4. Quartz Mountain

Younger rhyolite domes of the High Lava Plains (China Hat and East Butte) offer few exposures of the internal structure, and older domes (like Glass Buttes) feature good exposures where the rhyolite is pervasively devitrified but poor exposures of fresh in-place glass. Quartz Mountain is just right.

Quartz Mountain is a dome complex composed of two main eruptive units (Fig. 9): an older phorphyritic rhyolite (Table 1); and a younger aphyric rhyolite(Table 1). At the southwest flank of Quartz Mountain are rhyolites (Table 1) and perhaps dacites of Sixteen Butte, which seem to be older than the Quartz Mountain units.

Exposed in the 10 m high cliff at this place is the aphyric rhyolite of Quartz Mountain. The bulk of the outcrop is spherulitic devitrified flow-banded rhyolite. There are domains of pristine mahogany and black streaked obsidian

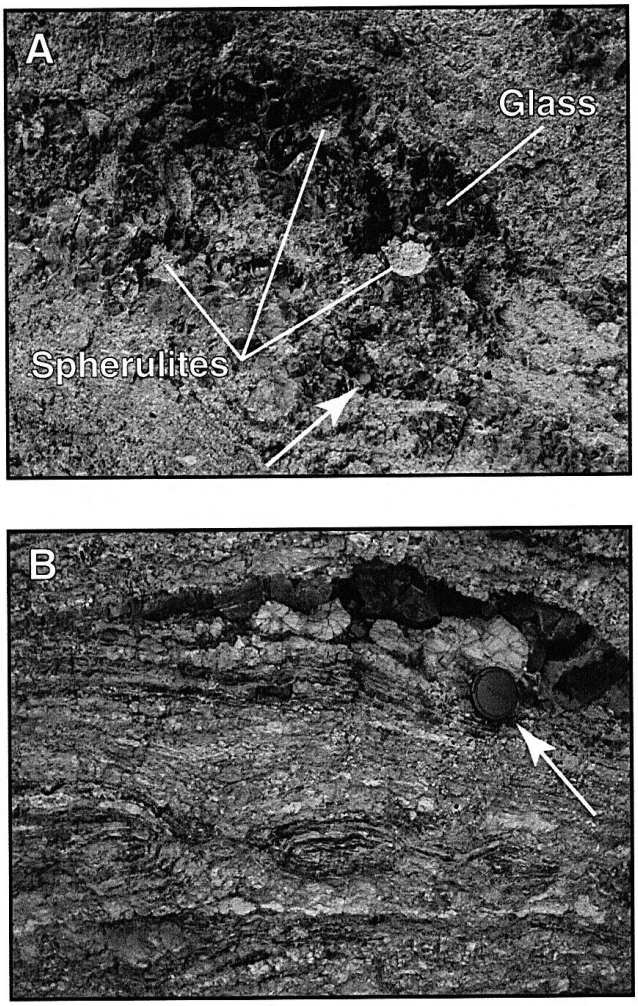

Figure 10. Photos of outcrop-scale features exposed in Quartz Mountain, Stop 4. Photo A shows the distribution of mahogany and black streaked obsidian and large intact spherulites. Photo B shows a train of spherulites and convolute flow banding. Arrows point to lens cap (5 cm) for scale.

with spherulites up to 10 cm (Fig. 10A). Flow banding is convolutely folded in places (Fig. 10B). This outcrop is probably representative of the distribution of glass, spherulite, and devitrified rhyolite in High Lava Plains domes, and it is easy to see how further weathering would disaggregate obsidian-bearing domains.

Continue along same road.

55.2 Go left at T intersection and stay left (avoiding borrow pit on the right into breccia that was mined for opal; L.A. Chitwood, personal communication).

56.4 At intersection with USFS 23 (yield sign), go left.

At intersection of USFS 23 and 2320, turn right, south. Fox Butte is the basaltic scoria cone on the east side of the intersection.

60.8 Go right toward Derrick Cave following the powerline south, not left toward Aspen Flat. The hills to the east are a cluster of rhyolite domes, from NW to SE, 2.4 Ma Long Butte, Squaw Mountain, Squaw Butte, and 3.7 Ma Squaw Ridge, all part of the age-progressive rhyolite trend. *Note: The place names that include "Squaw" are likely to be changed in accordance with a new place-names policy.*

63.7 The road forks. Stay under the power line.

65.2 At intersection, go straight, not right crossing under power line. The hill on the right is Buzzard Rock, another rhyolite center. Road soon splits, bear left.

66.6 The road has a three-way fork, take center fork. Young basalts from edge of Devils Garden basalt field are on the right.

67.0 Hot-tub sized spatter vent that is part of a NW-striking alignment of vents in several en echelon segments. Part of Devils Garden. The large parking area is access to Derrick Cave, a lava tube related to the Devils Garden. Potholes lava vents are on strike to NW.

67.7 Large spatter cones called "The Blowouts" that are part of the vent system for Devils Garden. As you continue south, the mafic scoria cone to the east is Ludi Butte, the rhyolite hills include Homestead Butte. Continue straight south. The hill west of the small settlement is Hogback Butte, another rhyolite dome.A bit farther along, the valley opening ahead is a basin that hosted Pleistocene Fort Rock Lake. Phreatomagmatic activity produced maars and tuff rings, some of which filled with lava to form table mountains. The distant symmetrical pointed peak is Hager Mountain, a 6 Ma rhyolite dome.

73.8 Go straight at intersection with Lake County Road 5-12C.

75.5 Go left on Lake 5-12B in the direction of

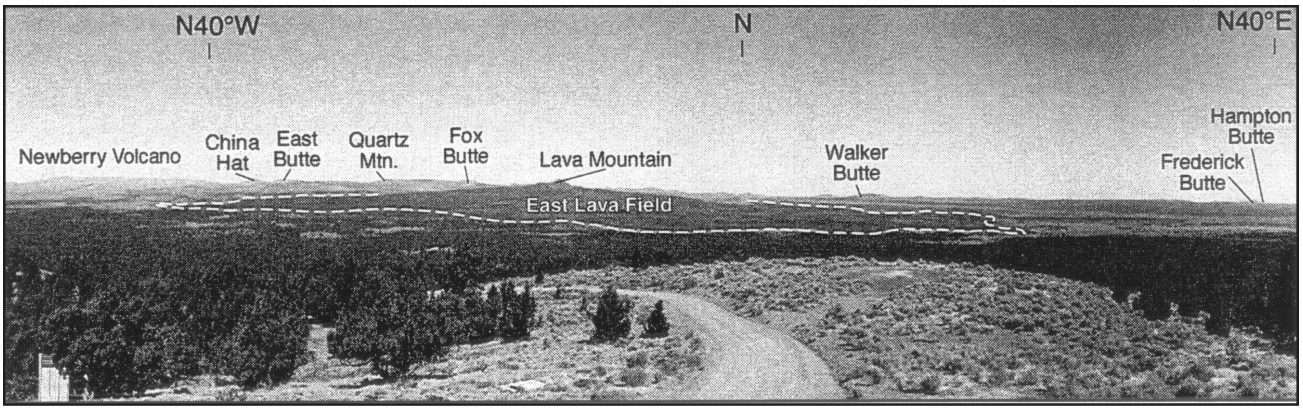

Figure 11. Photo looking north from the Green Mountain fire lookout. Noted are rhyolite domes and prominent cinder cones. The margins of the East Lava Field are highlighted by the dashed line.

Green Mountain. Road becomes gravel. Ahead and left you can see Lava Mountain, which is a cluster of scoria cones atop a broad shield of aa flows called the East Lava Field, which is Quaternary (post-Mazama) basalt.

82.1 Turn right, south, onto improved gravel road toward Green Mountain.

85 STOP 5. Green Mountain Fire Lookout.

Stop 5. Green Mountain Lookout

Green Mountain is a basalt shield that fed the lava flow at the next stop, Crack-in-the-Ground, about 740,000 years ago (Jordan, 2002). The fire lookout offers a panoramic overview of the western High Lava Plains and the northwestern Basin and Range. Points of interest in the western High Lava Plains are shown in Figure 11. East of the panorama shown in Figure 11 are the following volcanic buttes of the central High Lava Plains: Glass Buttes (two lumps at N70°E), Round Butte (N80°E), Paiute Butte (pointed butte at N82°E), Wagontire Mountain (S87°E), Horsehead Mountain (S74°E), Elk Mountain (S73°E), Little Juniper Mountain (S70°E), and Horse Mountain (S61°E). To the south is Christmas Valley with Table Rock, and in the background is Winter Rim (a Basin and Range escarpment). To the southwest note Fort Rock, a palagonitized tuff ring.

From this location we have an excellent view of the East Lava Field to the north (Fig. 6 and 11). At the center of the lava field is the Lava Mountain vent complex, the source of the East Lava Field. Obscured from our view by the east summit of Green Mountain is the Four Craters Lava Field, with its four aligned vents that give it its name (Fig. 6). Like the East Lava Field, the Four Craters Field is a post-Mazama aa basalt. It is compositionally identical to the East Lava Field, and the NW-trend of the four craters projects to the position of Lava Mountain. These relationships suggest that a single pulse of magmatism may have produced the Four Craters and East Lava Fields. We will get a closer look at the Four Craters Lava at the next stop.

85.4 Lunch at campground below the lookout.

85.9 Take right fork. Left fork is Green Mountain East.

89.9 Reaching the margin of the Four Craters lava. Note distinct aa flow morphology. Take a right.

91.1 STOP 6. Crack-in-the-Ground.

Stop 6. Crack-in-the-Ground

This locality (Fig. 12) features a great northwest-trending crack, Crack-in-the Ground, developed in the Green Mountian lava (740 ± 59 ka; Jordan, 2002). Volcanologists visiting this feature tend to view it as volcanogenic, and structural geologists tend to view it as tectonic. Pezzopane and Weldon (1993) recognized that the crack coincides with a Quaternary normal fault trace that extends beyond the crack to the north and south, strong evidence for a tectonic interpretation. In places the crack is clearly developed in more than one lava flow, further evidence for a tectonic origin. About 10 m of vertical displacement lies between rocks south-

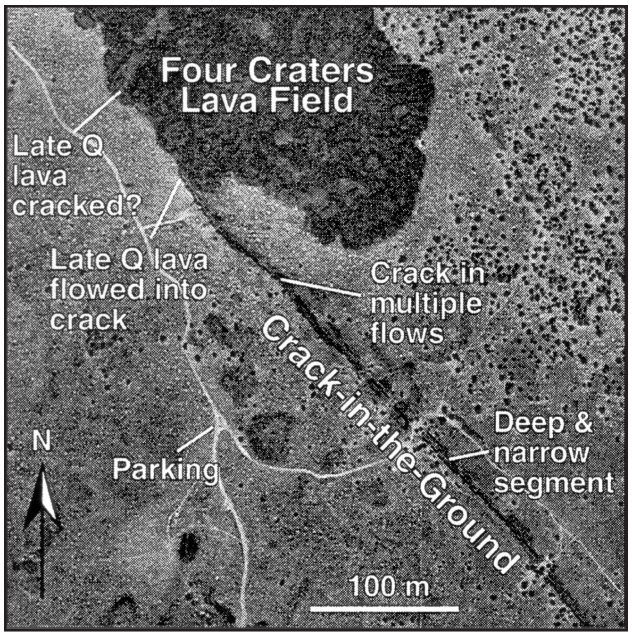

Figure 12. Annotated air photo of the Crack-in-the-Ground (Stop 6) showing locations described in the text. Note the incursion of the late Quaternary Four Craters lava into and over the crack at the north.

west (high) and northeast (low) of the crack. The crack has developed in what is essentially the upper hinge of a monocline generated by displacement on a steep normal fault below.

From the parking area, head east on the marked trail to Crack-in-the Ground. At the crack, go right (SE) and enter the crack. In this segment, the crack is deep and narrow, and irregularities on opposite sides of the crack clearly match. Then reverse your path and proceed northwest. View the crack from within, and also from the east side to appreciate the generally monoclinal structure that has formed here. In the crack, look for places where more than one flow has been cracked. Follow the crack until you reach the Four Craters lava. The lava can be clearly seen to flow into the crack at this point. Continue along the southwestern margin of the Four Craters lava. Pezzopane and Weldon (1993) suggest that the Four Craters lava has itself been cracked (though to a lesser degree than the Green Mountain lava), indicating Holocene displacement on this structure. We, however, have not observed unambiguous evidence for development of the crack in the younger lava.

From Crack-in-the-Ground, proceed south to the Christmas Valley Highway.

98.4 Go east, left, on Christmas Valley Highway. Driving east one can see rims of Basin and Range faults striking NNE with escarpments losing height as they approach the High Lava Plains. About 12 miles east, the most prominent double escarpment is Burma Rim (Fig. 13). The large mountain due east is Horse Mountain, a huge pile of peralkaline crystal-poor rhyolite lavas (Table 1). Elk Mountain is north of the highway, east of Burma Rim. You will cross a northern ridge of Horse Mountain before the road drops into Alkali Flat. The ridge is defined by a scarp of the Brothers Fault Zone oriented northwesterly. Alkali Rim on the far side of the valley, in contrast, is a NNE-striking Basin and Range fault that becomes Abert Rim to the south.

132.3 Intersection of Christmas Valley Highway and US 395. Turn south, right.

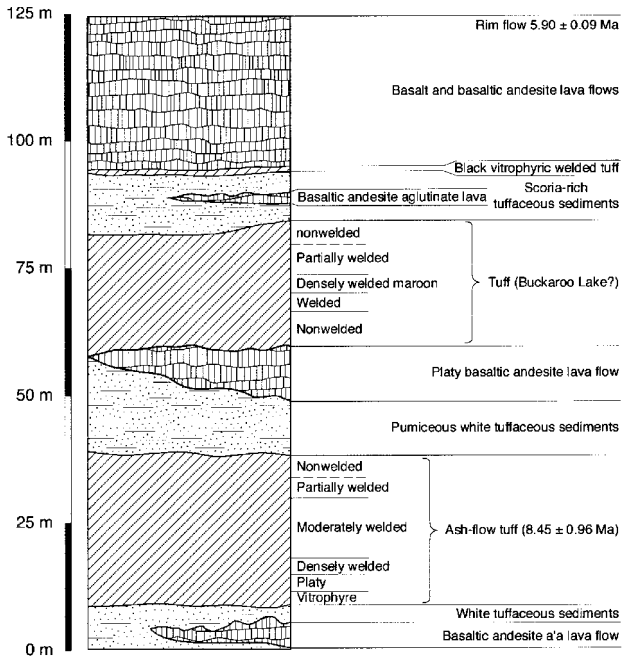

Figure 13. Composite section of rocks exposed at Burma Rim. We will not visit this section but provide a stratigraphic description because it is representative of the geology exposed in the many fault scarps we are passing to the south.

139.3 Turn left onto a dirt track.

139.7 STOP 7. Alkali Rim (Fig. 14). Hike up to the rim to the right side of the modest gully (reddish unit discernable at the top). Section of rheomorphic Rattlesnake Tuff, tuffaceous deposits, basalt lava, and valley filling tuff of Buckaroo Lake.

Stop 7. Alkali Rim

Low in the section are bold outcrops of densely welded Rattlesnake Tuff that is rheomorphic, devitrified, and lithophysal. A paleolake terrace is cut onto these. The tuff grades up into densely welded and vitric facies. Although eutaxitic folation is evident, up section the dense glass becomes pumiceous, not vitroclastic. This is interpreted to be the inflated carapace (revesiculation) of rheomorphic tuff that acted essentially as a lava flow. Steep plunges in the rheomporphic lineation suggest that topographic relief existed at the time of eruption (7.1 Ma). The top of the tuff grades into an ashy section that becomes increasingly pumice-rich up section. The pumices bear biotite and are unrelated to the Rattlesnake Tuff. The nearest biotite bearing silicic units in the region are at Palomino Butte and Elk Mountain.

Over the tuffaceous section (8 m thick) is a colluvial deposit (4 m thick) that includes clasts of various facies of Rattlesnake Tuff, some rounded. The colluvium is overlain by rimrock of basalt (primitive high-alumina olivine-tholeiite; sample 93.1ba, Table 2). The basalt drapes into a small paleovalley that is exposed in the head of the gully. The valley is filled in with tuff of Buckaroo Lake (6.78 Ma) that is zoned from marginal vitric and nonwelded facies to vitric partially welded with fiamme. Color gradation from light tan to brownish over 1 meter at the base of the tuff (observable locally near the paleovalley axis) appears to be more due to compositional variation than to an increase in welding.

Tuff of Buckaroo Lake crops out also along ridge marking the west side of Alkali Lake Valley and may crop out farther west and northwest. Compositional and lithological similarity with the 3.6 Ma tuff exposed at Stop 14, which may reach into the same general area of the central High Lava Plains, currently prevents a clear assignment to one or the other tuff.

Return to US 395

142.6 At the highway, turn north, right, toward Burns. The evening light is ideal to see fault scarps. Rimrocks are mainly basalt of the Rattlesnake Tuff.

151.7 Wagontire Mountain to the left and a rimrock of tuff of Buckaroo Lake. To the

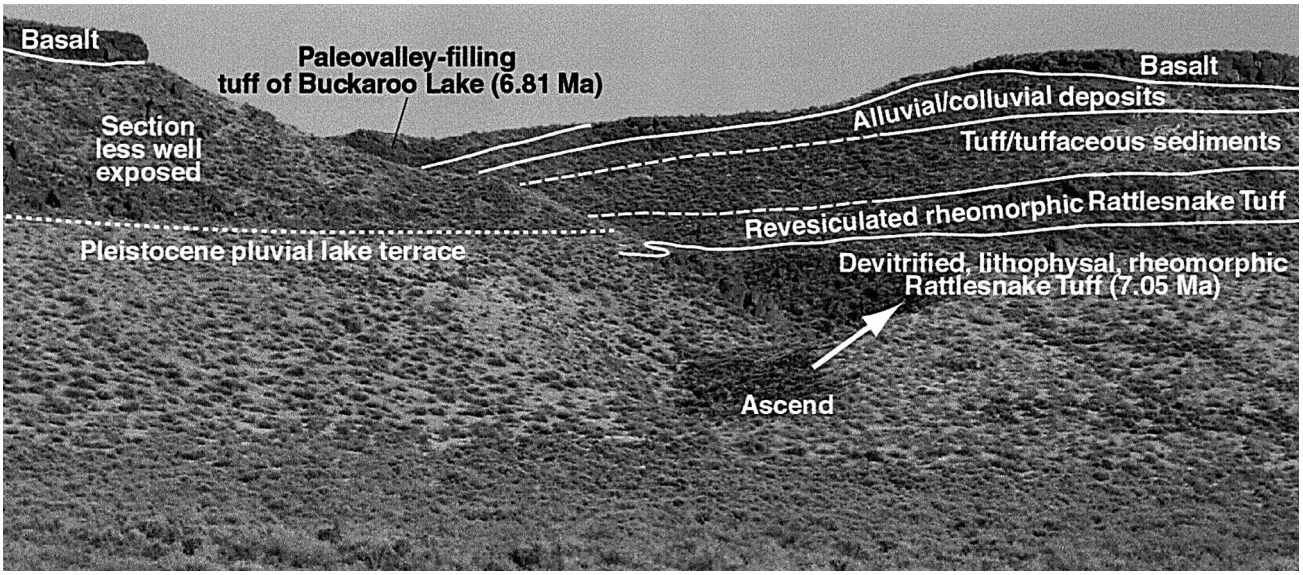

Figure 14. Photo of Alkali Rim at Stop 7, showing the distribution of different units and different facies of the Rattlesnake Tuff described in the text. Also note the pluvial lake terrace developed against the rim scarp.

right, Horsehead Mountain in background, and a rimrock of basalt. Sharply defined solitary butte to the northeast is Iron Montain, a rhyolite complex of 2.7 Ma, younger than domes of the age progression and one of the few exceptions to the trend.

170.5 Pass southeast entrance to Oregon State University Agricultural Station.

175.4 2.45 Ma basalt.

176.3 Southeast end of Juniper Ridge. Shields Butte basaltic andesite ahead. Stacks of flows to the north are calc-alkaline basaltic andesite.

180.6 Intersection of US 395 with US 20. Go right.

200.7 Road cuts through Rattlesnake Tuff. To the right, look at the capping basalt flows that are part of the field that fed the Wrights Point Flow, which protrudes into Harney Basin. It is an example of inverted topography. Tuffaceous sediment underlies it.

207.8 In Burns take left to stay on US 20.

208.3 The Silver Spur Motel. Rest your spurs here.

DAY 2

0 Depart Burns from the Silver Spur Motel. Go north on US 395.

1.4 At intersection, go left, staying north on US 395. After a few miles, you are going up a canyon that exposes the three large ignimbrite sheets of the Harney Basin region. Ignimbrites are more abundant in the east and central High Lava Plains than in the western part.

7.5 Tuffaceous sediment exposed in road cut on the west is part of the sediment between the 9.6-Ma Devine Canyon Tuff and the 8.1-Ma Prater Creek Tuff. The Rattlesnake Tuff (7.1 Ma) makes up the rimrock.

9.1 Turn and pull into the wide area on the west shoulder of the road at Milepost 61.

STOP 8. Overview of Harney Basin Ignimbrites

Excellent exposures of Harney Basin ignimbrite stratigraphy. The lowermost cliff is the Devine Canyon Tuff separated from the overlying Prater Creek Tuff by poorly exposed tuff and tuffaceous sedimentary rocks. The Rattlesnake Tuff caps the sequence. The bulk of the ignimbrites are composed of high-silica rhyolites that range from the peralkaline Devine Canyon Tuff to the peralkaline-metaluminous Rattlesnake Tuff and form important regional stratigraphic and structural markers.

Intercalated tuffaceous sediment at Stop 8 thins until it is completely missing about 60 km southward from here. There, the Rattlesnake Tuff directly overlies the Devine Canyon Tuff. Similarly, the sediment thins westward and northward suggesting that an active basin existed between 9 and 7 Ma around Burns, reaching into what is now the southern termination of the Blue Mountain Uplift (Walker and Robinson, 1990).

Devine Canyon Tuff

The Devine Canyon Tuff is crystal-rich and originally covered more than 18,600 km^2 of southeastern Oregon, with a total volume of approximately 195 km^3 (Greene, 1973). It is characterized by 10-30 percent phenocrysts of alkali feldspar and quartz, with sparse clinopyroxene. It ranges from nonwelded to densely welded; most commonly it occurs as greenish-gray stony devitrified tuff. The thickness is about 30 m near the type section about 0.5 km NE of the confluence with Poison Creek and corresponds with the observed maximum thickness (Greene, 1973). An $^{40}Ar/^{39}Ar$ age of 9.68±0.03 Ma was obtained from sanidine separates (Jordan and others, in prep). At this location, the tuff is partially welded and pumice-rich with pumice fragments up to 30 cm.

Prater Creek Tuff

The Prater Creek Tuff is mainly a devitrified, crystal-poor ash-flow tuff. Exposures of the type section (designated by Walker, 1979) can be seen from US 395 on the walls of Poison Creek, where the maximum thickness is 12 m. Lithologic variations can be seen in reference sections along Prater Creek, about 5 km east of Poison Creek. The type section consists chiefly of pale grayish-red devitrified tuff with grayish-pink gas cavities to 2 cm in diameter. Flattened devitrified pumice fragments occur throughout but are not abundant.

Alkali feldspar and quartz are sparse, and the tuff contains rare lithic fragments (Walker, 1979). Devitrified whole-rock tuff gave an age of 8.48±0.05 Ma (Jordan and others, in prep.).

Rattlesnake Tuff

Nonwelded to densely welded pumice- to ash-rich tuff with spherulitic, lithophysal, devitrified, and vapor-phase crystallization zones characterize the Rattlesnake Tuff. The phenocryst content is 1% or less throughout the bulk of the tuff and consists mainly of alkali feldspar, Fe-rich clinopryoxene, quartz, magnetite, and fayalite. Where pumiceous, the tuff commonly has distinctive white, gray, black, and banded pumice clasts set in a salt-and-pepper matrix of white and gray glass shards. Typically, the tuff occurs as 10-20-m-thick cliff-forming rimrock, and it likely originally covered 35,000 km^2 (Fig. 15). The maximum thickness is about 70 m. Weighted mean age of 15 single-crystal $^{40}Ar/^{39}Ar$ analyses of alkali feldspar yielded an age of 7.05±0.01 Ma (Streck and Grunder, 1995). Maximal run-out distances as based on today's outcrop remnants is about 150 km to the north and south from its likely source area in the western Harney Basin (Streck and Grunder, 1995). The Rattlesnake Tuff is among the most far-traveled ignimbrites known (Wilson and others, 1995).

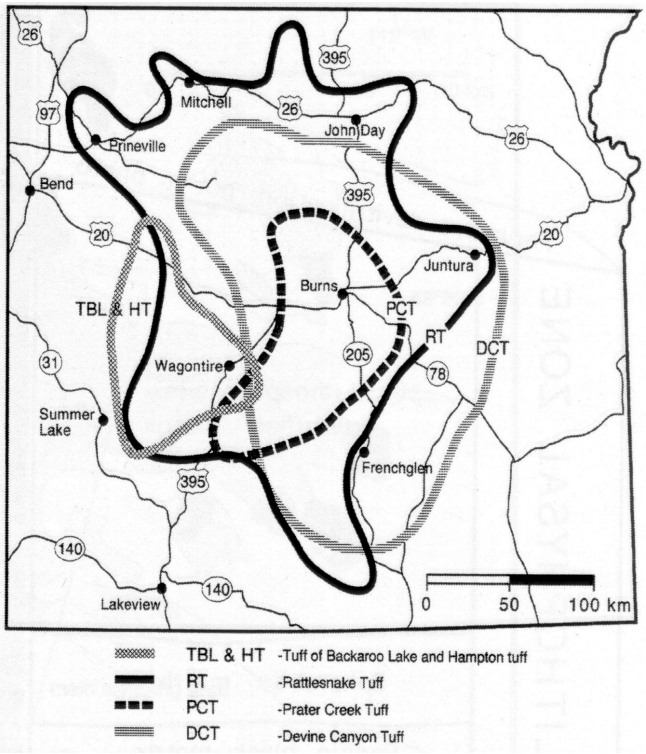

Figure 15. Distribution of major late Miocene ignimbrites in eastern Oregon that vented from the High Lava Plains. Data source: Rattlesnake Tuff (RST), Streck and Grunder (1995), Streck and others (1999); Devine Canyon Tuff (DCT), Green (1972); Prater Creek Tuff (PCT), Walker (1979); tuff of Hampton and tuff of Buckaroo Lake-like; Walker and others (1986); outcrop distributions envelops for DCT, PCT, and tuff of Hampton and tuff of Buckaroo Lake-like have been modified or approximately established by fieldwork of M.J. Streck and A.L. Grunder, unpublished.

Proceed south.

11.0 Tuffaceous sediment in the same road cut suitable for viewing from the other side of the vehicle.

12.3 Pull off on left shoulder. STOP 9.

STOP 9. Rattlesnake Tuff

The Rattlesnake Ash-flow Tuff (Walker, 1979), here referred to as the Rattlesnake Tuff (RST), is named for the original type locality on Rattlesnake Creek (John Day Valley), about 100 km north from here. The total thickness of the tuff at Stop 1 is 22 m. It is a highly zoned section. The underlying pale-orange to buff-colored, fine-grained, poorly consolidated tuffaceous sedimentary sequence is an ubiquitous slope-forming unit throughout the Harney Basin.

The lowermost white 1-m-thick finely laminated deposit, likely deposited by pyroclastic surges (Fig. 16), consists almost entirely of clear glass shards; it was likely a precursor event to the main pyroclastic eruption(s) that formed the Rattlesnake Tuff. This is conformably overlain by 0.5 m of nonwelded vitric tuff with "mixed" shard matrix (clear and brown rhyolitic glass shards) and 7 to 10% white pumice fragments to 2 cm in diameter. In some places, the transition from the lower laminated deposits to the unwelded tuff is gradational, and the transition may be exaggerated by the change from white to mixed shard matrix. Bubble-wall shards can be seen in both the unwelded and surge deposit. The unwelded zone grades abruptly to 0.5 m of partially welded vitric tuff, overlain by 1 m of black vitrophyre. The 20-m-thick capping cliff-forming

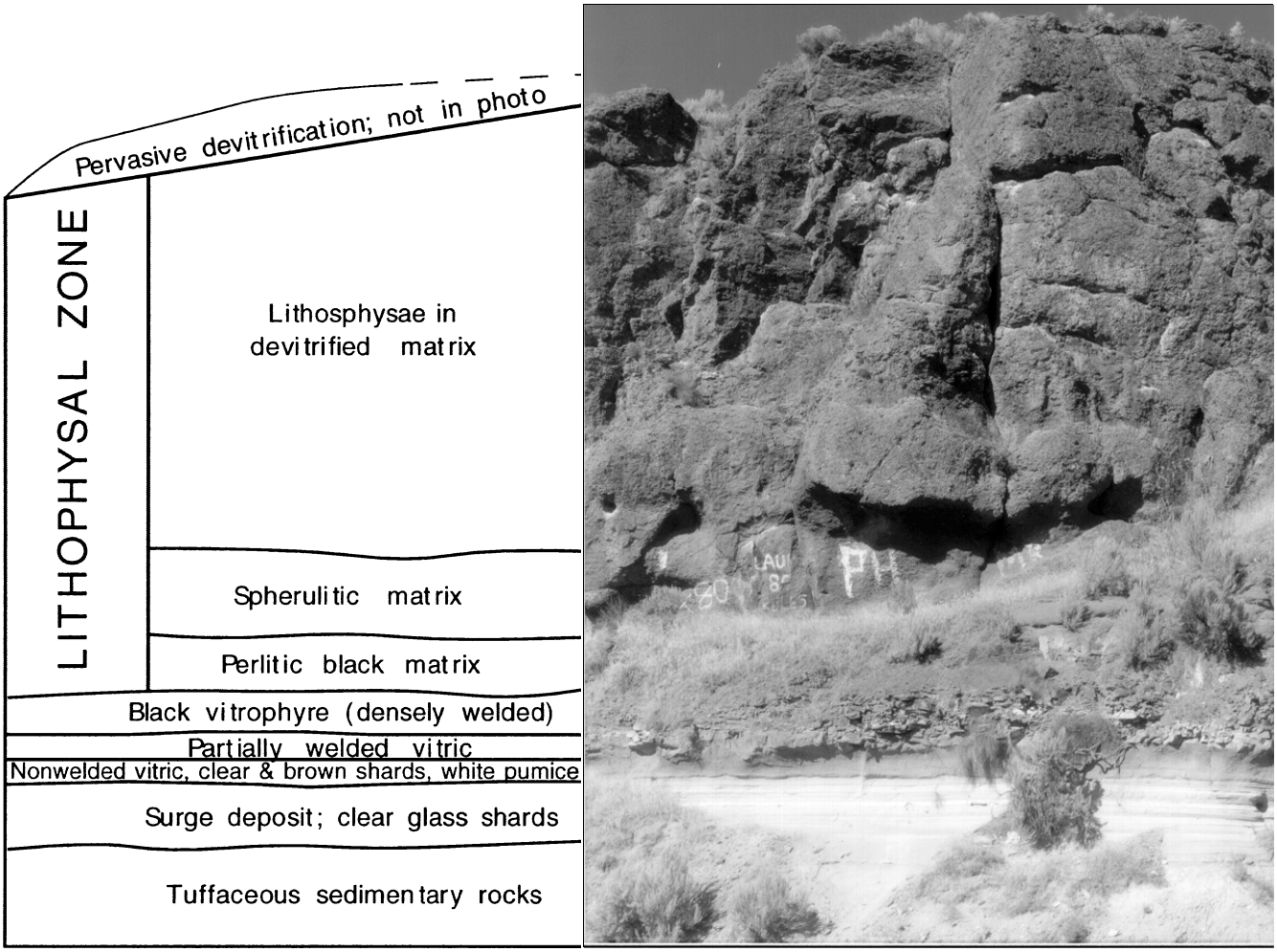

Figure 16. Lithologic variation in the Rattlesnake Tuff at its type locality on Highway 395 (Stop 9). Facies descriptions are in Streck and Grunder (1995).

unit is entirely lithophysal tuff. The lower 4 m of this section is divided into a perlitic black-matrix base and an upper part with a spherulitic matrix. The upper 15 m are entirely lithophysae in a devitrified matrix and are capped by float of pevasively devitrified tuff. Just across the highway (east) from this place, float on top of the cliff-forming Rattlesnake Tuff also includes upper vitric partially welded tuff indicating proximity to the inferred original top of the unit.

15.8 Continue right on US 395.
Go through Burns staying on US 395, heading west toward Bend (Fig. 17).
34.9 Turn left onto wide improved gravel road.
37.0 Hill on the right is a mafic vent that produced trachybaslt, strongly enriched in incompatible trace elements (HBA6, Table 2).
38.3 Go left on small dirt track that goes between two big buttes that make up Palomino Butte. Pull up about 0.3 miles, STOP 10.

STOP 10. Palomino Buttes

The Palomino Buttes are an example of the westward-younging rhyolites. They are a complex of flows that issued from at least three vents. They are an example of fairly crystal-rich rhyolite lava and are unusual in that they contain substantial biotite. Domes of this type include Elk Mountain, passed on Day 1, and are

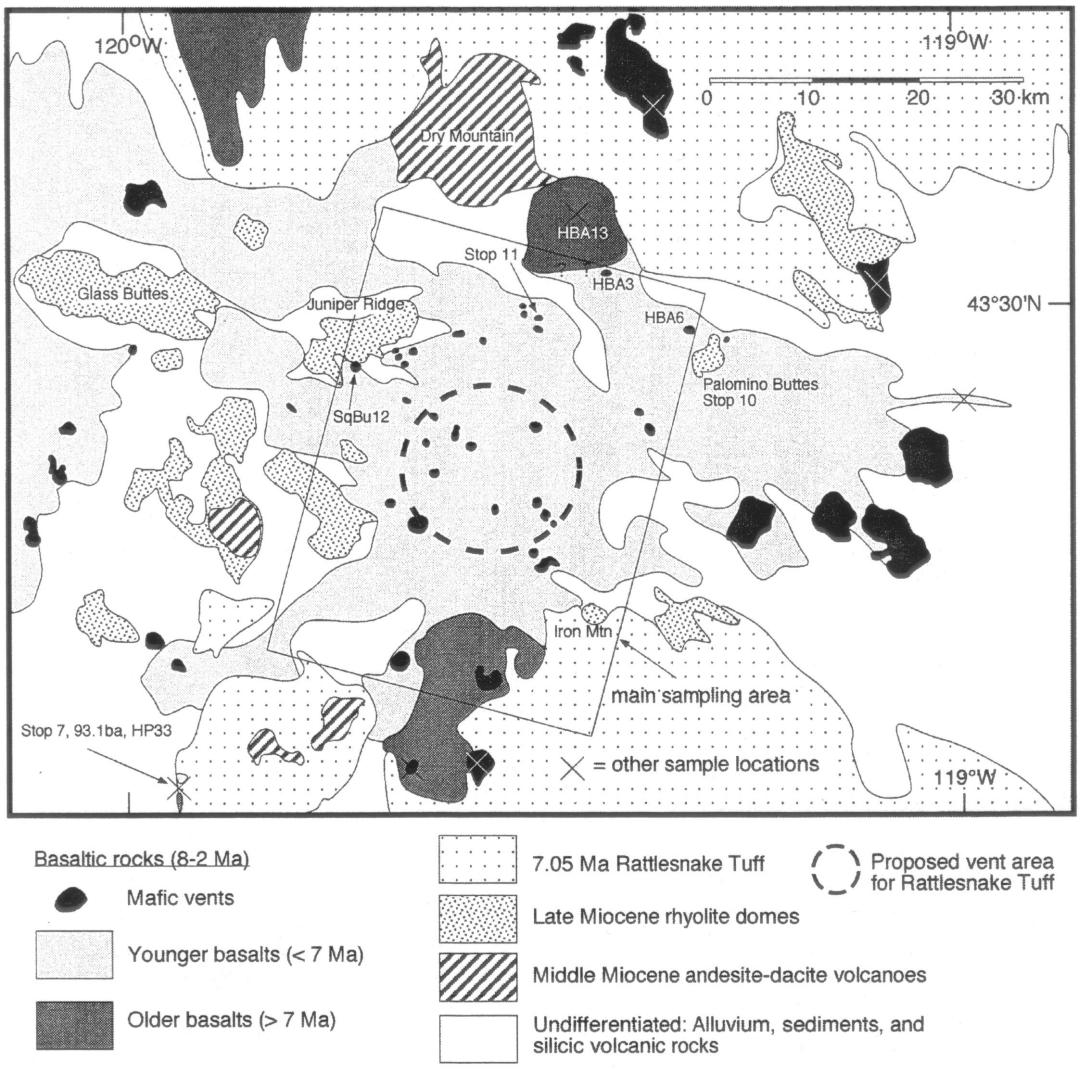

Figure 17. Simplified geologic map of the central High Lava Plains (modified from Walker, 1991). Rectangle delineates main sampling area for lavas shown in Fig. 19. Locations for some basalt samples of Table 2 are shown.

distinct from crystal-poor to aphyric domes in that they are richer in Ca relative to Fe (Fig. 18).

Return to gravel road and go north to the main highway, US 395.

42.3 At US 395, turn left, to continue west.

48.0 To the north is a mafic vent where basaltic trachyandesite erupted that is compositionally transitional between the iron-enriched trachytic and calc-alkaline basaltic trends (HBA 3, Table 2).

53.1 Intersection between US 395 and US 20. Go left, south, on US 395.

Shields Butte is on the right.

54.7 At the top of the first rise, go left on a cinder road that leads to STOP 11 and a cinder quarry. Have a look at the big bombs as you climb the back wall of the quarry for the view.

STOP 11. Overview of Mafic Volcanism

This stop is near the western margin of the Harney Basin, and several mafic vents and lava sequences can be viewed that span a wide range of compositions over a small area. Late Miocene to Quaternary mafic volcanism of the western Harney Basin and vicinity can be characterized by two end-member evolutionary trends. Starting with primitive high-alumina olivine tholeiite, one trend goes to andesite with calc-alkaline affinities and the other trend develops into iron-enriched and trachyandesitic

compositions that can be strongly enriched in incompatible trace elements (Fig. 19). Compositions transitional between calc-alkaline and iron-enriched trachytic occur as well.

Shields Butte is a pile of lavas, many agglutinated, and is part of the scoria cone exposed here. Shields Butte is uplifted along Brothers Fault Zone structures. The composition here is basaltic andesite with 52.8% SiO_2 and a calc-alkaline affinity (HBA16, Table 2, is from lava flows of Shields Butte across the road).

The view from the hill that makes the east side of the quarry includes the following (sweeping northward and westward from our last stop at Palomino Butte): (1) Palomino Butte at azimuth S75°E; (2) the subdued hill at azimuth S85°E corresponds to a mafic vent of very incompatible-trace-element enriched trachyandesite (HBA6, Table 2); (3) the 5.44±0.10 Ma mafic vent of basaltic trachyandesite HBA3 (N55°E) that is transitional between calc-alkaline and the most enriched basaltic trachyandesite; (4) scarps through a stack of calc-alkaline basaltic andesite flows (N40°E, HBA13) that grade into basalt near the base of the section (basal flow was dated at 7.60±0.11 Ma); (5) Dry Mountain (N20°W), a middle Miocene andesitic center; (6) Shields Butte (N45°W); (7) Juniper Ridge (N80°W to S45°W), a rhyolite dome complex that is 6.87 Ma in the east and 5.70 Ma in the west; and (8) Paiute Butte (2.37±0.04 Ma) is the sharp butte that peaks up (at S80°W) behind Juniper Ridge; it erupted lavas of very enriched basaltic trachyandesite (SqBu-12, Table 2).

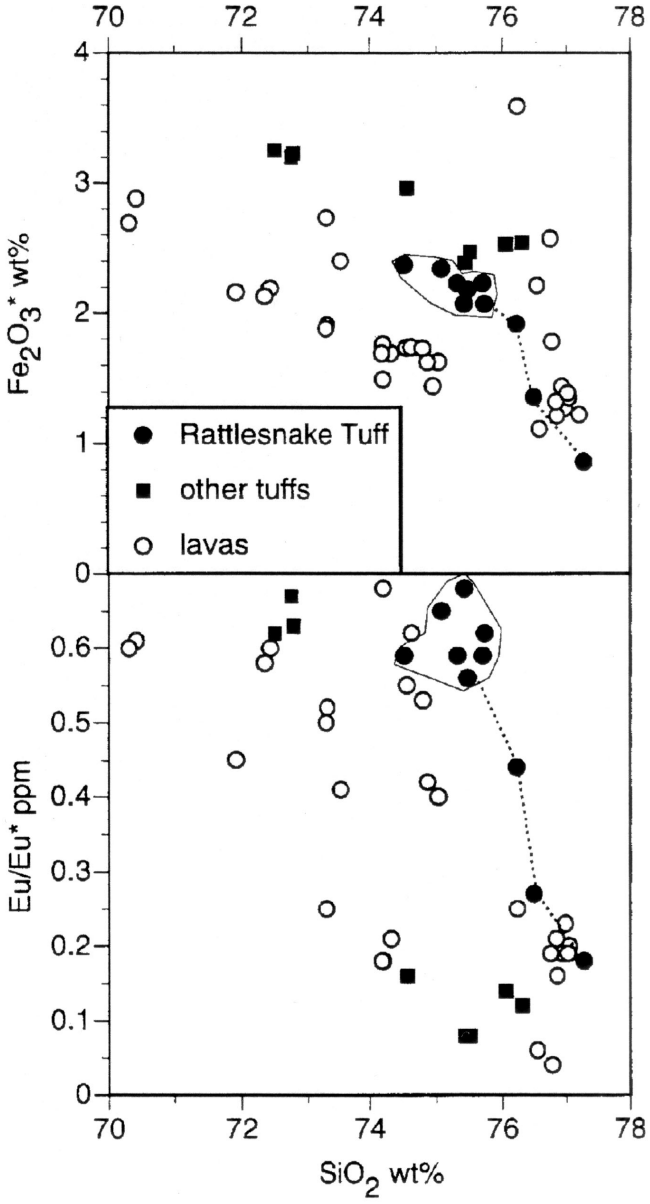

Figure 18. Chemical composition of rhyolitic lavas and tuffs from the central High Lava Plains. Chemical variation trends within the Rattlesnake Tuff (RST) are based on whole-rock pumice compositions and dictate magma differentiation compatible with nonmodal crystal fractionation (Streck and Grunder, 1997). Other tuffs include Devine Canyon Tuff (DCT), Prater Creek Tuff (PCT), and tuff of Hampton; and lavas include Elk Mountain, Horse Mountain, Juniper Ridge, Palomino Butte, Burns Butte, and Iron Mountain. Data sources: Streck and Grunder (1997); M. Streck and A. Grunder, unpublished data. Eu* is the Eu concentration predicted by projection of trends in adjacent rare-earth elements.

Return to the main highway.

55.3 Turn north on US 395.

56.8 At intersection with US 20, go west on US 20.

~62 Chickahominy Reservoir on the right, where typical high-aulmina olivine tholeiite basalt is exposed. Dry Mountain to the northwest. The Rattlesnake Tuff makes up most of the rimrock to the north. Glass Buttes is ahead, and Juniper Ridge is on the left.

64.8 Improved gravel road on the left goes to quarry in glomeroporphyritic basaltic andesite that is part of east Juniper

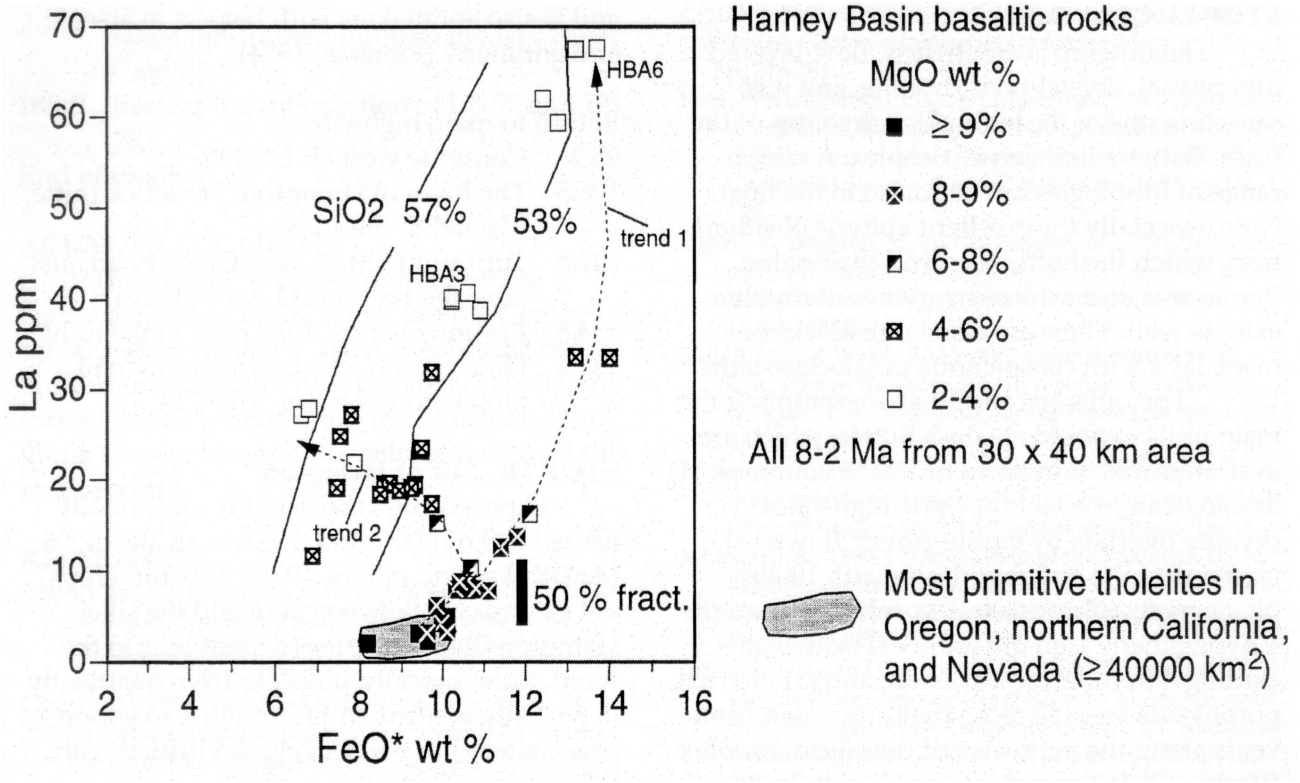

Figure 19. Chemical compositions of mafic lavas from the central High Lava Plains. Most primitive central HLP compositions overlap with other primitive compositions from Oregon, N. California, and N. Nevada. Evolved mafic magmas indicate two end-member trends; trend 1 follows an iron-enrichment trend developing trachytic compositions associated with strong incompatible-element enrichment, and trend 2 follows a calc-alkaline trend associated with more silica enrichment but less incompatible-element enrichment.

Ridge. This area is one of the few silicic centers that has substantial andesite and dacite.

67.2 Turn left onto OSU Agricultural Experimental Station. Improved gravel road.

As you approach the flank of Juniper Ridge, a great stack of basaltic lava is exposed in a NW-striking scarp. As you ascend the scarp, the basaltic stack is banked against rhyolite lavas (cryptic outcrop) of western Juniper Ridge.

68.8 STOP 12 is where road turns sharply south. Turn around and park on right shoulder.

STOP 12. Juniper Ridge

Here basalt banks onto rhyolite (low-silica variety) of western Juniper Ridge. The banking relationship is not directly exposed, but rhyolite crops out on the east side of the road, and basalt is exposed at the same altitude on the west side. At both eastern and western Juniper Ridge, most-evolved rhyolites are derived from least-evolved rhyolites by crystal fractionation (on the order of 50% crystallization). Dacite and andesite of eastern Juniper Ridge are derived by combined assimilation of lower silica rhyolite and fractional crystallization of high-alumina olivine-tholeiite. Rare dacite at western Juniper Ridge formes by mixing of high-alumina olivine-tholeiite and most-evolved rhyolite (MacLean, 1994).

Return to the main highway.

72.3 Go west on US 20. Glass Buttes directly ahead.

92.6 GI Ranch mailbox on the right. Go left onto dirt road. Go through wire fence, bear left.

93.9 STOP 13 is outcrop of stony rhyolite and diverse float in small draw off of Glass Buttes.

STOP 13. Glass Buttes

The outcrop is devitrified, flow-layered, lithophysal, crystal-poor rhyolite, and it is sampling one of the high-silica rhyolites of the Glass Buttes silicic dome complex. A wide range of lithologies can be found in the float. Note especially the excellent aphyric obsidian from which the buttes received their name. Pumiceous and oxidized varieties of rhyolite exist as well. There are also large blocks of a mafic lava with conspicuous plagioclase laths.

The outcrops and float are sampling the main units exposed at Glass Buttes, which are in stratigrahic order from oldest to youngest: (1) lithologically variable aphyric high-silica rhyolite overlain by biotite-phyric flows; (2) phyric rhyolite and rhyodacite with 10-40% phenocrysts (plagioclase ± hornblende ± augite ± hypersthene ± quartz and FeTi oxides), including a rhyodacitic intrusion; and (3) internal porphyritic basaltic rocks that originated from vents along the perimeter of the silicic complex (Roche, 1987). Several internal basalt flows show strong geochemical and petrographic evidence of contamination by silicic rocks (Roche, 1987).

From east to west, the main buttes are Eastern Glass Buttes, Round Top Butte (behind Eastern Glass Butte), Little Glass Butte, and Glass Butte. Radiometric age determination at Glass Buttes yielded K-Ar ages of 4.91±0.73 (MacLeod and others, 1976), 5.5±0.3, 5.8±0.3, 5.8±0.3, and 7.7±0.4 Ma (Phillips Petroleum Co, cited in Johnson, 1984). The oldest age of 7.7 Ma was derived from a sample proximal to a hydrothermally altered area, and it is therefore suspect (Benoit, written commun, cited in Johnson, 1984)

The eastern end of Glass Buttes is hydrothermally altered at the surface. Alteration is localized along northwest-trending normal faults and occurs primarily as opalite replacement of rhyolite glass with associated cinnabar, alunite, hematite, hyalite and clay-rich vein material (Johnson, 1984). Alteration identified in the subsurface by means of four stratigraphic test holes drilled by the Phillips Petroleum Co was interpreted to be related to an older hydrothermal system (Johnson, 1984). Carbonate, pyrite, quartz, and minor chlorite occur in vugs and fractures, and they partially replace subsurface basalt. Pyrite contains up to 13 ppm Au and is also anomalous with respect to arsenic and antimony (Johnson, 1984)

Return to main highway.

95.2 Continue west on US 395.

106.5 The town of Hampton. Frederick Butte (dacite) to the south.

127.5 Turn right onto Camp Creek Road, just after the Brothers Oasis rest area.

134.5 Pavement ends. Take road to the right.

135.6 Outcrops on left come close to road. Stop before the rise. STOP 14.

STOP 14. Tuff of Hampton

Exposed cliffs consist of the informally named tuff of Hampton that has an age of 3.6 Ma (Walker and others, 1974). This tuff crops out extensively between here and the silicic Hampton Butte complex (distant hills to the west). Lithologically, it ranges from incipiently to partially welded and from vitric to vapor-phase altered to pervasively devitrified with lithophysae. The tuff is typically pumiceous with tan, black, and banded pumice clasts and the maximum outcrop thickness is less than 10 m. Here at Stop 14, the thickness is 6.5 m and the average size of the five largest pumice clasts and lithic fragments is 34 cm and 2.5 cm, respectively. The tuff of Hampton is lithologically similar to the Rattlesnake Tuff but, in general, the Hampton is darker and its light pumice fragments are always tan and not white as in the Rattlesnake. Tan pumices, as is bulk tuff, are low-silica rhyolitic (72 wt% SiO_2) and dark pumices are dacitic (66 wt% SiO_2) (M. Streck, unpublished data; Table 3). On the other hand, the tuff of Buckaroo Lake (see Stop 7) is as dark as the tuff of Hampton and compositionally overlaps strongly with it (Fig. 15).

Bulk tuff contains 5% phenocryst composed largely of plagioclase (3.5%), green (Fe-rich?) clinopyroxene (1%) and oxide(s) (0.5%). Pumice clasts are more crystal-poor ranging from 1-2% in rhyolitic to less than 1% in dacitic pumice. Matrix glass is of two populations with light brown shards making up 99% and dark brown glass 1%.

Retrace route to US 20.

143.7 Continue west on US 20.

164 Sediment in road cut to the north. This lake sediment is from the Pleistocene

lake that drained through the Dry River Canyon.

185.5 Back at the intersection of US 97 and US 20.

End of roadlog.

ACKNOWLEDGMENTS

This research was supported by the National Science Foundation and the Geological Society of America. We recognize the contributions of our partners in the High Lava Plains Project, Jenda Johnson and Jim MacLean. We thank George Moore for a helpful review of this manuscript.

REFERENCES

Armstrong, R.L., Leeman, W.P., and Malde, N.E., 1975, K-Ar dating, Quaternary and Neogene rocks of the Snake River Plain, Idaho: American Journal of Science, v. 275, p. 225-251.

Camp, V.E., 1995, Mid-Miocene propagation of the Yellowstone mantle plume head beneath the Columbia River basalt source region: Geology, v. 23, p. 435-438.

Carlson, R.W., and Hart, W.K., 1987, Crustal genesis on the Oregon Plateau: Journal of Geophysical Research, v. 92, p. 6191-6206.

Chitwood, L.A., 1994, Inflated basaltic lava—Examples of processes and landforms from central and southeast Oregon: Oregon geology, v. 56, p. 11-20.

Christiansen, R.L., 1993, The Yellowstone Hot Spot: Deep mantle plume or upper mantle melting anomaly?: Transactions of the American Geophysical Union, v. 76, p. 602.

Christiansen, R.L., and McKee, E.H., 1978, Late Cenozoic volcanic and tectonic evolution of the Great Basin and the Columbia intermontane regions: Geological Society of America Memoir 152, p.283-311.

Clayton, R.W., 1989, Kinematics of the northern Basin and Range, Oregon: Geological Society of America Abstracts with Programs, v. 21, no. 5, p. 66.

Diggles, M. F., Conrad, J.E., and Soreghan, G.S., 1990, Geologic map of the Diablo Mountain Wilderness Stady Area, Oregon: U.S. Geological Survey Miscellaneous Field Studies Map MF-2121, scale 1:48,000.

Draper, D.S., 1991, Late Cenozoic bimodal magmatism in the northern Basin and Range Province in southeastern Oregon: Journal of Volcanology and Geothermal Research, v. 47, p. 299-328.

Fiebelkorn, R.B., Walker, G.W., MacLeod, N.S., McKee, E.H., and Smith, J.G., 1983, Index to K-Ar age determinations for the State of Oregon: Isochron West, v. 37, p. 3-60.

Greene, R.C., Walker, G.W., and Corcoran, R.E., 1972, Geologic map of the Burns Quadrangle, Oregon: U.S. Geological Survey Miscellaneous Geologic Investigations Map I-680, scale 1:250,000.

Hamilton, W.B., 1989, Crustal geologic processes of the United States, *in* Pakiser, L.C., and Mooney, W.D., Geophysical framework of the continental United States: Geological Society of America Memoir 172, p. 743-781.

Hart, W.K., Aronson, J.L., and Mertzman, S.A., 1984, Areal distribution and age of low-K, high-alumina olivine tholeiite magmatism in the northwestern Great Basin: Geological Society of America Bulletin, v. 95, p. 186-195.

Hearn, T., Beghoul, N., and Barazangi, M., 1991, Tomography of the western United States from regional arrival times: Journal of Geophysical Research, v. 96, p. 16369-16381.

Hill, B.E., and Taylor, E.M., 1989, Oregon central High Cascades pyroclastic units in the vicinity of Bend, Oregon: U. S. Geological Survey Open File Report 89-645, p. 51-54.

Johnson, J.A., 1995, Geologic evolution of the Duck Creek Butte eruptive center, High Lava Plains, southeastern Oregon: Oregon State University MS Thesis, 151 p.

Johnson, J.A., 1998, Geologic map of the Frederick Butte volcanic center, Deschutes and Lake Counties, south-central Oregon: U.S. Geological Survey Open-File Report 98-208, scale 1:40,000.

Johnson, J. A., and Grunder, A.L., 2000, The making of intermediate composition magma in a bimodal suite: Duck Butte Eruptive Center, Oregon, USA: Journal of Volcanology and Geothermal Research, v. 95, p. 175-195.

Johnson, M.J., 1984, Geology, alteration, and mineralization of a silicic volcanic center, Glass Buttes, Oregon: Portland State University MS Thesis, 127 p.

Jordan, B.T., 2001, Reconciling the misfit between the Yellowstone Plume trace and global plate motion models: Channelized and pancake plume flow on basal lithospheric topography: Eos, v. 82, p.1218.

Jordan, B.T., 2002, Basaltic volcanism and tectonics of the High Lava Plains, southeastern Oregon: Oregon State University PhD Dissertation, 218 p.

LaBas, M.J., Le Maitre, R.W., Streckeisen, A., and Zanettin, B., 1986, A chemical classification of volcanic rocks based on the total-alkali-silica diagram: Journal of Petrology, v. 27, p. 337-362.

Lawrence, R.D., 1976, Strike-slip faulting terminates the Basin and Range Province in Oregon: Geological Society of America Bulletin, v. 87, p. 846-850.

Linneman, S.K., and Meyers, J.D., 1990, Magmatic inclusions in Holocene rhyolites of Newberry Volcano, central Oregon: Journal of Geophysical Research, v. 95, p. 17677-17699.

MacLean, J.W., 1994, Geology and geochemistry of Juniper Ridge, Horsehead Mountain and Burns Butte: Implications for the petrogenesis of silicic magmas on the High Lava Plains, southeastern Oregon: Oregon State University MS Thesis, 141 p.

MacLeod, N.S., Walker, G.W., and McKee, E.H., 1975, Geothermal significance of eastward increase in age of upper Cenozoic rhyolitic domes in southeastern Oregon: U.S. Geological Survey Open-File Report 75-348, 21 p.

MacLeod, N.S., and Sherrod, D.R., 1988. Geological evidence for a magma chamber beneath Newberry Volcano, central Oregon: Journal of Geophysical Research, v. 93, p. 10059-10066.

MacLeod, N.S., and Sherrod, D.R., 1992, Reconnaissance geologic map of the west half of the Crescent Quadrangle, Deschutes, and Crook Counties, Oregon: U.S. Geological Survey Miscellaneous Investigations Map I-2215, scale 1:250,000.

MacLeod, N.S., Sherrod, D.R., Chitwood, L.A., and Jensen, R.A., 1995, Geologic map of Newberry Volcano, Deschutes, Klamath, and Klamath Counties, Oregon: U.S. Geological Survey Miscellaneous Investigations Map I-2455, scale 1:62,500 and 1:24,000.

McKee, E.H., and Walker, G.W., 1976, Potassium-argon ages of late Cenozoic silicic volcanic rocks, southeastern Oregon: Isochron/West, no. 15, p. 37-41.

Parker, D., and Armstrong, R.L., 1972, K-Ar dates and Sr isotope initial ratios for volcanic rocks of the Harney Basin, Oregon: Isochron/West, no. 5, p. 7-12.

Pezzopane, S. K., and Weldon, R.J., 1993, Tectonic role of active faulting in central Oregon: Tectonics, v. 12, p. 1140-1169.

Pickthorn, L.B.G., and Sherrod, D.R., 1990, Potassium-argon ages from the Klamath Falls area, south-central Oregon: Isochron/West, no. 55, p. 13-17.

Pierce, K.L., and Morgan, L.A., 1992, The track of the Yellowstone Hotspot: Volcanism, faulting, and uplift, *in* Link, P.K., Kuntz, M.A., and Platt, L.B., eds., Regional geology of eastern Idaho and western Wyoming: Geological Society of America Memoir 179, p. 1-53.

Roche, R.L, 1987, Stratigraphic and geochemical evolution of the Glass Buttes complex, Oregon: Portland State University MS Thesis, 99 p.

Sherrod, D.R., and Smith, J.G., 1990, Quaternary extrusion rates of the Cascade Range, northwestern United States and southern British Columbia: Journal of Geophysical Research, v. 95, p. 19,465-19,474.

Smith, R.B., and Braille L.W., 1994, The Yellowstone hotspot: Journal of Volcanology and Geothermal Research, v. 61, p. 121-188.

Streck, M.J., and Grunder, A.L., 1995, Crystallization and welding variations in a widespread ignimbrite sheet: The Rattlesnake Tuff, Eastern Oregon: Bulletin of Volcanology, v. 57, p. 151-169.

Streck, M.J., and Grunder, A.L., 1997, Compositional gradients and gaps in high-silica rhyolites of the Rattlesnake Tuff, Oregon: Journal of Petrology, v. 38, p. 133-163.

Streck, M.J., and Grunder, A.L., 1999, Enrichment of basalt and mixing of dacite in the rootzone of a large rhyolite chamber: Inclusions and pumices from the Rattlesnake Tuff, Oregon: Contributions to Mineralogy and Petrology, v. 136, p. 193-212.

Streck, M.J., Johnson, J.J., and Grunder, A.L., 1999, Field guide to the Rattlesnake Tuff and High Lava Plains near Burns, Oregon: Oregon Geology, v. 61 p. 64-76.

Streck, M.J., 2002, Partial melting to produce high-silica rhyolites of a young bimodal suite: Compositional constraints among rhyolites, basalts, and metamorphic xenoliths from the Harney Basin, Oregon: International Journal of Earth Sciences, in press.

Stimac, J.P., 1996, Rock magnetic and paleomagnetic characteristics of the late Miocene Rattlesnake and Devine Canyon Ash-Flow Tuffs, eastern Oregon: University of Oregon PhD Dissertation, 185 p.

Thelin, G.P., and Pike, R.J., 1991, Landforms of the conterminous United States: A digital shaded-relief portrayal: U.S. Geological Survey Miscellaneous Investigations Map I-2206, scale 1:3,500,000.

Thompson, R.N., and Gibson, S.A., 1991, Subcontinental mantle plumes, hotspots, and pre-existing thinspots: Journal of the Geological Society of London, v. 148, p. 973-977.

Vallier, T.L., and Brooks, H.C., eds., 1986, Geology of the Blue Mountains region of Oregon, Idaho, and Washington: U.S. Geologicial Survey Professional Paper 1435, 93 p.

Walker, G.W., 1974, Some implications of late Cenozoic volcanism to geothermal potential in the High Lava Plains of south-central Oregon: Ore Bin v. 36, p. 109-122.

Walker, G.W., 1979, Revisions to the Cenozoic stratigraphy of Harney Basin, Oregon: U.S. Geological Survey Bulletin 1475, 35 p.

Walker, G.W., and Repenning, C.A., 1965, Reconnaissance geologic map of the Adel Quadrangle, Lake, Malheur, and Harney Counties, Oregon: U.S. Geological Survey Miscellaneous Investigations Map I-446, scale 1:250,000.

Walker, G.W., Peterson, N.V., and Greene, R.C., 1967, Reconnaissance geologic map of the east half of the Crescent Quadrangle, Lake, Deschutes, and Crook Counties, Oregon: U.S. Geological Survey Miscellaneous Investigations Map I-457, scale 1:250,000.

Walker, G.W., and Robinson, P.T., 1990, Cenozoic tectonism and volcanism of the Blue Mountains Region, *in* Walker, G.W., ed., Geology of the Blue Mountains Region of Oregon, Idaho, and Washington, U.S. Geological Survey Professional Paper 1437: 119-135.

Walker, G.W., and MacLeod, N.S., 1991, Geologic map of Oregon: U.S. Geological Survey, scale 1:1,000,000.

Wilson, C.J.N., Houghton, B.F, Kamp, P.J.J., and McWilliams, M.O., 1995, An exceptionally widespread ignimbrite with implications for pyroclastic flow emplacement: Nature, v. 378, p. 605-607.

North-Central Oregon Cascades: Exploring Petrologic and Tectonic Intimacy in a Propagating Intra-Arc Rift

Richard M. Conrey, Department of Geology, Washington State University, Pullman, Washington 99164; conrey@mail.wsu.edu

Edward M. Taylor, Department of Geosciences, Oregon State University, Corvallis, Oregon 97331; taylore@geo.orst.edu

Julie M. Donnelly-Nolan, U.S. Geological Survey, Menlo Park, California 94025; jdnolan@usgs.gov

David R. Sherrod, U.S. Geological Survey, Hawaii National Park, Hawii 96718; dsherrod@usgs.gov

INTRODUCTION

The Cascade Range in northern Oregon is one of the world's most accessible magmatic arcs, near several major urban centers, and traversed by several highways and a vast network of logging roads. During the past 2 decades new geologic mapping has provided a much more detailed view of the history of the arc. Most of the regional mapping has been accomplished by David Sherrod and his collaborators (Sherrod and Smith, 2000; Sherrod, 1991; Sherrod and Scott, 1995; Sherrod and others, in press). Detailed new mapping of major stratocones has been done by several others (Conrey, 1991; Scott and others, 1997). Selected quadrangles have been mapped in detail by Sherrod and Conrey (unpub map of the Breitenbush Hot Springs 15-Minute Quadrangle), and Conrey (unpub maps of the Fort Butte and Whitewater River 15-Minute Quadrangles). In addition, geothermal exploration during the 1980s resulted in the drilling of several deep boreholes that help provide a three dimensional view of the arc (Conrey and Sherrod, 1988; Hill, 1992). These new map and drilling results have been accompanied by extensive geochemical analyses, such that a database of several thousand x-ray fluorescence (XRF) bulk-rock analyses (for both major and trace elements) has been created.

Allen (1966) proposed that the High Cascade Range in Oregon is confined to a continuous arc-parallel graben. Taylor (1981) and Smith and others (1987) documented the existence of a graben that developed starting about 5 Ma in north-central Oregon. The Hood River Valley in northern Oregon is also clearly produced by extensional faulting, but the structure is a half, not a full graben (Williams and others, 1982). A synthesis of new map, age, and geochemical data from northern Oregon demonstrates that the High Cascade Graben is discontinuous, structurally segmented, and time-transgressive, and thus resembles a propagating rift (Conrey and Sherrod, in preparation). Three structural segments are present, progressively younger northward. The segment boundaries coincide with major stratocones, which are long-lived (>5 m.y.) centers of intermediate and silicic volcanism. The southern segment, the object of this field trip, extends from Three Sisters to Mt Jefferson and exhibits a graben-within-graben structural style. The central segment, between Mt Jefferson and Mt Hood, is a full graben. The northern segment coincides with the Hood River Valley from Mt Hood to the Columbia River. Geothermal drill-core data suggest a total subsidence of 3 km in the southern segment and 1 km in the central segment. The northern half graben exhibits the least subsidence. Extension rates derived from subsidence-area balance range from 0.2 to 3.0 mm/yr, with the highest rates along the southern segment, early in its history.

This field trip provides a broad overview of the graben in north-central Oregon and is intended to illustrate some of the intimate connections between petrology and tectonism.

Field Guide to Geologic Processes in Cascadia: Oregon Department of Geology and Mineral Industries Special Paper 36, 2002.

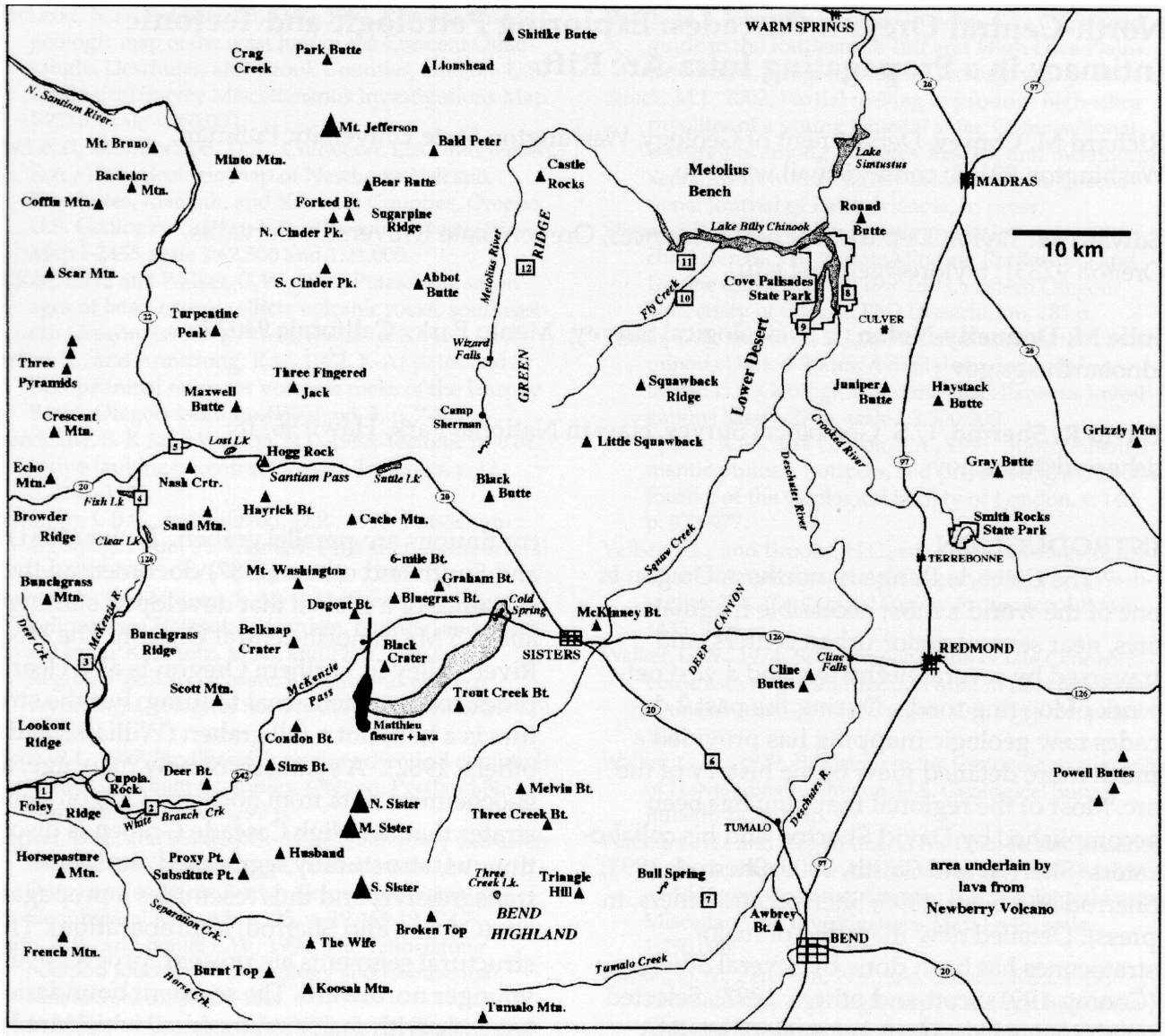

Figure 1. Geographic features of the central Oregon Cascade Range. Most field trip stops are located by numbered squares. See Figure 11 for the location of Stop 13.

The trip begins in Corvallis and returns there after traversing a loop utilizing Santiam Pass.

RELATION OF EXTENSION TO VOLCANISM

The formation of the High Cascade Graben postdates a long history of arc volcanism in northern Oregon. The most prevalent type of volcanic rock prior to the development of the rift was andesite of middle to late Miocene age (to early Pliocene in northern Oregon). These rocks accumulated at rather low rates from 15 to 8 or as young as 5 Ma all along the arc in northern Oregon. Basalt, basaltic andesite, and rhyolite were rarely erupted during this time; andesite, often amphibole-bearing, was by far the most common rock produced.

The initial indication of rifting in each segment of the arc was the eruption of voluminous lavas similar to midocean-ridge basalt (MORB) with a very low K content (Stops 1 and 9). Along with these low-K basalts, abundant basaltic andesite and large-volume pumiceous silicic ash-flow tuffs were erupted. Aphyric Fe-rich intermediate rocks are also common in these sequences, especially along the southern segment. Andesite is also common and often shows spectacular evidence of magma mixing. Amphibole is nearly absent. Eruption rates were dramatically higher during the accumulation of

these volcanic piles compared with the preceding Miocene rocks. Typically the high eruption rates lasted for some 2-3 million years, and as they declined, structural foundering of the axis of the arc commenced. So much volcanic material was erupted prior to the foundering that much of the older arc was buried. During or after the foundering, the rift-related rock package was uplifted along the rift flanks (especially the western side), and thus it now caps the ridges on both sides of the graben.

Profound geochemical differences distinguish volcanism related to rifting and that related to tectonic quiescence. Large ion lithophile (LIL) and high field strength (HFS) elements are invariably enriched in silicic Cascade rift-related rocks. Rift-related sequences generally include rocks with high FeO*/MgO ratios and lower Sr concentrations, factors that suggest a lower average pressure during magmatic evolution. Modelling of these differences suggests that they may be due in part to an increase in crustal temperature during rifting. A rise in crustal temperature is to be expected, as heat flow commonly increases during extension (Lachenbruch and Sass, 1978). Models of silicic rocks generated during rift-related crustal partial melting require granulite residues, whereas "normal" crustal partial melting is consistent with an amphibolite residue. A change in the protolith between rifting and quiescent conditions is almost certainly involved as well, because the mafic amphibolite composition that partially melted to yield "normal" low-K silicic melts cannot produce the high-K rift-related melts with an increase in temperature and degree of partial melting. The lower Sr of rift-related magma, combined with its higher LIL content, suggests a more enriched (tonalitic?) midcrustal source, probably containing biotite in addition to amphibole prior to partial melting. In contrast, a deeper, less enriched amphibolite source, with an average composition similar to the average Cascade basalt, can be modelled as the protolith for "normal" silicic magmas. Rifting may therefore be responsible for a crustal temperature rise high enough to partially melt enriched midcrustal rocks. Such melting could be facilitated by a shallower average emplacement depth for intruded mafic magma during rifting compared with quiescent conditions, where mantle-derived magma is likely stalled at deep crustal levels. Another factor to consider is the likelihood that rift-related mafic magmas are dryer on average than "normal" arc magmas and thus would promote hotter dryer conditions in their surrounding zones of partial crustal melting, leading to increased crustal temperature and a higher degree of partial melting in wall rocks adjacent to intruded sills or dikes.

ROAD LOG AND FIELD GUIDE—DAY 1

Cumulative mileage is listed at left; boldface interval mileage is given at the end of each entry. For viewpoint stops, the azimuth of prominent volcanoes or other geographic features is given. Analyses (x-ray fluorescence) of samples for which the labels (in parentheses) are given in the text can be found in Tables 1–3 at the back of this paper. Field trip stop locations and geographic features of the central Cascades are shown in Figures 1 and 11.

Mileage

0.0 Begin mileage log at Oregon 126-105 junction east of Springfield. Reach this junction by driving east on Oregon 126 from I-5 (take exit 194A–Hwy 126 Springfield) and proceed to the second stoplight (the junction is signed McKenzie River , Bend), get in left lane and turn left to continue on Oregon 126. **5.0**

5.0 Cross McKenzie River. **1.3**

6.3 Walterville junction. Approximately 2.3 miles due west of this junction is a road cut in basalt (MR-19) dated (K-Ar) at 28.9 ± 0.3 Ma (Emily Verplanck in Walker and Duncan, 1989). **4.8**

Western Cascade Arc Basalt

The Western Cascades in northern Oregon remain largely unmapped and unsampled in detail. In southern Oregon, older Cascade rocks form a conformable, gently east-dipping, homoclinal sequence broken only by minor faulting (Sherrod, 1991). By contrast, in northern Oregon, Western Cascade rocks are locally strongly folded (limbs dip up to 50°), and include both large-offset normal and lateral faults (Priest and others, 1987; Beeson and others, 1989). In addition, a major angular unconformity may be widespread in the north-

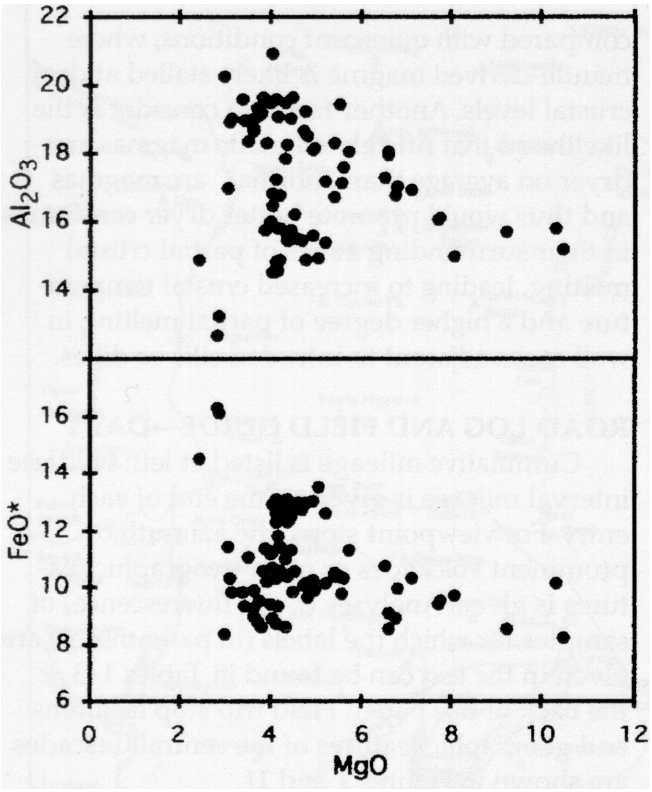

Figure 2. Al_2O_3 and FeO* versus MgO for Western Cascade basalt samples (SiO_2 < 52.5) from northern Oregon (data from Lux, 1981; Ritchie, 1987; R.M. Conrey, unpub. data). Augite-olivine fractionation will buffer FeO* and increase Al_2O_3, whereas plagioclase-dominated fractionation will result in Fe-enrichment and decreasing Al_2O_3. Magnetite phenocrysts are not present in these basalts.

ern Oregon Cascades, separating west-dipping rocks of 20-25 Ma from east-dipping older rocks (Priest, 1990).

Basalt in the Western Cascades is typically arc-like, with abundant phenocrysts of highly calcic plagioclase (including anorthite; Ritchie, 1987), augite (in places cm size), and olivine. At present it is not possible to subdivide the older rocks reliably other than in local areas, but compilation of reconnaissance chemical data for basalt from a broad region reveals a consistent pattern of Al_2O_3 vs MgO (Fig. 2). The most primitive basalts (for example, NSR-1) are consistently Al-poor, regardless of the fact that they are plagioclase phenocryst-rich. Petrologic arguments have been used to infer that substantial (approx 2%) H_2O is present in such magma, which is phenocryst-rich due to volatile saturation induced crystallization at shallow pressure as the magma rises to the surface (Conrey and others, 1997). A high H_2O content is consistent with the presence of anorthite and abundant augite. Water-rich basalt crystallizes augite and olivine before plagioclase, consistent with the rise of Al_2O_3 with declining MgO (Fig. 2), followed by its fall as plagioclase begins to dominate. Nearly all arcs have a similar pattern (unpub. compilation of R.M. Conrey).

11.1 Road cut on left in basalt (MR-20) is dated (K-Ar) at 26.8 ±0.3 Ma (E.P Verplanck, in Walker and Duncan, 1989). **8.1**

19.2 Goodpasture Covered Bridge. Road cut on left is in a small body of propylitically altered diorite or gabbro (Walker and Duncan, 1989). Across river to south (not visible) is a large, thick terrace-gravel deposit, probably of considerable age as it forms a bench 60 meters or more above river level. **1.3**

20.5 Another relict river terrace of similar height on the left. **5.4**

25.9 Approximate contact with the Nimrod Granite, a 5 km diameter, fine- to medium-grained, shallow intrusive body (Peck and others, 1964; Walker and Duncan, 1989). The stock is a true granite, with 4.1% K_2O, and graphic groundmass intergrowths of K-spar and quartz (Buddington and Callahan, 1936). It has a K-Ar age of 15.9 ± 0.2 Ma (Sutter, 1978); this age should be viewed critically (it is likely too young) as low-grade propylitic alteration is pervasive. **3.9**

29.8 Another gravel terrace remnant on the left, and the approximate eastern contact of the Nimrod Granite. **4.4**

34.2 Cross Blue River. **2.9**

37.1 Junction with road to Saddle Dam on Blue River Reservoir. View ahead is of westernmost Lookout Ridge, capped by Matuyama age intracanyon basalt (K-Ar age 1.68 ± 0.16 Ma; Priest and others, 1988). **1.1**

38.2 View of Castle Rock to right. This prominent knob is capped by over 150 meters of sparsely phyric andesite with a K-Ar age of 9.3 ± 0.4 Ma (Priest and others, 1988). Two possible origins are suggested: a plug dome, or a thick valley fill. Similarity to clearly paleovalley-filling andesite on Lookout Ridge to the north suggests the latter origin is more likely. If so, the base of the andesite sequence marks the floor of an ancestral McKenzie River Valley, 600 meters

higher than the modern valley floor. **0.5**

38.7 Junction with Road 19 to Cougar Reservoir along the South Fork McKenzie River. **1.1**

An Older Graben Boundary in the Western Cascades?

Cougar Reservoir is coincident with a major north-trending down-east normal fault (Priest and others, 1988) and a prominent residual gravity low (Blakely, 1994). The gravity low extends northward nearly to the Columbia River, and coincides with most of the major tributary junctions in the Western Cascades, as well as with a change in topographic style visible in digital elevation model (DEM) images. Topography west of the gradient is highly dissected, with much less dissection to the east. Perhaps this largely unexplored boundary marks the western margin of an older Cascade graben, 20-25 million

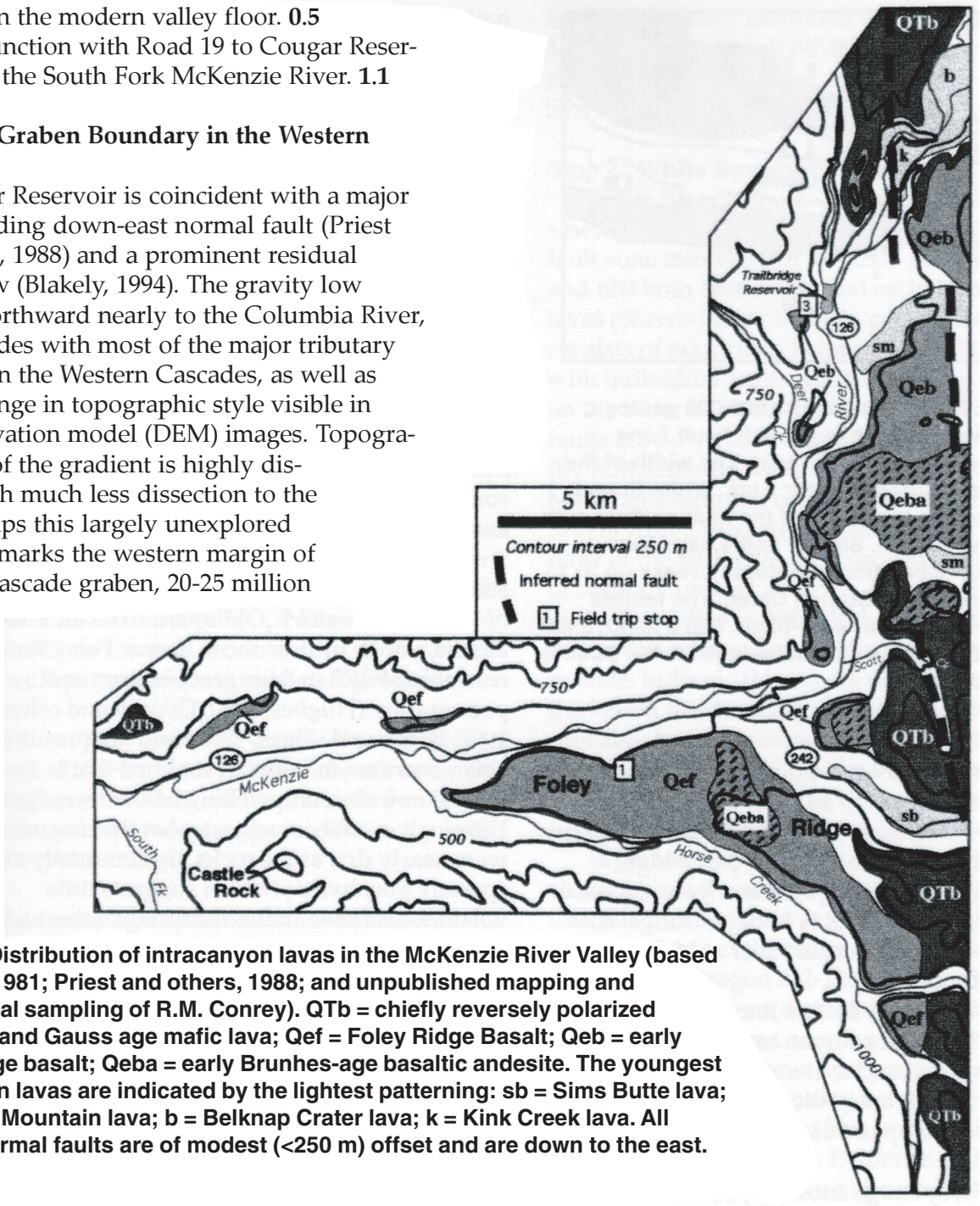

Figure. 3. Distribution of intracanyon lavas in the McKenzie River Valley (based on Taylor, 1981; Priest and others, 1988; and unpublished mapping and geochemical sampling of R.M. Conrey). QTb = chiefly reversely polarized Matuyama and Gauss age mafic lava; Qef = Foley Ridge Basalt; Qeb = early Brunhes age basalt; Qeba = early Brunhes-age basaltic andesite. The youngest intracanyon lavas are indicated by the lightest patterning: sb = Sims Butte lava; sm = Scott Mountain lava; b = Belknap Crater lava; k = Kink Creek lava. All inferred normal faults are of modest (<250 m) offset and are down to the east.

years old. Rocks of that age in the Western Cascades tend to be Fe-rich, similar to rocks associated with the present graben. The unconformity mapped by Priest (1990) noted above is evidence for an episode of pronounced uplift at about 20-25 Ma. As shown below, formation of the younger modern graben was linked to significant uplift.

39.8 Another view of Castle Rock. **2.0**

41.8 View left is of the main part of the east-trending elongate Lookout Ridge, capped by 6-8 Ma lavas that were derived chiefly from sources east of the ridge (now downfaulted and buried beneath younger cover) and that flowed westward down an ancestral McKenzie Valley (E.M. Taylor, in Priest and others, 1988). The topographic inversion represented by these paleovalley-filling lavas suggests not only extensive erosion but also profound uplift of the

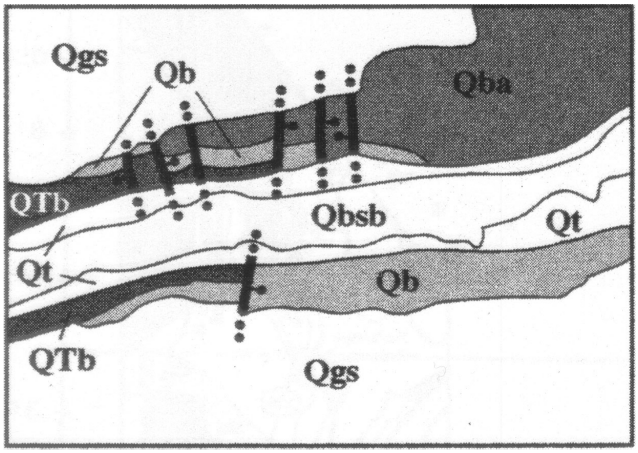

Figure. 4. Part of the Bend 1:100,000 geologic map showing the White Branch Fault Zone (Sherrod and others, in press). The width of the fault zone is approximately 2 km. White Branch Youth Camp is just north of the fault on the south side of the canyon. Similar faults have been mapped in Separation and Horse Creeks up to 15 km south of White Branch Creek. The faulted blocks are invariably east-tilted. Qtb = Matuyama-age rocks; Qb, Qba = Brunhes-age rocks; Qbsb = Sims Butte lava.

Western Cascades during intra-arc rifting (Priest, 1990; see Stop 13). **1.1**

42.9 Foreground ridge on left is underlain by basalt identical to that on Foley Ridge, a likely early Brunhes-age intracanyon sequence. Still in the background is Lookout Ridge. **0.9**

43.8 Cross McKenzie River at McKenzie Bridge. **2.3**

46.1 McKenzie Bridge Ranger Station. Foley Ridge, a large intracanyon tongue of mafic lava, is visible ahead and to the right. **0.5**

46.6 Turn R onto Foley Ridge Road. **0.5**

47.1 Outcrop of Foley Ridge basalt (FR-3).

Stop 1. Foley Ridge Intracanyon Basalt and View of Lookout Ridge.

Foley Ridge is a large tongue of intracanyon basalt and interbedded fluvial conglomerate that partially fills the McKenzie River Valley (Fig. 3). Its age is not directly known but is inferred from correlation among intracanyon benches along the McKenzie drainage. Older, dated intracanyon lavas occur at higher altitudes (Fig. 3) around the McKenzie River Valley (for example, the Lookout Ridges, the oldest of which is visible to the north across the valley), and all lavas in Foley Ridge have normal magnetic polarity (determined with a fluxgate magnetometer); thus Foley Ridge is likely of early Brunhes age (0.6-0.8 Ma). Priest and others (1988) and Flaherty (1981) both correctly traced a large tongue of Foley Ridge lava to the southeast up Horse Creek. However, they mapped prior to the advent of automated x-ray fluorescence equipment, and they did not recognize that Foley Ridge lava also extends northeast for some distance up the McKenzie drainage above Scott Creek (Fig. 3). Intracanyon benches of equivalent height above the modern McKenzie River, presumably of similar age, and underlain by geochemically diverse basalt, can be traced north to the vicinity of Trailbridge Reservoir. There the lavas seem to have flowed from sources to the east and to have been faulted down to the east.

Among the most certain indications of rifting in the Oregon Cascades was the eruption of low-K (<0.5 wt% K_2O) tholeiitic basalt. These basalts, which include those here at Foley Ridge, resemble MORB in their geochemistry and petrography (Hughes, 1990; Conrey and others, 1997; Bacon and others, 1997) and are presumably generated in a similar manner, that is, by extension-induced upwelling of shallow mantle. Petrologic evidence suggests that the magmas were nearly dry, as the rocks are commonly very sparsely porphyritic (which suggests little volatile-saturation induced crystallization) and contain plagioclase phenocrysts whose composition is consistent with crystallization under dry conditions (Conrey and others, 1997). The Foley Ridge lava is of interest because it represents the final pulse of such basalt from the southern rift segment in central Oregon; younger basalt there is not of the low-K variety.

Return to Oregon 126. **0.4**

47.5 Turn R (east). **1.1**

48.6 Junction with road to airfield on right. Now crossing the buried trace of the first major down-east normal fault that defines the western boundary of the graben. This fault seems to curl to the SW and intersect a WNW-trending normal fault at a right angle south of here. NW- and WNW-trending faults are abundant only along this part of the graben, are on strike with the Brothers Fault Zone, and thus may be an extension of that broad right-lateral fault system. **0.5**

49.1 Turn R onto McKenzie Pass Hwy 242.

Road cuts in till around this junction mark the westward limit of late Wisconsin glacial ice flowing down White Branch Canyon from the Three Sisters. **0.4**

49.5 View of Foley Ridge to the right (south) and similar intracanyon lavas ahead (east) forming a bench north of the McKenzie River. **1.9**

51.4 On the left young lavas from Sims Butte (unit **sb** in Fig. 3) are buried beneath forest and moss. **1.3**

Latest Pleistocene Sims Butte Lava on Valley Floor

The highway traverses young (approx 15 ka; W.E. Scott, unpub data, in Sherrod and others, in press) lava from Sims Butte, a cinder cone on top of the White Branch Creek headwall, for the next 12 miles. Sims Butte Lava is nearly aphyric basaltic andesite (97-104U), ranging in composition from 52 to 54.5% SiO_2. Nine analyses of Sims Butte Lava so far do not reveal any simple spatial pattern of chemical heterogeneity.

52.7 View ahead of Cupola Rock, a thick stack of chiefly Matuyama-age basalt and minor conglomerate. Back and to the right you can make out equivalent rocks in cliffs on the south side of the valley. **1.3**

Matuyama-age Basalt Benches Inboard of the Western Graben Margin

Cupola Rock and its equivalents south of the highway here comprise a thick stack of reversely polarized basalt lavas. Single flows are typically only a few meters thick but some are 10 m or more, and generally they are resistant to erosion and form steep cliffs. Priest and others (1988) mapped these lavas as the "basalt of Roney Creek" (a drainage south of the White Branch) and the "basalt of Cupola Rock". More recent work (R.M. Conrey, reported in Sherrod and others, in press) has not found division of the rocks into two sequences possible. Benches of similar rocks extend along the base of the Western Cascade scarp for some 12 km south of here and nearly 7 km north. The base of the sequence is dated at 2.4 ± 0.3 Ma (Priest and others, 1988) in Scott Creek (see mileage 64.4) and has normal polarity, presumably Gauss-age rocks. The top is poorly dated at 0.88 ± 0.33 Ma (Priest and others, 1988).

54.0 A gently east-tilted (5-7°) section of Matuyama-age basalt (97-89, 97-93) is visible on the left through the trees. **1.5**

55.5 Entrance to White Branch Youth Camp.

Stop 2. White Branch Fault Zone

White Branch Youth Camp marks the axis of a newly discovered Quaternary fault zone. This fault zone trends north for 12-16 km and cuts and tilts both Matuyama and early Brunhes-age lavas (Sherrod and others, in press). The zone consists of many en echelon strands (Fig. 4), with individual faults typically having offsets on the order of 50-100 m. Most but not all of the faults are down-east. These faults were found (by R.M. Conrey) while mapping out the Matuyama-Brunhes contact west of the Three Sisters with a fluxgate magnetometer. Offset on most of the faults has been proved with the aid of several hundred analyses. Proving the offset in the field often is difficult due to a lack of distinctive marker lavas. One characteristic is notable: individual lavas are usually much thicker on the downthrown side of a fault, probably because scarps were present during emplacement. Poorly exposed conglomerate lies throughout the faulted section, presumably due to banking up of debris flows against scarps.

A graben-within-graben structural style characterizes the southernmost part of the Cascade Intra-arc Rift, as suggested by this fault zone. We crossed the outer, older graben boundary near the Oregon 242-126 junction. That boundary fault zone drops 5-6 Ma rocks at the crest of the Western Cascades more than 1 km. Here we are at the inner and younger graben boundary, which downdrops stacks of Gauss and Matuyama lava that had ponded up against the outer graben margin. Evidence will be presented at Stop 12 for a mirror relationship on the eastern graben boundary, and at Stop 4 for the significant northward continuation of faults similar to those of the White Branch Fault Zone along the western graben boundary.

Return to Oregon 242-126 junction. **6.4**

61.9 Turn R (north) on Oregon 126. **1.0**

62.9 Road on left leading to Belknap Hotsprings (recommended!). The junction marks the trace of the major down-east fault (offset about 600 m) that downdrops the fault block noted below at mileage 66.0. It is no

accident that Belknap and Foley Hotsprings lie on the traces of two of the largest graben-bounding faults. Hillside to right is underlain by basalt of Foley Ridge, overlain by basaltic andesite that vented nearby. **1.5**

64.4 Scott Creek Road to the right (**recommended side trip**). **0.2**

Scott Creek Road Gauss-Normal Basalt Section

Up this road a short distance is downfaulted lava dated at 6.4 ± 0.2 Ma (Armstrong and others, 1975). Rocks with similar ages cap the ridges of the Western Cascades (see Priest and others, 1988). Approximately 0.7 mi up the road, begin about 1 mile of exposures of coarse conglomerate, pillow basalt, and some bedded palagonite (Taylor, 1981). These rocks are overlain by basaltic lava of more subaerial aspect dated variously at 2.35 ± 0.14, 2.2 ± 0.1, and 2.6 ± 0.1 Ma (Armstrong and others, 1975; Priest and others, 1988). The section is chiefly normally polarized and can be mapped beneath the chiefly reversely polarized basalt of Cupola Rock (Priest and others, 1988). Thus the Scott Creek exposures are likely Gauss normal in age. There are two possible explanations for the lava-water interactions: they may mark the trace of an ancestral Scott Creek or McKenzie River during Gauss time, or they may be due to ponding of drainage and creation of lakes by normal faulting here at the graben margin (Taylor, 1981).

64.6 Road 2650 to left (**recommended side trip**). **0.4**

Side Trip Up Frissell Point Road

Road 2650 leads over the McKenzie River and up a downfaulted block west of the river that is capped by Foley Ridge lava on its SE end. The lowermost road cut on this road exposes distinctive plagioclase-rich basalt that was mapped by E.M. Taylor (in Priest and others, 1988) in an east-west paleovalley at the crest of Lookout Ridge (and thus 5-6 Ma). The basalt is downfaulted to river level here. The bench is capped by the Trailbridge Ignimbrite and aphyric Fe-rich basalt identical to that at Stop 3. A powerline crosses the road on the bench providing a good view of Foley Ridge and the surrounding area. The road (which continues up to Frissell Point) is usually blocked past the ignimbrite; if this road is ever opened again, it would provide easy access to good exposures of the Lookout Ridge section.

65.0 The bench visible ahead is capped by Foley Ridge lava. **0.3**

65.3 Columnar jointed basal intracanyon basalt lava (97-51) underlain by fine grained sediment and cobble conglomerate, in turn underlain by older rocks equivalent to the Western Cascade ridge-capping sequence. This fresh, normally polarized lava represents the base of a likely early Brunhes-age intracanyon sequence equivalent to Foley Ridge. If Foley Ridge in part had a source northeast of here, then this would be the best candidate for the paleodrainage along which the lavas flowed into the McKenzie Valley. **0.7**

66.0 Road cuts on right for approx the next 0.4 mi are in a downdropped block of lava that almost certainly matches the Western Cascade ridge-capping section at the crest of Lookout Ridge west of the highway. These lavas are capped by a bench (noted at mileage 65.0) of normal-polarity basaltic lava that is identical in all respects to that on Foley Ridge. **1.2**

67.2 Turn L on (unsigned) Deer Creek Road. **0.2**

67.4 Cross McKenzie River. **0.8**

68.2 Bear R over bridge. Ridge ahead is a tilted (dips east 30°) fault block of lava that is likely downdropped from near the crest of the Western Cascade ridge line to the west, or is slightly younger than the crestal rocks and was confined inside the developing western graben boundary fault zone. The ridge is capped on its southern end by an intracanyon bench likely similar in age to Foley Ridge. **0.5**

68.7 Bear R at junction. Left fork is along Deer Creek, which coincides with a NW-trending, down-NE, normal fault. Initial chemical data on matching lava across the creek suggest that the offset across the fault is on the order of 150-200 m. **0.3**

69.0 Stay left. **0.8**

69.8 Stay on main road. **0.3**

70.1 A small north-trending normal fault is exposed in the road cut on the left in Fe-rich basalt. **0.4**

70.5 Switchback. Knob to right in trees is capped by tilted Trailbridge Ignimbrite, and the switchback marks the trace of a small-offset

north-trending down-west normal fault. **0.3** 70.8 Road cut in tilted Trailbridge Ignimbrite and roadside quarry in underlying Fe-rich basalt.

Stop 3. Tilted Rocks in the Western Boundary Fault Zone.

This stop illustrates some of the complexity of the western graben boundary fault zone, and also provides a view eastward into the graben. The view from here includes the following (labeled by azimuth):

34 **Three Fingered Jack**: A large, glacially dissected basaltic andesite shield volcano (Davie, 1980), believed, on the basis of lava-till field relations and lack of Three Fingered Jack clasts in circa 150 ka Jack Creek age moraines, to be younger than that glaciation, and clearly older than the Wisconsin glaciations (Scott and others, 1996). An age of 100-150 ka is therefore indicated.

35-41 **Sand Mountain chain of cones**: Source of much of the Holocene lava in the Clear Lake area—see Stop 4.

68 **Mt Washington**: Glaciated remnant of a large basaltic andesite shield volcano with a well exposed, resistant central plug (analysis number 95-185; see the tables for the parenthetical analyses). The progressive glacial erosion and increase in dissection with age of High Cascade shield volcanoes is well documented (Sherrod, 1986; Scott and others, 1996). Mt Washington once looked like Belknap Crater or Scott Mountain.

68 **Bunchgrass Ridge**: Broad forested ridge of normally polarized basaltic andesite, with a steep glacially eroded southern flank in front of Mt Washington.

105 **Scott Mountain**: Relatively young basaltic shield volcano (99-37). Has been glaciated but not heavily eroded.

100 and 120: **Unnamed, N-trending forested ridges** of likely Brunhes age basalt (mapped as unit **Qeb** in Fig. 3). A Brunhes age is indicated by the normal polarity of all exposed lava, which seems to be derived from diverse source vents; correlation with the Brunhes portion of the Robinson Lake Road section at the west end of Bunchgrass Ridge; and position above the modern valley floor similar to that of Foley Ridge The north trend of the ridges is likely due to down-east normal faults on their eastern side. If this interpretation is correct, it further illustrates the graben-within-graben style of this part of the intra-arc rift, similar to that noted at the White Branch Fault Zone.

135 **The Husband**: The dark, cliffy peak is a large plug in the core of the deeply eroded remains of a large Brunhes age basalt to basaltic andesite shield volcano.

145 **Proxy and Substitute Points**: The two summits are the NNW-elongate eroded core of yet another large basaltic andesite shield of Brunhes age. Lava erupted from these vents covers a broad area north of Separation Creek (Sherrod and others, in press).

175 East tilted fault block mentioned when crossing Deer Creek at mileage 68.2.

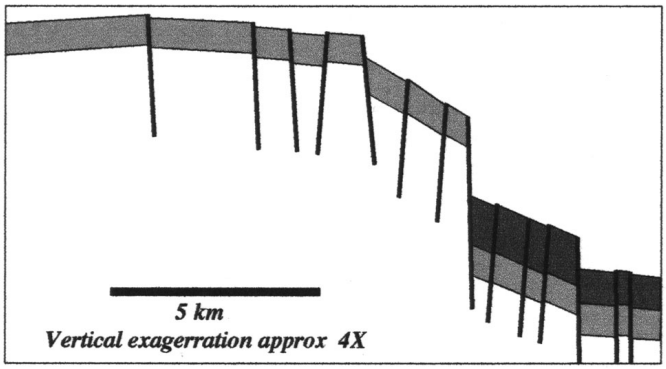

Figure. 5. Schematic east-trending cross section of the western graben boundary fault zone. West of the fault zone 5-8 Ma ridge-capping lava and sediment (light pattern) in west-draining paleochannels has been uplifted. A broad zone of modestly eastward tilted blocks cut by small offset faults lies between the unfaulted ridge caps and the major faults that define the graben boundary. Significant eastward tilting accompanied the development of the large offset faults. Younger rocks (dark pattern) banked against the fault scarp are also tilted and faulted. Individual blocks within the zone of major offset are riven by many small faults.

180 Distant skyline is of 5-8 Ma Western Cascade ridge-capping rocks, including Horsepasture Mountain, west of the Horse Creek Fault Zone (western boundary of the graben) and south of the McKenzie River Valley.

Tilted Fault Blocks and Graben Asymmetry

The tilted exposures here are part of a 10 km broad zone of invariably east-tilted fault blocks that collectively define the western graben boundary (Fig. 5). Numerous faults compose this complex zone, and the stratigraphy is still poorly known, so as yet little is known structurally other than the location of the larger faults. Some fault blocks seem to be riven by dozens of small faults between those with larger offsets that define the blocks. The consistent east tilting reflects a fundamental structural asymmetry in the graben, as tilted blocks in the center of the graben (tilted Matuyama- and Brunhes-age sections along White Branch Creek), and at the east graben margin also dip eastward (sediment on the flank of Green Ridge at mileage 56.4, Day 2). Another fundamental asymmetry is that significant uplift can be demonstrated on the west side of the graben, but not on the east (see Stop 13). The western graben-bounding escarp-

ments are over 300 meters higher than the crest of Green Ridge. The structural and topographic asymmetry, and evidence for broad uplift of the Western Cascades (Fig. 12), suggests that a broad updoming west of here occurred during rifting, perhaps in response to the rise of heated lower and middle crustal rocks in the manner of a metamorphic dome.

Trailbridge Ignimbrite

The tilted (21° E) basaltic andesite (97-114) Trailbridge Ignimbrite (Taylor, 1981; Priest and others, 1988) is exposed here with a densely welded, glassy, inclusion-poor base and an overlying less densely welded and inclusion-rich top. Taylor (1981) includes a fuller description and interpretation of this interesting deposit, which has a K-Ar age of 5.5 ± 0.2 Ma (Armstrong and others, 1975). The ignimbrite contains abundant phenocrysts of plagioclase, with lesser olivine and pyroxene, and is similar (but not identical) in bulk composition to overlying plagioclase-rich and olivine-bearing basaltic andesite lavas. The evidence that this deposit is a mafic ash-flow tuff includes the following: variation in degree of welding in the deposit, inclusion of abundant unsorted lithic fragments, and in some outcrops porous basal and top exposures and apparent layering. The ignimbrite can be traced for at least 10 km (as can the underlying Fe-rich basaltic lava), but it has not been found outside the margin-boundary fault zone. This suggests it was erupted during the development of the zone, when earlier west-flowing drainages were truncated in favor of south-flowing ones. The K-Ar age thus likely dates the inception of structural disruption along this part of the graben boundary. The unusual nature of the deposit could be due to eruption along a steep fault scarp, which would have favored catastrophic failure of vent and flow material perhaps leading to a pyroclastic flow. In addition, structural foundering could have led to rapid disruption (and thus rapid eruption) of a shallow magma body. Pyroclastic flow may have been induced by very rapid effusion.

Distribution of Fe-rich Basalt in Space and Time in the Cascades

An aphyric Fe-rich basalt (97-60) is exposed in a roadside quarry here, beneath the Trailbridge Ignimbrite. Fe-rich rocks commonly are nearly devoid of phenocrysts, but rarely they are also phenocryst-rich. This rock has high total Fe, Ti, P, and V, and low Al and Mg, with a high FeO*/MgO ratio of 2.8 that would result in its classification as tholeiitic. Such Fe- and V-rich basalts are common in the Deschutes Formation and are also found in age-equivalent or slightly younger ridge-capping rocks in the Western Cascades. Similar Fe- and V-rich basalt is common in Gauss- and Matuyama-age basalt in central Oregon, but is lacking in basalt of Brunhes age. Elsewhere along the rift to the north, such basalt is exceedingly rare, even in thick stacks of lava erupted during peak times of volcanic production.

The Fe- and V-enrichment likely has a simple genesis: crystal fractionation dominated by plagioclase, similar to that in midocean-ridge basalt where V is also incompatible during fractionation. The necessary conditions for such fractionation are low pressure (< 8 kb) and dry magma. Many of the low-K tholeiitic basalts could have been quite dry as magmas and thus have undergone such fractionation. The confinement of Fe- and V-rich basalt to the southern part of the rift, and the loss of such basalt there during the Brunhes as extension rates seem to have waned, suggests that conditions appropriate for its genesis are only reached at rates of extension on the order of 1-3 mm/yr. At lower extension rates, little basaltic magma seems to stagnate in isolated, middle to upper crustal chambers.

V- and Fe-enrichment is not the norm, even at the southern end of the rift where rates of extension are highest. Rather, the predominant pattern there, as elsewhere, is approximately constant V with declining MgO. This pattern is easy to generate with high-pressure (> 8 kb) crystal fractionation of clinopyroxene and olivine, due to the high distribution coefficient of V in clinopyroxene. Wet magmas also crystallize this assemblage even at modest pressure. Because at least the low-K tholeiites, which lie all along the rift, were likely fairly dry, the buffered V pattern suggests that much of the basalt intruded into the crust during rifting ponds in the lower crust or at the Moho. Basalt that reaches the surface there evidently undergoes some crystallization (and contamination?), increasing its volatile content to the point where

it is eruptable. At rates of extension of less than 1 mm/yr, virtually all of the basaltic magma is initially trapped at deep levels.

Turn around and return to Oregon 126. **3.5**

74.3 Turn L on Oregon 126. **1.7**

76.0 Olallie Campground entrance. The hillside visible to the right through trees is underlain by a stack of normally polarized lavas, chiefly basaltic, that is likely age-correlative with Foley Ridge, as it forms a bench at a similar height above the river (unit **Qeb** in Fig. 3). The lavas do not match those in Foley Ridge, but one of them does match with a lava in the Robinson Lake Road section (see below), which is above the apparent Matuyama–Brunhes boundary, further support for the interpretation that the lavas are early Brunhes in age. **0.3**

76.3 Olallie Creek Road on right. The toe of a basaltic lava from Scott Mtn (unit **sm** in Fig. 3) is exposed a short distance up this road. **1.3**

77.6 Trailbridge Ignimbrite exposed to right of highway opposite Trailbridge Reservoir. Ridge west of the reservoir is capped in part by this unit. **0.5**

78.1 Road to Trailbridge Campground on left. Road continues on to Smith Reservoir on the west side of a prominent, fault-controlled, north-trending ridge visible from Stop 5. **0.2**

78.3 Springs on right emerge from a flow unit or flow contact in young basalt of uncertain derivation (either equivalent to intracanyon lavas discussed in following description, or from the vicinity of Scott Mtn). The lower flow seems to overlie a (reworked?) till that contains both highly angular and highly rounded cobbles. **0.6**

78.9 Basaltic intracanyon lava (normally polarized) overlain by well-bedded lacustrine sediment and coarse cobble conglomerate, in turn overlain by till (see next description) The basalt is probably equivalent to the intracanyon lava package seen at mileage 79.5 (unit **k** in Fig. 3). **0.2**

79.1 Till, likely part of a lateral moraine extending from the southern glacially eroded flank of Bunchgrass Ridge east of the highway. Ice and lava from Scott Mtn leaked through a gap between Bunchgrass Ridge and the unnamed north-trending ridges of normally polarized lava south of Olallie Creek visible from Stop 3. **0.4**

79.5 Road cuts for about the next mile are in a tongue of late Brunhes-age intracanyon basalt (unit **k** in Fig. 3; KC-1). **1.3**

80.8 Robinson Lake Road to right. The Brunhes–Matuyama boundary occurs approx 0.4 mi up this road. A section of lavas 0.5 mi SW of this junction also includes the boundary. Matching of lava in that section with exposures west of the McKenzie River demonstrates significant down-east faulting of Matuyama- and early Brunhes-age lava (in this case on the order of 100-125 m). **1.3**

82.1 Highway crosses distal basaltic lava erupted from Belknap Crater (unit **b** in Fig. 3). Some Sand Mtn lava also leaked through this gap but is almost totally buried by younger Belknap lava. Forested knob uplava is likely an erosional remnant of early Brunhes-age basalt, probably similar in age to Foley Ridge. **0.1**

82.2 Exposures of reversely polarized basaltic andesite lava. At this location the lava has been dated by K-Ar at 1.1 ± 0.2 Ma (Armstrong and others, 1975). **0.3**

82.5 Road cut on right is in reversely polarized basaltic andesite. These lavas are identical in composition and appearance to lava that caps the ridge west across the McKenzie River. The implied offset is approx 250 m, evidence for significant down-east faulting coincident with the river, first suggested by Walter Avramenko (1981). The bench west of the river is broken by many north-trending, small-offset normal faults. The downdropped block on this side of the river is also north-trending and likely faulted off on its eastern side. **0.8**

83.3 Road to left to Koosah Falls and Icecap Campground just north of Carmen Reservoir. Koosah Falls formed at the terminus of lava erupted from the Sand Mtn chain. **0.2**

83.5 Ridge visible to west is capped with Matuyama-age lava. **0.1**

83.6 Sahalie Falls. Falls are due to a steep flow front in basaltic lava from the southernmost Sand Mtn cone. The lava is well exposed north of the falls along the highway. **0.6**

84.2 Cross McKenzie River just before road to Coldwater Cove Campground. Basaltic lava from the southernmost cone in the Sand Mtn chain is exposed around the road junction (95-20). **0.4**

84.6 Road cut in reversely polarized lava

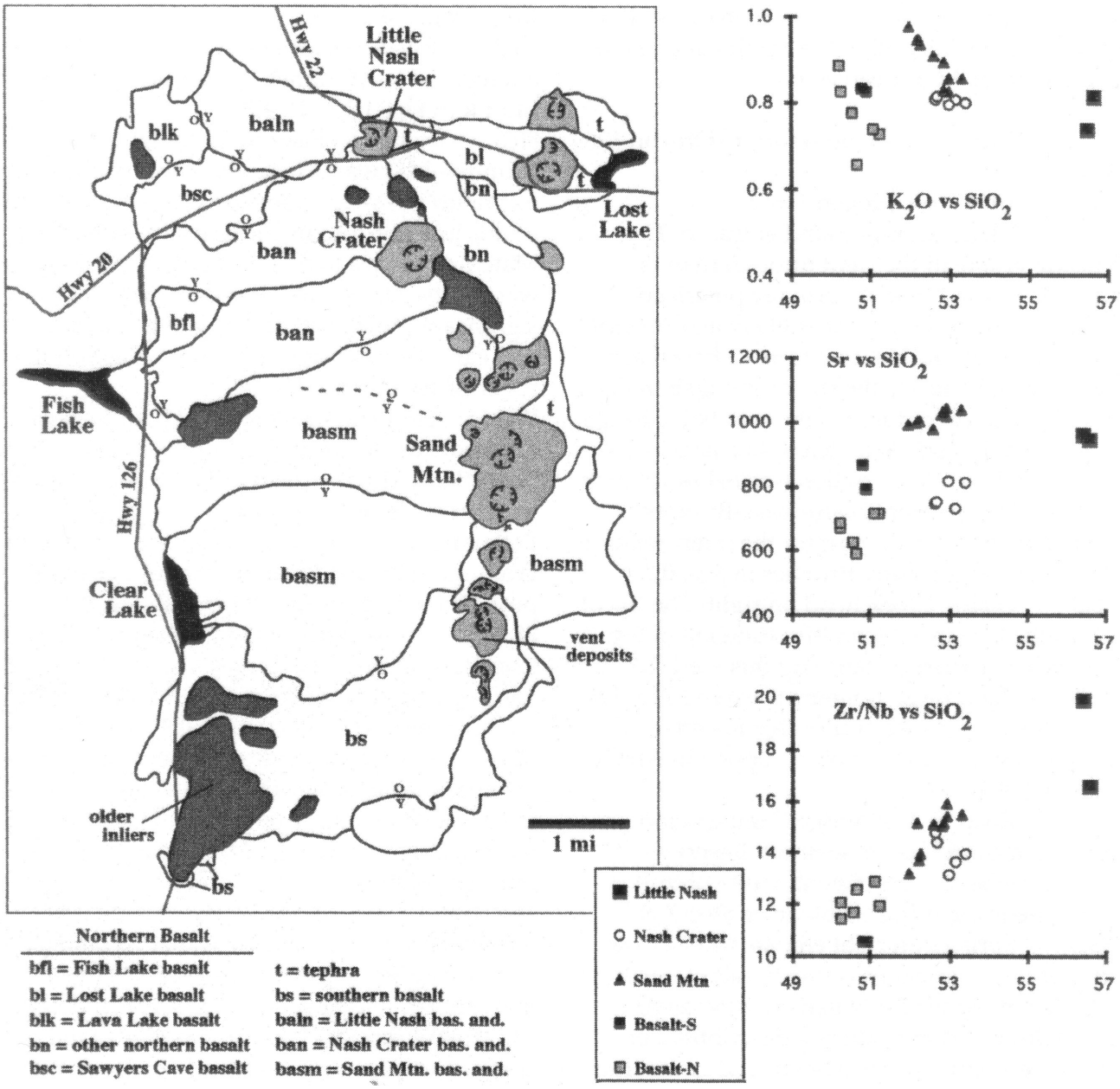

Figure. 6. Left panel is a geologic map of the Sand Mountain–Nash Crater lava field (E.M. Taylor, in Sherrod and others, in press). Relative age relations between adjacent lavas are indicated. Right panel shows selected geochemical variations, all plotted versus SiO_2.

opposite Clear Lake. **0.5**

85.1 Clear Lake Road on the right. Clear Lake was dammed by lava from Sand Mtn. A drowned forest in the lake has yielded ^{14}C ages of 2705 ± 200 yr (Benson, 1965) and 2750 ± 45 yr (a new accelerator mass spectrometer (AMS) age; Licciardi and others, 1999). **0.7**

85.8 Road cut on left is in very sparsely olivine-phyric alkaline basaltic andesite (97-113), likely of early Brunhes age. This lava is faulted and equivalent to that at mileage 86.7 on the east side of the Fish Lake Fault (see Stop 4 for discussion). Polarity here seems to be normal. The offset of this lava across the fault is small, on the order of 30-50 m. **0.4**

86.2 Cross trace of the Fish Lake Fault on the low ground. **0.5**

86.7 Road cut on right is in alkaline basaltic andesite, equivalent to that at mileage 85.8. The outcrop caps a small fault block east of the Fish Lake Fault. **0.2**

86.9 Road to right leads to margin of Sr-rich

basaltic andesite lava (95-18) from Sand Mtn in approx 0.4 mi. A further 0.4 mi along the road takes you close to the Eugene Water & Electric Board (EWEB) 1 drill site. **0.4**

87.3 Turn L into Fish Lake Campground.

Stop 4. Holocene Lavas of the Sand Mountain–Nash Crater Chain

The first subject of this stop is the geochemical heterogeneity in the Holocene Sand Mountain–Nash Crater chain, whose vent system is about 10 km long. The vent alignment chiefly trends N5E, but the latest eruptions at Nash and Little Nash Craters are on a N25W trend from Sand Mtn. The lava field erupted basalt and basaltic andesite (Fig. 6) for perhaps as long as 2000 years. The earliest lavas were basaltic, erupted from both the northern (95-1) and southern ends of the chain. A ^{14}C age of 3850 ±215 yr (Taylor, 1968) is believed to date the earliest northern basaltic lava near Lava Lake. A ^{14}C age of 1950 ± 150 yr of the cinder cone SW of Lost Lake also dates basalt from the northern end of the chain. The younger age does not seem to be consistent with the stratigraphy, however, if the older age is correct. Basalt at the southern end of the chain seems to have dammed the McKenzie River drainage, and thus to be dated by ^{14}C ages of 2705 ± 200 (Benson, 1965) and 2750 ± 45 yr (accelerator mass spectrometer age; Licciardi, 1999) of trees in a drowned forest in Clear Lake, 3 km south of here (see mileage 85.1). Following the basaltic eruptions, the central part of the chain, including Sand Mtn, erupted Sr-rich basaltic andesite (Fig. 6). These lavas are dated by a ^{14}C age of 2990 ± 300 yr (Taylor, 1968) near the east shore of Clear Lake. The next to last activity occurred at Nash Crater, which erupted basaltic andesite (95-2; Fig. 6) with a maximum age of 2590 ± 150 ^{14}C yr (W.E. Scott, in Sherrod and others, in press). Eruption of Little Nash Crater, which produced the most evolved rock in the chain (Fig. 6), postdates Nash Crater. Better age control is desirable.

Several puzzling features of the geochemical variations among the lavas are illustrated in Fig. 6. It seems difficult to interrelate any of the eruptive sequences. For example, northern basalt is commonly less evolved than southern basalt, but any potential fractionation relationship would have difficulty accounting for the lower Zr/Nb of southern basalt (Fig. 6). Possibly some fractionation relation exists between some northern basalt and Nash Crater basaltic andesite, but why does the K_2O content of the two overlap? Little Nash lava is even more problematic; it has the highest SiO_2, but the K_2O content is similar to that of Nash Crater. Finally, the Sr-rich basaltic andesite of Sand Mtn shows some interesting variations, but what does it mean when K_2O falls as SiO_2 rises, whilst Zr/Nb increases? If these relations suggest a mixing process, rather than fractionation, what are the end members and how were they created? Answers to these puzzles should help to address questions about basaltic andesite genesis in the Cascades, especially the generation of Sr-rich basaltic andesite.

Evidence for Post-1.9 Ma Faulting Along the Western Graben Boundary

The geology of the Bunchgrass Mtn–Browder Ridge–Echo Mtn–Smith River area was first examined in detail by Avramenko (1981). He recognized the pronounced tilting associated with faulting along the western graben boundary, and also the evidence for young offset on faults coincident with the upper McKenzie River. We have found more evidence for young faulting, especially in the EWEB 1 drill core.

Much of Fish Lake, and the area west of the lake along Hackleman Creek (see mileage 88.3 on Day 2), is underlain by a distinctive fingernail-sized plagioclase and (smaller) olivine-bearing basalt (97-112 in Table 3) and some east-tilted (5-8°) fine and coarse grained sediment. It is likely that minor faults cut the lava and sediment package. The lava is normally polarized with a K-Ar age of 1.89 ± 0.10 Ma (Black and others, 1987), which suggests it may be of Olduvai age. One of the first geothermal exploration wells drilled in the Cascades, EWEB1, was spudded in approximately 1.2 km SE of Fish Lake Campground in Holocene lava from Sand Mtn. The well was drilled with a rotary cone, not a diamond core, and the cuttings therefore consist of sand-sized grains mixed with grains derived from all higher levels in the hole. Only a very few cuttings were preserved for alteration studies by Terry Keith of the U.S. Geological Survey. She graciously provided the remains of her samples, and several were hand picked and analyzed by XRF. A sample from the 440 foot level of the core (which attracted atten-

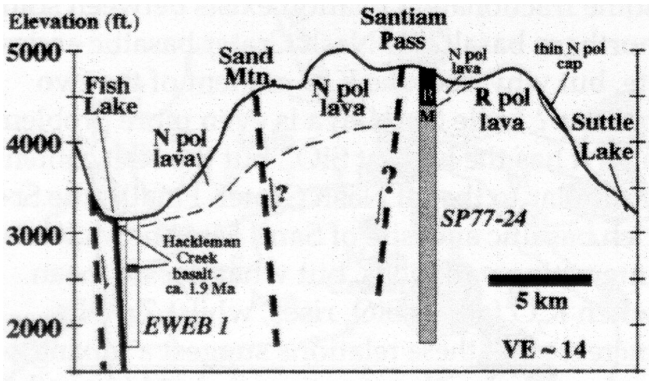

Figure. 7. Cross section from Fish Lake over Santiam Pass to Suttle Lake. Two geothermal boreholes help constrain the geometry. The Fish Lake Fault is the solid black line. Inferred faults are dashed. Note the asymmetry in surface geology across Santiam Pass, suggestive of a fault coincident with the pass (and see mileage 99.5 below). Hill (1992) proposed the fault beneath the Sand Mtn vent alignment.

tion from its log description and was fortunately saved by Terry) was rich in large plagioclase and olivine phenocrysts, and proved to be compositionally identical to the dated basalt from Fish Lake. A mass balance was required to demonstrate the correlation, as it was impossible to select the correct proportion of plagioclase and olivine grains in the picked core sample, which is groundmass-rich. Subtraction of 15% calcic plagioclase and 5% olivine from the Fish Lake sample matches the core sample for all but the hydration-mobile alkali elements (Table 3). There is little doubt, therefore, that the lava exposed on the northern shore of Fish lake is downfaulted approx 150 m by a fault (the Fish Lake Fault in Fig. 7) that likely passes beneath the campground.

Return to Oregon 126. **0.1**

87.4 Turn L onto Oregon 126. **0.7**

88.1 View right of Nash Crater and Sand Mtn **0.8**

88.9 Stay right at junction of Oregon 126 and US 20 (head E on US 20). **0.4**

89.3 View ahead of Three Fingered Jack. **0.8**

90.1 Parking for a short trail to Sawyers Cave, a lava tube in early Nash Crater basalt. **0.5**

90.6 At right curve, the road is in lava from Little Nash Crater (95-7). **0.3**

90.9 Basaltic andesite lava from Nash Crater along road to the right. The road follows the contact between lava from Nash and Little Nash Crater here for a short distance. **0.5**

91.4 Turn L onto side road. Follow cinder road to top of Little Nash Crater to its southwesternmost point. **0.6**

92.0 Top of Little Nash Crater.

Stop 5. Overview of Western Graben Margin from Little Nash Crater

Several features of the western graben margin, and some geology within the graben, are visible from this stop. Note the highly dissected nature of the western graben escarpment due to glacial erosion. As will be seen from Stop 12, the eastern graben escarpment is considerably less eroded, as it was both lower (by approx 300 m) than the western scarp and protected by the rain shadow of the Cascades, so it was never glaciated. The high degree of glacial dissection (and greater vegetative cover) has made the geology of the western margin harder to decipher as much of the original geometry of the ridge-capping deposit has been destroyed. On the positive side, all parts of the west-side section are accessible; on the east side the deeper parts of the section generally are still buried.

Another feature evident from this vantage is the rather modest slope of the western scarp, which is much less steep than the eastern escarpment along Green Ridge (Stop 12). The slope is modest because it is essentially a dip slope, underlain by E-tilted fault blocks. The steepest parts of the scarp are just east of the higher summits and generally coincide with major faults. The modest slopes east of those steeper scarps are underlain by E-tilted fault blocks in a zone that is usually about 5 km wide (Fig. 5). Faulting affects even the sections exposed on the higher summits, as those are generally tilted a few degrees eastward, as seen from here in Scar and Bachelor Mtns.

Finally, a sense of the young N-trending faulting along the upper McKenzie River can be gained from the distant view of the N-trending ridge between Carmen and Smith Reservoirs (see below). The ridge is capped chiefly by reversely polarized, Matuyama-age lava that has down-faulted equivalents east of the McKenzie River (Avramenko, 1981; R.M. Conrey, unpub. mapping).

The thumbnail geologic descriptions of the western Cascade ridge-cap sections below (identified by azimuth) rely on published work by Avramenko (1981), Black and others (1987), Priest and others (1987), and unpublished mapping by R.M. Conrey.

343 **Bachelor Mtn**: Triangular-shaped peak with broad open southwest flank. Composed chiefly of a stack of diverse mafic lava with some clearly near-vent deposits cut by several dikes. The summit lava has a K-Ar age of 6.35 Ma (Priest and others, 1987). The section exposed on the southwest flank has been faulted and dips gently eastward, the sense of dip is visible from here.

337 **Coffin Mtn**: Mesa-like appearance and hence name is due to capping by a very thick (100 m) mildly alkaline basaltic andesite lava flow. The thickness of the capping lava is unusual and suggests either an intracanyon relationship or ponding of lava against a fault scarp. If the latter is true, the lava likely erupted during initial development of the western graben boundary.

322 **Scar Mtn**: Banded appearance is due to dark lava overlying pale sedimentary rocks. The latter include round and imbricated cobble conglomerate that indicates a westward flow direction. The sediments can be traced to the west for some distance along the axis of the ancestral Middle Santiam River, marked by (now topographically inverted) ridge-capping lava that can be followed all the way to the Willamette Valley along the high ridges just north of the modern drainage (see Stop 13). The section at Scar Mt has been faulted and tilted gently eastward; the tilt is evident from this vantage point.

302-338 **Three Pyramids**: Sharp peaks on a dissected north-trending ridge. The ridge-top section comprises approx 650 m of mafic lava. A mafic lava near the top of the South Pyramid has a K-Ar age of 6.27 Ma (Black and others, 1987).

271-283 **Crescent Mtn:** Well named for its shape due to glacial erosion; a large glacial cirque opens to the east. The ridge-top section is almost exclusively mafic lava with some rare dacite (Black and others, 1987). The section is apparently thinner (400 m) than that underlying Three Pyramids and Echo Mtn.

253 **Echo Mtn**: Underlain by nearly 650 m of diverse mafic lavas, including at least one interbedded vent deposit. Section is cut by numerous N- to NW-trending mafic dikes. K-Ar ages include one of 7.22 Ma near the base of the exposed mafic lavas, and another of 5.77 Ma near the top (Black and others, 1987). A further age of 6.28 Ma was obtained from a downfaulted block. US 20 passes between Echo Mtn and Browder Ridge.

236 **Browder Ridge**: An elongate east-trending ridge with a thick section of mafic lava similar to Echo Mtn Section includes several vent deposits and is cut by numerous dikes. The break in slope at the eastern foot of Browder Ridge coincides with a major fault, which separates gently E-tilted rocks from steeply E-tilted ones (Avramenko, 1981).

221 **Bunchgrass Mtn**: The second summit south of Browder Ridge, the first is Wildcat Mtn, underlain by at least 450 m of ridge-cap section, dominated by mafic lava but including some pumiceous ash-flow tuff, intermediate lava, and sediment. Round cobble conglomerate is locally present similar to that at Scar Mtn. The sediment seems to mark the channel of the ancestral South Santiam River, which can be traced westward from Bunchgrass Mtn through Squaw Mtn, Twin Buttes, and Soapgrass Mtn (the latter summits visible from Stop 13) for approx 20 km. The section exposed at Bunchgrass Mtn has been faulted and is tilted gently (5-10°) eastward.

200 **Ridge between Carmen and Smith Reservoirs** (middleground, not skyline): A 3 km long diversion tunnel between Carmen and Smith Reservoirs quarried beneath the ridge penetrated a steeply E-tilted (20-30°) lava-dominated section cut by numerous normal faults (Avramenko, 1981). The east end of the tunnel transects approx 400 m of E-dipping fine- and coarse-grained sediment similar to that mapped from Fish Lake north to Marion Forks (Black and others, 1987), seen on the side trip along Lava Lake Rd from mileage 86.3 —Day 2.

155 **Nash Crater**: Holocene cinder cone, source of much of the lava around Santiam Junction (see Stop 4).

147 **N end of Sand Mountain chain**: Holocene cinder cone, part of the linear chain of Sand Mtn cones (see Stop 4).

141 **Mount Washington.**

122 **Hoodoo Butte**: Late Pleistocene cinder cone that was preserved in the lee of Hayrick Butte from ice flowing westward off of Santiam Pass (E.M. Taylor, in Sherrod and others, in press).

118 **Hayrick Butte** (partially obscured by Hoodoo Butte): Tuya form suggests that this andesite (NSH-4) dome was erupted beneath an ice cap sometime during the (late) Brunhes. The composition is incompatible-element poor similar to that of North Sister-type basaltic andesite (Hughes and Taylor, 1986).

108 **Potato Hill**: Likely the highly eroded remnant of a basaltic andesite shield volcano of Brunhes age (normally polarized; K-Ar age 0.44 ± 0.12 Ma; Armstrong and others, 1975) centered on the plug on its eastern end.

89-99 **Lost Lake cinder cone chain**: Chain of three Holocene cinder cones that dams drainage to create Lost Lake. The ^{14}C age of a cone SW of Potato Hill, thought to be similar in age to these cones, is 1950 ± 150 yr BP (Taylor, 1968; see Stop 4)

60 **Three Fingered Jack.**

53 **Maxwell Butte**: A young Sr-rich basaltic andesite shield that is glaciated but still relatively uneroded. The distal lavas are unglaciated and are cut by Oregon 22 north of Little Nash Crater (Black and others, 1987).

Return to US 20. **0.6**

92.6 Turn L (east) on US 20. **0.7**

93.3 Bear R at Santiam Junction to remain on US 20 (east). **0.7**

94.0 Road cut at left in basalt (NSH-5)

erupted from the Lost Lake cones. **0.5**

94.5 On left is flank of one of the cinder cones that dam Lost Lake. Jackpine Rd to the right leads to a K-Ar dated lava (0.44 ± 0.12) on the west end of Potato Hill in 0.3 mile. **0.6**

95.1 Lost Lake on left, formed by ponding of drainage behind the chain of cinder cones west of the lake. **1.0**

96.1 Road cut on left is in thick, glassy, Sr-rich basaltic andesite lava (CM-1) from a vent near Craig Lake southeast of Maxwell Butte. The physical character of this lava (including fan-like columnar joints) suggests it may have been an intraglacial eruption. View SE (ahead and right) is of Hogg Rock. **1.5**

97.6 Curve around south side of Hogg Rock (MJ-#058), likely also an andesite tuya as suggested by its steep, glassy sides and flat top (Davie, 1980). Hogg Rock is dated at 90 ± 20 ka (Hill, 1992), which would place its eruption in the early Wisconsin. Both Hogg Rock and Hayrick Butte have incompatible-trace-element-poor compositions similar to North Sister-type basaltic andesite (Hughes and Taylor, 1986). The prominent cliffy outcrop to the right is the basaltic andesite plug at the east end of Potato Hill. **0.4**

98.0 View right of Hayrick Butte and Mt Washington. **1.5**

99.5 Santiam Pass. **0.2**

A Fault Coincident with Santiam Pass?

The geology suggests that a north-trending, down-west normal fault coincides with Santiam Pass. South of the highway is a N-trending vent alignment 3 km long of three small basaltic cones that may mark the trace of a buried fault. The presence of a fault is suggested by the high level of Matuyama-age rocks east of the pass and the fact that west of the pass Brunhes-age rocks are exposed all the way to the western graben boundary (Fig. 7). The Matuyama section is diverse and not derived from a single source (Hill, 1992), so the presence of older rocks at a high altitude east of the pass cannot be ascribed to the built-up flank of a large single volcano.

99.7 Spur road at right opposite Douthit Spring shortly leads to the spud location of the Santiam Pass drill hole. **0.4**

Santiam Pass Drill Hole

A geothermal and deep-drilling exploration corehole just south of the highway was drilled to 3040 feet (Hill, 1992). The core sampled mainly basaltic andesite (consistent with surface exposures) lava and dikes from many diverse vents, but also encountered rare basalt, andesite, and coarse sediment, probably debris flows. K-Ar ages reported for samples from the core are all compromised by the presence of nearby normally polarized and likely Brunhes-age dikes (similar to the dike noted at mileage 100.4) transected by the core that would have slightly reheated rocks in their vicinity causing loss of radiogenic Ar and lower apparent ages. Fortunately, a magnetic record of the core was made by Brittain Hill using a fluxgate magnetometer, and that record suggests that the core bottoms in early Matuyama-age rocks below the Olduvai after traversing the Brunhes and the late Matuyama including the Jaramillo. Surface exposures confirm the shallow level at which the Brunhes–Matuyama transition is encountered in the core (Fig. 7). In contrast, Hill (1992) accepted the ages at face value and concluded that the normal polarity interval far downhole is the Jaramillo. The age of this core is critical to subsidence estimates within the graben.

100.1 Road cut in normally polarized mafic lava. **0.3**

100.4 Normally magnetized basaltic andesite lava (98-26) in road cut on the left. This is the second curve east of Santiam Pass. **0.1**

Apparent Tectonic Fractures in Brunhes-age Lava on Santiam Pass

The lava exposed at mileage 100.4 is locally fractured but apparently not faulted. Two N-trending vertical fracture zones seem to be tectonic in origin. One zone is a narrow (0.5 m) band of rock shattered into pencil- and fist-sized pieces; the other is a 3-4 m wide zone broken into vertical, plate-like fragments 15 cm wide. On the west end of the outcrop is a flared dike surrounded by bedded cinder (probably the stump of a vent) that is similar in composition to the lava.

100.5 Reversely magnetized lava on the left in road cut. This lava underlies the fractured lava discussed above. From here east to the

western end of Suttle Lake all lava in road cuts is reversely polarized and Matuyama in age (K-Ar age 0.72 ± 0.19 Ma; Hill, 1992). **0.5**

101.0 View ahead of Black Butte, a reversely polarized basaltic andesite shield of Matuyama age (K-Ar age of 1.4 ± 0.3 Ma; Hill, 1992) that is relatively uneroded because it was never glaciated. **1.8**

102.8 Cache Mtn, a small basaltic andesite shield covered with trees, is visible to right. The age of Cache Mtn is uncertain as its lavas are normally polarized but its K-Ar age is 0.90 ± 0.05 Ma (Armstrong and others, 1975). A much younger eruption of primitive K-rich basalt (TFJ-1; Hughes and Taylor, 1986; Conrey and others, 1997) built a cinder cone on top of Cache Mtn; the lava mostly flowed down its southern flank. **0.2**

103.0 Viewpoint (**optional stop**) on south side of highway allows leisurely examination of distant Black Butte, Mt Washington, and Cache Mtn **1.3**

104.3 Final road cuts in lava are of normally polarized basaltic andesite erupted from a cinder cone approx 2 km west of here (Sherrod and others, in press). **0.1**

104.4 From here east for almost the next 2 miles, road cuts are in till of the lateral moraine on the north side of Suttle Lake, visible at right through the trees as you descend the grade. **1.6**

106.0 Second Suttle Lake turnoff on right. Green Ridge is visible ahead for 0.25 miles after this junction. **0.4**

106.4 Till on right marks the end of the late Wisconsin terminal moraine belt. **0.5**

106.9 Jack Lake Rd on left. Junction is underlain by very poorly exposed outwash related to the Suttle Lake moraines (Sherrod and others, in press). **1.4**

108.3 Poor road cuts for the next 0.5 mi or so are in fresh, normally polarized basalt. **1.3**

109.6 Camp Sherman junction. Black Butte is obvious north of the highway. **2.0**

111.6 Black Butte Ranch entrance. **1.0**

112.6 Road climbs onto fault block of Deschutes Fm (see below) lava cut by strands of the Tumalo Fault Zone that also cut Black Butte. **0.1**

112.7 View right of Black Crater over Black Butte Swamp. **1.0**

113.7 Indian Ford junction. Road drops off Deschutes Fm fault block. **1.2**

114.9 Cold Springs cutoff road. From here to Sisters the road crosses poorly exposed Suttle Lake outwash (late Wisconsin). **4.2**

119.1 Hwy 242 junction on west side of the town of Sisters. Continue east on Hwy 20. **0.3**

119.4 Elm Street junction (road to Three Creek Lake). If needed, restrooms and water are available at Sisters Village Green two blocks to the right. **0.2**

119.6 From the east side of Sisters the view to east is of McKinney Butte, a 3.3 ±0.2 Ma (Armstrong and others, 1975) vent of nearly aphyric, very Fe-rich andesite (95-89). The west side of the butte facing you is cut by a strand of the NNW-trending Tumalo Fault Zone, a complex zone of small-offset normal faults. Sisters is built on a sediment-filled basin ponded up by the fault zone. **0.3**

119.9 Stay R on US 20 at junction with Redmond Hwy 126. **1.2**

121.1 Prominent bend in highway marks the location of the major down-west normal fault (buried here) that cuts McKinney Butte and defines the east side of the Sisters Basin. **1.2**

122.3 Road cut at bend is in lava of the Deschutes Fm **0.5**

Deschutes Formation—A Record of Intra-arc Rifting

The Deschutes Formation is a thick deposit of lava, sediment, and tuff derived from the Cascades during the onset of intra-arc rifting (Taylor, 1981; Smith and others, 1987). It covers much of north-central Oregon east of the graben. A widespread basalt near the base of the deposit has an Ar-Ar age of 7.42 ± 0.22 Ma (Smith and others, 1987). The top of the formation is approx 5 Ma, based on numerous Ar-Ar and K-Ar ages (Armstrong and others, 1975; Smith, 1986). In this area there are only two K-Ar ages, both from capping lavas, and these are 4.9 ± 0.4 Ma (Armstrong and others, 1975) and 4.7 ± 0.1 Ma (Hill, 1991). The Deschutes Fm is thus the east-side equivalent of the uplifted ridge-capping sequence west of the graben. A prominent volcanic ridge must have lain along the axis of the arc during the emplacement of both formations, because the individual lavas and tuffs in the Deschutes Fm were emplaced in east- to northeast-flowing drainages, the mirror image of their west-flowing west-side counterparts. The Deschutes Fm is one of the best-

mapped arc-rift-related formations anywhere; literally hundreds of individual flows and tuffs have been traced (Conrey, 1985, Smith, 1986, and references therein to several theses done at Oregon State University under Ed Taylor's direction). In this area and generally in the southern Deschutes Basin, the paleodrainage was to the northeast, whereas farther north at Green Ridge, the paleodrainages were east-flowing (see Stop 10 and Bend Highland discussion below).

122.8 Outcrop to right of highway is in the Brunhes-age Plainview Basalt (95-37), a widespread unit mostly northeast of the highway. **1.1**
123.9 Highway curves around another resistant outcrop of Deschutes Fm lava. **0.4**
124.3 Yet another curve in Deschutes lava. **0.6**
124.9 Gist Road junction. **1.4**
125.5 Plainview; road ahead traverses irregular contact between Plainview Basalt and glacial outwash. Cline Buttes visible to left; Bend Highland to right. **2.3**
127.8 Fryrear Rd. junction; Deschutes Fm cropping out right of road. **1.3**
129.1 Cascade Viewpoint on Hwy 20.

Stop 6. Overview of Three Sisters Area and Bend Highland

The viewpoint lies on glacial outwash; most of the small buttes visible in the near and middle ground are underlain by Deschutes Fm lava or cinder as a significant number of eroded vents occur east of the Tumalo Fault Zone (Taylor and Ferns, 1994). The Bend Highland (see below) is the prominent skyline ridge to the south that extends east of the Three Sisters. Other prominent features are as follows (again by azimuth):

340 **Squawback Ridge**: A mildly alkaline basaltic andesite shield built east of the Green Ridge escarpment on top of the Deschutes Fm. Squawback Ridge is Gauss age (normal polarity; K-Ar age 2.9 ± 0.2; Armstrong and others, 1975; Conrey, 1985).

337 **Bald Peter**: Faulted and glacially eroded remnant of a reversely polarized basaltic andesite shield (the central plug is well exposed), K-Ar age 2.2 ± 0.2 Ma (Armstrong and others, 1975); see Stop 12.

333 **Little Squawback Ridge**: Cousin to Squawback Ridge and probably similar in age as it is highly weathered with virtually no outcrop.

330 **Mt Jefferson**: A major stratocone constructed at the southern margin of a widespread (approx 150 km^2) field of intermediate and silicic volcanic rocks extending back to at least 1 Ma (Conrey, 1991). Such long-lived andesite- and dacite-dominated volcanic centers are spaced 60-70 km apart along the northern Oregon Cascade arc (Mt Hood, Mt Jefferson, South Sister). In between these centers intermediate or silicic rocks are rare. The broken skyline ridge south of Mt Jefferson includes several features described at Stop 12.

321 **Black Butte.**

312 **Three Fingered Jack.**

293 **Mt Washington.**

285 **Black Crater**: A relatively uneroded and thus late Pleistocene (estimated 50 ka) basaltic andesite (99-35) shield volcano with several flanking cinder cones. The "crater" is a shallow cirque. A N-trending, down-west normal fault was mapped across the western flank of Black Crater just west of Windy Point by Steve Bacon (1996). A fault is a possible explanation for the small, talus-covered scarp on the flank of the cone. It is of interest that the mapped fault is on strike with the 6 km long Matthieu Lake fissure vent between Black Crater and North Sister (Fig. 1). The fissure eruption must have been dike-fed, and the dike could have followed a fault to the surface.

281 **Trout Creek Butte**: A broad, flat-topped, normally-polarized basaltic andesite shield volcano (Taylor, 1987).

280 **Millican Crater**: A basaltic andesite cinder cone on the south flank of Black Crater (Taylor, 1987).

276 **Matthieu Lake fissure vent**: A 6 km long, N10E-trending chain of cones which erupted Fe-rich basaltic andesite (95-156) cinders, bombs, and lava that flowed far (> 15 km) to the east (Fig. 1). Glaciated but overlies Black Crater so age is likely 30-40 ka.

262 **North Sister**: A large basaltic andesite (95-131) shield volcano; the oldest of the Three Sisters. Regional stratigraphy and bracketing ages suggest a 100-200 ka age. The central plug, a large number of dikes, and a palagonitic complex on the NE side of the volcano have been exposed by glacial erosion (E.M. Taylor, unpub. mapping).

260 **Melvin Butte**: A rhyolite dome with a high-silica composition (74% SiO_2) similar to the Bend Pumice (Taylor and Ferns, 1995; Hill, 1991).

258 **Middle Sister**: A complicated, poorly known cone with abundant dacite lavas (95-133), stacks of intermediate rocks including Fe-rich varieties (95-132), and abundant plagioclase-rich basaltic andesite (95-135).

251 **Unnamed butte** beneath the Middle Sister–South Sister saddle: A rhyolite dome with a high-silica composition (74% SiO_2) similar to the Bend Pumice (Taylor and Ferns, 1995; Hill, 1991)

248 **South Sister**: The youngest of the Three Sisters (basal age of 90 ± 10 ka; Hill and Duncan, 1990), although there may be some overlap in time with lava erupted from the Middle Sister. South Sister is chiefly andesite, but it also erupted basaltic andesite and rhyodacite. A compositional gap extends from 66-72% SiO_2 (Wozniak, 1982; Hill, 1991). Silicic rocks there differ from Middle Sister and Bend

Highland silicic rocks in that they bear traces of amphibole and have lower heavy-rare-earth element and Y contents, and lower Zr concentrations. The intermediate and silicic rocks at Middle Sister and on the Bend Highland have the typical amphibole-absent geochemical patterns associated with rifting. The South Sister, in contrast, has a pattern more akin to that found in extension-absent, amphibole-bearing rocks. The change with time may reflect the decline of extension rates in central Oregon and consequent crustal cooling. All silicic rocks from the Bend Highland are likely older than approx 200 ka (Hill and Duncan, 1990). In addition, all of the silicic rocks in the Devils Lake Borehole, drilled 10 km south of the South Sister are certainly older than South Sister, and are of the Middle Sister type.

246 **Three Creek Butte**: A rhyolite dome with a high-silica composition (74% SiO_2) similar to the Bend Pumice (Taylor and Ferns, 1995; Hill, 1991).

242 **Snow Creek cinder cone**: Glaciated remnant of an Fe-rich basaltic andesite cinder cone near the headwaters of Snow Creek (Taylor, 1978).

239 **Broken Top**: A large, heavily dissected basaltic andesite shield volcano, with a crater open to the south (Taylor, 1978).

237 **Tam McArthur Rim**: Prominent cirque headwall above the Three Creek Lakes comprised of diverse lava including basaltic andesite, dacite, and rhyodacite (Taylor, 1978). Several large dikes beneath the rim suggest that most of the lava was vented locally. Hill and Duncan (1990) obtained a K-Ar age of 213 ± 9 ka on a thick rhyodacite lava that caps the section.

223 **Triangle Hill**: A prominent cone-shaped hill on the east end of the Bend Highland. Triangle Hill is a 340 ± 20 ka andesitic cinder cone (Hill, 1991; Hill and Duncan 1990), which overlies the probable vent for the Bend Pumice and Tumalo Tuff, a large rhyolitic pyroclastic deposit east of the Bend Highland dated at 440 ± 6 ka (Lanphere and others, 1999). Several rhyolite domes and mafic-intermediate cinder cones lie in a 3 km diameter circle centered on Triangle Hill (Sherrod and others, in press). The circle corresponds to a prominent negative gravity anomaly.

205 **Unnamed cinder cone** on east flank of Bend Highland: A basaltic andesite cinder cone that fed a small lava flow.

58 **Cline Buttes**: A large rhyolite dome complex recently Ar-Ar dated at 6.14 ± 0.06 Ma (M.A. Lanphere, in Sherrod and others, in press). Cline Buttes were long thought to be a source vent for the John Day Fm (19-39 Ma) in east-central Oregon, but groundwater investigations (by Marshall Gannett and Ken Lite) suggest that they are relatively unaltered and highly permeable, in sharp contrast with most John Day age rocks in central Oregon. Cline Buttes may have served as a source vent for silicic pyroclastic volcanism in the Deschutes Fm, and are one indicator of the tremendous breadth of the vent field during intra-arc rifting. Vents of 5-8 Ma lie from far out into the Western Cascades to as far east as Cline Buttes, a cross-arc distance of some 70 km. The distant Gray Butte, Smith Rocks, and Powell Buttes truly are all source areas for John Day age rocks.

Are the Bend Highland and Brothers Fault Zone Connected?

The Bend Highland (a term suggested by Larry Chitwood at the Bend USFS office) is a prominent, broad, WNW-trending ridge of young volcanic rocks that extends southeast of the Three Sisters some 20 km toward Bend. All surface exposures on the highland are of normal-polarity rocks (Sherrod and others, in press) and one drill core penetrates 1200 feet of Brunhes-age rocks (see CEBH-7 corehole below). Thus the highland is capped with a thick welt of Brunhes-age rocks. Because the highland trends WNW, Brunhes-age lavas are channelized in northeast-flowing drainages on its northern flank. This situation seems to have existed for a considerable time, as 5.0 Ma Deschutes Fm lavas northeast of the highland (including the exposures along US 20) were also channelized along northeast-flowing paleodrainages. The Brunhes-age ash-flow tuffs (Desert Springs, Tumalo Tuff, Shevlin Park—see below) with sources on or near the highland have counterparts in the petrologically similar and even more numerous and voluminous ash-flow tuffs of the Deschutes Fm. Several of the older tuffs can be traced from the Deschutes Basin upstream along the Deschutes River and its tributary creeks a considerable distance back to the southwest where they are truncated by the Tumalo Fault Zone. Their map distribution therefore suggests that they had sources in the vicinity of the modern Bend Highland (Smith and Taylor, 1983; Smith, 1986). These considerations suggest that the Bend Highland has been a long-lived feature of central Cascade geology.

The Brothers Fault Zone is a broad WNW-trending zone of small offset en echelon normal faults that extends for some 240 km across eastern Oregon (Lawrence, 1976; Walker and Nolf, 1981). North of the zone, Cenozoic and pre-Cenozoic rocks are exposed in northeast- and east-trending anticlines in the Ochoco and Blue Mountains. South of the zone only Cenozoic rocks are exposed, and they are broken and tilted by NNE-trending normal faults, some of which have formed major escarpments. Basin and Range faults south of the Brothers Fault Zone either die upon reaching the zone or merge into it. West-northwest extension of the

Basin and Range south of the zone, and its absence to the north, strongly suggests that the Brothers is a major right-lateral fault zone (Lawrence, 1976). It likely is a broad zone of lateral disruption, not a single fault like the classic San Andreas. The Brothers Fault Zone is of considerable antiquity (Walker and Nolf, 1981); the tectonic pattern in east-central Oregon has remained unchanged since at least the middle Miocene (Hooper and Conrey, 1989).

The Brothers Fault Zone may extend along its long WNW strike through the Cascade Range beneath the Bend Highland and the Three Sisters to the complex set of northwest-trending faults at the graben margin around the area of the McKenzie River bend at Foley Ridge. These faults perhaps connect farther along strike to WNW-trending right-lateral faults beneath the southern Willamette Valley (Yeats and others, 1996). A buried Brothers Fault Zone beneath the Bend Highland would explain the highland's orientation, longevity, the presence of two uniquely WNW-trending vent alignments there, and account for the ability of both silicic and mafic magma to easily penetrate the crust along the length of the highland over a span of many millions of years.

Bend Highland Drill Hole

A geothermal exploration corehole (California Energy Bend Highland CEBH-7) drilled on top of the highland south of Triangle Hill penetrated 3430 feet of volcanic rocks, predominantly lava, but including some silicic domes, pyroclastic rocks, and lahars. The lithologies in the hole are notable for their similarity to rocks exposed at the surface on the Bend Highland, namely, mafic lavas, intermediate rocks including Fe-rich varieties, and silicic lavas, domes, and pyroclastics. The CEBH-7 corehole intersected the Brunhes-Matuyama boundary at a depth of approximately 1200 ft, and we interpret the lower, chiefly reversely polarized portion of the core to be of Matuyama age. Unfortunately, alteration affects all of the rocks below the 1870 ft level, so the ages obtained from this core are almost certainly too young (a common problem in Cascade coreholes). If our age assumptions are correct, large offset (1 km or more) normal faulting must lie between the highland and Deschutes Fm lavas exposed in an inlier at Bull Springs (K-Ar age 4.7 ± 0.1 Ma; Hill, 1991) only 5 km northeast of the corehole. This interpretation is supported by a large down-west offset in layered conductivity anomalies measured with magnetotellurics that coincides with our postulated fault zone (Livelybrooks and others, 1989).

Continue east on US 20. **0.5**

129.6 Ditch exposes outcrop of early Brunhes age Desert Spring Tuff on both sides of highway. **2.7**

Desert Spring Tuff

The rhyodacitic Desert Spring Tuff is the oldest of three voluminous Brunhes age pyroclastic deposits (including the Bend Pumice–Tumalo Tuff and the Shevlin Park Tuff) on the east flank of the Bend Highland (Taylor, 1981). The erupted volume is thought to be on the order of 2 km^3 (Hill, 1991), but this is a very rough estimate, as much of the tuff has been buried by younger eruptions, and the tuff is not uniform in thickness but rather was emplaced in channeled and faulted topography. Correlative distal Rye Patch Dam Ash is thought to be approx 0.63 Ma, based on interpolation of lake-core sedimentation rates (Rieck and others, 1992). The Desert Springs was likely vented from chemically and petrographically equivalent domes near Tumalo Lake (compare pumice 96-20 with dome B217 in Table 1), approximately 18 km SSW of here, consistent with its map distribution (Fig. 8) and NNE- to ENE-trending pumice imbrication (assumed flow direction; Mimura, 1984). The domes are among the lowest normally polarized exposures along Tumalo Creek (Sherrod and others, in press), which suggest an early Brunhes age, consistent with the expected age of the tuff. The tuff contains large dark pumice (locally with blebs of lighter glass) bearing approx 10% of 5-7 mm plagioclase phenocrysts, and also those of orthopyroxene, clinopyroxene, magnetite, ilmenite, and apatite (Hill, 1991). The chemical signature is notable for its high Rb (80-90 ppm), unlike most other silicic rocks in central Oregon.

132.3 Couch Market Rd junction. Awbrey Butte on the outskirts of Bend ahead. Awbrey is a small mafic shield thought to be of Deschutes Fm age, but is undated. **0.8**

133.1 Pinehurst Rd. junction. Laidlaw Butte,

believed to be a Deschutes Fm vent, is on the right. **0.5**
133.6 Powell Buttes, visible in the distance from here at 10-11 o'clock, is a dome complex of the John Day Fm (19-39 Ma). **0.6**
134.2 Road cuts expose Tumalo Tuff (see below). **0.6**
134.8 Turn R on Tumalo State Park Rd. Note the gravel quarry operation along the Deschutes River here. Tumalo Tuff is exposed in the valley walls on both sides of the river. Ahead is Awbrey Butte. **0.8**
135.6 Deschutes Fm lava in road cut. **0.1**
135.7 Desert Spring Tuff in road cut. **0.1**
135.8 Turn R on Tumalo Reservoir Rd. **0.1**
135.9 Turn L on Johnson Rd. **0.1**
136.0 Desert Spring Tuff in road cut; the tuff forms bluffs along the Deschutes River left of road in Tumalo State Park. **0.3**
136.3 Tumalo Tuff in road cuts for the next 0.3 mi. **0.9**
137.2 Road climbs onto lava rim over Tumalo Tuff. **0.8**
138.0 Sharp L corner at junction with Tyler Rd—stay on Johnson Rd. **1.4**
139.4 Tumalo Butte, a small mafic vent left of the road. **0.8**
140.2 Turn R on Bull Springs Rd just down from crest of hill; follow pavement west. Warning signs on this private road are due to active quarry operations. **1.0**
141.2 Turn R on gravel road 4606 before entrance to quarry. This quarry contains some excellent exposures of Shevlin Park Tuff overlain by a bimodal airfall tephra, but at the time of writing it is largely backfilled. **0.2**
141.4 Lava cut by road may be equivalent to 178J andesite noted below. **0.2**
141.6 Road drops off lava flow. **0.1**
141.7 Nose of andesite lava flow (178J) on left. **0.4**
142.1 Outcrop of yet another lava, this one a basaltic andesite (179J) dated at approx 350 ka (M.A. Lanphere, unpub. data, 2000). **0.6**
142.7 Road cut exposes 179J basaltic andesite lava overlain by Shevlin Park Tuff. **0.1**
142.8 North rim of gully is underlain by densely welded Shevlin Park Tuff, sometimes quarried here for ornamental stone. **0.2**
143.0 Turn L on gravel road 4605. **0.2**
143.2 Stay left on main road. **0.3**
143.5 Turn L on poor gravel road and follow it right upstream (west) for 0.25 mi to a junction where you can turn around and park. **0.1**
143.6 Lava on right is poorly known. **0.1**
143.7 Stop at Columbia Canal irrigation ditch.

Stop 7. Shevlin Park Tuff at Columbia Canal

Walk up the canal bed. If water fills the canal, many features can still be seen by walking up the canal-parallel road for a few hundred meters and then cutting back into the canal from above.

The irrigation ditch contains one of the best exposures of the Shevlin Park Tuff and by far the best exposure of the Columbia Canal airfall pumice. The Tumalo Tuff also is well exposed. A shallow channel seems to have been eroded in the Tumalo Tuff (440 ka), which was partially filled by a flow front of the 179J basaltic andesite (350 ka; noted at mileage 142.1 above). The Columbia Canal airfall then accumulated in the channel, and the top was fluvially reworked and mixed with vesicular flow-top fragments from the lava. The Shevlin Park Tuff (260 ka, see below) was then emplaced in the channel, where it overlies beveled, reworked Columbia Canal pumice. The base of the tuff locally contains abundant fragments of the 179J lava. The tuff comprises multiple flow units here: a lower pumice-rich flow overlain by a thinner pumice-poor zone, in turn overlain by an upper pumice-rich flow that contains a local band of accumulated pumice.

What is the relationship, if any, between the Shevlin Park Tuff and the Columbia Canal airfall pumice? Chemically, silicic pumice in the tuff is similar but not identical (especially in some trace-element concentrations) to the airfall pumice (Sarna-Wojcicki and others, 1989; Conrey and others, 2001a). Mineralogically the two are also quite similar, with the exception that the airfall pumice contains slightly more Fe-rich orthopyroxene (Conrey and others, 2001a).

Shevlin Park Tuff

This tuff is the youngest of the three major Brunhes-age pyroclastic deposits east of the Bend Highland (Fig. 8; Taylor, 1981; Conrey and others, 2001a). The volume of the tuff is difficult to calculate, due to erosion and burial by younger eruptions, but must be at least several km^3. New $^{40}Ar/^{39}Ar$ data on plagioclase indicate

an age of 260 ± 15 ka (Lanphere and others, 1999). A Bend Highland source for the tuff is indicated by a radial distribution of pumice imbrication (assumed equal to flow direction) centered on the highland (Mimura, 1984) and an increase in degree of welding and pumice size toward the highland (Hill, 1991). Earlier workers suggested a source beneath Triangle Hill (Mimura, 1984; Hill and Taylor, 1990). However, it is highly unlikely that the source was the Triangle Hill area because new age dates put the eruption 80 ka after the construction of Triangle Hill, the Shevlin Park Tuff drapes the dated cinder cone, and no chemically equivalent domes or lavas there match with the Shevlin Park. We suggest instead that the Shevlin Park source was near lava or near-vent welded agglutinates east and southeast of Three Creek Lake, 5-6 km west and southwest of Triangle Hill (Fig. 8). The welded agglutinate nearest Three Creek Lake is petrographically and chemically similar to pumice clasts in the Shevlin Park (compare agglutinate B277 with pumice 99-62A in Table 1), and is heterogeneous as well. The relative age of the near-vent agglutinate is correct: it is overlain by Tam MacArthur Rim rhyodacite dated at 213 ± 9 ka (Hill and Duncan, 1990). A source near Three Creek Lake can account for the radial distribution of the Shevlin Park around the Bend Highland, and especially for the westernmost Shevlin Park outcrop in Squaw Creek (Fig. 8).

Some earlier workers recognized two tuffs that we have found geochemically difficult to separate, and thus we feel that the older of the two tuffs, the Century Drive Tuff of Taylor (1981) is likely just an initial flow unit of the Shevlin Park eruption. Paleomagnetic investigation supports our interpretation: the Shevlin Park and Century Drive Tuffs have the same magnetic directions within error limits (Duane Champion, in Conrey and others, 2001a). The correlation is bolstered by the fact that the magnetic direction is a somewhat unusual one for a Brunhes-age deposit. The purpose of our detailed geochemical sampling initially was to characterize the tuffs so that we could distinguish them from lithologically similar Newberry tuff, and also to determine how many large-volume ash-flow tuffs were erupted from the vicinity of the Bend Highland, as that has obvious implications for volcanic-hazard evaluation.

The Shevlin Park Tuff is dark ("black pumice flow" of Mimura, 1984) due to the presence of black andesitic pumice and glass. In good exposures, the tuff commonly includes two flow units, both of which are pumice-rich, but the lower unit has few pumice clasts larger than 1-2 cm, whereas large pumice is common in the upper flow unit. Some quarry exposures have as many as four flow units, some as thin as 1 meter. In photographs taken by Ed Taylor of now backfilled quarry exposures, the contact between the lower and upper flow units (then called the Century-Shevlin contact), seems to be marked by surge-bed deposits. In places, lower flow units of the tuff are channeled as deep as several meters, and filled with the overlying flow unit.

The bulk composition of the heterogeneous Shevlin Park Tuff is dacitic; earlier workers characterized it as andesitic (Taylor, 1981), but we have found a high proportion of dacitic and rhyodacitic pumice in the tuff. The tuff is compositionally bimodal, with black pumice clasts ranging from 55-62% SiO_2, and commonly paler silicic pumice from 64-68% (99-62E, G, and A). Rare banded pumice is present with compositions in the gap between 62 and 64% SiO_2. Lower flow units of the tuff seem to contain more silicic pumice, whereas the upper flow units contain a mixture of both silicic and mafic pumice. Pumice is sparsely porphyritic and contains phenocrysts of plagioclase, clinopyroxene, orthopyroxene, olivine, magnetite, and ilmenite (Hill, 1991; Conrey and others, 2001a). The compositional variations in the tuff can be modeled with a combination of magma mixing, which generates the wide spread in SiO_2 and variation in incompatible trace element ratios, and crystal fractionation, which is necessary to account for the variations of P_2O_5 and incompatible trace element concentrations in the more mafic pumice. Our model suggests a magma chamber where mixing occurred between mafic and silicic magmas accompanied by significant crystal fractionation of the mafic magma. An alternative interpretation would be one of three-component mixing, with one mafic component considerably more fractionated than the other.

Retrace route back to US 20 at Tumalo.

9.0

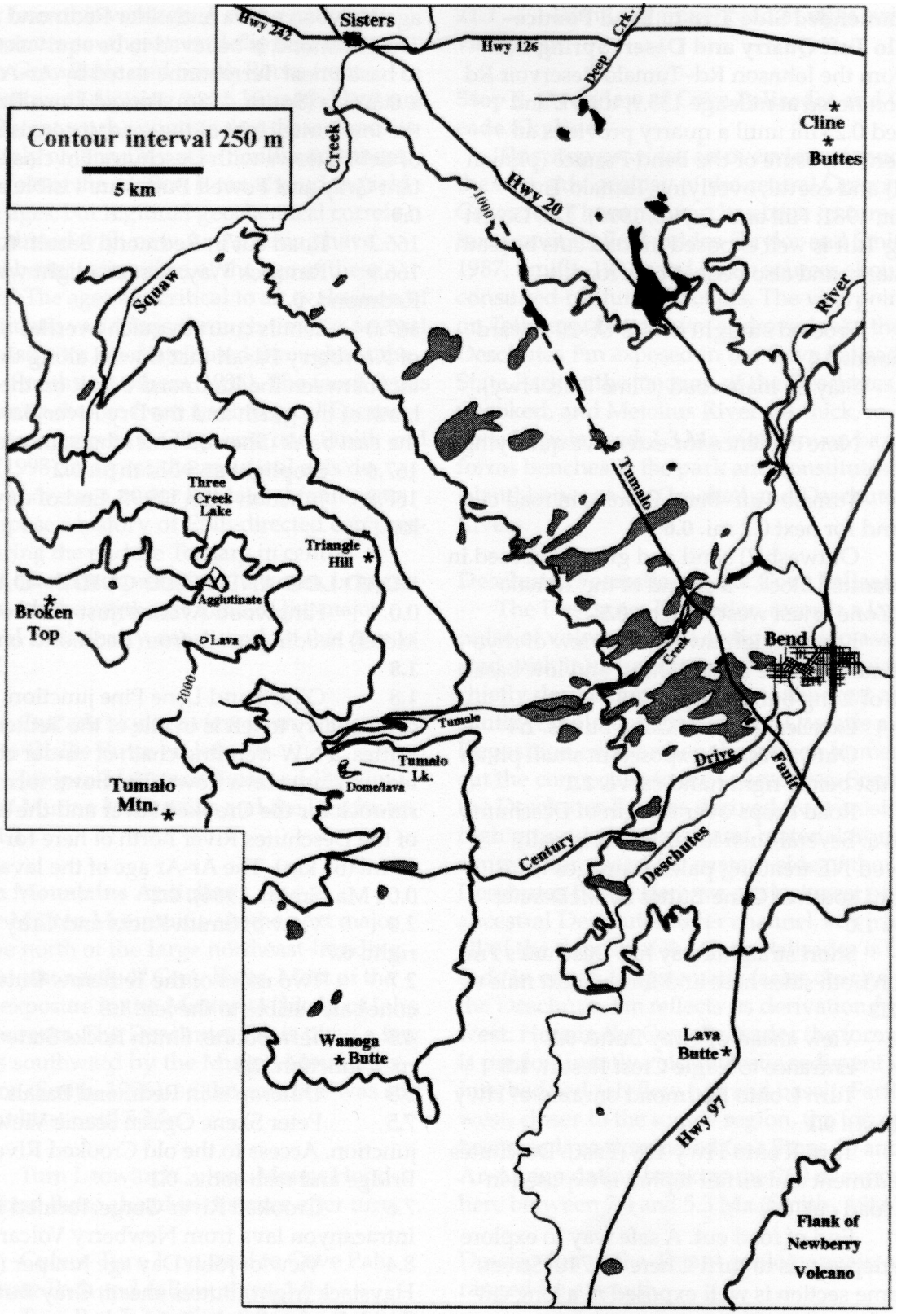

Figure. 8. Distribution of Shevlin Park (light gray pattern) and Desert Springs (black) Tuffs east of the Bend Highland in central Oregon. Potential source or near-source deposits for the Shevlin Park Tuff near Three Creek Lake are indicated. The radial distribution of the Shevlin Park about the Bend Highland suggests a highland source; a source at or near Three Creek Lake would be more likely to generate the distribution shown than one at Triangle Hill. A dome or lava near Tumalo Lake is likely the source of the Desert Spring Tuff.

Recommended Side Trip to Bend Pumice–Tumalo Tuff Quarry and Desert Spring Tuff

From the Johnson Rd–Tumalo Reservoir Rd junction noted at mileage 135.9, turn L and proceed 0.25 mi until a quarry provides an excellent exposure of the Bend Pumice (plinian airfall) and coeval, overlying Tumalo Tuff (Taylor, 1981; Hill and Taylor, 1990). The Desert Spring Tuff is well exposed in road cuts beneath the quarry and also beneath the road.

152.7 Proceed straight across US 20 toward Redmond. **0.4**
153.1 Stay on main road (Cline Falls Hwy). **0.3**
153.4 Note evidence for extensive quarrying. **0.2**
153.6 Tumalo Tuff–Bend Pumice in road cut here and for next 0.2 mi. **0.6**
154.2 Outwash(?) sand and gravel exposed in an upfaulted block—a strand of the Tumalo Fault Zone is just west of here. **0.5**
154.7 Long straightaway with view of rhyolite domes of Cline Buttes ahead and low basalt shield of Long Butte to right. **1.3**
156.0 Excellent view of Cline Buttes. **1.4**
157.4 Outwash sand exposed in small pit on right just before right hand curve. **1.1**
158.5 Road drops over margin of Deschutes Fm lava. Several such lavas that originally followed NE-trending paleodrainages were mapped south of Cline Buttes by McDannel (1989). **1.0**
159.5 Short straightaway has Deschutes Fm lava on both sides here and for the next mile or two. **2.3**
161.8 View ahead of Gray Butte. **0.3**
162.1 Entrance to Eagle Crest Resort. **1.0**
163.1 Turn L onto Redmond onramp of Hwy 126 (East). **0.1**
163.2 Turn R onto Hwy 126 (East). Deschutes Fm sediment and airfall tephra is exposed in deep road cut. **0.3**
163.5 End of road cut. A safe way to explore these deposits is to turn L here on 74th Street; the same section is well exposed in a long cut along that street. **0.0**
163.5 Cross Deschutes River. **0.1**
163.6 Entrance to Cline Falls State Park. Road climbs onto the margin of young basalt from Newberry Volcano. **2.0**
165.6 Helmholtz Way junction. **0.2**
165.8 Crossing the contact between Brunhes-age Newberry lava and older Redmond Basalt. The Redmond is believed to be equivalent in age to basalt near Terrebonne dated by Ar-Ar as 3.56 ± 0.30 Ma (Smith, 1986). Forked Horn Butte is the low butte right of the road; it consists chiefly of debris flows with Deschutes Fm clasts. Distant Gray and Powell Buttes are visible ahead. **0.9**
166.7 Road cut in Redmond Basalt. **0.2**
166.9 Rimrock Way; first stoplight west of Redmond. **0.1**
167.0 Tennis court in gulch overlies a tongue of Newberry Basalt that flowed along the contact between the Redmond Basalt on the west bank of the gulch and the Dry River Basalt on the east bank (Sherrod and others, in press). **0.6**
167.6 Stoplight at S Ninth St. **0.2**
167.8 Junction with US 97. End of day 1 road log.

ROAD LOG AND FIELD GUIDE—DAY 2

0.0 Kingwood Avenue (just past Hub Motel) heading north from Redmond on US 97. **1.8**
1.8 O'Neil and Lone Pine junction. Cinder cone quarry to left is in one of the Tetherow Buttes, a NW-trending chain of cinder cones that fed two large lava flows. The flows form the rimrock for the Crooked River and the east side of the Deschutes River north of here for approx 40 mi (65 km). The Ar-Ar age of the lava is 5.31 ± 0.04 Ma (Smith, 1986). **0.2**
2.0 View of Smith Rocks and Gray Butte on right. **0.7**
2.7 Two more of the Tetherow Butte cinder cones are visible to the left. **1.8**
4.5 Terrebonne; Smith Rocks State Park road junction. **0.8**
5.3 Outcrop is in Redmond Basalt. **2.2**
7.5 Peter Skene Ogden Scenic Viewpoint junction. Access to the old Crooked River Gorge Bridge and restrooms. **0.1**
7.6 Crooked River Gorge, formed in intracanyon lava from Newberry Volcano. **0.8**
8.4 View of John Day age Juniper (left) and Haystack (right) Buttes ahead; Gray Butte and Smith Rocks to right. **2.1**

John Day Age Rocks and Structures in Central Oregon

The age of tuff and lava in the Gray Butte–Smith Rocks area has long been a puzzle. The southward apparent dip of the section should be

evident from this vantage. A major anticlinal axis separates southeastward-dipping rocks beneath Gray Butte and Smith Rocks from northwestward-dipping rocks beneath Haystack Butte. Recent work suggests that these deposits are entirely of John Day age (Smith and others, 1998). Most of the section is too altered to yield reliable ages, but regional geochemical correlation combined with new Ar-Ar dating have allowed better estimation of the age of these deposits. The ages are critical to an evaluation of paleoclimatic variations through time, as several plant fossil sites are distributed throughout the section (Smith and others, 1998). The fossil floras document a change from a subtropical Eocene climate to a temperate Oligocene one. Smith and others (1998) interpret the anticlinal axis described above as a major left-lateral fault zone, and propose a history of ENE-directed compression during the middle Tertiary in central Oregon. Their interpretation, however, is inconsistent with the northeast trend of the major anticlinal axis; clearly, more work in this area is needed.

10.5 Cascade skyline view from Three Sisters to Olallie Butte on left. **3.0**
13.5 Juniper–Haystack Butte saddle. View ahead of Mutton Mountains and the Deschutes Basin. **1.1**

Mutton Mountains Anticline

The Mutton Mountains are the next major anticline north of the large northeast-trending anticline just north of Gray Butte. Most of the visible exposure in the Muttons is likely of John Day age rocks. The Deschutes Fm is tilted a few degrees southward by the Mutton Mountains Anticline (Smith, 1986), so the anticline was still active at least until 5 Ma.

14.6 Turn L toward Culver. Mount Hood and Round Butte ahead in distance after turn. **2.6**
17.2 Culver. Turn L on road to Cove Palisades State Park and follow signs. **1.0**
18.2 Turn R at T junction. **0.9**
19.1 Turn L toward Cove Palisades. **0.5**
19.6 Sharp right turn; stay on main road. **0.5**
20.1 Turn L toward Cove Palisades. **0.3**
20.4 Turn R toward Round Butte Dam overlook. **0.7**
21.1 Turn L on gravel road at right curve to viewpoint.

Stop 8. Overview of Cove Palisades and Cascade Skyline

This stop provides an overview of much of the east-side geology of the central Oregon Cascades. The same stop has been featured in two previous field guides (Taylor and Smith, 1987; Smith, 1991), and those sources should be consulted for further details. The viewpoint is on Tetherow Butte Lava, and overlooks the Deschutes Fm exposed in the Cove Palisades State Park at the junction of the Deschutes, Crooked, and Metolius Rivers. A thick, reversely-polarized, 1.3 Ma intracanyon basalt forms benches in the park and constitutes the island between the Crooked and Deschutes Rivers.

Deschutes Formation at the Cove Palisades

The Deschutes Formation records a large pulse of volcanism and sedimentation associated with intra-arc rifting. The deposit was chiefly derived from sources to the west and southwest along the pregraben Cascade axis. Deposition ended when the graben formed and cut the connection to the source area. Some of the Deschutes Fm was derived from erosion of high ground to the east, and material from those sources dominates the eastern side of the Deschutes Basin. Here we are just west of the ancestral Deschutes River channel, so virtually all of the deposit at the Cove Palisades is Cascade in origin. A systematic facies change within the Deschutes Fm reflects its derivation from the west. Here in the Cove Palisades the formation is predominantly volcaniclastic sediment with interbedded ash-flow tuff and basalt. Farther west, closer to the source region, the formation becomes lava-dominated (see Stops 10 and 12). Ar-Ar age dating brackets the 200 m exposure here between 7.4 and 5.3 Ma (Smith , 1986)

Description of the distant geology, again arranged by azimuth.

10 **Round Butte**: A small alkaline basalt (RB-10) shield volcano that overlies the Deschutes Fm. Ar-Ar age is 3.97 ± 0.05 Ma (Smith, 1986).

350 **Mutton Mountains.**

337 **Mt Hood and high ground to its SE**: Mt Hood is the next stratocone north of Mt Jefferson, and has been a locus

of intermediate and silicic volcanism for at least 8 m.y. (Conrey and Sherrod, in prep.). The high ground visible to the southeast of Mt Hood is capped chiefly by Pliocene andesite and dacite, derived from sources near the modern cone. Note the regular 60-70 km spacing of andesitic stratocones in north-central Oregon from South Sister to Mt Jefferson to Mt Hood. This pattern seems to be one of considerable longevity and also coincides with the structural segmentation of the graben.

330 **Mt Wilson and Beaver Butte**: Mt Wilson (left) is a reversely-polarized basaltic andesite shield, banked up against a small silicic dome complex of Gauss normal age at Beaver Butte (Sherrod and Scott, 1995). Not obvious from this vantage, the Long Ridge fault scarp extends south from Beaver Butte. The fault zone cuts rocks chiefly of Gauss-normal age (>2.3 Ma), but Matuyama-age rocks overlie the fault traces with no offset (R.M. Conrey, unpub map of the Fort Butte 15' Quad.).

315 **Fort Butte**: A small andesitic shield volcano, likely of Matuyama age.

304 **Olallie Butte**: A young, slightly glaciated basaltic andesite shield volcano (Conrey, 1991). The lava is similar in composition to North Sister lava.

293 **N end of Green Ridge**: The dissected remains of a large pyroxene- and hornblende-bearing andesite volcano centered near Castle Rocks (Wendland, 1988). K-Ar dating suggests an age of approx 8 Ma (Armstrong and others, 1975); the volcano is overlain unconformably by Deschutes Fm lava and tuff.

295 **Lionshead and Shitike Butte**: Lionshead is underlain by a large flow of very sparsely amphibole-phyric rhyodacite (MJ-1127Y; Yogodzinski 1985) with an Ar-Ar age of 2.27 ± 0.05 Ma (Smith 1986). Shitike Butte is a dome of very similar material. Similar rhyodacite lavas and domes underlie an area of approximately 100 km^2 north of Lionshead in the Fort Butte 15 Minute Quadrangle (R.M. Conrey, unpub mapping and data). The fact that the Gauss- and early Matuyama-age rocks of Lionshead and Bald Peter are at such high altitude so close to the Cascade crest is an indication that offset along the Green Ridge Fault Zone declines dramatically northward, thus defining a segment boundary.

286 **Mt Jefferson.**

272 **South Cinder Peak**: The conspicuous summit on the skyline south of Mt Jefferson is a Holocene(?) cinder cone that fed a small basalt lava which flowed down to the SW of the cone.

290-250 **Green Ridge**: A nearly 30 km long fault escarpment that bounds the eastern margin of the High Cascade Graben. The ridge comprises the proximal correlative of the 5.0-7.5 Ma rocks of the Deschutes Fm exposed in the Cove Palisades (Taylor, 1981; Smith and others 1987). Much of the formation in this area was emplaced along east-trending drainages leading from Green Ridge.

259 **Three Fingered Jack.**

247 **Squawback Ridge.**

239 **Black Butte.**

237 **Little Squawback.**

229 **Black Crater.**

223-218 **Three Sisters.**

213 **Broken Top and the Bend Highland.**

208 **Mt Bachelor**: A large basaltic andesite shield volcano at the northern end of a 25 km long, north-trending chain of late Pleistocene mafic vents (Scott and Gardner, 1992).

186 **Cline Buttes.**

180 **Newberry Volcano**: The enormously broad mafic Newberry Shield can be seen on a clear day.

157-142 Juniper–Gray Butte area.

Age Propagation of Rifting

This overview provides an along-arc view of nearly the entire east flank of the Cascade Range in northern Oregon. Geology similar to that found here along the southernmost graben segment, with an east-side pulse of rift-related volcanism and sedimentation, followed by foundering of the arc axis, lies all along the arc visible from here north. The geology is similar but is not coeval; the eastside deposits are progressively younger farther north, and their volumes diminish considerably. The graben structures also young progressively northward; thus the graben resembles a propagating rift (Conrey and Sherrod, in prep).

Return to Cove Palisades Park road. **0.8**

21.9 Turn R. **0.1**

22.0 Entrance to Cove Palisades State Park. **0.1**

22.1 Quarry on right in Tetherow Butte lava (RB-66). Note the glassy irregular jointing that suggests flow over wet ground or into water. **0.5**

22.6 Crooked River Campground loop junction marks the top of the intracanyon lava bench. From here down the grade, sediment and ash-flow tuff of the Deschutes Fm are exposed (see Smith, 1991 for a detailed description). **0.2**

22.8 Ash-flow tuff exposed here is the Cove Ignimbrite Member of Smith (1986). **0.1**

22.9 An unnamed ash-flow tuff. **0.7**

23.6 Entrance to marina and swimming area. Restrooms. **0.8**

24.4 Excellent exposure of the basal contact of the intracanyon lava at a small waterfall. **0.6**

25.0 Conspicuous landslide block to the right. Also note the shallow channel-filling nature of lavas exposed across the reservoir. **0.3**

25.3 Interesting ash-flow tuff deposit with round cobbles and boulders enclosed in its base. Clearly this tuff flowed along an old stream

drainage, probably the ancestral Crooked or Deschutes. **0.4**

25.7 Crooked Arm Bridge. **0.3**

26.0 Rough road over active landslide. **0.9**

26.9 The Ship. The upper ash-flow tuff exposed here is the Cove Ignimbrite (Smith, 1986). **0.3**

27.2 Entrance to Deschutes Campground. It and the nearby marina are built on a large landslide. **1.5**

28.7 Deschutes Arm Bridge. **0.3**

29.0 Pull carefully off onto left shoulder opposite road cut in basaltic lava.

Stop 9. Primitive Deschutes Formation Basalt on Deschutes Arm Grade

The basalt (96-79) exposed here is notable for several features that are common to primitive basalt in the Deschutes Fm. Note the physical evidence for fluid emplacement in the form of pahoehoe lobes, which suggest this was very dry and hot magma. Petrologic evidence from similar basalt also supports the interpretation that the magmas were dry (Conrey and others, 1997). Also note the conspicuous vesicle pipes, cylinders, and sheets, all apparently related to late mobilization of gas-rich melt or fluid near the end of crystallization of the basalt. Vesicle cylinders especially are ubiquitous in low-K basalt in the Deschutes Fm and are generally lacking in other basalt types. The lava was able to raft small bodies of sediment, perhaps by invading unconsolidated low-density material.

Other features of interest here are the well-exposed basal contacts of the intracanyon lava benches and a younger normally-polarized intracanyon basalt upstream in the Deschutes drainage. Those with an interest in sediment can walk up the grade to examine continuous exposures of varied fluvial and volcaniclastic beds in the Deschutes Fm. This sediment is part of the arc-adjacent alluvial-fan facies of the formation described in detail in the earlier field guide by Smith (1991).

Resume travel up the grade. **1.3**

30.3 Road climbs onto upper Canadian Bench Basalt mantled by minor sediment. This very extensive basalt (GR-236) sheet caps much of the western side of the Cove Palisades and can be traced toward its source nearly to the crest of Green Ridge (Conrey, 1985). The channels of the Crooked and Deschutes Rivers are controlled by the contact of this basalt with Tetherow Butte Basalt. **0.5**

30.8 Lake Chinook Village Store. Stay on main paved road. **1.0**

31.8 Straightaway offers good view of Squawback Ridge left ahead. **0.4**

32.2 Right-angle right turn—stay on pavement. **0.6**

32.8 Cross contact with Fly Lake Basalt, which overlies Canadian Bench Basalt and can also be traced almost to the crest of Green Ridge (Conrey, 1985). The Fly Lake has prominent glomerocrysts of plagioclase and olivine, and it thus is easy to map against the very sparsely porphyritic Canadian Bench Basalt. The road is on Fly Lake Basalt from here to Fly Creek grade. **0.4**

33.2 Right-angle left turn—stay on paved road. **1.2**

34.4 Road changes to gravel after Three Rivers housing development. **3.6**

38.0 Around paved right turn is an excellent exposure of Fly Lake Basalt (GR-208-2) atop baked paleosol and fluviatile sediment. To the left across Fly Creek is a section of Deschutes Fm lava, ash-flow tuff, and sediment. The tonguelike lava outcrop is due to topographic inversion of hard lava that originally filled an east-flowing drainage. Fly Creek cuts NE across the E-trending grain of the Deschutes Fm deposits due to diversion of originally eastward drainage by construction of the two Squawback shield volcanoes. **0.3**

38.3 Top of Six Creek Tuff. **0.2**

38.5 Basal contact of Six Creek Tuff. Pull carefully onto the left shoulder.

Stop 10. Six Creek Tuff and the Deschutes Formation on Fly Creek Grade

The informally named **Six Creek Tuff** exposed here has excellent exposures in that drainage (Conrey, 1985). The tuff was emplaced in an east-trending paleochannel (Fig. 9), as was virtually all of the lava that over- and underlies the tuff (Conrey, 1985). The total thickness here is approx 25 m, and the base is well exposed. The tuff thickens westward and is nearly 100 m thick on the west flank of Green Ridge. The tuff comprises several flow units; lag deposits with <2 m boulders are found between flow units in the west-flank exposure. The tuff is bimodal in

composition (Aubin, 2000), with black, Fe-rich andesite scoria (98-136) and white, rhyodacite pumice (GR-13). The scoria and pumice clasts display mineralogic, bulk geochemical, and isotopic evidence for incomplete mixing of magmas, either shortly before or during eruption (Aubin, 2000). Aubin (2000) reports a plagioclase Ar-Ar age of 5.38 ± 0.06 Ma from this tuff. Aubin (2000) demonstrated a systematic decline upward in large ion lithophile element concentration in the silicic end-members of the tuffs exposed at Green Ridge; the Six Creek Tuff is the most LIL-poor of the six ash flows studied.

At **Fly Creek**, the character of the Deschutes Fm differs from that seen in the Cove Palisades. The formation is no longer sediment-dominated, but contains abundant ash-flow tuff (five separate tuffs crop out on the Fly Creek Grade) and several basaltic and Fe-rich intermediate lava flows. The change reflects the fact that Fly Creek is nearly 15 km closer to the source for these deposits. From here west the formation becomes progressively more lava-dominated. A slowdown in the deposition rate of the upper part of the Deschutes Fm is thought to be responsible for the development of paleosols on interfluves above the Six Creek Tuff horizon (Smith and others, 1987; Smith, 1991; Dill, 1992). The sudden onset of paleosol development is thought to reflect the onset of graben subsidence, with interfluves becoming sediment-starved due to foundering of the source area (Smith and others, 1987).

Resume travel down Fly Creek Grade. **0.1**

38.6 Unnamed silicic ash-flow tuff in road cut has been found on the west flank of Green Ridge approx 15 km due west of here (R.M. Conrey, unpub data). **0.2**

38.8 Road cut in dacitic Meadow Creek Tuff of Aubin (2000). This tuff is widespread but poorly exposed on the east flank of Green Ridge as far east as Fly Creek. It may be correlative with the chemically similar, but more highly welded, Candle Creek Tuff, which is found on the west flank of Green Ridge approx 14 km west of here. **0.3**

39.1 Road cut in Fly Creek Tuff (Conrey, 1985; Smith, 1986; Aubin, 2000). See next stop. **0.3**

39.4 Road cuts in Balanced Rocks Tuff of Smith (1986) and Aubin (2000). See next stop.

39.9 Airfall tephra in road cut. **0.4**

40.3 Basalt of Big Canyon (Smith, 1986; Dill, 1992) crops out on both sides of Fly Creek. This basalt can be traced from just west of Fly Creek east to the outskirts of Madras, a distance of some 23 km. **0.5**

40.8 Pavement ends at outcrop of welded Fly Creek Tuff. **0.2**

41.0 Road 1170 junction—continue straight ahead. **0.1**

41.1 At end of road cut turn R on dirt road and stay left at Y junctions. **0.2**

41.3 Balanced Rocks overlook.

Stop 11. Balanced Rocks

The Balanced Rocks comprise caps of resistant, welded Fly Creek Tuff on eroded pillars of unwelded Balanced Rocks Tuff. Speculation as to their origin and stability will no doubt be rife among even a small group of geologists. The view includes the now familiar Mt Jefferson, the northern end of Green Ridge, and Olallie Butte. Some idea of the large amount of post-Deschutes Fm incision can be gained from noting that the conspicuous elongate ridge to the southwest (Gunsight Ridge—see mileage 43.2 below) is underlain by lava overlying cobble conglomerate. The paleodrainage was clearly at a much higher altitude than the modern streams. Also notable from here are intracanyon benches of Matuyama-age basalt in the Metolius River Valley. This lava originated within the graben and flowed along the Metolius Valley around the northern end of Green Ridge. Its upstream equivalent is visible from the next stop and has been found in the Abbot Butte corehole (Stop 12; Table 3). Some interesting volcaniclastic sediment, including a layer with abundant accretionary lapilli, intervenes between the two tuffs.

Balanced Rocks Tuff

The Balanced Rocks Tuff comprises multiple flow units in a single cooling unit (Smith, 1986; Aubin, 2000; Hoodoo Tuff of Conrey, 1985). The distribution of the tuff is not as well defined as that of the Six Creek Tuff, due to burial by younger Deschutes Fm deposits, but the source was undoubtedly from the west, as suggested by its east-elongate outcrop pattern (Fig. 9). The tuff contains abundant mixed and banded

pumice clasts; one notable variety has small (< 1 cm) blobs of pale silicic glass within dark intermediate glass. Some pumice is banded on a micrometer scale, whereas other pumice has coarser bands. The mineralogy and bulk pumice chemistry support a petrogenetic interpretation involving incomplete mixing of two diverse magmas (Aubin, 2000). The Balanced Rocks Tuff is the richest in LIL-element concentration of the tuffs studied by Aubin (2000). Rare partially melted fragments of granite and potassically altered tuff are found in the Balanced Rocks Tuff (R.M. Conrey, unpub. data; Conrey, 1985, mistakenly termed these granulites). The fragments are similar in their bulk chemistry to potassically altered rock encountered at the deepest level of the 3 km deep Sunedco drill hole near Breitenbush Hot Springs (Priest and others, 1987; Conrey and Sherrod, 1988; R.M. Conrey, unpub data). This correspondence suggests that the magma chamber that fed the Balanced Rocks Tuff may have been at very shallow depth (< 3 km). Aubin reports a plagioclase Ar-Ar age of 5.56 ± 0.06 Ma for the tuff. The near equivalence of this age with the Six Creek Tuff age suggests that the middle and upper parts of the Deschutes Fm may have been very rapidly deposited, as suggested also by Smith (1991).

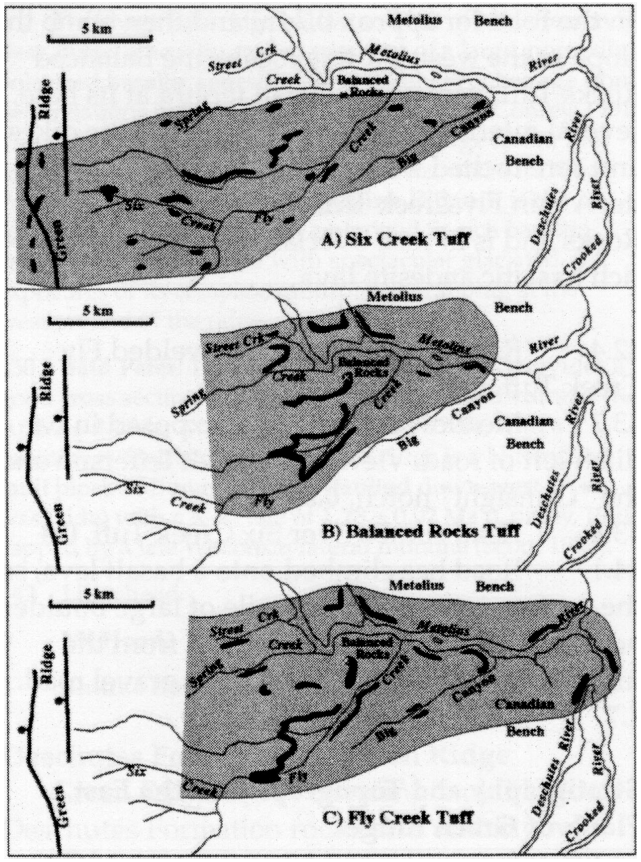

Fig. 9. Distribution of three Deschutes Fm ash-flow tuffs at Green Ridge (adapted from Smith, 1986, with additions by R.M. Conrey). Black pattern indicates outcrop; gray pattern is inferred extent. See Stops 10 and 11 for tuff descriptions. Note that all of the tuffs have similar east-elongate distributions, which suggests that the source volcanoes were all west of Green Ridge. Virtually all of the lava and tuff at Green Ridge flowed down an east-trending paleodrainage (Conrey, 1985).

Fly Creek Tuff

The typically welded Fly Creek Tuff is notable for its large rhyolitic pumice fragments (GR-380), evident in this exposure. The upper, less welded part of the tuff (eroded off here) contains abundant basaltic andesite scoria in addition to the pumice, and thus complete exposures resemble the classic silicic to mafic zonation seen in many ash-flow tuffs. The distribution of the Fly Creek Tuff is consistent with its derivation from a source west of Green Ridge (Fig. 9). Study of the geochemical variation in the tuff has shown that the rhyolite pumice is homogeneous, but the mafic scoria is quite variable, with a range from less evolved and P-poor (GR-427-7) to more fractionated and P-rich (GR-699; Aubin, 2000). The P-rich scoria has elevated middle rare-earth element concentrations, consistent with a genesis involving the resorption of approx 2% apatite at some point in its evolution (Aubin, 2000).

Return to Metolius River Rd. **0.2**

41.5 Turn L on Metolius River Rd. **0.1**

41.6 Turn R on road 1170 at end of cut. **0.1**

41.7 Road descends over welded Fly Creek Tuff. **0.2**

41.9 Junction with side road to left (**recommended side trip**)—stay on 1170. **0.5**

Side Trip to Balanced Rocks Tuff above Fly Creek Ranch Site

Excellent exposures of the Balanced Rocks Tuff are accessible by following this side road for approx 0.5 mi and parking near the site of the old Fly Creek Ranch. From there walk south

on the road for approx 0.2 mi and then climb the slope to the west. At this locale, the Balanced Rocks Tuff displays an airfall tephra at its base, several internal flow-unit contacts, clastic dikes, and rare melted wall-rock fragments and granite. A thin Fly Creek Tuff overlies the Balanced Rocks and is in turn overlain by an aphyric, Fe-rich basaltic andesite lava.

42.4 Road climbs back onto welded Fly Creek Tuff. **0.8**
43.2 Meadow Creek Tuff is exposed in bar ditch left of road. View right of Mt Jefferson and the "Gunsight" notch. **0.6**
43.8 Road climbs over Six Creek Tuff. **0.3**
44.1 Road has climbed onto a basalt lava, so the surface is now flat. The pile of large boulders near the road junction are derived from the underlying flow. Stay on the main gravel road. **1.7**

Stratigraphy and Topography on the East Flank of Green Ridge

West from mileage 44.1 to the crest of Green Ridge the road climbs onto a thickening stack of Deschutes Fm lavas. Short, steep gradients represent flow fronts or margins, whereas longer flats are flow-top surfaces. Erosion of these originally eastward-flowing lavas has resulted in an east-trending "ribbed" topography, and the "ribs" are underlain by harder lavas. The topography thus serves as a handy mapping tool, and so long as the adjacent lavas are easily distinguished, mapping is easy in this terrain.

45.8 Bear L at junction. Squawback Ridge visible to left. **0.7**
46.5 Straight at junction with Road 11. Road number changes to 1180. **0.7**
47.2 Note the stepped straightaway ahead where the road climbs over lava flow fronts. **0.7**
47.9 Now flat again on a flow surface. **1.2**
49.1 Stay right at junction. **0.1**
49.2 Bear left at junction and stay on Road 1180. **0.7**
49.9 Straight at junction with Road 1150. Road changes number again—now 1140. **1.0**
50.9 Bear left at junction with Road 1149. **0.5**
51.4 Bear right on red-cindered road 1490 at 1140–1490 junction. A **recommended side trip** left on Road 1140 leads to some of the more interesting Deschutes Fm lavas on Green Ridge. **0.1**

Side Trip to Mixed and Megacryst-bearing Lavas on Green Ridge

From the junction at mileage 51.4 bear L (south) on Road 1140 for 1.4 mi to a junction. Turn R, and in another 0.2 mi turn L at next junction to stay on 1140. An additional 0.2 mi leads to a low mound of float on the left. The float is of spectacularly mixed andesite, with two distinct populations of plagioclase (heavily resorbed An30-40, and clear An80-85; Conrey, 1985; R.M. Conrey, unpub data) and overgrowths of clinopyroxene on corroded hypersthene. From this location another 1.9 mi south along Road 1140 leads to a sharp left turn with outcrop and float of basaltic andesite lava bearing large resorbed crystals of andesine, and rare resorbed ilmenite and aluminous orthopyroxene (megacryst lava of Conrey, 1985; R.M. Conrey, unpub data).

51.5 Bear right at junction to stay on Road 1490. **0.4**
51.9 Crest of Green Ridge. **0.7**
52.6 Stop at second hairpin corner.

Stop 12. Eastern Graben Margin on Green Ridge

The view west from here toward the crest of the High Cascades, and south along the Green Ridge Escarpment, is a dramatic illustration of the results of intra-arc rifting. From here many volcanic features are evident at listed azimuths:

197 **Three Sisters.**

201 **Black Crater.**

212 **Belknap Crater**: Holocene mafic shield volcano (BKP-5). Belknap's age is probably best indicated by a new accelerator mass spectrometer ^{14}C age of 2635 ± 50 yr (Licciardi and others 1999). A prior sample from the same location suggested a much younger age, ca. 1800 yr BP, as did samples from the western margin of the Belknap lava field (Taylor, 1965). Presumably the earlier samples were contaminated with younger carbon, a common difficulty in ^{14}C dating. Early erupted basaltic lavas spread over 12 km west of the cone, and over 9 km eastward. Later basaltic andesite was erupted from the central crater and several flank vents.

217 **Mount Washington.**

The **Wizard Ridge Horst** (informal name) is visible in the middle ground west of the Metolius River in front of Mt Washington and Black Crater. On the NE side of the horst toward you is a flat bench of reversely polarized Matuyama-age basaltic lava (dated 3 km to the N at 1.6 ± 0.3 Ma; Armstrong and others, 1975), lava (97-267, MJ-CC5

and 6, see Table 3), and coarse sediment. Similar lava forms intracanyon benches downstream along the Metolius River nearly to its junction with the Deschutes River (seen at Stop 11; from here if you look north along the Metolius, most of the visible outcrop west of the river is made of these benches). On the W and NW side of the horst is a **3 km long chain of four Brunhes-age basaltic cinder cones** presumably overlying a N15W dike (and fault); the lavas (97-294) drape the horst and the Matuyama-age bench. The northernmost cone is on line with Three Fingered Jack.

230 **Hayrick Butte.**

245 **Three Fingered Jack.**

270 **Abbot Butte**: Low forested andesite dome (CC-16) in middle ground with broad ridges of dacite lava (97-269) extending to the SE. Normally polarized, plagioclase-rich intermediate lava overlies a small flow of basaltic andesite (97-271). Linear chemical variations with SiO_2 for all elements, and presence of olivine and quenched mafic inclusions, suggest an origin via magma mixing. The basaltic andesite lava seems to be plagioclase accumulative (~22 wt% Al_2O_3), and all of the lavas contain conspicuous plagioclase-olivine glomerocrysts. A geothermal core hole (Unocal 82-3) was spudded 3 km due S of Abbot Butte (see below).

276 **South Cinder Peak.**

291 **North Cinder Peak**: Prominent cliff (with cindery slopes on its southern side) underlying the peak is the glacially eroded and exposed crater fill or plug of a small Sr-rich basaltic andesite (ML-19, ML-29) shield volcano. Concentrations of Sr and incompatible elements decline up section in the volcano, whilst SiO_2 increases slightly. The geochemical, isotopic, and petrographic evidence suggest Sr-rich basaltic andesite was mixed with shoshonite to generate the range of compositions found in the lavas (Conrey and others, 2001b).

293 **Forked Butte**: Large basaltic andesite (CC-51) Holocene cinder cone that fed multiple lavas. Age is believed to be ca. 6400 ^{14}C yr based on interpolation of sedimentation rates in Cabot Lake (Scott, 1977). The obvious Holocene lava (south of the south ridge of Bald Peter) is from an **unnamed breached cinder cone** between Bear Butte and Sugarpine Ridge (see below) that is barely visible from here (it often has a small snow patch on it that persists late in the year). The lava from that cone is similar in composition to the final erupted Forked Butte lava (Conrey, 1991).

305 **Goat Peak**: A rhyodacite dome (MJ-354) on the south flank of Mt Jefferson.

313 **Mt Jefferson**: Recent $^{40}Ar/^{39}Ar$ analyses of plagioclase separates has indicated a 20.5 ± 5 ka age for lava comprising the uppermost part of the cone visible above the prominent Whitewater Glacier. A dome complex on the north flank of the mountain draped by the summit lava has an age of 28 ± 8 ka (M.A. Lanphere and R.M. Conrey, unpub. data). These ages are both "late Wisconsin", and consistent with physical evidence (steep, glassy flow margins, and finger-like distribution of tongues of multiple lava flows) suggesting the volcano was encased in ice during its last major eruptive period (Conrey, 1991).

The sharp bare ridge below and left of Mt Jefferson is **Bear Butte**, a heavily eroded remnant of a large, normally polarized basaltic andesite shield (likely Brunhes age from field relations but K-Ar age is 2.46 ± 0.26 Ma; Conrey, 1991). The broad ridge with many dead trees (large recent fire) south of Bear Butte (and between the azimuths for Goat Peak and Forked Butte) is **Sugarpine Ridge**. It is the remnant of a large, normally polarized Sr-rich basaltic andesite (ML-122) shield with spectacular glaciated exposures of its complex, multiple central plug at the western end of the ridge.

330 **Bald Peter**: The steep, faulted west flank provides a good cross section of a basaltic andesite shield volcano (K-Ar 2.2 ± 0.2 Ma; Armstrong and others 1975), with a prominent central plug. The south ridge is a N-trending fault block of E-trending lava (faulted down-west on its west side) with a K-Ar age of 1.28 ± 0.02 Ma (Conrey, 1991), capped by a late Wisconsin lateral moraine (Scott, 1977).

342 **Lionshead.**

0 **Mt Hood.**

3 **Shitike Butte.**

Deschutes Formation at Green Ridge

Green Ridge is a N-trending fault block of Deschutes Formation rocks and underlying amphibole-bearing andesite of the approx 8 Ma Castle Rocks Volcano (Armstrong and others, 1975; Wendland, 1988). That volcano is exposed only at the northernmost end of the ridge. The exposed Deschutes Fm section at Green Ridge is at least 500 m thick, and consists predominantly of diverse lavas, with a significant number of interbedded ash-flow tuffs, and minor, poorly exposed sediment (Conrey, 1985). Diverse lavas at Green Ridge include basalt, low-K tholeiite, basaltic andesite and andesite (both including Fe-rich varieties), rare dacite, and one rhyodacite (Conrey, 1985). Six of the ash-flow tuffs have been examined in detail (Aubin, 2000). Ar-Ar ages near the base and top of the exposed section are 7.27 ± 0.08 Ma and 5.27 ± 0.04 Ma, respectively (Smith, 1986). The base of the formation is not exposed, but presumably is not far beneath the oldest dated horizon. Approximately 200 mapped lavas and tuffs are known at Green Ridge (Conrey, 1985), all of which seem to have originally flowed down east-trending paleodrainages. The Deschutes Fm can be traced from Green Ridge eastward into the Deschutes Basin at the Cove Palisades some 30 km, where it is predominantly sediment, not lava, but still several hundred meters thick (Stops 8 and 9). The bulk of the Deschutes Fm at Green Ridge was derived from sources west of

the ridge, as shown by the facies change within the formation, and by mapping dozens of lavas and tuffs up their paleoslopes back to the west (Conrey, 1985). Some idea of the decline in eruption rates from Deschutes to Brunhes time can be gained by considering that the Brunhes-age High Cascade wedge does not uniformly reach even to the Metolius River, whereas the Deschutes Fm wedge extends some 30 km east of the Metolius. The Deschutes Fm is also much more voluminous than the other rift-related sequences northward along the arc.

The emplacement of the Deschutes Fm clearly required high eruption rates for over 2 million years. There was unlikely to have been any significant normal faulting during the rapid aggradation of over 500 meters of section. The first sign of faulting was the development of thick soil profiles on interfluves, found in the uppermost Deschutes Fm section in the Deschutes Basin (Smith and others, 1987). The soil development reflects sediment starvation, probably related to the onset of normal faulting that ponded earlier drainage (and perhaps to declining eruption rates as well; it may have been a coupled effect). Faulting seems to have begun about 5.3 Ma (Smith and others, 1987). There may well have been extension during the period of aggradation, but if so, it was taken up either by ductile faulting, with no brittle surface expression, or by diking. The latter could have resulted in several kilometers of extension. Consider the number of eruptions evidenced at Green Ridge, and the similar number of their west-side ridge-cap cousins. Both Green Ridge and the west-side ridge caps are some 15 km from the presumed arc axis at 5-8 Ma (assumed coincident with the modern axis), so their sections only record the larger, farther traveled, volcanic materials of the older arc. All told, therefore, thousands of eruptions took place along a short span of the arc from 5-8 Ma. If each was fed by a dike only 2 meters wide, then the total extension from diking could have been on the order of 2-3 km. A decline in eruption rate toward the end of Deschutes time may have led to the onset of brittle faulting, due to the inability of diking to keep pace with extension.

Abbot Butte Core Hole and Evidence for Graben-within-graben Faulting Style

The Abbot Butte drill hole (Unocal 82-3) provides some constraints on the offset history of the eastern graben margin. The core intercepted chiefly basaltic lava interbedded with coarse- and fine-grained sediment, probably including a significant component of glacial outwash in the upper part of the hole. K-Ar ages of the core are 1.35 ± 0.07 Ma at 1240 ft and 1.49 ± 0.06 Ma at 1741 ft (Priest, 1990). The latter sample is of slightly altered rock, and the age is likely a bit too young. The former age is of very fresh material and has the best yield of radiogenic Ar, so is probably the more reliable. The Brunhes–Matuyama boundary is at a downhole depth of about 200 m. Basalt in the core hole is compositionally and petrographically similar to basalt exposed in a reversely polarized, Matuyama-age bench (1.6 ± 0.3 Ma; Armstrong and others, 1975) west of the Metolius River (Table 3). Similar benches are found along the Metolius Valley for a considerable distance downstream and are visible from Stop 11. These correlations suggest significant offset of Matuyama-age rocks and a graben-within-graben structural style (Fig. 10) mirroring the same style on the west side of the graben.

Evolution of the Mt Jefferson Area with Time

Long-term changes in the composition of intermediate and silicic rocks are evident in the Mt Jefferson area based on detailed mapping and sampling there. As noted in the Introduction, silicic centers in the Cascades seem to be very long-lived features. The area surrounding Mt Jefferson has been a locus of intermediate and silicic volcanism for the past 4 to 5 million years and was likely a locus during the deposition of the Deschutes Fm (and equivalent ridge caps west of the Cascade crest) as far back as 7 Ma. Abundant silicic and intermediate rocks are found in the Deschutes Fm along the northern end of Green Ridge and north of there for several kilometers, exposed in canyons on the Warm Springs Indian Reservation. Such rocks are absent on the south end of Green Ridge, which suggests a major silicic center in the vicinity of Mt Jefferson during Deschutes Fm time. Northwest of Mt Jefferson about 7 km, several domes and near-vent airfall deposits are exposed in and around the area of Crag Creek. One of the uppermost lavas in that area has been dated at 3.95 ± 0.05 Ma (Conrey, 1991). Northeast of the mountain, the Gauss-age center around Lionshead has been described above.

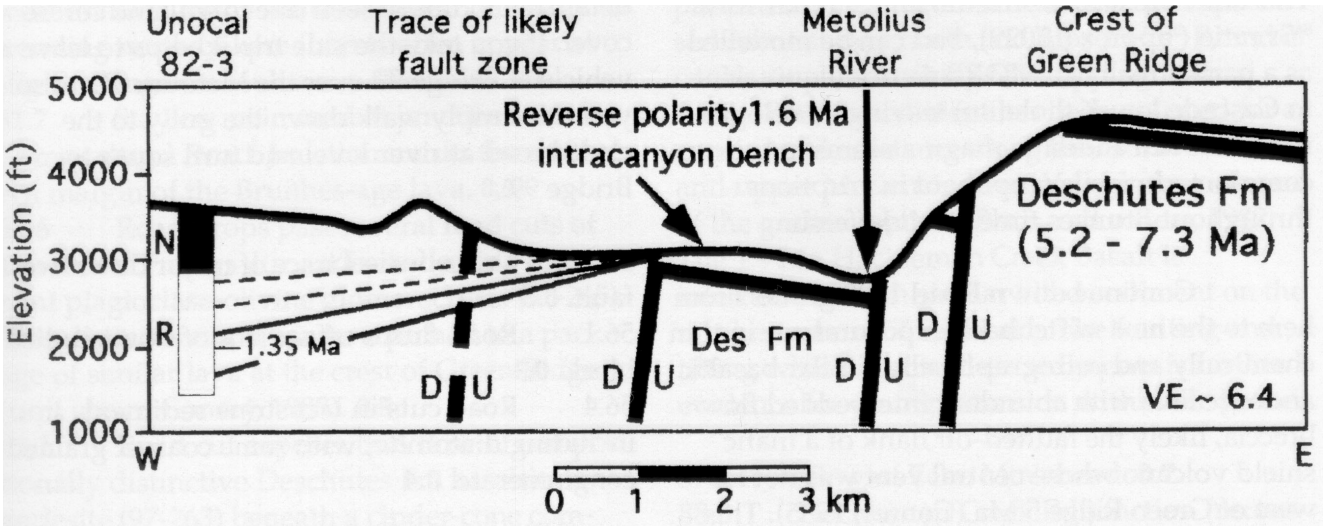

Figure. 10. Cross section across the Green Ridge Fault Zone to Abbot Butte (Unocal 82-3) core hole (Conrey and Sherrod, in prep.). Deschutes Fm rocks are downdropped by two major faults east of the Metolius River and one buried fault west of the northward strike extension of Wizard Ridge. The latter must have a very large offset because the Deschutes Fm is completely buried west of that fault. The Deschutes rocks must be downdropped a total of approx 3 km to satisfy the constraints provided by the Abbot Butte core hole. Correlation of Matuyama-age lavas in the core hole with surface exposures in a reversely-polarized intracanyon bench (Table 3) implies maximum offset on the order of 300-500 m of 1.0-1.5 Ma age rocks, depending on the paleoslope (here assumed equivalent to the present one; a lower gradient paleoslope would imply lower total offset). This offset likely occurred on a fault that coincides on strike to the north with the faulted off south ridge of Bald Peter. The largest offset fault that downdrops the Deschutes rocks could have only offset Matuyama-age rocks a small amount, as such rocks are present west of that fault. The zone of active faulting apparently has moved inward since the downfaulting of the Deschutes Fm; thus the structural style is a Quaternary graben within a Pliocene graben.

There is a systematic decline in the concentration of incompatible elements with time, consistent with declining mid(?)-crustal temperature. In other words, the temperature was likely higher during intra-arc rifting, and it seems to have declined as the extension rate dropped backed to much lower values. The decline of incompatible-element concentration is coupled to a rise in the modal proportions of amphibole in silicic rocks. Amphibole phenocrysts are virtually absent in Crag Creek (and Deschutes Fm) rocks, sparse in Lionshead rocks, and common in Mt Jefferson rocks.

Middle and Deep Crustal Melting Beneath Mt Jefferson—A Legacy of Rifting

Melting models for silicic magma at Mt Jefferson during Brunhes time suggest that the magma source is a midcrustal amphibolite with a bulk composition similar to that of average Cascade basalt (Conrey and others, 2001b). The low Y and heavy rare-earth element contents of Brunhes-age rhyodacite (MJ-556) at Mt Jefferson require amphibole-bearing residues. Rhyodacite is rather uniform in its Sr isotopic character with initial $^{87}Sr/^{86}Sr$ ratios of approx 0.7033. According to the geophysical model of the Cascades proposed by Stanley and others (1990), such rhyodacite could be generated at a depth of 25-30 km, where crustal temperature is on the order of 850-900°C. The geophysical model includes a lower, chiefly underplated mafic granulite crust at a temperature of 1000-1100°C. Intra-arc rifting probably played a major role in the development of the hot mafic underplate. Sr-rich (800-1200 ppm) andesite (MJ-696) at Mt Jefferson may have resulted from partial melting of mafic granulite at 1050 °C (Conrey and others, 2001b).

This andesite has a nonradiogenic initial $^{87}Sr/^{86}Sr$ ratio (approx 0.7029), and can be modelled as a partial melt of a MORB source (equivalent to Cascade low-K tholeiite) leaving an eclogite residue. Such andesitic magma seems to be a common admixed component in eruptions throughout Brunhes time at Mt Jefferson.

Continue down Road 1490 grade. From here to the next switchback exposures are in thin chemically and petrographically similar basaltic andesite lava with abundant interbedded flow breccia, likely the faulted-off flank of a mafic shield volcano whose central vent was not far west of Green Ridge 5 Ma (Conrey, 1985). This lava overlies the Candle Creek Tuff and is downfaulted and exposed below the road at mileage 55.4. **1.2**

53.8 View of northern end of Green Ridge, underlain by the large Castle Rocks andesitic complex (Wendland, 1988), and in part overlain by lava of the Deschutes Fm. The Deschutes lava includes a locally palagonitized alkaline basaltic andesite. **0.4**

54.2 Switchback with road cut in Deschutes Fm low-K tholeiitic basalt (GR-520). **1.0**

55.2 Pumice (98-225) washing out of road cuts here is from Mt Jefferson. Of two pumices here, the main amphibole-phyric one is correlative with an extensive air-fall pumice whose main dispersion axis was nearly due east of Mt Jefferson, and which has been found as far east as Arco, Idaho (Smith, 1986; Walder and others, 1999). **0.2**

55.4 Just after "DIP" sign, cross gully cleaned out by debris flow during the winter of 1995-96. **Recommended side trip. 0.1**

100 Percent Exposure of Candle Creek Tuff and Flanking Normal Faults

The debris flow in this gully started at the base of the thick, informally named Candle Creek Ash-flow Tuff (Aubin, 2000), 100 m higher than the road, and scoured the gully clean below the road. Exposures below the road include downfaulted Candle Creek Tuff and over- and underlying packages of basaltic andesite. In addition, two normal faults, which lack topographic expression and were thus unexpected, are exposed flanking the Candle Creek Tuff. The presence of these minor faults suggests that the graben-bounding fault zones are complex in detail, detail rarely seen due to soil and forest cover. If you take the side trip it helps to leave a vehicle at Bridge 99 over the Metolius River so you can simply walk down the gully to the closed road at river level and turn south to Bridge 99.

55.5 Cross buried trace of major down-west fault. **0.6**

56.1 Road drops off surface of downfaulted block. **0.3**

56.4 Road cuts in lacustrine sediment, including diatomite, with some coarser grained conglomerate. **0.4**

East-tilted Pliocene Sediment on Flank of Green Ridge

The sediment exposed at mileage 56.4 tilts eastward 8-10° toward a major fault only a few hundred meters to the east. The sediment overlies downdropped Deschutes Fm lava and was likely formed due to ponding of east-flowing drainage during the development of a north-trending fault scarp. Similar east-tilted sediment (dips to 20°) is known at the foot of Green Ridge where Jack Creek empties into the Metolius River (Smith, 1986). Diatoms in this sediment are of Pliocene age (J.P. Bradbury, in Smith, 1986).

56.8 The road cut is in platy-jointed, aphyric, Fe-rich andesite (98-222) in a downfaulted block of the Deschutes Fm The lava can be matched compositionally to a lava at the crest of Green Ridge 1.5 km to the east. The fault block has dropped approx 500 m along a major N-trending fault 400 m east of this outcrop. **0.6**

57.4 Turn R on Metolius River Road. **2.3**

59.7 Road on right to Wizard Falls and fish hatchery. Wizard Falls formed at the northern toe of a primitive Brunhes-age lava. **0.9**

60.6 Northern margin of the young olivine-bearing, primitive calc-alkaline basaltic lava (GR-773; Conrey and others, 1997). This lava emerged from a cinder cone overlying a fault on the flank of Green Ridge about 1.5 km SE of here. The road traverses the nearly flat flow surface for the next 0.25 mi. To the right is Wizard Ridge, a horst of Deschutes Fm lava. The horst is at a slight change in direction of the Green Ridge Fault Zone, from a few degrees

west of north to the south of here to virtually N-trending north of here (horsts often appear at slight changes in fault zone direction). **1.1**
61.7 Stay on main road at junction with Campground Road. Junction marks the southern margin of the Brunhes-age lava. **0.9**
62.6 Road drops past several road cuts of Deschutes Fm basaltic andesite bearing prominent plagioclase-olivine glomerocrysts (97-265). This distinctive unit can be matched to a package of similar lava at the crest of Green Ridge (unit gba of Conrey, 1985). **0.5**
63.1 Road cut exposes thin flow of compositionally distinctive Deschutes Fm basaltic andesite (97-263) beneath a cinder-cone complex. Lava with identical composition and petrography (sparse, small plag-oliv glomerocrysts) lies at the crest of Green Ridge 3 km to the east and also at the top of another fault block 1.5 km to the east (Mark Ferns and R.M. Conrey, unpub. data). The total fault offset across at least two major faults here is approximately 600 m. **0.5**
63.6 Cinder-cone complex in road cut. View of Three Fingered Jack to right and Black Butte ahead. The cinder complex (block 97-262) overlies downfaulted lava that can be matched with 5 Ma Deschutes Fm lava at the crest of Green Ridge to the east. It likely formed during the initiation of faulting along the Green Ridge Fault Zone. **0.4**
64.0 Turn R at Camp Sherman junction. **0.1**
64.1 Turn L at T. **0.3**
64.3 Bear R over bridge spanning Metolius River in colorful downtown Camp Sherman. **0.5**
64.8 Proceed straight through junction onto gravel Road 1216. **3.3**
68.1 Turn L onto paved Jack Lake Rd. **1.0**
69.1 Turn R at junction with Hwy 20 and retrace your route west over Santiam Pass. **13.2**
82.3 Bear L onto Hwy 20/126 at Santiam Junction. **3.4**
85.7 Stay straight on Hwy 20 at Hwy 20/126 junction. **0.2**
85.9 Sediment on R. **0.4**
86.3 Lava Lake Rd. junction (**recommended side trip**). **1.3**

Tilted and Faulted Sediment along Lava Lake Road

Tilted and faulted sediment can be examined in a road cut 1.4 mi up this road (stay R on pavement at Y junction at 1.0 mi). The exposed sediment strikes north and dips 15-20° E, and is cut by small N-striking 65E-dipping normal faults. Similar sediment has been mapped for a considerable distance along the North Santiam and upper McKenzie River Valleys, just inboard of the graben margin (Black and others, 1987). The 1.9 Ma Hackleman Creek Basalt is interbedded with similar tilted sediment on the northern shore of Fish Lake. The faulting and tilting which affects these sediments is further evidence for young extension within the graben.

87.6 View of Echo Mtn ahead. **0.7**
88.3 Hackleman Creek Rd junction (**recommended side trip**). **0.4**

Porphyritic Hackleman Creek Basalt

The very porphyritic, 1.9 Ma basalt (Table 3) along the shores of Fish Lake and in the EWEB 1 drill hole can be seen in a road cut 1.1 mi up this road. At 0.35 mi stay on main road; at 0.6 mi bear L at Y; at 0.7 mi bear R at junction.

88.7 Browder Ridge ahead. **0.6**
89.3 Junction with gravel Forest Service Rd 2065 marks the axis of a major fault zone (Avramenko, 1981) that separates steeply and gently east-dipping sections. **0.6**
89.9 Lost Prairie Campground entrance. Browder Ridge to left. **2.1**
92.0 Iron Mtn visible ahead. **1.6**
93.6 Tombstone Pass. **0.6**
94.2 Deer Creek Rd junction. Leads to trailhead for Iron Mtn Lookout (**recommended side trip**). **1.1**

Side Trip to Iron Mountain Lookout

The Iron Mtn Lookout Trail offers exposures of near-vent mafic ridge-cap lavas and a fine view. In the early summer this is a wonderful place for wildflowers, some quite rare.

95.3 Sign “Slides Next 7 Miles”. Landslides are common in the Western Cascades due to the prevalence of clay in altered and weathered, originally glass-bearing rocks. **1.0**
96.3 Conspicuous altered green ash-flow tuff in road cut. **0.8**
97.1 Carefully pull off onto left shoulder.

Stop 13. Overview of Topographically Inverted

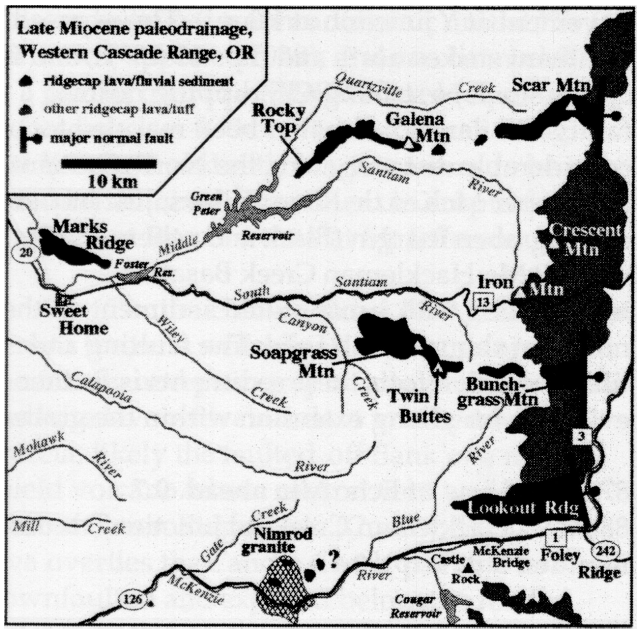

Figure. 11. Map of late Miocene (5-8 Ma) paleodrainage in the Western Cascades (Santiam drainages based on Walker and Duncan, 1989, and reconnaissance mapping by D.R. Sherrod and R.M. Conrey; McKenzie drainage from E.M. Taylor, in Priest and others, 1988). The ancestral course of the Middle Santiam River is marked by ridge-cap deposits between the modern river and Quartzville Creek. The ancestral South Santiam is marked by ridge-caps south of the modern drainage. The ancestral McKenzie drainage lay along Lookout Ridge; the distal end of the drainage is not known but may be marked by suspected ridge-capping mafic lava above Nimrod (Peck and others, 1964). The fault pat-tern is simplified close to the graben. Field trip stops 1, 3, and 13 shown by numbered squares.

Ancestral South Santiam River Channel

The view from here includes Squaw Mtn to the southeast and Twin Buttes to the southwest. The 5-8 Ma ridge-capping deposits of lava and fluvial sediment that compose those summits once filled the ancestral South Santiam River channel (Fig. 11). The cliffy Jumpoff Joe is composed of older rocks. The proximal deposits of both the South and Middle Santiam River paleochannels at Bunchgrass and Scar Mtns, respectively, were visible from Stop 5 (see Fig. 11).

Priest (1990) argued that the Western Cascades were uplifted in the early Pliocene during the tectonic events that created the High Cascade Graben. The uplift decreases westward away from the Cascades toward the Willamette River, which has served as a semistable base level at least since the middle Miocene. Recent work corroborates Priest's idea and quantifies the amount of uplift. A cross section of the Middle Santiam Paleodrainage (Fig. 12) suggests a broad zone of uplift, some 30 km wide, with uplift on the order of 700 m. Similar cross sections can be drawn through all the major rivers that traverse the Western Cascades. While we don't as yet recognize the downstream end of the ancestral McKenzie River, the upstream relationship at Lookout Mtn is similar to that of Galena Mtn and Scar Mtn. Thayer (1939) mapped the downstream end of an ancestral North Santiam River, and noted that it had a much higher gradient than the modern stream. The same relationship is found in the Clackamas River drainage and also along the Columbia River. Tolan and Beeson (1984) have long argued that the Cascades in the Columbia River Gorge were uplifted approximately 700 m during the late Pliocene or Quaternary. Estimates of uplift on the east flank of the graben are all much less

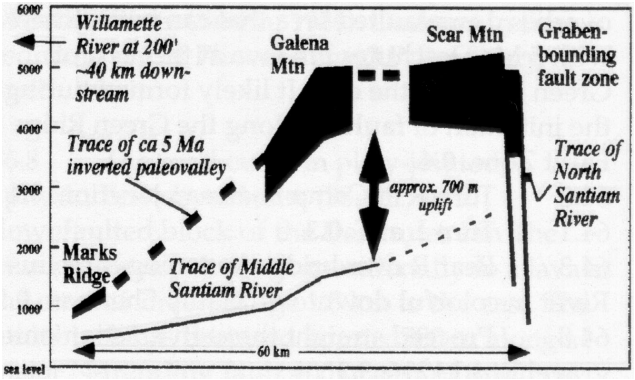

Figure. 12. Middle Santiam River cross section in the Western Cascade Range (Conrey and Sherrod, in prep). The ancestral river channel is defined by an inverted paleovalley that extends from Marks Ridge to Galena Mt (established through mapping and chemical and petrographic correlation; R.M. Conrey and D.R. Sherrod, unpub data). East from Galena Mtn discontinuous ridge-cap exposures of mafic lava and interbedded fluvial sediment extend to Scar Mtn The amount of uplift suggested is on the order of 700 m, if the base of the Scar Mtn sequence (presumably the paleovalley floor) is chosen as the reference datum. Note that the geometry suggests a broad zone of uplift extending some 30 km west of the graben margin.

than the west-side values. In addition, the crestal altitude of the western graben-flank escarpments are always higher (by more than 300 m) than the eastern flank scarps. For the same modern base levels, this suggests that significantly more uplift occurred on the west side of the rift.

Resume travel west on US 20. **1.8**
98.9 View left of Twin Buttes—Soapgrass Mtn ridge line just before sharp right curve. **1.6**
100.5 "Bump" sign—major landslide here. **2.4**
102.9 House Rock Campground junction. **1.9**
104.8 Upper Soda. **6.4**
111.2 Gordon Road junction. Sign indicates Twin Buttes Trail (**recommended side trip**). **4.7**

Twin Buttes Trail

Good exposures of ridge-capping basalt interbedded with cobble conglomerate can be seen from the Twin Buttes Trail. The trailhead can be reached from this junction in approx 14 mi by following Forest Service Rd 2032 (take R at junction of Gordon Rd with Rd 2032 in approx 1.5 mi).

115.9 Junction with road to Cascadia State Park (restrooms). **2.5**
118.4 Quarry. **0.8**
119.2 Outcrop dated at 25 Ma (Lux, 1982). **1.5**
120.7 Major curve. **2.0**
122.7 Major curve. **0.8**
123.5 Outcrop dated at 17 Ma (Lux, 1982). **0.3**
123.8 Outcrop dated at 24 Ma (Sutter, 1978). **0.5**
124.3 Quartzville Rd junction. **0.4**
124.7 Outcrop in deep road cut dated 25 or 18 Ma (Lux, 1982), take your pick. **1.4**
126.1 Foster Lake viewpoint (**optional stop**). From here the eastern end of Marks Ridge is visible to the NW. From Foster west to Sweet Home the right skyline is Marks Ridge. **4.5**

Marks Ridge—The Distal Ancestral Middle Santiam Channel Fill

Marks Ridge is a topographically inverted ridge-cap lava made of thick, glassy, and wildly fan-jointed basaltic andesite (94-92), underlain by cobble conglomerate (Karl Wozniak, personal commun., 2001). The lava has a K-Ar age of 4.5 ± 0.3 Ma (E.P. Verplanck, in Walker and Duncan, 1989). Exposures of Marks Ridge lava are easily accessible from the Pleasant Valley Rd junction at mileage 130.6. Turn R over the South Santiam River and proceed approx 5 mi on Ridgeway Rd to a conspicuous quarry (ignore turns onto Berlin Rd and North River Drive). Alternatively, turn L onto Berlin Rd and try to gain access to a quarry on the right after some 2 mi.

The Marks Ridge lava is chemically and petrographically similar to lava that caps Galena Mtn (94-91; Figs. 11 and 12). The obvious intracanyon-filling nature of both lavas supports the interpretation that they represent the same flow and thus define the course of the ancestral Middle Santiam River. Several additional flow packages have been physically traced from Galena Mtn to Rocky Top, thus demonstrating that west-trending paleodrainage passed beneath Galena Mtn (D.R. Sherrod and R.M. Conrey, 1994, unpub. mapping on private logging lands). A lava beneath the capping flow on Galena Mtn has a K-Ar age of 6.3 ± 0.1 Ma (E.P. Verplanck, in Walker and Duncan, 1989). That age is more consistent with other ridge-cap ages farther east; the Marks Ridge age is likely somewhat too young due to the presence of abundant groundmass glass, which is not a very tight Ar bottle.

130.6 Pleasant Valley Rd junction on western outskirts of Sweet Home. (**Recommended side trip to Marks Ridge**). **12.0**
142.6 First stoplight at Walmart on outskirts of Lebanon. **0.7**
143.3 Turn L on Airport Rd. **3.5**
146.8 Turn L on Hwy 34. End of Road Log. Proceed west to Corvallis.

ACKNOWLEDGMENTS

We acknowledge the assistance and knowledge of Peter Hooper; Charles Calica of the Tribal Council of the Confederated Tribes of Warm Springs; Larry Chitwood and Robert Jensen of the Deschutes National Forest; Ken Lite and Marshall Gannett of the U.S Geological Survey; George Priest, Gerry Black, Mark Ferns, and Neil Woller of the Oregon Department of Geology and Mineral Industries; Cynthia Gardner and Willie Scott of the Cascades Volcano Observatory; Mike Valentine; Karl Wozniak; and Dana Johnston, who invited us to write a 1-day field trip for the *Margins 2000* meeting in Eugene that forms the nucleus of this guide. Editorial comments by George Moore significantly improved our presentation.

Table 1. Selected X-ray Fluorescence Analyses[a] (Major Elements Wt% Oxide; Trace Elements ppm) of Cascade Range Rocks—Day 1

Unit	Sample[1]	Mileage	Source[2]	SiO_2	Al_2O_3	TiO_2	Fe_2O_3*	MnO	CaO	MgO	K_2O	Na_2O	P_2O_5
W Cascades	**MR-19**	6.3	1	50.37	15.99	1.61	10.56	0.18	10.30	7.62	0.52	2.61	0.23
W Cascades	**NSR-1**	6.3	2	51.04	15.12	0.80	9.11	0.15	10.77	10.32	0.39	2.18	0.13
W Cascades	**MR-20**	11.1	1	49.63	19.48	1.36	10.86	0.17	11.07	4.41	0.33	2.55	0.15
Foley Ridge	**FR-3**	47.1	1	48.98	16.98	1.35	10.13	0.17	9.34	9.18	0.51	3.07	0.30
Sims Butte	**97-104U**	51.4	1	53.68	17.21	1.22	8.46	0.14	7.86	6.48	0.97	3.74	0.25
White Branch R pol	**97-89**	54.0	1	49.27	16.84	1.89	11.84	0.19	9.59	6.33	0.47	3.19	0.38
White Branch R pol	**97-93**	54.0	1	49.37	18.03	1.45	9.96	0.17	10.07	6.98	0.36	3.30	0.32
Basal Brunhes int/cyn	**97-51**	65.3	1	51.08	17.66	1.32	9.64	0.16	8.92	6.82	0.87	3.20	0.32
Mt Washington	**95-185**	70.8	1	52.69	18.25	1.21	8.67	0.14	8.80	5.24	0.83	3.81	0.36
Scott Mtn	**99-37**	70.8	1	50.47	17.01	1.60	9.73	0.15	8.98	7.09	0.92	3.62	0.42
Trailbridge Ignimbrite	**97-114**	70.8	1	53.08	17.58	1.36	9.14	0.15	9.25	4.46	0.82	3.88	0.28
Fe-rich beneath Tmi	**97-60**	70.8	1	52.00	15.58	2.23	12.38	0.19	8.15	3.96	0.67	4.34	0.48
Late Brunhes int/cyn	**KC-1**	79.5	1	51.67	17.91	1.07	8.80	0.14	8.95	7.06	0.58	3.50	0.30
Early Sand Mtn	**95-20**	84.2	1	50.88	16.49	1.60	9.20	0.14	9.35	7.53	0.83	3.62	0.37
S of Fish Lk	**97-113**	85.8	1	54.69	17.50	1.56	9.08	0.13	7.10	3.52	1.82	4.07	0.53
Sand Mountain	**95-18**	86.9	1	52.21	17.24	1.30	8.66	0.14	9.32	6.23	0.94	3.58	0.38
Early Nash Crater	**95-1**	87.3	1	50.54	16.72	1.42	9.29	0.15	8.93	8.32	0.78	3.49	0.35
Nash Crater	**95-2**	87.3	1	52.65	17.93	1.29	8.45	0.14	8.48	5.74	0.82	4.11	0.39
Little Nash Crater	**95-7**	90.6	1	56.42	18.56	1.07	7.03	0.11	7.60	3.79	0.74	4.38	0.29
Hayrick Butte	**NSH-4**	92.0	1	59.78	18.28	0.68	6.07	0.11	6.21	3.28	1.07	4.40	0.12
Santiam Jnct	**NSH-5**	94.0	1	50.21	16.82	1.39	9.39	0.15	9.07	8.36	0.83	3.44	0.34
Craig Lake	**CM-1**	96.1	1	53.55	18.05	1.03	7.36	0.12	8.55	5.90	1.06	4.06	0.32
Hogg Rock	**MJ-#058**	97.6	1	59.48	18.28	0.68	6.21	0.11	6.46	3.54	0.96	4.18	0.11
Santiam Pass N pol	**98-26**	100.4	1	53.86	17.93	1.12	8.20	0.13	8.25	5.30	0.90	3.99	0.31
Cache Mtn	**TFJ1**	102.8	2	49.80	16.14	1.14	8.94	0.14	9.63	9.33	1.41	3.10	0.37
McKinney Butte	**95-89**	119.6	1	59.26	14.31	1.53	10.41	0.35	4.38	1.73	0.98	6.52	0.52
Plainview Basalt	**95-37**	122.8	1	52.44	18.09	1.35	8.67	0.15	8.65	5.76	0.75	3.89	0.26
Black Crater	**99-35**	129.1	1	54.12	18.02	1.07	8.04	0.13	8.67	5.22	0.88	3.56	0.28
S Matthieu Lake	**95-156**	129.1	1	54.66	16.95	1.53	9.85	0.15	7.32	3.90	0.94	4.41	0.28
North Sister	**95-131**	129.1	1	53.01	18.96	1.05	8.11	0.12	8.91	5.02	0.64	3.99	0.19
Middle Sister	**95-133**	129.1	1	64.06	16.03	0.92	6.00	0.14	3.31	1.28	1.72	6.20	0.34
Middle Sister	**95-132**	129.1	1	54.43	16.39	1.73	10.62	0.16	7.35	3.59	0.86	4.58	0.30
Middle Sister	**95-135**	129.1	1	54.80	17.67	1.38	8.69	0.13	7.84	4.15	1.10	3.98	0.25
Desert Spring Tuff	**96-20**	129.6	1	68.32	14.78	0.66	4.53	0.10	2.08	0.81	3.32	5.24	0.17
Tumalo Lake dome	**B217**	129.6	3	68.22	14.90	0.65	4.43	0.09	2.10	0.86	3.18	5.40	0.17
Brunhes lava	**178-J**	141.7	4	60.26	16.66	1.11	7.15	0.13	5.38	2.65	1.67	4.63	0.36
Brunhes lava	**179-J**	142.1	4	54.09	17.59	1.20	8.45	0.14	8.67	5.08	0.84	3.64	0.29
Three Crk Lk agglut	**B277**	143.7	3	66.98	15.47	0.81	4.56	0.10	2.66	0.86	2.53	5.81	0.22
Shevlin Park Tuff	**99-62A**	143.7	1	67.59	15.62	0.77	4.02	0.12	2.41	0.88	2.34	6.08	0.19
Shevlin Park Tuff	**99-62E**	143.7	1	61.79	16.06	1.25	6.68	0.14	4.48	2.02	1.67	5.55	0.37
Shevlin Park Tuff	**99-62G**	143.7	1	57.59	16.30	1.51	8.81	0.15	6.05	2.92	1.26	5.05	0.35

[a]All analyses except 178-J and 179-J acquired at the Washington State University Geoanalytical Laboratory; Donnelly-Nolan data is from the U.S. Geological Survey.
[1]RC or RMC prefixes removed (Conrey samples); S95 or SHES95 prefixes removed (Sherrod data); AUB prefixes removed (Aubin data).
[2]Sources: 1: Conrey, unpub; 2: Conrey and others., 1997; 3: Sherrod, unpub; 4: Donnelly-Nolan, unpub; 5: Aubin, 2000; 6: Conrey, 1991.
*Total Fe as Fe_2O_3. Major element analyses are normalized to 100%.
nd = not determined.

REFERENCES

Allen, J.E., 1966, The Cascade Range volcano-tectonic depression of Oregon: Oregon Department of Geology and Mineral Industries Transactions of the Lunar Geological Field Conference, p. 21-23.

Armstrong, R.L., Taylor, E.M., Hales, P.O., and Parker, D.J., 1975, K-Ar dates for volcanic rocks, central Cascade Range of Oregon: Isochron/West, no. 13, p. 5-10.

Aubin, W.A., 2000, Ignimbrites of the Deschutes Formation: A record of crustal melting and magma mixing: Washington State University MS Thesis, 125 p.

Avramenko, W., 1981, Volcanism and structure in the vicinity of Echo Mountain, central Oregon Cascade Range: University of Oregon MS Thesis, 156 p.

Bacon, C.R., Bruggman, P.E., Christiansen, R.L., Clynne, M.A., Donnelly-Nolan, J.M., and Hildreth, W., 1997, Primitive magmas at five Cascade volcanic fields: Melts from hot, heterogeneous sub-arc mantle: Canadian Mineralogist, v. 35, p. 397-423.

Table 1. Selected X-ray Fluorescence Analyses[a] (Major Elements Wt% Oxide; Trace Elements ppm) of Cascade Range Rocks—Day 1 (continued)

Unit	Sample[1]	Mileage	FeO*/MgO	Ni	Cr	Sc	V	Ba	Rb	Sr	Zr	Y	Nb
W Cascades	**MR-19**	6.3	1.25	51	262	41	273	126	7	437	114	19	9.6
W Cascades	**NSR-1**	6.3	0.79	99	405	39	225	136	6	398	82	14	5.6
W Cascades	**MR-20**	11.1	2.22	7	48	38	296	82	8	366	74	19	6.8
Foley Ridge	**FR-3**	47.1	0.99	181	360	36	205	210	7	396	115	26	8.2
Sims Butte	**97-104U**	51.4	1.18	111	190	23	184	275	17	423	128	22	6.7
White Branch R pol	**97-89**	54.0	1.68	67	161	31	294	282	2	384	142	35	8.8
White Branch R pol	**97-93**	54.0	1.28	80	172	33	242	224	2	412	117	26	6.6
Basal Brunhes int/cyn	**97-51**	65.3	1.27	84	139	27	214	269	11	502	121	23	7.4
Mt Washington	**95-185**	70.8	1.49	57	55	21	180	363	12	536	163	24	10.0
Scott Mtn	**99-37**	70.8	1.23	111	185	21	204	351	11	683	156	26	13.2
Trailbridge Ignimbrite	**97-114**	70.8	1.84	8	63	30	243	341	8	668	113	20	5.0
Fe-rich beneath Tmi	**97-60**	70.8	2.81	0	13	32	335	271	6	549	104	27	5.8
Late Brunhes int/cyn	**KC-1**	79.5	1.12	122	170	25	173	314	8	526	129	21	9.3
Early Sand Mtn	**95-20**	84.2	1.10	110	222	25	213	370	11	798	167	22	15.7
S of Fish Lk	**97-113**	85.8	2.32	0	15	20	235	1110	38	986	211	28	11.8
Sand Mountain	**95-18**	86.9	1.25	63	140	26	187	494	10	1007	171	22	12.2
Early Nash Crater	**95-1**	87.3	1.01	162	304	23	206	319	10	632	148	23	12.6
Nash Crater	**95-2**	87.3	1.33	103	103	29	180	372	9	759	172	23	11.9
Little Nash Crater	**95-7**	90.6	1.67	25	27	9	130	397	8	970	164	19	8.2
Hayrick Butte	**NSH-4**	92.0	1.66	34	26	13	106	276	14	515	103	14	4.2
Santiam Jnct	**NSH-5**	94.0	1.01	163	318	21	182	320	10	690	143	22	12.4
Craig Lake	**CM-1**	96.1	1.12	88	95	20	179	408	9	1171	152	15	5.0
Hogg Rock	**MJ-#058**	97.6	1.58	38	34	21	96	248	13	550	100	11	4.6
Santiam Pass N pol	**98-26**	100.4	1.39	79	95	21	168	336	9	778	128	19	8.8
Cache Mtn	**TFJ1**	102.8	0.86	190	341	30	177	739	7	1575	143	20	4.9
McKinney Butte	**95-89**	119.6	5.41	0	6	38	99	909	14	232	121	42	10.8
Plainview Basalt	**95-37**	122.8	1.36	84	63	21	214	298	10	517	124	24	9.1
Black Crater	**99-35**	129.1	1.39	50	94	22	170	372	11	568	147	23	7.4
S Matthieu Lake	**95-156**	129.1	2.27	9	21	27	287	353	14	519	139	23	8.6
North Sister	**95-131**	129.1	1.45	72	56	26	196	227	6	585	107	19	5.2
Middle Sister	**95-133**	129.1	4.24	5	0	13	36	571	25	335	228	38	11.8
Middle Sister	**95-132**	129.1	2.66	7	33	30	317	332	14	492	133	25	7.4
Middle Sister	**95-135**	129.1	1.88	38	62	30	210	324	18	496	142	24	7.8
Desert Spring Tuff	**96-20**	129.6	5.04	7	3	9	26	730	88	172	302	46	17.5
Tumalo Lake dome	**B217**	129.6	4.66	9	0	12	29	718	88	182	305	46	17.5
Brunhes lava	**178-J**	141.7	2.43	9	nd	nd	nd	510	24	508	203	26	9.0
Brunhes lava	**179-J**	142.1	1.50	26	nd	nd	nd	327	19	484	129	20	8.0
Three Crk Lk agglut	**B277**	143.7	4.79	9	19	16	45	704	48	284	287	39	16.4
Shevlin Park Tuff	**99-62A**	143.7	4.13	3	1	14	17	679	44	282	260	38	13.3
Shevlin Park Tuff	**99-62E**	143.7	2.97	1	6	17	111	524	30	419	195	34	11.1
Shevlin Park Tuff	**99-62G**	143.7	2.72	2	13	28	208	423	21	496	155	30	8.9

[a]All analyses except 178-J and 179-J acquired at the Washington State University Geoanalytical Laboratory; Donnelly-Nolan data is from the U.S. Geological Survey.
[1]RC or RMC prefixes removed (Conrey samples); S95 or SHES95 prefixes removed (Sherrod data); AUB prefixes removed (Aubin data).
[2]Sources: 1: Conrey, unpub; 2: Conrey and others., 1997; 3: Sherrod, unpub; 4: Donnelly-Nolan, unpub; 5: Aubin, 2000; 6: Conrey, 1991.
*Total Fe as Fe_2O_3. Major element analyses are normalized to 100%.
nd = not determined.

Bacon, S.N., 1996, Quaternary volcanic and glacial stratigraphy of Black Crater, outside Sisters, Oregon: Humboldt State University Senior Thesis, 55 p.

Beeson, M.H., Tolan, T.L., and Anderson, J.L., 1989, The Columbia River Basalt Group in western Oregon: Geologic structures and other factors that controlled flow emplacement patterns: Geological Society of America Special Paper 239, p. 223-246.

Benson, G.T., 1965, The age of Clear Lake, Oregon: Ore Bin, v. 27, p. 37-40.

Black, G.L., Woller, N.M., and Ferns, M.L., 1987, Geologic map of the Crescent Mountain area, Linn County, Oregon: Oregon Department of Geology and Mineral Industries Map GMS-47, scale 1:62,500.

Blakely, R.J., 1994, Extent of partial melting beneath the Cascade Range, Oregon: Constraints from gravity anomalies and ideal-body theory: Journal of Geophysical Research, v. 99, p. 2757-2773.

Buddington, A.F., and Callaghan, E., 1936, Dioritic intrusive rocks and contact metamorphism in the

Table 2. Selected X-ray Fluorescence Analyses[a] (Major Elements Wt% Oxide; Trace Elements ppm) of Cascade Range Rocks—Day 2

Unit	Sample	Mileage	Source	SiO_2	Al_2O_3	TiO_2	Fe_2O_3*	MnO	CaO	MgO	K_2O	Na_2O	P_2O_5
Round Butte	**RB-10**	21.1	1	51.86	16.71	1.70	10.51	0.16	8.14	5.52	1.16	3.70	0.55
Lionshead	**MJ-1127Y**	21.1	1	67.56	15.99	0.66	4.26	0.09	3.02	0.81	1.84	5.59	0.18
Tetherow Butte	**RB-66**	22.1	1	50.84	13.77	2.51	14.35	0.24	8.50	4.54	0.84	3.82	0.59
W arm Bridge	**96-79**	29.0	1	47.43	17.19	0.89	10.04	0.18	11.75	9.98	0.13	2.29	0.12
Canadian Bench	**GR-236**	30.3	2	49.57	17.67	0.86	9.55	0.16	11.04	8.45	0.24	2.37	0.09
Fly Lake	**GR-208-2**	38.0	1	50.06	17.37	0.88	9.45	0.17	11.11	8.02	0.32	2.53	0.09
Six Creek Tuff	**98-136**	38.5	5	55.32	16.47	1.88	9.80	0.16	7.22	3.21	1.02	4.42	0.50
Six Creek Tuff	**GR-13**	38.5	1	67.77	15.80	0.55	4.40	0.13	2.09	0.63	2.21	6.30	0.13
Fly Creek Tuff	**GR-380**	41.3	1	70.50	15.12	0.39	3.03	0.08	1.50	0.51	4.12	4.61	0.14
Fly Creek Tuff	**GR-427**-7	41.3	1	52.75	16.67	1.45	10.19	0.14	8.97	5.39	0.87	3.35	0.23
Fly Creek Tuff	**GR-699**	41.3	1	53.68	16.93	1.97	9.95	0.15	7.42	3.64	0.92	4.41	0.93
Belknap Crater	**BKP-5**	52.6	1	52.89	17.91	1.24	8.27	0.14	8.73	5.73	0.85	3.88	0.36
Wizard Ridge vent	**97-294**	52.6	1	51.26	18.28	1.34	8.99	0.13	8.51	6.90	0.77	3.51	0.30
Abbot Butte	**CC-16**	52.6	1	58.26	18.45	0.75	6.36	0.10	6.78	4.05	0.94	4.18	0.13
Abbot Butte	**97-269**	52.6	1	64.41	16.58	0.50	4.81	0.08	4.52	3.06	1.60	4.35	0.10
Abbot Butte	**97-271**	52.6	1	53.95	22.26	0.64	5.78	0.09	9.34	3.79	0.62	3.41	0.12
N Cinder Peak	**ML-19**	52.6	6	55.49	18.65	1.11	7.06	0.11	8.09	4.29	0.87	4.02	0.31
N Cinder Peak	**ML-29**	52.6	6	56.09	18.53	1.06	6.93	0.11	7.93	4.27	0.74	4.08	0.25
Forked Butte	**CC-51**	52.6	6	54.02	17.73	1.22	8.27	0.13	8.06	5.29	0.90	4.04	0.33
Goat Peak	**MJ-354**	52.6	6	68.51	15.83	0.48	3.61	0.08	2.80	1.09	2.13	5.37	0.09
Sugarpine Ridge	**ML-122**	52.6	6	56.61	18.54	1.06	6.51	0.10	7.72	4.29	0.76	4.15	0.28
Mt Jefferson area	**MJ-556**	52.6	6	69.34	15.52	0.41	3.42	0.07	3.18	1.12	2.06	4.79	0.09
Mt Jefferson area	**MJ-696**	52.6	6	58.54	18.66	0.87	5.77	0.09	7.12	3.68	0.71	4.37	0.19
Deschutes Fm	**GR-520**	54.2	1	51.08	16.73	1.30	11.59	0.16	9.69	6.20	0.17	2.95	0.11
Mt. Jefferson	**98-225**	55.2	1	70.38	15.59	0.44	3.30	0.07	2.52	0.82	2.19	4.57	0.11
Deschutes Fm	**98-222**	56.8	1	59.04	16.89	1.36	7.96	0.12	6.00	2.23	1.31	4.65	0.43
Wizard Falls	**GR-773**	60.6	2	49.06	15.42	1.57	11.25	0.17	9.21	9.53	0.47	2.92	0.39
Deschutes Fm	**97-265**	62.6	1	52.72	17.58	1.34	9.89	0.15	8.16	5.42	0.96	3.35	0.43
Deschutes Fm	**97-263**	63.1	1	52.01	17.71	1.46	10.29	0.17	8.08	5.27	0.87	3.55	0.59
Deschutes Fm	**97-262**	63.6	1	54.70	17.23	1.33	9.38	0.12	7.30	5.23	1.05	3.37	0.30
Marks Ridge	**94-92**	126.1	1	53.57	16.57	1.80	9.70	0.17	8.22	4.39	1.07	3.94	0.58
Galena Mtn	**94-91**	126.1	1	53.87	16.65	1.75	9.53	0.17	8.06	4.32	1.10	4.00	0.55

[a]All analyses except 178-J and 179-J acquired at the Washington State University Geoanalytical Laboratory; Donnelly-Nolan data is from the U.S. Geological Survey.
[1]RC or RMC prefixes removed (Conrey samples); S95 or SHES95 prefixes removed (Sherrod data); AUB prefixes removed (Aubin data).
[2]Sources: 1: Conrey, unpub; 2: Conrey and others, 1997; 3: Sherrod, unpub; 4: Donnelly-Nolan, unpub; 5: Aubin, 2000; 6: Conrey, 1991.
*Total Fe as Fe_2O_3. Major element analyses are normalized to 100%.
nd = not determined.

Cascade Range in Oregon: American Journal of Science, v. 30, p. 421-449.

Conrey, R.M., 1985, Volcanic stratigraphy of the Deschutes Formation from Green Ridge to Fly Creek, north-central Oregon: Oregon State University MS Thesis, 349 p.

Conrey, R.M., 1991, Geology and petrology of the Mt Jefferson area, High Cascade Range, Oregon: Washington State University PhD Dissertation, 357 p.

Conrey, R.M., Donnelly-Nolan, J.M., Taylor, E.M., Champion, D., and Bullen, T., 2001a, The Shevlin Park Tuff, central Oregon Cascade Range: Magmatic processes recorded in an arc-related ash-flow tuff: Eos, v. 82, p. F1345.

Conrey, R.M., Hooper, P.R., Larson, P.B., Chesley, J., and Ruiz, J., 2001b, Trace element and isotopic evidence for two types of crustal melting beneath a High Cascade volcanic center, Mt Jefferson, Oregon: Contributions to Mineralogy and Petrology, v. 141, p. 710-732.

Conrey, R.M., and Sherrod, D.R., 1988, Stratigraphy of drill holes and geochemistry of surface rocks, Breitenbush Hot Springs 15-Minute Quadrangle, Cascade Range, Oregon, *in* Sherrod, D.R., ed., Geology and geothermal resources of the Breitenbush–Austin Hot Springs area, Clackamas and Marion Counties, Oregon: Oregon Department of Geology and Mineral Industries Open-File Report O-88-5, p. 15-29.

Conrey, R.M., and Sherrod, D.R., in preparation, Propagating rift in the Cascade Range of Oregon and Washington.

Conrey, R.M., Sherrod, D.R., Hooper, P.R., and Swanson, D.A., 1997, Diverse primitive magmas in the Cascade Arc, northern Oregon and southern Washington: Canadian Mineralogist, v. 35, p. 367-396.

Davie, E.I., 1980, The geology and petrology of Three Fingered Jack, a High Cascade volcano in central Oregon: University of Oregon MS Thesis, 137 p.

Table 2. Selected X-ray Fluorescence Analyses[a] (Major Elements Wt% Oxide; Trace Elements ppm) of Cascade Range Rocks—Day 2 (continued)

Unit	Sample	Mileage	FeO*/MgO	Ni	Cr	Sc	V	Ba	Rb	Sr	Zr	Y	Nb
Round Butte	**RB-10**	21.1	1.71	66	113	27	186	347	19	479	191	33	18.1
Lionshead	**MJ-1127Y**	21.1	4.77	6	0	11	39	487	28	342	167	25	8.0
Tetherow Butte	**RB-66**	22.1	2.84	0	15	45	373	361	10	369	130	44	6.1
W arm Bridge	**96-79**	29.0	0.91	174	286	42	214	63	2	163	83	24	5.6
Canadian Bench	**GR-236**	30.3	1.02	140	279	43	232	125	5	270	73	25	2.0
Fly Lake	**GR-208-2**	38.0	1.06	103	220	44	233	113	8	317	81	26	2.0
Six Creek Tuff	**98-136**	38.5	2.75	1	16	24	223	307	11	562	142	23	9.7
Six Creek Tuff	**GR-13**	38.5	6.32	5	0	8	13	683	28	252	270	37	15.8
Fly reek Tuff	**GR-380**	41.3	5.34	7	0	8	1	813	61	163	291	37	14.6
Fly Creek Tuff	**GR-427-7**	41.3	1.70	36	109	28	264	291	16	739	119	25	6.3
Fly Creek Tuff	**GR-699**	41.3	2.46	0	8	29	187	300	14	648	123	28	7.0
Belknap Crater	**BKP-5**	52.6	1.30	68	125	27	179	307	13	542	153	23	13.2
Wizard Ridge vent	**97-294**	52.6	1.17	134	180	20	178	301	7	630	128	20	12.1
Abbot Butte	**CC-16**	52.6	1.41	54	53	17	130	273	13	536	96	15	4.6
Abbot Butte	**97-269**	52.6	1.41	70	45	5	72	466	32	391	118	13	5.8
Abbot Butte	**97-271**	52.6	1.37	54	87	12	96	211	10	653	64	9	3.7
N Cinder Peak	**ML-19**	52.6	1.48	47	38	20	146	353	8	1362	169	15	7.5
N Cinder Peak	**ML-29**	52.6	1.46	51	52	21	154	288	8	1047	150	16	7.3
Forked Butte	**CC-51**	52.6	1.41	77	114	29	169	285	13	595	138	19	9.9
Goat Peak	**MJ-354**	52.6	2.99	26	0	6	49	650	32	460	221	15	13.0
Sugarpine Ridge	**ML-122**	52.6	1.36	48	48	16	133	214	7	1294	158	14	5.9
Mt Jefferson area	**MJ-556**	52.6	2.75	28	13	6	54	491	43	399	124	15	9.0
Mt Jefferson area	**MJ-696**	52.6	1.41	37	34	19	120	193	4	1202	123	11	4.0
Deschutes Fm	**GR-520**	54.2	1.68	65	179	26	214	124	1	395	83	23	2.0
Mt Jefferson	**98-225**	55.2	3.62	6	0	2	38	613	32	306	178	16	7.8
Deschutes Fm	**98-222**	56.8	3.21	1	6	19	171	452	19	566	163	28	11.3
Wizard Falls	**GR-773**	60.6	1.06	223	334	33	187	220	6	701	174	27	10.0
Deschutes Fm	**97-265**	62.6	1.64	58	91	22	200	381	16	541	145	26	9.7
Deschutes Fm	**97-263**	63.1	1.76	61	114	19	205	458	10	523	191	32	12.1
Deschutes Fm	**97-262**	63.6	1.61	91	160	18	155	298	21	420	131	31	6.7
Marks Ridge	**94-92**	126.1	1.99	13	54	30	253	406	12	600	132	29	9.9
Galena Mtn	**94-91**	126.1	1.98	15	49	30	240	422	14	587	138	29	10.2

[a]All analyses except 178-J and 179-J acquired at the Washington State University Geoanalytical Laboratory; Donnelly-Nolan data is from the U.S. Geological Survey.
[1]RC or RMC prefixes removed (Conrey samples); S95 or SHES95 prefixes removed (Sherrod data); AUB prefixes removed (Aubin data).
[2]Sources: 1: Conrey, unpub; 2: Conrey and others, 1997; 3: Sherrod, unpub; 4: Donnelly-Nolan, unpub.; 5: Aubin, 2000; 6:Conrey 1991.
*Total Fe as Fe_2O_3. Major element analyses are normalized to 100%.
nd = not determined.

Dill, T.E., 1992, Stratigraphy of the Neogene volcanic rocks along the lower Metolius River, Jefferson County, central Oregon: Oregon State University MS Thesis, 343 p.

Flaherty, G.M., 1981, The Western Cascade—High Cascade transition in the McKenzie Bridge area, central Oregon Cascade Range: University of Oregon MS Thesis, 178 p.

Hill, B.E., 1991, Petrogenesis of compositionally distinct silicic volcanoes in the Three Sisters region of the Oregon Cascade Range: The effects of crustal extension on the development of continental arc silicic magmatism: Oregon State University PhD Dissertation, 235 p.

Hill, B.E, 1992, Geology and geothermal resources of the Santiam Pass area of the Oregon Cascade Range, Deschutes, Jefferson, and Linn Counties, Oregon: Oregon Department of Geology and Mineral Industries Open-File Report O-92-3, 61 p.

Hill, B.E, and Duncan, R.A., 1990, The timing and significance of silicic magmatism in the Three Sisters region of the Oregon High Cascades: Eos, v. 71, p. 1614.

Hill, B.E, and Taylor, E.M., 1990, Oregon Central High Cascade pyroclastic units in the vicinity of Bend, Oregon: Oregon Geology, v. 52, p. 125-126, 139-140.

Hooper, P.R., and Conrey, R.M., 1989, A model for the tectonic setting of the Columbia River basalt eruptions: Geological Society of America Special Paper 239, p. 293-306.

Hughes, S.S., 1990, Mafic magmatism and associated tectonism of the central High Cascade Range, Oregon: Journal of Geophysical Research, v. 95, p. 19,623-19,638.

Hughes, S.S., and Taylor, E.M., 1986, Geochemistry, petrogenesis, and tectonic implications of central High

Table 3. Comparison of bulk chemical analyses of Matuyama-age lavas and drill core (major elements in wt% and trace elements in ppm)

Sample	Candle Crk lava **97-267**	Abbot Butte core **817' depth**	Candle Crk lava **MJ-CC5**	Abbot Butte core **1,065'depth**	Candle Crk lava **MJ-CC6**	Abbot Butte core **1,259' depth**	Hackleman Crk basalt **97-112**	Mixing calculation	EWEB 1 core **440' depth**
SiO_2	51.63	51.58	51.30	51.06	48.96	48.34	47.78	48.09	48.12
Al_2O_3	18.06	17.70	17.30	17.47	17.00	17.02	18.39	16.83	16.97
TiO2	1.41	1.41	1.46	1.50	1.46	1.49	1.32	1.64	1.62
Fe_2O_3*	10.04	10.22	10.70	10.86	11.24	10.95	10.88	12.20	12.36
MnO	0.16	0.16	0.17	0.16	0.17	0.18	0.17	0.21	0.19
CaO	8.22	8.07	8.36	8.02	9.51	9.65	10.02	9.62	9.64
MgO	5.38	5.39	5.71	5.63	7.84	8.37	7.71	7.29	7.28
K_2O	0.88	0.89	0.79	0.76	0.32	0.33	0.23	0.28	0.40
Na_2O	3.69	4.04	3.73	4.02	3.22	3.39	3.13	3.38	2.98
P_2O_5	0.54	0.53	0.49	0.50	0.28	0.28	0.36	0.45	0.44
Ni	60	60	74	72	141	138	129		110
Cr	87	70	100	88	261	239	177		160
Sc	23	25	28	28	32	38	27	33	36
V	188	211	196	211	221	222	218	260	251
Ba	375	356	332	324	152	101	213	256	273
Rb	12	9	9	8	1	1	1		3
Sr	580	578	515	530	367	350	535		449
Zr	160	166	164	165	118	113	113	136	133
Y	26	29	30	27	28	27	26	31	30
Nb	12.0	12.7	12.7	12.9	6.3	5.2	7.3	8.8	8.8
Ga	20	22	20	22	14	18	18		20
Cu	81	50	97	53	86	61	107		106
Zn	104	97	103	98	84	78	108		117

Candle Creek area samples 97-267, MJ-CC5 and CC-6 are sparsely porphyritic reverse-polarity lavas exposed at surface; CC-5 overlies CC-6. Abbot Butte drill core samples (all reversely polarized and sparsely porphyritic) that most closely match the surface lavas are shown.

Hackleman Creek basalt is coarsely plagioclase- and olivine-bearing and normally polarized (see Stop 4). EWEB-1 core sample from 440 feet is coarsely plagioclase- and olivine-bearing. A mass balance calculation is shown in which 5 wt% olivine (Fo_{77}) and 15 wt% plagioclase (An_{75}) were subtracted from sample 97-112. The result is nearly identical to the hand-picked drill core sample (sum of $r^2 = 0.23$). The main contribution to the residual sums are the alkali elements, which may be hydrated or slightly altered in the glassy groundmass. 20% increases in concentration of the highly incompatible elements Ba, Zr, Y, and Nb are also shown. Compatible trace elements are all qualitatively consistent with the match.

Cascade mafic platform lavas: Geological Society of America Bulletin, v. 97, p. 1024-1036.

Lachenbruch, A.H., and Sass, J.H., 1978, Models of an extending lithosphere and heat flow in the Basin and Range Province: Geological Society of America Memoir 152, p. 209-250.

Lanphere, M.A., Champion, D.E., Christiansen, R.L., Donnelly-Nolan, J.M., Fleck, R.J., Sarna-Wojcicki, A.M., Obradovich, J.D., and Izett, G.A., 1999, Evolution of tephra dating in the western United States: Geological Society of America Abstracts with Programs, v. 31, p. A-73.

Lawrence, R.D., 1976, Strike-slip faulting terminates the Basin and Range province in Oregon: Geological Society of America Bulletin, v. 87, p. 846-850.

Licciardi, J.M., Kurz, M.D., Clark, P.U., and Brook, E.J., 1999, Calibration of cosmogenic ^{3}He production rates from Holocene lava flows in Oregon, USA, and effects of the Earth's magnetic field: Earth and Planetary Science Letters, v. 172, p. 261-271.

Livelybrooks, D.W., Clingman, W.W., Rygh, J.T., Urquhart, S.A., and Waff, H.S., 1989, A magnetotelluric study of the High Cascades Graben in central Oregon: Journal of Geophysical Research, v. 94, p. 14,173-14,184.

Lux, D.R., 1981, Geochronology, geochemistry, and petrogenesis of basaltic rocks from the Western Cascades, Oregon: Ohio State University PhD Dissertation, 171 p.

Lux, D.R., 1982, K-Ar and 40Ar-39Ar ages of mid-Tertiary volcanic rocks from the Western Cascade Range, Oregon: Isochron/West, no. 33, p. 27-32.

McDannel, A.K., 1989, Geology of the southermost Deschutes Basin, Tumalo Quadrangle, Deschutes County, Oregon: Oregon State University MS Thesis, 166 p.

Mimura, K, 1984, Imbrication, flow direction, and possible source areas of the pumice-flow tuffs near Bend, Oregon, U.S.A: Journal of Volcanology and Geothermal Research, v. 21, p. 45-60.

Peck, D.L., Griggs, A.B., Schlicker, H.G., Wells, F.G., and Dole, H.M., 1964, Geology of the central and northern parts of the Western Cascade Range in Oregon: U.S. Geological Survey Professional Paper 449, 56 p.

Priest, G.R., 1990, Volcanic and tectonic evolution of the Cascade Volcanic Arc, central Oregon: Journal of Geophysical Research, v. 95, p. 19,583-19,599.

Priest, G.R., Black, G.L., Woller, N.M., and Taylor, E.M., 1988, Geologic map of the McKenzie Bridge Quad-

rangle, Lane County, Oregon: Oregon Department of Geology and Mineral Industries Map GMS-48, scale 1:62,500.

Priest, G.R., Woller, N.M., and Ferns, M.L., 1987, Geologic map of the Breitenbush River area, Linn and Marion Counties, Oregon: Oregon Department of Geology and Mineral Industries Map GMS-46, scale 1:62,500.

Rieck, H.J., Sarna-Wojcicki, A.M., Meyer, C.E., and Adam, D.P., 1992, Magnetostratigraphy and tephrochronology of an upper Pliocene to Holocene record in lake sediments at Tulelake, northern California: Geological Society of America Bulletin, v. 104, p. 409-428.

Ritchie, B., 1987, Tholeiitic lavas from the Western Cascade Range, Oregon: University of Oregon MS Thesis, 94 p.

Sarna-Wojcicki, A..M., Meyer, C.E., Nakata, J.K., Scott, W.E., Hill, B.E., Slate, J.L., and Russell, P.C., 1989, Age and correlation of mid-Quaternary ash beds and tuffs in the vicinity of Bend, Oregon, *in* Scott, W.E., Gardner, C.A., and Sarna-Wojcicki, A.M., eds., Guidebook for field trip to the Mount Bachelor–South Sister–Bend area, central Oregon High Cascades: U.S. Geological Survey Open-File Report 89-645, p. 55-62.

Scott, W.E., 1977, Quaternary glaciation and volcanism, Metolius River area, Oregon: Geological Society of America Bulletin, v. 88, p. 113-124.

Scott, W.E., and Gardner, C.A., 1992, Geologic map of the Mount Bachelor volcanic chain and surrounding area, Cascade Range, Oregon: U.S. Geological Survey Miscellaneous Investigations Series Map I-1967, scale 1:50,000.

Scott, W.E., Gardner, C.A., Sherrod, D.R., Tilling, R.I., Lanphere, M.A., and Conrey, R.M., 1997, Geologic history of Mount Hood Volcano, Oregon—A field trip guidebook: U.S. Geological Survey Open-File Report 97-0263, 38 p.

Scott, W.E., Sherrod, D.R., and Taylor, E.M., 1996, Age of High Cascade shield volcanoes estimated using glacial record and degree of erosion: New view from Three Fingered Jack: Geological Society of America Abstracts with Programs, v. 28, p. 111.

Sherrod, D.R., 1986, Geology, petrology, and volcanic history of a portion of the Cascade Range between latitudes 43–44°N, central Oregon, U.S.A.: University of California Santa Barbara PhD Dissertation, 320 p.

Sherrod, D.R., 1991, Geologic map of a part of the Cascade Range between latitudes 43°-44°, central Oregon: U.S. Geological Survey Miscellaneous Investigations Series Map I-1891, scale 1:125,000.

Sherrod, D.R., and Scott, W.E., 1995, Preliminary geologic map of the Mount Hood 30- by 60-Minute Quadrangle, northern Cascade Range, Oregon: U.S. Geological Survey Open-File Report 95-219, 35 p., map scale 1:100,000.

Sherrod, D.R., and Smith, J.G., 2000, Geologic map of upper Eocene to Holocene volcanic and related rocks of the Cascade Range, Oregon: U.S. Geological Survey Geologic Investigations Series Map I-2569, scale 1:500,000.

Sherrod, D.R., Taylor, E.M., Ferns, M.L., Scott W.E., Conrey R.M., and Smith G.A., in press, Geologic map of the Bend 30 by 60 Minute Quadrangle, central Oregon: U.S. Geological Survey Geologic Investigations Series Map I-2683, scale 1:100,000.

Smith, G.A., 1986, Stratigraphy, sedimentology, and petrology of Neogene rocks in the Deschutes basin, central Oregon: A record of continental margin volcanism and its influence on fluvial sedimentation in an arc-adjacent basin: Oregon State University PhD Dissertation, 464 p.

Smith, G.A., 1991, A field guide to depositional processes and facies geometry of Neogene continental volcaniclastic rocks, Deschutes Basin, central Oregon: Oregon Geology, v. 53, p. 3-20.

Smith, G.A., Manchester, S.R., Ashwill, M., McIntosh, W.C., and Conrey, R.M., 1998, Late Eocene–early Oligocene tectonism, volcanism, and floristic change near Gray Butte, central Oregon: Geological Society of America Bulletin, v. 110, p. 759-778.

Smith, G.A., Snee, L.W., and Taylor, E.M., 1987, Stratigraphic, sedimentologic, and petrologic record of late Miocene subsidence of the central Oregon High Cascades: Geology, v. 15, p. 389-392.

Smith, G.A., and Taylor, E.M., 1983, The central Oregon High Cascade Graben: What? Where? When?: Geothermal Resources Council Transactions, v. 7, p. 275-279.

Stanley, W.D., Mooney, W.D., and Fuis, G.S., 1990, Deep crustal structure of the Cascade Range and surrounding regions from seismic refraction and magnetotelluric data: Journal of Geophysical Research, v. 95, p. 19,419-19,438.

Sutter, J.F., 1978, K/Ar ages of Cenozoic volcanic rocks from the Oregon Cascades west of 121°30': Isochron/West, no. 21, p. 15-21.

Taylor, E.M., 1965, Recent volcanism between Three Fingered Jack and North Sister, Oregon Cascade Range: Ore Bin, v. 27, p. 121-147.

Taylor, E.M., 1968, Roadside geology, Santiam and McKenzie Pass Highways, Oregon, *in* Dole, H.M., ed., Andesite Conference Guidebook: Oregon Department of Geology and Mineral Industries Bulletin 62, p. 3-34.

Taylor, E.M., 1978, Field geology of SW Broken Top Quadrangle, Oregon: Oregon Department of Geology and Mineral Industries Special Paper 2, 50 p., map scale 1:24,000.

Taylor, E.M., 1981, Central High Cascade roadside geology—Bend, Sisters, McKenzie Pass, and Santiam Pass, Oregon, *in* Johnston, D.A., and Donnelly-Nolan, J., eds., Guides to some volcanic terranes in Washington, Idaho, Oregon, and northern California: U.S. Geological Survey Circular 838, p. 55-83.

Taylor, E.M., 1987, Field geology of the northwest quarter of the Broken Top 15 Minute Quadrangle, Deschutes County, Oregon: Oregon Department of Geology and Mineral Industries Special Paper 21, 20 p., map scale 1:24,000.

Taylor, E.M., and Ferns M.L., 1994, Geology and mineral resource map of the Tumalo Dam Quadrangle, Deschutes County, Oregon: Oregon Department of Geology and Mineral Industries Map GMS-81, scale 1:24,000.

Taylor, E.M., and Ferns, M.L., 1995, Geologic Map of the Three Creek Butte Quadrangle, Deschutes County, Oregon: Oregon Department of Geology and Mineral Industries Map GMS-87, scale 1:24,000.

Taylor, E.M., and Smith, G.A., 1987, Record of early High Cascade volcanism at Cove Palisades, Oregon: Deschutes Formation volcanic and sedimentary rocks,

in Hill, M.L., ed., Cordilleran Section: Geological Society of America Centennial Field Guide, v. 1, p. 313-315.

Thayer, T.P., 1939, Geology of the Salem Hills and the North Santiam River Basin, Oregon: Oregon Department of Geology and Mineral Industries Bulletin 15, 40 p.

Tolan, T.L., and Beeson, M.H., 1984, Intracanyon flows of the Columbia River Basalt Group in the lower Columbia River Gorge and their relationship to the Troutdale Formation: Geological Society of America Bulletin, v. 95, p. 463-477.

Walder, J.S., Gardner, C.A., Conrey, R.M., Fisher, B.J., and Schilling, S.P., 1999, Volcano hazards in the Mount Jefferson region, Oregon: U.S. Geological Survey Open-File Report 99-24, 14 p.

Walker, G.W., and Duncan, R.A., 1989, Geologic map of the Salem 1 by 2° Quadrangle, western Oregon: U.S. Geological Survey Miscellaneous Investigations Series Map I-1893, scale 1:250,000.

Walker, G.W., and Nolf, B., 1981, High Lava Plains, Brothers Fault Zone to Harney Basin, Oregon, *in* Johnston, D.A., and Donnelly-Nolan, J., eds., Guides to some volcanic terranes in Washington, Idaho, Oregon, and northern California: U.S. Geological Survey Circular 838, p. 105-118.

Wendland, D.W., 1988, Castle Rocks: A late Miocene eruptive center at the north end of Green Ridge, Jefferson County, Oregon: Oregon State University MS Thesis, 196 p.

Williams, D.L., Hull, D.A., Ackermann, H.D., and Beeson, M.H., 1982, The Mt Hood region: Volcanic history, structure, and geothermal potential: Journal of Geophysical Research, v. 87, p. 2767-2781.

Wozniak, K.C., 1982, Geology of the northern part of the southeast Three Sisters Quadrangle, Oregon: Oregon State University MS Thesis, 98 p.

Yeats, R.S., Graven, E.P., Werner, K.S., Goldfinger, C., and Popowski, T.A., 1996, Tectonics of the Willamette Valley, Oregon: U.S. Geological Survey Professional Paper 1560, p. 183-222.

Yogodzinski, G.M., 1985, The Deschutes Formation–High Cascades transition in the Whitewater River Area, Jefferson County, Oregon: Oregon State University MS Thesis, 165 p.

Geology and Geomorphology of the Lower Deschutes River Canyon, Oregon

Robin A Beebee, Department of Geological Sciences, University of Oregon, Eugene, Oregon 97403; rbeebee@darkwing.uoregon.edu

Jim E. O'Connor, U.S. Geological Survey, 10615 SE Cherry Blossom Drive, Portland, Oregon 97216; oconnor@usgs.gov

Gordon E. Grant, U.S. Forest Service Pacific Northwest Research Station, Corvallis, Oregon, 97331; gordon.grant@orst.edu

INTRODUCTION

This field guide is designed for geologists floating the approximately 80 kilometers (50 miles) of the Deschutes River from the Pelton–Round Butte Dam Complex west of Madras to Maupin, Oregon. The first section of the guide is a geologic timeline tracing the formation of the units that compose the canyon walls and the incision of the present canyon. The second section discusses the hydrology, morphology, and formation of the present river channel. The third section is a river log, describing sights and stops for a 3-day floating field excursion.

GEOLOGIC HISTORY OF THE DESCHUTES BASIN

The northward-flowing Deschutes River joins the Columbia River approximately 160 km east of Portland, Oregon, draining a 26,900 km^2 basin that is bounded to the east by the Ochoco Mountains, to the west by the Cascade Range, and to the south by the Klamath and Great Basin Divides (Fig. 1). The basin is formed in sedimentary, igneous, and metamorphic rocks ranging from 250 million to 1.3 thousand years old, but most rocks are Tertiary and Quaternary lavas or other eruptive materials emplaced during the past 65 million years (Fig. 2). Along the route that we will be floating, the present canyon and river course reflect a 20 million year struggle among volcanic, tectonic, and fluvial processes. Since incision of the canyon of the Deschutes River during the Pliocene, lava dams, landslide dams, lahars, and exceptional floods have pinned the river between armored boundaries that were resistant even to the greatest floods of historical times. The cumulative result of the geology, climate, hydrology, and catastrophic past of the drainage basin is a river of remarkably uniform flow in an unusually stable channel.

Clarno and John Day Volcanism: 54–22 Million Years Ago

The central Deschutes Basin and Ochoco Mountains are underlain by volcanic, volcaniclastic, and sedimentary rocks of the Eocene Clarno Formation and the latest Eocene to early Miocene John Day Formation. These rocks formed 54 to 22 million years ago during a stage of subduction-zone volcanism predating and early in formation of the Cascade Range, and consist of lavas of various compositions, volcanic-ash flows, tuffaceous sedimentary rocks, and clay-rich paleosols. Erodible tuffaceous units and cliff-forming basalt of the John Day Formation also underlie younger Tertiary and Quaternary rocks in the valley of the lower Deschutes River (Fig. 2). Where the river has cut through these tuffs, canyon walls are particularly susceptible to landsliding, and all of the large landslide complexes in the lower Deschutes Basin are within these units.

Columbia River Flood Basalt: 17–14.5 Million Years Ago

Between 17 and 14.5 million years ago, flows of the Columbia River Basalt Group (CRBG) buried the northern and northeastern portions of the lower Deschutes River Basin with lava up to 600 meters deep. These lavas, which cover a total of 165,000 km^2, issued from numerous vents in eastern Washington, western Idaho, and eastern Oregon. Contemporaneous

Field Guide to Geologic Processes in Cascadia: Oregon Department of Geology and Mineral Industries Special Paper 36, 2002.

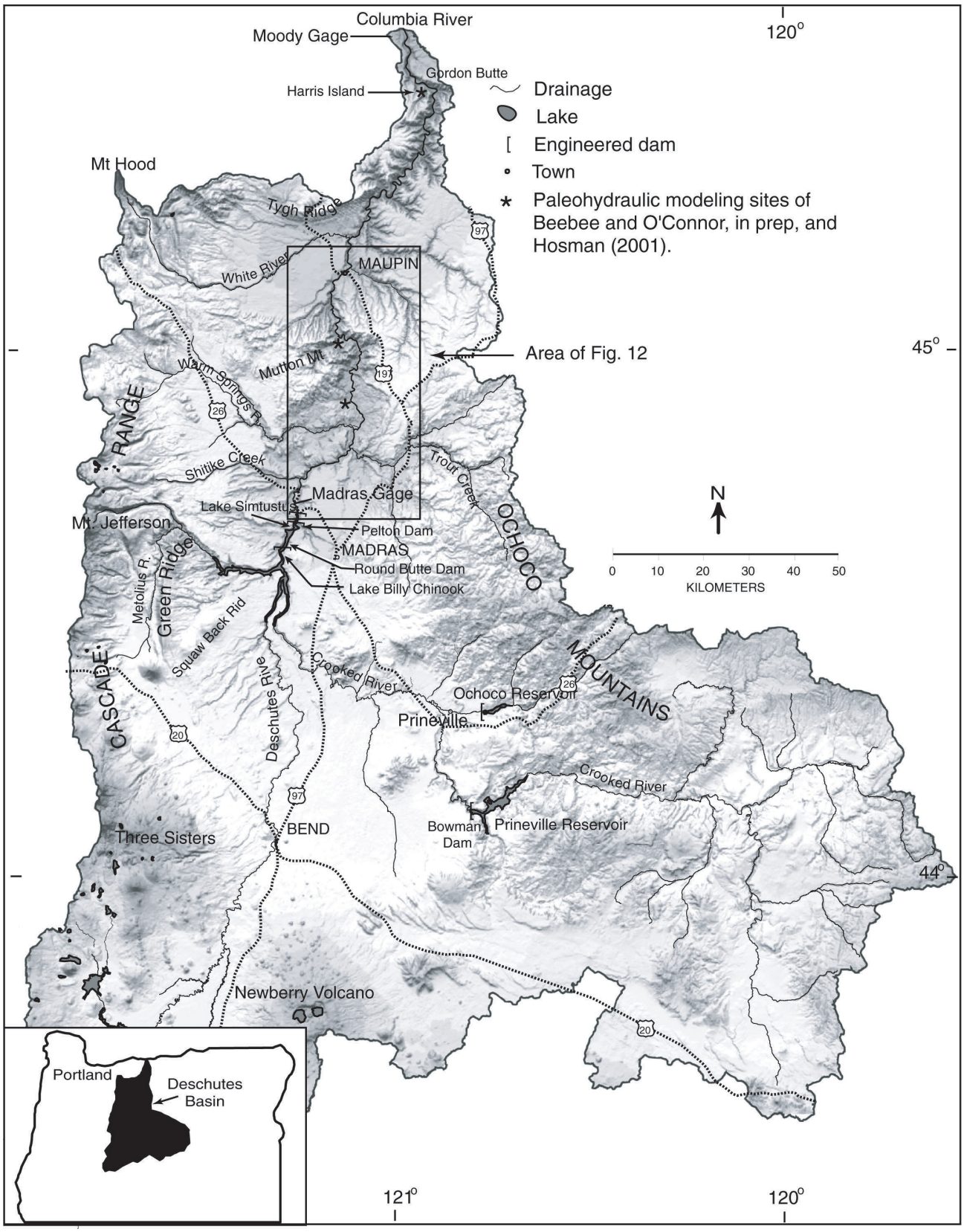

Figure 1. Drainage basin map of the Deschutes River.

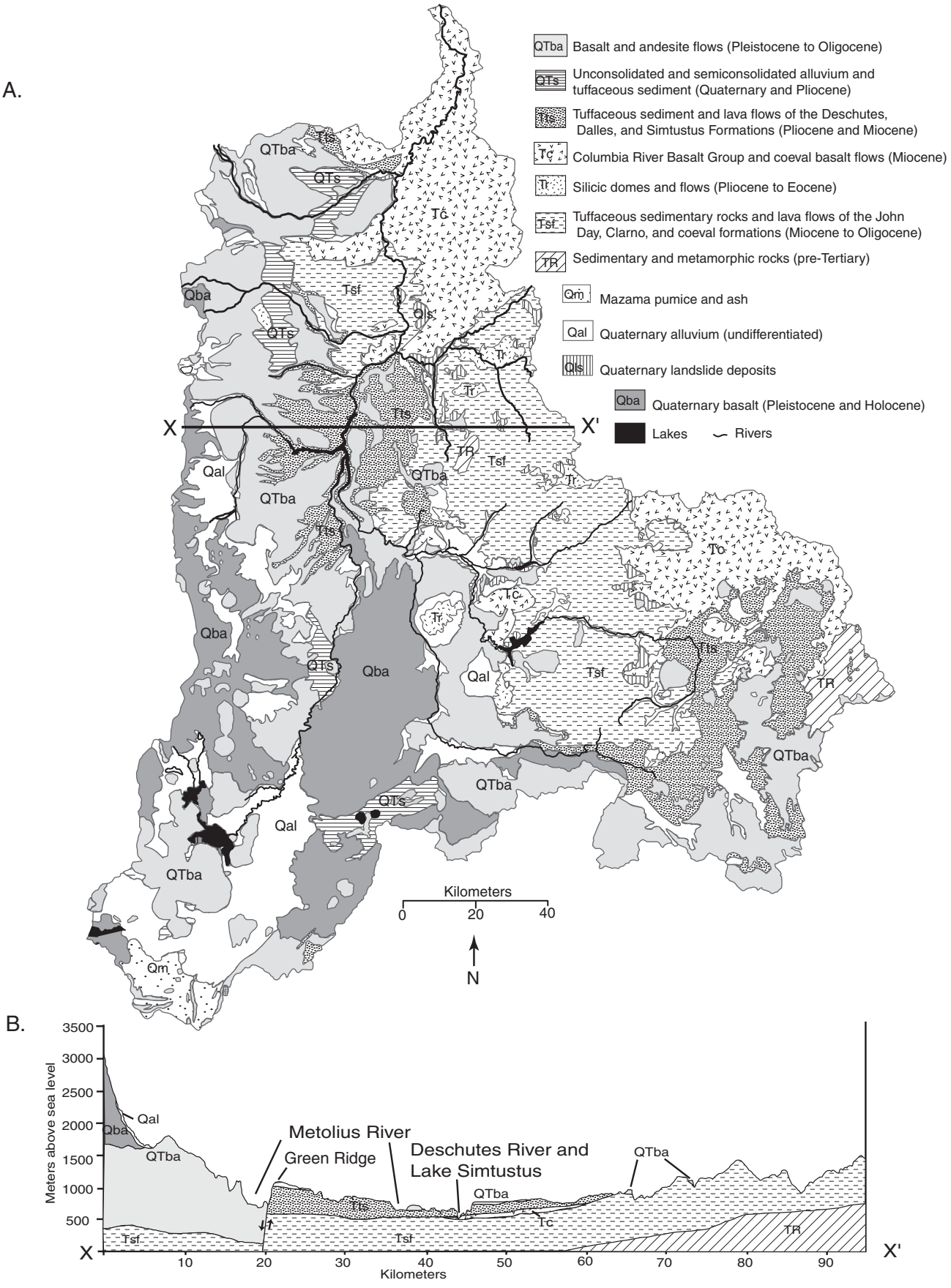

Figure 2. A. Geology of the Deschutes Basin generalized from Walker and McLeod (1991). B. Geologic cross section along line X to X' after Smith (1986).

Prineville Basalt, distinguished by elevated P_2O_5 and Ba, flowed from vents near the Bowman Dam site on the Crooked River and mingled with CRBG flows traveling south from the Columbia River (Hooper and others, 1993). The distribution of CRBG and contemporaneous basalts suggests that the geometry of the Deschutes Basin as a northward drainage between the Ochoco Mountains and the ancestral Cascade Range had been established by 17 million years ago (Smith, 1986).

A Very Different Deschutes River: 12–4 Million Years Ago

Following the emplacement of the Columbia River Basalt Group, volcanic debris from Cascade Range volcanism began to fill the Deschutes Basin between Bend and Trout Creek (Smith, 1986). These deposits, which constitute the Deschutes Formation, consist of ignimbrites, lahar deposits, ash-flow and air-fall tuffs, fluvial sediments, and basalt flows emplaced between 12 and 4 million years ago. Similar sedimentary units interbedded with volcanics were deposited south of Tygh Ridge and along the Columbia River. These are known as the Dalles Formation, which is generally analogous to the Deschutes Formation. Most of the silicic volcanic rocks in the Deschutes Formation were erupted from the ancestral Cascade volcanoes, with minor input from vents to the east, while mafic vents within the Deschutes Basin supplied basaltic lava (Smith, 1986; Hayman, 1983).

Gravel of the ancestral Deschutes River within the Deschutes Formation indicates that between 7.4 and 4 million years ago, the river was situated similarly to the modern Deschutes River, but instead of flowing through a narrow canyon, it spread out across a broad plain several hundred meters higher than its present altitude, continually aggrading and retrenching in response to influxes of volcanic material from the west (Smith, 1986). The distribution and thickness of fluvial and volcaniclastic deposits in the Deschutes Formation suggest that the ancestral Deschutes River switched from a mostly aggrading channel to a mostly degrading channel near the present position of Lake Simtustus, due to a northward decrease in volcanic sediment supply from the ancient Cascades and to uplift in the northern part of the basin (Hayman, 1983; Smith, 1982).

Sinking Volcanoes and Local Lava: 6–4 Million Years Ago

The Deschutes Formation was capped by basalt flows from vents in the central Deschutes Basin near Round Butte Dam and Squaw Back Ridge between 6 and 4 million years ago. The lavas cover broad upland surfaces, indicating that the Deschutes River and its tributaries had not yet cut deep canyons. At the same time, westward extension caused the Pliocene Cascade volcanic platform to sink several hundred meters. Green Ridge is a local bounding scarp of the High Cascade Graben (Fig. 2B). The eruptive style of the Cascade Range volcanoes shifted from silicic to generally less explosive mafic volcanism (Smith and Priest, 1983), and material shed from them no longer had a direct route to the Deschutes Basin. The Deschutes River began to cut back down through layers of lava and sediment around 4 million years ago, incising to near-present altitudes near Round Butte by about 1.2 million years ago (Smith, 1986).

Lava Dams at Both Ends: 1.6–0.7 Million Years Ago

Between 1.2 and 0.7 million years ago, basaltic lava from Newberry Volcano to the south repeatedly flowed into the Crooked River Gorge and partially filled the Crooked, Deschutes, and Metolius Canyons at the present location of Lake Billy Chinook (Sherrod and others, in press), damming the river and forcing it to cut a new channel around the flow margins. The river was similarly dammed during the Quaternary by an undated basalt flow from Gordon Butte that entered the canyon about 8 km upstream from the Columbia River confluence (Newcomb, 1969).

Bend–Tumalo Eruptions: 400,000 Years Ago

Huge volumes of silicic volcanic rocks erupted around 400,000 years ago from vents in the Bend–Tumalo area (Hill and Taylor, 1989). Thick accumulations of the Bend Pumice remain in the upper Deschutes Basin, and several terrace deposits preserved in the lower Deschutes Canyon contain the pumice. Pyroclastic flow deposits on a gravel terrace near Shitike Creek indicate that the river was locally clogged with sediment during or shortly after these eruptions (Hayman, 1983). The Bend Pumice has been found in terraces as far downstream as

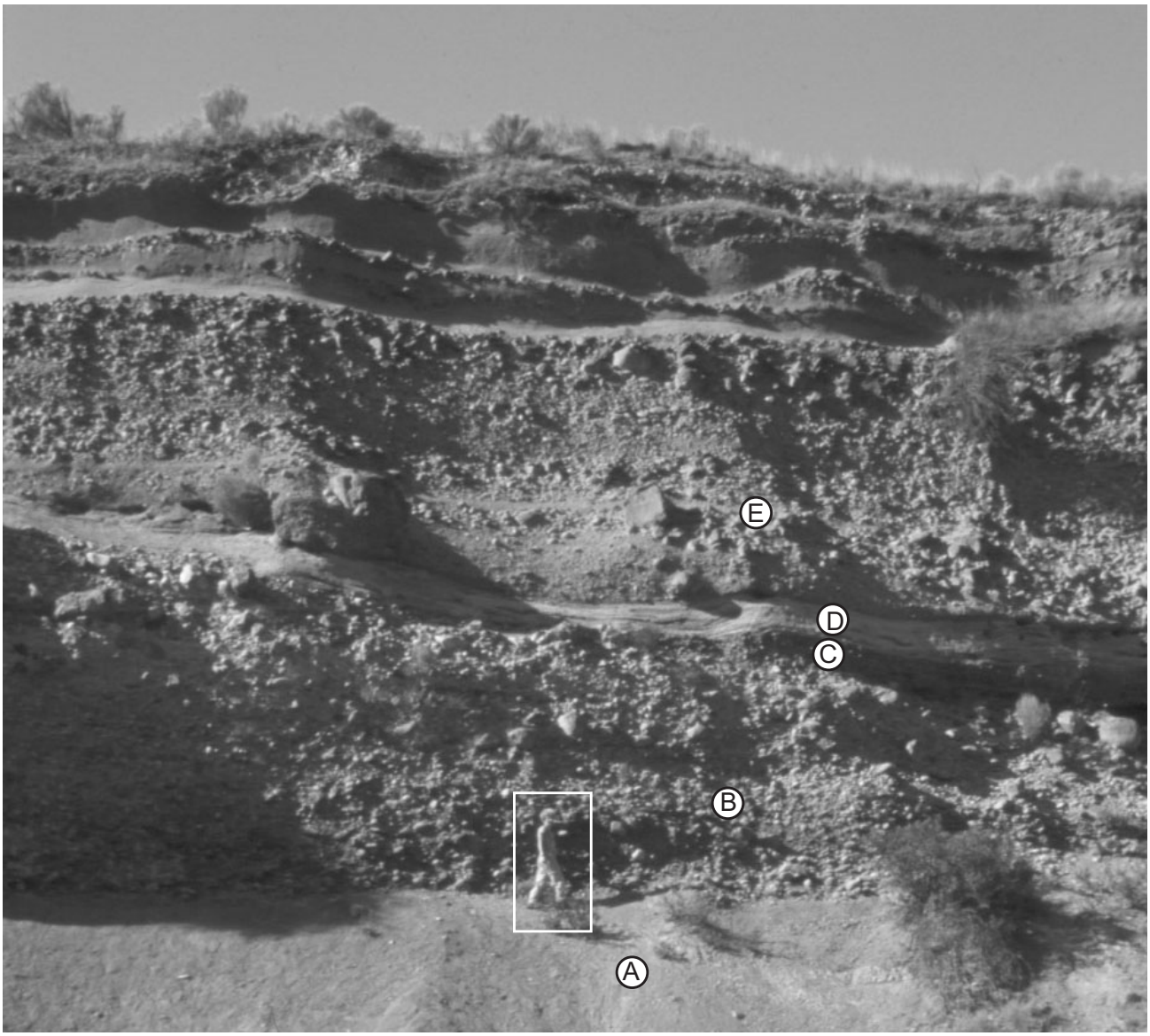

Figure 3. South Junction Terrace, River Mile 83.5 (Stop 3). A. Tilted strata of the John Day Formation. B. Fluvial gravel. C. Fluvial sand. D. Ashy lahar. E. Gravelly lahar. Unit E contains pumice clasts from a roughly 100,000 year old Mt Jefferson eruption (O'Connor and others, in press). The person is 1.68 m tall.

River Mile (RM) 31, suggesting that before this eruptive cycle, the river may have aggraded throughout much of its length.

Mt Jefferson Lahar: 100,000 Years Ago

Along the lower 50 kilometers of the river, gravelly lahar deposits approximately 15 meters above the current river level contain pumice from a 100 ka eruption of Mt Jefferson. This lahar traveled at least 200 kilometers from its source, apparently a record for the Cascade Range (J.E. O'Connor and A.M. Sarna-Wojcicki, unpub data, 2000). Pumice and ash-rich lahar deposits from the Mt Jefferson eruption are also interbedded in fluvial gravel 50 meters above river level near the Warm Springs River confluence (Fig. 3).

Pleistocene Landslide Dams and Outburst Floods: 40,000–10,000 Years Ago

Although undoubtedly impressive at the time, volcanic eruptions during the Quaternary have left far less of a mark on the modern channel of the Deschutes River than have landslides from the canyon walls. Uplift of the Mutton Mountains, along with changes in base

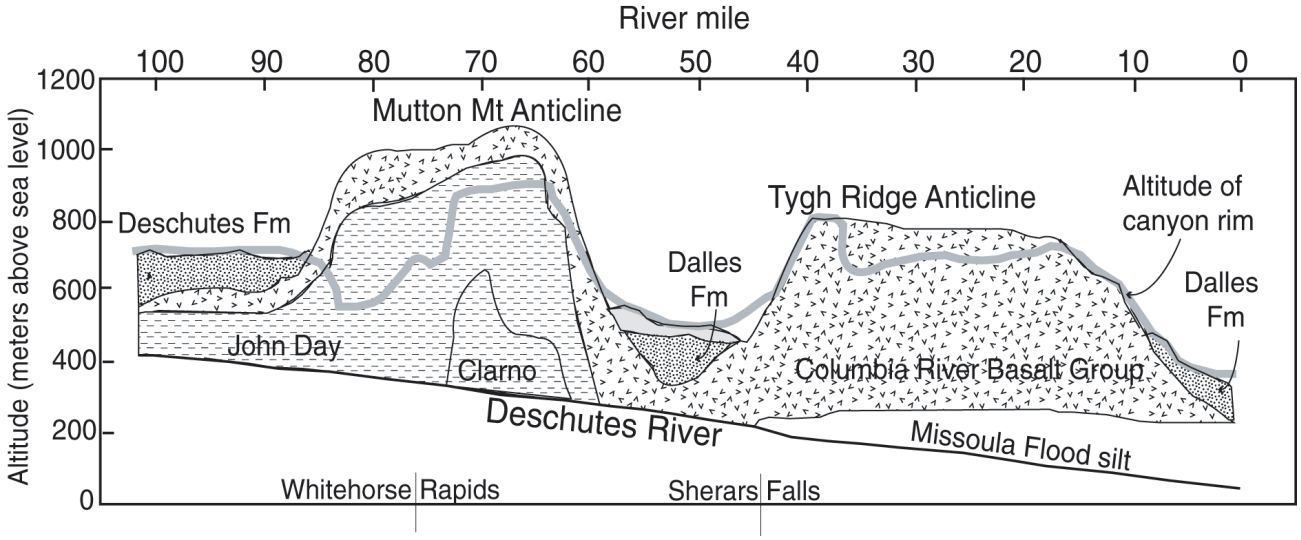

Figure 4. Longitudinal profile of the lower Deschutes River showing the exposed geology of the canyon. The gray line represents the altitude of the canyon walls superimposed on the total relief of the surrounding visible geologic formations and structures. Patterns follow Figure 2.

level and sediment delivery, have caused the Deschutes River to cut a deep canyon through alternating resistant lava flows and soft volcaniclastic sediment (Fig. 4). Between the Pelton–Round Butte Dam Complex and North Junction (RM 70), the river cuts through the soft sediment of the John Day Formation, capped by lava of the John Day Formation, the Columbia River Basalt Group, and the Deschutes Formation. This sequence of lithologies is particularly susceptible to slope failure, and mass-movement deposits ranging from single slump blocks to hummocky landscapes covering 50 square kilometers dominate the valley walls along this segment of the river. Many of these blocks likely have been slowly slumping throughout incision of the river, but several landslides were rapid enough to dam it during the Pleistocene. These include Whitehorse Rapids Landslide (The Pot) that created Whitehorse Rapids (RM 79-75), the large debris flow near Dant (RM 64), and the landslides that delivered boulders to Wapinitia and Boxcar Rapids at RM 55-53 (Fig. 5). Trout Creek Rapids may also be the remnant of a landslide dam or breach deposit. Few dates constrain these mass movements and resulting floods, but they all seem to have occurred during the Pleistocene, based on the amount of surface erosion and weathering of boulders in the deposits. Whitehorse Rapids Landslide seems to be the youngest large mass movement, and its persistent influence on the channel is difficult for boaters to ignore. Whitehorse Rapids, which drops 12 meters over less than 1 kilometer, is the remains of the landslide dam, and high bouldery deposits directly downstream from the rapids were deposited when the dam failed catastrophically (Figs. 6, 7). The presence of airfall tephra from the 7.6 ka eruption of Mt Mazama (Zdanowicz and others, 1999) in a closed depression in the landslide hummocks suggest that the Whitehorse Rapids Landslide occurred prior to that time. Radiocarbon dates from flood deposits downstream from Whitehorse Rapids indicate that the landslide dam breached catastrophically at least once between about 40 ka and 3.8 ka (O'Connor, Curran, and others, in press).

Missoula Floods: 15,000–12,000 Years Ago

When ice dams impounding Glacial Lake Missoula failed repeatedly in the Pleistocene, floodwater traveled down the Columbia River and backed up in tributaries to an altitude of approximately 300 meters above sea level in the vicinity of the Deschutes River. Slackwater silt and ice-rafted boulders were deposited on the banks of the Deschutes River as far south as

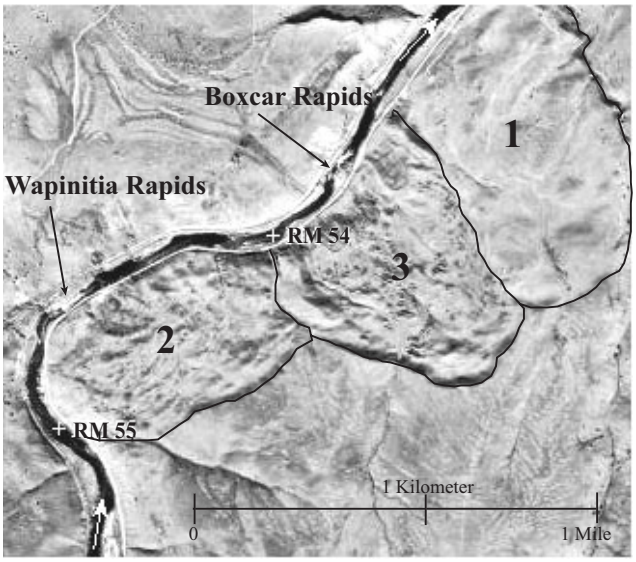

Figure 5. Air photo of overlapping landslides numbered 1–3 (oldest to youngest) at River Mile 55–53, and the rapids they created.

Maupin (Orr and others, 1992). The effects of the Missoula Floods are not evident upstream from Maupin, but its tan silt up to several meters thick mantles the banks of the Deschutes River downstream from about RM 50.

Outhouse Flood: 4100–2800 Years Ago

Bouldery cobble bars, massive sand deposits, and stripped bedrock surfaces 5 to 19 meters above summer low flow stages along the lower Deschutes River were left by at least one exceptional Holocene flood that was substantially larger than any historic flow (Figs. 8, 9). The Outhouse Flood, named for Bureau of Land Management toilet facilities built on many of its bouldery deposits, occurred during the middle Holocene, between 4.1 and 2.8 ka (Beebee and O'Connor, in press). Because of the disparity in flow magnitude between the largest historic flows and the discharge indicated by the high and coarse-grained Outhouse Flood deposits, we originally interpreted the Outhouse Flood to be the result of some sort of dam breach within the basin, similar to but more recent than that caused by th breaching of the Whitehorse Rapids Landslide. However, no obvious middle Holocene breach site has been located, and step-backwater modeling of three reaches at River Miles 82, 65, and 11 indicates that discharge increased substantially downstream in a manner similar to historical storm floods (Fig. 10). Hence our current interpretation of these features is that they were formed by an exceptional meteorological flood with a discharge 2–3 times as great as any flood of record.

Old Maid Lahar: Approx AD 1800

Mt Hood's Old Maid eruptive cycle about AD 1800 produced at least one lahar that entered the Deschutes River via the White River. Its volume was meager compared to lahars from the Bend–Tumalo and Mt Jefferson eruptions, but remnant gray pebbly sands lie near the White River confluence at RM 47, well above the stages of floods during the past 200 years.

Historical Flood: AD 1861

According to written accounts and geomorphic evidence, the rain-on-snow flood in December 1861 was the largest historical flood in the lower Deschutes Basin (Anonymous, 1861). Studies of the Crooked River suggest that the 1861 flood was the biggest flood in that drainage during the entire Holocene (Levish and Ostenaa, 1996). The stratigraphic position of deposits from the 1861 flood at the lower Deschutes River also shows that it was larger than recent floods in 1964 and 1996 (Fig. 8), which were regulated upstream by dams.

Ochoco Dam: AD 1920

The engineered Ochoco Dam near Prineville closed in 1920, providing flow regulation in the Crooked River part of the Deschutes Drainage Basin.

The Dalles Dam: AD 1956

The Dalles Dam on the Columbia River closed in 1956, flooding the mouth of the Deschutes River and Celilo Falls on the Columbia River.

Bowman Dam: AD 1960

Bowman Dam on the Crooked River closed in 1960, providing flood control and water storage in the Crooked River Basin.

Pelton–Round Butte Dam Complex and Flood: AD 1964

The Pelton-Round Butte Dam Complex was completed in 1964, creating Lake Billy Chinook. In December 1964, a rain-on-snow event produced record floods on the Crooked

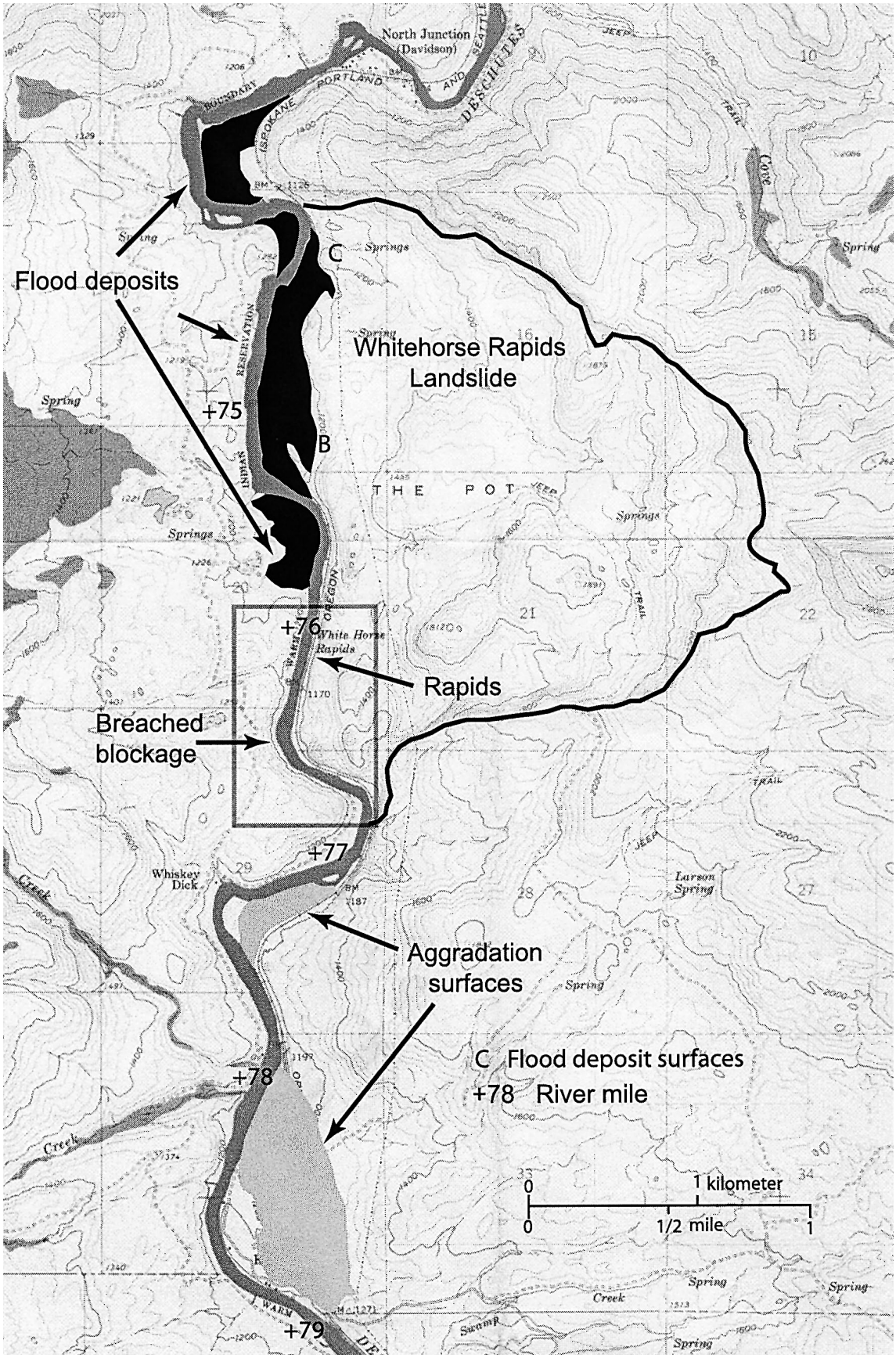

Figure 6. Geomorphic features related to the dam produced by the Whitehorse Rapids Landslide and the area of its outburst flood deposits plotted on the U.S. Geological Survey Kaskela 7.5-Minute Quadrangle.

and Deschutes Rivers. Because Lake Billy Chinook was not yet full, the Pelton–Round Butte Dam Complex provided some flood control. Presently, the dam is operated for hydropower and recreation but does not provide flood control because it is kept full.

Historical Flood: AD 1996

The February 1996 flood was caused by a rain-on-snow event similar to the one in 1964. Although this flood was regulated by the Ochoco and Bowman Dams, Lake Billy Chinook was already full, and the flood wave passed through the Pelton–Round Butte Dam Complex without attenuation. The 1996 and 1964 floods were similar in discharge, and they are calculated to have a recurrence interval of about 100 years in light of both the gaged record and the stratigraphic record of flooding during the past 2000 years (Hosman and others, in press).

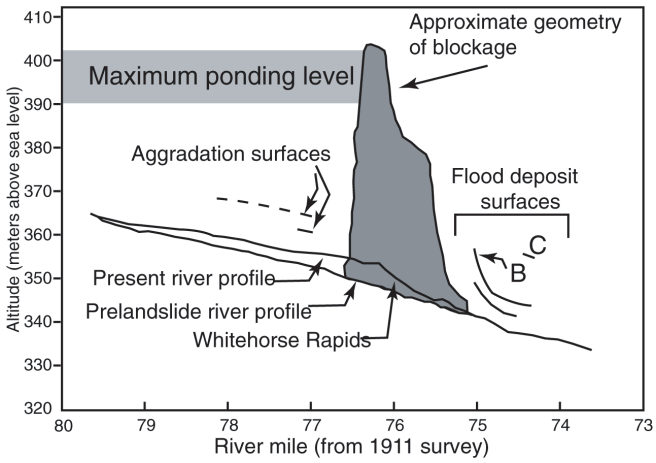

Figure. 7. Diagram of the breach site of the Whitehorse Rapids blockage showing the probable former river profile and the profile after the blockage. Surfaces B and C are labeled on Figure 6.

QUATERNARY GEOMORPHOLOGY AND HYDROLOGY

Many of the geomorphic studies described in this field guide were conducted in conjunction with Federal Energy Regulatory Commission's relicensing of Portland General Electric's Pelton–Round Butte Dam Complex. The earliest studies were begun in 1995 to determine the specific effects of the dams on the downstream hydrology, channel form, and aquatic habitat. The unexpected conclusion, first described in a pair of Oregon State University theses, was that the dam had little apparent influence on physical aspects of the river downstream from Lake Billy Chinook (McClure, 1998; Fassnacht, 1998). These results differ from studies of other regulated rivers that showed significant changes in channel and floodplain sedimentation, and consequently aquatic habitat, in the decades following impoundment (Andrews and Nankervis, 1995). The absence of such effects on the Deschutes River inspired follow-up studies aimed at providing overall understanding of important geomorphic processes controlling valley-bottom and channel conditions (Curran and O'Connor, in prss; Grant and others, 1999; O'Connor, Grant, and Haluska, in press). The conclusion of these latter studies is that the interruption of sediment and water flux by the dam complex has been minor compared to natural flow regulation and sediment trapping upstream of the dam. The river's steady discharge has been noted since the very first studies of the Deschutes River and is one of its most remarkable aspects. For example, Russell (1905) wrote

> The Deschutes is of especial interest to geographers, as it exhibits certain peculiarities not commonly met with. Although flowing from high mountains on which precipitation varies conspicuously with seasonal changes and where snow melts rapidly as the heat of summer increases, its volume, throughout a large section of its course, is practically constant throughout the year.

The young unincised volcanic terrain provides natural flow regulation in the southern and western parts of the drainage basin (Fig. 2). There, precipitation and snowmelt drain into porous aquifers and discharge from voluminous cold springs months to decades later (Manga, 1996). Snowpack, lakes, and a few glaciers in the Cascade Range also store and release seasonal precipitation, further dampening month-to-month variation in discharge. The resulting steady flow of the Deschutes River is striking when compared with flow characteristics of the neighboring John Day and Willamette Rivers (Fig. 11). Peak gaged flows on the Willamette

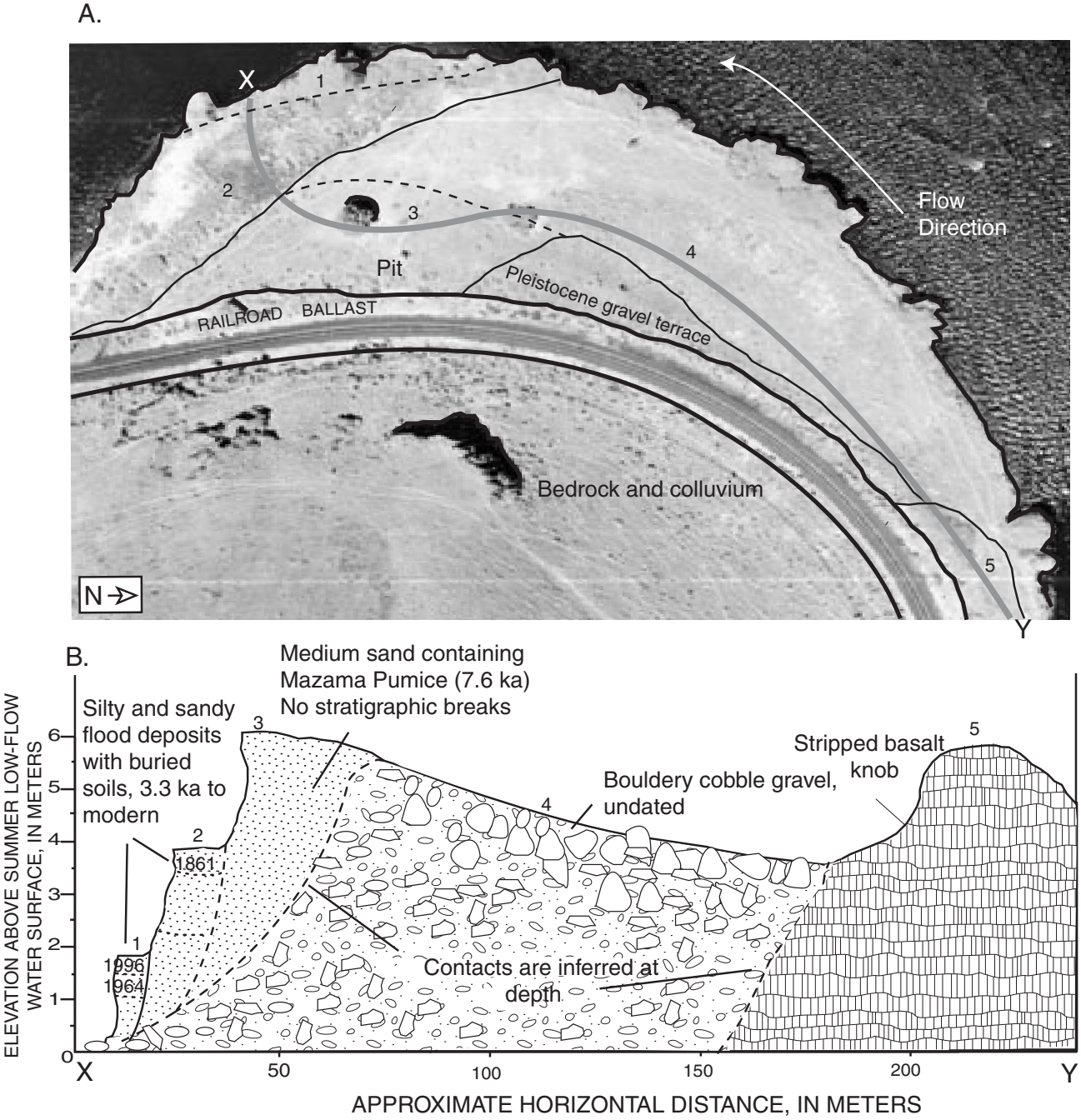

Figure 8. A. Air photo of an Outhouse Flood bar near Dant, River Mile 65 (Stop 7). B. Cross section of the flood bar along line X to Y.

and John Day Rivers were more than 20 times the river's mean flow, whereas peak gaged flow (in Feb 1996) on the Deschutes River was less than 5 times the mean flow.

Fluvial erosion and transport of sediment in the basin is hindered by the lack of integrated surface drainage and high-discharge events in the young volcanic terrain. A 1998 survey of the sediment trapped in the arms of Lake Billy Chinook revealed that the Deschutes and Crooked Rivers had been delivering less bedload over the previous 34 years than any other river of comparable size reported in the world literature (O'Connor and others, in prep). With little incoming sediment to trap and little floodwater to store, the Pelton–Round Butte Dam Complex has not resulted in such downstream impacts as bed coarsening,depth reduc-

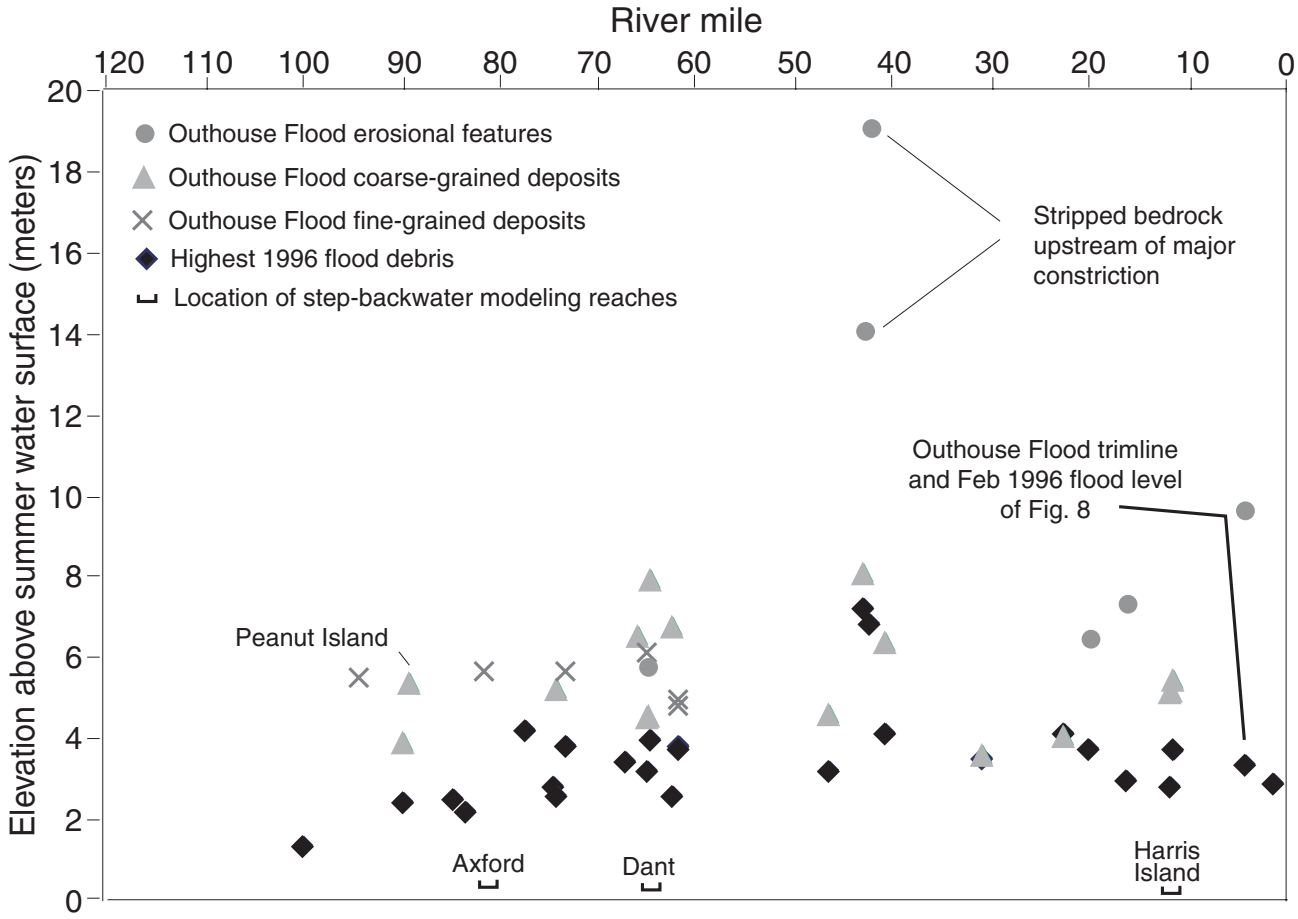

Figure 9. Comparison of the surveyed heights of paleostage evidence from the February 1996 flood and the Outhouse Flood.

tion, or channel narrowing (Fassnacht and others, in prep).

Studies spanning the 1996 flood concluded that this event, which was the largest in 135 years, did not substantially affect the channel form. The resilience of the channel boundaries is a testament to the magnitude of the previous events that shaped them relative to the modern hydrologic regime. Mass movements and high-magnitude paleofloods (such as the Outhouse Flood) transported sediment into the channel that has been immobile for thousands of years. As an indication of how influential these former high-magnitude events have been, 35% of all alluvial surfaces flanking the lower 160 kilometers of the Deschutes River were deposited by the Outhouse Flood alone, and they haven't been reworked for at least 3,000 years. Similarly, 11 of the 23 named rapids on the river are composed of coarse alluvium introduced into the channel by either the Outhouse Flood or by Pleistocene mass movements, and they were not significantly modified by historical floods (Curran and O'Connor, in prep). For the time being, the canyon that was clogged by hot ash and lava, dammed by landslides, and carved out by floods, houses a remarkably stable, subdued, and indeed, ineffective river.

RIVER LOG

Field trip stops are shown on Figure 12. Distances are given in river miles (RM), which are measured from the mouth of the river and interpolated from river miles marked on 7.5-minute U.S. Geological Survey topographic quadrangles. The directions "river right" and "river left" assume you are looking downstream to the north.

Between the Metolius River and North Junction (RM 69), the entire left (west) bank of the Deschutes River is on the Warm Springs Indian Reservation and is accessible by permit

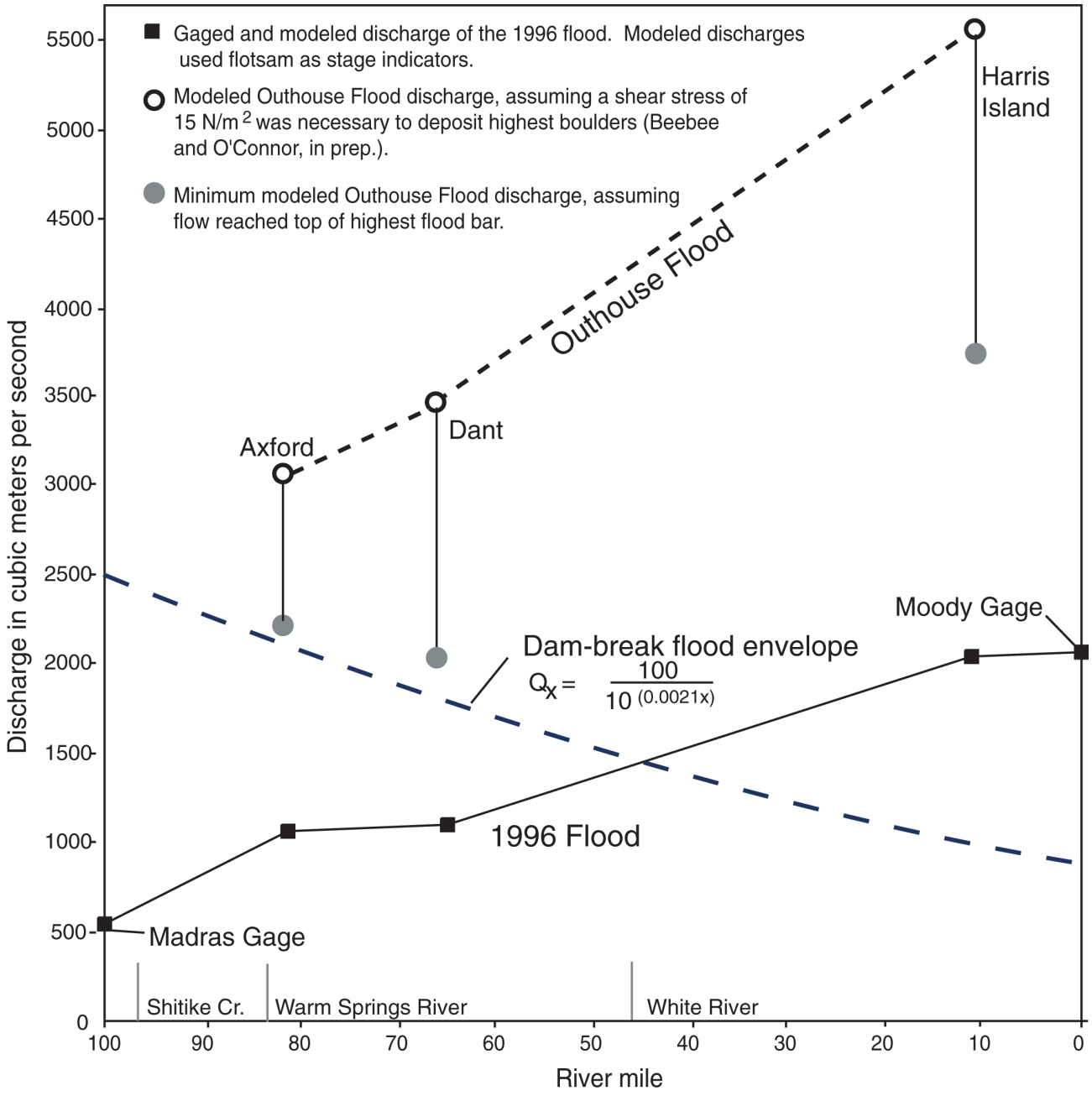

Figure 10. Comparison of modeled discharges of the Outhouse Flood with gaged and modeled discharges of the February 1996 storm flood. Envelope defining the peak discharge attenuation of historical dam-breach floods is from Costa (1988). In this equation, x is the distance downstream from the breach in km, and Qx is percentage of discharge at the breach.

only. Although the majority of riverbanks are public land, some stops involve private property, and permission of the landowners should be obtained prior to entering. As a State Scenic Waterway and a National Wild and Scenic River managed by the Bureau of Land Management, the Deschutes River has certain restrictions for trip size and collecting that should be followed. Most importantly, the Deschutes River is a whitewater river in the area covered by this field guide and should be floated only by experienced whitewater rafters or as part of a professionally guided expedition.

The U.S. Geological Survey 7.5-minute quadrangles that cover the course of the trip are, in downstream order, Madras West, Eagle Butte, Gateway, Kaskela, Dant, Maupin SW, Tygh Valley, and Maupin. Useful geologic maps from

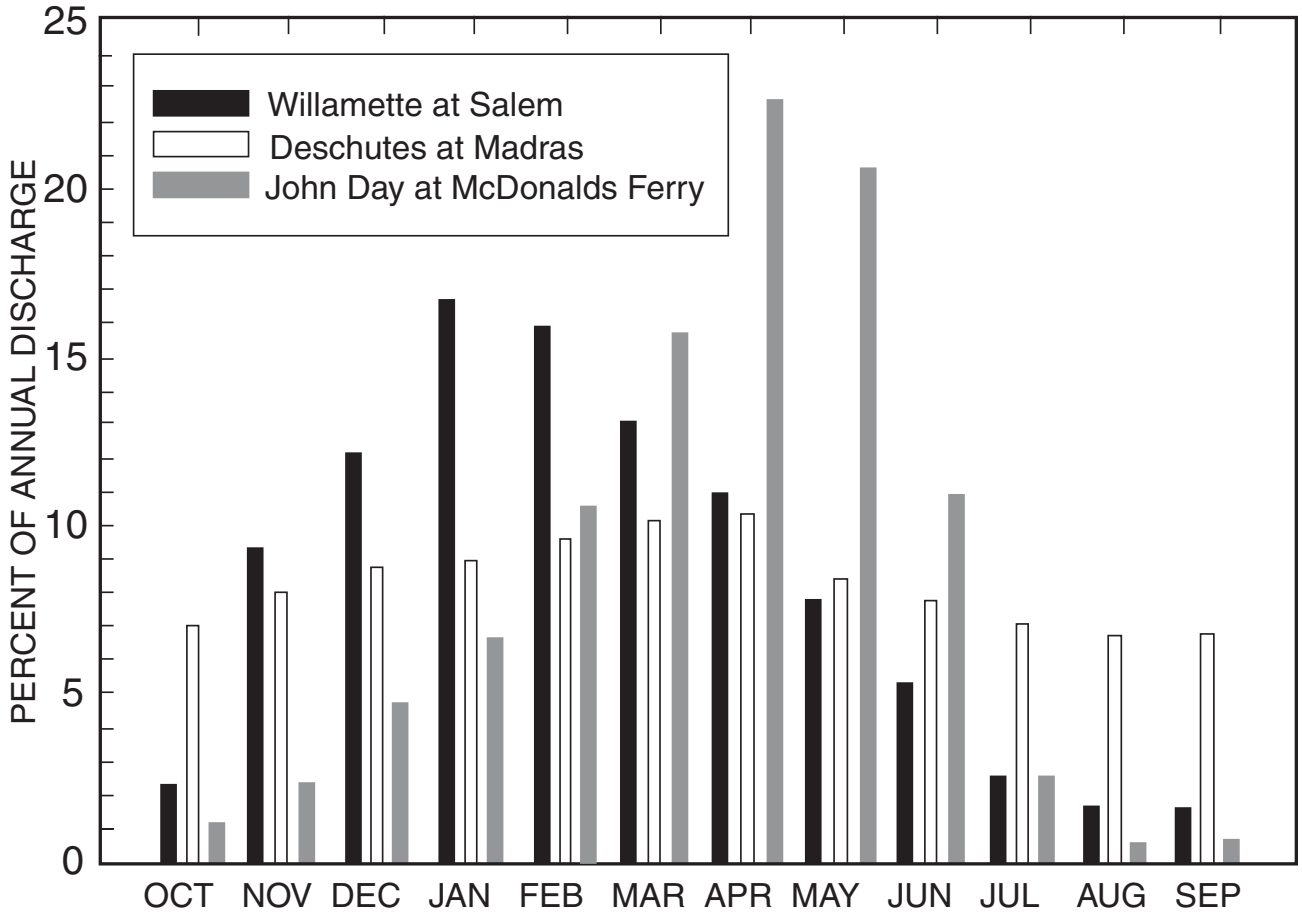

Figure 11. Bar graph showing mean monthly discharge of the Deschutes River, John Day River, and Willamette River.

which we have drawn much of the information presented about the pre-Quaternary geology include Smith (1987, 1:24,000-scale mapping of the Madras West and Madras East Quadrangles), Smith and Hayman (1987, 1:24,000-scale mapping of the Eagle Butte and Gateway Quadrangles), Waters (1968, reconnaissance geologic map of the Madras 15-Minute Quadrangle—covering the Eagle Butte, Gateway, and Kaskela 7.5-Minute Quadrangles along the trip route), and Bela (1982, 1:250,000-scale compilation of The Dalles 1x2-Degree Quadrangle—including the Dant, Tygh Valley, Maupin SW, and Maupin 7.5-Minute Quadrangles along the trip route).

RM 100.1: Reregulation Dam

We will embark just below the Reregulation Dam, which stores flow fluctuations due to power generation at the Round Butte and Pelton Dams upstream, releasing almost natural flows. These three dams are jointly owned and operated by Portland General Electric and the Confederated Tribes of Warm Springs. Pelton Dam (which impounds Lake Simtustus approximately 4 kilometers upstream) and the Reregulation Dam were constructed in the late 1950s, and Round Butte Dam (which impounds Lake Billy Chinook approximately 16 kilometers upstream) was constructed in the early 1960s. Total power generation capacity is 427 megawatts. Note that this property is owned by Portland General Electric and is not open to the public.

RM 100: U.S. Geological Survey gaging station (Deschutes River near Madras). Cross-section geometry extracted from discharge measurements over the period of 1957-1998 shows little change in channel morphology (Fassnacht and others, in prep).

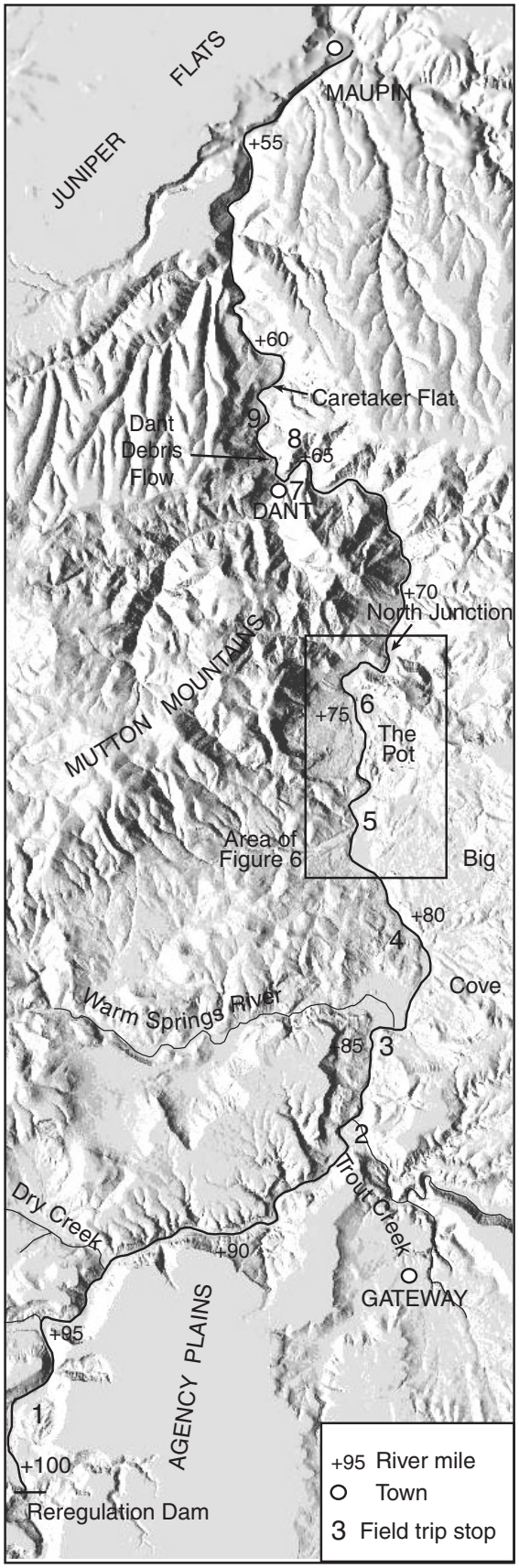

Figure 12. Field trip route with stops and river miles on a U.S. Geological Survey 10-meter digital elevation model (DEM).

RM 99: Quaternary terrace near river level and large slump complex upslope, both on river right.

RM 98: Stop 1. Disney Riffle

This has been the site of both geomorphic and ecologic investigations examining downstream effects of the dams. These studies have revealed surprisingly few effects on channel morphology, bedload transport, or bed texture. No evidence of channel degradation or bed coarsening below the dams has been observed, which we attribute to the unusually steady flow regime, very low rates of sediment supply above the dam, low frequency of bedload transport, and resistant channel boundaries. Evidence for low transport frequency is observed in salmon-generated dunes just downstream from this site along the margin of the right-hand island. These redds have not changed position or amplitude in the 15 years since they were last occupied.

RM 97: Highway 26 crossing. Public boat launch on river right, Shitike Creek confluence on river left. Quaternary terraces on river right contain pyroclastic flows from the Bend–Tumalo eruptions.

RM 95: Mecca Flat and public boat launch on river right. Light-colored layers exposed in erosion gullies on both sides of the river are tuffaceous sedimentary rocks of the John Day Formation. The John Day Formation is overlain by two Prineville basalt flows (middle Miocene), which in turn are overlain by poorly exposed Deschutes Formation and capped by the 5.3 Ma Agency Plains basalt flow.

RM 94: Dry Creek confluence on river left. The small channel circling the island at the tributary mouth is an important spawning area for resident rainbow and steelhead trout.

RM 93.5: Thin sedimentary beds of the Simtustus Formation are exposed between two Prineville basalt flows near the canyon rim on both sides of the river.

RM 90: Talus-covered slump complexes appear on both sides of the river.

RM 89: Peanut (Big) Island is a large boulder bar deposited by the Outhouse Flood in a local channel expansion. This is the most upstream feature confidently attributed to the Outhouse Flood, and it stands 5.3 meters above typical low-flow water level.

RM 88: Stop 2. Gateway Recreation Area

This boulder-studded alluvial surface on river right is interpreted as another Outhouse Flood bar, although local mass movements probably contributed some of the angular boulders. From this point until we enter the Mutton Mountain Anticline at RM 70, the canyon walls retreat into an undulating mass of ancient slump blocks composed of John Day Formation tuff and interbedded lava flows. The slump complex on river right between RM 85 and RM 75 is known as Big Cove. Smaller slump blocks directly downstream from Trout Creek may have impinged on the channel.

RM 87: Trout Creek Rapids. Boulders that make up Trout Creek Rapids were either part of a landslide that encroached on the channel, or outwash from a breached landslide dam.

RM 86: The tracks of the Burlington Northern Santa Fe Railroad descend Trout Creek to near river level and follow the Deschutes River for the remainder of their course to the Columbia. Originally constructed as the Oregon Trunk Line in 1910, this is one of two separate railroad lines that flanked the Deschutes River during the early 20th Century.

RM 83.5: Stop 3. South Junction Campground

Take out at the sandy bar on river right 200 meters downstream from the Warm Springs River confluence, then walk back upstream on the railroad tracks to the terrace exposure in the railroad cut (Fig. 3). Watch for the Burlington Northern Santa Fe coming around the bend. Lahar deposits in this terrace contain pumice from a roughly 100 ka eruption of Mt Jefferson. This terrace may correlate with Jefferson pumice-bearing bearing terraces downstream from RM 35.

Stop 4. Axford Flood Deposits

A sequence of fine-grained flood deposits several meters thick with dates spanning 7,000 years is exposed in a cutbank at the downstream end of the alluvial surface on river left. This site on Warm Springs Reservation property has been used for paleohydraulic modeling of the largest floods of the past several thousand years (Hosman, 2001; Hosman and others, in prep; Beebee and O'Connor, in prep).

RM 79: Kaskela Ranch on river right. This terrace and the surfaces downstream may represent aggradation behind the dam made by the Whitehorse Rapids Landslide (Figs. 6, 7).

RM 78.5: Stop 5. Whiskey Dick

Camp on river right. This gravel terrace, which was extensively quarried for railroad ballast during 1910-1912 railroad construction, is one of a series of terraces upstream from the Whitehorse Rapids Landslide (Fig. 6). None of these terraces has been dated, but we interpret them to be the result of aggradation behind a river blockage formed by the Whitehorse Rapids Landslide.

RM 77: Stop on river right and scout Whitehorse Rapids. Whitehorse Rapids are the largest rapids between Madras and Maupin, and over which the river drops about 12 meters in less than 1 kilometer. These rocky rapids are the remains of a landslide dam that breached catastrophically during the Pleistocene.

RM 76: Stop 6. The Pot

Take out on river right (Fig. 6) and climb up among the hummocks and knobs of The Pot to look at the landslide and breach site. Just downstream from the rapids, boulder bars, levees (on both sides of the river), and scoured divides are evidence that at least one large flood resulted from a breach of the landslide dam. A radiocarbon date on charcoal that accumulated in a small closed depression formed by a flood bar yielded an age of 3,820±240 ^{14}C yr ago, providing a minimum date for the outburst flood.

RM 74.5: Optional Stop

A railroad cut on river right exposes bouldery foresets containing Mt Jefferson pumice and charcoal dated at 38,760±540 ^{14}C yr ago, reinforcing the maximum date on the

outburst flooding from the Whitehorse Rapids Landslide dam.

RM 74–73.5: The river curves around an enormous gravel and boulder bar on river right, probably a landslide-dam breach deposit.

RM 73: North Junction. Due to sheer cliffs, land acquisition difficulties, and intervention by the Federal Government, two competing railroad lines laying track on either side of the river joined forces to construct a single line on the east bank between North Junction and South Junction. The east-bank line, originally constructed by the Oregon–Washington Railroad and Navigation Company, was gradually abandoned, and for the rest of the course of the field trip the old railbed serves as a road on river right. Between here and RM 54, this road and much of the right bank is privately owned.

RM 72: The river enters the Mutton Mountains, which are composed of uplifted John Day and Clarno Formations capped by flows of the Columbia River Basalt Group. The John Day and Clarno Formations here are composed of rhyolitic to andesitic lava flows, and they are far more resistant than the soft tuffaceous sedimentary facies upstream. Uplift of the Mutton Mountains has caused the river to incise a deep, narrow, meandering canyon in this reach. Several vacation homes on river right between RM 70 and 57 were damaged during the 1996 flood.

RM 69: Leaving Warm Springs Reservation on river left.

RM 66: Large Outhouse Flood bar on river right.

RM 65: Stop 7. Dant

Camp on river left, across the river from an old railroad tunnel. Several meters of fine-grained flood deposits, capped by 1964 and 1996 flood sands, are exposed in the cutbank at the downstream end of this bar (Fig. 8). A silt line deposited by the 1861 flood is preserved within a higher adjacent sequence, providing a paleostage indicator for estimating discharge. Sand deposited by the Outhouse Flood mantles the top of the flood bar but is not exposed in the cutbank. A trench dug near the BLM outhouse here revealed at least 2 meters of medium sand with reworked pieces of Mazama tephra, indicating that the Outhouse Flood is probably younger than Mazama's age of 7.6 ka.

RM 64.5: A large Outhouse Flood boulder bar noses into the channel on river right. The abandoned grade above the community of Dant on river left leads to the dormant Lady Francis Perlite Mine, which was developed in the 1940s.

RM 64: Buckskin Mary Rapid is composed of remnant boulders from the Dant Debris Flow (river left).

RM 63.75: Stop 8. Dant Debris Flow Overlook

Wear sturdy shoes or boots for this stop! Take out on river right at a wooden sign marked *Trail*. Hike 100 m up the road toward Buckskin Mary Rapid and up a steep trail that leads up a talus slope between two cliffs. Enjoy the spectacular view of a massive Pleistocene debris flow that temporarily blocked the channel. Sandy deposits exposed in a railroad cut 300 m upstream may have been deposited when a lake formed behind the blockage. Bend Pumice in the lacustrine deposits indicates that the blockage was formed during or after the Bend–Tumalo eruptions of about 400 ka.

RM 63.4: Four Chutes Rapids formed by fluvially transported landslide debris.

RM 62.5: Stop 9. Type Outhouse Flood Bar

The giant bar on river left may have first formed during breaching of the Dant Debris Flow. Angular boulders at the upstream edge do not seem to have been transported far from their source. The Outhouse Flood may have left the rounded boulders on the top of the bar (near the outhouse), and historical floods deposited and scoured the fresh pebbles and cobbles on the upstream and downstream margins of the bar. Note the bent young "clipper ship" juniper trees, deformed by the flood of February 1996 as well as much older trees perhaps deformed by the 1861 flood. A cobble bar with a lower surface (mantled by railroad camp debris) is appended to the downstream end of the Outhouse Flood bar and was perhaps deposited by the 1861 flood.

RM 62: Caretaker Flat on river right has exposures of fine-grained and gravelly flood deposits. The visible white layer in the cutbank is an accumulation of tephra from the 7.6 ka eruption of Mt Mazama. A sand and gravel lens, stratigraphically between the Mazama tephra and a charcoal accumulation dated at 2,850±50 ^{14}C yr ago, is inferred to be an Outhouse Flood deposit. This surface was not overtopped by the February 1996 flood, but a lower surface, inset into the flat at the downstream end, records several floods of February 1996 magnitude during roughly the past 1,000 years.

RM 58.5: The John Day Formation dives below river level as the river enters the structural basin between the Mutton Mountains and the Tygh Ridge Anticline. For the remainder of the Deschutes River's course to the Columbia, the river-level bedrock is the Columbia River Basalt Group. The 4.9 Ma Juniper Flats basalt flow caps the left valley wall.

RM 55–54: Wapinitia and Boxcar Rapids are at the eroded toes of two overlapping landslides (Fig. 5). Note giant boulders cluttering the banks near Boxcar Rapids.

RM 51.5: Maupin City Park take out on river right.

ACKNOWLEDGEMENTS

This field trip guide has benefited from reviews by Janet Curran and Pat McDowell.

REFERENCES

Andrews, E.D., and Nankervis, J.M., 1995, Effective discharge and the design of channel maintenance flows for gravel-bed rivers, *in* Costa, J.E., Miller, A., Potter, K.W. and Wilcock, P.R., eds., Natural and Anthropogenic Influences in Fluvial Geomorphology: American Geophysical Union Geophysical Monograph 89, p. 151-164.

Anonymous, 1861, Letter from The Dalles dated Dec 9: Salem Oregon Statesman, December 23, 1861, p. 1.

Beebee, R.A., and O'Connor, J.E., in press, The Outhouse Flood: A large Holocene flood on the lower Deschutes River, Oregon, *in* Grant, G.E., and O'Connor, J.E., eds., Deschutes River geomorphology, hydrology, and sediment transport: American Geophysical Union Water Science and Application Series.

Bela, J.L., 1982, Geologic and neotectonic evaluation of north-central Oregon: The Dalles 1x2-Degree Quadrangle: Oregon Department of Geology and Mineral Industries Geological Map Series GMS-276, scale 1:250.000.

Costa, J.E., 1988, Floods from dam failures, *in* Baker, V.R., Kochel, R.C., and Patton, P.C., eds., Flood geomorphology: New York, John Wiley and Sons, p. 439-464.

Curran, J.H., and O'Connor, J.E., in press, Formation and evolution of valley-bottom and channel features, lower Deschutes River, Oregon, *in* Grant, G.E., and O'Connor, J.E., eds., Deschutes River geomorphology, hydrology, and sediment transport: American Geophysical Union Water Science and Application Series.

Fassnacht, H., 1998, Frequency and magnitude of bedload transport downstream of the Pelton–Round Butte Dam Complex, lower Deschutes River, Oregon: Oregon State University MS Thesis, 311 P.

Fassnacht, H., McClure, E.M., Grant, G.E., and Klingeman, P.C., in press, Downstream effects of the Pelton–Round Butte Hydroelectric Project on bedload transport, channel morphology, and channel-bed texture, Deschutes River, Oregon, *in* Grant, G.E., and O'Connor, J.E., eds., Deschutes River geomorphology, hydrology, and sediment transport: American Geophysical Union Water Science and Application Series.

Grant, G.E., Fassnacht, H., McClure, E.M., and Klingeman, P.C., 1999, Downstream effects of the Pelton–Round Butte hydroelectric project on bedload transport, channel morphology, and channel-bed texture, Deschutes River, Oregon, Pelton–Round Butte hydroelectric project: Portland General Electric, FERC no. 2030, 111 p.

Hayman, G.A., 1983, Geology of a part of the Eagle Butte and Gateway Quadrangles east of the Deschutes River, Jefferson County, Oregon: Oregon State MS Thesis, 97 p.

Hill, B.E., and Taylor E.M., 1989, Oregon central High Cascade pyroclastic units in the vicinity of Bend, Oregon, *in* Scott, W.E., Gardner, C.A., and Sarna-Wojcicki, A.M., eds., Guidebook for field trip to the Mount Bachelor–South Sister–Bend Area, central Oregon High Cascades: U. S. Geological Survey Open-File Report 89-645, p. 51-54.

Hooper, P.R., Steele, W.K., Conrey, R.M., Smith, G.A., Anderson, J.L., Bailey, D.G., Beeson, M.H., Tolan, T.L., and Urbanczyk, K.M., 1993, The Prineville Basalt, north-central Oregon: Oregon Geology, v. 55, p. 3-12.

Hosman, K.J., 2001, Stratigraphic reconstruction of paleoflood frequencies and magnitudes, lower Deschutes River, Oregon: Central Washington University MS Thesis.

Hosman, K.J., Ely, L.L., and O'Connor, J.E., in press, Paleohydrology of late Holocene and historic floods on the lower Deschutes River, Oregon, *in* Grant, G.E., and O'Connor, J.E., eds., Deschutes River geomorphology, hydrology, and sediment transport: American Geophysical Union Water Science and Application Series.

Levish, D.R., and Ostenaa, D.A., 1996, Applied paleoflood hydrology in north-central Oregon: Guidebook for field trip 2, April 19-21, 1996, Cordilleran Section Meeting, Geological Society of America: U.S. Bureau of Reclamation Seismotectonic Report 96-7.

Manga, M., 1996, Hydrology of spring-dominated streams in the Oregon Cascades: Water Resources Research, v. 32, p. 3435-2439.

McClure, E.M., 1998, Spatial and temporal trends in bed material and channel morphology below a hydroelectric dam complex, Deschutes River, Oregon: Oregon State University MS Thesis, 85 p.

Newcomb, R.C., 1969, Effect of tectonic structure on the occurrence of ground water in the basalt of the Columbia River Basalt Group of The Dalles area, Oregon and Washington: U.S. Geological Survey Professional Paper 383-C, 33 p.

O'Connor, J.E., Curran, J.H., Beebee, R.A., Grant, G.E., and Sarna-Wojcicki, A.M., in press, Quaternary geology and geomorphology of the lower Deschutes River Canyon, Oregon, *in* Grant, G.E., and O'Connor, J.E., eds., Deschutes River geomorphology, hydrology, and sediment transport: American Geophysical Union Water Science and Application Series.

O'Connor, J.E., Grant, G.E., and Haluska, T.L., in press, Overview of geology, hydrology, geomorphology, and sediment budget of the Deschutes River Basin, Oregon, *in* Grant, G.E., and O'Connor, J.E., eds., Deschutes River geomorphology, hydrology, and sediment transport: American Geophysical Union Water Science and Application Series.

Orr, E.L., Orr, W.N., and Baldwin, E.M., 1992, The Geology of Oregon: Dubuque, Kendall/Hunt, 254 p.

Russell, I.C., 1905, Preliminary report of the geology and water resources of central Oregon: U.S. Geological Survey Bulletin 252, 138 p.

Sherrod, D.R., Taylor, E.M., Ferns, M.L., Scott, W.E., Conrey, R.M., and Smith, G.A., in press, Geologic map of the Bend 30 by 60 Minute Quadrangle, Deschutes, Jefferson, Lane, Linn, and Crook Counties, central Oregon: U.S. Geological Survey Open File Report.

Smith, G.A., 1982, Late Cenozoic structure on the Columbia Plateau: Implications for tectonics in the Pacific Northwest: Eos, v. 63, p. 1116.

Smith, G.A., 1986, Stratigraphy, sedimentology, and petrology of Neogene rocks in the Deschutes Basin, central Oregon: A record of continental-margin volcanism and its influence on fluvial sedimentation in an arc-adjacent basin: Oregon State University PhD Dissertation, 464 p.

Smith, G.A., 1987, Geologic map of the Madras West and Madras East Quadrangles, Jefferson County, Oregon: Oregon Department of Geology and Mineral Industries Geological Map Series GMS-45, scale 1:24,000.

Smith, G.A., and Hayman, G.A., 1987, Geologic map of the Eagle Butte and Gateway Quadrangles, Jefferson and Wasco Counties, Oregon: Oregon Department of Geology and Mineral Industries Geological Map Series GMS-43, scale 1:24,000.

Smith, G.A., and Priest, G.R., 1983, A field trip guide to the central Oregon Cascades: Oregon Geology, v. 45, p. 119-138.

Walker, G.W., and McLeod, N.S., 1991, Geologic map of Oregon: U.S. Geological Survey, scale 1:500,000.

Waters, A.C., 1968, Reconnaissance geologic map of the Madras Quadrangle, Jefferson and Wasco Counties, Oregon: U. S. Geological Survey Miscellaneous Geologic Investigations Map I-555.

Zdanowicz, C.M., Zielinski, G.A., and Germani, M.S., 1999, Mount Mazama eruption: Calendrical age verified and atmospheric impact assessed: Geology, v. 27, p. 621-624.

Hydrogeology of the Upper Deschutes Basin, Central Oregon: A Young Basin Adjacent to the Cascade Volcanic Arc

David R. Sherrod, U.S. Geological Survey, Hawaii National Park, Hawaii 96718; dsherrod@usgs.gov

Marshall W. Gannett, U.S. Geological Survey, 10615 SE Cherry Blossom Drive, Portland, Oregon 97216; mgannett@usgs.gov

Kenneth E. Lite, Jr., Oregon Water Resources Department, 158 12th Street NE, Salem, Oregon 97310, kenneth.e.lite@wrd.state.or.us

INTRODUCTION

The upper Deschutes Basin encompasses about 11,700 km^2 of the Deschutes River drainage basin in central Oregon (Fig. 1). Chiefly draining the east flank of the Cascade Range, the upper Deschutes Basin extends northward from a drainage divide near Chemult that separates it from the Klamath Basin to the south. The eastern margin of the basin lies along the south part of the Ochoco Mountains and through the crest of Newberry Volcano. The northern boundary is near Warm Springs, northwest of Madras.

The upper Deschutes Basin is underlain by Quaternary and Tertiary volcanic and sedimentary rocks. The occurrence and movement of ground water and the interaction of ground water and streams are controlled by the distribution of permeability within the depositional sequence. The permeability distribution reflects the age, lithology, and depositional environment of the strata, along with the subsequently imposed geologic structure.

The crest of the Cascade Range, including a broad upland area east of the Three Sisters, is the principal source of recharge for the groundwater system. The average annual rate of recharge from precipitation in the upper Deschutes Basin is estimated to be roughly 108 m^3/s (3,800 ft^3/s) (Gannett and others, 2001).

Ground water moves eastward from the Cascade Range and then generally northward through permeable Quaternary and upper Tertiary deposits. North of Madras, the permeable deposits thin out against relatively impermeable lower Tertiary deposits of the John Day and Clarno Formations (Fig. 2), forcing nearly all the northward-flowing ground water to discharge into the Deschutes River and its tributaries. This massive amount of ground-water discharge, exceeding 60 m^3/s (2,000 ft^3/s) near the confluence of the Deschutes and Crooked Rivers, is the principal reason for the remarkably stable flow of the Deschutes River.

Participants on this trip will explore the visible and conceptual aspects of the regional ground-water hydrology of the upper Deschutes Basin, including the interaction between ground water and streams. The trip follows the general direction of ground-water flow northward from the headwaters of spring-fed streams at the margin of the Cascade Range to the principal regional discharge area near Lake Billy Chinook.

This guidebook describes a 2-day trip. Day 1 begins in the La Pine Subbasin (uppermost Deschutes Basin) and proceeds through Bend, concentrating chiefly on the hydrologic controls created by Quaternary stratigraphy and structure (Fig. 3). Day 2 examines strata of the Deschutes Formation from Bend to Madras and the geologic factors that influence regional ground-water discharge.

A road log for each day is at the end of the field-trip guide. The metric system is used for all scientific aspects of the guidebook except altitude and water discharge rate, which are given in both meters and feet (altitude) and cubic meters per second and cubic feet per second (rate) owing to the widespread familiarity with U.S. traditional units in these matters. The road log is reported in miles to match most car odometers.

Field Guide to Geologic Processes in Cascadia: Oregon Department of Geology and Mineral Industries Special Paper 36, 2002.

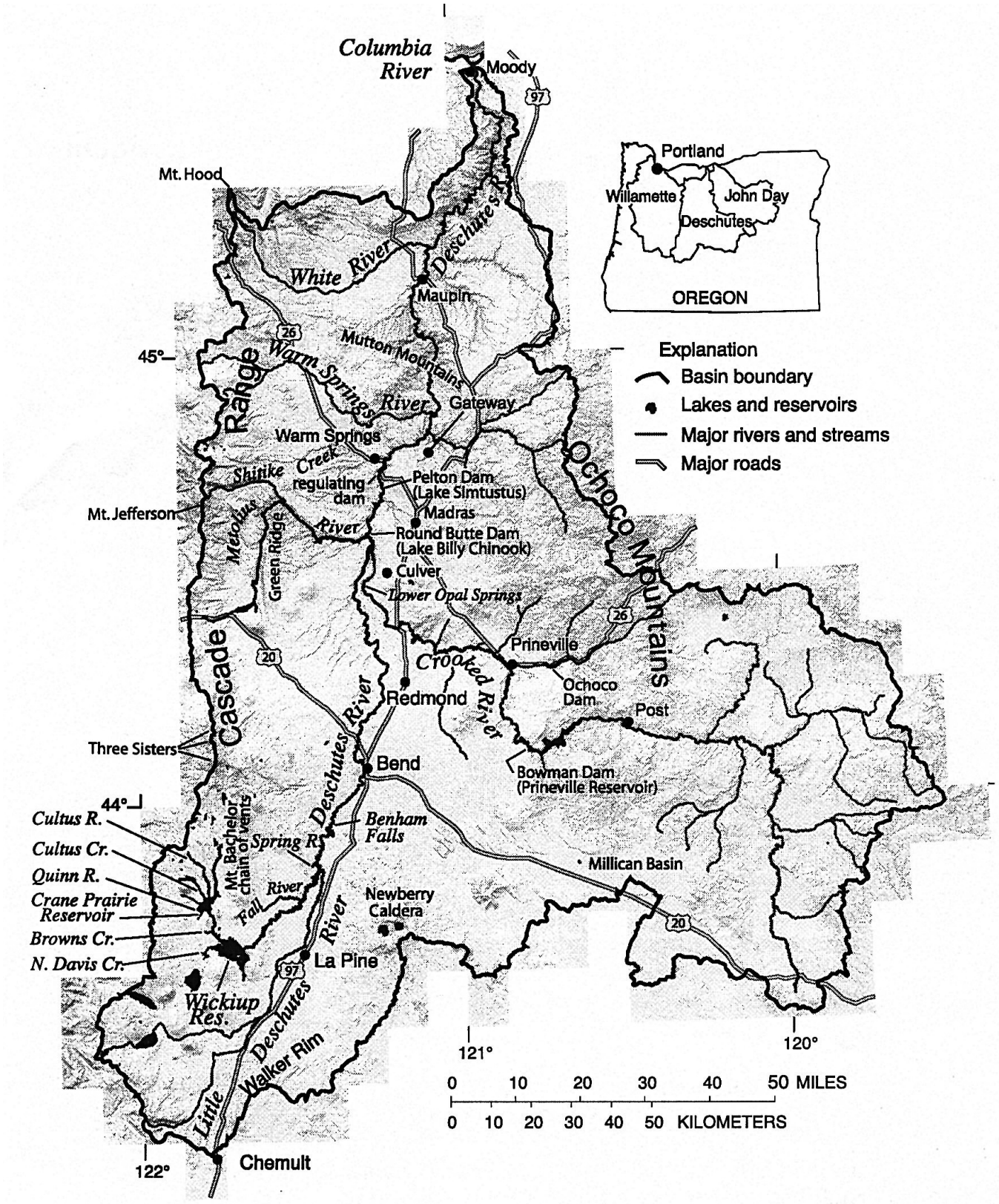

Figure 1. Extent of the Deschutes Basin (bold line), major rivers, and geographic features named in the text. Extent of the upper Deschutes Basin is shown on Figures 5 and 11.

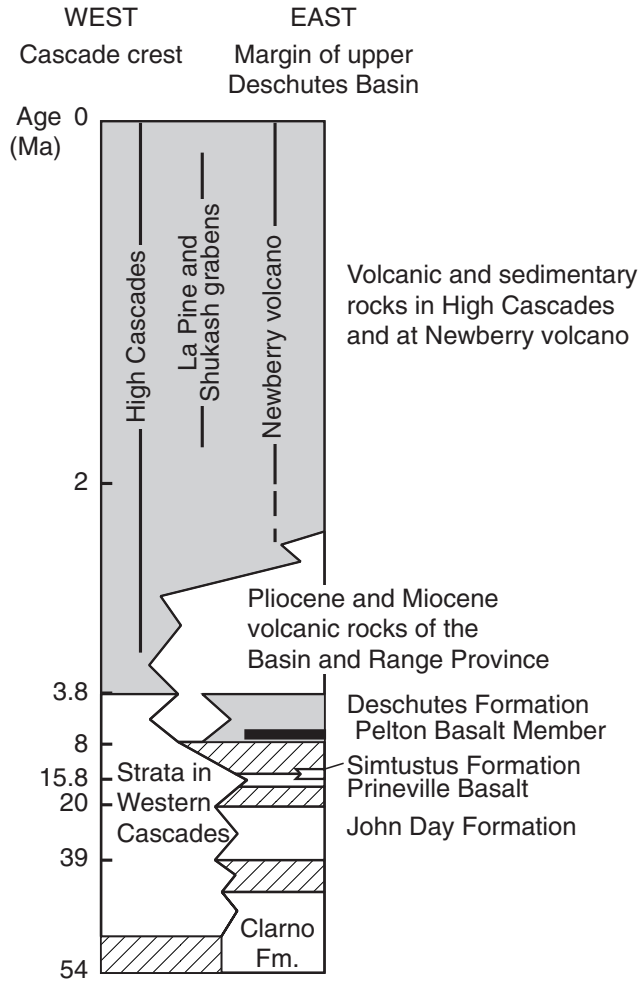

Figure 2. Generalized stratigraphic column for the upper Deschutes Basin. Shaded boxes show stratigraphic units visited on this trip. Open boxes, not visited. Diagonal pattern indicates nondeposition. Several names have descriptive geographic value but do not designate formally defined stratigraphic units.

Regional-scale geologic maps may aid travelers wishing a more thorough understanding of the geology along the trip route. Day 1 stops are within the area of the west half of the Crescent 1 by 2 Degree Quadrangle (MacLeod and Sherrod, 1992) and the Bend 30 by 60 Minute Quadrangle (Sherrod and others, in press). Maps of the Mount Bachelor volcanic chain (Scott and Gardner, 1992) and Newberry Volcano (MacLeod and others, 1995) provide more detail around the margins of Day 1 travel. A road map of the Deschutes National Forest is helpful for navigating the maze of Forest Service and county roadways during Day 1.

Most Day 2 stops are within the Bend Quadrangle (Sherrod and others, in press). The most northerly stops, however, are in an area that lacks regional-scale geologic mapping. Several 1:24,000-scale maps cover the northern part of the trip, including those by Smith (1987a, b), Smith and Hayman (1987), and Ferns and others (1996a). The Geologic Map of Oregon (scale 1:500,000, Walker and MacLeod, 1992) would also be helpful in the northern area.

ACKNOWLEDGMENTS

This acknowledgment has been 25 years in the making. Our deepest appreciation goes to Larry Chitwood, Rick Conrey, Mark Ferns, Kyle Gorman, Bob Jensen, Norm MacLeod, Bob Main, Andrei Sarna-Wojcicki, Willie Scott, Gary Smith, Ed Taylor, and George Walker for richly gestured discussions that have proved fundamental to our understanding of the geology and hydrology of the Deschutes Basin. Joy Gannett assisted in checking the driving instructions. This guidebook was reviewed for accuracy by Larry Chitwood and Bill McFarland and edited by George Moore for final publication. We thank them all.

DAY 1

Synopsis, Uppermost Deschutes Basin

Day 1 of this trip focuses on the uppermost Deschutes Basin, including the margin of the Cascade Range and the La Pine Subbasin (Fig. 3). This area is characterized at the surface by broad flatland areas and interspersed volcanic buttes. Relief increases toward the basin margins owing chiefly to volcanic buildup. The buttes, which consist of cinder cones, small shield volcanoes, and sparse silicic domes, are characteristic Cascade Range eruptive centers. From them have issued the numerous lava flows, predominantly basaltic andesite, seen in road cuts and river banks. A few tuff cones and maars resulted from eruptions during times when ground water saturated the upper strata or when shallow lakes occupied part of the basin. Silicic domes are scattered among the basalt and basaltic andesite vents; these range in composition from dacite to rhyolite. Pyroclastic-flow deposits are exposed sporadically, limited

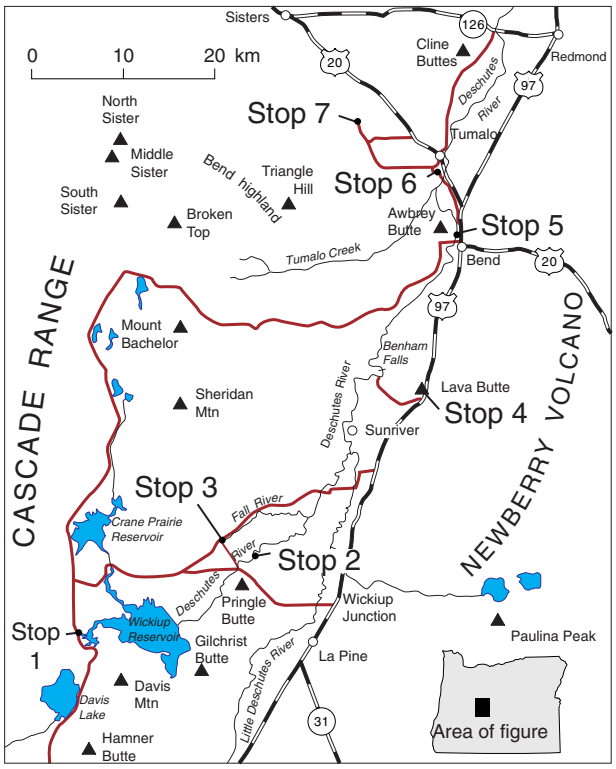

Figure 3. Route and stops for Day 1 of the field trip.

in extent, andesitic to rhyolitic in composition, and partially welded to nonwelded.

Sedimentary rocks, although rarely exposed, fill a substantial part of the La Pine Subbasin. The beds range from lacustrine to fluvial silt, sand, and gravel. We examine some of these beds at Pringle Falls (Stop 2). Sand- and gravel-rich strata are locally abundant and form important aquifers, especially near the town of La Pine.

Sedimentation occurred in the lowland created by the growth of adjacent volcanoes, as might be surmised by a casual glance at the landscape. Less obvious are within-basin horst-and-graben structures characteristic of the Basin and Range Province.

Precipitation and Orographic Effects

Much of the High Cascades in Oregon is a broad ridge whose topographic crest is defined by volcanoes along the axis of the Cascade Range. The range crest is a fundamental orographic barrier whose flanks receive precipitation from prevailing air flow across the North Pacific Ocean. The uppermost Deschutes Basin differs from other parts of the Cascade Range in Oregon by virtue of two additional substantial volcanic ridges east of the range crest—the Mount Bachelor chain of vents and Newberry Volcano.

Perhaps equally important hydrologically is a broad volcanic upland adjacent to the Cascade Range crest east of the South Sister. Known informally as the Bend Highland, this area encompasses 160 km^2 of terrain in excess of 1,830 m (6,000 ft) altitude, including Broken Top Volcano, Tam MacArthur Rim, and Triangle Hill. The infiltration of snowmelt and rainfall into the Three Sisters region and Bend Highland is the principal source of recharge to a ground-water system that dominates the hydrology of the Deschutes Basin. This extensive area of high altitude is unique in the Cascade Range in Oregon. In contrast, the upper Klamath River, which drains a comparably sized basin adjacent to the Cascade Range south of the Deschutes Basin has only about one-third of the mean discharge of the Deschutes River at Madras.

Ground-Water Flow in the Uppermost Basin

Much of the upper Deschutes Basin lacks a developed and integrated stream system. Permeability of the late Pleistocene and Holocene lava flows is high, so precipitation (including rapid snowmelt) tends to infiltrate the ground and not run off in established channels. Permeable lava of the Cascade Range encroaches eastward onto or interfingers with relatively impermeable fine-grained sedimentary strata in the La Pine Subbasin. Consequently, ground water flowing from the Cascade Range eastward through the permeable lava is likely to be diverted to the surface wherever it encounters fine-grained sedimentary strata. Ground water commonly issues abruptly from large springs in the lava along the west margin of the La Pine Subbasin, creating creeks and rivers flowing fully at 3 to 6 m^3/s (100-200 ft^3/s) within a few tens or hundreds of meters from their origin (Gannett and others, 2001).

Table 1. Altitude, Temperature, Discharge, and Isotopic Data for Selected Springs in the Upper Deschutes Basin (James and Others, 2000).

Spring name	Alt (m)	Alt (ft)	Temp (°C)	Disch (m^3)	$\delta^{18}O$ (‰)	$\delta^{18}O$ (‰)	^{14}C (% mod C)
Browns Creek	1332	4369	3.8	1.1	-13.9	-16.4	115.3
Cultus River	1356	4448	3.4	1.8	-14.1	-15.8	113.9
Fall River	1286	4219	6.1	4.2	-14.2	-11.8	110.9
Lower Opal Springs	597	1959	12.0	6.8	-15.3	-12.7	60.0
Metolius River	920	3018	8.2	3.1	-14.7	-11.5	61.3
North Davis Creek	1323	4340	3.4	—	-14.1	-15.8	114.0
Quinn River	1354	4442	3.4	0.7	-13.7	-16.5	112.3
Snow Creek	1378	4521	5.5	0.8	-14.1	-12.9	111.1
Spring River	1268	4160	8.0	3.5	-14.6	-11.5	67.5

Stop 1—Springs at North Davis Campground (Altitude 1,323 m; 4,340 ft)

Drive into North Davis Campground and try to find parking near Campsite 13. Walk north into the shallow drainage of North Davis Creek.

Numerous springs issue from lava flows exposed along North Davis Creek, a tributary to what is now the Davis Creek Arm of Wickiup Reservoir (Fig. 4). Streamflow measurements show that the Davis Creek Arm gains approximately 5.4 m^3/s (190 ft^3/s) from ground-water inflow over a distance of 3 km. Much of this flow comes from the spring complex of North Davis Creek seen at this stop. This spring complex is typical of several spring complexes along the margin of the Cascade Range in the southernmost Deschutes Basin. Similar full-fledged creeks take form over equally short distances along Browns Creek and at the heads of Quinn, Cultus, Fall, and Spring Rivers (Fig. 5). The total discharge from spring complexes in the area of Wickiup and Crane Prairie Reservoirs averages close to 17 m^3/s (600 ft^3/s).

The springs of North Davis Creek and similar springs in the area represent the westernmost (topographically highest) area of copious ground-water discharge in the Deschutes Basin. Temperature and isotopic data suggest that water emerging from these springs follows relatively short flow paths (James and others, 2000). Spring temperatures (about 3.5°C) essentially match the mean annual temperatures at the recharge altitudes as inferred from oxygen isotope ratios, indicating little or no geothermal warming (Table 1). Isotopes of carbon and noble gases show no evidence of magmatic volatile content (James and others, 2000).

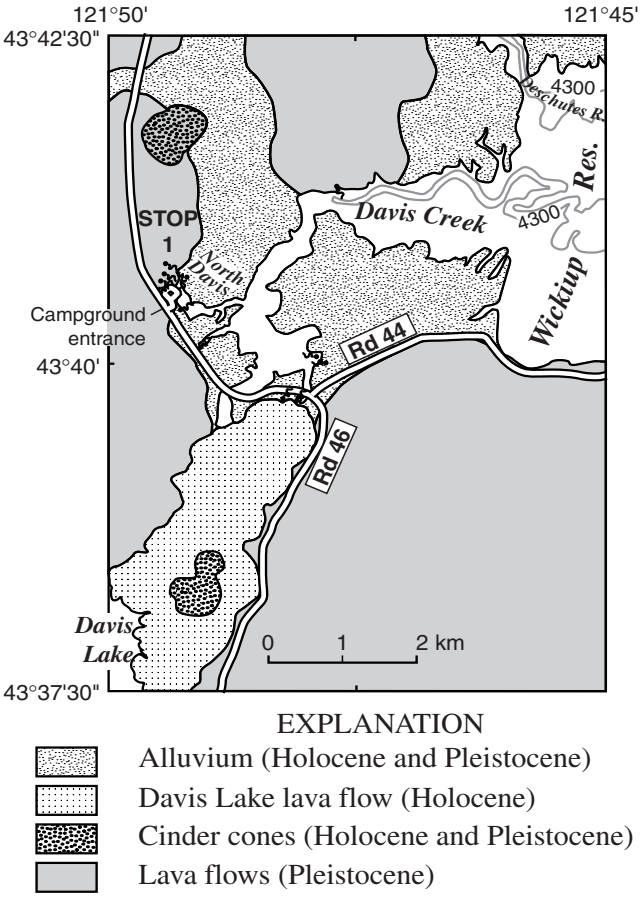

Figure 4. The area of North Davis Creek, Stop 1 (geology from MacLeod and Sherrod, 1992).

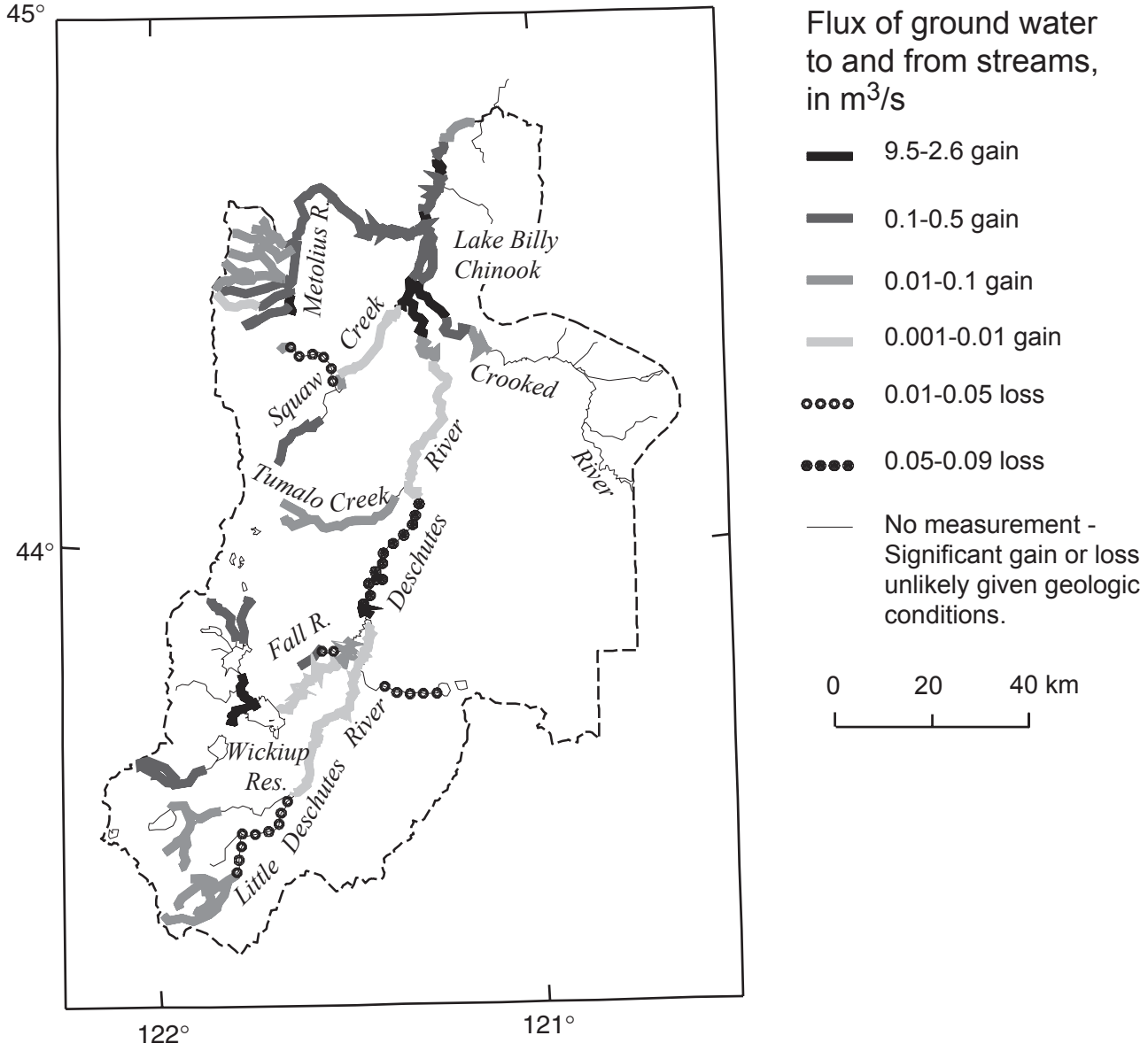

Figure 5. Estimated gain and loss rates for selected stream reaches in the upper Deschutes Basin, Oregon (from Gannett and others, 2001).

Stop 2—Pringle Falls Sedimentary Sequence (Altitude 1,295 m; 4,250 ft)

The Deschutes River at Pringle Falls has eroded through fine-grained sediment approximately 20 m thick. The falls themselves, more a dangerous rapid than a waterfall, are in an underlying basalt lava flow. The geologic exposure at Pringle Falls is unique because of the thickness of sedimentary strata exposed at the surface. Most of the upper basin is barely incised, which limits the extent of exposure for poorly indurated beds. The Mazama Ash, a Holo-cene tephra deposit erupted from Mount Mazama (Crater Lake), 100 km south-southwest, thickly blankets much of the area; it is about 70 cm thick in the Pringle Falls area. Even the few good sedimentary exposures are draped by colluvium from interbedded or capping lava flows. The floors of some reservoirs have been exposed during drought years, providing the only other sites where sedimentary strata may be viewed extensively.

Our stop is at the east end of the Pringle Falls area, one of two excellent exposures (Fig. 6). The other site is on private land to the west at the base of Pringle Falls. The deposits at Pringle Falls are thin-bedded, nearly

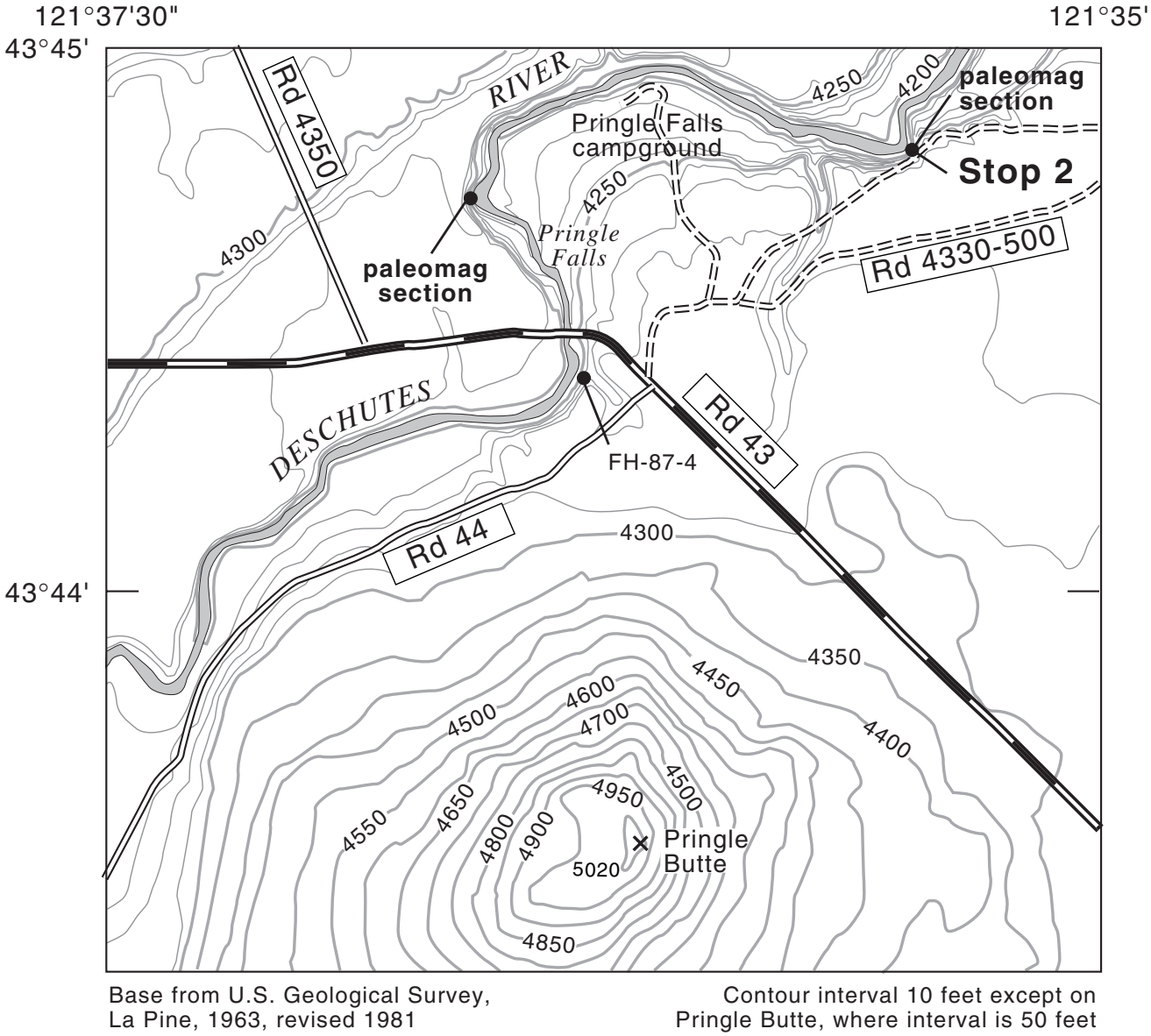

Figure 6. The Pringle Falls area, Stop 2.

undeformed lacustrine and fluvial mud, silt, and sand (Fig. 7). Gravel caps the sedimentary sequence. The beds are well exposed locally where the Deschutes River undercuts and maintains oversteepened banks.

The sedimentary sequence contains several fallout tephra layers. Pumice bed D, about 3.5 m above river level (Fig. 7), has an $^{40}Ar/^{39}Ar$ age of 218±10 ka (Herrero-Bervera and others, 1994; A.M. Sarna-Wojcicki, written commun., 2001). The lacustrine sequence also contains the Pringle Falls geomagnetic polarity episode, which occurred between about 218±10 and 169±17 ka (Herrero-Bervera and others, 1994). The latter age is obtained by regional correlation of lacustrine paleomagnetic data from Tule Lake, Calif. The polarity episode was determined from paleomagnetic directions of the lacustrine sediment at the west and east sites (Herrero-Bervera and others, 1989; Herrero-Bervera and Helsey, 1993).

The Pringle Falls sedimentary sequence is exposed on the north flank of a north-northeast-trending horst marked by Pringle and Gilchrist Buttes. This horst separates the La Pine Graben on the east from the Shukash Graben on the west (Fig. 8). The La Pine Graben is a lowland with numerous water wells that provide some understanding of the thickness and lithology of the strata there. Water wells in the La Pine

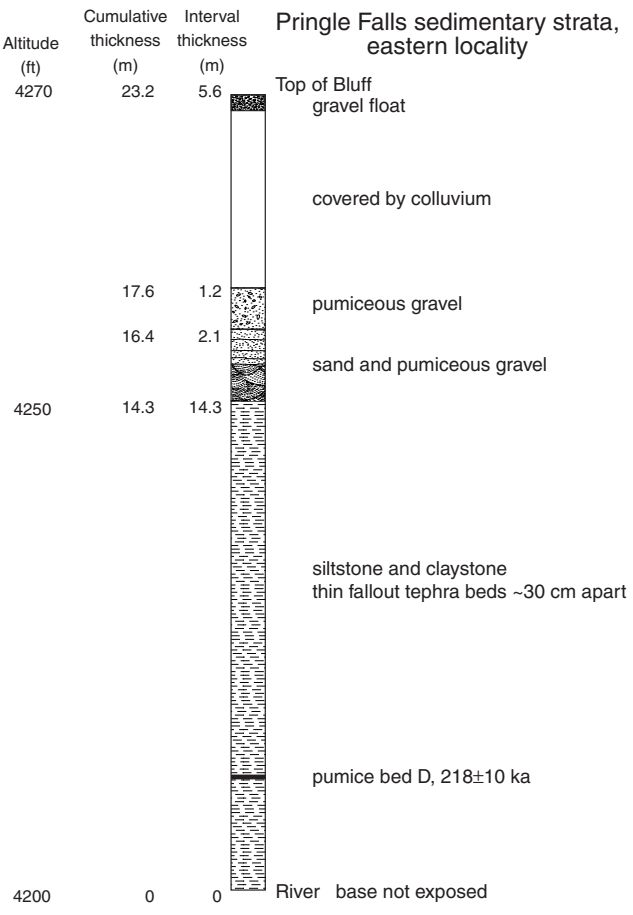

Figure 7. Stratigraphic section for the east exposure, Pringle Falls area, Stop 2.

Graben have penetrated as much as 395 m of sediment before encountering lava flows (Fig. 8; Couch and Foote, 1985). A well drilled at the Fall River Fish Hatchery, roughly 5.8 km north of Pringle Falls, penetrated fine-grained sediment to a depth of 150 m, and below that, interbedded basalt and cinders to a depth of 172 m. The thickest parts of the sedimentary fill, which may be as thick as 0.7-1.0 km (Gettings and Griscom, 1988), probably coincide with a -150 mGal gravity anomaly (Fig. 8). Deep holes drilled on the upper west flank of Newberry Volcano encountered no lacustrine deposits, and the alluvial strata on the volcano are complexly interbedded with primary volcaniclastic deposits. Therefore the volcano probably has formed an eastern buttress to basin-filling sediment for a substantial period of time (MacLeod and others, 1995). In contrast, the Shukash Graben has been obscured topographically by the growth of small shield volcanoes and cinder cones (Fig. 8). No deep water-well data are available from the Shukash Basin.

Although undated, the inception of the La Pine and Shukash Grabens likely began in late Pliocene or early Pleistocene time. The Chemult Graben, which may be of similar age, lies 30 km to the south (Fig. 8). An age from a lava flow capping the Chemult Graben's east rim (Walker Rim) is 2.33 Ma (Table 2), suggesting that the Chemult, and by analogy, the La Pine Grabens are younger. An age of 0.61 Ma was obtained from Gilchrist Butte, a normal-polarity shield at the south end of the horst between the La Pine and Shukash Grabens (Table 2). Gilchrist Butte lava has been faulted, so at least some of the faulting is younger than 0.6 Ma.

Other ages from the Pringle Butte–Gilchrist Butte Horst are thought meaningless, or at best, difficult to interpret. Ages ranging from 6.7 to 8.2 Ma were obtained from lava flows exposed on the horst (Hawkins and others, 1989). One of these samples was collected 150 m upstream from the Pringle Falls road bridge (FH-87-4, Fig. 6); it yielded an age of 6.9±0.8 Ma. These ages are much too old in view of the geomorphic landforms preserved by the volcanic vents along the horst. Gilchrist Butte buries most of the rhyolite dome of Eaton Butte, age 3.68±3.3 Ma (Table 2), which lies on its west flank. The large analytical error renders this age almost useless for determining the age of bedrock in the Pringle Butte–Gilchrist Butte Horst.

The geographic and geologic setting of the Pringle Falls sedimentary sequence suggests that a natural dam for the La Pine Subbasin may have once existed 23 km northeast, where lava flows from Newberry Volcano have ponded against Cascade Range lava flows north of Sunriver. Subsequent deformation along faults that bound the Pringle Butte–Gilchrist Butte Horst has probably elevated the sedimentary section slightly. This interpretation relies on a comparison of altitudes around the basin: 4,200 ft, where the dam might have existed north of Sunriver, and 4,250 ft at the top of the Pringle Falls lacustrine section (Fig. 6). The basin between Pringle Falls and Sunriver lacks remnant geomorphic surfaces that might correspond to an

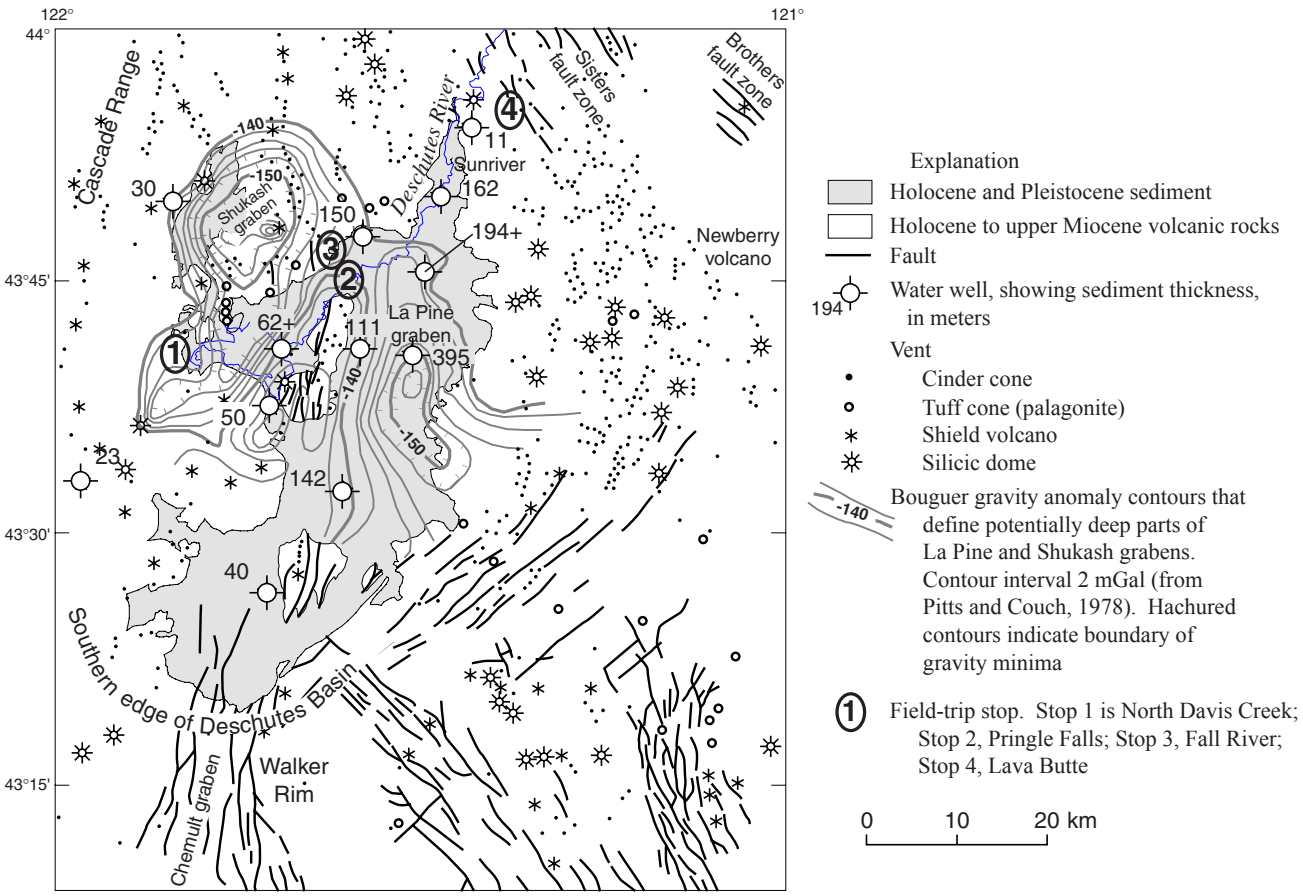

Figure 8. Map showing water wells, volcano-tectonic structure, and extent of grabens defined by gravity anomalies in the upper Deschutes Basin (from MacLeod and Sherrod, 1992).

extensive sediment sequence with an upper surface at 4,250-ft altitude; hence our reasoning that the Pringle Falls section has been elevated in response to uplift on the horst.

The fine-grained sediment exposed at Pringle Falls and inferred at depth from drilling data and geophysical studies is hydrologically significant. The low permeability of the sediment contrasts sharply with that of the lava flows and pyroclastic deposits to the east and west. As mentioned previously, the numerous springs on the west margin of the La Pine Subbasin are believed to result from eastward-flowing ground water diverted to the surface upon encountering these low-permeability deposits. The low permeability affects flow in the vertical direction as well. The area underlain by these fine-grained sedimentary deposits is characterized by a shallow water table, with the depth to water commonly less than 3 m.

Stop 3—Fall River Headwater Springs (Altitude 1,305 m; 4,280 ft)

Fall River is one of the larger spring-fed tributaries to the Deschutes River. Virtually the entire flow of Fall River originates from springs near its headwaters. Fall River springs emerge from Pleistocene basaltic andesite lava at the contact with Pleistocene alluvial and lacustrine sediment, presumably similar to deposits exposed at Pringle Falls (Stop 2). The Fall River headwaters are one of two spring complexes along the northwest margin of the La Pine Graben that discharge water that has followed intermediate-length flow paths. The other spring complex is that of Spring River, 16 km northeast of the springs at Fall River.

Temperatures of the Fall River and Spring River springs (6.1 and 8.0°C respectively, Table 1) are significantly warmer than mean annual temperatures at recharge altitudes inferred from oxygen isotope ratios, indicating the water

Table 2. Potassium-argon and $^{40}Ar/^{39}Ar$ isotopic ages of volcanic materials discussed in the text

Age (Ma)	Quality	Geologic unit or geographic location	Lat. (N)	Long. (W)	Rock type	Material dated	Reference
Volcanic rocks of High Cascades or Basin and Range provinces							
0.093±0.011	+	South Sister, early-erupted lava on northeast flank	44°08.29'	121°43.20'	Dacite	Whole rock	Hill and Duncan, 1990; Hill, 1992
0.61±0.05	+	Gilchrist Butte	43°38.75'	121°39.15'	Basalt	Whole rock	Sherrod and Pickthorn, 1989
*1.19±0.08	+	Bas. of The Island, intracanyon flows in Crooked River	44°25.96'	121°14.48'	Basalt	Whole rock	Smith, 1986a
1.43±0.33	+	Black Butte, 1 km northeast of summit	44°24.41'	121°37.53'	Basaltic andesite	Whole rock	Hill and Priest, 1992
2.33±0.09	+	Walker Rim (east side, Chemult graben)	43°16.20'	121°44.05'	Basalt	Whole rock	Sherrod and Pickthorn, 1989
3.68±3.3	-	Eaton Butte	43°38.6'	121°41.2'	Basalt	Whole rock	Fiebelkorn and others, 1983
Pliocene basalt and basaltic andesite							
2.9±0.2	+	Summit, Squaw Back Ridge shield volcano	44°28.70'	121°28.59'	Basaltic andesite	Whole rock	Armstrong and others, 1975
*3.56±0.30	+	Basalt of Redmond	44°23.20'	121°13.02'	Basalt	Whole rock	Smith, 1986a
Deschutes Formation							
3.97±0.05	+	Basalt of Round Butte	44°37.29'	121°11.80'	Basalt	Whole rock	Smith, 1986a
4.7±0.1	+	Deschutes Formation lava, near Bull Spring	44°06.63'	121°29.22'	Basaltic andesite	Whole rock	Hill, 1992
4.9±0.4	+	Lava flow at top of Deep Canyon grade (Oreg. Hwy 126)	44°17.38'	121°24.80'	Basaltic andesite	Whole rock	Armstrong and others, 1975
*5.06±0.03	+	Bas. andesite of Steamboat Rock, Deschutes Formation	44°21.45'	121°16.03'	Basaltic andesite	Whole rock	Smith, 1986a; Smith and others, 1987a
*5.31±0.05	o	Basalt of Tetherow Butte	44°32.70'	121°15.07'	Basaltic andesite	Whole rock	Smith, 1986a
*5.43±0.05	o	Basalt of Lower Desert	44°31.05'	121°18.57'	Basalt	Whole rock	Smith, 1986a
*5.77±0.07	+	Basalt of Opal Springs, Deschutes Formation	44°26.11'	121°14.50'	Basalt	Whole rock	Smith, 1986a; Smith and others, 1987a
*6.14±0.06	+	Rhyolite of Cline Buttes, Deschutes Formation	44°15.89'	121°17.50'	Rhyolite	Plagioclase	Sherrod and others, in press
*6.74±0.20	+	Rhyodacite southwest of Steelhead Falls, Deschutes Fm.	44°23.21'	121°22.44'	Rhyodacite	Plagioclase	Sherrod and others, in press
*7.42±0.22	+	Pelton Basalt	44°39.97'	121°12.10'	Basalt	Whole rock	Smith and others, 1987
John Day Formation							
*28.82±0.23	+	Gray Butte rhyolite, basal vitrophyre	44°24.30'	121°06.79'	Rhyolite	Anorthoclase	Smith and others, 1998
28.3±1.0	+	Powell Buttes dome	44°11.86'	120°58.03'	Rhyolite	Anorthoclase	Evans and Brown, 1981
*27.62±0.63	+	West end of Haystack Reservoir, quarry	44°29.87'	121°09.37'	Welded tuff	Sanidine	Smith and others, 1998
*29.57±0.17	+	West end of Haystack Reservoir, quarry	44°29.76'	121°09.36'	Welded tuff	Sanidine	Smith and others, 1998
*29.53±0.09	+	West end of Haystack Reservoir, quarry	44°29.85'	121°09.28'	Hydromagmatic tuff	Sanidine	Smith and others, 1998
30.8±0.5	+	Northeast of Gray Butte	44°26.10'	121°05.40'	Basalt (intrusion)	Whole rock	Fiebelkorn and others, 1983
*32.49±0.30	+	Tuff of Rodman Spring, at Rodman Spring	44°27.83'	121°06.91'	Fallout lapilli tuff	Sanidine	Smith and others, 1998

Grouped by stratigraphic unit and generally arranged from youngest to oldest. Ages are K-Ar unless preceded by *, which are 40Ar/39Ar. Symbols indicating "quality" show usefulness of age in stratigraphic interpretations: +, age thought meaningful; o, age probably meaningful but accuracy may be far poorer than indicated by the reported precision; -, age meaningless (owing to large analytical error) or incorrect (on basis of our knowledge obtained by all ages and regional stratigraphic relationships). Positional datum is NAD 27. Lithologically, material dated is lava except where noted

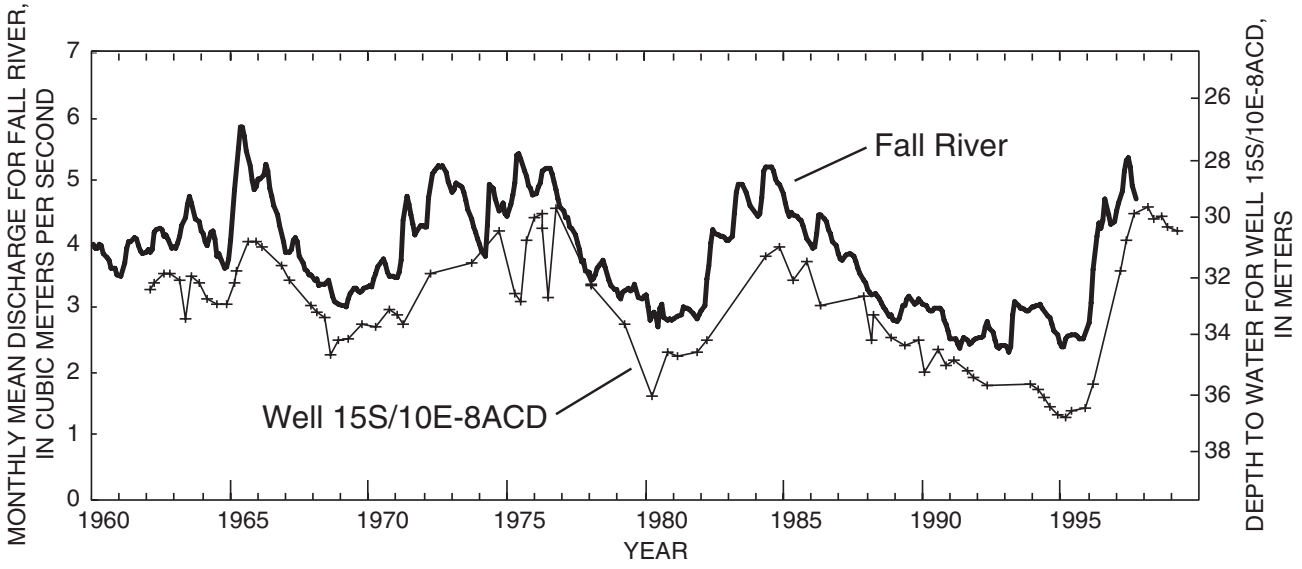

Figure 9. Hydrograph showing monthly mean streamflow of Fall River and the depth to water in a well near the margin of the Cascade Range at Sisters, about 60 km to the north.

has picked up geothermal heat along its flow path (Manga, 1998; James and others, 2000). Analysis of isotopes of carbon and noble gases indicates that the water of Spring River contains magmatically derived volatiles (James and others, 2000).

Stream-gage data show that Fall River has little seasonal variation; mean monthly flow varies only about 5 percent from the mean annual flow. On a decadal scale, however, the flow of the Fall River springs varies by a factor of more than two (Fig. 9). These decadal fluctuations correspond to climate cycles and snow-pack trends in the Cascade Range (Gannett and Lite, 2000; Gannett and others, 2001). Climate fluctuations represented by discharge variations in Fall River springs represent the largest transient signal in the hydrology of the upper Deschutes Basin. This pattern of variation occurs in spring discharge and water-table fluctuations throughout the basin (for example, Fig. 9).

Stop 4—Top of Lava Butte (Altitude 1,529 m; 5,016 ft)

A couple hundred large and small volcanoes and nearly two-thirds of the upper Deschutes Basin may be seen from the splendid vista atop Lava Butte. A simplified compass wheel shows the declination and distance to many features visible on a clear day from the lookout (Fig. 10).

Lava Butte itself is a Holocene cinder cone that erupted basaltic andesite lava flows. It lies at the downslope end of Newberry Volcano's northwest rift zone, which was active most recently between about 5,900 and 6,400 ^{14}C yr BP (MacLeod and others, 1995). A radiocarbon age of 6,160±70 ^{14}C yr BP was obtained from charcoal collected beneath Lava Butte's tephra plume where exposed in a highway road cut northeast of the butte (Chitwood and others, 1977).

Lava flows of the northwest rift zone merge with lava flows from the Cascade Range, forming the northern limit of the La Pine Subbasin today and probably for a substantial part of the subbasin's history. As mentioned at the Pringle Falls stop, lava flows probably formed natural dams in the past. Emplacement of the Lava Butte flow about 7,100 calendar years ago diverted the Deschutes River, forcing the river to establish a new channel along the west margin of the lava flow.

The topographic gradient increases abruptly north of this contact between the lava of Newberry Volcano and the Cascade Range, from relatively flat in the sediment-filled basin south of here to northward sloping to the north. The stream gradient reflects this topographic change. The Deschutes River drops a mere 0.48 m/km along the 71-km reach between Wickiup Reservoir and Benham Falls. North of Benham Falls the gradient steepens dramatically to 8.7

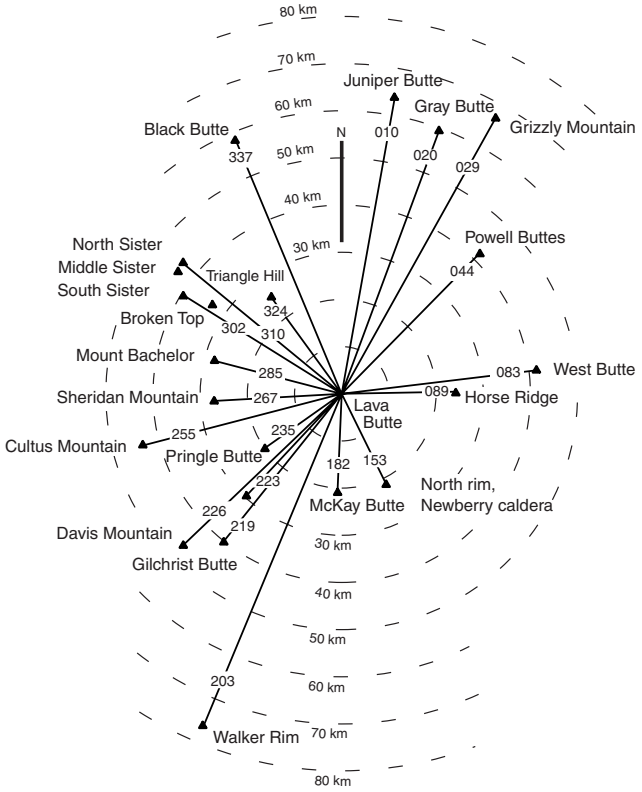

Figure 10. Compass wheel showing direction and distance to selected geographic features visible from the top of Lava Butte, Stop 4.

m/km along the 18.5-km reach to Bend.

The slope of the water table also increases north of Benham Falls, but to an even greater degree. The water table is roughly 3 m below the land surface in much of the La Pine subbasin. Starting at Sunriver, 8 km south of Lava Butte, the water table slopes northward so steeply that at Bend the depth to water is 170-200 m below the land surface. Near the river at Benham Falls, the water table is at an altitude of about 1,260 m (4,135 ft) and 1.5 to 5 meters below the land surface (Fig. 11). In downtown Bend, the water table is at an altitude of 940 m (3,080 ft) and the land surface is 1,110 m (3,630 ft)

The northward-increasing depth to water in this area has implications for the interaction of ground water and streams. South of Sunriver, the Deschutes River system commonly gains due to ground-water discharge, and major spring complexes are common. North of Sunriver, the streams lose water to the ground-water system as ground-water levels drop far below stream levels. For example, stream-gage data from the 1940s and 1950s showed that the Deschutes River lost an average of 0.68 m^3/s (24 ft^3/s) between Sunriver and Benham Falls. The average loss between Benham Falls and Lava Island, about 12 km downstream, was 2.3 m^3/s (83 ft^3/s). Most of the loss likely occurs where the channel crosses or is adjacent to the lava flows from Lava Butte. This lava is sufficiently young that fractures have not been sealed by sediment. Water easily leaks through the stream bed or channel walls into underlying lava flows.

In stops farther north we will see that conditions are reversed, and the regional water table is above river level, causing ground water once again to discharge to streams. The relation between topography and ground-water level in the upper Deschutes Basin is shown diagrammatically in Figure 12.

The rate of leakage from the Deschutes River in the Benham Falls area is proportional to the river stage and hence to streamflow (Gannett and others, 2001). The higher the stage, the greater the rate of loss. The ground-water level near the river varies in response to variations in the leakage rate. Continuous-recorder hydrographs show how the water table responds to changes in streamflow (Fig. 13). The stage and discharge in the Deschutes River in this reach are controlled by reservoir operations upstream. Streamflow is highest from April to October as water is routed down from the reservoirs to canal diversions near Bend. The water level in well 19S/11E-16ACC, about 150 m from the river near the Benham Falls parking area, rises and falls rapidly in response to river stage. Abrupt changes in streamflow usually become apparent in the well within a few to several days. These effects are much less pronounced, however, in wells farther from the river. The water level in well 18S/11E-21CDD, about 1.6 km from the river, also fluctuates in response to river stage, but the fluctuations are subdued, and the hydrograph is nearly sinusoidal, showing only the slightest inflections in response to abrupt changes in streamflow. In addition, the peaks and troughs in the hydrograph of well 18S/11E-21CDD lag those of well 19S/11E-16ACC by 1 to 2 months (Fig. 13).

Lithologic and geophysical logs from wells provide limited stratigraphic information for the Lava Butte area. The drillers' log from

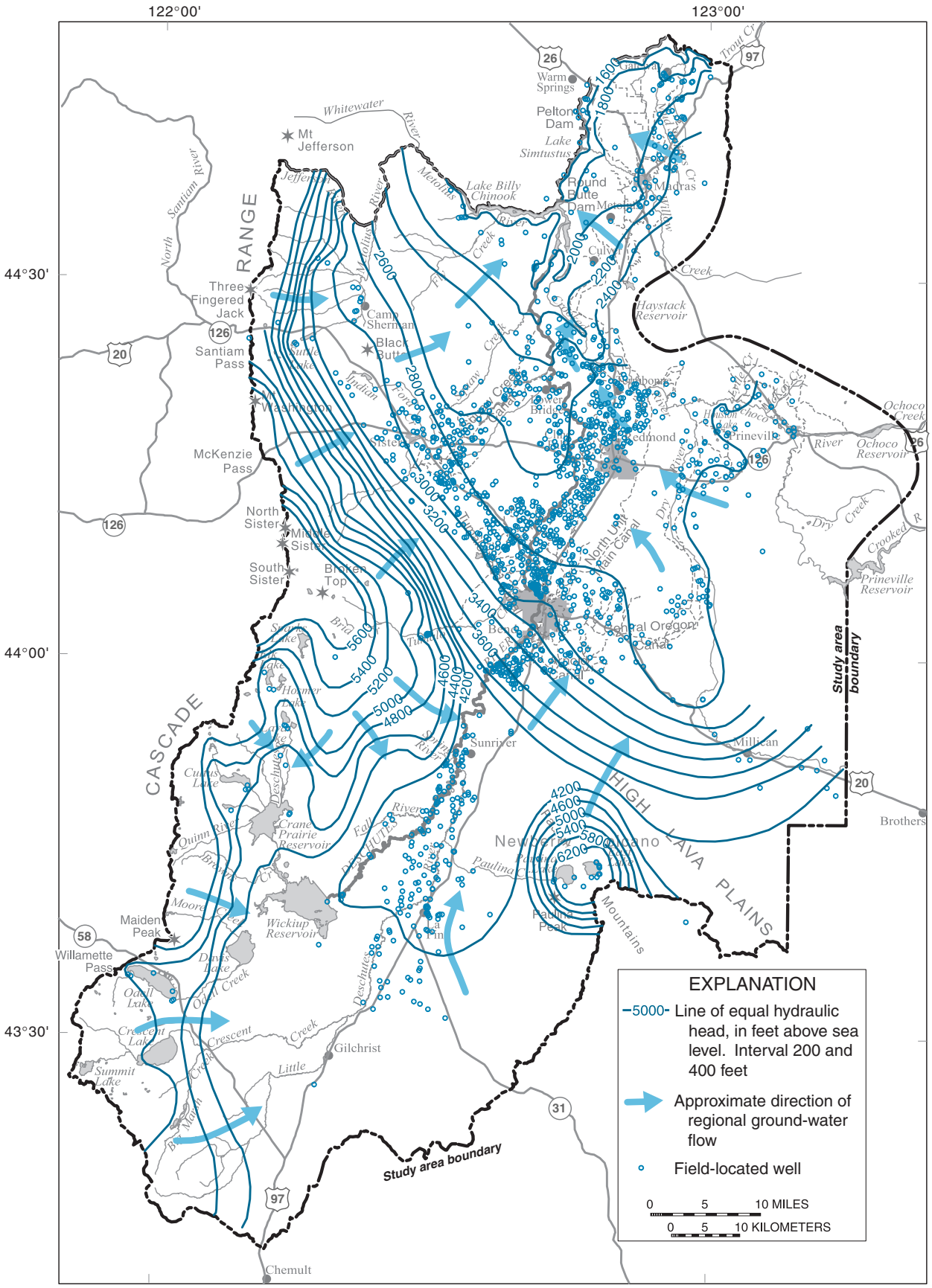

Figure 11. Map showing generalized lines of equal hydraulic head and ground-water flow directions in the upper Deschutes Basin (from Gannett and others, 2001).

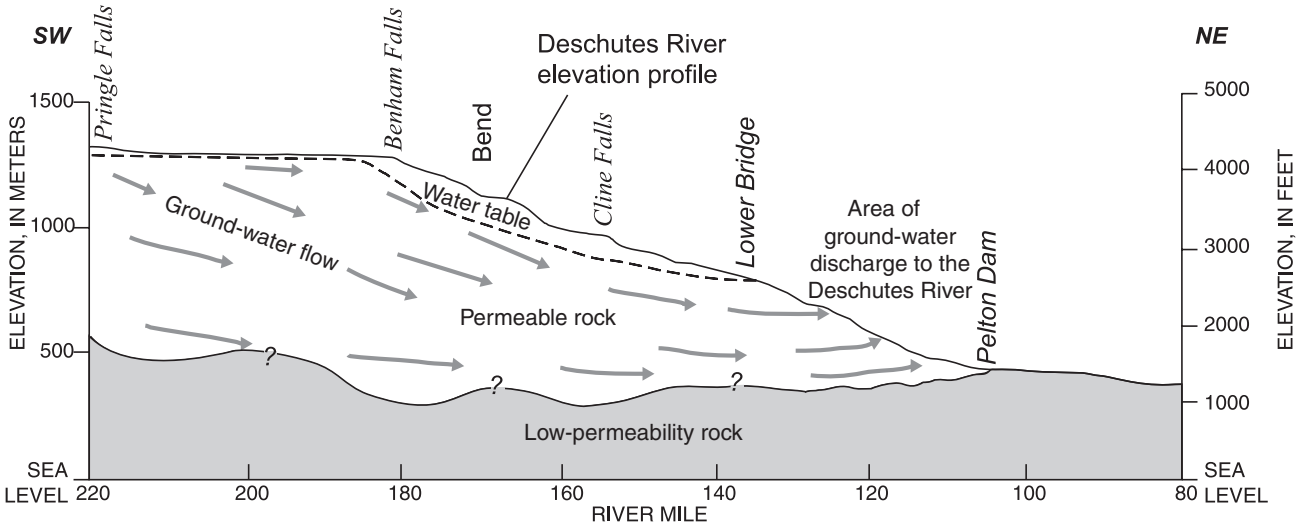

Figure 12. Diagrammatic section showing the effect of geology and topography on ground-water discharge along the Deschutes River from Benham Falls to Pelton Dam.

the well at the Lava Lands Visitor Center, just south of the butte, describes a more or less monotonous stack of interbedded lava and cinders to a depth of 155 m. The drillers' log for a test well east of US 97 shows predominantly lava and cinders to a depth of 91 m, underlain by 12 m of tan sandstone, in turn underlain by 12 m of white pumice. A gamma-ray log (Fig. 14; K.E. Lite, Jr., unpub data) indicates that these latter strata are silicic, so we interpret the "sandstone" and pumice to be the Tumalo Tuff and the Bend Pumice (described at Stop 6). Although ambiguous, descriptions for the 19.5-m section below the silicic deposits suggest interbedded lava and sediment. At the base of Lava Butte, the water table is at about 1,251 m (4,104 ft), and it lies about 122 m below the land surface.

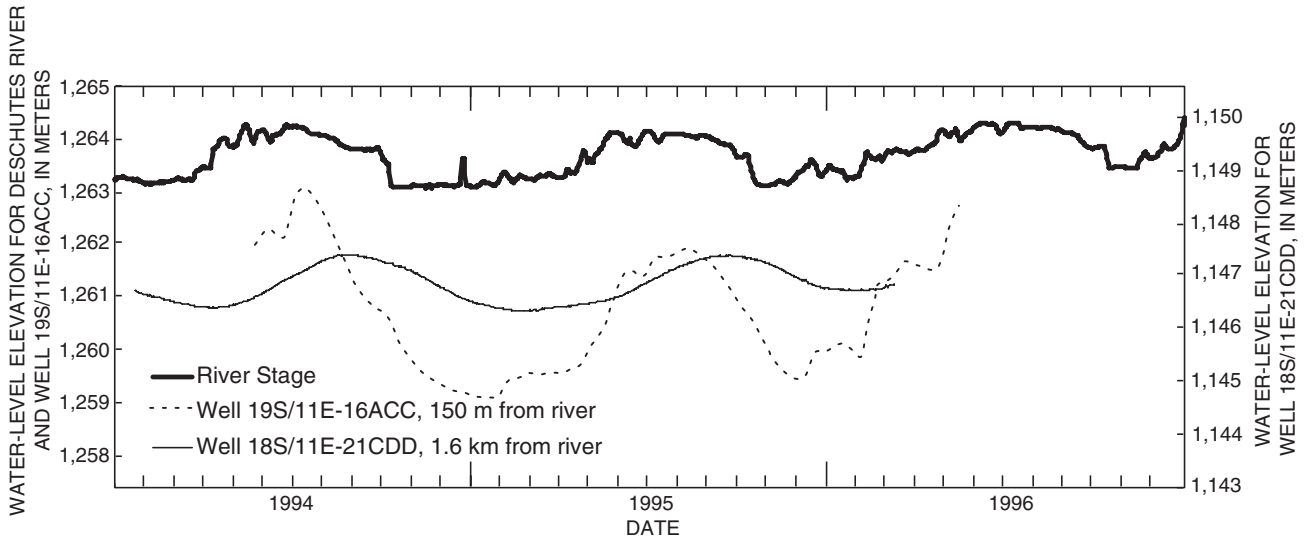

Figure 13. Hydrograph showing the relation between the stage of the Deschutes River at Benham Falls and water levels in wells 150 and 1,600 m from the river.

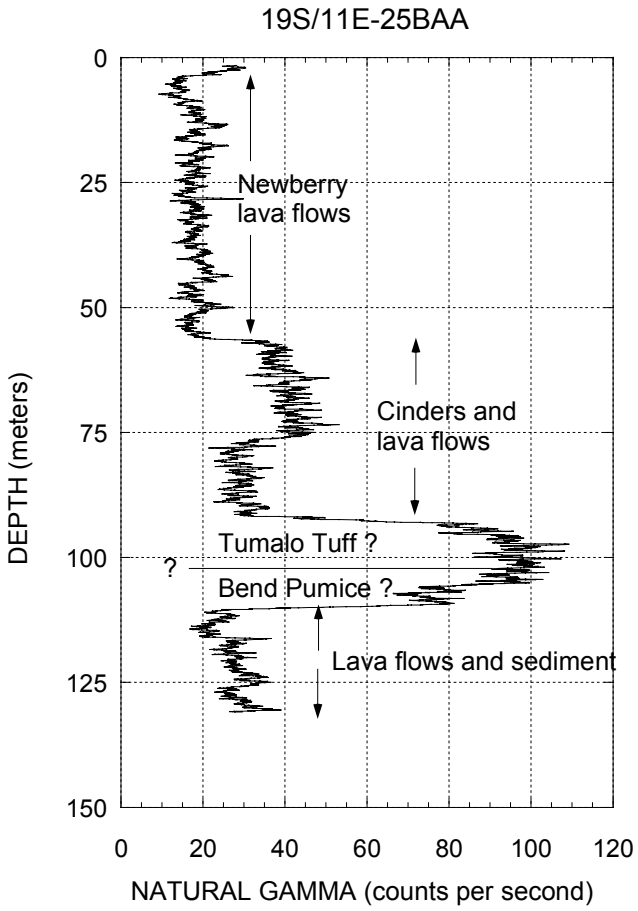

Figure 14. Natural gamma-ray log and inferred stratigraphy in a well east of US 97 near Lava Butte, Stop 4.

Stop 5—Surface-Water Diversions in Bend (Altitude 1,085 m; 3,560 ft)

At this stop we can see the dam and headgates for diversion into the North Unit and Pilot Butte Canals (Fig. 15). The dam, near River Mile 165, was constructed in the early 1900s as part of the diversions (K.G. Gorman, oral commun, 2001). It also once served as a hydropower impoundment. Some of the original power-generating equipment is visible downstream from the dam.

During the irrigation season, water is diverted from the Deschutes River between Lava Butte and Bend into irrigation canals at a rate of approximately 57 m^3/s (2,000 ft^3/s) (Gannett and others, 2001). The average annual rate is about 28 m^3/s (1,000 ft^3/s). The North Unit and Pilot Butte Canals account for roughly half the total diversion. Most canals are unlined and leak considerably. Overall transmission losses approach 50 percent and are even greater where the canals cross fractured Pleistocene lava. Water lost from canals infiltrates and recharges the ground-water system. Although the canals lose large amounts of water, the Deschutes River north of Bend shows little or no loss. The probable reason for the lack of stream leakage is that lava in the stream channel north of Bend is sufficiently old that fractures have been sealed by sediment.

Total canal losses north of Bend approach a mean annual rate of 14 m^3/s (500 ft^3/s), which is a substantial flux of water, more than 10 percent of the long-term average recharge from precipitation in the entire upper Deschutes Basin, about 108 m^3/s (3,800 ft^3/s) (Gannett and others, 2001). Ground-water flow directions

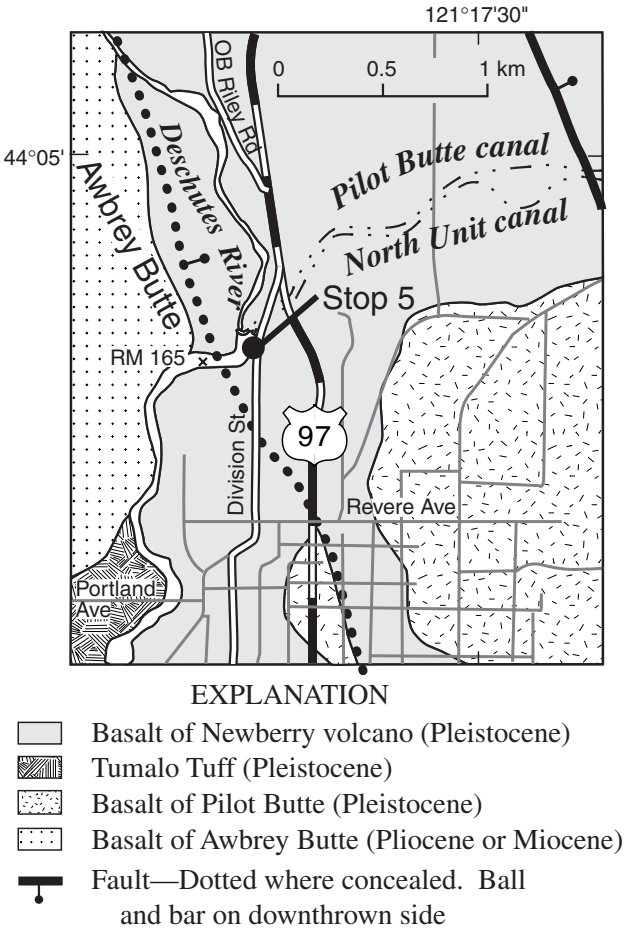

Figure 15. Map showing the Deschutes River diversions for the North Unit and Pilot Butte Canals near Bend, Stop 5 (geology from Sherrod and others, in press).

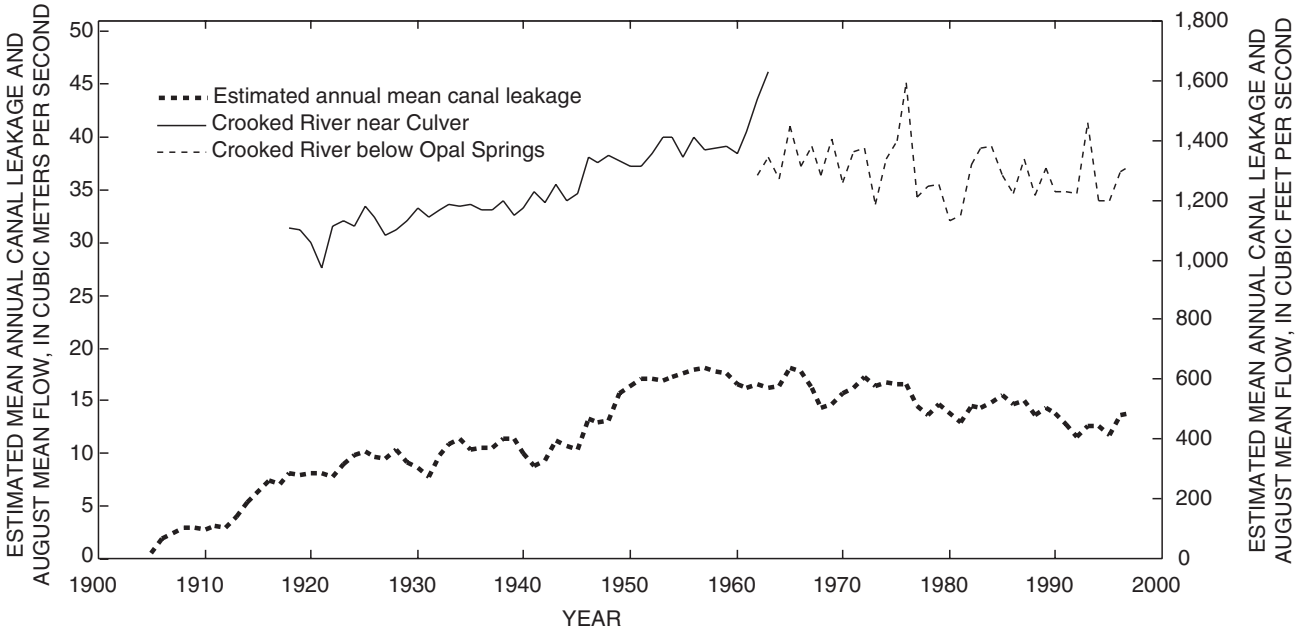

Figure 16. Hydrograph showing estimated canal losses north of Bend and August mean discharge of the Crooked River.

inferred from head maps (Fig. 11) suggest that the lost canal water flows toward the lower Crooked River. Comparing rates of estimated canal losses with long-term streamflow records confirms that this is the case. Figure 16 shows the estimated annual mean canal losses from 1905 to 1998. Also shown are the August mean flows of the lower Crooked River for the same period. During August, flows of the lower Crooked River are due almost entirely to spring discharge, and variation in August mean flow is a good proxy for variation in ground-water discharge (baseflow). As shown in Figure 16, baseflow to the lower Crooked River increased in a manner similar to the estimated canal losses throughout most of the past century. This relation has implications for water management. Efforts to conserve water by lining the canals may result in reduced streamflow in the lower Crooked River.

Many wells in the Bend area have static water levels greater than 200 m below the land surface. Some wells, however, have depths to water ranging from 30 to 60 m. Many of these shallower saturated zones are artificially recharged from canal leakage and deep percolation of irrigation water. Historic data are insufficient to determine precisely how much shallow ground water is canal derived and how much might result from natural stream leakage.

Ground-water levels show varying rates of response to changes in canal flow depending on the permeability of the bedrock, as described in detail by Gannett and others (2001). For example, the static water level in a well 5 km southeast of here, drilled in fractured lava 1 km from the Arnold Canal, responds within a matter of days to canal operation (Fig. 17A).

In contrast is a well on the north side of Redmond that spudded into the 3-4-Ma basalt of Dry River and yields water from underlying sedimentary strata of the Deschutes Formation. The water level in this well, 0.4 km west of the Pilot Butte Canal, has a greater lag time and a more subdued response (Fig. 17B). It begins to respond 2 months after canal operation begins and peaks 1 to 2 months after the canals are shut off for the year.

Stop 6—Sisters Fault Zone Outcrop, Tumalo Reservoir Road (Altitude 1,006 m; 3,300 ft)

This stop shows in cross section a minor fault of the Sisters Fault Zone. The quarried exposure shows Bend Pumice (fallout tephra), Tumalo Tuff (pyroclastic flow), and overlying gravel deposits cut by a steep northwest-striking fault with offset less than 4 m, down on

the northeast side. The Tumalo Tuff is about 0.4 Ma in age, on the basis of ages by both conventional K-Ar (Sarna-Wojcicki and others, 1989) and step-heating $^{40}Ar/^{39}Ar$ methods (Lanphere and others, 1999). The capping gravel deposit is undated. Thus the latest fault motion here is known only to be younger than 0.4 Ma. Exposed in adjacent road cuts are older deposits, including the underlying Desert Spring Tuff, which is 0.6 Ma in age.

The north-northwest-trending Sisters Fault Zone comprises nearly 50 mapped faults across a breadth of 5-15 km. The total length of the zone is 60 km, and our stop here is about midway along it. The principal strand, the Tumalo Fault, extends nearly continuously for 47 km. Its trace passes 5.5 km southwest of this stop and will be visited at Tumalo Dam (Stop 7). The Tumalo Fault has displaced Pliocene lava flows of the Deschutes Formation by at least 60-70 m of normal separation at Tumalo Dam. Quaternary lava flows younger than 0.78 Ma in the same area have escarpments of only 6-10 m.

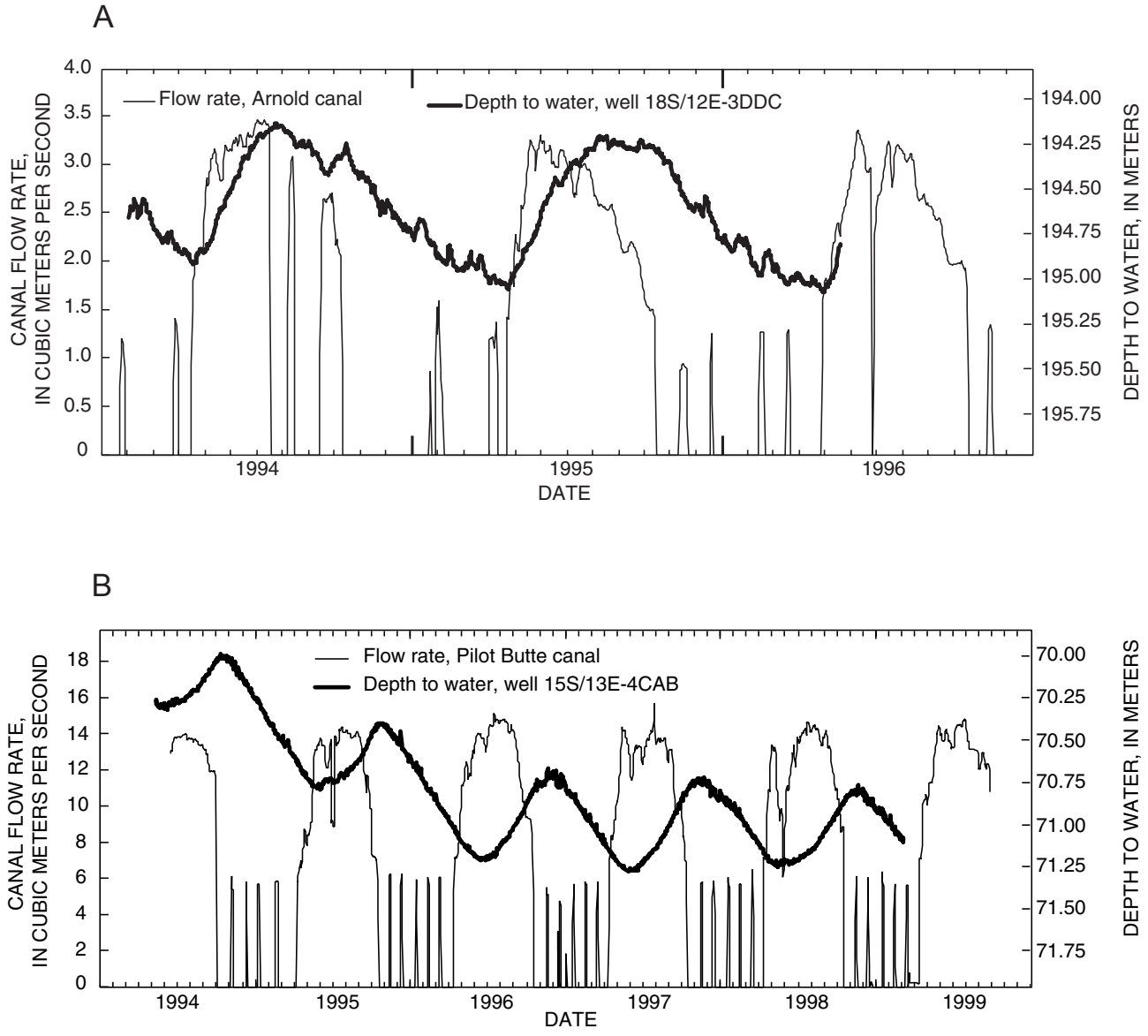

Figure 17. Hydrographs showing the relation between ground-water fluctuations and canal operation. *A.* Well and canal water fluctuations in highly permeable late Quaternary lava flows at Bend. *B.* Well and canal water fluctuations in early Pliocene and Miocene lava flows and sedimentary strata at Redmond.

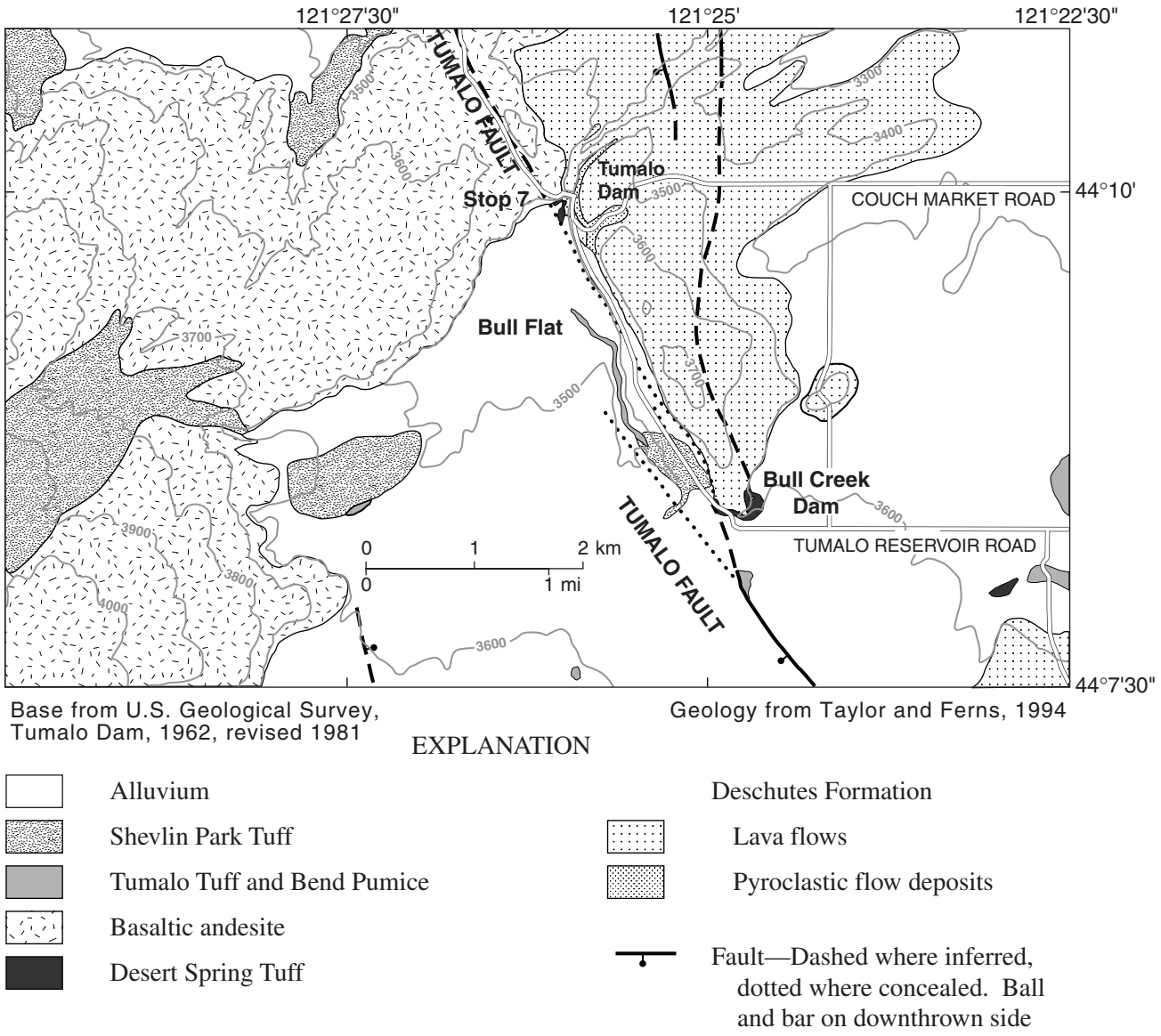

Figure 18. Map showing geology of the Bull Flat–Tumalo Dam area, Stop 7.

The Sisters Fault Zone is roughly on trend with a pronounced ground-water gradient (high-head-gradient zone) that characterizes the Deschutes Basin northwest from Bend for 60 km to Suttle Lake in the Cascade Range (Fig. 11). The fault zone and ground-water gradient are displaced from each other by roughly 10 km, however, with the ground-water gradient lying closer to the topographic slope of the Cascade Range. There is no evidence that the Sisters Fault Zone has a measurable effect on the distribution of ground water.

This observation is unsurprising stratigraphically, because the upper Miocene and lower Pliocene strata of the Deschutes Formation on the upthrown side of faults along the zone are similar in permeability to upper Pliocene and Pleistocene deposits along the downthrown side. Thus, permeability contrasts across the faults likely are few. Ground-water damming would occur only if these faults had created substantial gouge, or if fault offsets occurred rapidly enough or were sufficiently great to create numerous or extensive closed basins.

Ground-water levels in this area are elevated slightly due to canal losses and irrigation (Gannett and others, 2001). The water table is at an altitude of about 930 m (3,050 ft), and depths to water range from 60 to 120 m de-

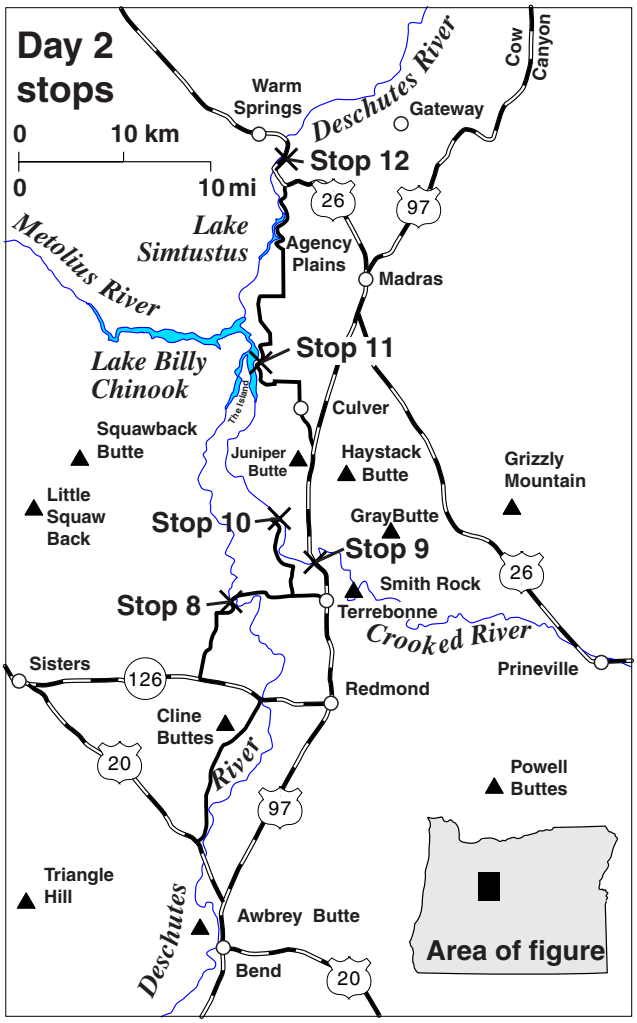

Figure 19. Route and stops for Day 2 of the field trip.

pending on land-surface altitude and proximity to the river.

Stop 7—Bull Flat and Tumalo Dam (Altitude 1,067 m; 3,500 ft)

Our travel northwest to here has been along the Tumalo Fault. En route we passed by the small Upper Tumalo Reservoir and its impoundment, Bull Creek Dam. Continuing 3.5 km farther, the road crosses Tumalo Dam, then resumes its northwest course along the fault. Tumalo Dam obstructs an unnamed drainage. Bull Flat is the treeless basin upstream from the dam. The water-table altitude is about 840 m (2,750 ft) in this area and depths to water in wells average about 150 m.

At Stop 7 we can see the geomorphic and stratigraphic contrast across the Tumalo Fault (Fig. 18). On the northeast (upthrown) side are Pliocene strata of the Deschutes Formation. They are chiefly basaltic andesite lava flows. An andesitic ignimbrite (62 percent SiO_2; Smith, 1986a) is interlayered in the Deschutes sequence and visible in the road cut at the east dam abutment. The Deschutes units exposed here are probably about 4-5 Ma in age, although no isotopic ages have been reported from this area. Offset of at least 70 m is indicated by the height of the Deschutes Formation ridge northeast of the fault and the absence of Deschutes Formation strata at the ground surface southwest of the fault. Cross sections by Taylor and Ferns (1994) suggest that the Deschutes Formation is buried by 50 m of volcaniclastic deposits in the downthrown block, in which case the dip separation is 120 m.

On the southwest (downthrown) side is alluvium that floors Bull Flat. Middle Pleistocene pyroclastic-flow deposits are exposed sporadically where they have banked against Deschutes Formation strata of the upthrown block or where alluvium is thin on the floor of Bull Flat. The ~0.6-Ma Desert Spring Tuff likely has been displaced several meters here, because no outcrops of the tuff are found on the downthrown side but they are present on the upthrown block of the Tumalo Fault near the dam. Displacement of younger pyroclastic-flow deposits is difficult to quantify, because the pyroclastic flows may have overtopped topographic barriers and been deposited across a wide altitude range.

Bull Flat is an alluvial basin that likely has received sedimentary and volcanic deposits during at least the past million years. Neither the depth nor lithology of the subsurface fill is known. The rate of stream incision across the Tumalo Fault in this area has kept pace with the rate of uplift, however, because the distribution of all pyroclastic flows of 0.6 Ma and younger suggests that they escaped through channels cut through the upthrown block.

The west dam abutment is a Cascade Range basaltic andesite lava flow. Topographic escarpments only 6–10 m high mark the trace of the Tumalo Fault across this flow. It possesses normal-polarity thermal-remanent magnetization and is thought to be younger

SIDEBAR 1. THREE BUTTES—70 YEARS OF UNCERTAINTY RESOLVED

Three volcanic buttes of previously uncertain age lie within a few kilometers of the Deschutes River between Redmond and Madras (Fig. 20). Our travel takes us by Cline Buttes, a prominent rhyolite dome complex west of Redmond. Less prominent is Forked Horn Butte, which lies 6 km east of Cline Buttes and may be visible along the drive. The third butte, which won't be visible, is an unnamed sprawling mass of rhyodacite lava southwest of Steelhead Falls, 15 km north of Cline Buttes. Each had been assigned to stratigraphic units several million years older than the Deschutes Formation (Stearns, 1931; Williams, 1957; Stensland, 1970; Robinson and Stensland, 1979; Smith, 1986a). By contrast, our mapping and dating have determined that these buttes are late Miocene in age and part of the Deschutes Formation.

The rhyolite of Cline Buttes has an isotopic age of 6.14±0.06 Ma (Table 2). Most rocks at Cline Buttes are hydrothermally altered, but the dated sample came from fresh obsidian in a quarry on the east flank. Forked Horn Butte is a knob within an extensive debris-avalanche deposit. It is undated isotopically, but it underlies the 3.68-Ma basalt of Redmond and overlies sedimentary strata in the Deschutes Formation. The rhyodacite southwest of Steelhead Falls is fairly fresh and homogeneous throughout. It has an age of 6.74±0.20 Ma (Table 2).

Depth to water in the Cline Buttes area averages 90 to 120 m on the south side and 60 to 100 m on the north side. The water-table altitude is 823 to 838 m (2,700 to 2,750 ft). Hydrologic evidence indicates that the rhyolite of Cline Buttes and the rhyodacite southwest of Steelhead Falls are fairly permeable relative to the surrounding terrain, a finding in keeping with their age (Ferns and others, 1996b; M.W. Gannett, unpub. data). Sparse head data from wells shows that the northward gradient steepens adjacent to Cline Buttes, suggesting higher relative permeability. In addition, substantial ground water discharges to the Deschutes River from springs issuing from the rhyodacite exposed in the canyon north of Steelhead Falls (Ferns and others, 1996b).

These late Miocene ages and stratigraphic assignments lead to a different view of the breadth and thickness of Deschutes Formation strata in the central part of the basin. Instead of thinning against steptoes, the Deschutes Formation extensively blankets the central basin with a thickness of 300-460 m. Indeed, the Deschutes Formation may be as thick as 500-600 m if measured from the summit of Cline Buttes.

than 0.78 Ma. The lava flow is overlain upslope by the 0.2-Ma Shevlin Park Tuff.

The story of the Tumalo Dam and its reservoir is one of broken promises and unfulfilled dreams, like many that surround the land-grab development of the arid west. An excellent history of the Tumalo Project, which we retell in the following, is provided by Winch (1984-85).

In the 1890s, homesteaders were lured to this area by promises of free land and abundant water for irrigation. By 1913, however, the private developers had gone bankrupt, and the promised water and delivery canals had not materialized. The State of Oregon stepped in to fulfill promises made to the homesteaders and to the federal government. Tumalo Dam was part of an attempt to provide the promised irrigation water.

Prior to construction, some engineers expressed concern about the permeability of the strata bounding the reservoir. The dam, constructed in 1914, is a 22-m-tall earth-fill structure with a steel-reinforced concrete core. The outlet was a 2.5 by 2.5-m concrete-lined tunnel 123 m long. Flow through the outlet was to be controlled from a small house at the end of the dam. The reservoir was to cover 447 ha and to impound 24.66 x 10^6 m^3 of water. The dam was completed and the sluice gates closed on December 5, 1914.

The concerns of the engineers were confirmed early in the winter of 1915, as the reservoir, at only a fraction of its capacity, saw its water level falling 0.2 m per day. When runoff increased in March and April, and the water level started to rise, large sinkholes developed (perhaps along the Tumalo Fault) at the eastern margin of the reservoir not far from the dam. The largest sinkhole was 9 by 15 m across and 3 to 8 m deep, swallowing water at an estimated rate of 5.7 m^3/s (200 ft^3/s). Attempts to seal the

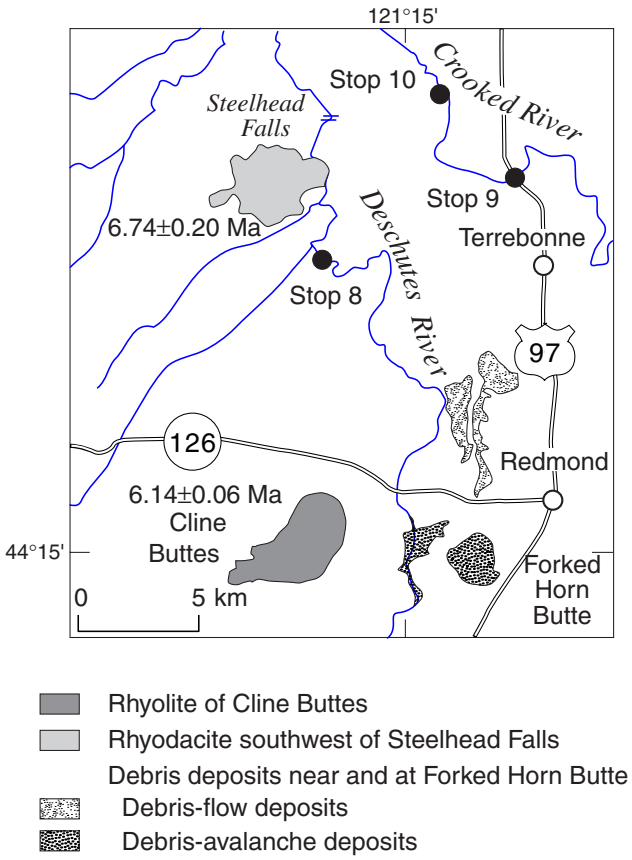

Figure 20. Cline Buttes, Forked Horn Butte, rhyodacite southwest of Steelhead Falls, and nearby debris deposits.

reservoir failed, and the Tumalo Dam has never been used.

DAY 2

Synopsis, Deschutes Basin from Bend to Madras

The traverse from Bend to Madras (Fig. 19) is within a broad valley dominated by a gently northward-sloping surface with scattered low hills. Many of the hills consist of cinder cones, small shield volcanoes, and silicic domes, mainly of the upper Miocene to Pliocene Deschutes Formation. Several small canyons form a northeast-trending topographic grain on the west side of the valley, exposing lava flows, ash-flow tuff, and sedimentary strata deposited as a result of volcanic eruptions during Deschutes time. We will drive down one of these canyons (Buckhorn) on our way to Lower Bridge (Stop 8).

The central and eastern surface in the southern part of the valley is flat and covered predominately with Pleistocene lava flows originating from Newberry Volcano, which forms part of the southeast basin margin. Some of the lava flows from Newberry traveled tens of kilometers and entered the ancestral Deschutes and Crooked Rivers as intracanyon flows. Remnants of these lava flows form conspicuous benches within the canyons of the Deschutes and Crooked Rivers in the northern part of the valley. The eastern boundary of the valley consists of hills of mainly silicic rocks of the Oligocene to Miocene John Day Formation.

The modern Deschutes and Crooked Rivers form shallow incised drainages in the southern part of the valley, but they have carved narrow deep canyons in the northern part. It is in these deep canyons where much of the section of the Deschutes Formation is exposed. Lava flows, ash-flow tuff, debris-flow deposits, and fluvial silt, sand, and gravel are exposed in cliffs along several kilometers of canyon walls. Our hike down into the canyon of the Crooked River (Stop 10) will be an opportunity to examine some of those deposits in detail. By about 7 km downstream from Round Butte Dam, the Deschutes River has cut through the entire thickness of the Deschutes Formation and exposed the underlying Simtustus Formation and Prineville Basalt. About 8 km downstream from that point, approximately at the regulator dam, the river has cut down to the John Day Formation.

The broad flat area between the canyon of the Deschutes River and Madras, known as the Agency Plains, is underlain by Deschutes Formation lava flows (the basalt of Tetherow Butte). These flows cover only the west side of the Agency Plains. The east side, including Madras, is underlain by fine-grained sedimentary deposits of the Deschutes Formation shed mainly from the uplands to the east.

Ground-Water Flow from Bend to Madras

Throughout the area between Bend and Madras, ground water flows generally northward through sediment and lava of the Deschutes Formation toward the confluence of the Deschutes and Crooked Rivers. The Pleistocene lava flows from Newberry Volcano and pyroclastic deposits from the Bend Highland

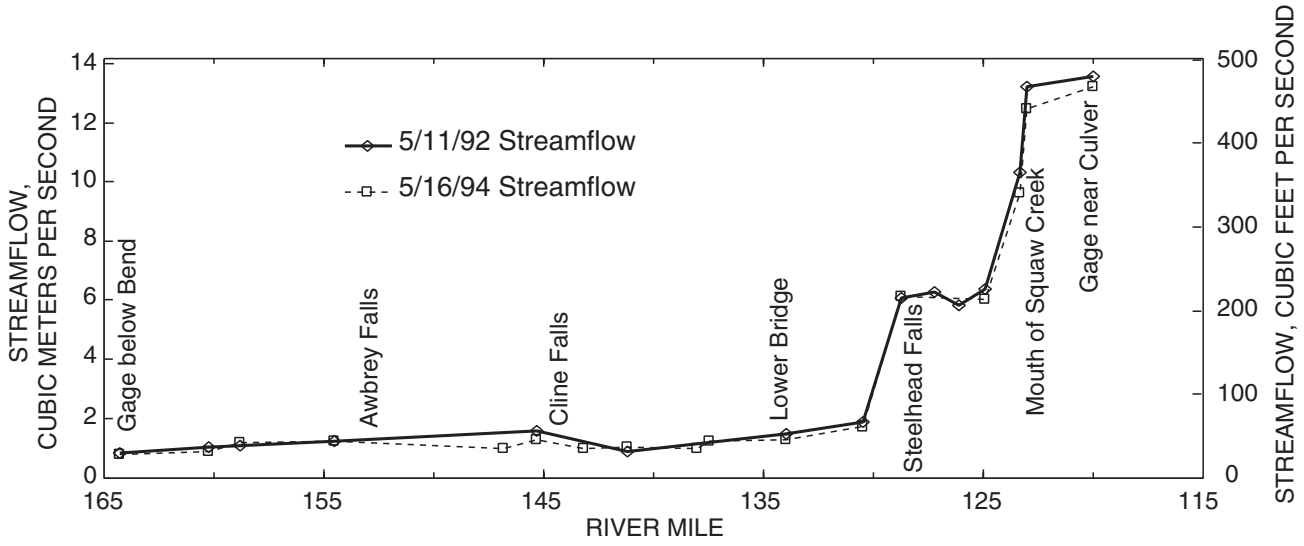

Figure 21. Graph showing gain in flow of the Deschutes River owing to ground-water discharge between River Miles 165 and 120, May 1992 and May 1994.

are largely unsaturated. The area around Bend extending north to Tumalo is characterized by a large vertical head gradient indicating strong downward flow. Shallow wells in the area commonly have static water levels less than 30 m below the land surface, whereas nearby deep wells may have depths to water exceeding 200 m. The presence of the shallow water table and the strong downward gradient is attributed to local and at least partly artificial recharge from canal and stream leakage. Such areas of artificial recharge and anomalously shallow saturated zones are far less common to the north around Redmond. The water table slopes gently northward from Bend toward the Deschutes–Crooked Rivers confluence area with a gradient of approximately 3.8 m/km (Fig. 11). The stream gradient, however, is somewhat steeper, averaging 6.2 m/km between Bend and Lower Bridge. As a consequence, the canyons of the Deschutes and Crooked Rivers intersect the regional water table several kilometers north of Redmond.

The Deschutes River intersects the regional water table at about Lower Bridge (Fig. 12; River Mile 134), and the Crooked River intersects the regional water table at about Trail Crossing (River Mile 20.6), about 2.1 km northeast of the US 97 bridge. Downstream from these sites, the altitude of the streams is below that of the regional water table, and ground water flows toward and discharges to the streams, resulting in dramatic increases in streamflow. Between the points where the Deschutes and Crooked Rivers intersect the regional water table and the point where the Deschutes River intersects the John Day Formation, the combined streams gain approximately 63 m^3/s (2,200 ft^3/s) from ground-water inflow (Gannett and others, 2001).

North of the regulator dam (at River Mile 100), the Deschutes Formation thins against the underlying units and pinches out by about River Mile 87. Below this point, the Deschutes River gains little if any flow from ground-water discharge, and the modest increases in flow that do occur are due to tributary inflow.

Stop 8—Lower Bridge, Where Ground Water Meets the Deschutes River (Altitude 770 m; 2,525 ft)

This stop is at the south side of the bridge on the left bank of the Deschutes River. It is about here where the Deschutes River has incised deeply enough to intercept the regional water table. Downstream from this point, the Deschutes River is below the regional water table, resulting in ground-water discharge to the river. Wells in the Lower Bridge area have static water levels coincident with the river level.

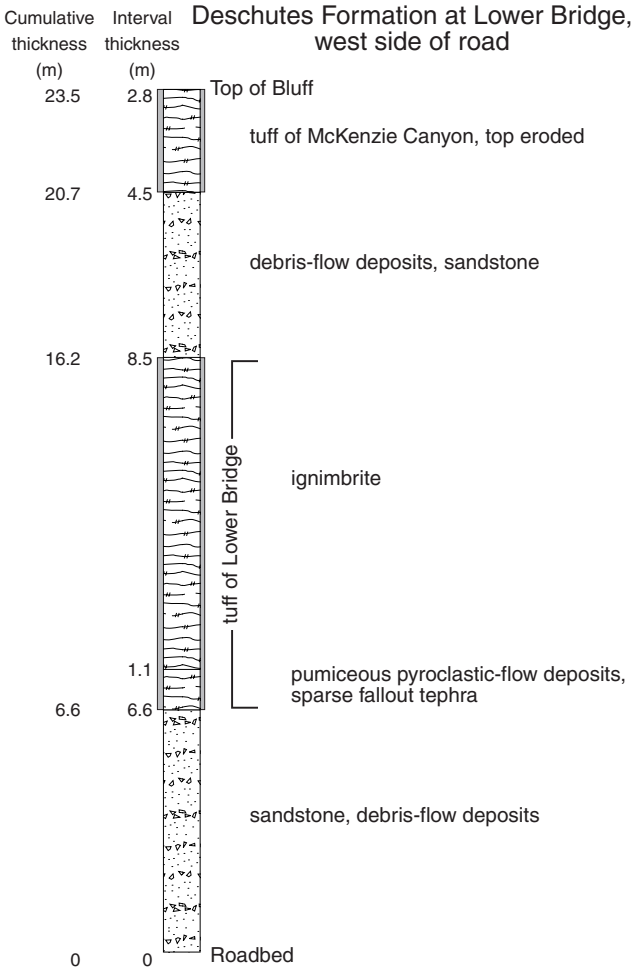

Figure 22. Stratigraphic section of the Lower Bridge area, Stop 8.

Streamflow measurements that are synoptic (gathered nearly simultaneously) show that the Deschutes River gains approximately 11.3 m^3/s (400 ft^3/s) from ground-water discharge between Lower Bridge and the stream gage just above Lake Billy Chinook near Culver (Fig. 21). About a quarter of this increase comes from ground-water discharge to the lower 3.2 km of Squaw Creek. Ground-water inflow is not uniform along the stream but emerges preferentially from permeable deposits such as coarse conglomerate and the fractured rhyodacite described in Sidebar 1 (Ferns and others, 1996b).

Exposures on the west side of the road provide easy access to about 24 m of the Deschutes sedimentary and volcanic sequence (Fig. 22). In the middle one-third is the tuff of Lower Bridge, about 8.5 m here, a typical thickness. At the top of the exposure is the tuff of McKenzie Canyon. It is only 2.8 m thick, but its top is eroded. The tuff of McKenzie Canyon commonly is 6-10 m thick in this part of the basin. Both units were erupted from vents in the Cascade Range. Neither tuff has been dated, but both were emplaced between about 5.77 and 5.06 Ma on the basis of their position above the basalt of Opal Springs and beneath the basaltic andesite of Steamboat Rock (Table 2). A gamma-ray log from a well about 1.3 km south of this exposure reflects the same stratigraphic section viewed at this stop (Fig. 23; K.E. Lite, Jr., unpub data). The principal water-bearing unit in the well is the sand and gravel deposit 12-25 m below the tuff of Lower Bridge.

Two Pleistocene stratigraphic units are widespread in the Lower Bridge area and visible from this stop. Poorly indurated earthy white diatomite caps the bluff west of our stop

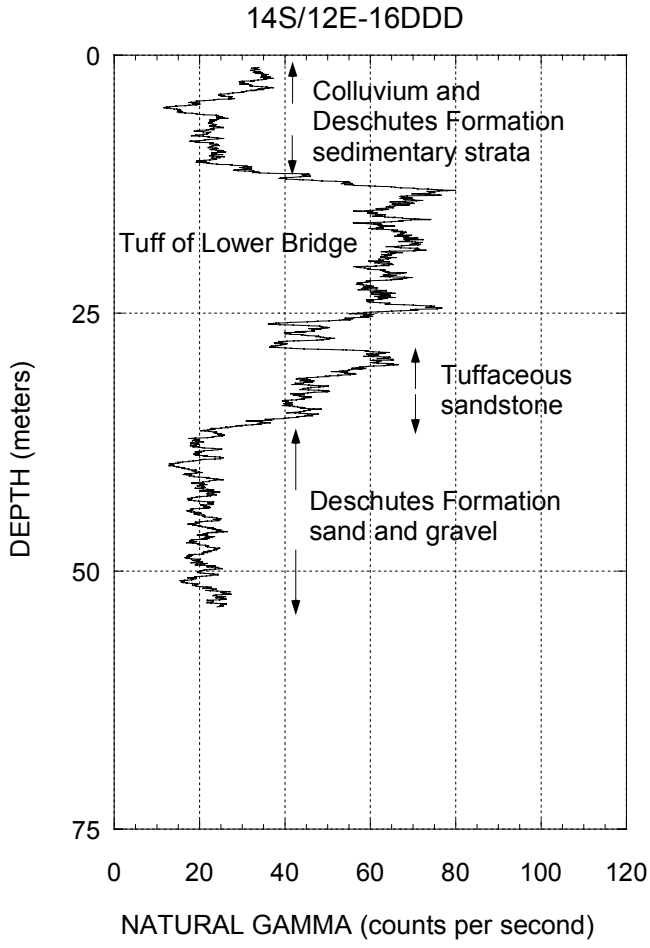

Figure 23. Natural gamma-ray log and inferred stratigraphy in a well near Lower Bridge, Stop 8.

and is also exposed in road cuts along the highway grade east from here. The diatomite has been mined extensively from the now-abandoned quarry above the bluff. Basalt from Newberry Volcano overlies the diatomite in several exposures.

The diatomite was once as thick as 20 m (Moore, 1937). Little of the original deposit remains, however, and the site is now mostly occupied by irregularly heaped overburden and waste from strip mining. Predominant diatom species are *Stephanodiscus niagarae* (K.E. Lohman in Moore, 1937) and *S. excentricus* (Smith and others, 1987), indicating a late Pliocene or Pleistocene age (Krebs and others, 1989). Volcanic ash bedded within the deposit has been tentatively correlated with the Loleta Ash (distal-fallout equivalent of the Bend Pumice) (Smith and others, 1987; A.M. Sarna-Wojcicki, oral commun, 1995), which is thought to be about 0.4 Ma in age. An alternative correlation with a 1.9-Ma ash bed found in drill core from a well near Tulelake, California (T-749, 191 m depth; Rieck and others, 1992), is nearly as satisfactory on the basis of statistical comparison coefficients (A.M. Sarna-Wojcicki, oral commun, 1995).

The age of the main diatomite body is probably middle Pleistocene, because the deposit fills a valley floor whose altitude is only slightly higher than the surface later mantled by basalt of Newberry Volcano. Presumably the prediatomite erosional stage is only slightly older than the basalt. Although overlain by the basalt of Newberry Volcano in road cuts northeast of Lower Bridge, earlier Newberry lava flows may have dammed the ancestral Deschutes River to create the lake in which the diatomite was deposited (Smith, 1986a).

Stop 9—Peter Skene Ogden Bridge (Older Bridge) and Adjacent New Bridge (Altitude 811 m; 2,660 ft)

US 97 crosses the Crooked River where middle Pleistocene basalt forms most of the canyon walls. These lava flows were erupted from vents on the north flank of Newberry Volcano and flowed north across the broad plain extending to Redmond. The lava poured into the canyon of the ancestral Crooked River 9 km southeast of the present Ogden Bridge and flowed downstream past the bridge site at least another 8 km—a distance of more than 55 km from the vent area. Lava flows also entered the Deschutes River and reached to Lake Billy Chinook, at least 65 km from the vent.

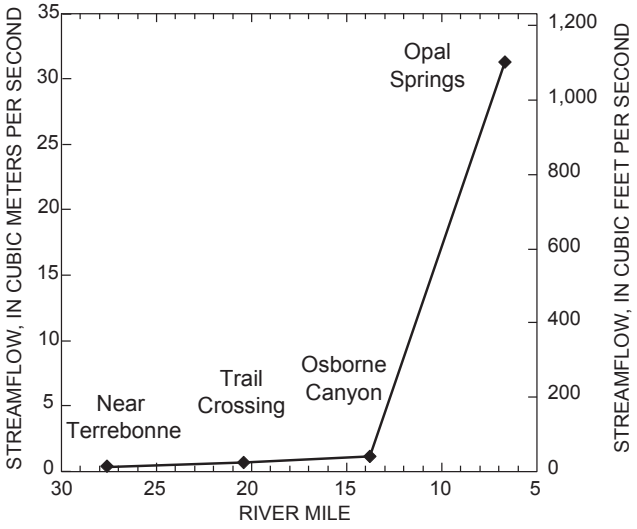

Figure 24. Graph showing gain in flow of the lower Crooked River owing to ground-water discharge between River Miles 28 and 7, July 1994.

The altitude of the Crooked River at the US 97 crossing is approximately 750 m (2,460 ft). At this level, the Crooked River has incised to the depth of the regional water table. Synoptic streamflow measurements gathered in 1994 (Fig. 24) show the Crooked River gaining about 2 m^3/s (70 ft^3/s) from ground-water discharge between Trail Crossing, about 3.2 km upstream from the US 97 crossing, to Osborne Canyon, about 7.2 km downstream. Along the 11.2-km downstream reach between Osborne Canyon and the gage above Lake Billy Chinook, the river gains an additional 28.3 m^3/s (1,000 ft^3/s), making this reach one of the principal ground-water discharge areas in the basin.

The hills to the east are underlain by southeast-dipping strata of the John Day Formation. They form the upthrown block of the Cyrus Springs Fault Zone (Smith and others, 1998). Rocks as young as the Prineville Basalt (15.8 Ma) were involved in the deformation, whereas the Deschutes Formation, the next youngest unit preserved, is undeformed. Thus the deformation occurred after early Oligocene and before late Miocene time. The deformation

SIDEBAR 2. WHAT WAS THE PATH OF THE ANCESTRAL DESCHUTES RIVER?

The Deschutes and Crooked Rivers of today were probably following similar paths before 1 Ma. The Crooked River is a long-lived system draining the southwest flank of the Ochoco Mountains. The geologic record for the Crooked River in the Deschutes Basin can be inferred back to about 6 Ma.

The Deschutes River history for the time back to 4 Ma is known only for its downstream reach north of Lower Bridge and Steelhead Falls. South (upstream) from there, the distribution of lava and pyroclastic flows indicate southwest-trending drainages, as if the Deschutes River may have had its source in the area of the Three Sisters. Evidence for an ancestral Deschutes path southward through the Bend area is buried, and there is no evidence that a river like the modern Deschutes flowed through the Bend area until sometime after 2 Ma.

As shown in Fig. 25A, the general path of the Deschutes and Crooked Rivers in late Miocene time is inferred from paleocurrent indicators, the orientation of intracanyon lava flows toward the basin's axis, and the position of older rocks forming a buttress to sediment transport and deposition along the east side of the basin (Stensland, 1970; Smith, 1986a). This alluvial region was choked by the basalt of Tetherow Butte about 5 Ma, forcing the ancestral Deschutes River westward to its present alignment (Fig. 25B).

The Crooked River subsequently established a course across the basalt of Tetherow Butte, incising a canyon from which it has never escaped. By about 3.5 Ma, the Crooked River upstream from the US 97 crossing was forced to follow its approximate current alignment near the foothills of the Ochoco Mountains owing to emplacement of the basalt of Dry River 3.5-4.0 Ma (Fig. 26).

Still unclear is when the Deschutes River expanded southeastward. The 3.56-Ma basalt of Redmond verged upon but did not enter the Deschutes River drainage northwest of Redmond. Instead it followed a path into the Crooked River drainage. Between 3 and 1 Ma, however, some Deschutes tributary reached southeast beyond Cline Falls and Redmond, judging from broad topographic incision northwest of Redmond. Also, the Redmond Channel, discussed later, probably was carved southeast through the Redmond area prior to about 1 Ma.

About 1 Ma, the basalt of The Island choked the lower Crooked River. This lava can be traced in patchy exposures along the walls of the Crooked River to within 600 m west of the US 97 bridge. The altitude along the lava's base shows that the Crooked River had cut down nearly to the present level by 1 Ma, but the basalt of The Island sheds little light on the paleoriver pattern, because nothing is known about its distribution beyond an already well-defined river valley.

The most recent intracanyon lava flows are part of the basalt of Newberry Volcano, which advanced across the Redmond Plain between 0.7 and 0.3 Ma. Some of these flows draped into and choked the canyon of the Crooked River, once again forcing the river northward to resistant bedrock. Today the Crooked River remains trapped in a deep gorge along the Smith Rock pathway. Other Newberry flows entered the Deschutes River system on each side of Forked Horn Butte (Fig. 27), the first rock-hard evidence we have that the Deschutes drainage was well developed south of Redmond.

One of the little-known features of the history of the Deschutes River is the 9-km-long Redmond Channel (Stensland, 1970). This gulch is only 6-12 m deep today, but its breadth is similar to the nearby modern gorge of the Deschutes River, which is 35 m deep. The Redmond Channel was carved after 3.5 Ma. It follows the contact between the basalt of Redmond and the basalt of Dry River, and in its lower reach, it cuts across the basalt of Redmond. The channel was then nearly filled with lava sometime after 0.7 Ma when the basalt of Newberry Volcano flowed into it. The Redmond Channel may mark the time when a river from the south (the head of the modern Deschutes River) first passed across the Bend area. We presume that the channel has an age of at least 1 Ma in order to account for the depth of erosion required by the breadth and length of its valley.

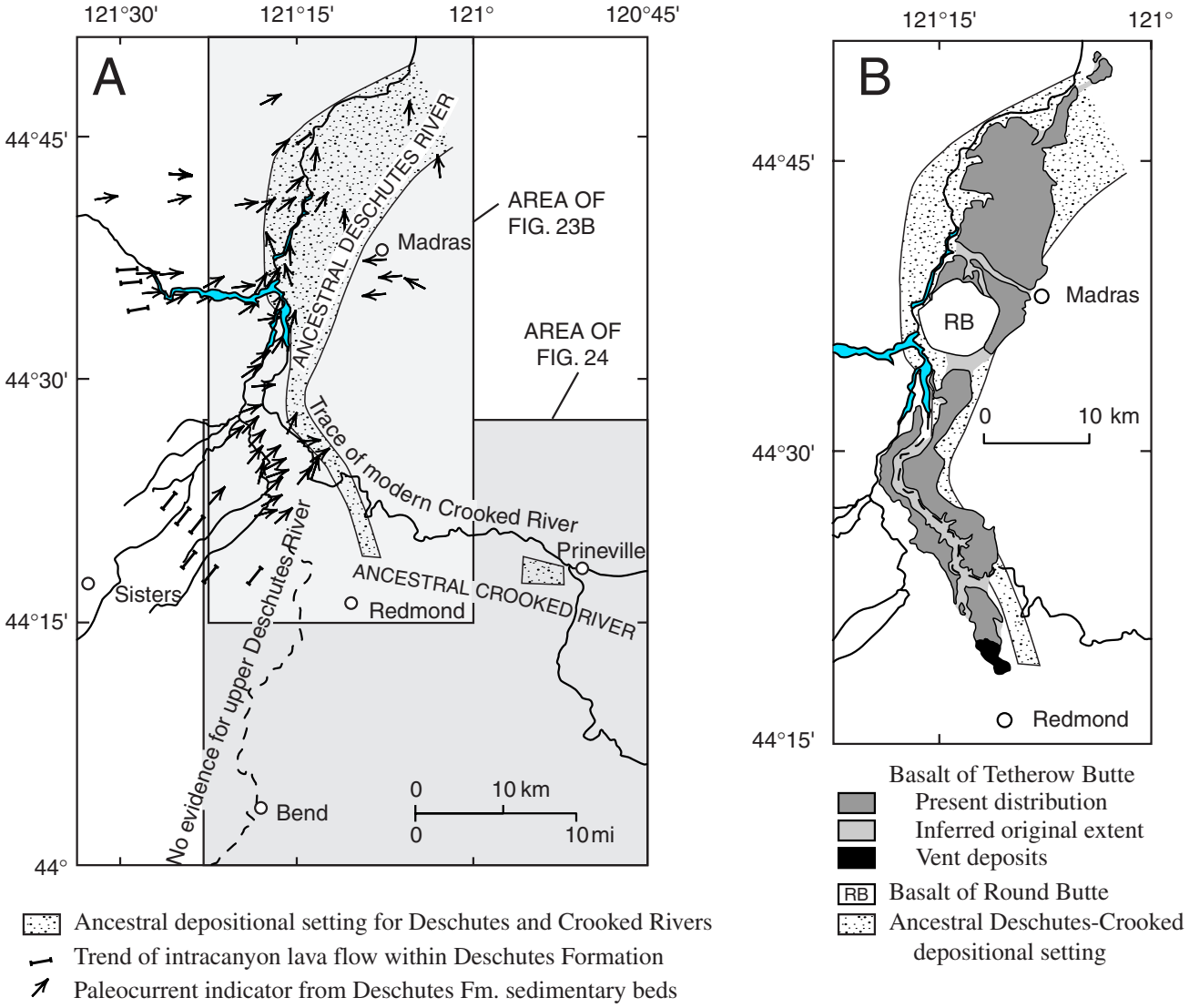

Figure 25. Maps showing path of the Deschutes and Crooked Rivers about 5 Ma, with modern rivers, tributaries, and Lake Billy Chinook shown for reference (data from Smith, 1986a). *A.* Extent of the Deschutes River depositional setting, and flow directions from paleocurrent and paleogeographic indicators. *B.* Extent of basalts of Tetherow Butte and Round Butte.

may be entirely middle or earliest late Miocene in age.

Rocks of the John Day Formation have low permeability because the tuffaceous material is mostly devitrified to clay and other minerals. Lava flows within the formation are weathered and contain abundant secondary minerals. The John Day Formation acts as a barrier to regional ground-water flow. It and age-equivalent Cascade Range strata are considered the lower boundary of the regional flow system throughout much of the Deschutes Basin. The overlying middle Miocene Prineville Basalt is locally fractured, contains permeable interflow zones, and is used as a source of water in some places.

Stop 10—Crooked River Gorge at Crooked River Ranch (River Altitude 670 m; 2,200 ft)

This stop includes a walk into the canyon of the Crooked River on a dirt access road known colloquially as the Hollywood Grade. Headworks for a flume system are preserved at the base of the grade. The term Hollywood stems from the use of this area for filming a major motion picture many years ago. Note: Access to the top of the road requires crossing private land, so check with the nearby motel

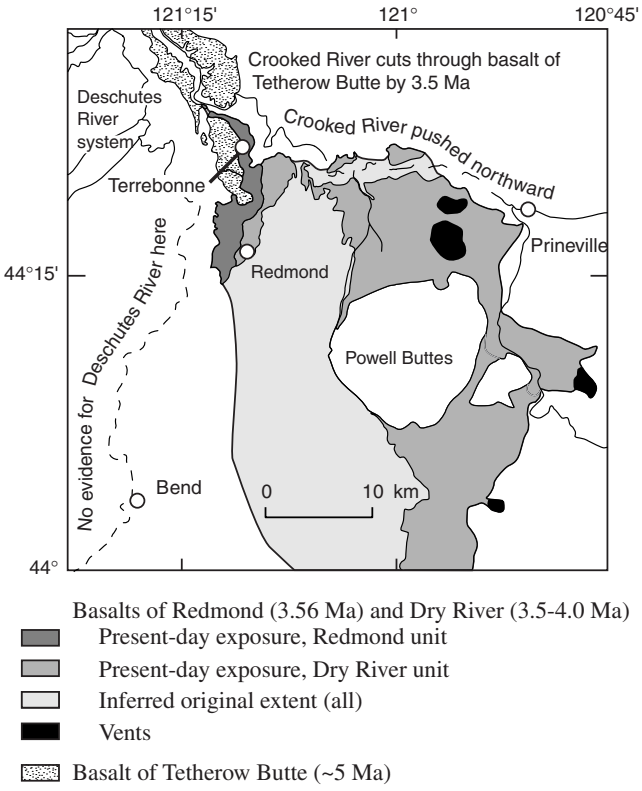

Figure 26. Extent of lava flows in the basalts of Redmond and Dry River across the Redmond Plain and into the ancestral canyon of the Crooked River.

staff or the office of Crooked River Ranch about permission.

The destination of this stop is about 2.4 km downstream from the top of the road, where we will encounter one of a large number of springs emerging from the canyon walls. Springs occur intermittently from about River Mile 13, just below Osborne Canyon, to Opal Springs, about River Mile 6.7. These springs issue from the 5.77-Ma basalt of Opal Springs. The Crooked River gains over 28 m^3/s (1,000 ft^3/s) from ground-water discharge through springs in the basalt of Opal Springs in this reach. Most prolific of these is Opal Springs itself, which discharges from the base of the basalt on the east bank of the river. Discharge from this single spring is estimated to be approximately 7 to 9 m^3/s (250 to 300 ft^3/s) (Stearns, 1931; Robert MacRostie, oral commun).

Isotope and temperature data (Table 1) indicate that the water from Opal Springs has followed a relatively long, deep flow path (Caldwell, 1997; James and others, 2000). The low tritium content indicates that the water was recharged prior to atmospheric testing of nuclear bombs in the early 1950s. Carbon and helium isotope data indicate that the water of Opal Springs contains a component of magmatic gas not present in many springs higher in the basin, such as those at North Davis Creek. Comparing the temperature of Opal Springs (12°C) with the mean annual temperature at the altitude of recharge inferred from oxygen isotope measurements indicates considerable geothermal warming (James and others, 2000).

About 170 m of Deschutes Formation strata are exposed across the valley in the area

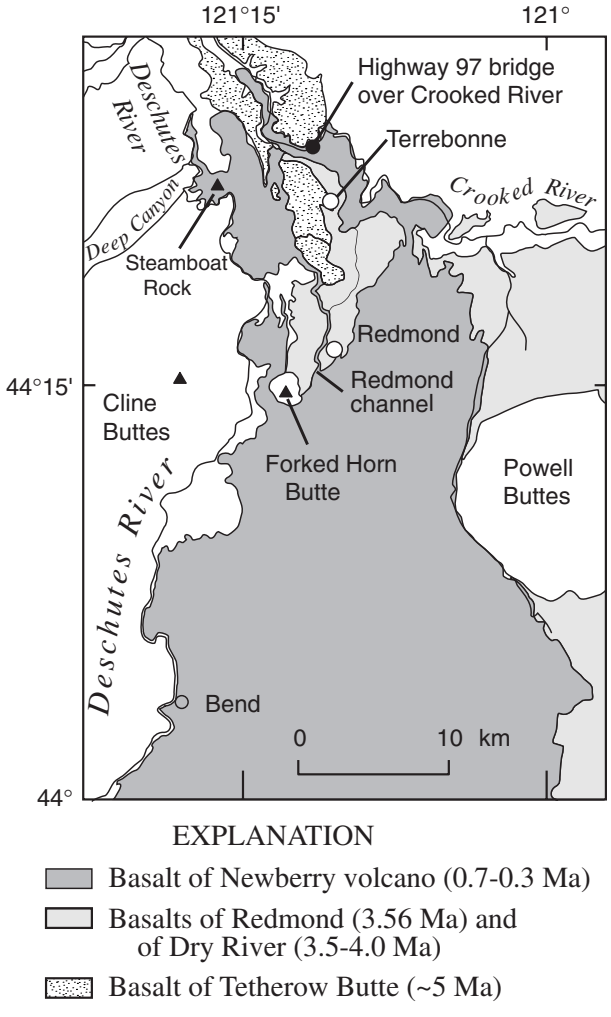

Figure 27. Extent of lava flows in the basalt of Newberry Volcano across the Redmond Plain and into the ancestral canyons of the Deschutes and Crooked Rivers.

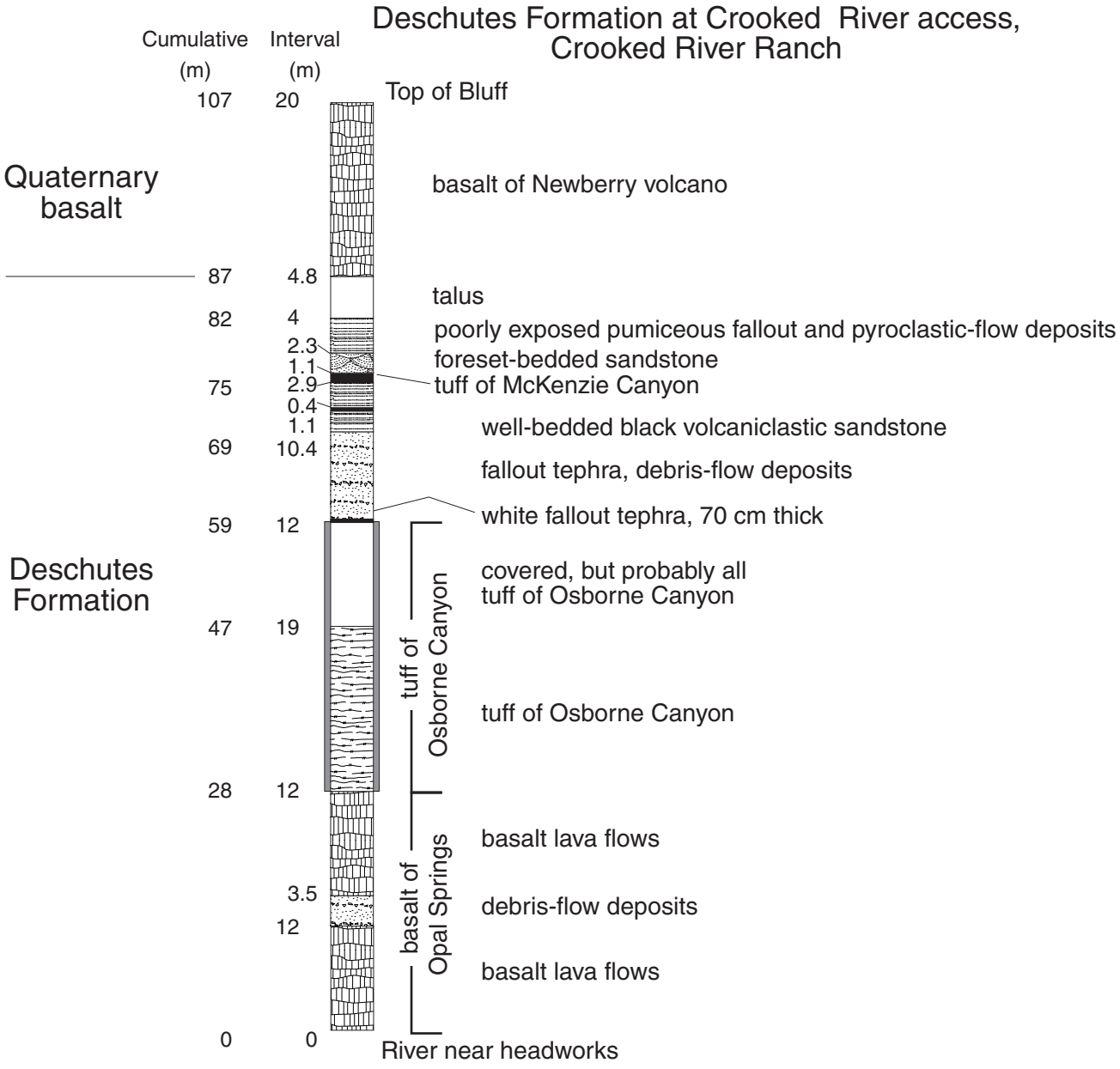

Figure 28. Stratigraphic section exposed along Hollywood Grade in the canyon of the Crooked River near Crooked River Ranch, Stop 10.

of this stop. At the top is the basalt of Tetherow Butte, a spectacularly jointed sequence of tholeiitic basalt 45-60 m thick. In the lower one-third of the valley wall is the orange-weathering tuff of Osborne Canyon, 20-30 m thick (Fig. 28). At the base of the sequence is the basalt of Opal Springs. The Opal Springs unit is exposed through 28 m, and it continues into the subsurface in this area. The basalt of Opal Springs is as thick as 40 m elsewhere in the basin (Smith, 1986a).

This part of the Deschutes Formation was deposited in less than 1 million years. The basalt of Opal Springs, at the canyon floor, has an isotopic age of 5.77±0.07 Ma (Table 2). The capping basalt of Tetherow Butte is probably younger than 5.04 Ma. It has an isotopic age of 5.31±0.05 Ma (Table 2), but it possesses normal-polarity thermal-remanent magnetization. An age younger than 5.04 Ma would agree with the currently accepted paleomagnetic time scale (Fig. 29).

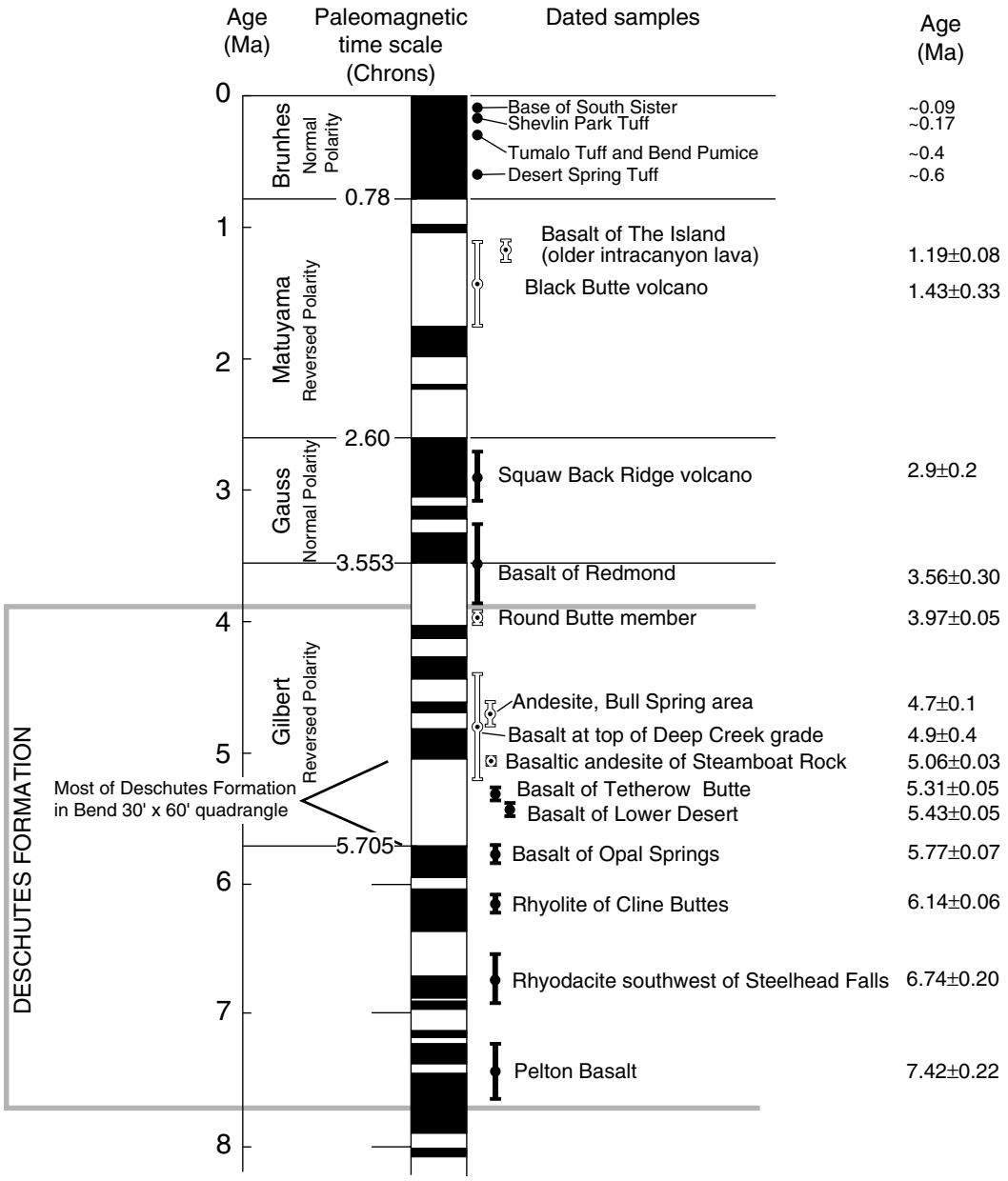

Figure 29. Correlation of selected dated samples with paleomagnetic time scale. Patterns show remanent magnetization: dark fill, normal polarity; white fill, reversed polarity. Bars showing age and standard deviation are similarly patterned. See Table 2 for references to age data. Remanent magnetization determined using portable fluxgate magnetometer (time scale from Cande and Kent, 1992).

Erosion along the ancestral canyon of the Crooked River has carved into and removed the basalt of Tetherow Butte and some underlying sedimentary beds from the area of our traverse. Quaternary intracanyon lava flows have invaded and partly refilled the inner canyon, creating the broad flat bench at Crooked River Ranch. The walk down the grade begins stratigraphically in the middle Pleistocene basalt of Newberry Volcano, then passes into sedimentary and volcanic strata of the Deschutes Formation (Fig. 28). The tuff of McKenzie Canyon, which we saw at Stop 7, lies partway down the grade. It is only 1–2 m thick and easily overlooked. Near the base of the grade is the conspicuous tuff of Osborne Canyon.

Directly beneath the tuff of Osborne Canyon is the basalt of Opal Springs. It comprises two lava-flow sequences, each containing

several flows of open-textured olivine basalt. The two flow sequences are separated by 3–6 m of debris-flow deposits and other sedimentary beds. The isotopic age for the basalt of Opal Springs, 5.77±0.07 Ma, came from lava in the lower sequence (Smith, 1986a).

Both the capping basalt of Newberry Volcano and the stream-flooring basalt of Opal Springs possess normal-polarity thermal-remanent magnetization. A third basalt sequence, with reversed-polarity magnetization, underlies the basalt of Newberry Volcano at the base of Hollywood Grade. Named the basalt of The Island for a prominent mesa at Cove Palisade State Park, it is lithologically similar to the basalt of Newberry Volcano and the basalt of Opal Springs. It has an isotopic age of 1.19±0.08 Ma (whole-rock, $^{40}Ar/^{39}Ar$, Smith, 1986a).

The basalt of The Island reputedly was erupted from Newberry Volcano (Peterson and others, 1976; Smith, 1986a; Dill, 1992), but the unit cannot be traced farther south toward Newberry than the area near the Crooked River Ranch (Sidebar 2). Thus, the upstream pathway for the reversed-polarity basalt must now be overlain entirely by normal-polarity basalt of Newberry Volcano. An observation that may argue against a Newberry source is that the upper surface of these flows lies at an altitude of roughly 730 m (2,400 ft) in most locations (Dill, 1992; Ferns and others, 1996a), which would be unlikely if the lava were flowing downstream along its entire extent. An alternative explanation, therefore, is that the basalt of The Island was erupted from some yet-to-be-found fissure vent downstream from (north of) the Crooked River Ranch and backed up along the Crooked River (Sherrod and others, in press).

Stop 11—Lake Billy Chinook Overlook (Reservoir Altitude 593 m; 1,945 ft)

Stop 11 provides a view of the canyons of the Crooked and Deschutes Rivers just upstream from their confluence. Lake Billy Chinook is impounded behind Round Butte Dam, which was completed in 1964. Our east-rim overlook is on the ~5-Ma basalt of Tetherow Butte (Smith, 1986a). Sedimentary rocks of the Deschutes Formation form most of the canyon walls. The far rim (west rim of the canyon of the Deschutes River) is capped by the basalt of Lower Desert (Smith, 1986a). The basalt of Lower Desert has normal-polarity magnetization. Its isotopic age is 5.43±0.05 Ma (Table 2), but its magnetization suggests that it too is about 5 Ma in age (Fig. 29). The narrow flat-topped ridge separating the Crooked and Deschutes Rivers is The Island, an erosional remnant of a reversely polarized 1.19-Ma intracanyon lava flow, the basalt of The Island. Our viewpoint rim is at an altitude of 786 m (2,480 ft). The pool altitude is 593 m (1,945 ft), and the canyon floor, now flooded, is about 488 m (1,600 ft). A photograph taken from this spot in August 1925 by Harold T. Stearns (Fig. 30) provides a glimpse of the prereservoir exposures. In Figure 30B, the conspicuous lava flows at the base of the canyon belong to the 7.42-Ma Pelton Basalt Member, the lowest lava-flow member of the Deschutes Formation (Stearns, 1931; Smith, 1986a).

The Pelton Basalt Member is considered to be the base of the Deschutes Formation as defined by Smith (1986a). It comprises several lava flows of olivine tholeiite, some with thin sedimentary interbeds (Smith, 1986a). A dated flow in the Pelton has an age of 7.42±0.22 Ma (Table 2). The Pelton Basalt is exposed today as far south as Round Butte Dam and was mapped another 6.4 km southward from the mouth of the Crooked River prior to impoundment of Lake Billy Chinook (Stearns, 1931). It is as thick as 30 m near Pelton Dam (Smith, 1987b).

As is the case for the basalt of Opal Springs, considerable ground water discharges from springs in the Pelton Basalt Member. Stearns (1931) observed that all the springs in the lower Crooked River below about River Mile 4 and along the Deschutes from its confluence with the Crooked River to below the confluence with the Metolius River issue from the Pelton. He noted a large spring issuing from it in the forebay of the power plant that once existed about 1.6 km upstream from this point. He also documented a line of springs extending 1.2 km along the west bank of the Deschutes River, about 0.8 km upstream from the Metolius River, with an estimated discharge between 2.3 and 2.8 m^3/s (80 and 100 ft^3/s). Ground-water discharge to Lake Billy Chinook is estimated from stream-gage data to be approximately 12 m^3/s (420 ft^3/s). Most of this

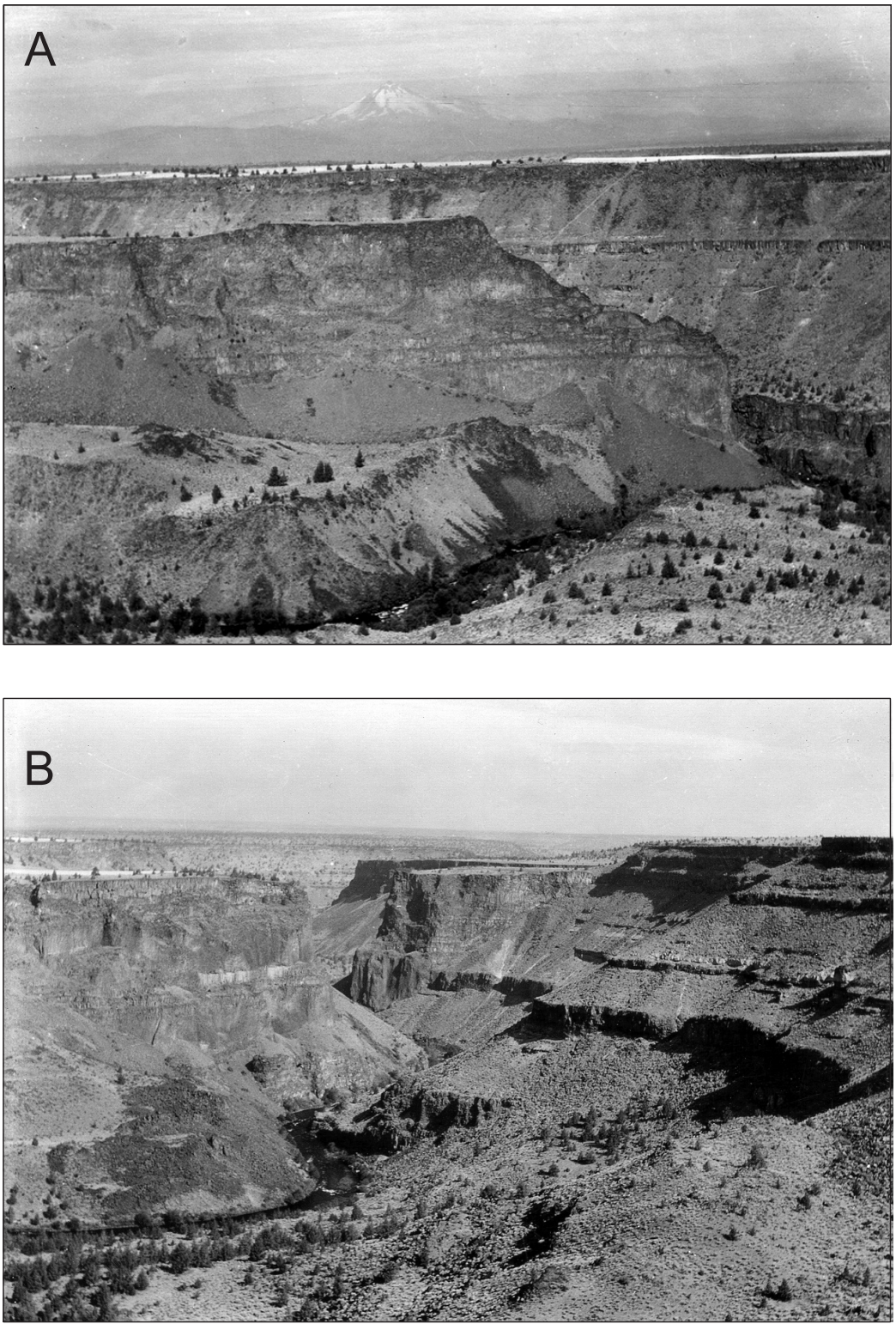

Figure 30. Photographs of the canyons of the Crooked and Deschutes Rivers from the SE 1/4 sec. 35, T. 11 S., R. 12 E. (Stop 11), taken by H.T. Stearns, August 1925, prior to inundation by Lake Billy Chinook. *A.* View west across the canyon of the Crooked River to The Island, and beyond it, to the west rim of the canyon of the Deschutes River. The Deschutes–Crooked confluence is at right side of photo in near ground, Mount Jefferson centered in background 45 km west-northwest. *B.* View north (downstream) into the canyon of the Deschutes River. The Deschutes–Crooked confluence is at lower left edge of photo.

discharge is likely from the Pelton (Gannett and others, 2001).

The Pelton Basalt Member extends in the subsurface south beyond its now-submerged exposure in the canyon. Wells drilled at river level near Opal Springs (River Mile 6.7) penetrated the Pelton at a depth of approximately 110 m. It proved to be a productive aquifer at this place. Wells encountered an artesian pressure in the Pelton Basalt Member of approximately 50 psi at the land surface and artesian flow rates of up to 0.32 m^3/s (5,000 gallons per minute).

The Pelton Basalt Member is the lowest sequence of lava in the Deschutes Formation, and although Smith (1987a,b) maps a thin section of Deschutes sediment underlying it, the Pelton is effectively the base of the permeable section in the Deschutes Formation. The Deschutes contact with underlying units is exposed about 8 km north of this stop. By that point, most of the ground water flowing from the upper basin in the Deschutes Formation has discharged to the river system. Depending on location, the Deschutes Formation may be seen in unconformable contact with the underlying middle Miocene Simtustus Formation or the upper Oligocene to lower Miocene John Day Formation (Fig. 2). Mapping by Smith (1987a, b) shows that the Simtustus Formation and Prineville Basalt typically separate the Deschutes and John Day Formations in the canyon of the Deschutes River. West of the canyon, the Deschutes Formation lies directly on the John Day Formation in many places.

The Simtustus Formation is a sequence of middle Miocene volcanogenic sandstone, mudstone, and tuff conformable on and interbedded with lava of the Prineville Basalt (Smith, 1986b). The Simtustus Formation, which is as thick as 65 m, was deposited across an area almost 20 km wide. Deposition occurred in response to drainage-system disruption by lava flows of the Columbia River Basalt Group and the Prineville Basalt (Smith, 1986b). The Simtustus Formation is exposed in areas ranging from the canyon of the Deschutes River to east of Gateway. Its hydrologic characteristics are unknown. Because of its location, limited areal extent, and relative thinness, it is a hydrologically insignificant stratigraphic unit.

The Prineville Basalt is a sequence of relatively evolved lava flows exposed sporadically across north-central Oregon. Of middle Miocene age, it includes flows with both normal- and reversed-polarity magnetization that are thought to have erupted during a short time period about 15.8 Ma when the Earth's magnetic field was changing polarity from reversed to normal (Hooper and others, 1993). In the Deschutes Basin, the Prineville Basalt is as thick as 200 m. It is exposed east of Powell Buttes, east of Smith Rock, and along the Deschutes River from Pelton Dam downstream toward Cow Canyon, 20 km northeast of Gateway (Smith, 1986a). The Prineville Basalt may underlie the Deschutes Formation in much of the east half of the basin. Stratigraphic separation between the two formations is relatively small, depending on the thickness of intervening middle Miocene strata of the Simtustus Formation.

The hydrologic characteristics of the Prineville Basalt are poorly known. It is generally less permeable than the Deschutes Formation, and we know of no published reports of major springs issuing from the unit. It is, however, used locally as a source of water from domestic wells and a few irrigation wells.

About 13 km north of this place, just below Pelton Dam, the John Day Formation is exposed in the canyon of the Deschutes River. The John Day Formation in this area consists primarily of light-colored tuff, lapillistone, fine-grained volcanic sandstone, and mudstone (Smith, 1987a, b). The John Day Formation has very low permeability and is considered the basement of the regional ground-water flow system (Sceva, 1968; Gannett and others, 2001). In contrast to the upper basin, little ground water discharges to the Deschutes River downstream from the point where it intersects the John Day Formation. The John Day Formation can be observed at optional Stop 12.

Stop 12—Canyon of the Deschutes River Near Warm Springs, Optional Stop (Altitude 421 m; 1,380 ft)

At this place the John Day Formation forms the lower canyon walls on either side of the Deschutes River. These strata have limited permeability. The permeable strata of the

Deschutes Formation are above the river at this point and thin abruptly northward. Virtually all of the regional ground-water flow has discharged to the Deschutes River and its tributaries upstream from this point. During the summer months, almost the entire flow of the Deschutes River at this place comes from ground-water discharge. Year-round, approximately 90 percent of the mean discharge of the Deschutes River here is attributable to ground water. In the 160 km between here and the mouth of the river, the Deschutes gains very little water from ground-water discharge, and its increases in flow are primarily from tributary streams.

ROAD GUIDE

Directions to Stop 1—Springs at North Davis Campground

From Bend: South on US 97 approximately 15 mi to Vandevert Road (6 mi south of entrance to Lava Lands Visitor Center). West on Vandevert Road 1.0 mi to South Century Drive. South on South Century Drive 1.1 mi to County Road 42 (which becomes Forest Road 42). West on Forest 42 for 23 mi to Forest 46. South on Forest 46 for 3.9 mi to North Davis Campground.

From Willamette Pass: Follow Oregon 58 southeast 5.5 mi beyond Odell Lake east access road to Crescent Cutoff Road. East on Crescent Cutoff Road (Forest 61) 3.2 mi to Forest 46. North 14.1 mi on Forest 46 to North Davis Campground.

From the south on US 97: In town of Crescent turn northwest onto Crescent Cutoff Road (County 61; may be marked as Ward Street in town). West on Crescent Cutoff Road 9 mi to Forest 46. North 14.1 mi on Forest 46 to North Davis Campground.

Directions from Stop 1 to Stop 2—Pringle Falls Sedimentary Section

Forest 46 north 3.9 mi to South Century Drive (Forest 42). East 9.3 mi to Burgess Road (Forest 43). East 3.6 mi to Forest 500 on left (north) side of the road after crossing Deschutes River. North on Forest 500 about 0.3 mi to fork. Veer left and follow road along power lines about 0.5 mi to where the road is adjacent to the Deschutes River.

Directions from Stop 2 to Stop 3—Fall River Headwater Springs

Return to Forest 43. Turn right, proceed west 0.6 mi to Forest 4350. North on Forest 4350 for 2.1 mi to Forest 42. East on Forest 42 about 0.1 mi to Fall River Guard Station. Turn into the guard station and park.

Directions from Stop 3 to Stop 4—Top of Lava Butte

Leave Fall River Guard Station and continue east 10.7 mi on Forest 42 to South Century Drive. North 1.1 mi to Vandevert Road. East 1.0 mi on Vandevert Road to US 97. North 6.0 mi on US 97 to Lava Lands Visitor Center. Depending on time of year, a fee may be charged to enter the center and its roads. Road leads approximately 1.7 mi to top of Lava Butte.

Directions from Stop 4 to Stop 5—Surface-Water Diversions in Bend

North 11.5 mi on US 97, which becomes the newly completed Bend Parkway through downtown Bend. Take Exit 137 (Revere Avenue—Downtown) straight through traffic signal onto Division Street. Proceed on Division Street 0.5 mi from traffic signal to Riverview Park's tiny parking area on west side of road. Diversion dam and headgates are seen just north of parking area.

Directions from Stop 5 to Stop 6—Sisters Fault Zone Outcrop, Tumalo Reservoir Road

North 0.2 mi on Division to intersection with US 97 business route. North 0.3 mi to O.B. Riley Road. West 4.1 mi on O.B. Riley Road to Tumalo Reservoir Road, which lies just beyond crossing of Deschutes River. West (left) 0.5 mi on Tumalo Reservoir Road, then park on road shoulder. Stop 6 is prominent exposure of pyroclastic deposits quarried north of road.

Directions from Stop 6 to Stop 7—Bull Flat and Tumalo Dam

West 0.6 mi on Tumalo Reservoir Road to T intersection. Left (west) 3.5 mi to where the road turns north and becomes Sisemore Road. North 2.3 mi on Sisemore Road (along the Tumalo Fault) to Tumalo Dam. Find place to park just west past the dam.

Directions from Stop 7 to Stop 8—Lower Bridge

Turn around and go east beyond Tumalo Dam 0.1 mi to Couch Market Road (Y intersection). East 3.5 mi to US 20. Southeast 2.4 mi to Cook Avenue in small town of Tumalo (see sign for Cline Falls State Park). North 10.3 mi on Cook Avenue (becomes Cline Falls Highway after a few blocks) to Oregon 126. West (toward Sisters) 3.7 mi on Oregon 126 to Buckhorn Road. North 4.2 mi on Buckhorn Road to Lower Bridge Road. East 1.6 mi to Deschutes River. Park just before crossing the bridge (south side).

Directions from Stop 8 to Stop 9—Peter Skene Ogden Bridge and Scenic Viewpoint

East 6.2 mi on Lower Bridge Road to US 97. North 2.4 mi on US 97 to wayside at Ogden Scenic Viewpoint. Pull into wayside, then walk to old highway bridge, which is now a pedestrian walkway.

Directions from Stop 9 to Stop 10—Crooked River Gorge at Crooked River Ranch

Return south 1.4 mi on US 97 to Wimp Way. West 0.3 mi on Wimp Way, which curves north to Ice Avenue. West 0.2 mi to 43rd Street. North 0.8 mi to a T intersection at Chinook Drive. West (then curves more or less north) 3.3 mi to Clubhouse Road. East and southeast 0.4 mi on Clubhouse Road past clubhouse and stores; park near chapel. Walk through parking lot for motel and hike into the canyon of the Crooked River on a road that starts beyond the gate south of the motel parking lot. The road crosses private property. Check at the office of the Crooked River Ranch for information on access to the road through the gate. Alternatively, check with motel for permission to follow the fence line north to the canyon rim, where the road is reached by an easy scramble. Watch for rattlesnakes.

Directions from Stop 10 to Stop 11—Lake Billy Chinook Overlook

Return to US 97 by retracing route from Stop 9. North 8.5 mi on US 97 to Culver Road. East, then north, 2.6 mi on Culver Road to C Street in town of Culver. Signs from here help by pointing route toward The Cove Palisades State Park. West 1.0 mi on C Street to Feather Drive. North 0.9 mi on Feather Drive to Fisch Lane. West 0.5 mi on Fisch to where it turns north and becomes Frazier. Follow Frazier 0.5 mi to intersection with Jordan Road. West on Jordan Road 0.3 mi to Mountainview (look for the sign to View Points). North on Mountainview, following it 2.1 mi along rim of the canyon of the Crooked River to third scenic viewpoint on left. Failure to turn onto Mountainview will result in a geologically rewarding drive into Cove Palisades State Park.

Directions from Stop 11 to Optional Stop 12—Canyon of the Deschutes River Near Warm Springs

Continue north on Mountainview about 2.2 mi to an intersection. Turn left and continue north on Mountainview 2.6 mi to a T intersection. Turn right on Belmont Lane and travel east 1.5 mi to Elk Drive. Left (north) on Elk Drive for 2.8 mi, where it turns left down into the canyon and becomes Pelton Dam Road. Follow Pelton Dam Road 6.8 mi north to its intersection with US 26. Turn left (north) on US 26 and go about 1.5 mi to where the canyon narrows. This is the stop. US 26 lacks pullouts in the area, and the road shoulder is narrow. Use extreme caution if disembarking to look at outcrops. A wayside and boat ramp about 0.7 mi north of this place provide an opportunity to examine the river.

REFERENCES CITED

Armstrong, R.L., Taylor, E.M., Hales, P.O., and Parker, D.J., 1975, K-Ar dates for volcanic rocks, central Cascade Range of Oregon: Isochron/West, no. 13, p. 5-10.

Caldwell, R.R., 1997, Chemical study of regional groundwater flow and ground-water/surface-water interaction in the upper Deschutes Basin, Oregon: U.S. Geological Survey Water-Resources Investigations Report 97-4233, 49 p.

Cande, S.C., and Kent, D.V., 1992, A new geomagnetic polarity time scale for the Late Cretaceous and Cenozoic: Journal of Geophysical Research, v. 97, p. 13,917-13,951.

Chitwood, L.A., Jensen, R.A., and Groh, E.A., 1977, The age of Lava Butte: Ore Bin, v. 39, p. 157-164.

Couch, R., and Foote, R., 1985, The Shukash and La Pine Basins: Pleistocene depressions in the Cascade Range of central Oregon: Eos, v. 66, no. 3, p. 24.

Dill, T.E., 1992, Stratigraphy of the Neogene volcanic rocks along the lower Metolius River, Jefferson County, central Oregon: Oregon State University MS Thesis, 343 p.

Evans, S.H., and Brown, F.H., 1981, Summary of Potassium/Argon dating—1981: U.S. Department of Energy, Division of Geothermal Energy DE-AC07-80-ID-12079-45, 29 p.

Ferns, M.L., Lite, K.E., Jr., and Clark, M.D., 1996b, Lithologic controls on groundwater discharge to the Deschutes River between Lower Bridge and Lake Billy Chinook, central Oregon: Geological Society of America Abstracts with Programs, v. 28, no. 5, p. 65.

Ferns, M.L., Stensland, D.E., and Smith, G.A., 1996a, Geologic map of the Steelhead Falls Quadrangle, Deschutes and Jefferson Counties, Oregon: Oregon Department and Geology and Mineral Industries Geological Map Series GMS-101, scale 1:24,000.

Fiebelkorn, R.B., Walker, G.W., MacLeod, N.S., McKee, E.H., and Smith, J.G., 1983, Index to K-Ar age determinations for the State of Oregon: Isochron/West, no. 37, p. 3-60.

Gannett, M.W., and Lite, K.E., Jr., 2000, Climate-driven fluctuations in hydraulic head and groundwater discharge to streams in the upper Deschutes Basin, Oregon: Eos, v. 81, no. 48, p. F531-F532.

Gannett, M.W., Lite, K.E., Jr., Morgan, D.S., and Collins, C.A., 2001, Ground-water hydrology of the upper Deschutes Basin, Oregon: U.S. Geological Survey Water Resources Investigation Report 00-4162, 77 p.

Gettings, M.E., and Griscom, A., 1988, Gravity model studies of Newberry Volcano, Oregon: Journal of Geophysical Research, v. 93, p. 10,109-10,118.

Hawkins, F.F., LaForge, R.C., and Gilbert, J.D., 1989, Seismotectonic study for Wickiup and Crane Prairie Dams, Deschutes Project, Oregon: U.S. Bureau of Reclamation Seismotectonic Report 89-2, 38 p.

Herrero-Bervera, E., and Helsey, C.E., 1993, Global paleomagnetic correlation of the Blake geomagnetic polarity episode, in Applications of paleomagnetism to sedimentary geology: SEPM Special Publication 49, p. 71-82.

Herrero-Bervera, E., Helsey, C.E., Hammond, S.R., and Chitwood, L.A., 1989, A possible lacustrine paleomagnetic record of the Blake episode from Pringle Falls, Oregon, U.S.A.: Physics of the Earth and Planetary Interiors, v. 56, p. 112-123.

Herrero-Bervera, E., Helsey, C.E., Sarna-Wojcicki, A.M., Lajoie, K.R., Meyer, C.E., McWilliams, M.O., Negrini, R.M., Turrin, B.D., Donnelly-Nolan, J.M., and Liddicoat, J.C., 1994, Age and correlation of a paleomagnetic episode in the western United States by $^{40}Ar/^{39}Ar$ dating and tephrochronology: The Jamaica, Blake, or a new polarity episode?: Journal of Geophysical Research, v. 99, p. 24,091-24,103.

Hill, B.E., 1992, Petrogenesis of compositionally distinct silicic volcanoes in the Three Sisters region of the Oregon Cascade Range: The effects of crustal extension on the development of continental arc silicic magmatism: Oregon State University PhD Dissertation, 235 p.

Hill, B.E., and Duncan, R.A., 1990, The timing and significance of silicic magmatism in the Three Sisters region of the Oregon High Cascades: Eos, v. 71, p. 1,614.

Hill, B.E., and Priest, G.R., 1992, Geologic setting of the Santiam Pass area, central Cascade Range, Oregon, *in* Hill, B.E., ed., Geology and geothermal resources of the Santiam Pass area of the Oregon Cascade Range, Deschutes, Jefferson, and Linn Counties, Oregon: Oregon Department of Geology and Mineral Industries Open-File Report O-92-3, p. 5-18.

Hooper, P.R., Steele, W.K., Conrey, R.M., Smith, G.A., Anderson, J.L., Bailey, D.G., Beeson, M.H., Tolan, T.L., and Urbanczyk, K.M., 1993, The Prineville Basalt, north-central Oregon: Oregon Geology, v. 55, p. 3-12.

James, E.R., Manga, M., Rose, T.P., and Hudson, G.B., 2000, The use of temperature and the isotopes of O, H, C, and noble gases to determine the pattern and spatial extent of groundwater flow: Journal of Hydrology, v. 237, p 100-112.

Krebs, W.N., Bradbury, J.P., and Theriot, E., 1989, Neogene and Quaternary lacustrine diatom biochronology, western U.S.A.: Palaios, v. 2, p. 505-513.

Lanphere, M.A., Champion, D.E., Christiansen, R.L., Donnelly-Nolan, J.M., Fleck, R.J., Sarna-Wojcicki, A.M., Obradovich, J.D., and Izett, G.A., 1999, Evolution of tephra dating in the western United States: Geological Society of America Abstracts with Programs, v. 31, no. 6, p. A73.

MacLeod, N.S., and Sherrod, D.R., 1992, Reconnaissance geologic map of the west half of the Crescent 1 by 2 Degree Quadrangle, central Oregon: U.S. Geological Survey Miscellaneous Investigations Series Map I-2215, scale 1:250,000.

MacLeod, N.S., Sherrod, D.R., Chitwood, L.A., and Jensen, R.A., 1995, Geologic map of Newberry Volcano, Deschutes, Klamath, and Lake Counties, Oregon: U.S. Geological Survey Miscellaneous Investigations Series Map I-2215, scales 1:62,500 and 1:24,000.

Manga, M., 1998, Advective heat transport by low-temperature discharge in the Oregon Cascades: Geology, v. 26, p. 799-802.

Moore, B.N., 1937, Nonmetallic mineral resources of eastern Oregon: U.S. Geological Survey Bulletin 875, 180 p.

Peterson, N.V., Groh, E.A., Taylor, E.M., and Stensland, D.E., 1976, Geology and mineral resources of Deschutes County, Oregon: Oregon Department of Geology and Mineral Industries Bulletin 89, 66 p.

Pitts, G.S., and Couch, R.W., 1978, Complete Bouguer gravity anomaly map, Cascade Mountain Range, central Oregon: Oregon Department of Geology and Mineral Industries Geological Map Series GMS-8, scale 1:125,000.

Rieck, H.J., Sarna-Wojcicki, A.M., Meyer, C.E., and Adam, D.P., 1992, Magnetostratigraphy and tephrochronology of an upper Pliocene to Holocene record in lake sediments at Tulelake, northern California: Geological Society of America Bulletin, v. 104, p. 409-428.

Robinson, P.T., and Stensland, D.E., 1979, Geologic map of the Smith Rock area, Jefferson, Deschutes, and Crook Counties, Oregon: U.S. Geological Survey Miscellaneous Investigations Map I-1142, scale 1:48,000.

Sarna-Wojcicki, A.M., Meyer, C.E., Nakata, J.K., Scott, W.E., Hill, B.E., Slate, J.L., and Russell, P.C., 1989, Age and correlation of mid-Quaternary ash beds and tuffs in the vicinity of Bend, Oregon, *in* Scott, W.E., Gardner, C.A., and Sarna-Wojcicki, A.M., eds., Guidebook for field trip to the Mount Bachelor–South Sister–Bend area, central Oregon High Cascades: U.S. Geological Survey Open-File Report 89-645, p. 55-62.

Sceva, J.E., 1968, Liquid waste disposal in the lava terrane of central Oregon: U.S. Department of the Interior, Federal Water Pollution Control Administration

Technical Projects Branch Report No. FR-4, 66 p., app. 96 p.

Scott, W.E., and Gardner, C.A., 1992, Geologic map of the Mount Bachelor volcanic chain and surrounding area, Cascade Range, Oregon: U.S. Geological Survey Miscellaneous Investigations Map I-1967, scale 1:50,000.

Sherrod, D.R., and Pickthorn, L.G., 1989, Some notes on the Neogene structural evolution of the Cascade Range in Oregon, *in* Muffler, L.J.P., Weaver, C.S., and Blackwell, D.D., eds., Geology, geophysics, and tectonic setting of the Cascade Range: U.S. Geological Survey Open-File Report 89-178, p. 351-368.

Sherrod, D.R., Taylor, E.M., Ferns, M.L., Scott, W.E., Conrey, R.M., and Smith, G.A., in press, Geologic map of the Bend 30 by 60 Minute Quadrangle, central Oregon: U.S. Geological Survey Miscellaneous Investigations Map I-2683, scale 1:100,000.

Smith, G.A., 1986a, Stratigraphy, sedimentology, and petrology of Neogene rocks in the Deschutes Basin, central Oregon: A record of continental-margin volcanism and its influence on fluvial sedimentation in an arc-adjacent basin: Oregon State University PhD Dissertation, 467 p.

Smith, G.A., 1986b, Simtustus Formation: Paleogeographic and stratigraphic significance of a newly defined Miocene unit in the Deschutes Basin, central Oregon: Oregon Geology, v. 48, p. 63-72.

Smith, G.A., 1987a, Geologic map of the Seekseequa Junction and a portion of the Metolius Bench Quadrangles, Jefferson County, Oregon: Oregon Department of Geology and Mineral Industries Geological Map Series GMS-44, scale 1:24,000.

Smith, G.A., 1987b, Geologic map of the Madras West and Madras East Quadrangles, Jefferson County, Oregon: Oregon Department of Geology and Mineral Industries Geological Map Series GMS-45, scale 1:24,000.

Smith, G.A., and Hayman, G.A., 1987, Geologic map of the Eagle Butte and Gateway Quadrangles, Jefferson and Wasco Counties, Oregon: Oregon Department of Geology and Mineral Industries Geological Map Series GMS-43, scale 1:24,000.

Smith, G.A., Manchester, S.R., Ashwill, M., McIntosh, W.C., and Conrey, R.M., 1998, Late Eocene–early Oligocene tectonism, volcanism, and floristic change near Gray Butte, central Oregon: Geological Society of American Bulletin, v. 110, p. 759-778.

Smith, G.A., Snee, L.W., and Taylor, E.M., 1987, Stratigraphic, sedimentologic, and petrologic record of late Miocene subsidence of the central Oregon High Cascades: Geology, v. 15, p. 389-392.

Stearns, H.T., 1931, Geology and water resources of the middle Deschutes River Basin, Oregon: U.S. Geological Survey Water-Supply Paper 637-D, p. 125-212.

Stensland, D.E., 1970, Geology of part of the northern half of the Bend Quadrangle, Jefferson and Deschutes Counties, Oregon: Oregon State University MS Thesis, 118 p.

Taylor, E.M., and Ferns, M.L., 1994, Geology and mineral resource map of the Tumalo Dam Quadrangle, Deschutes County, Oregon: Oregon Department of Geology and Mineral Industries Geological Map Series GMS-81, scale 1:24,000.

Walker, G.W., and MacLeod, N.S., 1992, Geologic map of Oregon: U.S. Geological Survey, scale 1:500,000.

Williams, H., 1957, A geologic map of the Bend Quadrangle, Oregon, and a reconnaissance geologic map of the central portion of the High Cascade Mountains: Oregon Department of Geology and Mineral Industries, scale 1:125,000 and 1:250,000.

Winch, M.T., 1984-85, Tumalo—Thirsty land: Oregon Historical Quarterly, v. 85, p. 341-374; v. 86, p. 47-79, 153-182, 269-297.

Paleobotanical Record of Eocene–Oligocene Climate and Vegetational Change Near Eugene, Oregon

Jeffery A. Myers, Department of Earth and Space Sciences, Western Oregon University, Monmouth, Oregon 97361; myersj@wou.edu

Paul R. Kester, Department of Earth and Space Sciences, University of Washington, Seattle, Washington 98195; pkester@u.washington.edu

Gregory J. Retallack, Department of Geological Sciences, University of Oregon, Eugene, Oregon 97403; gregr@darkwing.uoregon.edu

OVERVIEW

At least five paleofloras bracket the Eocene–Oligocene boundary near Eugene in the southern Willamette Valley of western Oregon. Most of the floras occur within 2 km from marine rocks bearing late Eocene (Galvinian) molluscan and decapod faunas (Rathbun, 1926; Steere, 1955; Hickman, 1969). Two of the floras, the latest Eocene Goshen Flora (Chaney and Sanborn, 1933) and the early Oligocene Willamette Flora (undescribed), have long been regarded as critical indicators of vegetational and climatic change across the Eocene–Oligocene transition (Wolfe, 1981, 1994). Until recently, very little work has focused on the stratigraphic or geochronologic relationships of the strata that bear plant fossils within the sequence. Recent work by G.J. Retallack and D.R. Prothero has established magnetostratigraphic and physical stratigraphic relationships among the paleofloras. P.R. Kester and J.A. Myers are currently evaluating the detailed depositional framework and taxonomic relationships of the Willamette Flora. These studies provide important constraints on the timing and magnitude of climatic and vegetational events during the latest Eocene and early Oligocene.

This field trip will overview the stratigraphic, chronologic, and facies relationships between the Goshen, Willamette, and recently discovered Coburg Floras, and interfingering rocks of the Eocene-Oligocene marine Eugene Formation.

Field Guide to Geologic Processes in Cascadia: Oregon Department of Geology and Mineral Industries Special Paper 36, 2002.

FIELD TRIP ROAD LOG

0.0. Set trip odometer to zero at the Oregon 34 bridge over the Willamette River in Corvallis.

Here, the Willamette River incises Holocene alluvium of the "Willamette" and "Rowland" Formations (Yeats and others, 1996), the former representing deposits of the great Missoula Flood events. Between 30 and 50 flood events carried sediment and rafted ice southward up the Willamette Valley to the vicinity of Eugene, leaving behind silt and lithologically exotic dropstones.

The Willamette Valley is fundamentally a broad, faulted syncline bordered on the west by the Coast Range Anticlinorium, and on the east by the uplifted, westward tilting Western Cascades. The Corvallis Fault and many smaller displacement faults cut Holocene sediment in the valley (Yeats and others, 1996). In the middle to southern part of the valley, the majority of faults, along with broad subsidiary folds, strike generally northeast.

Near Corvallis, approximately 100 meters of Pleistocene and Holocene sediment cover broadly folded middle Eocene to early Oligocene marine strata of the Eugene, Spencer, Yamhill, and Tyee Formations, which rest unconformably upon the ocean floor basalt of the Siletz River Volcanics (Fig. 1). The sequence reflects the accretion of ocean floor basalt to Oregon's western margin, and subsequent infilling of a forearc trough, beginning with deep marine turbiditic sandstone of the Tyee Formation during the early to middle Eocene, and terminating with shallow shelf deposits of the Eugene Formation during the late Eocene to early Oligocene. Volcanic rocks within the

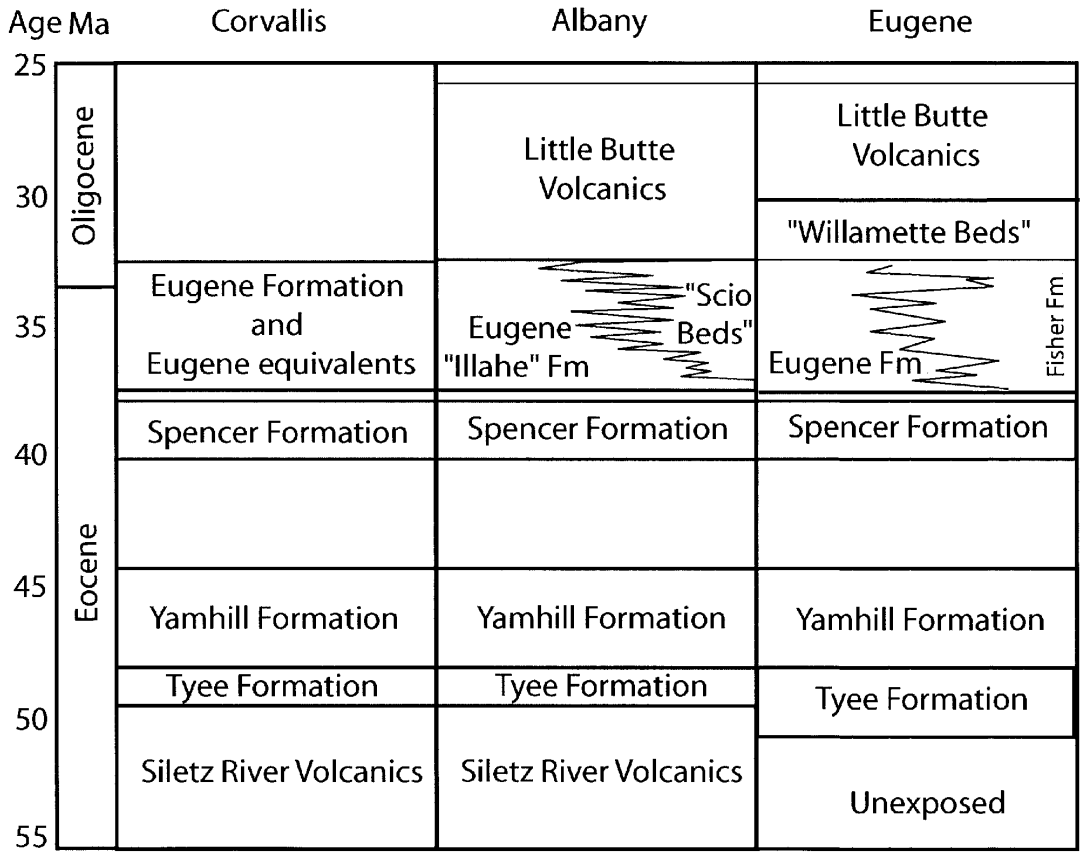

Figure 1. Stratigraphic relationships of Eocene and Oligocene rocks in the Willamette Valley (in part from Yeats and others, 1996).

Yamhill and younger formations record arc volcanism in the Western Cascades Arc, which commenced approximately 42 million years ago. By the middle Oligocene, agglomerate, breccia, and sandstone of the Western Cascades had infilled the forearc basin, and these rocks of the nonmarine Little Butte Volcanics lie conformably over older marine rocks. Uplift of the present Coast Ranges and deformation of the Willamette Valley along currently active structural features began during the latest Miocene.

Approximately 1.5 miles east of the Willamette River, we will cross the steeply-dipping Owl Creek Fault. This fault has produced approximately 120 meters of west-down offset in Pleistocene alluvium, but it apparently does not cut the Willamette Formation.

10.1 Enter I-5 Southbound

Many of the buttes to the east of I-5 are composed of flows and hypabyssal plugs of Oligocene–Miocene basalt of the Little Butte Volcanics of Peck and others (1964).

In the subsurface of this part of the valley, the Eocene–Oligocene Eugene Formation grades eastward into pumice-bearing, tuffaceous, nonmarine sandstone, which has been assigned variously to the "Mehama Volcanics", the "Scio Beds", and more recently (Peck and others, 1964) to the Little Butte Volcanics. The rocks are lithologically similar to and approximately coeval with the tuffaceous nonmarine Fisher Formation in the Eugene area, within which some authors (Yeats and others, 1996) have included them.

Eocene and Oligocene paleofloras are abundant in the midvalley east of Salem and Albany. These include the Sweet Home (Brown, 1950), Scio (Sanborn, 1949), Bilyeu (Klucking, 1964), and Thomas Creek (Eubanks, 1962; Klucking, 1964) Floras. The diverse Bilyeu Creek Flora compositionally resembles the latest Eocene Goshen Flora and is dominated by large-leaved tropical and near-tropical taxa. However, the Scio and Thomas Creek Floras include taxa common in Oligocene assemblages

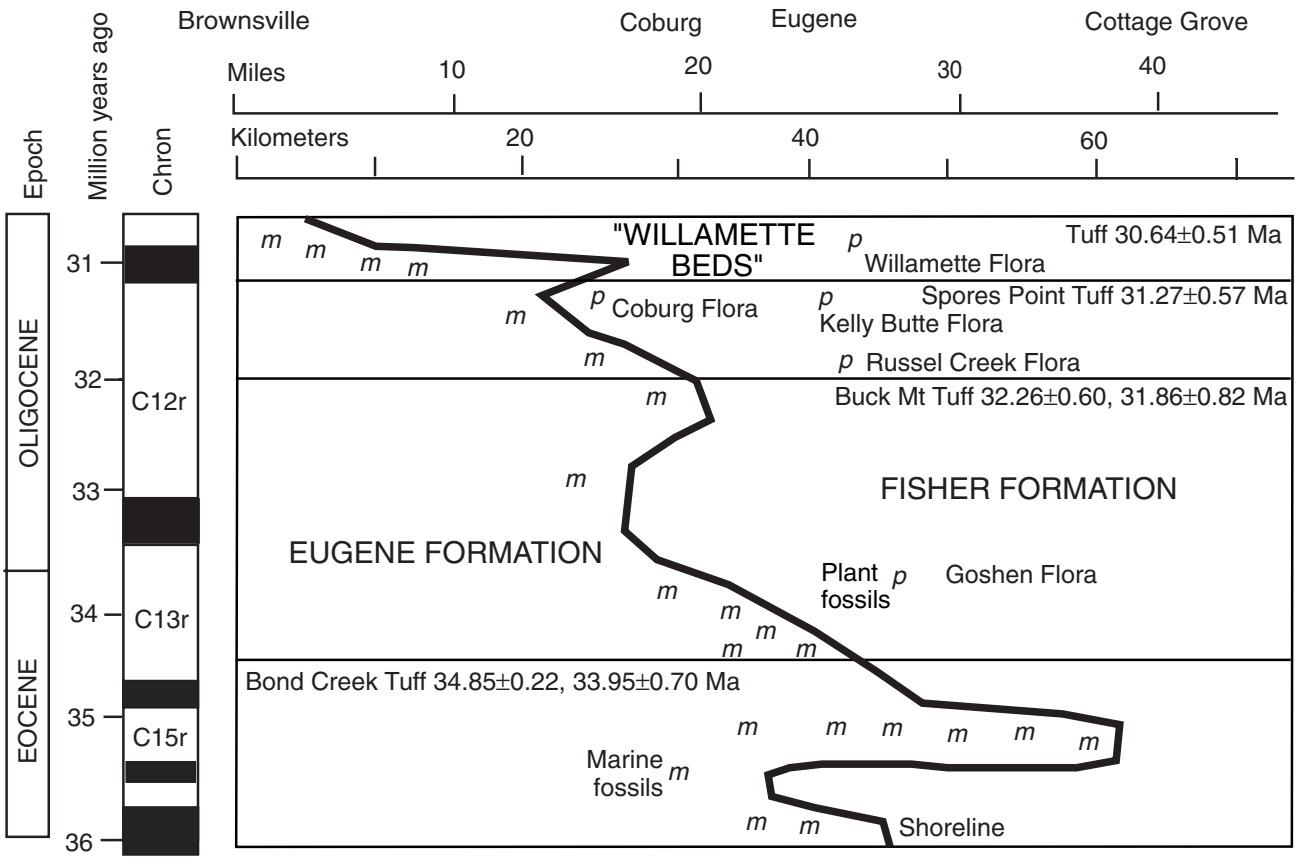

Figure 2. Correlation of rocks and fossil localities in the Eugene area. Magnetostratigraphy is from D.R. Prothero and G.J. Retallack (in prep). Localities for new $^{40}Ar/^{39}Ar$ dates are in Table 2.

from elsewhere in Oregon (such as *Acer, Alnus, Metasequoia, Pterocarya*, *Exbucklandia,* and others) that are not currently known from other low-elevation "Goshen-type" paleofloras in the Willamette Valley.

38.2 Ahead and to the left are the Coburg Hills. As we travel south toward Eugene, the Willamette Valley Synclinorium narrows to approximately 40 km in width. The steep face ahead of us is the scarp of a west-dipping normal fault on the eastern margin of the Willamette Valley Synclinorium. The Coburg Hills are composed of Western Cascades volcanic and sedimentary rocks, and shallow intrusives of the Little Butte Volcanics.

41.3 Excellent exposures of Little Butte Volcanics basalt flows and tuff are exposed on the cliff to the east of the freeway.

41.6 McKenzie River crossing.

46.2 Willamette River crossing.

50.3 Exit I-5 at the Goshen Exit (188A). Turn RIGHT at the bottom of the offramp. Continue one short block and turn LEFT on old HWY 99. Continue 2 miles to the freeway overpass.

52.5 Goshen Flora locality

STOP 1—I-5 NORTH ONRAMP SOUTH OF GOSHEN

Park well off the onramp just before it rises to the I-5 overpass.

Impressions of leaves, wood fragments, and rare reproductive structures comprising the Goshen Flora were first noted in 1920 by E.L. Packard, then of the University of Oregon, during construction of U.S. Highway 99 (Pacific Highway). R.W. Chaney and E.I. Sanborn monographed the flora in 1933, and type collections are housed at the U.C. Museum of Paleontology, Berkeley. Numerous revisions of

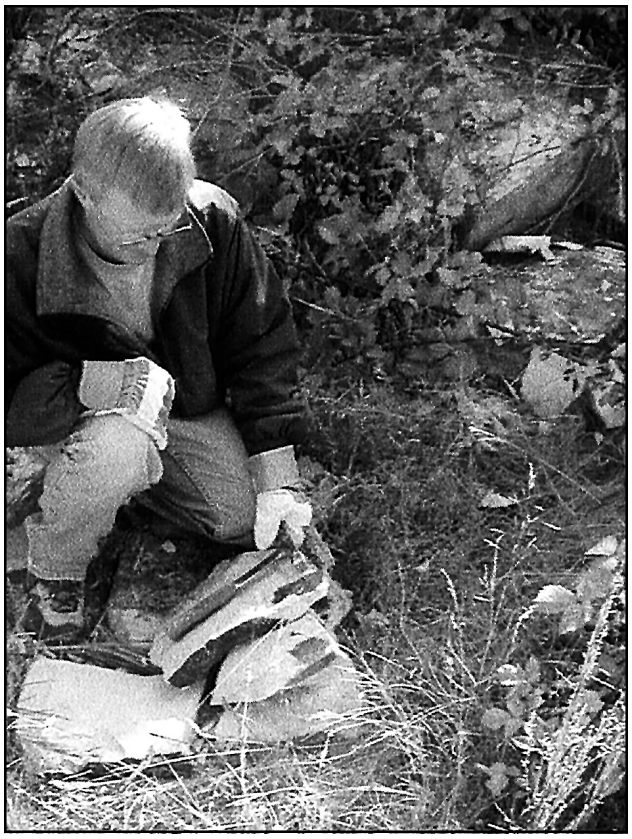

Figure 3. The Goshen Flora. Fossils are recovered from siltstone intervals. Pebble conglomerate is visible in the background.

individual taxa found in the Goshen Flora are scattered in the literature (Wolfe, 1977), but the flora would benefit from a thorough taxonomic review. Although the Goshen Flora has not been directly dated, recent $^{40}Ar/^{39}Ar$ dates from the Bond Creek Tuff, which underlies the Goshen Flora (Fig. 2), indicates that the flora must be younger than 34.85 ± 0.22 Ma (Kester, 2001). The flora is widely regarded to be latest Eocene in age, and was deposited prior to 33.7 Ma (Kester, 2001; Myers, in press).

The type locality of the Goshen Flora was covered during highway construction in the 1930s. However, several large blocks of tuffaceous sandstone and conglomerate from the original locality were brought to the surface during construction of a gas pipeline several years ago. A few parts of these blocks remain between the I-5 North onramp south of Goshen and the train tracks directly west of the onramp. Follow the cleared trail southwest from the onramp. The gray-brown blocks are scattered in the underbrush.

The Goshen Flora is contained in the late Eocene nonmarine Fisher Formation. Here, the Fisher Formation is composed predominately of yellowish-brown tuffaceous sandstone with pebble conglomerate stringers and finely-laminated carbonaceous intervals containing fossil plants (Fig. 3). Leaf impressions are found in pumiceous sandstone, which shows evidence of preburial weathering. Fossils are colored by a film of iron oxide which makes them stand out conspicuously against the light-colored matrix. The flora includes more than 50 taxa, including: Menispermaceae (*"Ficus" plinerva* Chaney and Sanborn), *Magnolia*, *Anona*, Lauraceae, Theaceae (*"Ilex" oregona* Chaney and Sanborn), *Allophyllus wilsoni* Chaney and Sanborn, *Meliosma aesculifolia* Chaney and Sanborn, *Meliosma goshenensis* Chaney and Sanborn, Anacardiaceae (*"Astronium" oregonum* Chaney and Sanborn), *Fagus oregona* (Chaney and Sanborn) Wolfe, Myrtaceae, *Cercidiphyllum*, *Plafkeria obliquifolia* (Chaney) Wolfe, *Florissantia speirii* (Lesquereux) Manchester, and *Platanus*. Some species found in the Goshen Flora are apparently limited in occurrence to the latest Eocene, including *Allophylus wilsoni* and *Meliosma aesculifolia*. These taxa are considered by Wolfe (1981) to be index species for a latest Eocene "Goshen-type" paleobotanical biozone.

Even without taxonomic revision, the Goshen Flora exhibits a strong floristic affinity to extant humid paratropical forests. This interpretation is supported by leaf physiognomic climate estimates, which yield a mean annual temperature (MAT) of about 19.5°C and annual precipitation in excess of 2300 mm/year, with no significant dry season.

On return to the vehicles, continue over the I-5 overpass. Turn LEFT on Peebles Rd, just to the east of the overpass.

54.6 Turn LEFT at Matthews Rd.

Very shortly after this you will turn LEFT at the intersection of Matthews Rd and Oregon 58. Warning: This is a very busy intersection.

Immediately move to the RIGHT lane and enter I-5 to Eugene.

55.5 Exit I-5 at the 188 B—(US 99 south) offramp

Continue to the base of the offramp and pull as far as possible onto the shoulder. Walk back up the offramp approximately 50 meters.

Figure 4. Overview of the freeway outcrop containing the Willamette flora. Fossil plants occur at two horizons. The primary fossiliferous interval is marked by the white line, and a second layer occurs near the top of the hill. The flora spans a range of depositional facies.

The Willamette Flora is exposed on the west-facing road cut above you (Fig. 4).

STOP 2. THE WILLAMETTE FLORA

The Willamette Flora has been mentioned in several brief taxonomic lists (Vokes and others, 1951; Brown, 1959; Meyer and Manchester, 1997), but it remains undescribed. The flora was originally collected from several localities. All of these but the freeway locality were destroyed during road construction. Large collections of the flora are housed at the U.C. Museum of Paleontology, Berkeley, the National Museum of Natural History, Washington, and the Condon Museum, University of Oregon.

The Willamette Flora occurs within a sequence of well-bedded, tuffaceous sandstone, mudstone, and pebble breccia, variously assigned to the lowermost interval of the Little Butte Volcanics (Wolfe, 1981) and to the Fisher Formation (Baldwin, 1981). The regularly bedded nature of the sequence, local occurrence of pumiceous tuff, and presence of carbon-rich horizons, closely resemble the Fisher Formation stratigraphically below it, whereas the presence of thick volcaniclastic debris flow deposits is characteristic of the Little Butte Volcanics. The contact between the Fisher Formation and the overlying Little Butte Volcanics likely is gradational. A $^{40}Ar/^{39}Ar$ date from near the top of the freeway exposure yielded an age of 30.64 ± 0.51 Ma (Kester, 2001).

The stratigraphic relationship between the Willamette Flora and the Goshen Flora, exposed not far to the south, is difficult to establish because of poor exposure and minor faulting. However, the distinctive well-bedded sequence containing the Willamette Flora can be followed north for several kilometers, where it includes fossilized upright tree stumps within debris flow deposits. The debris flow deposits comprise immature andesitic volcanics and suggest that the Willamette Flora grew in an unstable environment adjacent to increasingly active vents of the Western Cascades.

The flora is preserved in thinly and regularly bedded mudstone and coarse-grained sandstone. Excellent exposure at the freeway outcrop makes it possible to follow the fossiliferous bed for more than 100 meters along strike (Fig. 4). Fossils consist of black compressions in dark gray shale. Pervasive zeolitization makes the rocks difficult to cleave and quarry in slabs large enough to yield whole leaves, but with a little work excellent specimens can be recovered. At the south end of the outcrop, the

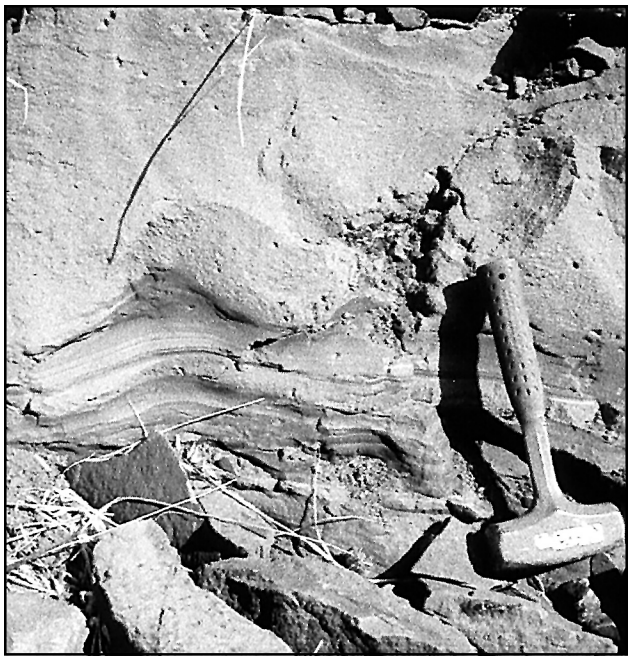

Figure 5. Soft-sediment deformation in thinly-laminated siltstone of the Willamette Flora fossiliferous interval. The overlying sequence is a volcaniclastic debris-flow deposit containing charcoalized wood.

fossiliferous interval is dominated by claystone, which we interpret to represent floodplain or lake-margin paleosols (Fig. 5). A lake-margin setting is compatible with the discovery of a fossil salamander *Palaeotaricha oligocenica* in these beds (van Frank, 1955). Near the north end of the outcrop, the fossil horizon consists of thinly-laminated mudstone. Plant fossils are superbly preserved, and the absence of fragmentation and evidence of preburial decay is suggestive of deposition in a midlake environment. Because the Willamette Flora spans lake-margin to midlake environments within a single outcrop, the flora provides an opportunity to examine facies-specific taphonomic and compositional biases.

We have recently examined all major collections of the Willamette Flora. At present we recognize approximately 60 taxa in the flora. A partial list is included in Table 1.

Many taxa seem to be holdovers from the warmer late Eocene (such as *Magnolia*, *Paleophytocrene*, Theaceae, *Meliosma*, *Fagus oregona*, and others). However taxa that are

Table 1. Preliminary List of Willamette Flora Taxa

Conifers
?Chamaecyparis sp.
Cunninghamia sp.
Fokeniopsis sp.
Gingko sp.
Keteleeria sp.
Metasequoia occidentalis (Newberry) Chaney
Pinus johndayensis Meyer and Manchester
Sequoia affinis Lesquereux
Tetraclinis sp.
?Torreya sp.
Angiosperms
Acer osmontii Knowlton
Alnus sp.
?Astronium sp.
Berhamniphyllum sp.
?Betula sp.
Cercidiphyllum/Joffrea sp.
Cinnamomophyllum sp.
Cercis maurerae Meyer and Manchester
Cedrela merrillii (Chaney) Brown
Crataegus merriamii (Knowlton) Meyer and Manchester
Cruciptera sp.
Exbucklandia oregonensis (Chaney) Brown
Fabaceae
Fagus oregona (Chaney and Sanborn) Wolfe
Florissantia sp.
?Hydrangia sp.
Juglandaceae
Lauraceae sp. (3 or more forms)
Magnolia sp.
Mahonia simplex
?Meliosma sp.
?Menispermaceae
Palaeophytocrene
Palaeocarya sp.
Plafkeria obliquifolia (Chaney) Wolfe
Platanus condonii (Newberry) Knowlton
Platanus exaspera Meyer and Manchester
Pterocarya sp.
Quercus consimilis Newberry
Quercus sp.
Rhus varians Lakhanpal
"Smilax"
?Theaceae
Ulmus sp.
?Zelkova sp.

Table 2. New $^{40}Ar/^{39}Ar$ Radiometric Dates for the Eugene Area, Oregon

Dated tuff	Location	Ma	Error ±
Dexter Tuff, NW of Jasper Railway Station	NW SE S10 T17S R2W	25.87	0.59
Tuff high above Willamette Flora near Goshen	SE SE S14 T17S R3W	30.64	0.51
Spores Point Tuff on river E of Spores Point	NW NW S10 T16S R3W	31.27	0.57
Buck Mountain Tuff at Short Mountain Landfill	NE NW S36 T17S R3W	31.86	0.82
Buck Mountain Tuff at Buck Mountain	SW NE S14 T15S R3W	32.26	0.6
Bond Creek Tuff in Willamette River	NW SE S32 T16S R3W	33.95	0.7
Bond Creek Tuff in Willamette River	NW SE S32 T16S R3W	34.85	0.22
Fox Hollow Tuff on Lorane Highway	SE NW S22 T17S R4W	40.98	0.56

Dates are from plagioclase by R.A. Duncan, Oregon State University.

taxonomically and numerically dominant in the flora are also found in the upland latest Eocene Cedarville Flora (Myers, 1998), the early Oligocene Bridge Creek Flora (Meyer and Manchester, 1997), and other Oligocene paleofloras from west of the Cascades (for example, the Rujada Flora, Lakhanpal, 1958). Shared taxa include *Sequoia affinis*, *Pinus johndayensis*, *Platanus condonii*, *Platanus exaspera*, *Quercus consimilis*, *Plafkeria obliquifolia*, *Rhus varians*, *Cedrela merrillii*, *Berhamniphyllum sp.*, *Crataegus merriamii*, Ulmaceae, and many others. One of the most unique aspects of the flora is the diversity of conifers in the assemblage.

The Willamette Flora reflects a mesic warm temperate mixed broadleaved and coniferous vegetational source. Leaf physiognomic estimates from the flora yield a mean annual temperature of 13.5°C and approximately 1500 mm of seasonal rainfall. Cold-month temperature did not approach freezing, whereas warm-month temperature remained moderate (less than 20°C). These climatic conditions are ideal for many conifer lineages, and they probably account for the large diversity of conifers in the Willamette Flora.

The Willamette Flora is both floristically and vegetationally very different from the 1 to 2 million year older Goshen Flora. The stark contrast between the two floras is one of the classic and most often cited examples of profound vegetational change in response to Eocene–Oligocene climatic cooling. However, our examination of large collections from the Willamette Flora indicate a less than 6°C decline in mean annual temperature between the Goshen Flora and the Willamette Flora. Cooling was concomitant with a significant decline in precipitation, particularly during the dry season. Although climatic change alone does not seem to account for the dramatic vegetational and floristic transition between the two floras, "threshold" cold month temperature or dry season precipitation changes, perhaps combined with increasing impacts of environmental disturbance between the late Eocene and early Oligocene, may account for the dramatic shift in the composition, diversity, and relative abundance of the taxa growing near the depositional centers.

Return to the vehicles and continue north on old Highway 99 toward Eugene.

57.3 Texaco Station—If anyone needs a rest stop, this is a good place.

Continue north on old Highway 99 to the I-5 North freeway onramp. Continue toward Eugene.

59.1 Exit Glenwood–Springfield. Continue to Franklin Blvd, and turn RIGHT. Continue to Pioneer Parkway, Springfield.

60.8 Pioneer Parkway, Springfield. From old downtown Springfield Main Street head south on Pioneer Parkway across the railway tracks and then uphill for 1/2 mile to a long and high new road cut into the hill of Willamette Heights overlooking the Willamette River (NE NE NW NW section 2 T18S R3W Lane County).

61.4 STOP 3. PIONEER PARKWAY SOUTH

These near-horizontal volcanic-lithic and glauconitic sandstone beds are the upper part of the Eugene Formation. This facies is nearshore-marine and beach, and it is near the point where marine sediment grades upward

into a nonmarine facies. A large permineralized log lies near the middle of the exposed section, and molds and casts of marine surf clams *Spisula eugenensis* can be seen low in the section down the hill toward Springfield. In places the shells form coquina beds. The classic fossil sites of the Eugene Formation along the railway in Glenwood, across the Willamette River to the west, can be seen from here. Although widely regarded as Oligocene, only faunas of the Eugene Formation here, in the Coburg Hills, near Brownsville, and in Salem now seem to be Oligocene. Down section to the west of Springfield these marine rocks are late Eocene.

The Eugene Formation interfingers with rocks of the Fisher Formation (Vokes and Snavely, 1948). Molluscan faunas within the Eugene Formation are tied to the Lincoln and Keasey West Coast local biozones, and are broadly tied to the Galvinian Stage (Armentrout, 1981), *Molopophorus gabbi* and *M. stephenson* zones (Durham, 1944), and the *Acila shumardi* zone of Schenck (1936). Recent magnetostratigraphic work by Prothero and Hankins (2001) places the Keasey Formation within Chrons C15n to C12r, approximately 35 to 32.8 Ma, or latest Eocene to early Oligocene in the Berggren and others (1995) chronology. This assignment agrees with radiometric dates from the Bond Creek Tuff (McBirney, 1978; Murray, 1994; Kester, 2001), which occurs within the Eugene Formation near Eugene to the west of us.

Return to the vehicles, make a U-turn at Dorris Rd, and return NORTH on Pioneer Parkway through Springfield to Oregon 126 to Eugene. Continue WEST on Oregon 126 and return to I-5 North.

65.9 Exit 195 Beltline Florence–Airport. Continue west to Coburg Rd. Turn right (north) on Coburg Rd.

69.8 You will cross the McKenzie River. Just north of the river, turn RIGHT on McKenzie View. Continue slowly up McKenzie View for a little less than 1 mile.

70.7 Pull left and park at the fenced road. *Be sure to lock the vehicles here.*

STOP 4. THE COBURG FLORA

Walk up McKenzie View approximately 200 m. On your left above the landslide barriers is an outcrop of the Eugene Formation, which overlies the Fisher Formation at this place. These Oligocene marine rocks are illustrated in Figure 2.

Climb down the steep slope to the McKenzie River. Ropes are provided, but the path can be very slippery.

At the river, continue north along the bank for approximately 50 meters. The Coburg Flora is exposed along the river bank here.

The Coburg Flora occurs within tan muddy fine-grained sandstone of the Fisher Formation. Fossils are preserved as dark compressions. Although the flora has not been extensively collected to date, extremely well-preserved leaves, fruits, and wood have been recovered. The Coburg Flora is undescribed, and the only mention of a "Coburg Flora" comes from a letter from C.W. Washburne to W.D. Smith (1917) referring to "a collection of

Figure 6. Stump in growth position within the Spores Point Tuff at the Coburg Flora locality.

Oligocene leaves made on the Vanduzen place, east of Coburg" (cited in an unpublished catalogue of fossils by Hergert, 1954). A small collection from this locality was made by Leroy Detling of the University of Oregon.

The Coburg Flora is an autochthonous untransported assemblage. Wood and other plant debris is mixed within a paleosol, and growth-position tree stumps are common (Fig. 6). The fossiliferous horizon of the Coburg Flora is conformably overlain by the Spores Point Tuff. The tuff seems to have been deposited rapidly upon the forest floor, entombing the community nearly intact. A $^{40}Ar/^{39}Ar$ date from the Spores Point Tuff yielded an age of 31.27 ± 0.57 Ma (Kester, 2001). The age of the tuff is particularly important, because the tuff is coeval with the Coburg Flora, and hence provides the only direct date for an early Oligocene flora west of the Cascades.

Preliminary collections from the Coburg Flora include plants tentatively recognized as Celastraceae, Theaceae, Lauraceae, Urticaceae?, and others. These plants are indicative of a warm, moist climate, and more closely resemble the Goshen Flora than the Willamette Flora, although the apparent difference may be a product of taphonomic or growth-habitat biases.

Return to vehicles and make a U-turn to return to Coburg Road.

Turn RIGHT on Coburg Road.

73.5 Downtown Coburg. Turn RIGHT on Pearl St.

74.2 Enter I-5 North.

103.6 Oregon 34 (Exit 228) to Corvallis

114.2 Approaching the Oregon 34 bridge over the Willamette River, look up to see the huge osprey nest at the top of the eastern central bridge support.

REFERENCES

Armentrout, J.M., 1981, Correlation and ages of Cenozoic chronostratigraphic units in Oregon and Washington, *in* Armentrout, J.M., ed., Pacific Northwest Cenozoic Biostratigraphy: Geological Society of America Special Paper 184, p. 137-147.

Baldwin, E.M., 1981, Geology of Oregon: Dubuque, Kendall/Hunt, 170 p.

Berggren, W.A., Kent, D.V., Swisher, C.C., and Aubry, M.P., 1995, A revised Cenozoic geochronology and chronostratigraphy, *in* Berggren, W.A., Kent, D.V., Aubry, M.P., and Hardenbol, J., eds., Geocronology, time scales, and global stratigraphic correlation: Society of Economic Paleontologists and Mineralogists Special Publication 54, p. 129-212.

Brown, R.W., 1950, An Oligocene evergreen cherry from Oregon: Washington Academy of Sciences Journal, v. 40, p. 321-324.

Brown, R.W., 1959, A bat and some plants from the Oligocene of Oregon: Journal of Paleontology, v. 33, p. 120-124.

Chaney, R. W., and Sanborn, E. I., 1933, The Goshen Flora of central Oregon: Carnegie Institution of Washington Publication 439, 237 p.

Dalrymple, G.B., 1979, Critical tables for conversion of K-Ar ages from old to new constants: Geology, v. 7, p. 558-560.

Durham, J.W., 1944, Megafaunal zones of the Oligocene of northwestern Washington: University of California Department of Geological Sciences Bulletin, v. 27, p. 101-211.

Evernden, J.F., and James, G.T., 1964, Potassium-argon dates of the Tertiary floras of North America: American Journal of Science, v. 262, p. 945-974.

Eubanks, W., 1962, The fossil flora of Thomas Creek: Ore Bin, v. 24, p. 26-27.

Hergert, H.L., 1954, Tertiary floras of Western Oregon and their geological significance: Oregon State University MS Thesis, 87 p.

Hickman, C.J.S., 1969, The Oligocene marine molluscan fauna of the Eugene Formation in Oregon: University of Oregon Museum of Natural History Bulletin, v. 16, 112 p.

Kester, P.R., 2001, Paleoclimatic interpretation from the early Oligocene Willamette Flora, Eugene, Oregon: University of Washington MS Thesis, 62 p.

Klucking, E., 1964, An Oligocene flora from the Western Cascades: University of Caliifornia Berkeley PhD Dissertation, 241 p.

Lakhanpal, R.N., 1958, The Rujada Flora of west central Oregon: University of California Publications in Geological Sciences, v. 35, 66 p.

McBirney, A. R., 1978, Volcanic evolution of the Cascade Range: Annual Review of Earth and Planetary Sciences, v. 6, p. 437-456.

Meyer, H.W., 1973, The Lyons Flora of northwestern Oregon: Ore Bin, v. 35, p. 37-51.

Meyer, H.W., and Manchester, S.R., 1997, Revision of the Oligocene Bridge Creek Floras of Oregon: University of California Publications in Geological Sciences, v. 141, 191 p.

Murray, R.B., 1994, Geology and mineral resources of the Richter Mountain 7.5 Minute Quadrangle, Douglas and Jackson Counties, Oregon: University of Oregon MS Thesis, 250 p.

Myers, J.A., 1998, Paleovegetational heterogeneity and the record of Eocene–Oligocene climate change in the interior Pacific Northwest: University of California Santa Barbara PhD Dissertation, 502 p.

Myers J.A., in press, Terrestrial Eocene–Oligocene vegetation and climate in the Pacific Northwest, *in* Prothero, D.R. ed., The marine Eocene–Oligocene transition: Cambridge University Press.

Peck, D.L., Griggs, A.L., Schlicker, H.G., Wells, F.G., and Dole, H.M., 1964, Geology of the central and northern parts of the Western Cascade Range in Oregon: U.S. Geological Survey Professional Paper 449, 56 p.

Prothero, D.R., and Hankins K.G., 2001, Magnetic stratigraphy and tectonic rotation of the Eocene–Oligocene Keasey Formation, northwest Oregon: Journal of Geophysical Research v. 105, p. 16,473-16,480.

Rathbun, M.J., 1926, The fossil stalk-eyed crustacea of the Pacific Slope of North America: U.S. National Museum Bulletin, v. 138, 155 p.

Sanborn E.I., 1949, The Scio Flora of western Oregon. Oregon State College Studies in Geology, no. 4, 29 p.

Schenk, H.G., 1936, Nuculid bivalves of the genus *Acila*: Geological Society of America Special Paper 4, 149 p.

Steere, M.J., 1955, Fossil localities of the Eugene area, Oregon: Ore Bin, v. 20, p. 51-59.

van Frank, R., 1955, *Palaeotaricha oligocenica*, new genus and species; an Oligocene salamander from Oregon: Breviora, v. 45, p. 1-12.

Vokes, H.E., and Snavely, P.D., Jr., 1948, The age relationships of the Eugene and Fisher Formations: Geological Society of the Oregon Country Geological Newsletter, v. 14, p. 38-41.

Vokes, H.E., Snavely, P.D., Jr., and Myers, D.A., 1951, Geology of the southern and southwestern border areas of the Willamette Valley, Oregon: U.S. Geological Survey Oil and Gas Investigation Map OM110.

Wolfe, J.A., 1977, Paleogene floras from the Gulf of Alaska region: U.S. Geological Survey Professional Paper 997, 108 p.

Wolfe, J.A., 1981, A chronologic framework for Cenozoic megafossil floras of northwestern North America and its relation to marine geochronology, *in* Armentrout, J.M., ed., Pacific Northwest biostratigraphy: Geological Society of America Special Paper 184, p. 39-47.

Wolfe, J.A., 1994, Tertiary climatic changes at middle latitudes of western North America: Palaeogeography, Palaeoclimatology, Palaeoecology, v. 108, p. 195-205.

Yeats, R.S., Graven, E.P., Werner, K.S., Goldfinger, C., and Popowski, T.A., 1996, Tectonics of the Willamette Valley, Oregon: U. S. Geological Survey Professional Paper 1560, p. 183-222.

Unraveling the Mystery of the Oligocene Flora at Sweet Home, Oregon: A Field Study for K–12 Teachers

Larry G. Enochs, Science and Mathematics Education, Oregon State University, Corvallis, Oregon 97331; enochsl@ucs.orst.edu

Lockwood DeWitt, 345 SW 11th Street, Corvallis, Oregon 97330; lockwooddewitt@hotmail.com

Erwin G. Schutfort, Radiation Center, Oregon State University, Corvallis, Oregon; schutfoe@rc.orst.edu

Peter Wampler, Geosciences, Oregon State University, Corvallis, Oregon; wamplerp@geo.orst.edu

The Earth is a vast cemetery where the rocks are tombstones on which the buried dead have written their own epitaphs.
Louis Agassiz

INTRODUCTION: K–12 GEOLOGY EDUCATION

Geology, the study of the Earth, is primarily a field science. Geologists observe the Earth and its processes, apply their knowledge and observations to the past, and develop a history of the Earth. For professional geologists, a rigorous field training program is required. Most K–12 teachers of earth science have had only limited field experience in geology, usually in the form of a few field trips for an introductory-level course in geology or earth science. Hence, most teachers are not prepared to teach earth science in the field. They must rely on textbooks and indoor laboratory experience. Therefore, teachers and students do not relate their classroom experiences to the "real" world outside of the classroom. They have only a limited experience, if any, in directly viewing and evaluating earth phenomena, and in collecting and analyzing field data or samples. The Earth itself is our most valuable, practical, and versatile laboratory for teaching earth science, yet it is rarely used for earth science instruction in our middle and junior high schools.

Field Guide to Geologic Processes in Cascadia: Oregon Department of Geology and Mineral Industries Special Paper 36, 2002.

Our motivation in leading this field trip and the associated workshop is to provide practicing earth science teachers the experience that many lack, and to extend the experience of others. The field trip will engage science teachers in scientific inquiry of the petrified wood found near Sweet Home, Oregon.

Recently, the National Research Council (NRC) published a book entitled *Inquiry and the National Science Education Standards: A Guide for Teaching and Learning*. The authors cite the need for inquiry activities in K-12 science classrooms. According to the National Research Council, students learn science best through such inquiry activities. These activities should be driven by five essential elements (National Research Council, 2000). These are (1) learners are **engaged** by scientifically oriented questions; (2) learners give priority to **evidence**, which allows them to develop and evaluate explanations that address scientifically oriented questions; (3) learners formulate **explanations** from evidence to address scientifically oriented questions; (4) learners **evaluate** their explanations in light of alternative explanations, particularly those reflecting scientific understanding; (5) learners **communicate and justify** their proposed explanations. The following vignette depicts how science teachers might proceed after discovering the plant fossils found in the field trip area; the sidebars denote science teaching processes recommended and highlighted by the NRC.

VIGNETTE: TEACHERS VISIT THE SWEET HOME FOSSIL FOREST

Teachers visiting with a friend south of the Sweet Home area see a fist-sized piece of petrified wood in the ditch by the road, and they are impressed by the color and preserved detail in the specimen. Looking more closely they find numerous pieces and realize that petrified wood is quite common in this small area. In their classes the next day they show the pieces of wood to their students, who are also fascinated by these unusual rocks. The students ask questions that the teachers themselves have pondered: "How old are these?" "Are there more out there?" "Why are they concentrated in this one area?" "Are they worth anything?" And so on. The teachers realize that some of these questions might have answers that they can discover along with their students.

Make observations

Exhibit couriosity; ask questions

The next time the teachers visit with their friend, they ask neighbors if petrified wood is common in the area. The neighbors say that similar fossils are found throughout the area, and people have been collecting them for decades. They learn of a paper that has been written about the petrified wood. Another neighbor tells about a local rock club that might be able to help answer some of the questions. A half hour of research at the nearby university library unearths the paper written in 1968 by Irene Gregory (1968). Gregory lists many types of fossil wood found in that part of Linn County and a few specific sites where it was collected. The paper also gives the approximate geologic age of Miocene for the petrified forest. Contact with rock club members results in opportunities to see spectacular samples of cut and polished wood.

The teachers realize that while a few of the simple questions have been answered, many more remain unanswered. "How was the wood preserved?" "Why is it on this side of the Willamette Valley, but not on the other side?" "What did the world look like when the wood was forming, and how is it different today?" The teachers decide they are willing to invest some time and effort in answering these questions.

The answers to initial questions lead to more questions

Another visit to the library yields more information on the geology of the Sweet Home area, and more articles describing petrified wood (Gregory, 1969a, b, 1970, 1972, 1973). A stop at the geology department of the local university connects her with people who can help with the terminology and concepts which are new, and yields more literature and references. The teachers conclude that despite the arcane terminology, their students would readily comprehend most of the *ideas*. After reviewing all the available literature, they realize that no one has answered many of the questions they are pondering about the petrified wood.

Broaden knowledge base through talking to experts and going to published literature

They ponder how they might use the mystery of the fossil wood in the classroom to involve students in answering the many unanswered questions. Although they are science teachers, they are painfully aware of the limits of their knowledge and experience. One of their university contacts provides them with the name of a graduate student willing to spend some time working with them. Together, they make a trip to the field, and discuss the interpretation of the rocks and fossils found there. In the lab, the teachers learn to make thin sections, and they start to develop a skill for wood identification.

Begin to involve students with research experience

They decide that making thin sections is an activity that their eighth graders could accomplish successfully, with a low level of expense. They take their students on day trips to the field to examine the rocks, take photos of outcrops, and collect specimens. The students begin to work on the wood. They make several hundred thin sections, identify dozens of wood varieties, and even discover a type previously unknown in the area. The students are fascinated by the microscopic detail visible in a "simple rock," and take great pride in writing an article that is published in

Further observations; use of technology to gather evidence for answering questions

Oregon's science teaching journal . The teachers and their classes answered some of the original questions and developed many more. They also learned that their interpretations are not the only interpretations possible—just the best explanations they have been able to develop with the information they have gathered.

Present findings to peers

They discover that the wood seems to have been preserved in several different ways. The plant materials were apparently entombed in sediment with abundant dissolved silica, which was deposited within the cells of the wood. The petrified wood doesn't occur in the Coast Range across the valley, because that area either lacked the volcanism of the Cascades, or was an environment where wood is unlikely to occur (such as in deep marine sediment). The environment where the wood formed seems to have been a relatively flat coastal plain, with low volcanoes close by to the east. The diversity of the types of wood identified makes the classes begin to wonder about the ecology of the Miocene forest. How can trees that seem to represent different climates and biomes occur in the same location? Remembering the original research by Gregory, they start to think about ways to support or refute the different hypotheses they developed to explain this mystery.

The following autumn, the teachers make a presentation at the annual Oregon Science Teachers Association meeting. They describe the process and activities done with their students. They explain their initial uncertainty about an ability to "actually do science," but with time, effort, and persistence, they discovered that "doing science" is achievable. They teach meeting participants how to polish a slice of rock and affix it to a slide, and provide materials so they can finish the thin sections and share the activity with their students. At the end of the presentation, the teachers put up a geologic map of Oregon marked with the locations and ages of known fossil wood sites. There is wood everywhere! Audience members come up to find the fossil wood locations near their schools. They are given a bibliography of articles dealing with paleobotany in Oregon. In the following weeks more than twenty teachers across the state go out to look at rocks… and in looking, they begin to see, with ever-increasing clarity, visions of a past world that they can share with their students

Continue dissemination of findings; involve others to broaden scope of addressable problems

...and the process never ends

TOWARD WOOD STUDY IN THE CLASSROOM

As the previous vignette shows, starting from scratch and doing geologic and paleontologic research with students in the classroom is demanding but rewarding. A great deal of the effort required by these dedicated, determined, (and fictional) teachers was glossed over. The balance of this paper details the field work and background information required to formulate and address scientific problems that arose in investigations of the Sweet Home Petrified Forest, includingthe following:

- Background and description of the collecting area
- Rocks of volcanic environments
- Geology and stratigraphy of the Sweet Home area
- Varieties of wood and other plants
- Sources of wood
- Preparation of thin sections of fossil wood
- Geochemistry of Petrified Wood

BACKGROUND AND DESCRIPTION OF THE COLLECTING AREA

When one thinks of petrified forests, Arizona comes to mind. Yet Oregon has its own petrified forests that span several geologic periods. This field trip will focus on the petrified forest in the area encompassing Sweet Home and Holley in Linn County, Oregon (Fig. 1).

The city of Sweet Home boasts a steady population of over 8,000 and covers approximately 6.5 square miles. Local industry includes timber and forest products, agriculture, electronics, and small manufacturing companies.

The primary collecting area for this trip is a small watershed south of Sweet Home, extending to Holley. Much of this drainage is intermittent and flows southward into the Calapooia River near Holley. The valley floor

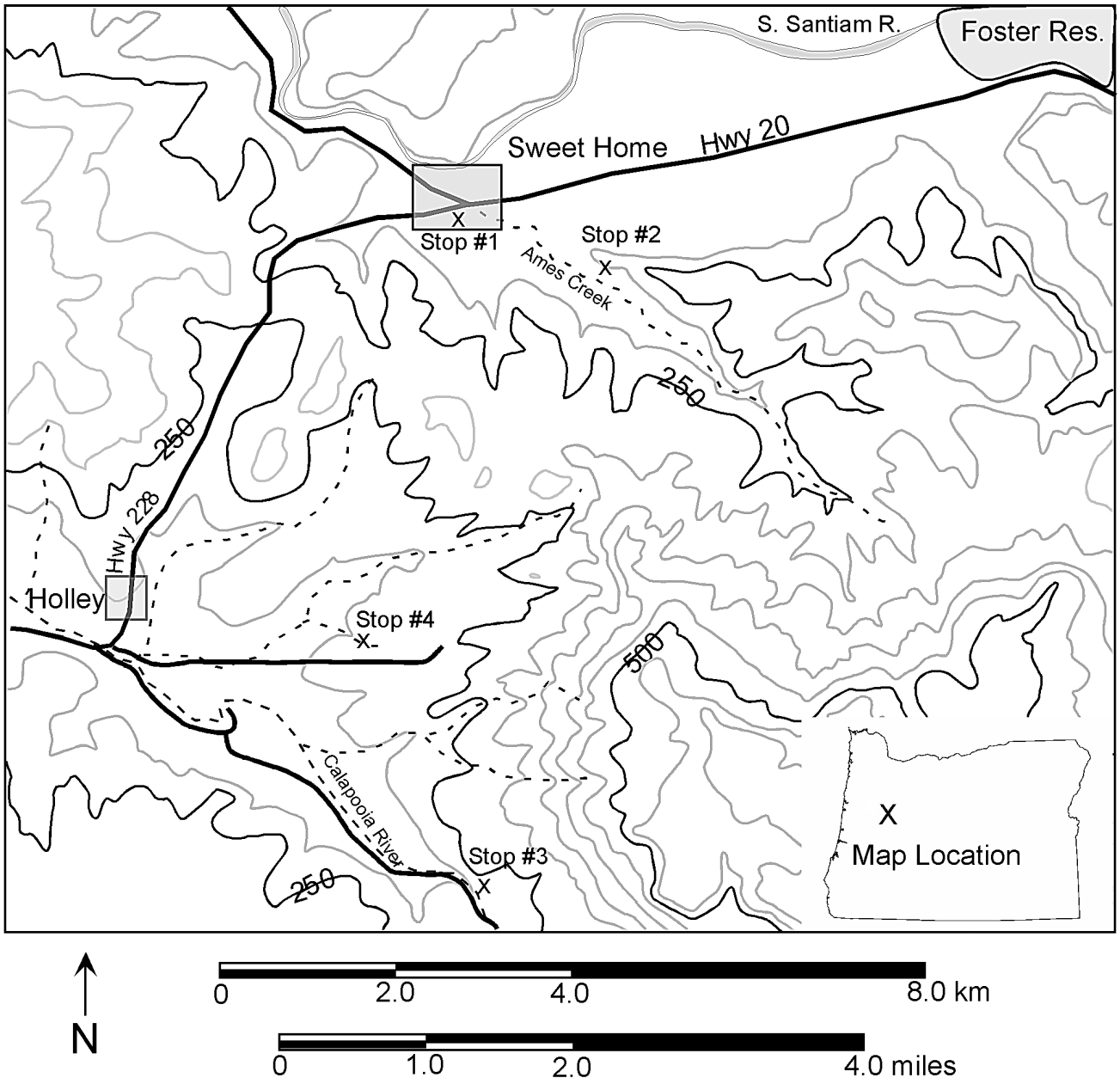

Figure 1. Location map.

contains large amounts of fossilized wood, and in some places the wood is closely packed. The margins of this drainage are composed of volcanic ash and tuff. Gregory (1968) posits that erosional processes carved the valley system and removed the ash particles, leaving the heavy silicified wood material behind as a lag product. The angular nature of the fossil wood indicates that it was likely a residual product and thus was not carried far. Richardson (1950) reported several large petrified stumps in the surrounding hillsides that seem to be in place.

ROCKS OF VOLCANIC ENVIRONMENTS

The Sweet Home area is overwhelmingly volcanic in origin; nearly all the rocks preserved in this region are derived in one way or another from material that erupted from volcanoes during the late Oligocene to early Miocene. Because of this, it is appropriate that we begin with an overview of the many different kinds of rocks that can form in such an environment.

When lava erupts from a volcano, it rapidly cools, forming small crystals. This fine grain is diagnostic of volcanic igneous rocks. The three most common volcanic rock types are

rhyolite, andesite, and basalt. Rhyolite tends to be glassy, medium to light in color, and commonly shows colors other than gray to black. It is high in silica (silicon dioxide), sodium, and potassium, and low in iron, calcium, and magnesium. Basalt is dark gray to (typically) black, and is nearly at the opposite end of the chemical spectrum from rhyolite: it is low in silica, sodium, and potassium, and high in iron, calcium, and magnesium. Andesite tends toward lighter grays than basalt, but is usually fairly dark, and is intermediate between basalt and rhyolite in chemical composition. Basalt and andesite weather to red and orange due to their iron content.

While lava flows are the rocks most commonly associated with volcanoes, other forms of lava can also be produced. If water or other gasses such as carbon dioxide are abundant in the erupting lava, the vapor pressure produced by these volatile substances can fragment the lava, as confining pressure decreases near the vent. The most familiar material produced by such a process is volcanic ash: fine, sand-grain sized particles of rapidly cooled lava. Because these particles cool very quickly on contact with the air they are generally glassy—mineral crystals do not have time to form and grow. Other materials include lapilli, (2 to 64 mm fragments, as defined by Fisher and Schminke, 1984) and bombs and blocks (fragments larger than 64 mm). As a group, these materials are called pyroclastic (from roots meaning "fire-broken").

One of geology's fascinating, albeit frustrating, characteristics is that the materials generally form along continua. Sedimentary rocks are defined as those that have been moved by some agent such as water, wind, or ice, then deposited in layers. Volcanic rocks are defined as those that have cooled and solidified from a melt that erupted onto the Earth's surface. So materials that have erupted from a volcano and *not* been moved by a transporting agent are strictly volcanic. But if they have been moved by wind, water, or ice, they are technically sedimentary. Thus, sedimentary rocks composed largely of fragments of volcanic rock are called volcaniclastic.

Transport of volcaniclastic sediment over significant distances by water or wind produces rounded volcanic fragments and strong sorting or segregation into layers of different particle-size groups known as bedding. A lack of rounding and bedding suggests that the materials are still close to their source. Volcanic debris flows, or lahars, can transport material long distances as a concrete-like slurry that usually lacks rounding of clasts (individual grains of sediment) and bedding.

The fossilized wood we will examine on this trip comes from poorly sorted, poorly bedded, and poorly rounded volcaniclastic materials. Nearly all this material ranges from sand- to pea-sized. It is unclear whether these rocks represent water-laid material that has undergone almost no transport (colluvium), or lahar deposits. Our best hypothesis at this writing is that much of the material was transported a short distance, perhaps deposited in a broad delta environment near an ancient shoreline. Some of the rocks may represent lahars, but the lack of coarse (larger than a few mm) fragments is an argument against this. Some may even represent pyroclastic materials that have undergone no transport: they may have erupted from a volcano, settled to the ground, and lithified in place. The one identified flow in this area is basalt, and the volcaniclastic sedimentary grains are dominantly intermediate in composition.

GEOLOGY AND STRATIGRAPHY OF THE SWEET HOME AREA

Beginning about 35 Ma (million years ago, mega-annums), volcanic eruptions became common and voluminous in the Western Cascades. Prior to this time, marine sediment had been deposited in the embayment that would become the Willamette Valley. Much of this material was volcaniclastic. Peck and others (1964) noted rare flows of basalt and andesite in these older rocks where they are exposed as the Colestin Formation in the southern part of the Western Cascades. This suggests that volcanism had been present prior to 35 Ma, but not abundant. Marine sedimentary rocks equivalent to the Colestin likely occur at depth in the Sweet Home area, but they are not exposed at the surface.

The western edge of active volcanism was approximately the same as the eastern edge of the Willamette Valley (see Fig. 2, after Orr and Orr, 1999). Peterson Butte, just west of Leba-

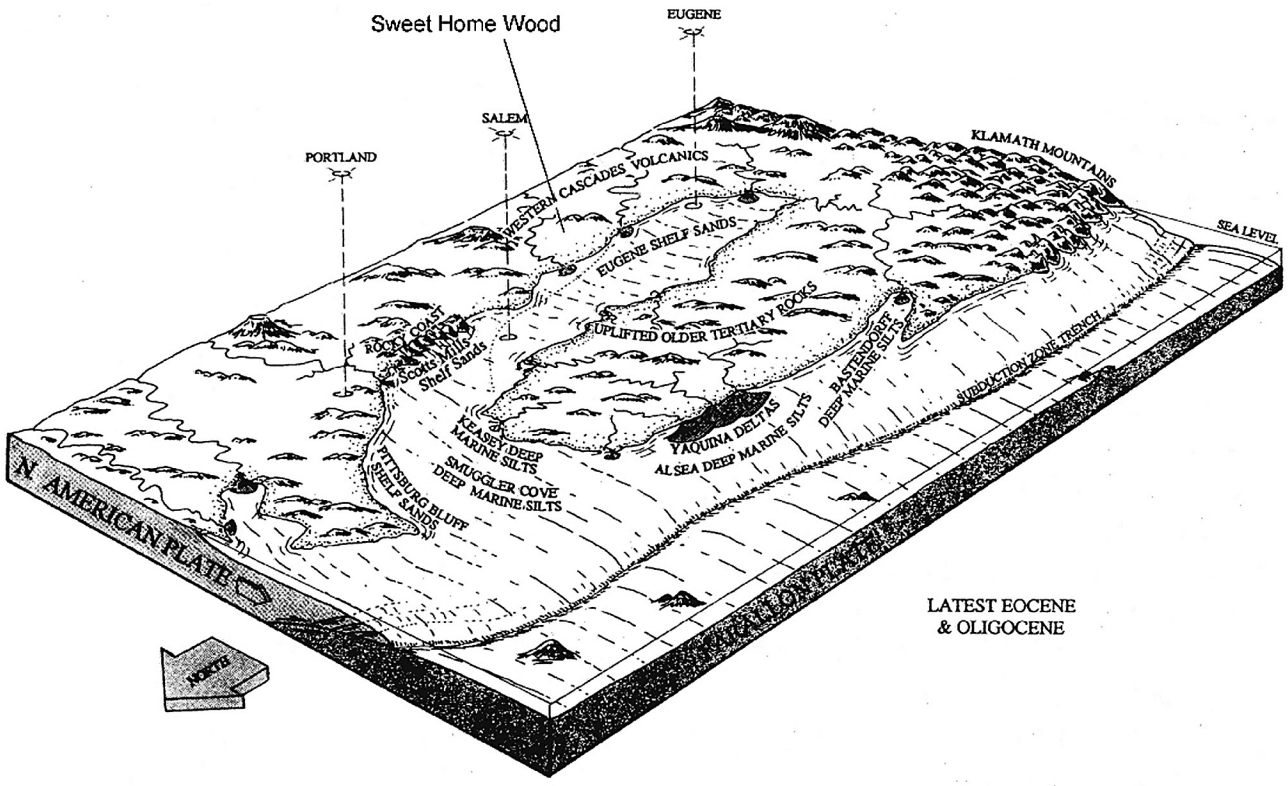

Figure 2, Oligocene geologic setting (after Orr and Orr, 1999).

non, is identified as the remains of volcano of this time. While the eastern edge of volcanism is largely hidden under younger material, it is clear that the width of the active area was substantially greater than the width of the modern High Cascades volcanism. Priest (1990) estimates that the width of the volcanic arc at this time, was three to four times the width of the modern arc.

During this first phase of Western Cascade volcanism, flows, pyroclastic material, and volcaniclastic sediment were produced rapidly. These deposits were named the Little Butte Volcanics by Peck and others (1964). Priest and others (1983) referred to this unit by the more descriptive "Early Western Cascades." It is within the nearshore deposits of this unit that we find the rich floras of middle Oligocene to early Miocene time.

By about 17 Ma, the volcanic front had moved substantially eastward; although flows may have reached toward this area, no active vents are believed to have been present. Also at this time, flows of the Columbia River Basalt Group reached as far south as Lebanon, but did not reach the Holley–Sweet Home area.

SOURCES OF WOOD

A long list of varieties of wood and other plants are reported from the Sweet Home Petrified Forest (Table 1). Gregory (1968) notes that even a cursory glance over the taxa identified from this flora reveals plants from widely varying climatic-ecologic environments. This presents a problem because they are clearly preserved together in a single assemblage. So how did these plants representing different climates come to be preserved together? Gregory's explanation is as follows:

> It is at once apparent that the list of identified specimens in table 1 represents members of several types of plant communities, some of which, by the durable nature of even unsilicified wood, may have been transported long distances from their place of growth.
>
> So as a departure from usual paleobontanical form, rather than attempt to reconstruct a picture of the physical growth environment of this fossil flora by separating its component parts into ecologic associations as we

Table 1. Varieties of wood and other plants reported from the Sweet Home Petrified Forest (Gregory, 1968; Orr and Orr, 1981; Richardson, 1950)

Abies (fir)
Acer (maple)
Actinidia
Aesculus (buckeye)
Alangium
Allophylus
Alnus (alder)
Alniphyllum
Betula (birch)
Carpinus (hornbeam)
Carya (hickory)
Cassia (senna)
Castanea (chestnut)
Castanopsis (chinquapin)
Catalpa
Cedrela (cedar)
Cercidiphyllum (katsura)
Chrysobalamus (cocoa plum)
Cinnamomum (camphorwood)
Cladrastis (yellow wood)
Cordia (geiger tree)
Carnus (dogwood)
Corylus (hazelnut)
Cupressus (cypress)
Diospyros (persimmon)
Equisetum
Entandrophragma
Fagus (beech)
Ficus (fig)
Fraxinus (ash)
Gleditsia (honey locust)
Gymnocladus (Kentucky coffee tree)
Hydrangea
Ilex (holly)
Juglans (walnut)
Larix (larch)
Libocedrus (cedar)
Liquidambar (sweet gum)
Magnolia
Meliosma
Nectandra (laurel)
Nyssa (tupelon)
Ocotea (lancewood)
Osmanthus (devilwood)
Phoebe
Pinus (pine)
Platanus (sycamore)
Populus (cottonwood)
Porana (morning glory)
Prunus (cherry)
Quercus (oak)
Reptonia
Rhammus
Salix (willow)
Sassafrass
Schima
Sequoia (redwood)
Sterculia
Taxodium (bald cypress)
Tetracera (liana vine)
Trochodendron
Trochodendroxylon
Ulmus (elm)
Umbellularia (laurel)
Viburnum

know them today, we shall instead speculate and theorize as to the possible origins of the species that have accumulated here:

1. Tropical woods present could well represent Eocene species—remnants of an earlier, warmer climate adapted to the later but still moderate Oligocene seacoast environment of our area, much as palms have adapted today to the climates of England and Scotland. Interesting correlations may be noted here with the Goshen Flora (Chaney and Sanborn, 1933).

2. Many trees were petrified *in situ,* having been covered by rapid and repeated falls of ash from erupting volcanoes nearby and to the east. At present, remains of some stand upright in several Sweet Home locations (Richardson, 1950). Notable among these are the sycamores (*Platanus*), typical stream-bank bottom land species. Tops of stumps of a large grove of sycamore trees are visible at ground level in a valley on the McQueen property where their bases have been covered by material eroded from the surrounding steep hillsides.

3. Westward-flowing streams, carrying quantities of pyroclastic debris originating from volcanoes to the east, constructed large deltas where they reached the coast. Specimens of fossil wood which show considerable transportation wear might well represent live woods of the time carried by flooded streams from the interior and deposited as a part of such deltas. Fossil woods of earlier Eocene time, transported and buried in a similar manner, could be present in Oligocene rocks in much the same way that the Cretaceous fern *Tempskya* is found in later Eocene Clarno deposits in the Greenhorn Mountains of northeastern Oregon. Here the fossilized wood was eroded from the enclosing rocks and redeposited in younger sediment.

4. Asiatic species reported to occur only rarely in Tertiary fossil woods could have arrived as random logs of driftwood by way of the sea. An example of this is *Actinidia*, not previously reported as a fossil wood and found at Holley thus far as a single specimen consisting of an almost complete trunk section. Logs transported as driftwood from offshore islands of the time (or from unlimited distances in the Eastern Hemisphere) and carried into the marine embayment may have been entrapped in coastal swamps and petrified after burial in stream sediments or falls of ash. Another wood — the Asiatic genus *Schima* of the tea family (Theaceae) — might have had such a source. The absence of branches and twigs and the preponderance of woods representing trees rather than shrubs help give credence to the idea that at least some of the material arrived at the locality as stripped-down, water-worn tree trunks.

5. Many of the specimens collected have inclusions of quartz pseudomorphs after halite (rock salt) crystals. We have found thus far, as did (Staples, 1950), that the inclusions were contained only in the fossil woods found as float and not in those petrified in place in the areas. A collected specimen of *Castanopsis indica*, or Indian sweet chestnut (Asiatic), whose structure shows it to be a portion of a large tree trunk, is almost completely replaced with quartz pseudomorophs after halite. The distribution of the halite indicates that the solution had access from all sides as in floating and might have been absorbed during a long period at sea.

Table 2: Preparing Thin Sections of Fossil Wood (Barefoot and Hankins, 1982; Enochs, 1984).

Using a diamond saw, cut a thin slice of the specimen to be sectioned (0.08 to 0.15 cm)
Grind a flat surface of the area to be sectioned with successive grits of 200, 400, and 600 mesh to ensure a smooth surface to be glued to the slide. Following each grinding step, wash the specimen to remove the coarser grit.
Frost one side of the petrographic slide with fine (600 grit) using a glass plate
Wash the specimen and slide to remove grit.
Attach the specimen to the frosted slide using epoxy.
Using fine (200, followed by 400, and finally 600) grit, grind the specimen on the glass plate until light passes through the specimen. Check the thickness frequently, and wash the grit off thoroughly before proceeding to the next finer grit. The thin slice should be ground to a uniform thickness. Continue to grind until the specimen is thin enough to observe the features of the wood. The thickness should be checked under the microscope to ensure that the features are clear.
Wash the thin section to remove all grit.
Attach a cover slip by adding a small amount of epoxy to the cover slip and placing it on the specimen.
Label the slide by writing on the frosted edge of the slide

Figure 3. Complex cell structure perhaps due to disease or decomposition.

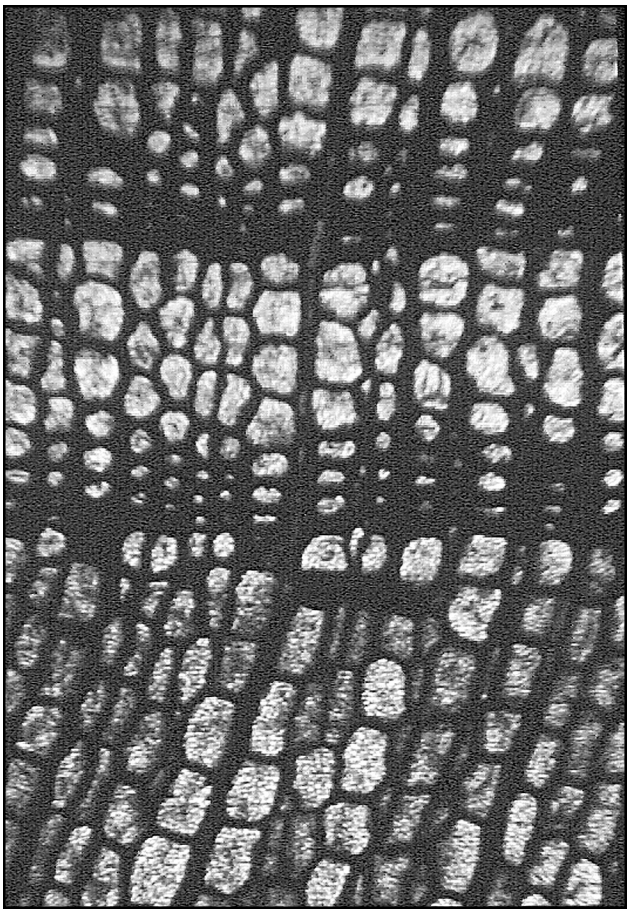

Figure 4. Detailed photo of cell structure

PREPARATION OF THIN SECTIONS OF FOSSIL WOOD

Thin sections provide a way to study rocks through a microscope in precisely the same way that prepared biologic specimens are studied. Microscopy is every bit as important in geology as in biology. But while nearly every public school student is expected to have at least rudimentary experiences with biologic microscopy, few people other than trained geologists have even heard of geologic microscopy, or petrography.

In addition to being a high-interest introduction to the techniques of petrography, fossil wood also provides an opportunity for students to view the microscopic world of plants. With practice, they can also begin to classify the wood taxa, allowing the students to address paleoecologic questions. Table 2 outlines the steps to prepare thin sections with students.

TEXTURES IDENTIFIED IN FOSSIL WOOD

Petrified wood is an abundant fossil throughout the geologic record from the late Paleozoic to present. It is generally found in three different depositional environments: pyroclastic sediments, hot springs, and sedimentary basins. The fossilization process may be different in these environments, and trace element geochemistry is a potential tool in their interpretation. Some previous workers interpreted petrification as a replacement process of original organic wood by silica. Others have argued that the wood was preserved through an impregnation of the organic materials. While the petrified wood from our area is silicified to a greater or lesser degree, it may also be replaced (less commonly) by other minerals such as calcite or iron oxides and hydroxides.

The diversity of the mineralized wood becomes readily apparent upon macroscopic

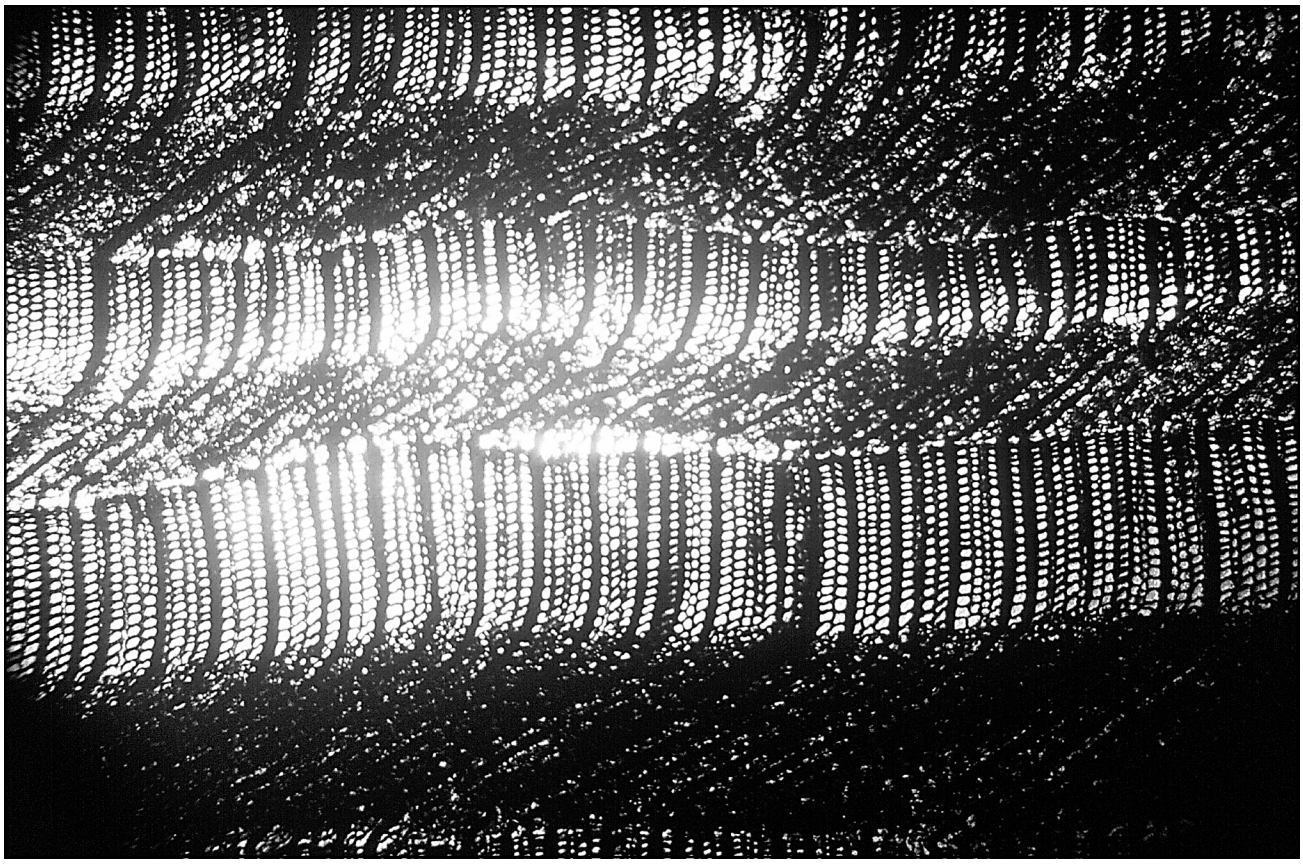

Figure 5. Contorted growth rings.

observation of hand specimens and petrographic analysis of thin sections. First, some samples have clearly been carbonized, turned to a charcoal-like material, at some point prior to silicification. Some of these samples are much like coal in their density and appearance, but more like peat in the sense that remnants of original cellular-scale structure are evident. Others are silicified, but are a jet-black color. Another nearby site, above Green Peter Reservoir, yields thoroughly silicified carbonized wood that can scratch steel, but smudges skin with a soot-like substance. These samples also show an unusual alternation between severely deformed and undeformed regions within growth rings. Second, based on density and hardness, distinct differences in the degrees of petrification are obvious—normally between samples, but sometimes within a single sample. Third, in samples which represent "fresh" (uncarbonized) wood, even an untrained eye can pick out distinct differences, such as the presence or lack of rays and ring pores, size and distinctiveness of growth rings, and other features that represent preserved anatomical features of the wood from the original type of tree (Fig. 3, 4, and 5). Fourth, coloration differences between separate samples and within single samples may represent one, or a combination of, factors such as trace element abundance, dissolution of minerals, oxidation, degree of replacement versus infilling, or other variables that may not have occurred to us.

FIELD TRIP STOPS

Stop 1. East Linn Community Museum

The city of Sweet Home is rightfully proud of its history and heritage. This small museum displays artifacts and memorabilia commemorating the town's past. Equipment used in the major industries of the area—logging and agriculture—has been restored and preserved. Two magnificent petrified logs are on display. These logs represent some of the finest of the petrified wood found in the Sweet Home–Holley area. One is about 2 1/2 feet in diameter by 8 feet high, and the other is

about 3 1/2 feet in diameter by 4 feet high. Macroscopic wood structures such as growth rings and rays are visible in the latter block, as are clues to the petrification process, such as quartz veins and pockets of quartz crystals.

Although many petrified trees were standing in this area 50 years ago, apparently in their life positions, few of these stumps remain due to aggressive and uncontrolled collecting. Damage caused by a few irresponsible collectors has left many land owners in this area with a negative image of anyone looking for petrified wood. Despite the tremendous amount of material collected, much remains buried in the soil and in some creek beds. For our purposes, smaller fragmentary material is sufficient, but it is impressive to see the size of some of the fossils that were once present. They also help us envision the kind of forests that were standing during early Cascade volcanism.

Stop 2. Ames Creek

Numerous recent road cuts along this stream allow us to see some representative volcaniclastic sediment, ranging from siltstone and sandstone to pebbly sandstone and sandy conglomerate. Some beds show a nearly complete lack of sorting, whereas others show fairly good sorting. This difference, as described earlier, can be ascribed to differing modes of deposition.

With this in mind (and remembering that the sediment was derived from the eruption, erosion, and redeposition of volcanic rocks), we can begin to envision the environment as it existed about 30 million years ago. Due to the widespread nature of angular deposits, the setting is probably not a narrow valley eroded into lava flows, but rather a broad coastal plain of the Oligocene sea that covered what is now the Willamette Valley. Streams coming down from nearby volcanoes to the east carried eroded material toward the shoreline and deposited it on the coastal plain. Occasionally, in response to a particularly wet season, a volcanic eruption, or after a forest fire denuded upstream areas, debris flows would rush down onto this plain and cover a large area rapidly and much deeper than would ordinarily occur. Burial likely included both driftwood carried by water and in-place forests. Large clasts are angular suggesting the sediment that contains the wood has not been transported far.

Substantial amounts of fossilized leaf material and abundant plant fragments have been found at here. As yet we have found no silicified wood, but local people have said that wood occurs in the drainage. We hope that identifiable leafy material can be used to corroborate the wood identification and provide a clearer picture of the paleobotany of the area. The plant material, combined with the angular nature of the sediment, are consistent with a gentle to nearly flat coastal plain covered by a vigorous plant community, subject to frequent inundation by water and burial under volcanic debris. Other rocks in the area clearly show that the sea lay nearby to the west and the axis of volcanism to the east. The immaturity of the sediment (lack of rounding and weathering) suggests that the sediment source was close by.

Stop 3. Abandoned Railroad Grade East of Holley

The rock here is similar to but more weathered than the rock we saw at Ames Creek. It also appears darker in tone, which suggests a composition that is more basaltic as a source for this sediment. The exposures along the first 1/4 mile of the grade are thoroughly weathered. Although we have seen a few rocks that are suggestive of fossil wood, the rock is so rotted that identification is difficult.

After crossing the small stream from the north, we come to a much better preserved exposure that displays numerous wood pieces. We have found several stumps in an upright position—suggesting that they actually grew in the spot where they are seen today. Upright fossils are typically strongly silicified. We also find numerous pieces of wood as fragments, and one horizontal log about 15 feet long. These latter fossils appear to have been carbonized either before or during burial and lithification, and they are not as silicified as the upright wood. One sample we have collected here shows a gradation from thoroughly mineralized on the outside to nearly unmineralized in the middle. The density and hardness differences are obvious with han-

dling. We have also found some preserved leaf material here, but not as much as at Ames Creek.

The host rock in which the fossils are preserved has poor to nonexistent sorting, bedding is indistinct, and the individual clasts range up to about pea or grape sized. The lack of larger fragments makes it difficult to consider these as lahar deposits, but the lack of sorting and bedding makes it difficult to consider them as having traveled any significant distance.

Stop 4. Private Land Near Holley

As has been noted previously, nearly all the petrified wood in this area has been found on privately owned land. Damage to fences, open holes, and theft caused by a few irresponsible collectors has left many landowners in this area unwilling to allow collecting on their property. To ensure that we will have continued access to this resource, we must avoid damage to the owner's operations and property. While we choose not to publicize the people who have generously granted us permission to collect on their land, we do wish to publicly acknowledge our gratitude.

The landscape at this stop is typical for areas in which we find wood: gently sloping with relatively low relief, well-developed soil, and numerous small streams. Petrified wood is primarily as float in the upper few feet of the soil; plowing commonly turns it over, and we see it in the tractor path. Because large chunks of rock are destructive to farm machinery, our host has tossed these chunks into a pile along the edge of the field.

After investigating this pile, we will walk down to the stream to see the abundant wood there, water level permitting. Along the stream, wood is abundant as blocks and boulders in the stream bed and banks. In the banks one can see the upper 3 to 4 feet of alluvium and colluvium and contrast it with the bedrock in the stream bottom. The bedrock here is much the same as we've seen elsewhere on the trip: coarse, poorly sorted, tuffaceous sandstone. Our present hypothesis is that erosion and in-place mass wasting are concentrating the wood fragments as they remove finer materials. We have found no fossils in the bedrock. The angular often dangerously sharp edges of the petrified wood show clearly that this material has undergone almost no transport.

REFERENCES

Barefoot, A.C., and Hankins, F.W., 1982, Specimen preparation, *in* Barefoot, A.C., and Hankins, F.W., eds., Identification of modern and Tertiary woods: London, Oxford University Press, p. 189.

Chaney, R.W., and Sanborn, E.I., 1933, The Goshen FLora of west central Oregon: Carnegie Institution of Washington Publication , 103 p.

Enochs, L.G., 1984, Preparation of thin sections in the junior high classroom: Earth Scientist, v. 1, no. 4, p. 17-19.

Fisher, R.V., and Schminke, H.-U., 1984, Pyroclastic rtocks: New York, Springer-Verlag, 472 p.

Gregory, I., 1968, The fossil woods near Holley in the Sweet Home Petrified Forest, Linn County, Oregon: Ore Bin, v. 30, p. 57-76.

Gregory, I., 1969a, Fossilized palm wood in Oregon: Ore Bin, v. 31, p. 93-110.

Gregory, I., 1969b, Worm-bored poplar from the Eocene of Oregon: Ore Bin, v. 31, p. 184-185.

Gregory, I., 1970, An ancient acacia wood from Oregon: Ore Bin, v. 32, p. 205-210.

Gregory, I., 1972, A fossil pine forest in the Blue Mountains of Oregon: Ore Bin, v. 34, p. 31-38.

Gregory, I., 1973, An ancient acacia wood from Oregon: Palaeobotanist, v. 20, p. 19-21.

National Research Council, 2000, Inquiry and the National Science Education Standards: A guide for teaching and learning: Washington, National Academy Press, 200 p.

Orr, W.N., and Orr, E.L., 1981, Handbook of Oregon plant and animal fossils: Eugene, 285 p.

Orr, E.L., and Orr, W.N., 1999, Oregon fossils: Dubuque, Kendall/Hunt Publishing Co., 381 p.

Peck, D.L., Griggs, A.B., Schlicker, H.G., Wells, F.G., and Dole, H.M., 1964, Geology of the central and northern parts of the Western Cascade Range in Oregon, U.S. Geological Survey Professional Paper 449, 56 p.

Priest, G.R., 1990, Volcanic and tectonic evolution of the Cascade Volcanic Arc, central Oregon: Journal of Geophysical Research, v. 95, p. 19,583-19,599.

Priest, G.R., Woller, N.M., Black, G.L., and Evans, S.H., 1983, Overview of the geology of the central Oregon Cascade Range, *in* Priest, G.R., and Vogt, B.F., eds., Geology and geothermal resources of the central Oregon Cascade Range: Oregon Department of Geology and Mineral Industries Special Paper 15, p. 3-28.

Richardson, H.E., 1950, The geology of the Sweet Home Petrified Forest: University of Oregon MS Thesis, 44 p.

Staples, L.W., 1950, Cubic pseudomorphs of quartz after halite in petrified wood, Oregon: American Journal of Science, v. 248, p. 124-136.

Luckiamute River Watershed, Upper Willamette Basin: An Integrated Environmental Study for K–12 Educators

Stephen B. Taylor, Earth and Physical Science Department, Western Oregon University, Monmouth, Oregon 97361; taylors@wou.edu

Bryan E. Dutton, Biology Department, Western Oregon University, Monmouth, Oregon 97361; duttonb@wou.edu

Pete E. Poston, Earth and Physical Science Department, Western Oregon University, Monmouth, Oregon 97361; postonp@wou.edu

INTRODUCTION

This field trip examines aspects of environmental science in the Luckiamute River Watershed, upper Willamette Basin, Oregon. A 1-day itinerary is designed for K–12 science educators with an interest in watershed studies and natural science disciplines (earth science, biology, chemistry).

Selected localities, natural features, and respective discussions for this field trip were derived from a 6-week Environmental Science Institute course convened during Summer 2001 at Western Oregon University. The institute course targeted undergraduate science majors, preservice education majors, practicing education professionals, and masters-level education students. The course was designed with four integrated science modules in geomorphology, field botany, paleoclimatology, and environmental chemistry. The geomorphology module focused on landscape analysis, geographic information systems, surficial mapping methodology, and field hydrology. The botany module emphasized characterization of riparian habitats, floristic changes over time, impacts of invasive plant species, and field monitoring methodologies. The paleoclimatology module included derivation of climate variables from modern and ancient flora, and examination of the Tertiary fossil record of the mid-Willamette Valley. The environmental chemistry module examined land use and water quality issues in the Willamette Basin, with a focus on aqueous chemistry, field measurement techniques, and pesticide contamination. Discussion topics of this field trip concentrate on the geomorphology, botany, and environmental chemistry of the Luckiamute Watershed. Selected aspects of the paleoclimatology module are covered in a companion paper in this volume (Myers and others, 2002). As this field trip and guidebook are sponsored by an alliance of geoscience organizations, the content emphasis is accordingly weighted toward a geologic perspective.

The field guide is organized into two principal sections. The first provides a literature review and background information on the regional setting of the Luckiamute River. The second is a detailed road log and stop description, with suggestions for field-based science-education activities.

The road log for this 1-day field trip begins at the north entrance to the CH2M Hill Alumni Center on the campus of Oregon State University, Corvallis. The trip consists of a 100+ mile loop through the Luckiamute Watershed via Philomath Boulevard, Kings Valley Highway (Oregon 223), Falls City Road, Monmouth Road, Helmick Road, Oregon 99W, and Soap Creek Road (Fig. 1). Field trip stops include those that are both scenic and scientific, with an emphasis on integrated environmental studies at the watershed scale.

PHYSIOGRAPHY

The Luckiamute River constitutes a part of the Willamette Basin in west-central Oregon (Fig. 2). This seventh-order watershed (Strahler, 1957) drains eastward from the Coast Range into the Willamette River and occupies a total drainage area of 815 km^2. The Luckiamute Basin is bounded by the Willamette River to the east, the crest of the Coast Range to the west, Green Mountain and Marys River to the south, and the Rickreall Creek Watershed to the north (Fig. 2). Land surface elevations range from 46 m (150 ft) at the confluence with the Willamette

Field Guide to Geologic Processes in Cascadia: Oregon Department of Geology and Mineral Industries Special Paper 36, 2002.

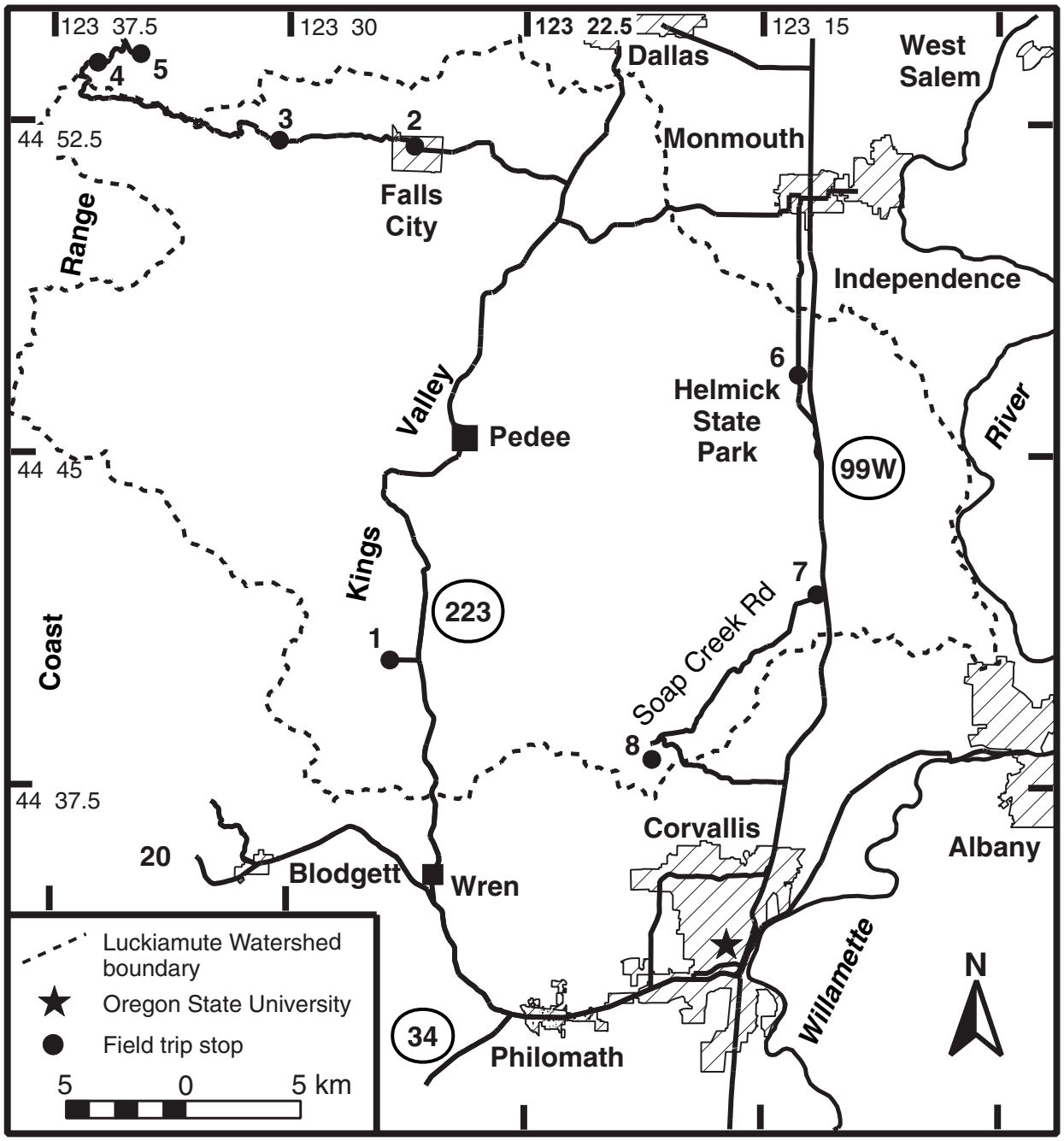

Figure 1. Location map and field trip route for the Luckiamute Watershed.

River to 1016 m (3333 ft) at Fanno Peak. The Luckiamute has an average gradient of 3 m/km, a total stream length of 90.7 km, and an average basin elevation of 277 m (910 ft) (Rhea, 1993; Slack and others, 1993). Fanno Ridge separates the watershed into two tributary subbasins, with the Little Luckiamute to the north and the main stem of the Luckiamute to the south (Kings Valley) (Fig. 2). Lower-order tributaries include Boughey Creek, Waymire Creek, Vincent Creek, Plunkett Creek, Woods Creek, Maxfield Creek, and Soap Creek.

The greater Willamette Valley extends northward 190 km from Eugene to Portland, Oregon. This lowland is up to 60 km wide, separating the Coast Range to the west from the Cascade Range to the east. Valley floor elevations range from 150 m (500 ft) to 3 m (10 ft), with an average gradient of 2 m/km (Slack and others, 1993).

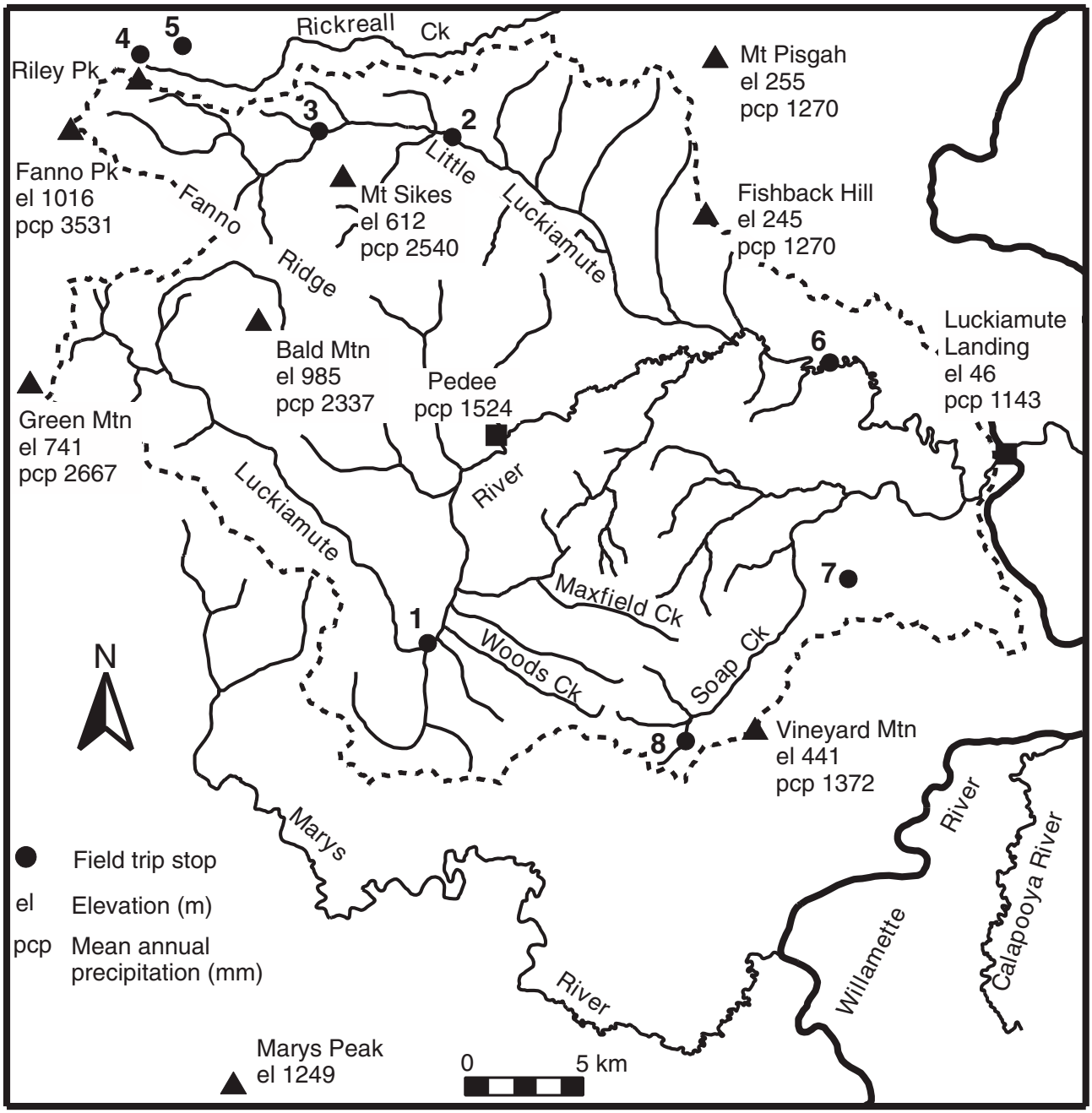

Figure 2. Physiographic map and spot annual precipitation for the Luckiamute Watershed.

TECTONIC SETTING

The Luckiamute Watershed is on a convergent tectonic margin where the Juan de Fuca Plate subducts eastward beneath North America. This subduction zone is associated with a long history of oblique convergence, tectonic accretion, arc volcanism, dextral shear, and clockwise rotation (Wells and others, 1984). Long-term rates of plate convergence average 3.5 to 4.0 cm/yr (Adams, 1984). Paleoseismic studies along coastal Oregon suggest that the region experiences large magnitude, subduction-style earthquakes with a recurrence interval of approximately 300 to 500 years (Darienzo and Peterson, 1990).

The western two-thirds of the Luckiamute River drains the central Oregon Coast Range (Fig. 2). This mountain system began to uplift between 15 and 10 Ma (Snavely and others, 1993) and it continues to be

neotectonically active (Adams, 1984). Thus the present-day relief in the Oregon Coast Range is a combination of net uplift due to plate convergence and vertical incision by surface processes (Kelsey and others, 1994).

Historic releveling surveys of western Oregon suggest that the western boundary of the Luckiamute is presently tilting eastward at a rate of approximately 1×10^{-8} rad/yr with a crustal shortening of 10^{-7} yr^{-1} (Adams, 1984). Although tilt data suggest that portions of the Luckiamute are neotectonically active, Mitchell and others (1994) reported no evidence for historic uplift in this part of the Coast Range. By comparing topographic relationships in this region to the southern Coast Range and the Olympics, Kelsey and others (1994) hypothesized that the subducting Juan de Fuca slab is likely segmented at the latitude of the Luckiamute.

The Willamette Valley proper represents a forearc basin situated between the Coast Range and the Cascade Volcanic Arc. The northern Coast Range forms a broad, north-plunging anticlinorium, with pre-Miocene strata dipping eastward toward the Willamette Valley (Yeats and others, 1996). The Cascades are associated with a long history of intermediate to mafic volcanism dating from late Eocene (40-35 Ma) to present. Arc volcanism has been narrowing and migrating eastward over time, with the geometry of High Cascade volcanoes controlled by the present-day subduction-zone configuration (Priest, 1990)

BEDROCK GEOLOGY

Yeats and others (1996) and Snavely and Wells (1996) provided comprehensive summaries of the bedrock geology in the Luckiamute region. The bedrock comprises an Eocene to Oligocene sequence of basaltic volcanic rocks, marine sedimentary rocks, and mafic intrusives of varying composition (Fig. 3). In ascending order, lithostratigraphic units include the Siletz River Volcanics (upper Paleocene to middle Eocene; 58-46 Ma), Tyee Formation (middle Eocene; 53-48 Ma), Yamhill Formation (middle and upper Eocene; 48-44 Ma), Spencer Formation (upper Eocene; 44-41 Ma), and undifferentiated mafic intrusions (middle Oligocene; 34-30 Ma). The Siletz River Volcanics are composed primarily of submarine basalt lava flows interbedded with breccia, sandstone, and siltstone. The Tyee Formation is characterized by an arkosic sandstone lithofacies, interpreted as deltaic and submarine fan deposits. The Yamhill Formation comprises interbedded siltstone and shale of marine origin. The Spencer Formation comprises arkosic sandstone, siltstone, and mudstone, interpreted as shallow marine deposits. Given the convergent tectonic setting, strata in the Coast Range portion of the Luckiamute are extensively faulted and fractured.

Bedrock map units are grouped into four lithospatial domains in the Luckiamute, as recognized on the basis of outcrop pattern (Fig. 3). These include the Siletz River Volcanics Domain (south), the Tyee Domain (west-southwest), the Yamhill–Intrusive Domain (north-northwest), and the Spencer–Valley Fill Domain (east). The Siletz River Volcanics Domain constitutes 19% of the watershed and is mainly seafloor basalt. The Tyee Domain (29% of total area) is underlain primarily by the Tyee Formation with local mafic intrusives supporting ridge tops. The Yamhill-Intrusive Domain occupies 23% of the watershed and is characterized by the outcrop of equal parts of the Yamhill Formation and mafic intrusives. The Spencer–Valley Fill Domain (29%) is underlain by a patchwork of Spencer Formation and Quaternary alluvium. Each of these bedrock spatial domains is associated with unique landform assemblages and surficial processes.

SURFICIAL GEOLOGY AND GEOMORPHOLOGY

Geomorphic systems of the Luckiamute Watershed can be divided into a valley-floor regime to the east and a hillslope-colluvial regime to the west (Fig. 4). The style of the surficial process and landform associations are controlled by topographic position, underlying bedrock geology, and resistance to erosion. Hillslope landforms and colluvial processes dominate the Siletz River, Tyee, and Yamhill–Intrusive Domains, whereas fluvial landforms and alluvial processes are characteristic of the Spencer–Valley Fill Domain.

Valley Floor–Fluvial Regime

The lower Luckiamute is characterized by a mix of alluvial stratigraphic units and geomorphic surfaces. Landforms include active channels, floodplains, fill terraces, and strath-pediment surfaces (McDowell, 1991). In addition to these fluvial landforms, the lower Luckiamute is associated with swaths of low-relief colluvial hillslopes supported by the Spencer Formation (Fig. 4). Present-day geomorphic conditions extend back to at least the Pliocene, the time at which the Willamette River eroded through intrabasinal divides, permitting

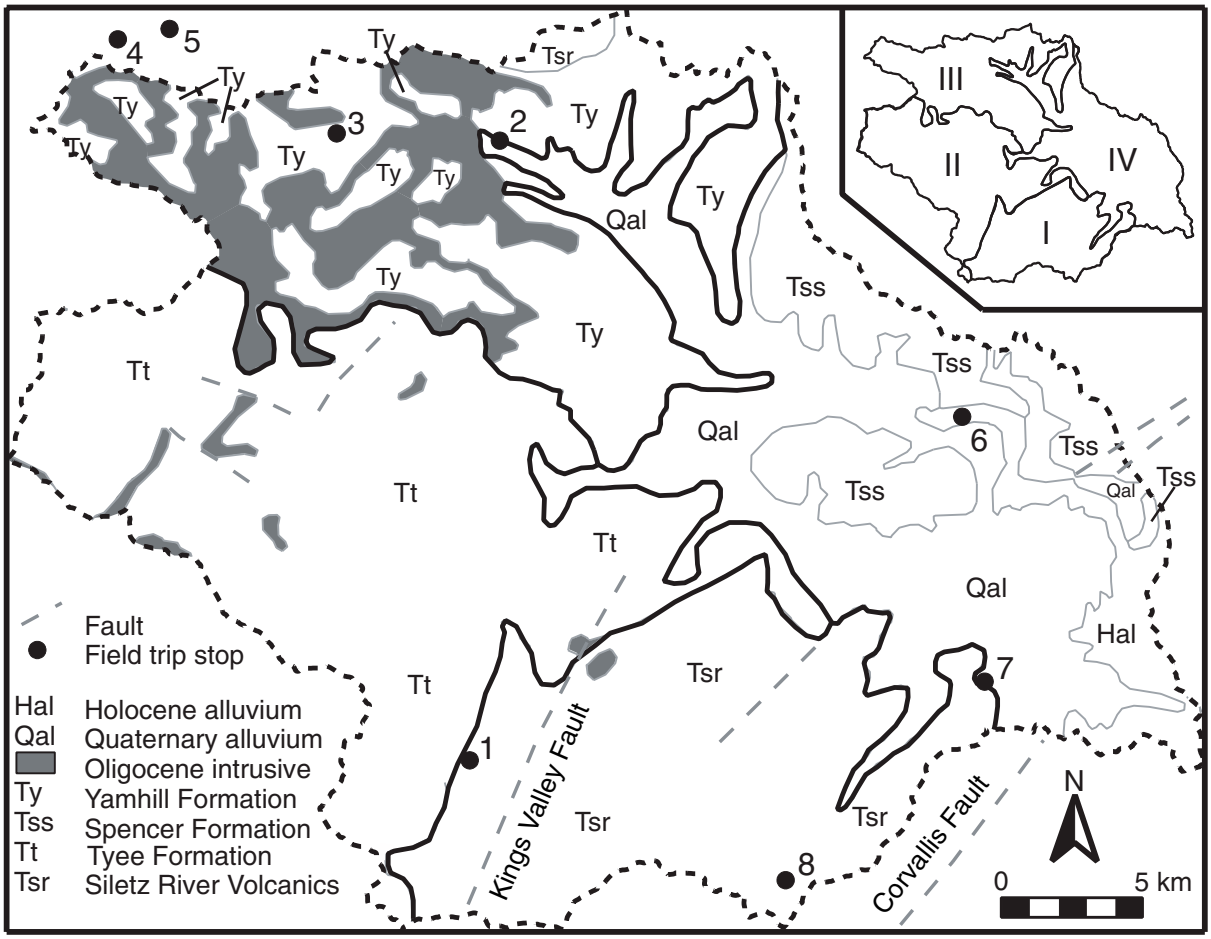

Figure 3. Bedrock geology of the Luckiamute Watershed (after Walker and MacLeod, 1991). Inset map shows grouping of recognized lithospatial domains: I = Siletz River Domain, II = Tyee Domain, III = Yamhill–Tertiary Intrusive Domain, IV = Spencer–Valley Fill Domain.

open drainage to the Columbia River (McDowell, 1991). Pleistocene through Holocene terrace development records a complex history of base level fluctuation, internal erosion-deposition cycles, and glacial-outburst floods (Missoula Floods) from the Columbia River system.

Maximum thickness of Pliocene to Holocene sedimentary fill in the mid-Willamette Valley is up to 150 m (Yeats and others, 1996). Balster and Parsons (1966) mapped terrace and floodplain surfaces in this region on the basis of topography and soil development. The active channel of the lower Luckiamute is incised 8 to 9 m below the floodplain, with higher level terrace surfaces at 12 to 15 m above the mean annual stage (Reckendorf, 1993). The higher-level terrace surfaces are covered with rhythmically-bedded, silty slack-water deposits of the Willamette Formation (Missoula Flood deposits, 13.5-12 ka). These late Pleistocene surfaces are inset with lower terrace and floodplain deposits that are predominantly Holocene in age (post-Missoula Flood, <12 ka) (Fig. 4; O'Connor and others, 2001).

Hillslope–Colluvial Regime

Parsons (1978) presented a geomorphic overview of the Coast Range portion of the Luckiamute. Small-scale intrusions and volcanic rocks support ridge tops and provide the resisting media for steep terrain. On average, hillslope gradients range from 25 to 30% with maxima up to 90%. Local relief is on the order of 300 to 500 m. Hillslope processes dominate this part of the Luckiamute Watershed, including slide, debris flow, creep, tree throw, and faunal turbation. Fluvial transport and erosion

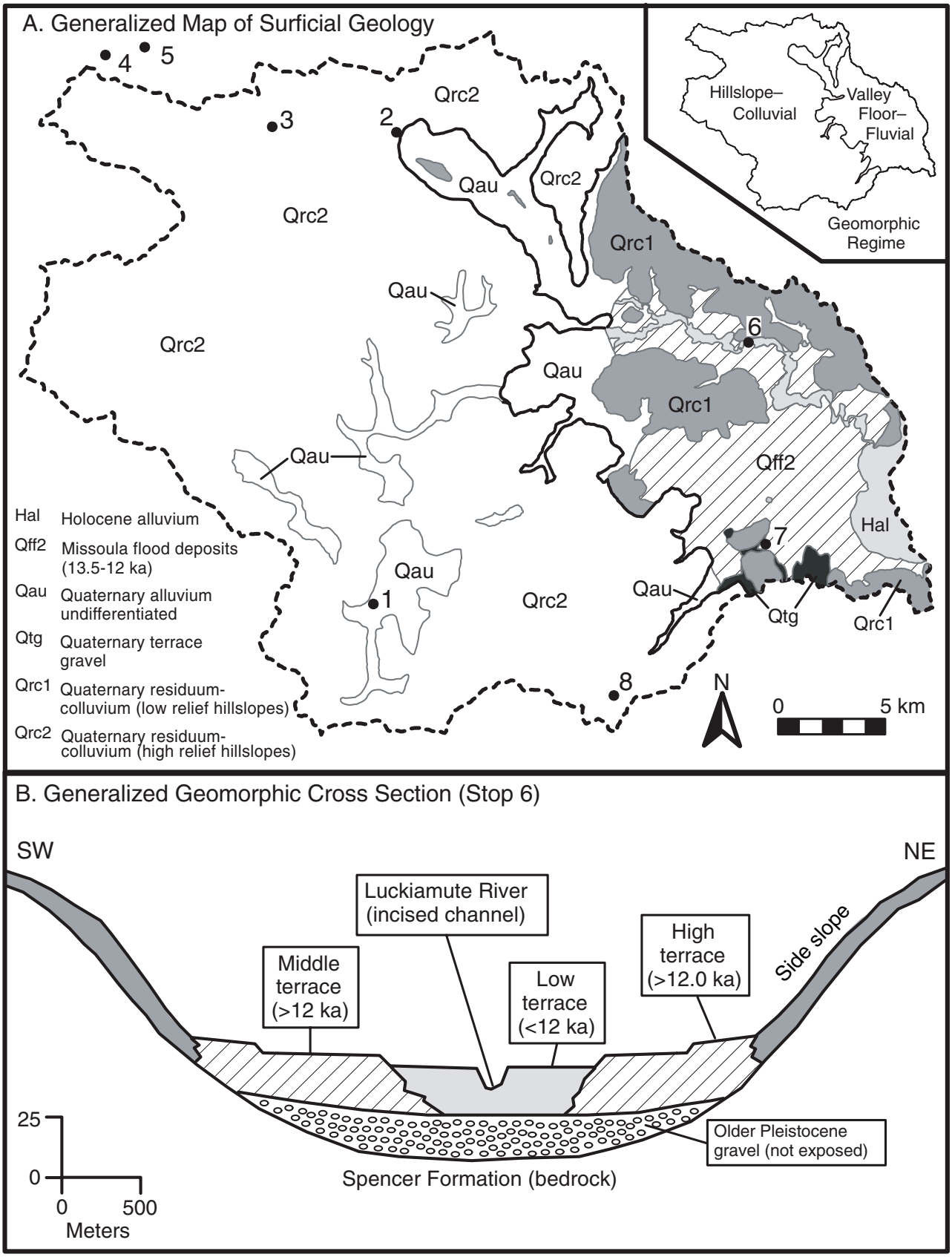

Figure 4. Surficial geology and geomorphology of the Luckiamute River Basin. Surficial map units are modified from O'Connor and others (2001), after Taylor and others (1996). Cross section shown in Frame B represents generalized landform elements at Helmick State Park (Stop 6).

occur in narrow, low-order tributary valleys. Upland landforms include ridge tops, side slopes, hollows, landslide scars, and dissected pediments. Narrow valley bottoms are geomorphically active, with channels, floodplains, low terraces, and small-scale debris fans (Balster and Parsons, 1968).

The Oregon Coast Range is noted for hazards associated with landslides, flooding, and debris flow activity (Gresswell and others, 1979; Robinson and others, 1999). The Oregon Department of Forestry (2000) has recently released a set of debris flow hazard maps for parts of the Luckiamute Watershed. These maps were derived from slope analysis of 30-meter digital-elevation models. Preliminary evaluation of the these hazard maps indicates that hillslopes underlain by the Tyee Formation are the most prone to debris flow (Table 1). The data suggest that bedrock lithology exerts a strong control on the style of hillslope process, soil development, and related landforms in the upland portion of the Luckiamute.

Table 1. Debris flow hazard potential ranked by lithospatial domain, Luckiamute Watershed (data derived from Robinson and others, 1999)

Lithospatial domain	Domain area (km^2)	Percent of domain area in hazard zone	Hazard rank
Tyee	241	38.1	1
Yamhill–Tertiary intrusives	193	24.6	2
Siletz River	151	30.2	3
Spencer–Valley Fill	229	0.7	4

Soil Associations

Geographic Information Systems (GIS) analyses of county soil surveys (Knezevich, 1975, 1982) yield distribution data for soil series, orders, and subgroups in the Luckiamute Basin. Inceptisols, Ultisols, and Mollisols are the most abundant soil orders in the watershed, representing 38%, 31%, and 24% of the total area, respectively. Inceptisols are typically composed of up to 50% lithic clasts and are associated with active hillslopes (>45% gradient). More deeply weathered Ultisols are common on metastable, lower-gradient hillslopes and pediment surfaces (Parsons, 1978). Representative subgroups include Haplohumults (31%), Xerochrepts (14%), Haplumbrepts (14%), Argixerolls (8%), and Haplaquolls (8%). Colluvial soil associations in the Coast Range portion include: (1) Jory, Peavine, Bellpine, Apt, and Honegrove (Haplohumults); and (2) Price, Ritner, Klickitat, Valsetz, Luckiamute, and Cruiser (Haplumbrepts and Cryochrepts). Down basin, alluvial soil associations include: (1) Woodburn, Coburg, Willamette, Malabon (Argixerolls); (2) Veneta, Willakenzie (Haploxeralfs); and (3) Waldo, Wapato (Haplaquolls). The spatial distribution of soil assemblages is ultimately controlled by geomorphic process. As such, Reckendorf (1973, 1993) emphasized their use as a primary criteria for floodplain mapping in the mid-Willamette Valley.

CLIMATOLOGY AND HYDROLOGY

Taylor and Hannan (1999) summarized historic climate data for western Oregon. The Luckiamute straddles Oregon Climate Zones 1 (Coastal Area) and 2 (Willamette Valley), with westerly Pacific marine air serving as the primary moisture source. Precipitation patterns are strongly seasonal with 75% of the annual total falling from October to March. Hydrometeorologic events are driven primarily by cyclonic and frontal storm systems. Rain-on-snow events are common at higher elevations.

Annual precipitation varies greatly from west to east across the Luckiamute Watershed, as governed by westerly airflow and a lee-side rain-shadow effect in the Coast Range. Annual precipitation in the watershed ranges from 3600 mm along the northwestern boundary to 1140 mm in the center of the Willamette Valley, a west-to-east precipitation gradient of 95 mm/km (Fig. 2).

The U.S. Geological Survey maintains a gauging station on the Luckiamute River at Helmick State Park (USGS Suver Station 14190500; Stop 6 on Fig. 1 and 2). The station is 18 km upstream from the basin outlet, with 650 km^2 of drainage area positioned above the monitoring point (approximately 80% of the total). Analysis of the stream-flow record reveals that flooding and high discharges directly correspond to seasonal precipitation patterns. During the winter season, average discharge is on the order of 50 m^3/s, whereas

summer months are typified by less than 3 m^3/s. The two peak discharges of record were observed at 700 and 620 m^3/s during December 1964 and February 1996, respectively. The 100-yr flood event at the Suver Station is marked by a discharge of 760 m^3/s (Waichler and others, 1997).

Waichler and others (1997) derived a rainfall-runoff model for the Luckiamute Watershed. They estimated an average annual precipitation of 1894 mm for the entire watershed, with a total input volume of 1.23×10^9 m^3. A water budget analysis indicates that 61% of the total annual rainfall is accounted for as runoff, whereas 39% is consumed in the form of evapotranspiration and groundwater flow.

VEGETATION

The Coast Range portion of the Luckiamute Watershed lies in the *Tsuga heterophylla* Zone of Franklin and Dyrness (1988). Dominant forest species include *Pseudotsuga menziesii* (Douglas fir), *Tsuga heterophylla* (western hemlock), and *Thuja plicata* (western red cedar), with a lesser occurrence of *Abies grandis* (grand fir). These species formed part of the classic old-growth timber stands that were logged extensively in the Pacific Northwest during the early 1900s. Disturbed valley zones are characterized by *Alnus rubra* (red alder) and *Rubus spp* (blackberry). *Acer macrophyllum* (big leaf maple) is a common late succession species in valley bottoms and hollows. Balds with meadow grasses and mosses occur locally along higher elevation ridge tops. Lower reaches of the Luckiamute Watershed lie in agricultural crop and pasture land, with local patches of mixed *Quercus garryana* (Oregon white oak) and urban mosaic species.

LAND USE AND ENVIRONMENTAL SETTING

Since European settlement, the predominant economic activities in the Willamette Valley have centered on agriculture in the lowlands and timber harvesting in upland forests. Over the past several decades, industrialization and rapid population growth have resulted in significant impact to the habitat and environmental quality of the region. Given that greater than 75% of all water use in the Willamette Basin is derived from surface sources, land-use and river quality issues are at the forefront of environmental planning in western Oregon.

Private timber companies own a large part of the upper Luckiamute, and 67% of the watershed is classified as forest. In contrast, the eastern valley section comprises a mix of agricultural lands (15% of total), native vegetation (3%), and urban development (1%) (Urich and Wentz, 1999). Primary commodities in the agricultural zones include grass seed, wheat, hay, oats, and mixed crops (clover, sweet corn, mint, alfalfa, filberts) (Wentz and others, 1998). As such, agricultural pesticides and fertilizers are the primary anthropogenic agents that can potentially impact surface and groundwater quality in the Luckiamute Basin.

Wentz and others (1998) presented a water-quality summary for the Willamette Basin, including smaller tributary systems such as the Luckiamute. The greatest potential for water-quality degradation in the lower Luckiamute is from fertilizer-related nitrates and pesticides (herbicides, insecticides, and fungicides). Documented nitrate impacts include nutrient loading, excessive aquatic plant growth, and eutrophication. Nitrate concentrations fluctuate according to seasonal rainfall-runoff patterns with annual maxima common during winter months. Pesticides are also routinely detected at significant concentration levels (3-14 ppb) in the Willamette and related tributaries. Commonly detected pesticides include atrazine, simazine, metochlor, deethylatrazine, diuron, and diazinon. Only atrazine and deethylatrazine are associated with forest-management practices in mountainous subbasins outside of the agricultural zones. Pesticide transport is either through direct advection in a dissolved state or via adsorption to fine-grained suspended sediments.

ROAD LOG AND STOP DESCRIPTIONS

Miles (approximate)

0.0	Depart Oregon State University's CH2M Hill Alumni Center toward the south and then right (west) onto Western Avenue.
0.5	Turn left (south) onto 35th Street.
0.6	Turn right (west) onto Philomath Boulevard (Highway 34/20), toward Philomath.
2.9	Note low-relief hillslopes of the Eocene Spencer Formation to the south (left) of Philomath Boulevard.
3.2	Crossing buried part of the Corvallis Fault, continue west on Highway 34/20 through Philomath, note Marys Peak in distance.

En Route to Stop 1

The drive west from Corvallis on Highway 34/20 provides spectacular views of the central Oregon Coast Range and Marys Peak. The field trip route in this area follows the Marys River drainage, an east-flowing fluvial system that serves as a principal water source for the city of Corvallis. Examples of late Quaternary floodplain and terrace surfaces are evident along the Marys River Valley in the vicinity of Philomath (Fig. 1 and 2).

At mileage point 3.2, Philomath Boulevard crosses the Corvallis Fault, a major thrust and strike-slip system that was active during the early Tertiary. This fault zone trends northeast, dips approximately 10° NW, and is associated with 11 to 13 km of crustal shortening (Yeats and others, 1996). The net result is the westward juxtaposition of the older lower Eocene Siletz River Volcanics next to younger Tertiary sedimentary strata (to the east). Snavely and others (1993) extended the Corvallis Fault offshore to the southwest, where it intersects a north-trending right-lateral strike-slip fracture referred to as the Fulmar Fault. Their offshore mapping suggests that the Corvallis Fault is a major geologic feature associated with convergent-margin tectonics.

Marys Peak is the highest point (1249 m) in the Oregon Coast Range and is supported by erosionally-resistant intrusive rocks of the Marys Peak Sill. Up to 390 m of Oligocene (29.9 Ma) gabbroic rocks intrude sandstone of the middle Eocene Tyee Formation (Yeats and others, 1996). The entire stratigraphic sequence is in turn cut by the Kings Valley Fault, a high-angle reverse fault with relatively limited throw (Walker and Macleod, 1991). High-elevation ridge tops of Marys Peak are associated with unique plant communities composed of mosses and grasses (Franklin and Dyrness, 1988).

5.7 Bear right (west) onto US 20, follow signs toward Newport.
9.7 Turn right (north) onto Kings Valley Highway (Oregon 223).
12.7 Kings Valley Highway crosses into the Luckiamute Watershed.
14.5 Kings Valley Highway bends from northeast to northwest at Plunkett Creek. The highway crosses the approximate position of the Kings Valley Fault at this point (Fig. 1 and 3).
16.0 Turn left (west) onto Luckiamute Road.
16.7 Proceed 0.7 mi on Luckiamute Road to **Stop 1**, bridge crossing Luckiamute River.

Stop 1. Kings Valley (Hoskins)

The main stem of the Luckiamute River forms the principal physiographic feature of Kings Valley. The Hoskins stop is just west of the Kings Valley Fault, which lies near the boundary between the Tyee and Siletz River Domains (Fig. 3).

Systematic geomorphic mapping forms the foundation upon which integrated watershed studies are constructed (Taylor, 1999). Kings Valley and the Coast Range at this stop provide a framework for discussion of a surficial mapping protocol in unglaciated, mountainous landscapes. Taylor and others (1996) devised a four-fold geomorphic mapping scheme in which units are delineated on the basis of age, origin (process), landform, and material (texture) (Table 2). The technique emphasizes the link between landforms and processes in landscapes dominated by hillslopes, mass wasting, and fluvial erosion. Hillslopes are characterized by colluvial diamicton (matrix supported gravel) with landforms subdivided into ridges, side slopes, hollows, and noses. Gravel-dominated valley bottoms are characterized by channel processes and debris flow activity. Valley-bottom landforms are subdivided into channels, floodplains, terraces, fans, and aprons. The four-fold nature of the mapping protocol lends itself particularly well to the layered approach of geographic information systems (GIS). Field trip participants are provided an opportunity to apply the systematic map protocol to the upper Luckiamute River drainage.

16.7 Return east to Kings Valley Highway
17.4 Turn left (north) onto Kings Valley Highway (Oregon 223)
Enter town of Pedee, continue north on Kings Valley Highway.
33.5 Turn left (west) onto Falls City Road.
37.8 Enter Falls City.
37.9 Turn right onto Black Rock Road.
38.0 Stop 2, Falls at Falls City (pull out on left side of road).

Stop 2. Falls at Falls City

Falls City lies at the domain boundary between the Spencer–Valley Fill Domain to the east, and the Yamhill-Intrusive Domain to the west (Fig. 3). The city is set along the Little Luckiamute River and has traditionally served as an access point for timber operations. Field Stop 2 is at the falls of the Little Luckiamute River, just west of town center (Fig. 2).

Table 2. Four-fold surficial-map protocol for unglaciated mountainous landscapes (after Taylor and others, 1996).

1. Age of surficial material

H = Holocene (<10,000 years old)
W = Wisconsin (89 to 10 ka)
I = Illinoian
P = Pleistocene undifferentiated
EP = early Pleistocene
MPl= middle Pleistocene
LP = late Pleistocene
Q = Quaternary undifferentiated
CZ = Cenozoic undifferentiated

2. Origin of surficial process

A. Hillslope
r = residuum (in situ regolith)
c = colluvium (mass wasting)
ds = debris slide
rf = rock fall or topple

B. Valley bottom
a = stream alluvium (normal flow)
hcf = hyperconcentrated flow
df = debris flow
sw = slackwater deposition

C. Lacustrine
l = lacustrine deposit, undiff.
lb = lake-bottom deposit
ld = lacustrine deltaic

D. Other
g = glaciofluvial, undifferentiated
go = glacial outwash
e = eolian
cr = cryoturbation
x = anthropogenic disturbance
f = artificial fill
rk = bedrock

3. Landform Units

A. Hillslope
n = nose
sl = side slope
h = hollow
veneer = <2 m of regolith
blanket = >2 m of regolith
bf = boulder field
bs = boulder stream
pg = patterned ground
tls = talus

B. Valley bottom
ch = channel
fp = floodplain (recurrence interval = ≤ 2-3 yr)
t = terrace (t1, t2 …tn; height above river)
f = fan
f-t = fan terrace (f1, f2 …fn; height above river)
a = apron (footslope deposit)
lo = lobe
lv = levee
ox = oxbow, abandoned channel

C. Other
ft = flow track (debris flow)
hm = hummocky topography
rb = rock block-slide deposit
x = excavated, fill, disturbed ground
d = delta

4. Material (composition and texture)

b = boulders (>256 mm clast supported)
c = cobbles (64-256 mm clast supported)
p = pebbles (4-64 mm clast supported)
g = gravel (>2 mm clast supported)
sg = mixed sand and gravel
s = sand (0.05-2.0 mm)
st = silt (0.002-0.05 mm)
cy = clay (<0.002 mm)
l = loam (mix of sand, silt, clay)
d = diamicton undifferentiated
bbd = very bouldery diamicton
bd = bouldery diamicton
cd = cobbly diamicton
pd = pebbly diamicton
ds = sandy matrix diamicton
dt = silty matrix diamicton
dy = clayey-matrix diamicton
rk = bedrock (modify by lithology)
rs = rotten stone, saprolite
tr = travertine
tu = tufa
ma = marl
og = organic-rich sediment
w = water
u = unkown

Figure 5. Falls City knickpoint along the Little Luckiamute River (Stop 2).

The falls represent a knickpoint or hydraulic step in the longitudinal profile of the Little Luckiamute. Total knickpoint relief is approximately 6 m (Fig. 5). Knickpoint zones along rivers represent significant perturbations in the hydraulic system, intimately related to base-level changes and lithologic discontinuities in the channel substrate (Wohl, 2000). The falls at Falls City are formed on resistant sedimentary lithofacies of the Yamhill Formation. North- to northeast-trending fractures are evident in bedrock pavement along the active channel and provide a strong control on knickpoint development. The Falls City knickpoint is eroding headward with time by processes of block plucking and wall-rock undercutting. Gravel tools generated by knickpoint erosion are in turn available for downstream channel abrasion. The presence of bedrock-lined channels and the relative absence of gravel alluvium suggest that the Little Luckiamute at this position is under capacity with respect to sediment load, that is, the total available stream power exceeds sediment load thresholds (Montgomery and others, 1996). This field stop provides access to readily observable river features that demonstrate concepts of landscape erosion and geomorphic work.

38.0 Continue west on Black Rock Road.
38.2 Bear left onto the gravel portion of Black Rock Road.
41.8 **Stop 3**, Black Rock (pull out where bridge crosses Little Luckiamute River).

Stop 3. Black Rock (Little Luckiamute)

Invasive plant species are problematic for both native and agricultural plant communities as they can compete for resources and displace competitors. Local extirpation of native plant species has obvious impacts on wildlife and natural habitats. Competition between plant species is a part of any habitat, but introduction of nonnative species disrupts relationships evolved among native plants and their communities within those specific habitats.

Table 3. Occurrence of common invasive plant species at selected field trip localities in the Luckiamute Watershed (BR = Black Rock—Stop 3; HSP = Helmick State Park—Stop 6; SSp = Sulphur Springs—Stop 8).

Species	Origin	Occurrence BR	HSP	SSp
Capsella bursa-pastoris (shepherdspurse)	Europe	X	X	X
Cichorium intybus (cichory)	Mediterranean		X	X
Cirsium arvense (Canada thistle)	Eurasia		X	X
Cirsium vulgare (bull thistle	Eurasia		X	X
Conium maculatum (poison hemlock)	Europe		X	X
Cytisus scoparius (Scotch broom)	Europe	X		X
Daucus carota (wild carrot)	Europe		X	X
Digitalis purpurea (foxglove)	Europe	X		X
Dipsacus fullonum (common teasel)	Europe	X	X	X
Hedera helix (English ivy)	Eurasia Africa	X		
Hypericum perforatum (common St Johnswort)	Europe		X	X
Lamium purpureum (purple deadnettle)	Europe	X	X	X
Leucanthemum vulgare (oxeye daisy)	Europe			X
Rubus armeniacus (Himalayan blackberry)	Armenia	X	X	X
Rumex acetosella (red sorrel)	Europe	X	X	X
Senecio jacobaea (tansy ragwort)	Europe	X	X	
Solanum dulcamara (bittersweet nightshade)	Europe		X	X
Tanacetum vulgare (common tansy)	Europe		X	X
Taraxacum officinale (dandelion)	Europe	X	X	X
Verbascum thapsus (common mullein)	Eurasia	X	X	X

Botanical survey techniques are critical for documenting the occurrence of invasive plant species and assessing their relative impact on the ecosystem. Three broad categories of survey methodologies include systematic (taxonomic), monitoring (as distinct from ecological), and ecological (Stiling, 1998). Common nonnative, invasive plant species at select Luckiamute field localities, including Black Rock, are listed in Table 3. Field trip participants are provided an opportunity to explore plant identification methods, botanical survey techniques, and their potential application in a classroom setting.

41.8 Continue west on Black Rock Road

42.3 Bear right at Y intersection, note quarry on right.

43.4 Proceeding on Black Rock Road. Please note that logging roads in this vicinity are narrow and steep, with limited sight distance and active log transport. Use extreme caution when driving this part of the route; citizens-band radio communication is recommended.

En Route to Stop 4

The field trip route west of Black Rock winds along hillslopes of the Coast Range that are intensively managed for forest production. This area is owned by private timber companies and is actively logged by clear-cut methodologies. Logging activities have a profound influence on vegetative plant communities and geomorphic processes. The route through this area follows the Luckiamute drainage divide and provides views of Laurel Mountain to the north of the watershed (Fig. 1 and 2).

Laurel Mountain forms a part of the crest of the Coast Range, with a maximum altitude of 1094 m (3589 ft). Average annual rainfall at the crest exceeds 3800 mm/yr (Taylor and Hannan, 1999). The southeast-facing hillslope of Laurel Mountain was subject to extensive slope failure and debris flow activity in response to a high-intensity, long-duration storm event in February of 1996 (Robinson and others, 1999). Extensive debris slide scars are evident as breaks in the forest canopy below the peak of Laurel Mountain to the north (right) of Black Rock Road. Debris slides were initiated on steep hillslopes (up to 90% gradient) underlain by rocks of the Yamhill-Intrusive Domain. Ten discrete slide zones produced a net landslide erosion rate of 42 m^3/ha over an area of 8.0 km^2,

Figure 6. Overview of Coast Range watersheds and mid-Willamette Valley (view to east from Stop 5).

one of the highest that was documented during the 1996 storm event (Robinson and others, 1999).

44.7 Three-way intersection, continue straight on center road, following contour.
45.7 Three-way intersection, continue straight on center road, following contour.
46.8 Bear left at Y intersection.
47.5 Continue straight at T intersection.
47.8 Continue straight at T intersection.
48.7 Bear right (north) at Y intersection, note **S-Line** tree marking. The road crosses over the Luckiamute drainage divide at this point, with Riley Peak directly to the east. **Stop 4,** road aggregate quarry.

Stop 4. Road Aggregate Quarry

Stop 4 is at a road aggregate quarry set in the Yamhill–Intrusive Domain (Fig. 1 and 3). The quarry provides an excellent exposure of Oligocene gabbro intruding Eocene Yamhill sedimentary strata. The rock assemblages are extensively fractured and typify the bedrock supporting this part of the Coast Range.

Oligocene igneous intrusives form erosionally resistant outcrops that tend to support ridge tops and steep hillslopes. Soil in this part of the Coast Range constitutes part of the Valsetz-Yellowstone complex, characterized by Inceptisols developed in gravelly diamicton (Knezevich, 1982). Quarry-wall exposures illustrate the high degree of rock weathering that is common in the Coast Range. Examples

of spheroidal weathering are readily evident. Chemical weathering acts on preconditioned joint blocks to create rounded, boulder-like forms. Clay alteration of feldspars results in volume expansion, differential rock stress, and spalling of joint planes (Easterbrook, 1999). The net result is to produce spherically weathered forms. Regolith deposits produced by spheroidal weathering can be misinterpreted as rounded gravel alluvium associated with river transport and represent a potential source of error in interpreting the origin of a geomorphic surface.

49.5 Continue north-northeast on S-Line.
50.4 Note road-maintenance shed on right.
50.6 Turn right (east) onto unnamed logging road; continue past Silver Falls area.
51.1 **Stop 5**, Coast Range drainage divide, overview of Willamette Valley.

Stop 5. Coast Range Drainage Divide

Although just north of the Luckiamute drainage divide, this stop provides a vantage point to view the crest of the Coast Range and mid-Willamette Valley (Fig. 6). Extensive logging and clear-cut forest practices are evident at this stop.

Numerous studies have linked the increased occurrence of landslides and debris flows in the Coast Range to logging and related road construction (Swanson and others, 1977; Ice, 1985; Sidle and others, 1985). Forest practices commonly lead to physical and biological alterations of hillslopes that may contribute to exceedence of landslide thresholds during the winter rain season. Logging-related parameters contributing to slope failure include decreased root strength, decreased evapotranspiration and increased pore pressure, alteration of snow melt patterns, oversteepening of slopes along road cuts, and hydraulic blowouts related to culverts (Robinson and others, 1999).

Stop 5 also provides an opportunity to discuss residuum as a surficial deposit. Residuum is a form of regolith that results from in-place weathering of bedrock with negligible components of downslope transport (Taylor, 1999). Gravel clasts in the regolith at this stop exhibit weathering rinds indicative of in-place chemical alteration, limited transport, and surface stability. Mills and Allison (1995) used clast weathering rinds as a relative dating tool for surficial deposits and as a method to interpret transport processes in colluvium-dominated landscapes. Similar approaches are applicable in the Coast Range.

51.1 Return to Falls City along previous route.
64.3 Falls City town center.
68.7 Turn right (south) onto Kings Valley Highway (Oregon 223).

En Route to Stop 6

The route from this point to Stop 6 is through the Spencer–Valley Fill Domain (Figure 3). The topography of this area is characterized by relatively flat floodplains and terraces punctuated by low-relief, rolling hills supported by the Spencer Formation (Fig. 4). Land use along this part of the route is dominated by agricultural production and local wood-lot management. Fertilizer and pesticide use are primary environmental factors that impact water quality in this part of the watershed. In addition, crop-management practices have profoundly influenced the occurrence and distribution of invasive plant species in the ecosystem.

Crop mapping in the upper Willamette Basin is very useful in estimating mass loading of pesticides and fertilizer compounds in the watershed (Anderson and others, 1997). Grass seed production in the region consumes the most land area and is the agricultural activity associated with highest rates of pesticide application. Atrazine, metochlor, and diuron are herbicides that are most commonly used and detected in water quality samples (Anderson and others, 1997). The drive between Stop 5 and Stop 6 provides an opportunity to view land-use practices in the mid-Willamette Valley and discuss associated environmental impacts.

The Polk County Flora Project at Western Oregon University is a long-term environmental assessment and monitoring program that focuses on native and invasive plant species in the regional ecosystem. The flora project provides a collaborative framework for faculty, students, and the local K-12 education community to conduct botanical surveys using geographic information systems (GIS), global positioning systems (GPS), and internet technologies. Field trip participants are provided an overview of the Polk County Flora Project with demonstrations of related activities.

69.6 Turn left (east) onto Monmouth Road, and follow signs toward Monmouth.
76.6 Enter city of Monmouth, turn right (east) onto Main Street.
76.9 Turn right (south) onto Knox Street (Helmick Road), continue south on paved highway.

81.7 **Stop 6**, Helmick State Park.

Stop 6. Helmick State Park

Helmick State Park lies along the lower Luckiamute River and is representative of the mid-Willamette Valley geomorphic setting (Fig. 4). Hillslopes to the north are underlain by sandstone lithofacies of the Spencer Formation. A flight of low- to mid-level fluvial terraces is readily observable as topographic breaks in agricultural fields directly south of the park entrance. These surfaces were mapped as Qtl (low terrace), Qtlm (low to middle terrace), and Qth (high terrace) by Bela (1981). The Luckiamute River is incised 8 to 9 meters below Qtl, the alluvial surface upon which the Helmick State Park facility is constructed. Suspended-sediment transport dominates this lower part of the Luckiamute, in marked contrast to the gravel-dominated reaches observed upstream at Stops 1 and 3.

The U.S. Geological Survey maintains the Suver stream gauging station at this stop (USGS Station 14190500). Historic river discharge and stage data form the basis for floodplain management in the Willamette Valley. The Suver station record extends back to 1941, for a total of 60 years of continuous river discharge monitoring. Kochel and Baker (1988) discussed the statistical limitations associated with relatively short duration gauge records, and promoted the use of paleohydrology as a method to extend such records back in time. Paleohydrology involves a series of geomorphic and quantitative techniques that are used to reconstruct prehistoric river conditions (for example, peak discharge and maximum flood stage) from preserved flood deposits. Slackwater deposits are typically composed of fine-grained suspended sediment that is deposited under low-flow velocities during overbank flood events. Slackwater sediment is preserved in sheltered low-energy areas along valley bottoms and provides a record of maximum flood stage. High-water levels can then be incorporated into slope-area equations to determine flood discharge. Field trip participants are afforded an opportunity to inspect the gauging station, examine historical discharge data, and reconstruct stages of past flood events.

The stop at Helmick State Park also provides an opportunity to examine the interaction between anthropogenic disturbance, geomorphic process, and distribution of invasive plant species. Agricultural lands and flood-disturbed zones along the mid-Willamette Valley have historically served as corridors facilitating the spread of invasive plant species throughout the region. The riparian zone and abandoned railroad grade directly north of the state park offer exceptional opportunities for identification of the species listed in Table 3, and for down-basin comparison to those observed at the Black Rock locality (Stop 3).

81.7 Continue south on Helmick Road.
83.8 Intersection of Helmick Road with Oregon 99W, continue south on 99W.
87.4 Turn right (west) onto Coffin Butte Road.
87.5 **Stop 7,** Coffin Butte Landfill.

Stop 7. Coffin Butte Landfill

Coffin Butte Landfill is an Environmental Protection Agency (EPA) Subtitle D refuse disposal facility that is operated by Valley Landfills Inc., of Corvallis. The landfill occupies approximately 700 acres of the former Camp Adair Army Training Facility. Active disposal cells are located at the head of an unnamed tributary to the Luckiamute, in a topographic saddle between Poison Oak Hill and Coffin Butte (Fig. 1 and 2). The unnamed tributary and associated wetlands drain eastward toward the E.E. Wilson National Wildlife Refuge. Hillslopes to the north and south of the facility are underlain by fractured and faulted oceanic basalt of the Siletz River Volcanics (Fig. 3). Basaltic lithofacies are overlain by 10 to 20 m of Pleistocene terrace gravel (Fig. 4).

Coffin Butte is the second largest landfill in Oregon with disposal rates ranging from 1200 to 1700 tons per day (Valley Landfills, personal communication). The refuse-disposal cells are designed as a series of stacked, interlocking subunits with a multiple-layer synthetic liner system. Environmental controls in the liner system include impermeable membranes, leachate recovery and leak detection, secondary containment, and methane extraction. A multilevel groundwater monitoring system is employed for leak detection, water quality compliance, and prevention of offsite contaminant migration. In addition, the Coffin Butte facility is equipped with an on-site waste water treatment plant and methane-based electrical generator (Valley Landfills, unpublished document). Field trip participants are presented an overview of landfill design technology, leachate chemistry, and water quality monitoring systems.

87.5 Continue west on Coffin Butte Road.
88.3 Turn left (south) onto Soap Creek Road.

Table 4. Field chemistry of Sulphur Springs and upper Soap Creek at Stop 8. Explanation of units: µS = microSiemens, SU = Standard pH units, mV = millivolt, ppm = parts per million.

Field parameter	Sulphur Springs	Soap Creek
Conductivity (µS/cm)	371	104
pH (SU)	6.7	7.3
Eh (mV)	-287	137
O_2(ppm)	1.2	10.0
CO_2(ppm)	15.0	4.0
Sulfide (ppm)	1.0	0.2
Total hardness (ppm)	280	90

89.0 Cross intersection with Tampico Road, continue straight (south) on Soap Creek Road.
92.6 Note historic Soap Creek School on left (east).
93.9 Turn right onto Sulphur Springs Road, continue straight on gravel portion.
94.1 **Stop 8**, Sulphur Springs (Baker Creek). Note footbridge and pullout on left.

Stop 8. Sulphur Springs (Baker Creek)

Stop 8 includes visits to two sites. The first is to the Sulphur Springs discharge point along the upper reaches of Soap Creek, and the second is to a mesoscale landslide site along Baker Creek (Fig. 1 and 2).

Sulphur Springs is a low-discharge spring located on the north bank of Soap Creek, directly upstream from the confluence with Baker Creek. Sulphur Springs was a popular recreation area in the late 1800s and early 1900s. Today the site constitutes part of the Oregon State University Research Forest facility. The spring emanates from a veneer of valley-bottom alluvium, overlying hydrothermally altered basalt of the Siletz River Volcanics (Fig. 3). The Siletz River Volcanics are highly fractured and associated with significant zeolitization. Zeolites are a group of hydrous-silicate minerals that commonly occur as secondary deposits in association with low-grade alteration. Water chemistry of Sulphur Springs was compared to that of Soap Creek using a basic set of field parameters, the results of which are shown in Table 4.

Field data suggest that water emanating from Sulphur Springs is strongly reducing and oxygen deficient compared to that of Soap Creek. Stagnant water surrounding the spring also displays active bubble release and gas discharge. The working hypothesis is that the gas discharge is generated by anaerobic bacteria in the form of hydrogen sulfide (H_2S) and methane (CH_4). The sulfur is likely derived from groundwater leaching of disseminated pyrite in the altered Siletz River Volcanics. Sulfate (SO_4^{-2}) is in turn converted to sulfide (S^{-2}) by bacteria under reducing conditions, with subsequent release of hydrogen sulfide (H_2S) gas. The methane (CH_4) forms from bacterial decay of organic matter in near-surface, oxygen-deficient water at the Sulphur Springs site. Field trip participants will be afforded an opportunity to directly measure a suite of field parameters, examine additional laboratory data, and formulate reactions that address the influence of bedrock geology on the geochemistry of surface water in the Luckiamute drainage.

The Baker Creek Landslide is 0.5 km south of the confluence between Baker Creek and Soap Creek (Fig. 2). The trail starts at the wooden footbridge and follows an abandoned forest road that was used for logging-related activities at McDonald Forest. The landslide scar disrupts the trail and is readily evident.

The landslide initiated on the fill-slope portion of the forest road and lies at the base of a zero- to first-order tributary draining from the adjacent hillslope to the east. The fresh nature of the scar (Fig. 7), sparse vegetative cover, and presence of invasive plant species (Table 3) suggest that the slope failed during a winter rainfall event within the past several years. Geometric analysis of the landslide scar yields a total transport volume of 750 to 800 m^3, the bulk of which is preserved as hummocky topography along the floodplain of Baker Creek. A complex motion of slide and flow is indicated by the presence of intact road base partially mixed with other debris. The landslide mass has in turn constricted the valley bottom, providing optimal conditions for beaver dam construction, ponding, and significant alteration of the hydrologic regime (Fig. 7).

Swanson and others (1990) emphasized the importance of ecologic links between geomorphic process, landforms, biotic systems, and forest-management practices in mountainous watersheds of the Pacific Northwest. Landslides represent a vegetative-disturbance regime that effect soil substrate conditions, nutrient availability, canopy shading (solar influx), riparian hydrology, and fish habitats.

Figure 7. Fresh landslide scar and deposits at Stop 8 along Baker Creek. Note constriction of valley bottom and beaver-dam ponding of drainage. View is from slide scar looking down gradient at snow-covered colluvial deposits.

Opening of the forest canopy by geomorphic disturbance results in extensive development of understory vegetation and multilayered forests (Swanson, 1980). A disturbed regolith provides germination sites for a wide variety of shade-intolerant native and nonnative species (Pabst and Spies, 1998). Flood disturbance of bottom land results in similar vegetative response along floodplain and channel zones (Hupp, 1988). An anthropogenic overprint is added to the system in the form of forest road construction which dramatically alters hillslope hydrology and increases the frequency of slope failure (Montgomery, 1994; Wemple and others, 2000).

The Baker Creek Landslide site provides an excellent mesoscale example of complex process-response between geomorphic and biotic system variables. The following is a summary of system interactions. The forest road was constructed by cut-and-fill methods along the lower segment of a hillslope adjacent to Baker Creek. A culvert was installed at the landslide site to divert water from the low-order hollow to the east. Surface and subsurface water accumulated at the culvert during a high-magnitude rainfall event. Increased pore pressure and the saturated weight of the road fill resulted in slope failure and mass transport to the valley bottom. Constriction of the floodplain provided optimal conditions for subsequent beaver-dam construction and alteration of the riparian hydrology. Beaver ponds dramatically decreased average daily discharge of Baker Creek, altering sedimentation patterns, channel geometry, and displacing the riparian habitat under saturated soil conditions (after Gurnell, 1998). Opening of the forest canopy resulted in the demise of shade-intolerant understory vegetation and incursion of nonnative plant species. The patchwork of

geomorphically disturbed hillslopes and valley bottoms in the Oregon Coast Range acts as a conduit for the dispersal of invasive species. The Baker Creek Landslide site represents one of thousands of similar localities in western Oregon and provides a model for the complex interaction between multiple physical and biological factors.

94.1 Return east on Sulphur Springs road.
94.3 Continue straight at turn-off to Soap Creek Road, toward top of ridge.
95.5 Lewisburg Saddle (Oregon State University, MacDonald Experimental Forest).
97.0 Turn left (east) onto Lewisburg Avenue.
98.1 Turn right (south) onto Oregon 99W, follow signs to Corvallis.
101.5 Return to OSU CH2M Hill Alumni Center.

CONCLUSION

The Luckiamute Watershed provides a platform from which to study integrated environmental systems in western Oregon. Active tectonics, extreme precipitation patterns, dynamic geomorphic systems, and intensive land use result in complex interactions between physical and biological components. The field stops and discussions provided in this guide represent a starting point from which science educators can incorporate integrated natural science curricula into their respective classrooms. The pursuit of such endeavors will be necessary to prepare scientifically literate citizens to make informed decisions about complex environmental-resource issues in the 21st Century and beyond.

ACKNOWLEDGEMENTS

The 2001 Environmental Science Institute (ESI) at Western Oregon University was sponsored by the College of Liberal Arts and Sciences, Division of Extended Programs, and the Oregon Collaborative for the Excellence in Preparation of Teachers (OCEPT). OCEPT is a science-education grant initiative in the state of Oregon hosted by Portland State University and sponsored by the National Science Foundation. Additional funding for field equipment was provided by the PT3 Project (Preparing Tomorrow's Teachers to Use Technology) at Western Oregon University, a campus-wide enterprise supported by the U.S. Department of Education. The M.J. Murdock Trust Partners in Science Program funded a portion of Taylor's work. Jeff Myers is acknowledged for his contributions to the Environmental Science Institute program and development of the paleoclimatology course module. Jeff Templeton, George Moore, and Ellen Moore graciously reviewed draft versions of the manuscript.

REFERENCES

Adams, 1984 , Active deformation of the Pacific Northwest continental margin: Tectonics, v. 3, p. 449-472.

Anderson, C.W., Wood, T.M., and Morace, J.L., 1997, Distribution of dissolved pesticides and other water quality constituents in small streams, and their relation to land use, in the Willamette River Basin, Oregon, 1996: U.S. Geological Survey Water-Resources Investigations Report 97-4268, 87 p.

Balster, C.A., and Parsons, R.B., 1966, A soil-geomorphic study in the Oregon Coast Range: Oregon Agricultural Experiment Station Technical Bulletin 89, 35 p.

Balster, C.A., and Parsons, R.B., 1968, Sediment transportation on steep terrain, Oregon Coast Range: Northwest Science, v. 42, p. 62-70.

Bela, J.L., 1981, Geology of the Rickreall, Salem West, Monmouth and Sidney Quadrangles, Marion, Polk, and Linn Counties, Oregon: Oregon Department of Geology and Mineral Industries, Geologic Map Series, GMS 18, scale 1:24,000.

Darienzo, M.E., and Peterson, C. D., 1990, Episodic tectonic subsidence of late Holocene salt marshes, northern Oregon, central Cascadia margin: Tectonics, v. 9, p. 1-22.

Easterbrook, D.J., 1999, Surface processes and landforms: Upper Saddle River, New Jersey, Prentice Hall, 546 p.

Franklin, J.F., and Dyrness, C.T., 1988, Vegetation of Oregon and Washington, second edition: Corvallis, Oregon State University Press, ed. 2, 216 p.

Gresswell, S., Heller, D., and Swanston, D.N., 1979, Mass movement response to forest management in the central Oregon Coast Ranges: U.S. Forest Service Pacific Northwest Experiment Station, Resource Bulletin PNW-84, 26 p.

Gurnell, A.M., 1998, The hydrogeomorphological effects of beaver dam-building activity: Progress in Physical Geography, v. 22, p. 167-189.

Hupp, C.R., 1988, Plant ecological aspects of flood geomorphology and paleoflood history, in Baker, V.R., and others, eds., Flood Geomorphology: New York, John Wiley and Sons, p. 335-356.

Ice, G., 1985, Catalog of landslide inventories for the northwest: National Council of the Paper Industry for Air and Stream Improvement, New York, Technical Bulletin 456, p. 87-102.

Kelsey, H. M., Engebretson, D. C., Mitchell, C. E., and Ticknor, R. L., 1994, Topographic form of the Coast Ranges of the Cascadia Margin in relation to coastal uplift rates and plate subduction: Journal of Geophysical Research, v. 99, p. 12,245-12,255.

Knezevich, C.A., 1975, Soil survey of Benton County Area, Oregon: U.S. Department of Agriculture, Soil Conservation Service, 119 p.

Knezevich, C.A., 1982, Soil survey of Polk County, Oregon: U.S. Department of Agriculture, Soil Conservation Service, 250 p.

Kochel, R.C., and Baker, V.R., 1988, Paleoflood analysis using slackwater deposits, *in* Baker, V.R., and others, eds., Flood Geomorphology: New York, John Wiley and Sons, p. 357-376.

McDowell, P. F., 1991, Quaternary geology of the Pacific margin—Willamette Valley, *in* Morrison, R. B., Quaternary nonglacial geology; Conterminous U.S.: Geological Society of America Geology of North America, v. K-2, p. 141-214.

Mills, H.H., and Allison, J.B., 1995, Weathering rinds and the evolution of piedmont slopes in the southern Blue Ridge Mountains: Journal of Geology, v. 103, p. 379-394.

Mitchell C.E., Vincent P., Weldon, R.J., II, and Richards M.A., 1994, Present-day vertical deformation of the Cascadia Margin, Pacific Northwest, United States: Journal of Geophysical Research, v. 99, p. 12,257-12,277.

Montgomery, D.R., 1994, Road surface drainage, channel initiation, and slope instability: Water Resources Research, v. 30, p. 1925-1932.

Montgomery, D.R., Abbe, T.B., Buffington, J.M., Peterson, N.P., Schmidt, K.M., and Stock, J.D., 1996, Distribution of bedrock and alluvial channels in forested mountain drainage areas: Nature, v. 381, p. 587-589.

Myers, J.A., Kester, P.R., and Retallack, G.J., 2002, Paleobotanical record of Eocene-Oligocene climate and vegetational change near Eugene, Oregon: Oregon Department of Geology and Mineral Industries Special Paper 36.

O'Connor, J.E., Sarna-Wojcicki, A., Wozniak, K.C., Polette, D.J., and Fleck, R.J., 2001, Origin, extent, and thickness of Quaternary geologic units in the Willamette Valley, Oregon: U.S. Geological Survey Professional Paper 1620), 52 p., map scale 1:250,000.

Oregon Department of Forestry, 2000, Western Oregon debris flow hazards maps: Oregon Department of Forestry Special Map Series, scale 1:24,000.

Pabst, R.J., and Spies, T.A., 1998, Distribution of herbs and shrubs in relation to landform and canopy cover in riparian forests of coastal Oregon: Canadian Journal of Botany, v. 76, p. 298-315.

Parsons, R.B., 1978, Soil-geomorphology relations in mountains of Oregon, U.S.A.: Geoderma, v. 21, p. 25-39.

Priest G.R., 1990, Volcanic and tectonic evolution of the Cascade Volcanic Arc, central Oregon: Journal of Geophysical Research, v. 95, p. 19,583-19,599.

Reckendorf, F.F., 1973, Techniques for identifying flood plains in Oregon: Oregon State University PhD Dissertation, 344 p.

Reckendorf, F. F., 1993, Geomorphology, stratigraphy, and soil interpretations, Willamette Valley, Oregon, in Kimble, J.M., ed., Proceedings of the Eighth International Soil Management Workshop: Utilization of Soil Survey Information for Sustainable Land Use: U.S. Soil Conservation Service, p. 178-199.

Rhea S., 1993, Geomorphic observations of rivers in the Oregon Coast Range from a regional reconnaissance perspective: Geomorphology, v. 6, p. 135-150.

Robinson, G.E., Mills, K., Paul, J., Dent, L., and Skaugset, A., 1999, Storm impacts and landslides of 1996: Final Report: Oregon Department of Forestry Forest Practices Technical Report 4, 145 p.

Sidle, R.C., Pearce, A.J., and O'Loughlin, C.L., 1985, Hillslope stability and land use: American Geophysical Union Water Resources Monograph 11, 223 p.

Slack, J.R., Lumb, A.M., and Landwehr, J.M., 1993, Hydro-climatic data network (HCDN): Streamflow data set, 1874-1988: U.S. Geological Survey Water Resources Investigations Report 93-4076, 85 p.

Snavely, P.D., Jr., Wells, R.E., and Minasian, D., 1993, The Cenozoic geology of the Oregon and Washington Coast Range and Road Log: Northwest Petroleum Association 9th Annual Field Trip: U.S. Geological Survey Open-File Report, OFR 93-189, 40 p.

Snavely, P.D., Jr., and Wells, R.E., 1996, Cenozoic evolution of the continental margin of Oregon and Washington, in Rogers, A.M., and others, eds., Assessing and reducing earthquake hazards in the Pacific Northwest: U.S. Geological Survey Professional Paper 1560, p. 161-182.

Stiling, P.D., 1998, Ecology: Theories and applications: Upper Saddle River, N.J., Prentice Hall, ed. 3, 638 p.

Strahler, A.N., 1957, Quantitative analysis of watershed geomorphology: American Geophysical Union Transactions, v. 38, p. 913-920.

Swanson, F.J., 1980, Geomorphology and ecosystems, in Waring, R.W., ed., Forests: Fresh perspectives from ecosystem analysis: Oregon State University, Proceedings of the 40th Annual Biology Colloquim, p. 159-170.

Swanson, F.J., Franklin, J.F., and Sedell, J.R., 1990, Landscape patterns, disturbance, and management in the Pacific Northwest, USA, *in* Zonneveld, R.S., and Forman, R.T., eds., Changing landscapes: An ecological perspective: New York, Springer-Verlage, p. 191-213.

Swanson, F.J., Swanson, M.M., and Woods, C., 1977, Inventory of mass erosion in the Mapleton Ranger District, Siuslaw National Forest: U.S. Dept. of Agriculture, Mapleton, Oregon, 75 p.

Taylor, G.H., and Hannan, C., 1999, The climate of Oregon: From rain forest to desert: Corvallis, Oregon State University Press, 211 p.

Taylor, S.B., 1999, Geomorphic controls on sediment-transport efficiency in the central Appalachians: A comparative geomorphic analysis of three watersheds underlain by the Acadian Clastic Wedge: West Virginia University PhD Dissertation, 334 p.

Taylor, S.B., Kite, J.S., and Kuhn, K., 1996, Surficial map criteria for unglaciated humid-mountainous landscapes—linkage of process and landform: An example from the Fernow Experimental Forest, Tucker County, West Virginia: Geological Society of America Abstracts with Programs, v. 28, p. 123.

Urich, M.A., and Wentz, D.A., 1999, Environmental setting of the Willamette Basin, Oregon: U.S. Geological Survey Water-Resources Investigations Report 97-4082-A, 20 p.

Valley Landfills, Inc., unpublished document, Coffin Butte Landfill, Benton County, Oregon, 4 p.

Waichler, S., Chang, S., Gochis, D., Healy, R., Rockhold, M., and Selker, J., 1997, Geography, precipitation, and streamflow of the Luckiamute River Watershed, Oregon: Oregon State University, Bioresource Engineering Department, on line at http://www.fsl.orst.edu/~waichler/lucki/luckihome.htm, updated June 1997.

Walker, G.W., and MacLeod, N.S., 1991, Geologic map of Oregon: U.S. Geological Survey, scale 1:500,000.

Wells, R.E., Engebretson, D.C., Snavely, P.D., and Coe, R.S., 1984, Cenozoic plate motions and the volcano-tectonic evolution of western Oregon and Washington: Tectonics, v. 3, p. 275-294.

Wemple, B.C., Swanson, F.J., and Jones, J.A., 2001, Forest roads and geomorphic process interactions, Cascade Range, Oregon: Earth Surface Processes and Landforms, v. 26, p. 191-204.

Wentz, D.A., Bonn, B.A., Carpenter, K.D., Hinkle, S.R., Janet, M.L., Rinella, F.A., Uhrich, M.A., Waite, I.R., Laenen, A., and Bencala, K.E., 1998, Water quality in the Willamette Basin, Oregon, 1991-1995: U.S.

Geological Survey Circular 1161, on line at http://water.usgs.gov/pubs/circ1161, updated June 25, 1998.

Wohl, E. E., 2000, Mountain rivers: American Geophysical Union Water Resources Monograph 14, 320 p.

Yeats, R.S., Graven, E.P., Werner, K.S., Goldfinger, C., and Popowski, T., 1996, Tectonics of the Willamette Valley, Oregon: U.S. Geological Survey Professional Paper 1560, v. 1, p. 183-222.

Miocene Molluscan Fossils and Stratigraphy, Newport, Oregon

Ellen J. Moore, Department of Geosciences, Oregon State University, Corvallis, Oregon 97331; ellen.moore@cmug.com

George W. Moore, Department of Geosciences, Oregon State University, Corvallis, Oregon 97331; mooreg@geo.orst.edu

INTRODUCTION

This field trip tours from Corvallis in the Willamette Valley west to the Pacific Coast at Newport, Oregon, a distance of 51 miles by highway (Fig. 1). We will inspect some of the Tertiary marine formations and volcanic rocks on the way to the coast and also at it. Of primary importance will be the collecting of Miocene marine mollusks in the Astoria Formation from beach cliffs near the mouth of Wade Creek.

The road log follows the stops in sequence. On May 12, 2002, however, high tide is at 1:42 p.m. Therefore, to precede the tide at Stop 4, we will go directly to the coast, and we will remain until 1:00 p.m. collecting fossils and having lunch at Wade Creek, Stop 4. Then we will visit the inland stops 2, 3, and 1, and return to Corvallis in time for the Convention Welcoming Party.

OVERVIEW OF REGIONAL GEOLOGY

The oldest rocks at Corvallis are the Eocene Siletz River Volcanics, which form the basement under the Tertiary rocks of the Coast Range and the Willamette Valley and crop out in the hills along the northwest side of the city. These volcanics, which formed about 51 million years ago at Corvallis, are composed mostly of basaltic pillows, breccia, and flows.

The hills are bounded by the Corvallis Fault, which passes northeast from just east of Philomath through the town of Lewisburg north of Corvallis. The Corvallis Fault is a major steeply dipping strike-slip and reverse fault that is no longer active. It also extends toward the southwest, and has a total mapped length of 50 km.

Field Guide to Geologic Processes in Cascadia: Oregon Department of Geology and Mineral Industries Special Paper 36, 2002.

The Tyee Formation is the oldest marine sedimentary unit on this field trip. It is middle Eocene west of Corvallis, and deposition began in the early Eocene farther south where the underlying Siletz River Volcanics are older. The Tyee is exposed in cuts along US 20 between Corvallis and Newport. It is about 2,000 meters thick and is composed of regular 1-meter-thick pairs of beds, usually including a thick micaceous fine-grained sandstone bed overlain by a thin carbonaceous siltstone bed.

The Tyee is a flysch deposit formed by turbidity currents, and it generally dips about 15° west. Flute casts are preserved from eroded molds on the underside of some of the coarser beds, and they indicate flow from the present south. But the Tyee Formation contains mica flakes not present in source rocks to the south. The turbidity currents are believed to have flowed from a mica source in metamorphic rocks in Idaho prior to clockwise rotation of the Coast Range by about 70° since the Eocene, as indicated by rotated paleomagnetic pole positions.

Near the coast, the Tyee is overlain by a series of younger sandstone, siltstone, and shale formations of Eocene, Oligocene, and Miocene age. Like the Tyee, these formations dip about 15° west. The westward dip of the west side of the Coast Range occurred rather abruptly near the beginning of the Pliocene Epoch. The cause is uncertain—in one hypothesis, Pliocene subduction understuffed buoyant material along the axis of the Coast Range.

The Tyee Formation is overlain with an angular unconformity by the marine Spencer Formation of late Eocene age, which also in places unconformably overlies the Siletz River Volcanics.

Francis Turner named the Spencer Formation in 1938. It is a marine sedimentary deposit lying under much of the City of Corvallis. The

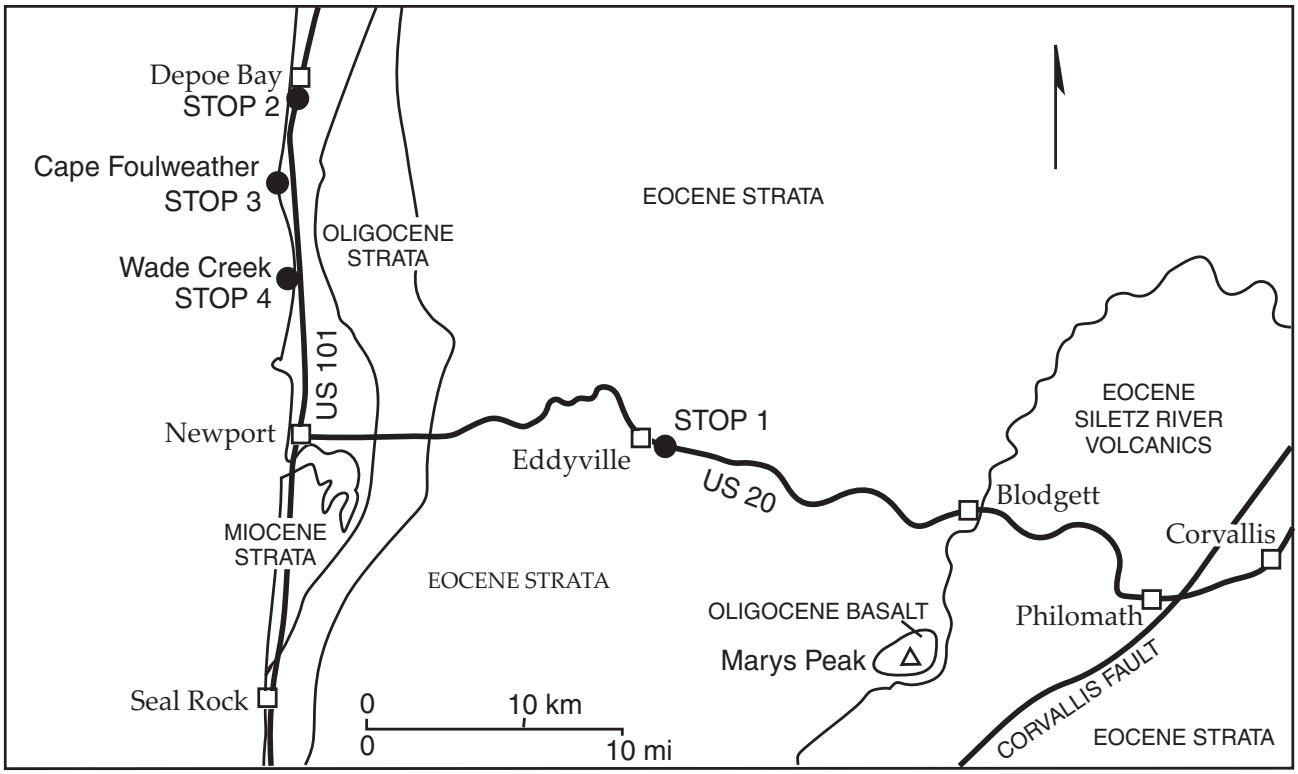

Figure 1. Simplified geologic map of the field-trip area showing the stops.

Spencer is mostly a deeply weathered sandstone with poorly preserved fossil mollusks, such as the bivalves *Corbula, Glycymeris, Pitar,* and *Solen*, and the gastropods *Conus, Crepidula, Ficopsis, and Whitneyella.*

The Spencer is exposed on the west side of the Willamette Valley to about 10 miles south of Eugene.

Mary's Peak, visible to the southwest from Corvallis, and the highest mountain in the Oregon Coast Range (1,249 m; 4,098 ft), is held up by an erosion-resistant basaltic sill of Oligocene age (30 Ma) intruded into the Tyee Formation.

FIELD TRIP

The field trip will begin at the north entrance to the CH2M Hill Alumni Center on the Oregon State University campus in Corvallis at 9:00 a.m. and proceed along US 20 to the coast at Newport. Distances are in miles; rock units in meters.

Road Log

0.0 Proceed south from the north entrance to Oregon State University's CH2M Hill Alumni Center on 26th Street near Western.

0.1 Cross Western Blvd. The Oregon State campus is underlain by sandstone of the late Eocene Spencer Formation. Terrace gravel overlies the Spencer, and that is overlain by the Willamette Silt, deposited by the catastrophic Missoula floods ending about 13,000 years ago. This road intersection has an altitude of 68 meters (224 feet). At its maximum, the water from the floods filled the Willamette Valley to a depth of 100 m (330 ft).

0.3 Turn right (west) on US 20 (Philomath Blvd).

2.1 Cross 53rd Street (stoplight).

3.2 Neabeach Hill to the left (south) is made of the Spencer Formation. The Corvallis Fault, which trends N 30° E, lies just to the northwest beyond the hill.

3.6 Clemens Mill Street to the right (north) lies approximately on the Corvallis Fault. An excellent exposure of the fault appears in the Mid Valley Gravel Quarry, 0.5 mi to the north. The fault is a boundary between the Spencer Formation and seafloor basalt of

Figure 2. Road cut in the Nye Mudstone 2 miles east of Newport on US 20, largely overtaken by vegetation since the photograph was made.

the Siletz River Volcanics, emplaced here during the middle Eocene. The vertical separation is more than 5,000 m (cutting out the intervening Tyee Formation). Slickensides show both dip-slip and left-lateral displacements, and basaltic boulders in the adjacent Spencer indicate that much of the displacement took place during the late Eocene (Goldfinger, 1990). Paleomagnetic pole positions indicate that these rocks have rotated about 70° clockwise since they were formed (Wells and Heller, 1988). Hence, the Corvallis Fault originally trended about N 40° W. It probably was a forearc thrust formed in an oblique subduction regime.

4.1 Sign saying "Welcome to Philomath".
5.0 Center of Philomath, 13th Street.
5.9 Junction where Oregon 34 leaves to southwest; continue west on US 20 to Newport.
6.7 Marys River.
9.8 Outcrop of the Siletz River Volcanics in the roadcut on the left (south)—the best exposure on this route. For the origin of the Siletz River Volcanics, we accept an analogy with the floor of the Gulf of California (Moore, 1984). An original coastal Pacific Northwest pulled away from the Klamath Mountains toward southern Alaska (like Baja California much later pulled away from mainland Mexico), leaving behind a tract of seafloor basalt, the Siletzia Terrane.
10.0 Kings Valley Road.
13.5 Approximate contact between the Siletz River Volcanics and the overlying Tyee Formation, about 2000 m thick, which forms a questa dipping gently toward the west.
14.2 Weigh station at right (north). Marys Peak to left. The hybrid poplar trees here are planted for paper and particle board. Several ages of Douglas fir are visible in former clearcuts.
15.4 Blodgett Country Store, Marys River.
19.9 Benton–Lincoln County line.
21.4 Burnt Woods Store, gasoline.
22.3 Ellmaker State Park, rest rooms.
23.3 Cline Hill Summit, 235 m (770 ft), highest point on this route.
27.5 Typical exposure of the Tyee Formation.
28.3 Slow before the Brush Trail road junction to

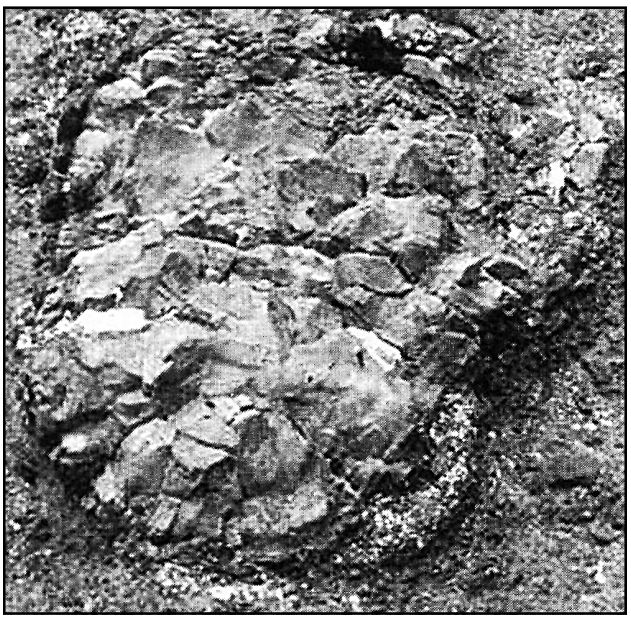

Figure 3. Basalt pillow about 1 meter in diameter exposed just north of the Oregon Coast Aquarium Gift Shop in Depoe Bay.

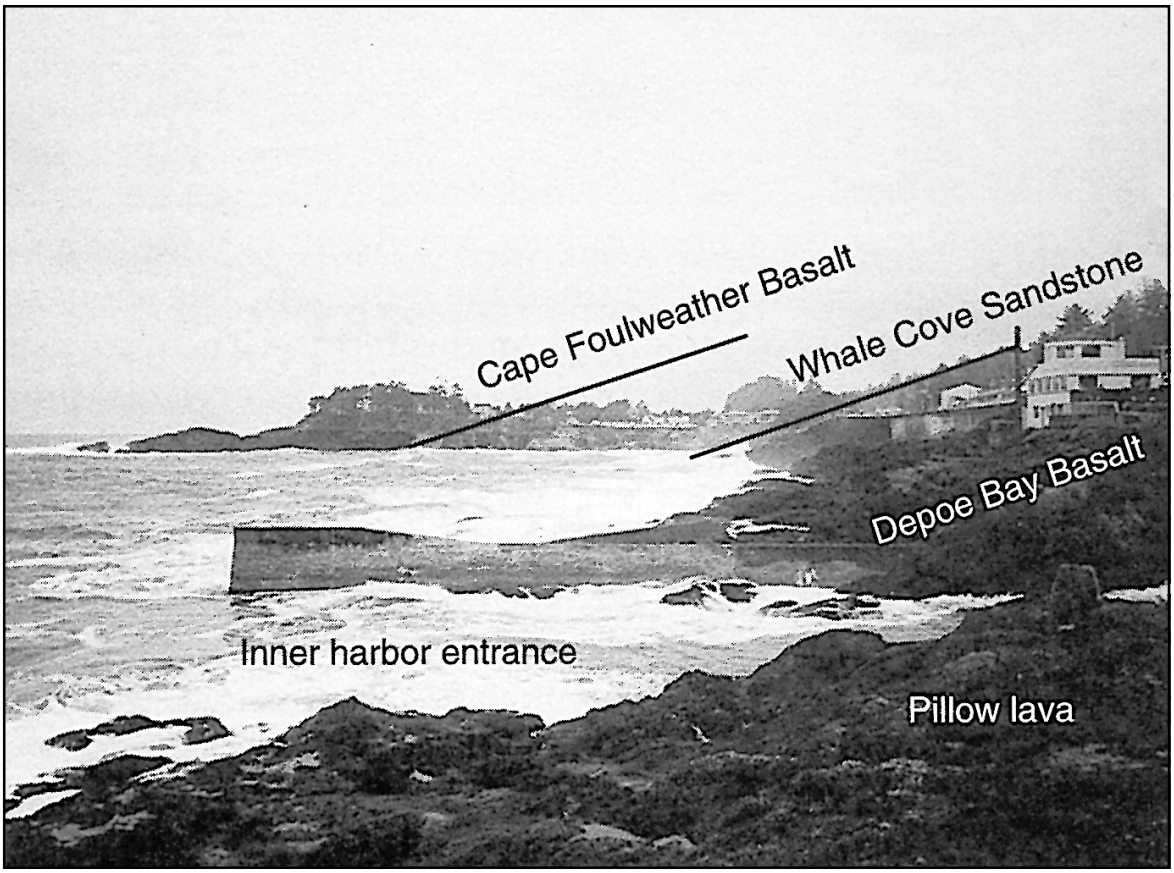

Figure 4. Looking toward the north end of Depoe Bay from the entrance to Depoe Bay's inner harbor, which is a breech through the Depoe Bay Basalt. Three geologic formations dip 15° toward the west, and a fourth, the Astoria Formation, lies out of the photograph to the right below the Depoe Bay Basalt. Erosion has hollowed out the Astoria to form the inner harbor.

the right (north), and park just before the junction. [If stopping from the west, Brush Trail is 2.1 miles from the Yaquina River bridge and railroad crossing at Eddyville. Pull down a sloping road shoulder to a flat area opposite Stop 1's road cut with Brush Trail ahead to the east. Watch for traffic when crossing US 20.]

Stop 1. Tyee Formation.

The outcrop of the marine Tyee Formation just west of Brush Trail was deposited in middle bathyl water depths. The Tyee dips 7° west here, and owing to its generally low west homoclinal dip, it constitutes the bedrock along the highway for 30 miles, approximately to the Toledo Exit. Note the conspicuous mica flakes in the sandstone beds. Five flute casts on the undersides of sandstone beds at this place fan by 40° and have an average azimuth of N 4° E, suggesting downslope flow from the present south on Eocene submarine fans. But paleomagnetic data indicate that these rocks have been rotated 70° clockwise since they were deposited. Therefore, most investigators believe the Eocene flow was from the east.

Molluscan fossils are rare in the Tyee Formation here, because most of them settled out of the turbidity currents farther up the paleoslope. Turner (1938, p.19) reports them in massive sandstone to the present south.

Resume driving west.

29.1 A world-class collection of automobile hubcaps on the building to the north.

30.4 Eddyville, railroad crossing, and Yaquina River. A tall exposure of the Tyee Formation, formerly one of the best, lies just west of

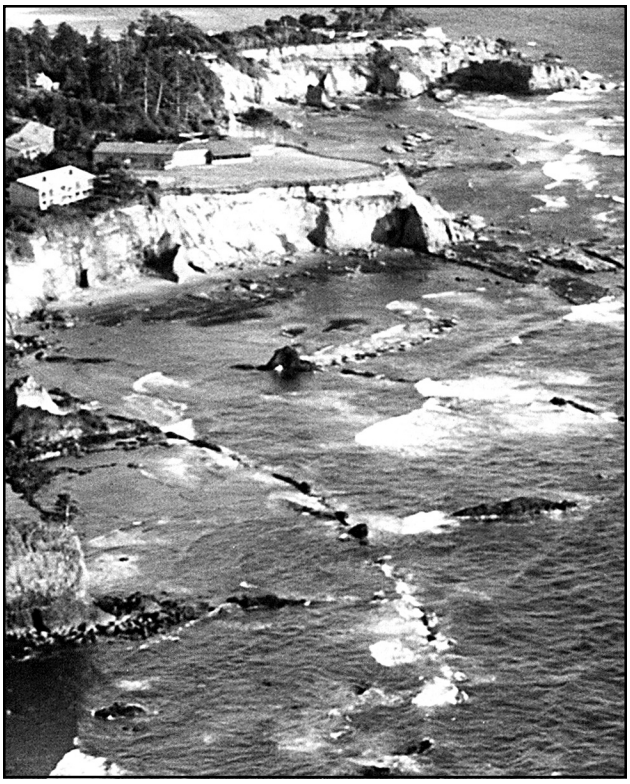

Figure 5. Curved and transverse invasive basaltic dikes exposed at low tide directly south of Cape Foulweather. The dikes penetrated downward into sediment that spread because of loading by the heavy basalt. Sandstone of the Astoria Formation, dipping 15° west, is exposed in the beach cliffs. The overlying Pleistocene terrace is about 80,000 years old.

Eddyville. Now it is nearly obscured by nonnative Scotch broom.

38.2 Elk City road to south.

41.0 Pioneer Mountain summit, 103 m (337 ft).

43.8 Toledo junction, south.

45.6 Siletz junction, north.

49.0 Nye Mudstone on the north side of the highway (Fig. 2). This exposure is now largely taken over by Scotch broom. The Nye Mudstone is well exposed along the north side of Yaquina Bay to the south. It is also exposed in beach cliffs south of Newport, on the ocean shelf beyond the beach at low tide both south and north of Newport, and as small patches of shale in the cliffs along Agate Beach at the north side of Newport. It is of early Miocene age and underlies the early and middle Miocene Astoria Formation. It contains mollusks that are characteristic of the Pillarian Molluscan Stage and the *Vertipecten fucanus* zone named by Warren Addicott (1976).

51.4 Junction of US 20 with US 101 in Newport; turn right (north).

52.0 Stoplight at 11th Street. If you wish to see the Nye Mudstone on your own, you may head west on this street and view it at **Jumpoff Joe**, and also see landsliding there. Take the trail to the beach north of the end of the street, then double back south to Jumpoff Joe. Some investigators say that the Nye Mudstone unconformably underlies the Astoria Formaton at Jumpoff Joe, whereas others say that the stratal disruption at the contact is due to Holocene landsliding.

54.1 Lighthouse Road, Yaquina Head Outstanding Natural Area (fee required), including an excellent interpretive center. The operating lighthouse is open to the public.

57.1 Wade Creek access road and parking. (This will be **Stop 4** on our return south.)

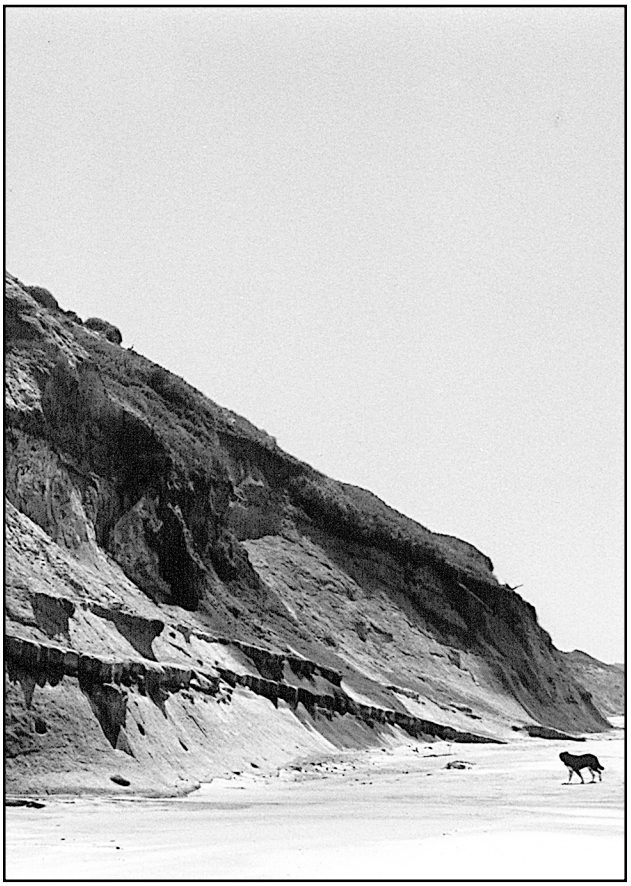

Figure 6. Headland south of Wade Creek exposing the Astoria Formation.

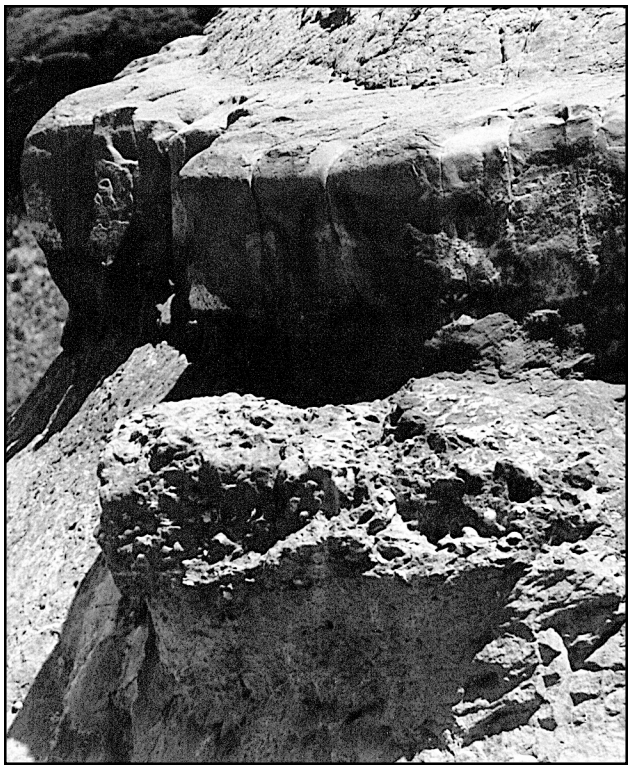

Figure 7. Exposure of the *Anadara* and Barren Layers.

57.7 Beverly Beach State Park. Rest rooms in the Day Use Area.
58.8. Otter Rock. Native rhododendrons.
60.6 Cape Foulweather. (This will be **Stop 3** on our return south.)
64.3 Bridge over harbor entrance to Depoe Bay.
64.4 Oregon Coast Aquarium Store (rest rooms).
64.5 Fisherman's Memorial. The highway has a wide spot here that may permit a U-turn. Otherwise turn right on Clarke Street, to Combs, to Collins, around the block, and back to the highway, to park facing south on US 101 near the Aquarium Store.

Stop 2. Depoe Bay

We will be here for about 1/2 hour. Rest rooms are downstairs in the Oregon Coast Aquarium Gift Shop.

Outside of the low stone wall along US 101 on the west side, just north of the Aquarium Gift Shop, the rocky slope exposes a remarkable display of pillow basalt (Fig. 3). Seawater chilled these sausage or pillow shaped bodies of basalt when they entered the Miocene sea. The basalt, part of the Columbia River Basalt Group, flowed all the way across the state from vents in eastern Oregon and Washington.

Modern wave erosion has cut cross sections through some of these 1 meter basalt pillows to show dull slowly cooled basalt inside. A shiny black 2-cm rind of basalt glass marks the perimeter of each pillow, where the chilling was almost instantaneous.

Four geologic formations are exposed at Depoe Bay, and they dip about 15° toward the sea (Fig. 4). The oldest and most landward is the Astoria Formation, which erosion has hollowed out to make Depoe Bay's inner boat harbor. It is overlain by the Depoe Bay Basalt, which forms a ridge serving as a protective barrier for the boat harbor between US 101 and the shoreline. Above that is the Whale Cove Sandstone, which can be seen as yellow-orange cliffs at the north and south ends of the outer bay. The youngest and most seaward formation is the Cape Foulweather Basalt, which forms

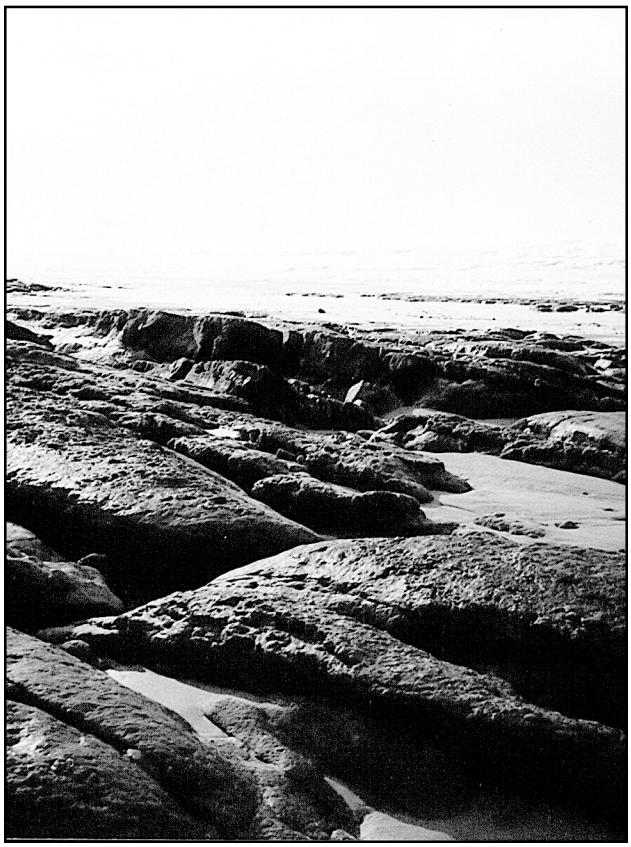

Figure 8. Reefs of the Astoria Formation at Stop 4 during the winter when the beach sand has moved offshore.

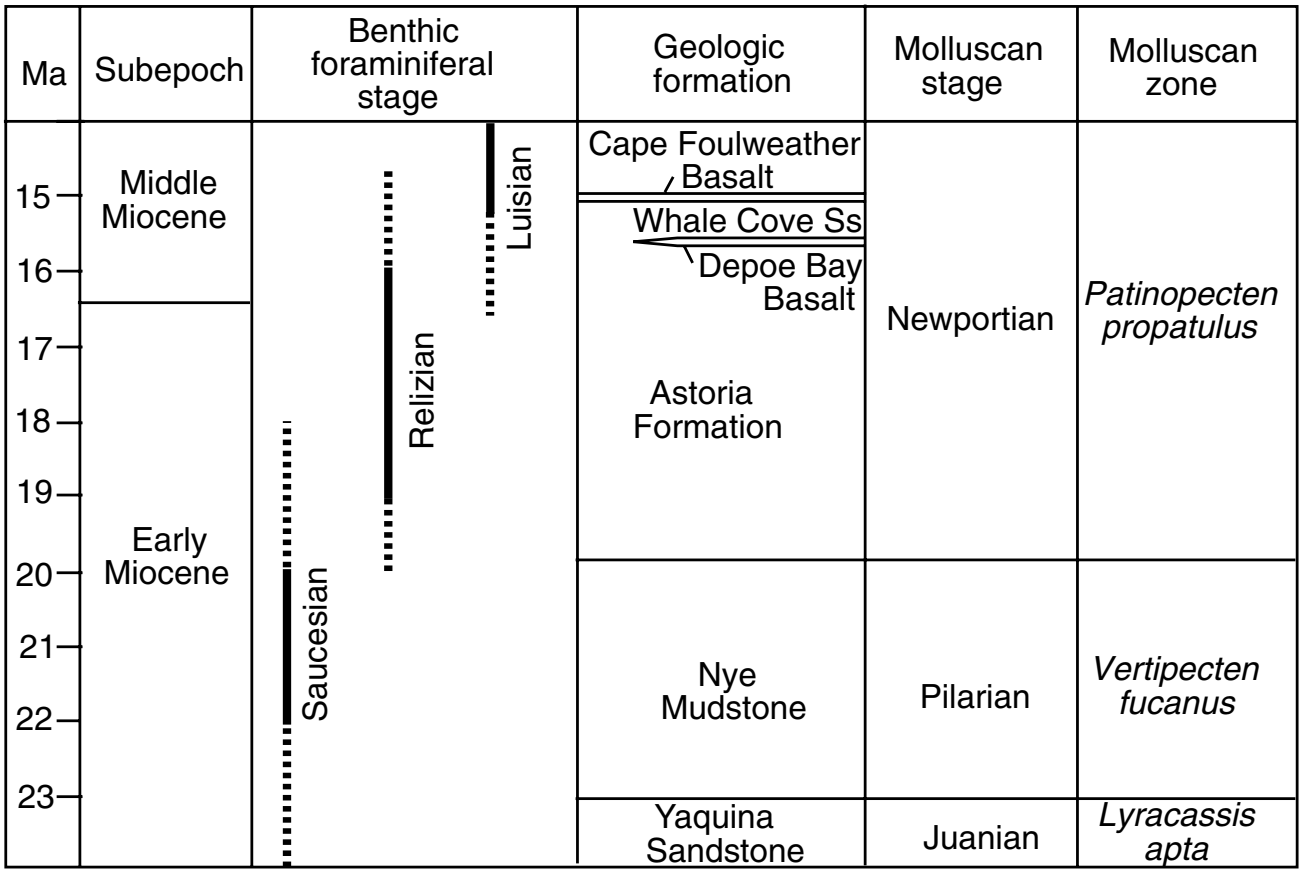

Figure 9. Chronostratigraphic position and correlation of the Miocene Pillarian and Newportian Molluscan Stages. Vertical dashes indicate possible extensions of the foraminiferal stages.

protective capes at the north and south entrances to the outer bay.

You will want to walk south past the Oregon Coast Aquarium Gift Shop to the highway bridge to see the underlying entrance to the harbor—"the smallest harbor in the world". Fishing boats speed toward the blind harbor entrance through heavy swells, blowing their horns to warn other boats not to start out. They then transit the narrow passage through the ridge of Depoe Bay Basalt into the inner harbor.

Two streams drain into the harbor, and their combined flow probably cut the passage through the basalt along a line weakened by a fracture.

Resume the trip by driving back toward the south.

68.3 Take the exit to the right (west) to Cape Foulweather.

68.6 Parking lot at Cape Foulweather.

Stop 3. Cape Foulweather

This will be a brief stop of 15 minutes.

On the south side of the parking lot is a view of curved and transverse invasive dikes exposed at low tide, and the Astoria Formation in the beach cliffs (Fig. 5). The Whale Cove Sandstone is visible from the north window of the gift shop as discontinuous sandstone bodies between the nearly merged Depoe Bay and Cape Foulweather Basalts.

Return to the highway.

68.8 Rejoin US 101 and turn south.

71.6 Entrance to Beverly Beach State Park (rest rooms).

72.3 Wade Creek parking, 0.7 miles south of Beverly Beach entrance road. The access

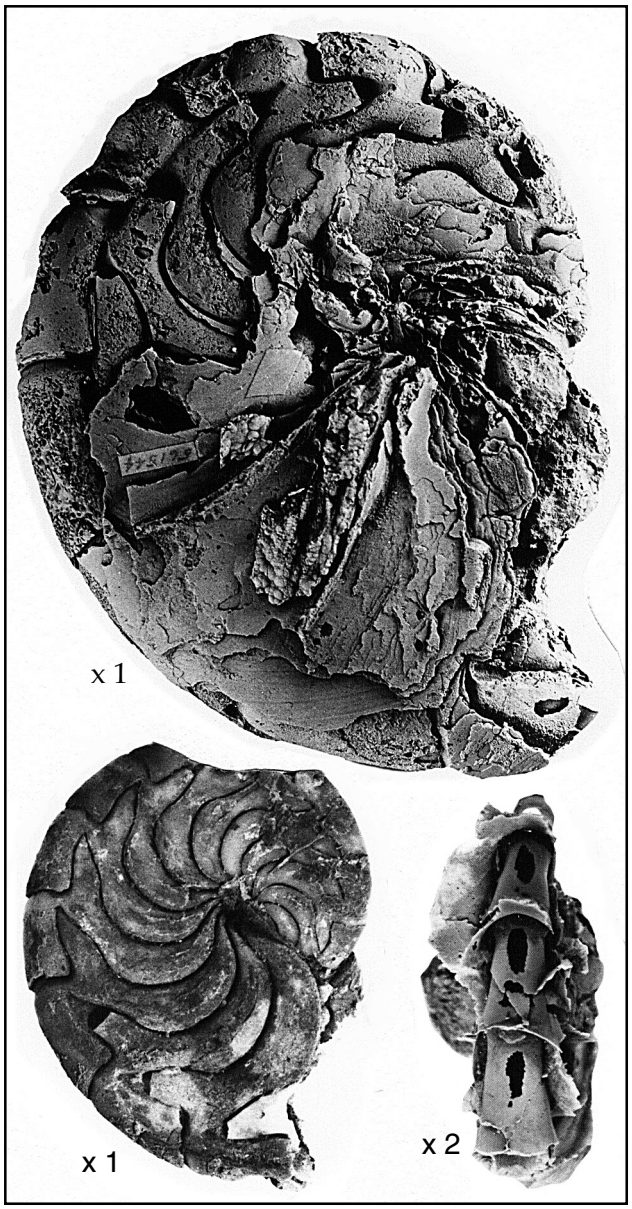

Figure 10. The cephalopod *Aturia angustata* (Conrad) from the Nye Mudstone characteristic of the Pillarian Molluscan Stage and the *Vertipecten fucanus* zone. *Aturia angustata* extends into the lower part of the Astoria Formation, and the species (and genus) became extinct approximately before deposition of the *Anadara* Layer, 17 million years ago.

road to the beach is at the south end of the long parking area.

Stop 4. Wade Creek

From the parking lot, proceed south down the gravel road to the beach and head south for about 150 meters (Fig. 6). Here and farther south you will see the *Anadara* Layer exposed in the Astoria Formation with the Barren Layer directly above it (Fig. 7).

The first fossils were collected from the type area of the Astoria Formation near the old fort at Astoria by John Townsend (1839). A few years later James Dana collected from the same locality. He spent several days in Astoria in 1841 after the shipwreck of the USN *Peacock* on the Columbia Bar during the U.S. Exploring Expedition under Charles Wilkes. Both of these collections were identified by Timothy Conrad (1848, 1849), and they were assigned to the Miocene, which had just been defined by Charles Lyell (1833). Thomas Condon (1880) was the first to apply the name "Astoria shales" to the formation.

Fossiliferous exposures of the Astoria Formation south of the type area are limited almost entirely to the sea cliffs along the Pacific Ocean between Tillamook Bay and Newport. In this distance of about 110 km, the Astoria is only intermittently exposed, much faulted, and repeated in fault blocks that form cliffs. Exposures are commonly interrupted by volcanic rocks and slides. The beds usually dip westward at angles around 15°. The maximum thickness of beds exposed in an uninterrupted section is 190 m, and few exposures are more than a few hundred meters long. Niem and others (1992) show the facies relations of the Astoria Formation in northwestern Oregon.

The strata exposed consist of fine-grained sandstone, siltstone, shale (ranging in silt and sand content), coarse-grained sandstone, conglomerate, and tuff. Silty fine-grained sandstone and calcareous silty shale generally predominate.

The sedimentary rocks in the Astoria Formation range considerably in induration. The well-indurated beds form ledges and cliffs along the coast, and the poorly indurated beds are undercut and often involved in slides. The westerly dip of these beds and the presence of hydroplastic shale in the underlying Nye Mudstone have caused large slides in the Newport area, some of which have destroyed buildings and roads. The exposures in the sea cliffs change in detail every winter from storms and high tides. At low tide, especially in the winter when the sand has moved out, the Astoria Formation is exposed as reefs (Fig. 8).

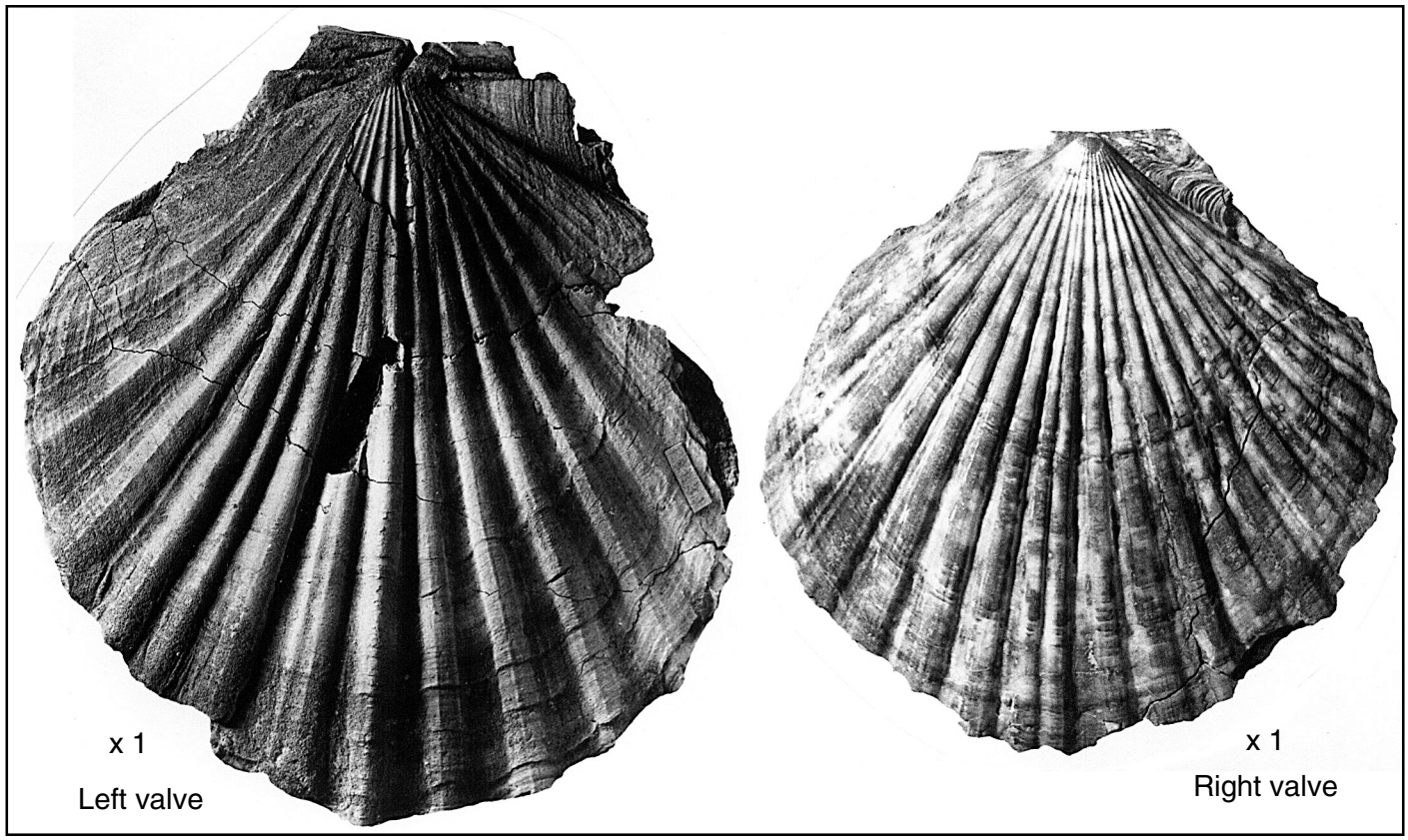

Figure 11. ***Vertipecten fucanus*** **(Dall), zonal fossil for the Pillarian Stage.** ***V. fucanus*** **is distinguished by elevated central and third ribs on the left valve.**

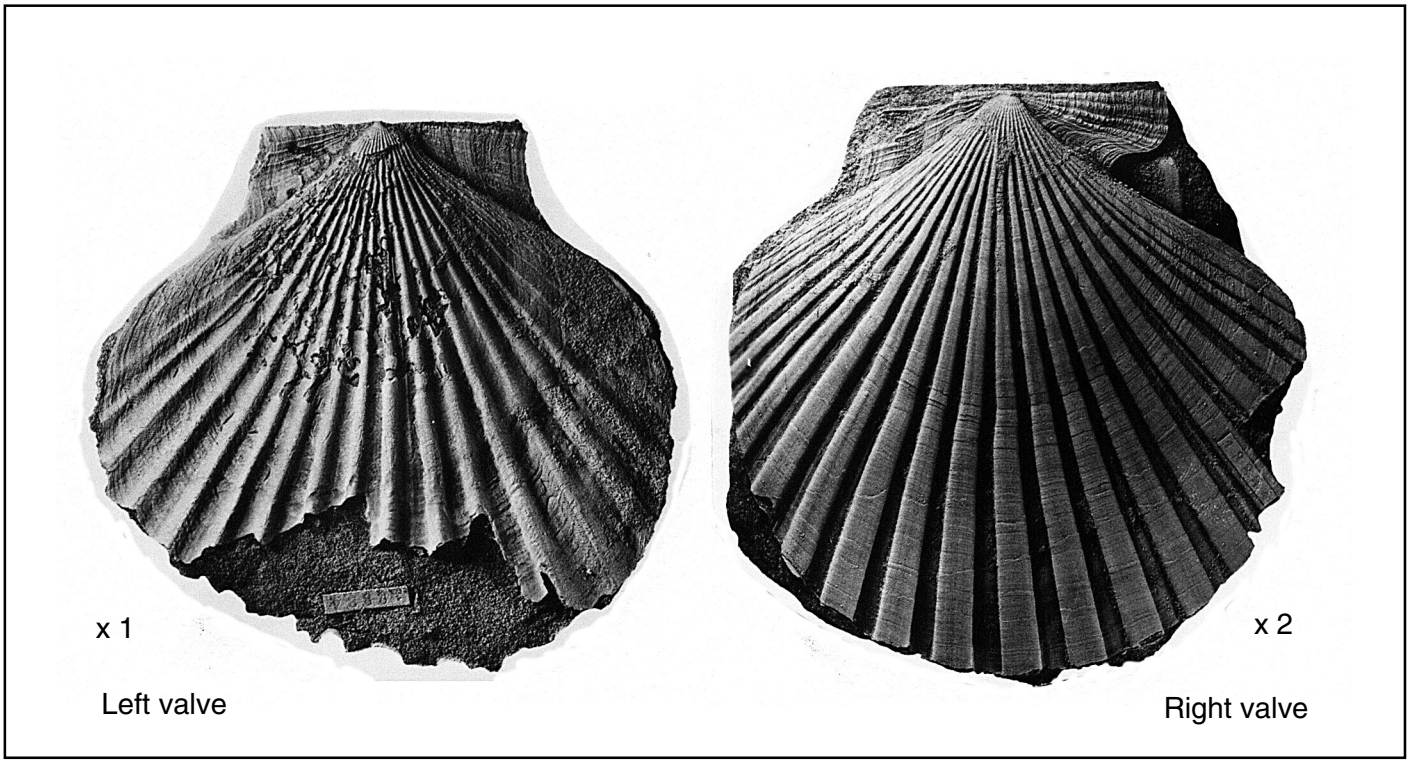

Figure 12. ***Patinopecten propatulus*** **(Conrad), zonal fossil for the Newportian Stage. This species lacks the raised ribs on the left valve that distinguish** ***Vertipecten fucanus*** **of the Pillarian Stage.**

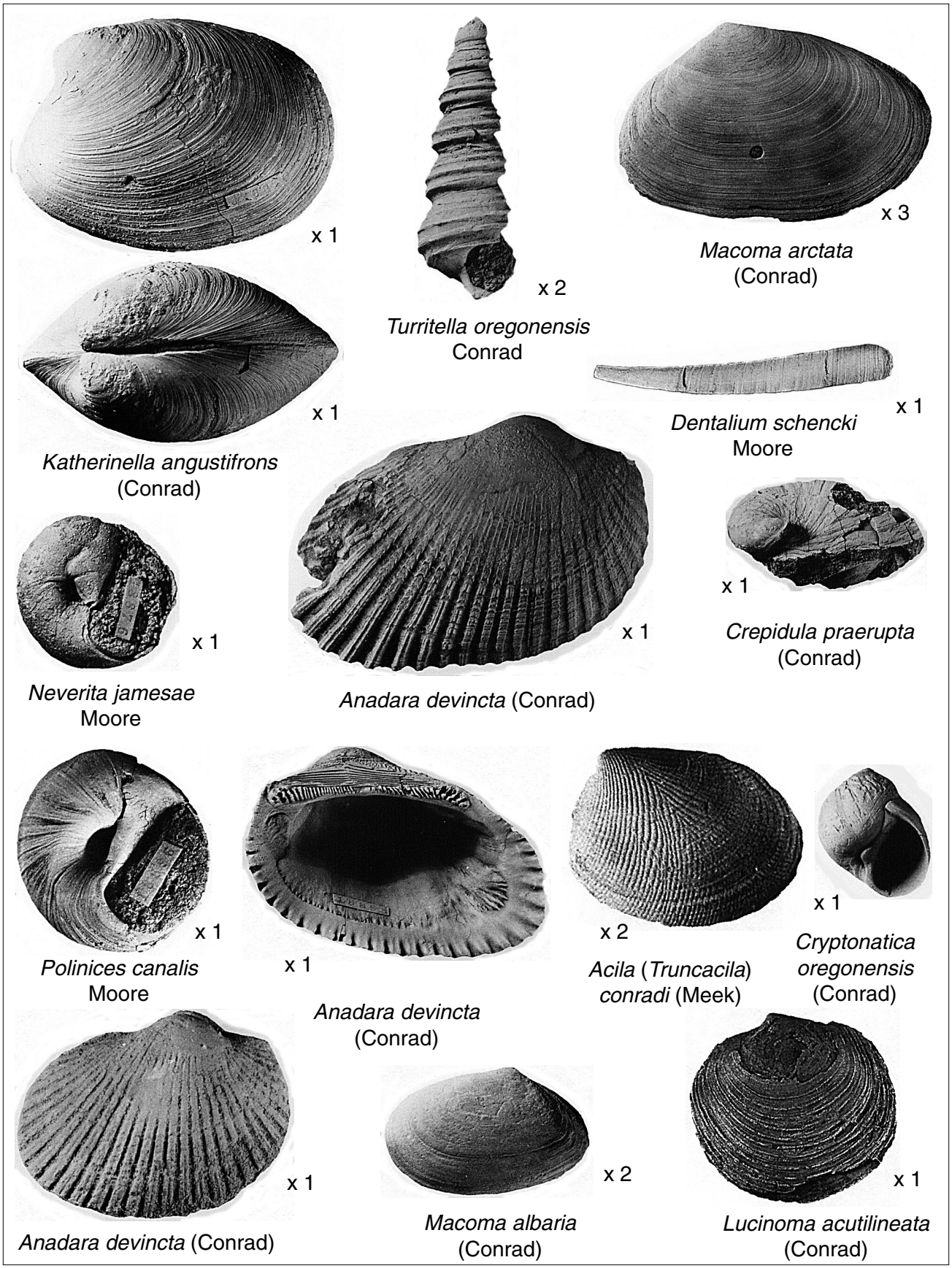

Figure 13. Mollusks from the Astoria Formation characteristic of the Newportian Molluscan Stage and the *Patinopecten propatulus* zone.

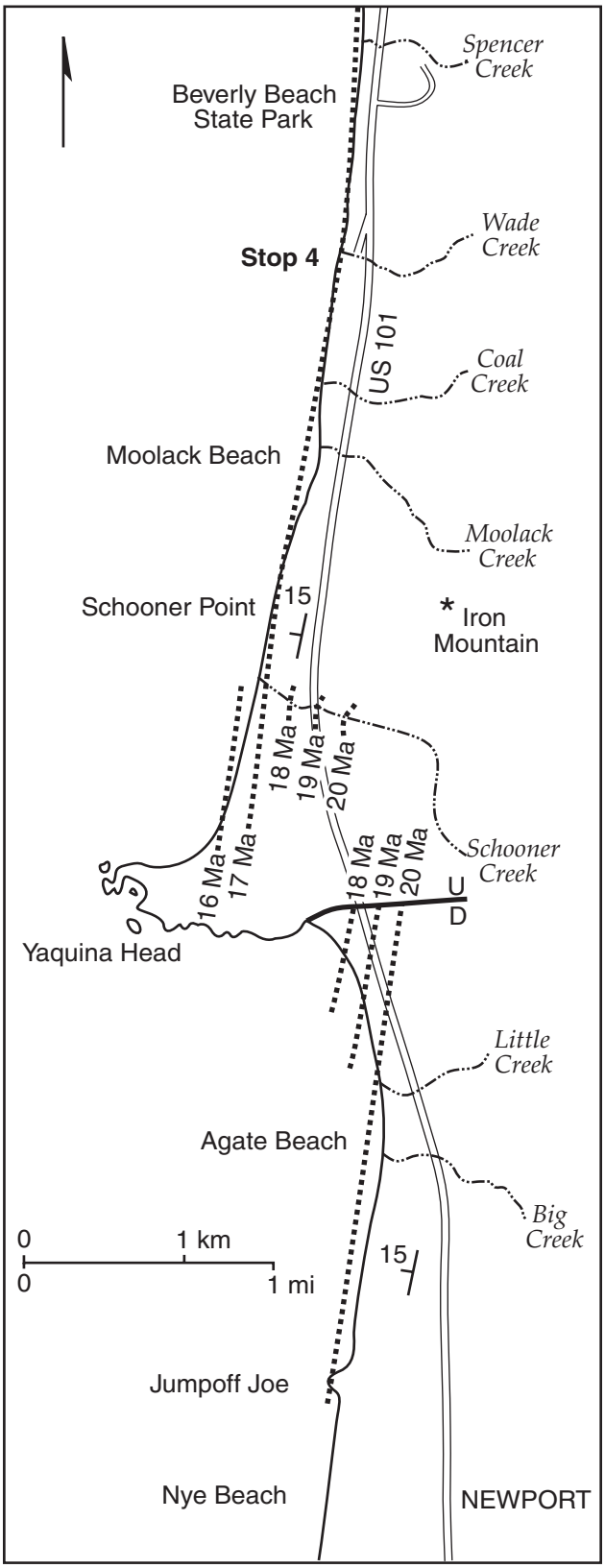

Figure 14. The Newport area showing Stop 4 at Wade Creek. Sedimentary rock ages are in million years ago (Ma). The Nye–Astoria contact is at about 20 Ma, and the *Anadara* Layer at 17 Ma (after Prothero and others, 2001).

In the Newport area, the Astoria Formation rests on the Nye Mudstone and is unconformably overlain by Pleistocene sand (Fig. 9–11).

Joseph Diller (1896) first assigned the rocks near Newport to the Astoria Formation. The geology of this area has since been studied by many geologists. References to most of these papers are cited in Moore (1963, 2000), Snavely and others (1976), and Snavely and Wells (1996).

Stop 4 shows some of the best exposures of the *Anadara* Layer (Moore, 1963, p. 17). It is a sandy siltstone unit 0.3 to 0.6 m thick in which *Anadara devincta* is very abundant, and the clams are so closely packed that they form a traceable layer. This is the most fossiliferous unit seen in the Astoria Formation. It is made up of well-indurated rock and is overlain with slight irregularity by 15 to 60 cm of a dark-greenish-gray silty fine-grained sandstone that is barren of fossils. The bottom contact of the *Anadara* Layer is irregular. The fossils in the *Anadara* Layer are well preserved and were certainly not moved any considerable distance. The shells in this layer are entire, and few shell fragments are present.

Most *Anadara* specimens are mature individuals of similar size, and most are articulated with the shells agape. The shells are not worn, and they usually are not broken. They are filled with sediment, and none are hollow or filled with crystals. The overlying Barren Layer has neither megafossils nor microfossils.

The *Anadara* Layer probably represents a storm deposit with no significant transport. Although it is a death assemblage, most of the specimens are articulated with the valves together, and some valves are closed. A significant number have paired shells that are slightly offset. Sediment compaction may have caused this after the ligaments decayed.

The *Anadara* and Barren Layers perhaps could be explained by a storm (or tsunami) that was so intense it took the sediment and clams into suspension, then allowed them to settle out, with the heavy shells (the *Anadara* Layer) at the base and the silty sandstone of the Barren Layer at the top.

The Astoria Formation belongs to the Newportian Stage. Originally dated as middle Miocene, the Newportian Stage was subse-

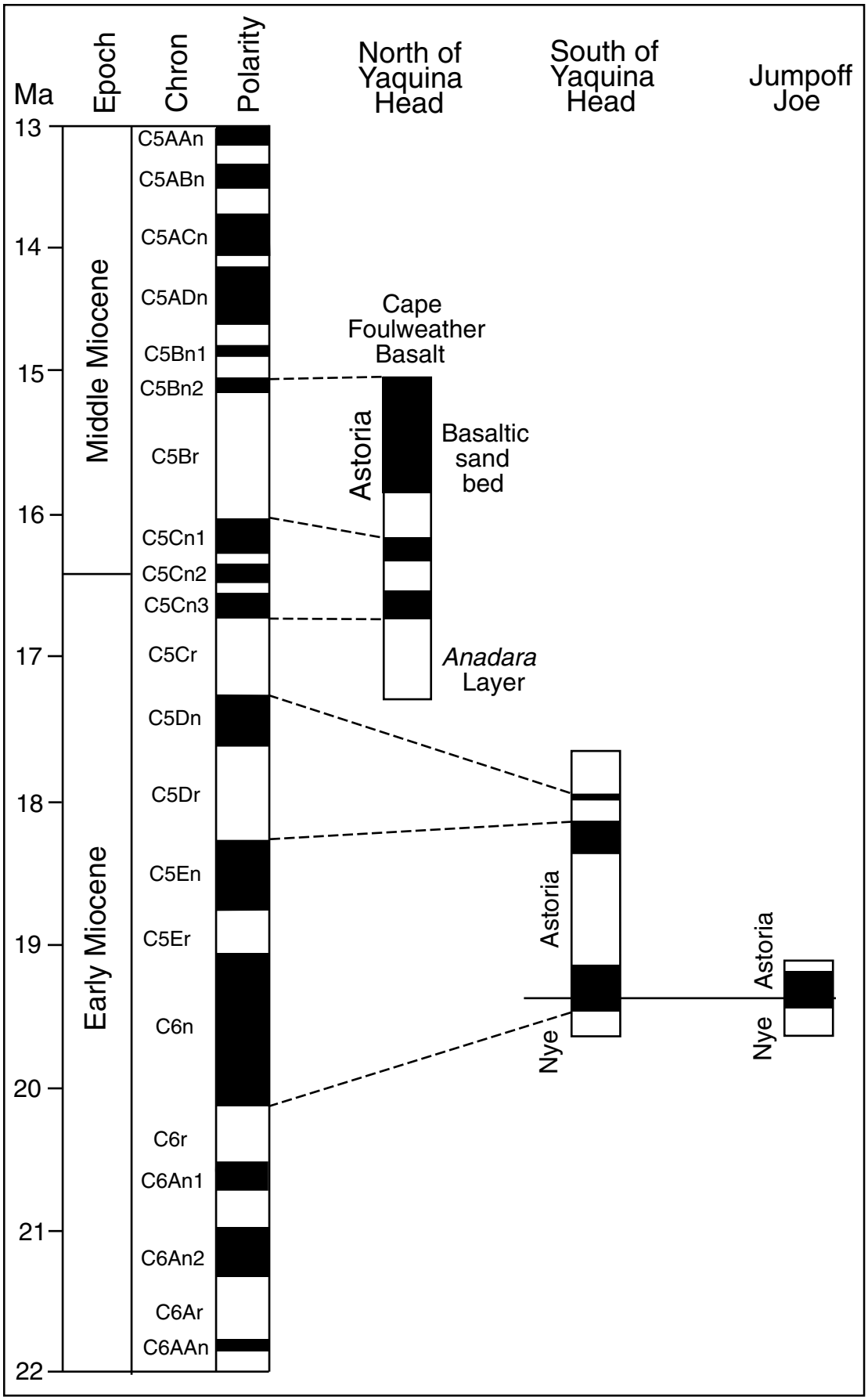

Figure 15. The magnetic polarity time scale of Berggren and others (1995) correlated with the Astoria Formation (after Prothero and others, 2001).

quently revised to include the late early Miocene (Moore and Addicott, 1987). The molluscan zone characteristic of the Newportian is the *Patinopecten propatulus* zone (Fig. 12-13).

Assemblages of Tertiary molluscan fossils generally permit dating to about plus or minus 2 million years. Recently the precision of the dating of the Astoria Formation at Newport was greatly increased by using the molluscan fossils to pin the age to a 4 million year interval, then matching that interval to a paleomagnetic-reversal stratigraphy measured in the rocks (Prothero and others, 2001).

During deposition of the Astoria Formation, the Earth's magnetic field reversed 10 times, as the North Magnetic Pole became the South Magnetic Pole and vice versa. These magnetic fields were naturally recorded by magnetic sand and silt grains in the formation.

We took small oriented rock samples spaced through the Astoria, and their magnetic polarities later were determined by a superconducting magnetometer (Fig. 14). The varied spacings of the normal and reversed rock samples were correlated with the reversal time scale of Berggren and others (1995). On this basis, our understanding of the age of the *Anadara* Layer, for example, was increased ten fold from a former precision of 17 ± 2 million years ago to 17.0 ± 0.2 million years ago (Fig. 15).

While we were preparing this field guide during the Fall of 2001, the Oregon Department of Transportation took positive action to remediate a situation that has plagued it for decades. Directly south of both Wade Creek and our fossil-collecting site, a large landslide was drilled to dewater it (Fig. 16). About 50 gently sloping pipes now drain to the base of the beach cliff from directly under US 101. They don't extend beyond the highway to avoid excessively lowering the landward water table.

Yaquina Head and its lighthouse form the skyline south of our stop. The Cape Foulweather Basalt, which flowed from eastern Oregon before uplift of the Coast Range, makes up the headland. Its 15° west dip can be seen in the profile of the head.

The Cape Foulweather Basalt directly overlies the top of the Astoria Formation at Yaquina Head. A basaltic sandstone with sideritic concretions lies about 50 meters below

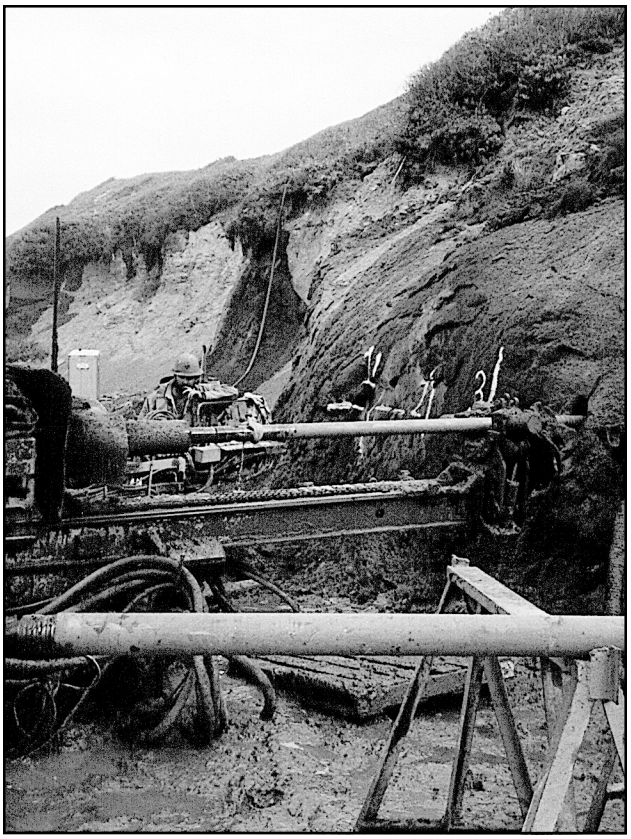

Figure 16. Drilling to dewater a landslide in the Astoria Formation south of Stop 4.

the top of the Astoria on the north side of the head. We think the basaltic sandstone correlates with the Depoe Bay Basalt, which did not reach this place as a flow. Hence the top part of the Astoria Formation at Yaquina Head is correlative with the Whale Cove Sandstone that lies between the Cape Foulweather and Depoe Bay Basalts, where both are present.

A final item of interest is an important fossil mammal locality known as the "Iron Mountain Beds". It is in the Astoria Formation at the beach cliff between our stop and Yaquina Head (Barnes, 1992).

Iron Mountain is an adjacent small prominence east of US 101. It is an invasive basalt body formed by downward lava movement in heavily loaded Astoria sediment. An invasive dike extends from Iron Mountain to the coast, and it makes large blocks on the beach just this side of Schooner Point, the first headland north of Yaquina Head. The blocks are barely visible from our stop.

On each side of the invasive dike, groundwater in the low cliffs has stained red

the (pholad-bored) Astoria Formation and overlying Pleistocene sand. The Miocene fossil mammals, commonly pinniped seals but also including terrestrial mammals, occur between the invasive dike and Schooner Point. They are in concretions in the unstained gray sandstone, and they lie about 20 meters below the 17 Ma *Anadara* Layer, which crops out at Schooner Point.

Consider the rising tide if you plan to make the run to Schooner Point or beyond. Please keep in mind our departure time of 1:00 p.m. at the van, and if you are caught by the tide, climb through a cliff-side yard, and walk along US 101 to the parking lot.

REFERENCES

Addicott, W.O., 1976. Neogene molluscan stages of Oregon and Washington, *in* Fritsche, A.A., ed., The Neogene Symposium; selected papers on paleontology, sedimentology, petrology, tectonics, and geologic history of the Pacific Coast of North America: Society of Economic Paleontologists and Mineralogists, Pacific Section, p. 95-115, 5 pls., 6 figs.

Addicott, W.O., 1977, Neogene chronostratigraphy of nearshore marine basins of the eastern North Pacific, *in* Saito, T., and Ujiie, H., eds., Proceedings of the First International Congress on Pacific Neogene Stratigraphy, Tokyo, 1976, Science Council of Japan: Tokyo, Kaiyo Shuppan C, p. 151-175.

Barnes, L.G., 1992, A new genus and species of middle Miocene enaliarctine pinniped (Mammalia, Carnivora, Otariidae) from the Astoria Formation in Oregon: Natural History Museum of Los Angeles County Contributions in Science, no. 431, p. 1-27.

Berggren, W.A., Kent, D.V., Swisher, C.C., III, and Aubry, M.-P., 1995, A revised Cenozoic geochronology and chronostratigraphy: SEPM Special Publication 54, p. 129-212.

Condon, T., 1880, Corrections of the geological maps of Oregon, *in* Cope, E.D., American Naturalist, v. 14, p. 457-458.

Conrad, T.A., 1848, Fossil shells from Tertiary deposits on Columbia River, near Astoria: American Journal of Science, ser. 2, v. 5, p. 432-433, 14 figs. [*Reprinted in* Dall, W.H., 1909, U.S. Geological Survey Professional Paper 59, p. 150-151].

Conrad, T.A., 1849, Fossils from northwestern America, *in* Dana, J.D., Geology: U.S. Exploring Expedition, 1838-1842, under the command of Charles Wilkes, v. 10, appendix 1, p. 723-728, atlas, pls. 17-21. [*Reprinted in* Dall, W.H., 1909, U.S. Geological Survey Professional Paper 59, p. 152-157].

Diller, J.S., 1896, A geological reconnaissance in northwestern Oregon: U.S. Geological Survey, 17th Annual Report, pt. 1, p. 441-520.

Goldfinger, C., 1990, Evolution of the Corvallis Fault and implications for the Oregon Coast Range: Oregon State University MS Thesis, 129 p.

Lyell, C., 1833, Miocene, *in* Principles of geology: London, John Murray, v. 3, p. 52-55, 57-58.

Moore, E.J., 1963, Miocene marine mollusks from the Astoria Formation in Oregon: U.S. Geological Survey Professional Paper 419, 109 p., 33 pls., 9 figs. [1964].

Moore, E.J., 2000, Fossil shells from western Oregon—A guide to identification: Chintimini Press, Corvallis, Oregon, 131 p., illus.

Moore, E.J., and Addicott,W.O., 1987, The Miocene Pillarian and Newportian (Molluscan) Stages of Washington and Oregon and their usefulness in correlations from Alaska to California: U.S. Geological Survey Bulletin 1664A, p. A1-A-13, 4 pls.

Moore, G.W., 1984, Tertiary dismemberment of western North America: 3rd Circum-Pacific Energy and Mineral Resources Conference Transactions, p. 607-612.

Niem, W.A., Niem, A.R., and Snavely, P.D., Jr., 1992, Western Washington–Oregon coastal sequences; Sedimentary embayments of the Washington–Oregon coast: Geological Society of America Geology of North America, v. G-3, p. 265-270, 314-319.

Prothero, D.R., Bitboul, C.Z., Moore, G.W., and Moore, E.J., 2001, Magnetic stratigraphy of the lower and middle Miocene Astoria Formation, Lincoln County, Oregon, *in* Prothero, D.R., ed., Magnetic stratigraphy of the Pacific Coast Cenozoic: Pacific Section SEPM Society for Sedimentary Geology Book 91, p. 272-283.

Snavely, P.D., Jr., McCloud, N.S., Wagner, H.C., and Rau, W.W., 1976, Geologic map of the Yaquina and Toledo Quadrangles, Lincoln County, Oregon: U.S. Geological Survey Miscellaneous Investigations Map I-867, scale 62,500.

Snavely, P.D., Jr., and Wells, R.E., 1996, Cenozoic evolution of the continental margin of Oregon and Washington: U.S. Geological Survey Professional Paper 1560, p. 161-182.

Snavely, P.D., Jr., MacLeod, N.S., and Rau,W.W., 1969, Geology of the Newport area, Oregon: Ore Bin, v. 31, no. 2-3, p. 25-72.

Townsend, J.K., 1839, Narrative of a journey across the Rocky Mountains to the Columbia River with a scientific appendix: Philadelphia, Henry Perkins, 352 p. [Jobanek, G.A., ed., 1999, Reprint : Corvallis, Oregon State University Press, 290 p.]

Turner, F.E., 1938, Stratigraphy and Mollusca of the Eocene of western Oregon: Geological Society of America Special Paper 10, 117 p., 22 pls.

Wells, R.E., and Heller, P.L., 1988, The relative contribution of accretion, shear, and extension to Cenozoic rotation in the Pacific Northwest: Geological Society of America Bulletin, v. 100, 325-389.

Pleistocene and Holocene Dunal Landscapes of the Central Oregon Coast: Newport to Florence

Curt D. Peterson, Geology Department, Portland State University, Portland, Oregon 97207; petersonc@pdx.edu
Darren L. Beckstrand, Cornforth Consultants, 10250 SW Greenburg Road, Portland, Oregon 97223; dbeckstrand@cornforthconsultants.com
Charley M. Clough, AMEC Earth and Environmental, 7477 SW Tech Center Drive, Portland, Oregon 97223
J. Courtney Cloyd, U.S. Forest Service, P.O. Box 3623, Portland, Oregon 97208; jcloyd@fs.fed.us
Jon M. Erlandson, Anthropology Department, University of Oregon, Eugene, Oregon 97403
Georg H. Grathoff, Geology Department, Portland State University, Portland, Oregon 97207
Roger M. Hart, College of Oceanographic and Atmospheric Sciences, Oregon State University, Corvallis, Oregon 97331
Harry M. Jol, Department of Geography and Anthropology, University of Wisconsin., Eau-Claire, Wisconsin 54702; jolhm@uwec.edu
David C. Percy, Geology Department, Portland State University, Portland, Oregon 97207; bjpd@pdx.edu
Frank F. Reckendorf, Reckendorf and Associates, 950 Market Street NE, Salem, Oregon 97301; frecken.@open.org
Charles L. Rosenfeld, Department of Geosciences, Oregon State University, Corvallis, Oregon 97331; rosenfec@geo.orst.edu
Phyllis Steeves, U.S. Forest Service, 4077 Research Way, Corvallis, Oregon 97333
Errol C. Stock, Griffith University, Brisbane, Queensland 4111, Australia; e.stock@mailbox.gu.edu.au

ABSTRACT

During this 2 day field trip we will traverse the broad dune sheets (0–100 ka in age) that mantle the narrow coastal plain (1–5 km in width) of the central Oregon coast. We will examine interstratified dunal paleosols and redox-boundary hardpans that control cut-slope stability, ephemeral wetlands, groundwater geochemistry, and archaeological site distributions. We will trek across active dunes, overview dunal archaeological sites, interpret ground-penetrating radar profiles, perform paleosol chronosequencing, and collect a thermoluminescence sample for dating.

INTRODUCTION AND BACKGROUND

Sustainable development issues in coastal plains of the West Coast are of increasing interest to growing coastal populations. Narrow coastal plains (1–5 km in width) are largely covered by dune deposits in Washington, Oregon, central California, and Baja California Sur (Fig. 1). Although the dune cover is relatively thin, typically 3-30 m in thickness, it impacts cut-slope stability, surface and groundwater quality, wildlife habitat, and the location of archaeological sites. Regional-scale reexaminations of coastal dunes in western North America are now underway by a large coalition of investigators (http://nwdata.geol.pdx.edu/SeaGrant/index.html).

William Cooper's 1958 and 1967 monographs on coastal eolian dunes of Washington, Oregon, and California completed one of the most comprehensive coastal geologic studies in the Pacific Northwest. From a field program spanning 22 years (1919 through 1941) he formulated creative insights about dune morphology and distribution on the West Coast. Since Cooper's seminal work, the technologies of radiocarbon (RC) dating, thermolumines-

Field Guide to Geologic Processes in Cascadia: Oregon Department of Geology and Mineral Industries Special Paper 36, 2002.

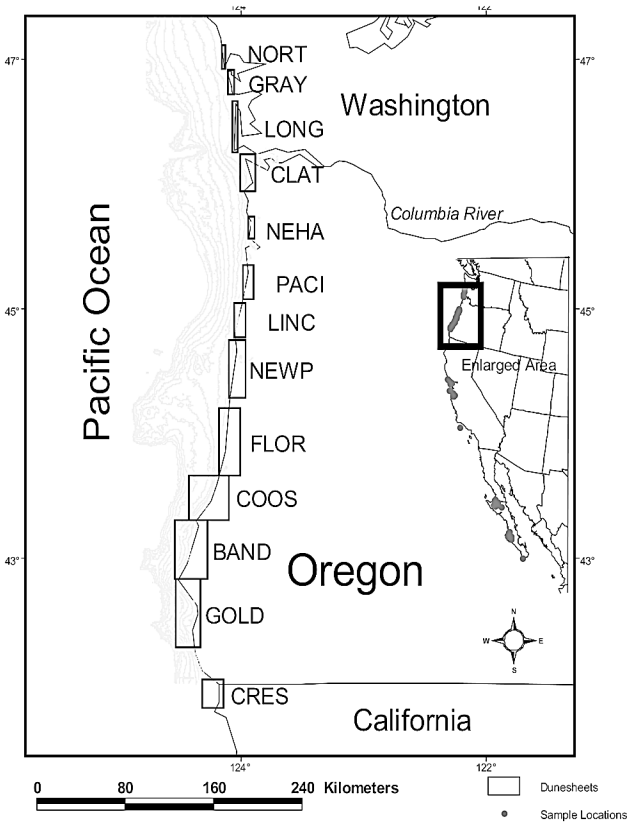

Figure 1. West Coast dune sites where dune dating (radiocarbon and thermoluminescence) is being performed (dots in Washington, Oregon, California, and Baja California Sur). Square boxes represent areas of dunesheet mapping in the Pacific Northwest.

cence (TL) dating, and digital ground-penetrating radar (GPR) have become available to extend our dating and subsurface-imaging capabilities.

Understanding of dunal landscape evolution on the central Oregon coast is also advancing from related studies in other disciplines. The related work includes recent studies of Quaternary sea-level change (Pirazzoli, 1993), coastal neotectonics (Muhs and others, 1992; Ticknor, 1993), coastal paleoclimate (Worona and Whitlock, 1995), and coastal archaeology (Erlandson and others, 1998).

Coastal dune studies in many countries have focused on late Holocene dune development. Dunes originate from posttransgressive remobilization of shelf sand and local redistribution through littoral drift (Pye and Rhodes, 1985; Short, 1987; Tooley, 1990; Illenberger and Verhagen, 1990). Holocene dune fields of the Oregon coast are generally restricted to embayments or the northern ends of littoral cells. Holocene dune ramps that allowed beach sand to reach sea-cliff tops (2–5 ka) are now largely eroded away, leaving unsupported slopes (Fig. 2). Similarly, the ongoing exposure of buried prehistoric forests that colonized middle Holocene wave-cut platforms (Fig. 3) indicate a net loss of sand from some littoral cells in recent time (Hart and Peterson, 1997).

In contrast to the narrowly restricted active dunes, the widespead stabilized dunes of the central Oregon coast originated in late-Pleistocene time (24–100 ka)(Fig. 4). These widespread dune sheets likely migrated onshore from continental-shelf sand exposed to eolian processes during lower sea-level stands (Fig. 1 and 5). Such lowstand origins have been proposed for some pre-Holocene coastal dunes in southern California (Orme, 1990) and Australia (Thom and others, 1994).

The long geologic histories of the Oregon dune sheets have led to interstratified loose sand and cemented paleosols and hardpans (Fig. 6). These different units complicate predictions of dunal slope stability, wetland regulatory status, and groundwater flow in dunal aquifers (Couch and others, 1980; Reckendorf, 1998). The forested dune sheets previously mapped as marine terrace deposits (Schlicker and others, 1973) climb up the foothills to altitudes of 100–150 m at distances of 1–6 km inland from the coast (Fig. 7a,b). Together, the Holocene and Pleistocene dunal landscapes cover about 80 percent of the coastal plain in the Newport and Florence areas.

This guide to a 2 day field trip between Newport and Florence, Oregon (Fig. 8) identifies about 2 dozen roadside stops where earth scientists can address the age, origin, and stratigraphic development of the dunal landscapes along the central Oregon coast. In addition, many of these stops provide critical exposures that prompt more informed consideration of dunal slope

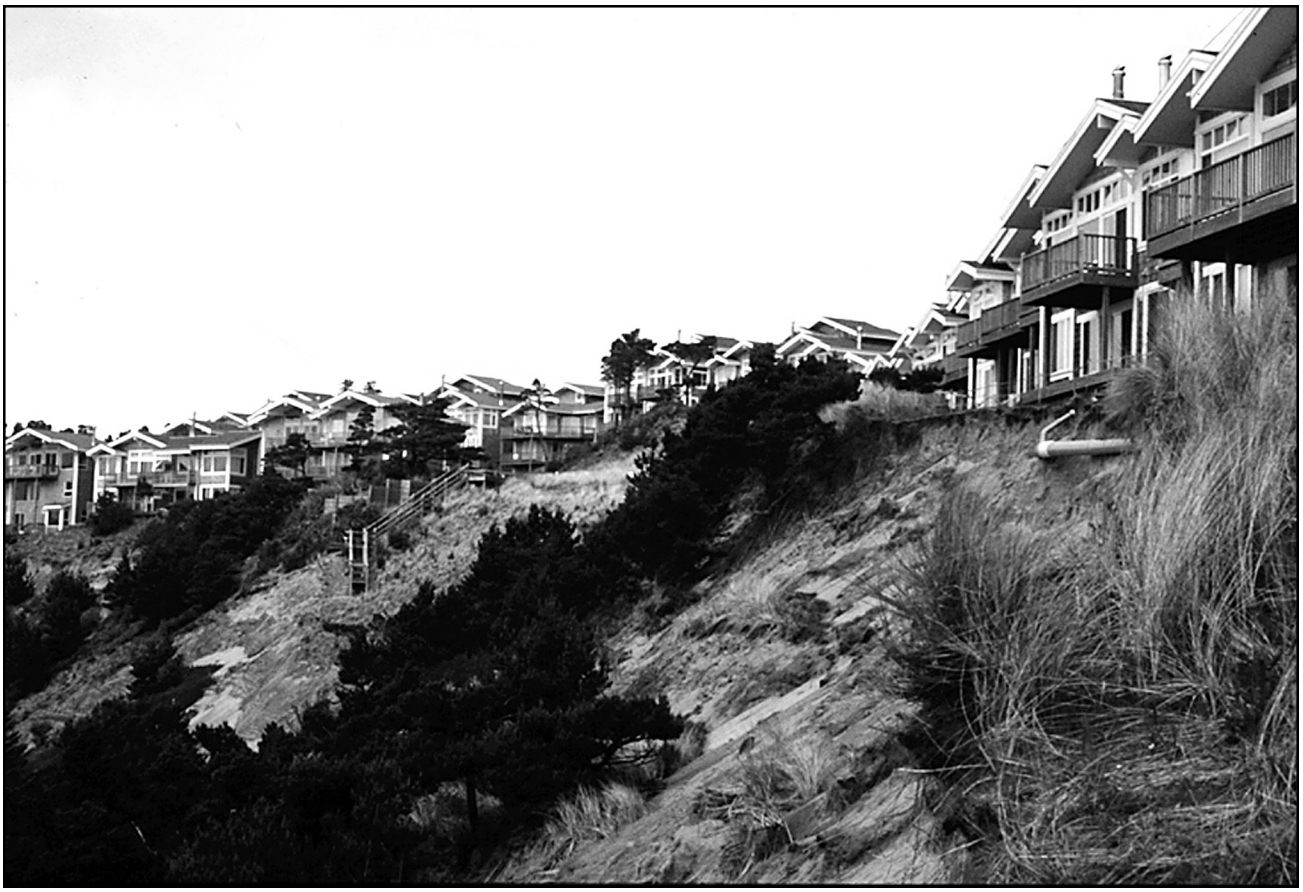

Figure 2. Digital image of The Capes development at Netarts Bay, Tillamook County, Oregon. The development extends onto a perched Holocene dune ramp that failed recently, leading to condemned structures and lawsuits.

stability, dunal aquifer management, and sustainable development in the coastal zone. We will appreciate input from field trip participants about specific field trip localities and broader sustainable-development issues on the coastal plain.

OVERVIEW OF ITINERARY

Day 1

The formal field trip starts in Newport, Oregon (Fig. 8). The first stop is at a beach-access trail that descends to the base of Pleistocene and Holocene dune deposits exposed in a sea-cliff section. We then complete a traverse to the east (3 km in length) tracing dunal deposits across the city of Newport. The Pleistocene dune sheets, generally ranging from 3 to 30 meters thick, cover marine terraces to the west and hillslope colluvium to the east. The surface features of uptown Newport, including topographic benches, valleys, and small ridges, reflect both episodic advances of the late Pleistocene dunes and intervening truncation by deflation. We will examine some geotechnical "successes" and "failures" in dealing with dunal cut-slope instabilities at Newport.

From Newport we drive south to Ona Beach for lunch and a brisk walk out to view a stratigraphic record of dunes (0–80 ka). This 30 meter vertical section extends from a basal wave-cut platform up to the Pleistocene–Holocene dunal contact. At this site we will also collect a thermoluminescence (TL) sample for dating one of the dune depositional sequences.

Continuing south toward Seal Rock we complete another eastward traverse (3 km in length) ending at the Pioneer Cemetery on the ridgeline. On a clear day we

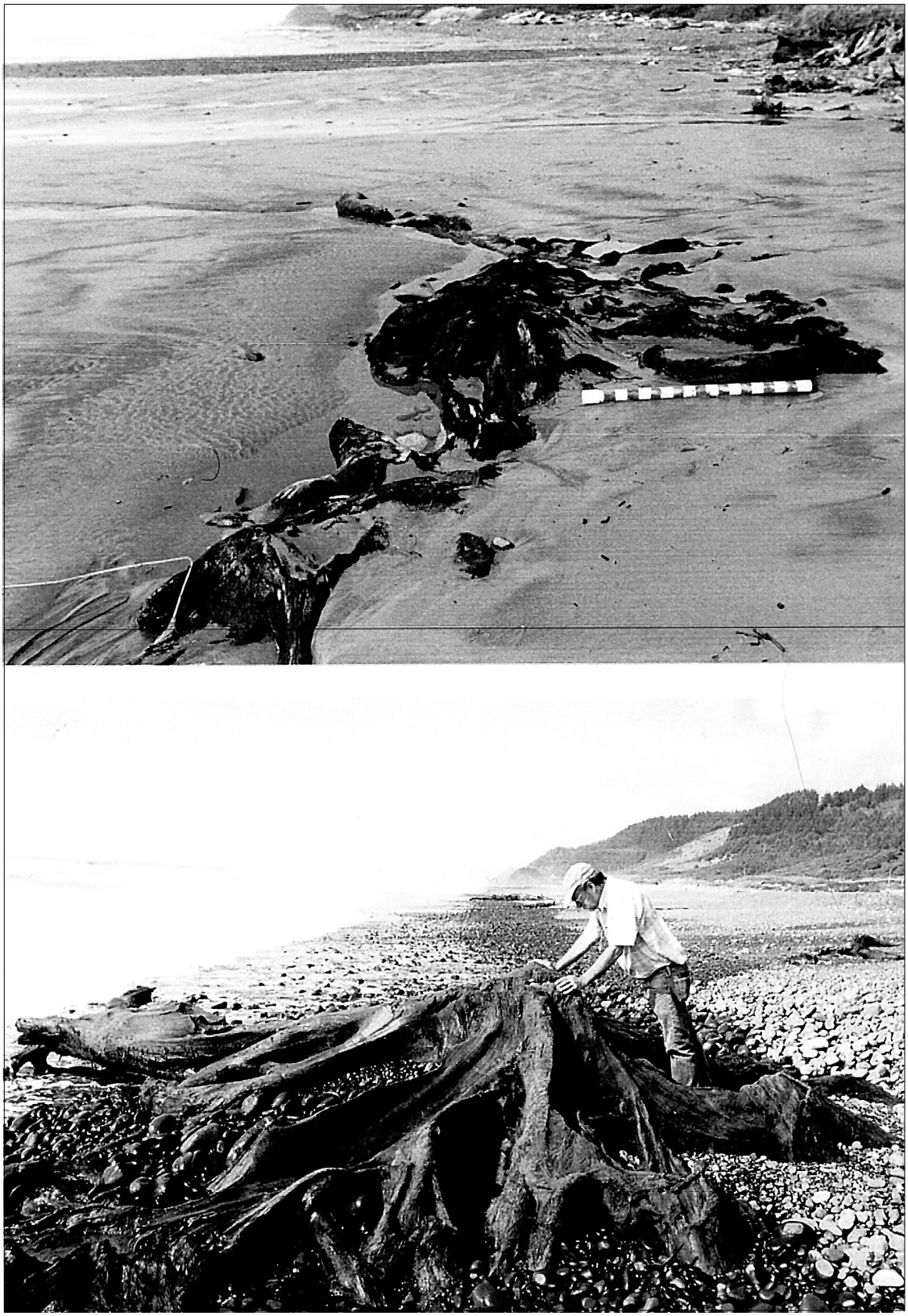

Figure 3. "Mystery" or swash-zone forest stump during summer (upper photo) and winter (lower photo) at the southern end of the Newport Littoral Cell. These forests grew on exposed Holocene wave-cut platforms in middle to late Holcoene time, prior to burial by a posttransgressive sand supply during late Holocene time. Progessive exposure of the stumps to marine-life degradation indicates a net loss of beach sand from this littoral cell in latest Holocene time.

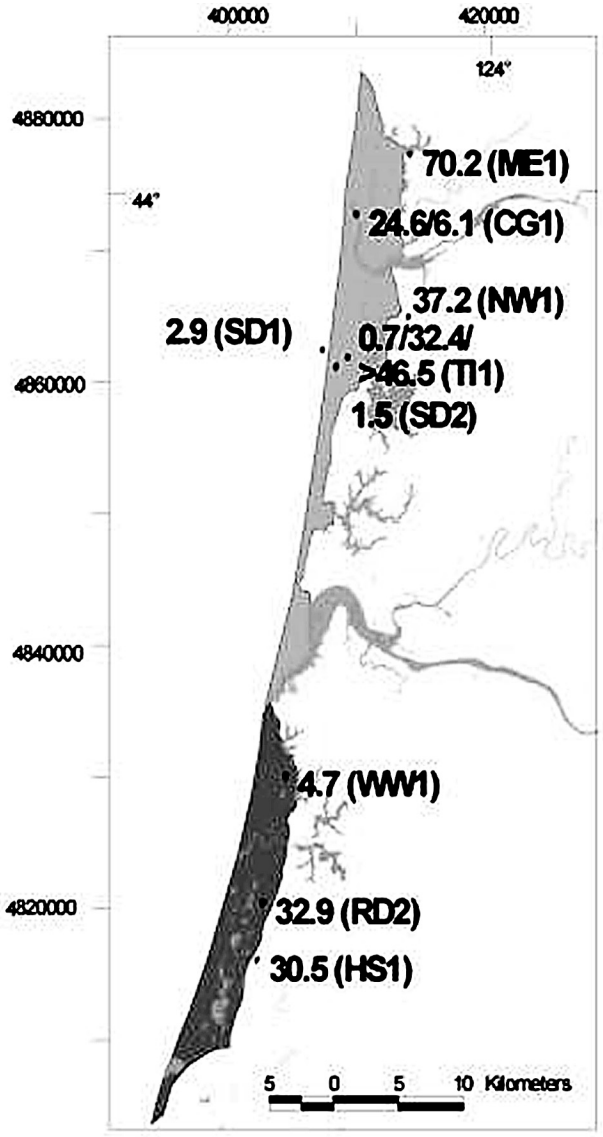

Figure 4. Map of dune ages from thermoluminescence dating (ME1-70.2 ka, CG1-24.6 ka, NW137.2 ka, TI1-32.4 ka, SD1-2.9 ka, SD2-1.5 ka, WW1-4.7 ka, RD2-32.9 ka, and HS1-30.5 ka) and radiocarbon dating (CG1-6.9 ka, TI1->467.5 ka, and 0.7ka) from the Florence and Coos Bay Dune Sheets in the Oregon Dunes National Recreation Area (ODNRA) (from Beckstrand, 2001).

should be able to gaze down the clear-cut dune ramps to the distant sea cliffs. We then can imagine the exposed dune sheets extending west 20–40 km across the inner continental shelf during lowstands of sea level.

Returning to US 101, we will continue south, shortly passing a Native American shell midden (0.3 ka) at Seal Rock. Short stops will be made to view dune cut-slope failures along US 101, dune-barrage ponds, marine-terrace deposits not covered by dunes, and "mystery" stumps in modern surf zones. Ongoing net erosion of the beach deposits episodically reveals the "mystery" stumps (generally 2–4 ka in age) during the winter months.

Our last formal stop of the day will be at a deflated dune section at Yachats, spanning 0–80 ka in age but only 7 meters in height. After this stop we drive 60 km south on US 101 to Florence. As we drive along the scenic Cape Perpetua to Heceta Head coastline, the tourists will be looking downslope at the crashing surf below, while we will be looking upslope at dunal remnants along the high cliffs.

We have arbitrarily mapped the distal dune sheets as distinct units separated along the coast by major headlands. However, the dune sheets were likely contiguous between major river valleys on the subaerial continental shelf during marine lowstand periods.

Day 2

From Oldtown Florence (Fig. 8) we will travel northwest to the Siuslaw Harbor Coast Guard Station. Bay-cliff exposures in this area reveal the contact between the uppermost Pleistocene deflation surface (>24 ka) and the overlying late Holocene dune sheet (<7 ka). We will continue north about 5 km to start another eastward traverse (6 km in length) at the Sutton Creek Recreational Area. Holocene dune cover extends some 2–3 km landward of the modern shoreline at the northern end of the Umpqua Littoral Cell. Holocene shoreline progradation here, possibly 0.5–1 km, accompanied the late Holocene posttransgressive sand surge and northward littoral transport in this cell. We will raise environmental issues about historic dune stabilization, wetland regulation, and barrage-pond water quality at short stops along the traverse.

US 101 marks the onset of late Pleistocene dunes exposed at the surface along this traverse, which continues eastward for

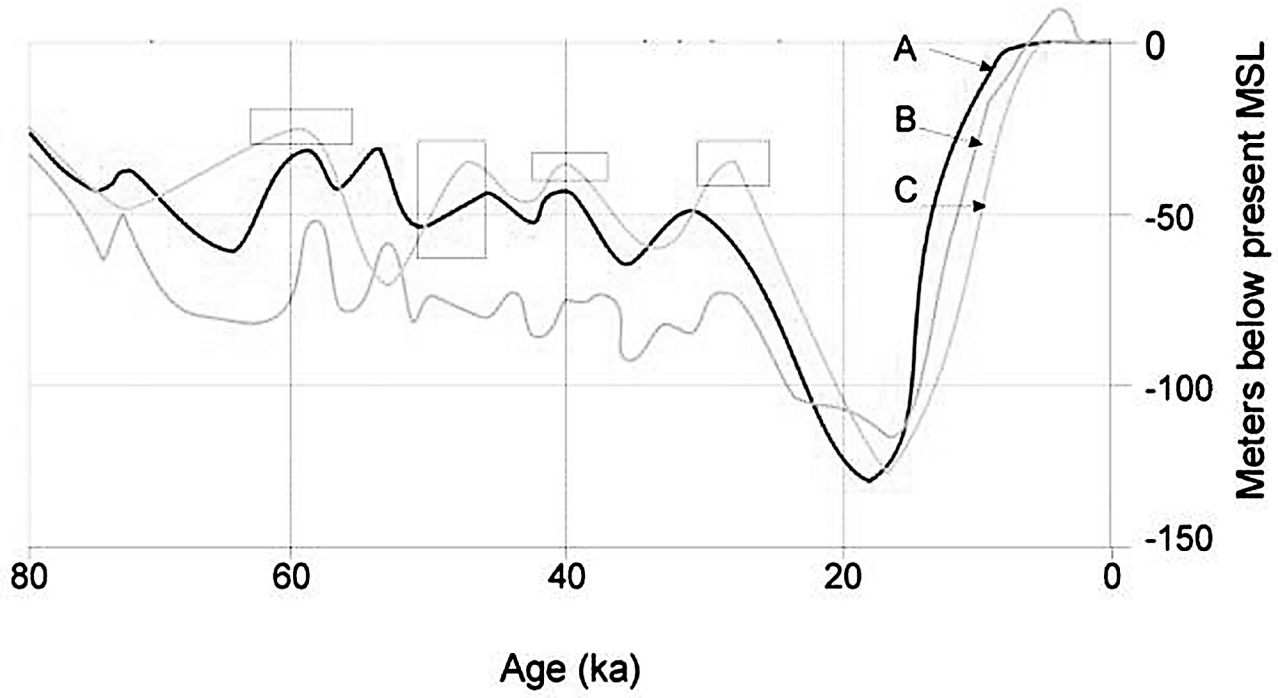

Figure 5. Published sea-level curves from a compilation by Pirazzoli (1993). Between 80 and 10 ka, the average sea level was about 50 meters below the present sea level. During the last glacial maximum (about 18 ka), sea level dropped 120–140 meters below the present level.

another 3 km to Mercer Lake. Mercer Lake is one of several smaller barrage lakes that flood pre-Holocene river valleys of the north Florence dune sheet. Gibbsite nodules precipitated in "old" dunal deposits (70 ka) around Mercer Lake, and they will be discussed in terms of interstratal groundwater geochemistry.

A short drive back to Florence and over the Siuslaw River Bridge to South Jetty Road, takes us into the active dune fields of the Oregon Dunes National Recreation Area (ODNRA) managed by the U.S Forest Service. We will complete another eastward traverse here, including an overview of an archaeological site (0.7–1.0 ka) developed on a young, intermittently exposed dunal paleosol (0.5–2 ka). Deep ground penetrating radar (GPR) profiles will be shown from recent surveys along this traverse. The traverse will continue east of US 101 at Woahink Lake to the easternmost extent of the late Pleistocene dunes (37 ka). The Pleistocene dune cover here extends 6–7 km inland from the modern coast (Figure 7b).

At the eastern edge of the Pleistocene dune sheet we will perform a soil-profile analysis for chronosequencing. Several large dunal barrage lakes occur in the southern part of the Florence Dune Sheet. At least one of these barrage lakes, Tahkenitch Lake, contains a nearby (upland) record of Native American occupation (8–0 ka). Efforts are underway to date some of the barrage-lake deposits in the Florence Dune Sheet and to establish the ages of initial impoundment (Jesse Ford, pers. comm., 2001).

The last formal stop of the field trip will be at the modern foredune in the Oregon Dunes National Recreation Area's Siltcoos Access Area. The base of the foredune is dated at 3 ka, indicating little or no net shoreline progradation since that time. However, some landward sand transport occurred until about 1.5 ka at the eastern margin of the existing deflation plain. The Siltcoos foredune site provides opportunities to discuss complex management issues in the ODNRA. Some of these

Figure 6. "Weeping sands" in late Pleistocene dunes with interstratified dunal paleosols serving as aquitards. Intrastratal groundwater deposition of hydroxides, clay, and other phases at paleosol redox boundaries serves to further cement the paleosol contacts.

issues include foredune breach experiments, snowy plover habitat, and European beachgrass stabilization of active dunes.

FIELD TRIP ROAD LOG, DAY 1

From Corvallis, Oregon, drive west 82 km (51 mi) on US 20 to coastal US 101 in Newport. The northern Coast Range drainages provide some of the sand that is ultimately blown onshore to build the dunes. However, dunal sand mineralogies of the central Oregon coast largely reflect volcanic arc and metamorphic provenances drained by larger rivers to the south such as the Umpqua, Rogue, and Klamath Rivers. Commingling of the different provenance mineralogies occurs on the inner continental shelf, which is a source of sand to the larger dune fields (Scheidegger and others, 1971; Beckstrand, 2001).

0.0 km (0.0 mi) Field trip starts at the intersection of US 20 and US 101 in Newport, Oregon (Fig. 8). Continue across the intersection due west 0.7 km (0.4 mi) on W Olive Street.

0.7 km (0.4 mi) Reach Stop 1 at the City Park (Donald A. Davis Park) above the sea cliff.

Stop 1: Donald Davis City Park Beach Trail (rest rooms)

From the parking area we will follow the paved trail past the flagpole as it winds down the sea cliff to the beach. We will examine the dune sequences in the sea cliff including from bottom to top (a) the wave-cut platform cut into the local bedrock, (b) Pleistocene dunes, and (c) a thin mantling of late Holocene dunes (regional dates of 1–3 ka by radiocarbon dating) above a conspicuous paleosol. The Newport wave-cut platform (lowest exposed platform) is dated at 80-85 ka by mollusk aminostratigraphy (Kennedy and others, 1982) This terrace age is thought to represent the last substantial marine highstand (isotope stage 5a) forming the Whisky Run Terrace of southwest Oregon (Muhs and others, 1992). The late Pleistocene dune sequence contains different types of paleosols as follows (1) Bw horizons (iron-stained accumulation), (2) Bh horizons (humate accumulation), (3) Bg horizons (chemically reduced glade or "gray" layers), and (4) Bt horizons (clay accumulation). The late Holocene dunes contain only Bw and Bh horizons, whereas the late Pleistocene sequences also include Bg and Bt horizons (Table 1).

The late Holocene dunes above the late Pleistocene topsoil must have originated from broad beaches and extensive dune ramps that climbed above the middle Holocene sea cliffs. The sea cliffs are now once again eroding, thereby undercutting both the Pleistocene and Holocene dune cover. Unstable dunal sea cliffs seem to fail

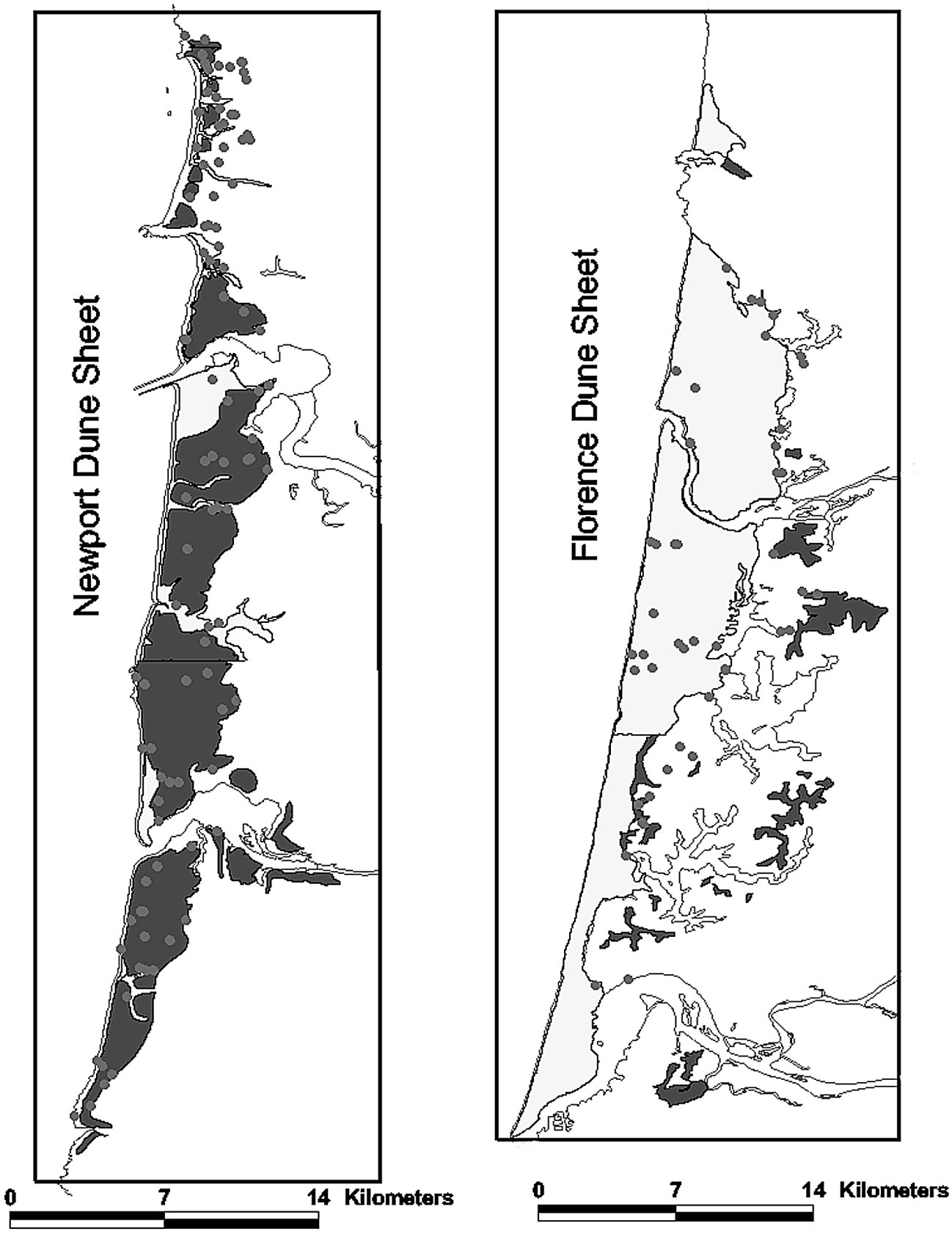

Figure 7. Quaternary dune and marine terrace deposits digitized from published geologic maps (http://nwdata.geol.pdx.edu/SeaGrant/index.html) showing dots where dune deposits have been profiled in the Newport (Figure 7a) and Florence (Figure 7b) Dune Sheets. Shaded units are shown in the legend.

unpredictably, due in part to the variably cemented Pleistocene dune strata. Creep along seaward-dipping failure plains in the shallow bedrock units further complicates the shoreline-erosion process in this area (George Priest, pers. comm., 2001).

2.3 km (1.4 mi) From Stop 1 return to the intersection of US 101 and US 20, then continue east on US 20 (E Olive St) 0.8 km (0.5 mi) to a stoplight intersection with NE Harney, and turn north (left) on NE Harney.

2.7 km (1.7 mi) Continue north 0.4 km (0.2 mi) on NE Harney to a stop-sign intersection with 7th Steet. Turn east (right) on 7th Street.

2.9 km (1.8 mi) Continue up the hill on 7th Street 0.2 km (0.1 mi) to Stop 2 at the Newport Middle School parking lot.

Stop 2: Newport Middle School Parking Lot

From the parking lot and playing fields of the Newport Middle School we will view the engineered dunal slopes to the east. Initial grades were too steep, resulting in rilling, gullying, and small slumps after winter rains. Mitigation steps included drainage-monitoring wells, slope-grading, geotechnical fabric covers, and reseeding.

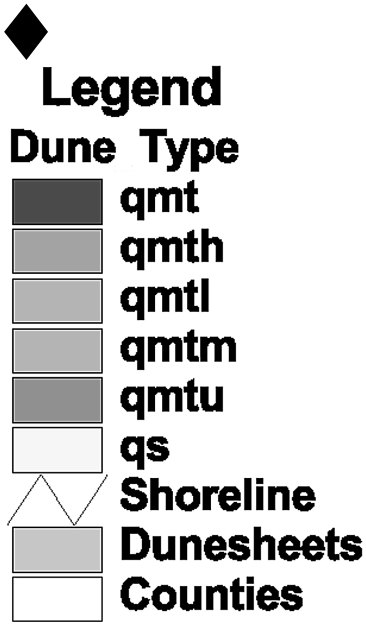

Side Trip: A side trip can be made to a dunal liquefaction site near the top of Big Creek Road in north Newport. From 7th Street continue several blocks west to Eads Road, then turn north (right) on Eads Road, and continue around Sam Case Elementary School to connect with Big Creek Road. The liquefaction site is at a Pleistocene dune outcrop in a road cut (west) at the intersection with the Frank Wade City Park entrance. Clastic dikes (>20 cm width) at the base of the exposed section transition to convolute bedding (1–3 m in thickness) in the middle of the section. The scale and setting of these features indicate significant ground shaking. A thermoluminescence (TL) date of the dune deposit (predating the liquefaction) is pending. Similar cosesimc liquefaction features are reported from dune deposits above marine terraces that are exposed in nearby sea cliffs (Peterson and Madin, 1997). Return to Stop 2.

3.2 km (2.0 mi) From Stop 2 return to NE Harney Street and turn south (left) to intersection with 3rd Street. Turn east (left) on 3rd Street.

4.2 km (2.6 mi) Continue east 1 km (0.6 mi) on 3rd Street, viewing dune deposit exposures in road cuts to Stop 3 at the Newport City Water Tank.

Stop 3: Newport Water Tank, 3rd Street Road Cut

After pulling off the road across from the Newport water tank, we will walk 50 m east (uphill) on 3rd Street to examine dune-deposit exposures in the north road cut. Stop 3 is within 0.5 km of the eastern limit of the preserved dune-sheet deposits in this area (Figure 7a). The Newport Dune Sheet maintains about the same width to the south, but it narrows to the north. The next dune sheet north, the Lincoln City Dune Sheet, averages only about 1 kilometer in width. Pleistocene dune sheets farther north of Lincoln City are increasingly narrow and discontinuous to the north. These trends suggest diminishing shelf-sand supply north of the Stonewall–

Table 1. Nye Beach Dunal Stratigraphic Section

', Estimated Error (2D,3D +-m), GPS Altitude (Alt m)
l), Auger (AU), Road Cut (RC), Sea Cliff (SC), Bay Cliff (BC), Slope (SL)

Leached Soil (E), Accumulation Soil (B), Sesquioxides'Fe+3' (Bw), Clays (Bt), Humates (Bh),
:ed Glade Layer (Bg), Oxidized Parent (Cox), Dune Parent (C), Colluvium (U),
;tuary (L), Beach Shoreface (S), Basal Conglomerate (M), Wave-cut Platform (W), Tertiary Bedrock (T)

: (cohesionless), cohesive (sticky/clumpy), peds (small concretions in matrix), blocky (cemented blocks)
U/L); Foresets (Bearing,Dip); Deformation=shear, liquefaction, bioturbation, etc.
:, Gibbsite, Allophane; Cultural=shell midden, firecracked rock, artifacts

Mapper
Roger Hart

UTM-E	EPE (m)	Alt (m)	Time GMT
415659	14	19	13:54 Local

Photos

Site Notes
Nye Beach, Newport. Section taken about 100 m north of beach access trail from Davis Park. Predicted swash tide level was 0.3 m (MLLW?). Above swash elevations: W (8.61 m), Holocene contact (17.19 m), top of section 19.94 m.

Thickness cm	Grain Size	Sed. Structure	Max.Color	Pen(kg/cm^2)	Cementation	Diagenesis	Cultural
10					loose		
140	FU-ML			0.5	loose		
10			5yr6/8 w5yr5/8				
110			10yr7/6 w10yr5/6	1			
60							
30							
90		Planar	10yr6/6 w10yr5/8	3.5	Peds	Top truncated by deflation	
6	FL						

Table 1. Nye Beach Dunal Stratigraphic Section

UTM-N=0000000, UTM-E=000000, Estimated Error (2D,3D +-m), GPS Altitude (Alt m)
Exposure=Active (AC), Trench (TR), Auger (AU), Road Cut (RC), Sea Cliff (SC), Bay Cliff (BC), Slope (SL)

Units=Dune (D), Organic Soil (A), Leached Soil (E), Accumulation Soil (B), Sesquioxides'Fe+3' (Bw), Clays (Bt), Humates (Bh),
Calcrete (Bc), Silcrete (Bs), Reduced Glade Layer (Bg), Oxidized Parent (Cox), Dune Parent (C), Colluvium (U),
Peat (P), Alluvial (V), Lagoonal/Estuary (L), Beach Shoreface (S), Basal Conglomerate (M), Wave-cut Platform (W), Tertiary Bedrock (T)

Cementation (soil structure)=loose (cohesionless), cohesive (sticky/clumpy), peds (small concretions in matrix), blocky (cemented blocks)
Grain Size (CU/L, MU/L, FU/L,VFU/L); Foresets (Bearing,Dip); Deformation=shear, liquefaction, bioturbation, etc.
Interstratal Diagenesis=Ortstein Fe, Gibbsite, Allophane; Cultural=shell midden, firecracked rock, artifacts

Dune Sheet	Date	Mapper
NEWP	5/26/00	Roger Hart

Zone/NAD	UTM-N	UTM-E	EPE (m)	Alt (m)	Time GMT
N10/83	4943091	415659	14	19	13:54 Local

Exposure	Depth (m)	Photos	Site Notes
SC	19		Nye Beach, Newport. Section taken about 100 m north of beach access trail from Davis Park. Predicted swash tide level was 0.3 m (MLLW?). Above swash elevations: W (8.61 m), Holocene contact (17.19 m), top of section 19.94 m.

Units	Subsurface cm	Thickness cm	Grain Size	Sed. Structure	Max.Color	Pen(kg/cm^2)	Cementation	Diagenesis	Cultural
HA	0-10	10					loose		
HDC	10-150	140	FU-ML			0.5	loose		
HDBw	150-160	10			5yr6/8 w5yr5/8				
HDCox	160-270	110			10yr7/6 w10yr5/6	1			
HA	270-330	60							
HBg	330-360	30							
PDBw	360-450	90		Planar	10yr6/6 w10yr5/8	3.5	Peds	Top truncated by deflation	
PDBg	450-456	6	FL						
PDBw	456-656	200		F.setEDip20			Cohesive	Allophane replaces roots	
PDBg	656-696	40		Planar					
PDCox	696-946	250	FU-ML	F.setEDip30	10yr5/8 w10yr5/6		Cohesive	Allophane replaces roots	
PDBg/P	946-988	42							
PDC	988-1068	80		Planar		4.5		Fe-Ortstein	
PS	1068-1128	60		Ripples			Coheisve		
PM	1128-1133	5	Cobbles						
PW	1133-1134	1							
T	1134-1943	809							

Perpetua Banks on the inner continental shelf, off the Newport–Florence area (Figure 1).

6.5 km (4.0 mi) From Stop 3 continue east 2.3 km (1.4 mi) on 3rd Street to intersect US 20. Turn west (right) back toward Newport.

9.1 km (5.6 mi) Continue west on US 20 to the intersection with US 101 in Newport. Turn south (left) on US 101.

22.6 km (14.0 mi) Continue south 13.5 km (8.4 mi) on US 101 to Stop 4 at Ona Sate Park.

Stop 4: Ona State Park (rest rooms)

From the parking lot at Ona State Park we will follow the beach access path across the Ona Creek pedestrian bridge to the beach. From the beach entrance we will walk 0.5–1 km south along the sea cliff viewing the dunal stratigraphy. This sea-cliff section provides one of the most complete exposures of the Newport Dune Sheet. The stratigraphic record of dunes in the 30 m vertical section extends between a basal wave-cut platform and the Pleistocene–Holocene dunal contact at the top of the sea cliff. The exposure includes from bottom to top: (1) the basal marine terrace, (2) Fe-Ox precipitates at aquitard boundaries, (3) 4–6 dunal "gray-layer" deflation surfaces, (4) allophane replacement of roots, and (5) the Pleistocene to Holocene contact soil. The age of the basal marine terrace here is not well constrained. Tichnor (1993) interprets the terrace to be the stage 5e highstand, 125 ka (Muhs and others, 1992). However, the shoreface and dunal straigraphy above the wave-cut platform at this locality do not seem to differ substantially from those at Stop 1 (north of Yaquina Bay) where the platform is reported to be that of the stage 5a highstand (80 ka). A basal dune TL date above the wave-cut platform from this site is pending, but an optically-stimulated luminescence date from a preserved upper-backshore deposit is required to date the terrace deposits directly.

The uppermost paleosol at the Pleistocene–Holocene contact seems to be correlated throughout the study area. This widespread period of dune stabilization is thought to represent reduced dune-sand supply from the continental shelf, possibly during the last glacial maximum or the early Holocene transgression. A present controversy amongst the project researchers is whether the "paleosol/gray layers", typically 4–6 in number, can be correlated throughout the dune-sheet deflation plains. For example, do the paleosol-deflation horizons correspond to sea-level fluctuations (Fig. 5), late Pleistocene climatic extremes, or random dune movements? Initial thermoluminescence dates that should help to constrain the timing of some sequences from this site are pending. We will bring sampling equipment to collect one additional TL sample from a sequence not yet dated in the Ona Beach section.

Side Trip: A side trip can be made from Ona Sate Park to the eastern limit of the preserved late Pleistocene dune sheet (Fig. 7a). From the intersection of N Beaver Creek Road and Ona State Park continue due east 1.7 km (1.0 mi) to the intersection of N Beaver Creek Road and S Beaver Creek Road, turn north (left) staying on N Beaver Creek Road. Continue 0.3 km (0.2 mi) on N Beaver Creek Road to view road cut exposure on the west side of the road. A TL date from this site is 103 ka. Return to Stop 4.

25.6 km (15.9 mi) From Stop 4 turn south (right) onto US 101 and continue south 3 km (1.9 mi) to Seal Rock State Park. Stop 5 is at the state park, which is on the west side of the highway.

Stop 5: Seal Rock State Park (rest rooms)

From the State Park parking lot we will follow the trail to the sea-cliff overlook. Then take the trail south down to the beach to view the dune sequence in the sea-cliff exposure. Can the "gray-layer horizons" at this stop be correlated with those at the previous stop at Ona State Park? A lack of paleosols, that is A or B horizons, directly above the allophane replaced roots, suggests that eolian deflation locally reduces the preservation of paleosol sequences. The

replacement of roots by allophane, semiordered aluminosilicate, 1:1.8 Si/Al ratio, was unexpected by us. We initially believed the white gelatinous replacement material to be amorphous silica or opal. Allophane was established by broad x-ray diffraction peaks at 3.3 and 2.25 angstroms (Grathoff and others, 2001). The mobilization of Al in the dunal groundwater will be discussed further at Stop 14.

25.8 km (16.0 mi) From Stop 5 continue 0.2 km south (0.1 mi) on US 101 to an uncontrolled intersection with Seal Rock Street. Turn east (left) on Seal Rock Street.

26.1 km (16.2 mi) Continue west on Seal Rock Street 0.3 km (0.2 mi) to an intersection with NW Cross Street. Turn east (left) on NW Cross Street.

24.5 km (15.2 mi) Continue east 2.9 km (1.8 mi) on NW Cross Street, which becomes a gravel road, and continue to the top of the ridge for Stop 6 at the Pioneer Cemetery.

Stop 6: Seal Rock Pioneer Cemetery

This stop represents the easternmost extent of the preserved late Pleistocene dune sheet in the Seal Rock vicinity (Fig. 7a). At a distance of several kilometers from the coast this dune-capped high ridge demonstrates the abundance of sand that was supplied to the late Pleistocene dune advances. By comparison, the posttransgressive highstand dunes (Holocene) barely ramped over the existing sea cliffs in this area. During most of the past 80,000 years the continental shelf was subaerially exposed to 40-80 m below present sea level (Fig. 5). That level corresponds to a distance of 10–20 km offshore from the present shoreline (Fig. 1). During the last glacial maximum the coastline, at –120 m, would have lain some 40 km offshore from the present Seal Rock coastline, possibly well beyond the reach of inland dune migration at this latitude. By 10 ka a shoreline at 50–60 m below present sea level (Peterson and Scheidegger, 1984) would still put the coastline at several tens of kilometers offshore. Early cultural sites associated with shorelines during those periods would be at least a full day's walking journey from the present sea cliffs at Seal Rock.

27.9 km (17.3 mi) From Stop 6, return to US 101. Turn south (left) on US 101, passing the Seal Rock shell midden, just 100 m south of the turn onto US 101.

This midden (0.2–0.3 ka) locally infills hollows in Pleistocene dune deposits east of the highway, but occurs at the top of overlying Holocene dune layers next to the sea cliff. The very young midden age and lack of dune cover over the midden suggest a coincidence of terminated dune-sand supply and onset of rocky-intertidal shellfish collection in latest Holocene time. Might this coincidence also correspond to the beach erosion that has left the late Holocene dune ramps along the local sea cliffs undercut in modern time? Additional work is needed to date the termination of Holocene dune supply and the onset of beach erosion in this area.

By comparison to the Seal Rock midden, some other sea-cliff shell middens, such as near Whisky Run Creek at the Bandon marine terraces, occur just prior to the late Holocene dune supply. Those middens sit upon the well-developed paleosol formed at the Holocene–Pleistocene dune boundary. That period corresponds to a generally rocky coastline that existed between the rapid sea level rise in early to middle Holocene time and the onset of posttransgressive dune inundation in middle to late Holocene time. The late Holocene influx of beach and dune sand (5–2 ka) probably limited rocky-intertidal shellfish collection to the protruding headlands in the central and southern Oregon littoral cells. An influx of littoral sand in middle to late Holocene time could account for midden abandonment at some dunal sea cliff sites that were adjacent to intertidal pools prior to the influx of Holocene beach sand.

33.6 km (20.9 mi) Continue south 5.7 km (3.5 mi) on US 101 to Stop 7.

En route, note the barrage ponds at 4.6 km (2.8 mi) and 5.2 km (3.2 mi) that are

trapped between Holocene parabolic dunes to the west of US 101 and Pleistocene dunes to the east of US 101. How are these ponds (>10 m above MSL) maintained during dry summer months in the porous dunal deposits? Upland groundwater seepage might supply some water to the ponds year-round. However, effective bottom seals, such as late Pleistocene paleosol aquitards, likely underlie the ponds, thereby reducing bottom discharge. Comprehensive water-balance measurements have yet to be completed for most of the dunal barrage ponds. Just beyond a highway sign "Alsea Bay North Wayside 1/4 mile" find a side street and park away from the highway. Walk 50 m northward on the west side of the highway shoulder to view the slope failure in the dunal deposit road cut on the east side of the highway.

Stop 7: US 101 Road Cut North of Alsea Bay Bridge

From the western side of US 101 we will view a road-cut exposure of late Pleistocene dunal deposits on the eastern side of US 101. Several slumps have occurred in this road cut causing traffic hazards. The engineered slope is locally stabilized by interstratified paleosols and iron-cemented hardpans. However, the same horizons serve as aquitards resulting in locally elevated pore pressures. Slope failures seem to follow undermining of Cox soil horizons below cemented Bw/Bt horizons. The Cox horizons are the uncemented parent dune sand. However, much deeper failure planes within the slope are indicated by sets of surface separation cracks (3–5 cm wide) located 10–15 m east of the present headwall. These features suggest slope failure that cuts through the different strata. Ground penetrating radar (GPR) profiles image the subsurface complexity of cross-cutting dunal foresets and paleosols to a depth of 20 m east of the road-cut exposure. Slope-failure mitigation involves monitoring wells, grading of slide toes, and monitoring for potential slump-block hazards on the highway shoulder (Bernard Kleutsch, pers. comm., 2000).

42.0 km (26.1 mi) From Stop 7 continue 8.4 km (5.2 mi) to Tillacum State Park on the west side of US 101. Inside the park turn north (right) into the north loop to reach Stop 8 at the beach access trail.

Stop 8: Tillacum State Park (rest rooms)

From the North Loop beach access trail we will walk several tens of meters to the beach. Although sand currently covers the wave-cut platform at this site, in situ tree stumps are episodically observed in the swash zone along the central Oregon coastline (Fig. 3). The stumps generally range in age from 2 to 4 ka (Hart and Peterson, 1997). The stumps represent a complex sequence of events starting with the early to middle Holocene erosion of the wave-cut platforms. Brief periods of middle to late Holocene emergence permitted the forest colonization of some platforms, particularly near freshwater creek mouths. However, an inundation of posttransgressive sand during late Holocene time killed and buried the trees. Subsequent beach erosion exposes the stumps to saltwater organisms that rapidly degrade the wood. Efforts are underway to monitor new exposures of stumps and platform forest soil layers as net beach erosion removes the sand cover after thousands of years of protective burial.

43.2 km (26.8 mi) From Stop 8, reverse course to head north 1.2 km (0.7 mi) on US 101 to the Reynolds Road intersection. Reynolds Road is unmarked, but it is on the opposite side (east) of US 101 from a large red beach house (west). Turn east (right) onto the narrow paved Reynolds Road.

47.5 km (29.5 mi) Continue east 4.3 km (2.7 mi) on Reynolds Road, passing dune-barrage creeks and associated riparian wetlands at 3.6 km (2.2 mi). The easternmost limit of the Pleistocene dune sheet is at 3.9 km (2.4 mi), and the marine terrace exposure at Stop 9 is 4.3 km (2.7 mi) from the US 101 intersection.

Stop 9: Reynolds Road Marine Terrace

From the narrow roadway we will observe shallow exposures of marine terrace

deposits in road cuts along the north side of the road. This terrace sequence includes beach sand and basal conglomerate above a wave-cut platform. The marine terrace exposure is east of the farthest advance of the late Pleistocene dune sheet. The topsoil on the marine terrace deposit is very well developed with a thick Bt horizon (clay accumulation) resulting from continuous exposure to surface leaching processes since deposition. The marine terrace deposits under the Pleistocene dunes to the west of this stop yield paleosols with thinner Bt horizons or only Bw horizons (sesquioxide accumulation). In the most seaward locations, preserved in the modern sea cliffs, the marine-terrace-top paleosol is commonly truncated or completely missing due to eolian deflation. Some investigators have assumed that the late Pleistocene dune sheets represent highstand deposits, that is to say that the dunes were deposited soon after formation of the wave-cut platform and shoreface deposition. However, existing TL dates from the Florence Dune Sheet (Fig. 4) suggest substantial time gaps (tens of thousands of years) between terrace formation at stage 5a or older (greater than 80 ka), and dunal topsoil development in late Pleistocene time (generally 20–40 ka).

51.8 km (32.1 mi) From Stop 9 return west 4.3 km (2.7 mi) to US 101. Turn south (left) on US 101.

58.5 km (36.3 mi) Continue south 6.7 km (4.2 mi) to Yachats, then turn west (right) on 7th Street.

58.8 km (36.5 mi) Continue 0.3 km west on 7th Street to Oceanview Drive, then turn south (left) and continue 50 m south to a small parking area (turnout) with a park bench at the sea cliff for Stop 10.

Stop 10: Yachats Oceanview Drive Sea Cliff

This is the last stop of Day 1. From the small parking turnout, follow a footpath heading south down to the beach. This short stratigraphic section (6–7 m) extends from a wave-cut platform to the Holocene–Pleistocene topsoil. Tichnor (1993) interprets the platform to correlate to the isotope stage 5e (125 ka) highstand, with possible reoccupation during the later stage 5c (105 ka) and stage 5a (80 ka) marine highstands. The original terrace age, and any subsequent reoccupation ages have yet to be confirmed by independent dating.

The truncated dunal section at Yachats includes 4–6 paleosol "gray-layer" deflation horizons. This shortened dunal section corresponds to a very narrow strip of Pleistocene dune cover in the Yachats area (less than 0.5 km in width) suggesting a lack of dune-sand supply. Local narrowing of the Pleistocene dune cover also exists in the northern Newport Dune Sheet at Agate Beach, the central Florence Dune Sheet near Woahink Lake (Stop 17) and the central Bandon Dune sheet west of Langlois. In the Woahink Lake area a high dune ridge (100 m) blocks sand advance to the east. Could westward high dune ridges, now removed by marine transgression, have similarly blocked sand advances in other narrow dune-sheet reaches?

Ground penetrating radar profiles were taken parallel to the sea cliff at this site. Paleosols, as thin as 2-3 cm, are clearly traced by continuous GPR reflections from cliff-parallel profiles. Maximum GPR penetration, to the wave-cut platform, increased where the profiles did not encounter the thick topsoil (Bw) horizon. A continuous stratigraphic section at this site has been permanently recorded by a new peel-making technique, using a cyanide-polymerizing grout from Japan. Several peels are on display at the Hatfield Marine Science Center, Newport, Oregon (Bill Hanshumaker, pers. comm., 2001).

59.1 km (37.7 mi) Return to US 101. Turn south (right) on US 101.

77.5 km (48.2 mi) Continue south on US 101 to reach Florence, viewing remnant dune deposits at 6.5 km (4.0 mi) Neptune State Park, 8.6 km (5.3 mi) Bob Creek Wayside, and 18.4-20.4 km (11.4-12.7 mi) Washburne State Park, among others. These dune remnants indicate that the Newport and

Florence Pleistocene dune sheets were likely contiguous between major river valleys on the inner continental shelf during marine lowstands. Small Holocene dune fields, which ramped up the middle Holocene sea cliffs, are now being undercut by net erosion along the small pocket beaches.

103.5 km (64.3 mi) At a distance of 26–26.5 km (16.1-16.5 mi) south of Yachats look for viewpoint turnouts on the southwest side of US 101 that overlook the northern end of the Florence Dune Sheet.

Lilly Lake, one of a half dozen dune-barrage lakes in the area, is at the foot of the Heceta Head headland and has a basal peat date of 3 ka (Briggs, 1994). Late Holocene peat and forest remnants have been observed at the modern beach just south of Lilly Lake. These wetland deposits exposed at modern beaches reflect some net erosion of the shoreline in recent time. A marine terrace back edge of unknown age is identified by sea stacks east of Lilly Lake. The sea stacks are on US 101 some 29 km (18 mi) from Yachats. Pleistocene dunes generally surface east of US 101, and they climb the foothills to heights of 100 to150 m at distances of some 5-6 km inland from the present coast (Fig. 7b).

118 km (73.3 mi) Continue south 15 km (9.3 mi) on US 101 to Florence on the Siuslaw River, which marks the end of Day 1.

FIELD TRIP ROAD LOG, DAY 2

0.0 km (0.0 mi) From the Oldtown Florence Loop under the bridge drive northwest 0.4 km (0.2 mi) on Kingwood Street to the intersection with Rhododendron Drive, turn west (left) on Rododendron Drive (Fig. 8).

4.9 km (3.0 mi) Continue 4.5 km (2.8 mi) northwest on Rhododendron Drive to the Coast Guard station, just past (north of) the 35th Street intersection. Turn west (left) off of Rhododendron Drive into the Coast Guard station and drive northwest 0.1 km (0.05 mi) to the visitors' parking lot for Stop 11.

Stop 11: Siuslaw Coast Guard Station

The access to this stop requires advance permission from the U.S. Coast Guard. The contact between overlying Holocene and underlying Pleistocene dune deposits can be viewed at several bay-cliff localities 0.5–1 km north and south of the Coast Guard station. Several key thermoluminescence (TL) and radiocarbon (RC) dates have been taken from dunal deposits at the Coast Guard Station site (Fig. 4). The bay-cliff exposure along this part of the Siuslaw River reveals a broad contact between a late Pleistocene deflation surface, about 24 ka (thermoluminescence), and overlying Holocene dunes, younger than 7 ka (radiocarbon). A Holocene radiocarbon-date sample at the contact (6,900±700 RCYBP Beta#84373) was taken from one of many stumps that were buried in situ, vertically standing, by the advance of the Holocene dunes. The radiocarbon date from the standing stump represents an approximate age of tree death that predates the major influx of Holocene dune sand.

5.2 km (3.2 mi) From Stop 11 return to Rhododendron Drive, then turn south (right) on Rhododendron Drive then abruptly (left) at the 35th Street intersection.

6.6 km (4.1 mi) Continue east 1.4 km (0.9 mi) on 35th Street, to reach the intersection with US 101. En route, note the recently active parabolic dunes. The elimination of virtually all active dunes in the Florence area by vegetative stabilization and other methods is both imminent and controversial (see discussion topics at next stop).
Turn north (left) on US 101.

11.8 km (7.3 mi) Continue north 5.2 km (3.2 mi) on US 101 to Campground Vista Road (Sutton Creek Campground Road) intersection. Turn west (left) on Campground Vista Road.

15.0 km (9.3 mi) Continue west 3.2 km (2.0 mi) on Campground Vista Road to Holman Vista Parking Lot (Sutton Beach Access) for Stop 12.

Stop 12: Holman Vista (Sutton Beach Access) rest rooms

At this stop we initially will examine one of the few dunal isopach maps in Oregon. Based on a seismic-refraction survey, three dunal aquifer layers are identified in the Florence Dunal Aquifer (Couch and others, 1980). For example, at the intersection of Campground Vista Road and US 101 the isopach map indicates (1) 6 m of unsaturated Holocene dune sand above (2) 20 m of saturated Holocene dune sand above (3) 20 m of semiconsolidated Pleistocene dune sand above (4) bedrock. The maps indicate substantial spatial variability of the different units' thickness throughout the dunal aquifer.

After discussing the dunal isopach map, we will walk out to the modern foredune (beach access trail) to view a variety of dunal habitats. We will examine the effects of nonnative vegetation such as European beachgrass *Ammophila arenaria* on different dunal environments. Until a decade ago the major goal of dune managers was the stabilization of active dunes (Carlson and others, 1991). However, environmental, recreational, and community sentiments are changing toward an appreciation of active and semiactive dunal landscapes. We will discuss efforts to recreate an active-dune habitat for threatened species such as the Snowy Plover. We also will discuss the potential impacts of vegetative stabilization on other recreational and aesthetic uses of active-dune landscapes.

18.2 km (11.3 mi) From Stop 12 return east 3.2 km (2.0 mi) on Campground Vista Road to the US 101 intersection. En route, view dune pine and rhododendron forests, dunal ponds, and wetlands on the Holocene dune fields. Turn north (left) on US 101.

18.4 km (11.4 mi) Continue north 0.2 km (0.1 mi) on US 101 to the Mercer Lake Road intersection. Turn east (right) on Mercer Lake Road.

18.5 km (11.5 mi) Continue east 0.1 km (0.05 mi) on Mercer Lake Road to the *Darlingtonia* Bogs State Park on the south side of the road for Stop 13.

Stop 13: *Darlingtonia* State Park (rest rooms)

At this stop we will take a short (50 m long) boardwalk to see some *Darlingtonia* bogs. *Darlingtonia* (pitcher plant) is a carnivorous plant that relies on the digestion of trapped insects for nutrients that are low in abundance in the bog soils. At this site we will discuss issues concerning federal regulation of dunal wetlands. Wetland species thrive in dunal bogs following rainy seasons, but they dry out at ephemeral wetland sites during drought periods. The ephemeral wetlands of dunal deflation hollows and gullies are temporarily formed by perched groundwater above paleosol aquitards. Federal regulations restrict development in the sensitive wetlands. Disputes arise when developers purchase land, but are then restricted from developing it when wetland species rejuvenate during wet years.

20.7 km (12.9 mi) Continue east 2.2 km (1.4 mi) on Mercer Lake Road to a turnout on the northwest side of the road. The small turnout at Stop 14 is adjacent to a prominent road cut at a sharp road bend on the southeast side of Mercer Lake. Watch for traffic hazards at this sharp road bend.

Stop 14: Mercer Lake Road Cut

From the turnout at the road bend at this stop we will carefully cross the road to examine gibbsite nodules and interstratal groundwater cementation of late Pleistocene dunes that date back to 70 ka (thermoluminescence) (Fig. 4). The top of this dune section has been truncated by mass wasting, and the lower units extend below the Mercer Lake water level. The full extent of this early dune advance is not known. However, younger late Pleistocene dunes, with less interstratal cementation, reach farther inland and to higher altitudes (see Side Trip below). The precipitation of gibbsite $Al(OH)_3$ in the coastal dunes came as a surprise to us, as this phase usually reflects extreme weathering in laterite. The

gibbsite occurs in the coarser sand where it precipitates as nodules or in cavity fills (1–2 cm diameter). The precipitation of gibbsite rather than kaolinite requires a low dissolved silica concentration, which was unexpected in these quartz-rich sand dunes (Beckstrand, 2001; Grathoff and others, 2001). Groundwater is apparently removing large amounts of Fe and Si from the aquifer, but the sinks or discharge areas of those two elements are not known. In addition to the gibbsite nodules, some late Pleistocene dune sections include gibbsite fracture fills, gibbsite replacement of lithic clasts, and gibbsite sheets between bedding planes.

Side Trip: An interesting side trip can be made from here to one of the higher altitude dune deposits in the Florence area. From Stop 14 continue 0.1 km (0.05 mi) east on Mercer Lake Road to an unmarked intersection. Turn south (right) on the gravel road (which turns into Chapman Road) and follow it 0.6 km (0.4 mi) uphill to an intersection with View Road. Alternatively, find another route to View Road. Turn east (left) on View Road, and then make an abrupt turn north (left) on Ocean View Road. Continue uphill 0.2 km (0.1 mi) and look for dune deposits in an east-side road cut near the top of Ocean View Road. The thin topsoil development and weak cementation of the Cox horizon here suggests a younger age for these late Pleistocene dunes than those of the Mercer Lake deposit at the bottom of the north slope at Stop 14. Return to Stop 14.

23.0 km (14.3 mi) From Stop 14 return 2.3 km (1.4 mi) west on Mercer Lake Road to the US 101 intersection. Turn south (left) on US 101.

30.5 km (18.9 mi) Continue south 7.5 km (4.7 mi) on US 101 to the Oregon 126 intersection in Florence.

33.0 km (20.5 mi) Continue south 2.5 km (1.5 mi) on US 101 through Florence, and over the Siuslaw River Bridge to the South Jetty Road intersection. Turn west (right) on South Jetty Road.

36.3 km (22.5 mi) Continue west 3.3 km (2.1 mi) on South Jetty Road to a north bend (right) in the road at the modern foredune. Turn around at the gravel-road intersection.

Solid-stem auger coring at this site recovered late Holocene beach shells and gravel at 7 m depth. Little or no net shoreline progradation has occurred at this site since the deposition of the beach shells (shell radiocarbon sample yet to be dated). Ground penetrating radar profiles, vibracores, and geoprobe cores from the adjacent deflation plain record subhorizontal deflation surfaces to at least 10 m depth. In this area the position of the middle Holocene paleoshoreline back edge has not been established. However, a deflation-truncated paleosol was encountered at 10 m depth at the eastern margin of the deflation plain (Goose Pasture Staging Area) about 1 km east of the foredune. Deeper GPR profiling will be required to establish the Holocene shoreline back edge, somewhere between the modern foredune and the Goose Pasture Staging Area.

38.5 km (23.9 mi) Return east 2.2 km (1.4 mi) on South Jetty Road to the South Jetty Staging Area entrance road south (left turn) for Stop 15.

Stop 15: South Jetty Road Staging Area 1 (rest room and lunch)

After lunch we will take a brisk walk to an overview of the South Siuslaw Dune archaeological site. This informal overview is 50 north of the entrance day-pass station, which was passed on the way into the South Jetty Staging Areas. The archaelogical site, dated at 0.7-1.0 ka (Minor and others, 2000) was developed on a weak paleosol that is being progressively buried and exposed on opposite sides of a deflation corridor between active transverse dunes. The deflation corridor can be viewed toward the base of the northward-descending dune field. Abundant fish bones, small spear points, and other artifacts are scat-

tered on the paleosol. Charcoal layers in the paleosol date from 0.5-2.3 ka (radiocarbon). Another paleosol 0.5 km to the east of the 0.5-2 ka paleosol dates at 4 ka. It is not known what caused the localized vegetative stabilization of the dunes during the temporary periods of soil development recorded at these active-dune sites.

Ground penetrating radar profiling was performed to test whether the buried cultural horizon, that is paleosol (0.5-2 ka), could be mapped under the active dunes. We will examine the GPR profiles of the cultural site from the overview. The GPR records show that the paleosol climbs to the south, as photographed in previous years of exposure, and that it merges with a perched groundwater surface at several meters depth. Both the paleosol and groundwater surface dip northward toward the Siuslaw River. Several dune reactivation surfaces are imaged at much greater depths in the subsurface. A continuous high-amplitude basal reflection occurs at a subsurface depth of 40 m. It is not known whether this basal reflection represents the Holocene–Pleistocene dunal contact, a fluvial terrace cut into the dunal substratum, or some other structure.

39.6 km (24.6 mi) Return 1.1 km (0.7 mi) to US 101 intersection. Turn south (right) on US 101.

42.1 km (26.1 mi) Continue south 2.5 km (1.5 mi) on US 101 to intersection with Woahink Road. Turn east (left) on Woahink Road.

45.2 km (28.1 mi) Continue east 3.1 km (1.9 mi) on Woahink Road to Stop 16 at dune deposits exposed in a north-side road cut. En route, examine oversteep cutbanks of Woahink Road and the subsequent slope failures of late Pleistocene dune deposits, some 1.6 km (0.9 mi) from the US 101 intersection.

Stop 16: Woahink Road Cut Exposure

At this stop we will briefly examine and record a soil profile taken in a road cut of the late Pleistocene dune deposits. This locality is near the eastern limit of late Pleistocene dune advance, and has been thermoluminesence (TL) dated at 37 ka (Figures 4 and 7b). Pleistocene dune-soil chronosequencing has been attempted in the study area, based on traditional methods of soil color, texture, and structure. However, the traditional indexes of soil development have not correlated well with measured deposit age (Beckstrand, 2001). Problems likely arise from soil truncation by deflation, loess deposition on existing soils, and variable redox conditions from changing groundwater level, among others.

For this study we have had success in using a combination of measurements taken from the preserved accumulation horizons in the dune topsoils. The measurements include (1) type of soil accumulation horizon (Bw, Bh, Bg, Bt, Bs/Bc); (2) thickness of preserved accumulation zone (<5, 5-20, 20-60, 60-120, >120 cm); (3) maximum apparent consolidation (loose, cohesive, peds, blocky, Cox-cemented); and (4) maximum consolidation measurements from penetrometer (1, 2, 3, 4, 5 kg/sq cm). Each of these parameters is scored (1–5), summed, and averaged by the number of parameters to yield a normalized accumulation horizon index (NAHI) of 1–5. Low NAHI values (1–2) generally correspond to late Holocene dune topsoils, whereas high NAHI values (4–5) typify Pleistocene dune topsoils. Where truncation has occurred at incomplete soil profiles, the parameter of accumulation-horizon thickness is not used. Where dune reactivation has buried soils producing multiple paleosols, the NAHI index provides only a limiting relative-age estimate. Ultimately, luminescence or radiocarbon dating is required to constrain the absolute age of the dune deposits. However, the NAHI system used in this study has proved useful to geologists, engineers, and archaeologists in discriminating between Pleistocene and Holocene dune deposits.

48.3 km (30.0 mi) Return west 3.1 km to US 101 intersection. Turn south (left) on US 101.

51.4 km (31.9 mi) Continue south 7.1 km (4.4 mi) on US 101 to intersection with Siltcoos Road (Siltcoos Campground and Beach Access). Turn west (right) on Siltcoos Road.

53.8 km (33.4 mi) Continue west 2.4 km (1.5 mi) on Siltcoos Road to Stop 17 at the Siltcoos Recreation Area foredune parking lot and beach access trail.

Stop 17: Siltcoos Recreation Area Foredune (rest rooms)

This is the last stop of Day 2 in the formal Field Trip Guide. We will walk a couple hundred meters north from the parking lot to a "foredune breach" experiment site. The artificial breach was completed a couple of decades ago to allow beach sand to be blown through the beachgrass-stabilized foredune, thereby rebuilding dunes on the deflation plain. We will observe and discuss the results of the experiment, particularly with respect to modern beach-sand supply. The basal foredune deposits have been vibracored and thermoluminescence dated (3 ka) at this locality. Deflation-plain deposits (dune sand) were also vibracored and TL dated (1.5 ka) at sites at the eastern margin of the existing deflation plain. Historic photos demonstrate at least 100 m of recent eastward deflation. The deflation occurs to groundwater level, and it leaves interannual records of "trailing linear-edge deflation troughs". Landward from the deflation plain, or about 1.5 km east of the foredune, we will observe Tree Island #1, where exposed paleosols date to late Pleistocene time, greater than 32 ka (thermoluminescence and radiocarbon)(Fig. 4). These exposed paleosols indicate a relatively thin veneer of Holocene sand above the late Pleistocene dune ridge. Current deflation of the late Pleistocene paleosols at the Tree Island site, and in nearby parabolic-dune deflation corridors, reflect the remobilization of the underlying late Pleistocene dune deposits to form new Holocene dunes.

We hypothesize the following scenario for dune development in this area: Late Pleistocene dune deposits by 30 ka accumulated as a broad high ridge (about 100 m above modern sea level) landward from a broad deflation plain (near present sea level). Early to middle Holocene transgression ravined the late Pleistocene deflation-plain deposits. Middle Holocene shoreline progradation followed posttransgression sand supply from onshore wave transport for several thousand years. Surplus sand was blown inland, mantling and locally reactivating the late Pleistocene dune ridge. With decreasing sand supply in latest Holocene time, the shoreline position stabilized or began to retreat. However, shoreward deflation continued to supply small transverse and parabolic dunes on the seaward side (Tree Island area) of the large dune ridge. Large areas of unstable active dunes continued to resist vegetative stabilization into late historic time (Cooper, 1958; Hunter and others, 1983). Nonnative beachgrass and shore pine planted in the middle part of the 1900s isolated and stabilized the active dunes. Deflation east of the foredune lowered the Holocene dune cover to the groundwater-surface level. Ongoing deflation continues to extend the deflation-surface wetlands (bogs) to the east. Finally, incipient European beachgrass colonization of the transverse and parabolic dunes on the large dune ridge has begun within the past couple of decades. The spread of European beachgrass onto the western slopes of the large dune ridge foretells the likely end of active dunal landforms in the Oregon Dunes National Recreation Area.

Several means of reactivating the vegetation-stabilized dunes are now under study in the ODNRA. These approaches to European beachgrass control include large-scale mechanical removal, expanded all-terrain vehicle (ATV) recreation, herbicides, burning, and handpicking. We will discuss the costs and relative effectiveness of these methods, and whether they can be sustained over large areas.

Side Trip: A short drive can be made from the Siltcoos Recreational Area entrance to the ODNRA Dunes Overlook Station by going south 4.1 km (2.5 mi) on US 101. The

U.S. Forest Service provides a handicap-accessible overlook of the dunes. On a clear day the view extends from the deflation plain landward of the foredune to climbing parabolic dunes "precipitating" (Cooper, 1958) into upland forests perched on late Pleistocene dunes. The late Pleistocene dunes are themselves ramped up against foothills of the Coast Range. Signboards at the overlook outline dune forms, habitats, and wildlife. Return to Stop 17.

Side Trip: A further side trip can be made to the Tahkenitch Landing archaeological site at Tahkenitch Lake, another 3 km (2 mi) south of the ODNRA Overlook. Three periods of dunal landscape development have been proposed for the Tahkenitch Lake area based on animal remains and other artifacts at the site (Minor and Toepel, 1986). The periods are (1) fishing camp—saline species in an estuary of the Tahkenitch Valley (8-5.2 ka by radiocarbon), (2) village—saline species and whalebones in a shallow estuary of the Tahkenitch Valley (5.2-3 ka), and (3) canoe landing—dune-barrage lake (3-0 ka). A controversy has arisen over the origin of the whalebones. If the whales swam up a moderately deep estuary to the site in late Holocene time, then the large dunes blocking the valley could not have developed until very late Holocene time. If the whalebones were scavenged from the beach and transported to the site, then the large dunes blocking most of the Tahkenitch Valley might have been in place by middle Holocene time. Analysis of long core records from the Tahkenitch Lake deposits could help resolve the timing of the estuary-to-lake transition. Return to Stop 17.

68.3 km (42.4 mi) From Stop 17 return east 2.4 km (1.5 mi) to the intersection with US 101. Turn north (left) on US 101, and continue north 12.1 km (7.5 mi) to the intersection of US 101 with Oregon 120 in Florence.

End of field trip guide.

ACKNOWLEDGEMENTS

This field trip guide is based in large part on field mapping performed by us, by study collaborators, and by student field assistants. Some of the student assistants include C. Alton, J. Brasseur, B. Burris, S. Cowburn, J. Jones, C. Knoepp, G. Peterson, S. Wacaster, and R. DeChaine. Support for this research has been provided by Griffith University, Brisbane, Australia (1996-present); the USFS Siuslaw National Forest (1997-present); the Oregon Dunes National Recreation Area (1996-1999); Oregon Department of Transportation (1999-present); Oregon Sea Grant 2000-02 (R/SD-04 NA650K); and Oregon Sea Grant 2002-04. George Moore provided editorial suggestions for the improvement of this field trip guide.

REFERENCES

Beckstrand, D.L., 2001, Origin of the Coos Bay and Florence Dune Sheets, south central coast, Oregon: Portland State University MS Thesis, 192 p.

Briggs, G.G., 1994, Coastal crossing of the elastic strain zero-isobase, Cascadia margin, south central Oregon coast: Portland State University MS Thesis, 251 p.

Carlson, J., Reckendorf, F., and Ternyik, W., 1991, Stabilizing coastal sand dunes in the Pacific Northwest: USDA Soil Conservation Service, Agriculture Handbook 687, 53 p.

Cooper, W.S., 1958, Coastal sand dunes of Oregon and Washington: Geological Society of America Memoir 72, 169 p.

Cooper, W.S., 1967, Coastal dunes of California: Geological Society of America Memoir 104, 131 p.

Couch, R., Cook, J., Gerald, C., Troseth, S., and Standing, W., 1980, Seismic measurements of the dunal aquifer of Florence, Oregon: Final Report to the Lane Council of Governments, Eugene, Oregon, 41 p.

Erlandson, J.M., Tveskov, M.A., and Byram, S., 1998, The development of maritime adaptations on the southern Northwest Coast: Arctic Anthropology, v. 35, p. 6-22.

Grathoff, G.H., Peterson, C.D., and Beckstrand, D.L., 2001, Coastal dune soils in Oregon, USA, forming allophane and gibbsite: 12th International Clay Conference Proceedings, Argentina, 8 p., in press.

Hart, R., and Peterson, C.D., 1997, Episodically buried forests in the Oregon surf zone: Oregon Geology, v. 59, p. 131-144.

Hunter, R.E., Richmond, B.M., and Alpha, T.R., 1983, Storm-controlled oblique dunes of the Oregon coast: Geological Society of America Bulletin, v. 94, p.1450-1465.

Kennedy, G.L., Lajoie, K.R., and Wehmiller, J.F. 1982, Aminostratigraphy and faunal correlations of late Quaternary marine terraces: Science, v. 299, p. 545-547.

Illenberger, W.K., and Verhagen, B.T., 1990, Environmental history of dating of coastal dunefields: South African Journal of Science, v. 86, p. 311-314.

Minor, R., Greenspan, R.L., Hughes, R.E., and Tasa, G. L., 2000, The Siuslaw Dune Site: Archaeology and environmental changes in the Oregon Dunes, *in* Losey, R.J., ed., Changing landscapes: Proceedings of the Third Annual Coquille CulturalPreservation Conference: North Bend, Oregon, Coquille Indian Tribe, p. 82-102.

Minor, R., and Toepel, K.A., 1986, The archaeology of the Tahkenitch landing site: Early prehistoric occupation on the Oregon coast: Eugene, Ore., Heritage Research Associates:, 46 p.

Muhs, D.R., Rockwell, T.K., and Kennedy, G.L., 1992, Late Quaternary uplift rates of marine terraces on the Pacific coast of north America, southern Oregon to Baja California Sur, Quaternary International, v.15-16, p. 121-133.

Orme, A.R., 1990, The instability of Holocene coastal dunes: The case of the Morro Dunes, California, *in* Nordstrom, K., Psuty, N., and Carter, B., eds., Coastal dunes: Form and process: New York, John Wiley and Sons, p. 315-336.

Peterson, C.D., and Madin, I.P., 1997, Coseismic paleoliquefaction evidence in the central Cascadia Margin, USA. Oregon Geology, v. 59, p. 51-74.

Peterson, C.D., and Scheidegger, K.F., 1984, Holocene depositional evolution in a small active-margin estuary of the northwestern United States: Marine Geology, v. 59, p. 51-83.

Pirazzoli, P.A., 1993, Global sea-level changes and their measurement: Global and Planetary Change, v. 8, p. 135-148.

Pye, K., and Rhodes, E.G., 1985, Holocene development of an episodic transgressive dune barrier, Ramsay Bay, North Queensland coast, Australia: Marine Geology, v. 64, p. 189-202.

Reckendorf, F., 1998, Geologic hazards of development on sand dunes along the Oregon Coast, *in* Burns, S., ed., Environmental, groundwater, and engineering geology applications from Oregon: Belmont, Calif., Star Publishing Company, p. 429-438.

Scheidegger, K.F., Kulm, L.D., and Runge, E.J., 1971, Sediment sources and dispersal patterns of Oregon continental shelf sands: Journal of Sedimentary Petrology, v. 41, p. 1112-1120.

Schlicker, H. G., Deacon, R. J., Olcott, G.W., and Beaulieu, J.D., 1973, Environmental geology of Lincoln County, Oregon: Oregon Department of Geology and Mineral Industries Bulletin 81, 171 p.

Short, A.D., 1987, Modes, timing and volume of Holocene cross-shore and aeolian sediment transport, southern Austalia: Coastal Sediments v. 87, p. 1925-1937.

Thom, B., Hesp, P., and Bryant, E., 1994, Last glacial "coastal" dunes in eastern Australia and implications for landscape stability during the Last Glacial Maximum: Palaeogeography, Palaeoclimatology, Palaeoecology, v. 111, p. 229-248.

Ticknor, R., 1993, Late Quaternary crustal deformation on the central Oregon coast as deduced from uplifted wave-cut platforms: Western Washington University MS Thesis, 70 p.

Tooley, M.J., 1990, The chronology of coastal dune development in the United Kingdom, in Bakker, W.M., Jungerius, P.D., and Kalin, J.A., eds., Dunes of the Eurpoean Coast: Catena Supplement, v. 18, p. 81-88.

Worona, M.A., and Whitlock, C., 1995, Late Quaternary vegetation and climate history near Little Lake, central Coast Range, Oregon: Geological Society America Bulletin, v. 107, p. 867-876.

Fluvial Record of Plate-Boundary Deformation in the Olympic Mountains

Frank J. Pazzaglia, Department of Earth and Environmental Sciences, Lehigh University, Bethlehem, Pennsylvania 18015; fjp3@Lehigh.edu

Mark T. Brandon, Department of Geology and Geophysics, Yale University, New Haven, Connecticut 06520; mark.brandon@yale.edu

Karl W. Wegmann, Washington Division of Geology and Earth Resources, Olympia, Washington 98504; karl.wegmann@wadnr.gov

TRIP OVERVIEW

We have constructed a 2-day field trip designed to exhibit the geology, geomorphology, and active tectonics of the Pacific coast of the Olympic Peninsula. The trip is organized around the following three major topics that should generate lively discourse on how to use and interpret basic field relationships in tectonic geomorphology research:

(1) What is a river terrace, how is it made, and what do river terraces tell us about active tectonics?

(2) What is driving orogenesis for the Olympic Mountain segment of the Cascadia Subduction Zone? Is it shortening parallel to the direction of plate convergence, shortening normal to the direction of plate convergence, or some combination of both? Are there any geomorphic or stratigraphic field relationships that can actually be used to track the horizontal movement of rocks and thus interpret the shortening history over geologic time scales?

(3) We know that uplift along Cascadia includes the effects of cyclic earthquake-related deformation, as well as long-term steady deformation. How do these different types of uplift influence incision and aggradation in the rivers of the Olympic Mountains?

The trip begins by building a Quaternary stratigraphic foundation along the western coast of the Olympic Peninsula, and then it works landward into the Clearwater River drainage. As far as possible, we will present the deposits in stratigraphic order, from oldest to youngest. Throughout the trip, we will show the data and reasoning for the spatial correlation of deposits, their numeric age, and the resulting tectonic implications. An important consideration in understanding deformation in this setting is how rocks move horizontally through the subduction wedge. We present geomorphic and stratigraphic data to help resolve the horizontal translation of rocks and thus provide constraints for shortening over geologic time scales.

Fluvial terraces are the main source of geologic and Quaternary stratigraphic data used in our tectonic interpretations. Terraces are landforms that are underlain by alluvial deposits, which in turn sit on top of straths, unconformities of variable lateral extent and local relief. Typically, a strath is carved into bedrock, but it can also be cut into older alluvial deposits. At the coast, we recognize straths and their accompanying overlying alluvial deposits, and then show how those features continue upstream into the Clearwater drainage. The straths and terraces are exposed because there has been active incision of the river into the rocks of the Olympic Peninsula. The most obvious conclusion is that river incision is a response to active rock uplift. But straths and terraces indicate that the incision history of at least one river has not been perfectly steady. There has been variability in external factors, such as climate or tectonics, which has modulated the terrace formation process. What we hope to demonstrate is that the variability in incision process and rate is primarily attributed to climate, but that continued uplift provides

Field Guide to Geologic Processes in Cascadia: Oregon Department of Geology and Mineral Industries Special Paper 36, 2002.

the means for long-term net incision of the river into the Olympic landscape.

The first day will be mostly dedicated to understanding the coastal stratigraphy in and around Kalaloch where many of our age constraints are located. The field relationships for permanent shortening of the Olympic Wedge will also be explored. The second day will be devoted to the Clearwater Drainage and an investigation of terraces of various size, genesis, and tectonic implication. We will consider the myriad of processes that have conspired to construct and preserve the terraces and the possible contributions of both cyclic and steady uplift.

INTRODUCTION

This field trip is about the use of Quaternary stratigraphy to measure tectonic deformation of the Olympic Mountains section of the Pacific Northwest Coast Range. An important motivation for understanding orogenesis here, and throughout the Coast Range, is the concern about the relationship of active deformation to seismic hazards associated with the Cascadia Subduction Zone. There is also interest in sorting the nature of the deformation, whether cyclic or permanent, and whether it involves mainly shortening parallel or perpendicular to the margin. Of particular interest is evidence of cyclic deformation related to large earthquakes at or adjacent to the subduction zone (Savage and others, 1981, 1991; Thatcher and Rundle, 1984; Dragert, 1987; Rogers, 1988; Atwater, 1987, 1996; Holdahl and others, 1987, 1989; West and McCrumb, 1988; Darenzio and Peterson, 1990; Atwater and others, 1991; Bucknam and others, 1992; Hyndman and Wang, 1993; Dragert and others, 1994; Mitchell and others, 1994). Fundamental to these studies is the distinction between short-term (10^2–10^3 yr) cyclic elastic deformation adjacent to the seismogenic subduction thrust and long-term (10^4–10^5 yr) permanent deformation associated with growth and deformation of the overlying Cascadia Wedge. Holocene deposits preserved in locally subsiding estuaries along the west coast of the Olympics provide good evidence of cyclic deformation related to large prehistoric earthquakes (Atwater, 1987, 1996). Seismogenic slip associated with these earthquakes, both on the subduction thrust and also on upper-plate faults, contributes to long-term deformation of the margin. However, it is difficult to separate elastic deformation, which is created and then recovered during each earthquake cycle, from the permanent deformation associated with fault slip. The earthquake cycle is probably partly decoupled from the permanent deformation, so we cannot easily integrate the effects of numerous earthquake cycles and arrive at the final long-term deformation. Furthermore, aseismic ductile flow, occurring within the deeper parts of the Cascadia Wedge, probably also contributes to deformation manifest over long time spans.

Pre-Holocene stratigraphy and structure provide the only records of sufficient duration to separate long-term permanent deformation from earthquake-cycle elastic deformation. For this reason, local active-tectonic studies have focused on deformation of Quaternary deposits and landforms, which are best preserved along the Pacific Coast and offshore on the continental shelf (Rau, 1973, 1975, 1979; Adams, 1984; West and McCrumb, 1988; Kelsey, 1990; Bockheim and others, 1992; Kelsey and Bockheim, 1994; Thackray and Pazzaglia, 1994; McCrory, 1996, 1997; McNeill and others, 1997; Thackray, 1998; McNeill and others, 2000). Mud diapirism, which is widespread beneath the continental shelf and along the west coast of the Olympics (Rau and Grocock, 1974; Rau, 1975; Orange, 1990), may be a local factor contributing to the observed deformation of Quaternary deposits.

In contrast, much less is known about the long-term deformation of the coastal mountains that flank the Cascadia margin (Fig. 1). The development and maintenance of the Oregon–Washington Coast Range as a topographic high suggests that it is an actively deforming part of the Cascadia plate boundary. Diverse geologic and geodetic datasets seem to indicate shortening and uplift both parallel (Wang, 1996; Wells and others, 1998) and normal (Brandon and Calderwood, 1990; Brandon and Vance, 1992; Brandon and others, 1998) to the direction of convergence (Fig. 2). This relationship is best documented in the Olympic Mountains (Fig. 1b, c), which, on a geologic time scale ($> 10^3$ yr), seems to be the fastest deforming part of the Cascadia forearc high. The Olympic Mountains occupy a 5800 km^2 area within the Olympic

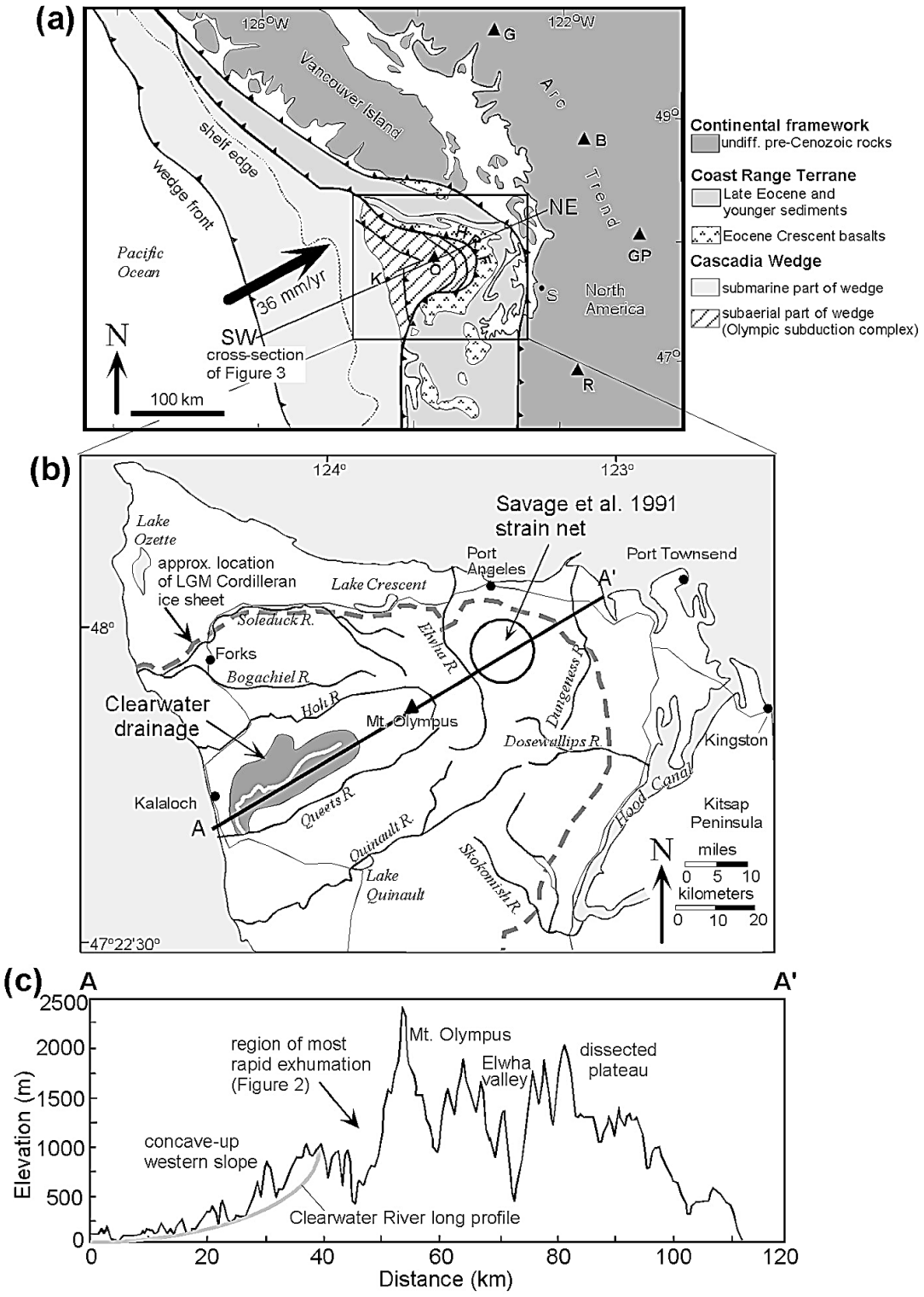

Figure 1. (a) Simplified geologic map of the Cascadia convergent margin, modified from Brandon and others (1998). HRF = Hurricane Ridge Fault, K = Kalaloch, S = Seattle, O = Mt Olympus, G = Mt Garibaldi, B= Mt Baker, GP = Glacier Peak, R = Mt Rainier. Beneath the Olympics, the convergence velocity of the Juan de Fuca Plate relative to North America is 36 mm/yr. at an azimuth of 54°, which is nearly orthogonal to the modern subduction zone (option 2 for Juan de Fuca/Pacific in DeMets and others, 1990, and "NA-PA Combined" in DeMets and Dixon, 1999). (b) Major drainages of the Olympic Peninsula. The gray dashed line marks the southern boundary of the last glacial maxima (LGM) of the Cordilleran Ice Sheet. (c) Topographic section across the Olympic Peninsula, parallel to the modern convergence direction (A-A' in b).

Peninsula. The central part of the range has an average altitude of ~1200 m, and reaches a maximum of 2417 m at Mount Olympus (Fig. 1c). The Olympics first emerged above sea level at ~18 Ma (Brandon and Vance, 1992), and they then seem to have quickly evolved into a steady-state mountain range, defined here by rock uplift rates that are closely balanced by erosion rates (Brandon and others, 1998). Fission-track-cooling ages indicate that the fastest erosion rates, ~0.8 m/k.y., are localized over the highest part of the range (Fig. 2). Rocks exposed there were deposited and accreted in the Cascadia Trench during the late Oligocene and early Miocene, and then exhumed from a depth of ~12 - 14 km over the past 16 m.y. Present-day rugged relief and high-standing topography are consistent with ongoing tectonic activity.

Geodetic and tide-gauge data (Reilinger and Adams, 1982; Holdahl and others, 1989; Savage and others, 1991; Mitchell and others, 1994) indicate that short-term uplift is very fast on the Olympic Peninsula, ranging from 1.2 to 3.2 m/k.y., with the highest rates along the west side of the peninsula (Fig. 2). These large rates probably include a significant component of earthquake-cycle elastic deformation, given that the Cascadia Subduction Thrust is presently locked. This conclusion is supported by geologic evidence that indicates insignificant long-term uplift or growth in coastal regions around the peninsula over the past 10 m.y. For instance, exposures of upper Miocene to lower Pliocene shallow-marine deposits locally crop out near modern sea level (Montesano and Quinault Formations; see Tq in Fig. 2) (Rau, 1970; Tabor and Cady, 1978a; Armentrout, 1981; Bigelow,

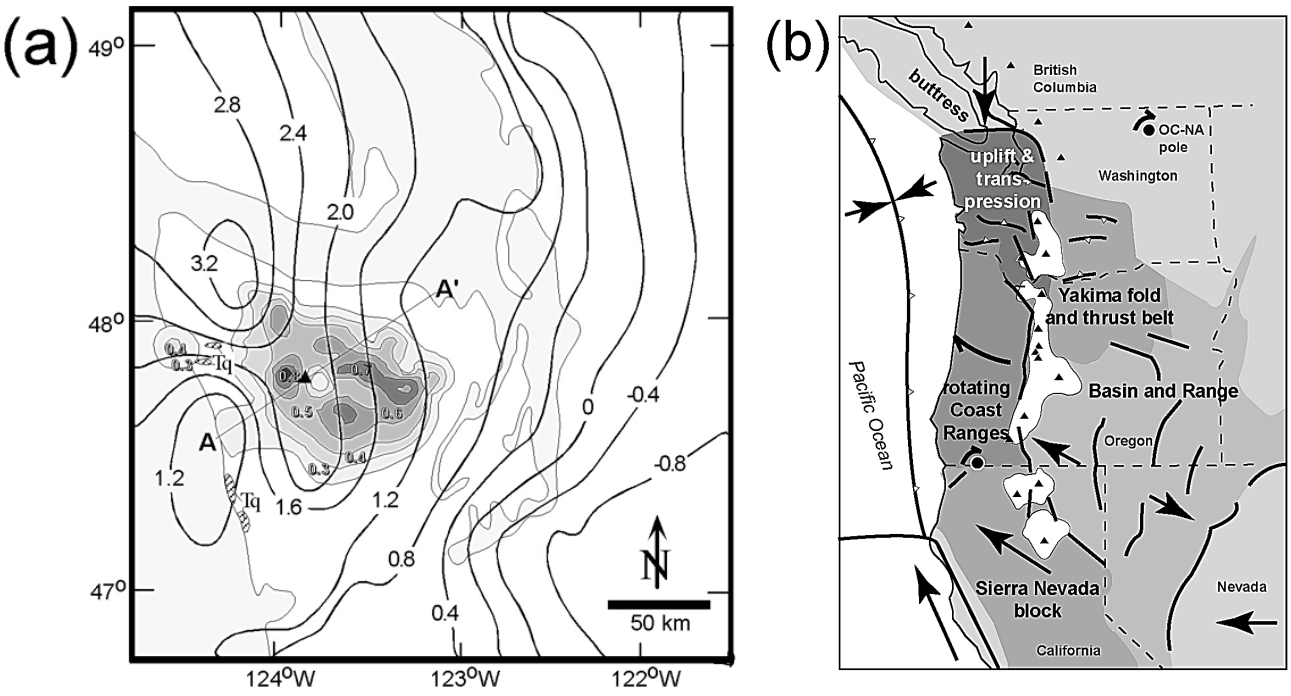

Figure 2. (a) Contour map showing short-term uplift rates (solid contour lines) as determined by geodetic measurements (Savage and others, 1991; Dragert and others, 1994) and long-term erosion rates (shaded contour intervals) as determined by fission-track thermochronology (Brandon and others, 1998, and M. Brandon and M. Roden-Tice, unpublished apatite fission-track ages). Rates are in mm/yr. Areas labeled Tq (diagonal-ruled pattern) along the west coast mark exposures of lower Pliocene shallow marine sediment of the Quinault Formation. The preservation of the Quinault and other adjacent nearshore units indicates slow long-term uplift and erosion along the west coast. (b) Relative motion of major tectonic blocks in the Pacific Northwest calculated from geodetic data with respect to the OC-NA pole. Arrows indicate relative block motion. Onshore white polygons and black triangles are volcanic deposits and volcanoes respectively. In this interpretation, uplift of the Olympic Mountains is accomplished by transpression between the Oregon Coast Ranges and a proposed Vancouver Island buttress. (Modified from Wells and others, 1998).

1987; Palmer and Lingley, 1989; Campbell and Nesbitt, 2000). These units currently sit within ~200 m of their original depositional altitude, which implies rock-uplift rates less than about 0.05 m/k.y. Slow long-term rock and surface uplift is also consistent with the preservation of extensive middle and lower Pleistocene deposits and constructional landforms along much of the west coast (Thackray and Pazzaglia, 1994; Thackray, 1998).

Our objective here is to use fluvial terraces to examine the pattern and rates of long-term river incision across the transition from the relatively stable Pacific Coast to the actively uplifting interior of the Olympic Mountains. We have focused on the Clearwater Drainage (Fig. 1b; Fig. 3), which remained unglaciated during the late Pleistocene and Holocene, and thus was able to preserve a flight of fluvial terraces. Each terrace records the shape and height of past long profiles, with the oldest record extending back into the middle Pleistocene. An important advantage of the Clearwater River is that its main channel has an orientation roughly parallel to the Juan de Fuca–North America convergence direction, and thus it is well situated to document shortening normal to the margin. We assess how fluvial terraces are formed in this setting and then use features of the terraces to estimate incision rates along the Clearwater long profile. Geologic relationships and geodetic data are used to examine the degree of horizontal shortening in the direction of plate convergence for the Cascadia Forearc High. The long fluvial history preserved in the Clearwater ensures that the unsteady deformation associated with the earthquake cycle is averaged out, leaving us with a record of long-term uplift. We show, however, that the earthquake cycle may play an important role in terrace genesis at the millennial time scale.

TECTONIC SETTING

The Cascadia subduction zone underlies a doubly vergent wedge (in the sense of Koons, 1990, and Willett and others, 1993). The change in vergence occurs at the crest of the Oregon-Washington Coast Range, which represents the forearc high. The doubly vergent system includes a prowedge (or proside) that overrides oceanic lithosphere and accretes turbidites of the Cascadia Drainage, and a retrowedge (or retroside) that underlies the east-facing flank of the Coast Range (Willett, 1999; Beaumont and others, 1999) (Fig. 4). This usage emphasizes the asymmetry of the underlying subduction zone, defined by subduction of the pro-plate (Juan de Fuca) beneath the retro-plate (North America).

Much of the Cascadia Forearc High is underlain by the Coast Range Terrane, a slab of lower Eocene oceanic crust (Crescent Formation and Siltez River Volcanics), which occurs as a landward-dipping unit within the Cascadia wedge (Fig. 1a) (Clowes and others, 1987). Accreted sediment that makes up the proside of the wedge reaches a thickness of 15-25 km at the present Pacific Coast (Fig. 1 and 4) and locally extends landward beneath the Coast Range Terrane. The Coast Range Terrane is clearly involved in subduction-related deformation, even though the rate of deformation is relatively slow when compared with the accretionary deformation occurring at the toe of the seaward wedge. Nonetheless, the Cascadia Wedge, by definition, includes all rocks that are actively deforming above the Cascadia Subduction Zone. Thus, the Coast Range Terrane cannot be considered a rigid "backstop", but instead represents a fully involved component of the wedge.

In the Olympic Mountains, the Coast Range Terrane has been uplifted and eroded away, exposing the Hurricane Ridge Thrust and the underlying Olympic Subduction Complex (OSC) (Fig. 1 and 3). The OSC is dominated by a relatively competent and homogeneous assemblage of sandstone and mudstone, with minor conglomerate, siltstone, and basalt (Tabor and Cady, 1978a, b). A large part of the OSC was formed by accretion of seafloor turbidites into the proside of the wedge, starting at about 35 Ma (Brandon and others, 1998). Where exposed in the Olympics, those accreted sediments are now hard well-lithified rocks. The steep rugged topography of the Olympics is supported by both basalt of the Coast Range Terrane and accreted sediment of the OSC, which suggests that there is little difference in their frictional strength. Uplift in the Olympic Mountains has been driven by both accretion and within-wedge deformation (Fig. 4) (Brandon and Vance, 1992; Willett and others, 1993, see stage 2 of their Fig. 2; Brandon and others,

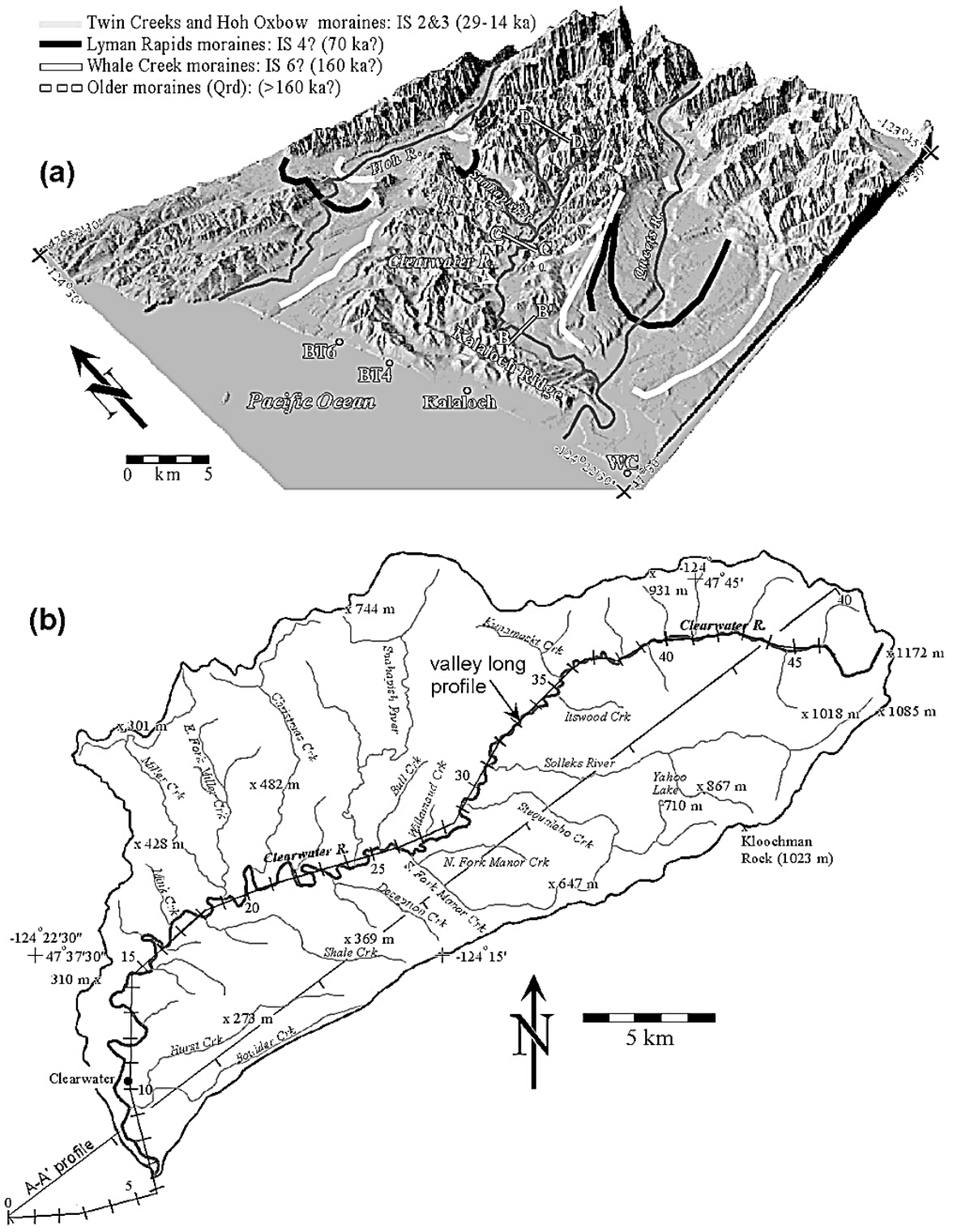

Figure 3. (a) Digital shaded-relief image (30 m-resolution DEM) showing the relation of the Clearwater Drainage to adjacent drainages and glacial deposits in the western Olympics (glacial data are from Thackray, 1996, 2001; Easterbrook, 1986). BT6, BT4, and WC mark Beach Trail 6, Beach Trail 4, and Whale Creek, where important stratigraphic relationships are exposed along the coast. Profiles B-B', C-C', and D-D' mark cross-valley sections of the Clearwater Valley, as presented in Fig. 8. (b) Map of the Clearwater drainage. The valley profile is shown as a crooked thin line with ticks marking valley kilometers from the mouth of the Queets River at the coast. The straight section (A-A' in Fig. 1 and 3) lies along the southeast side of the drainage. Final results were projected into A-A', which parallels the local convergence direction for the Cascadia Subduction Zone.

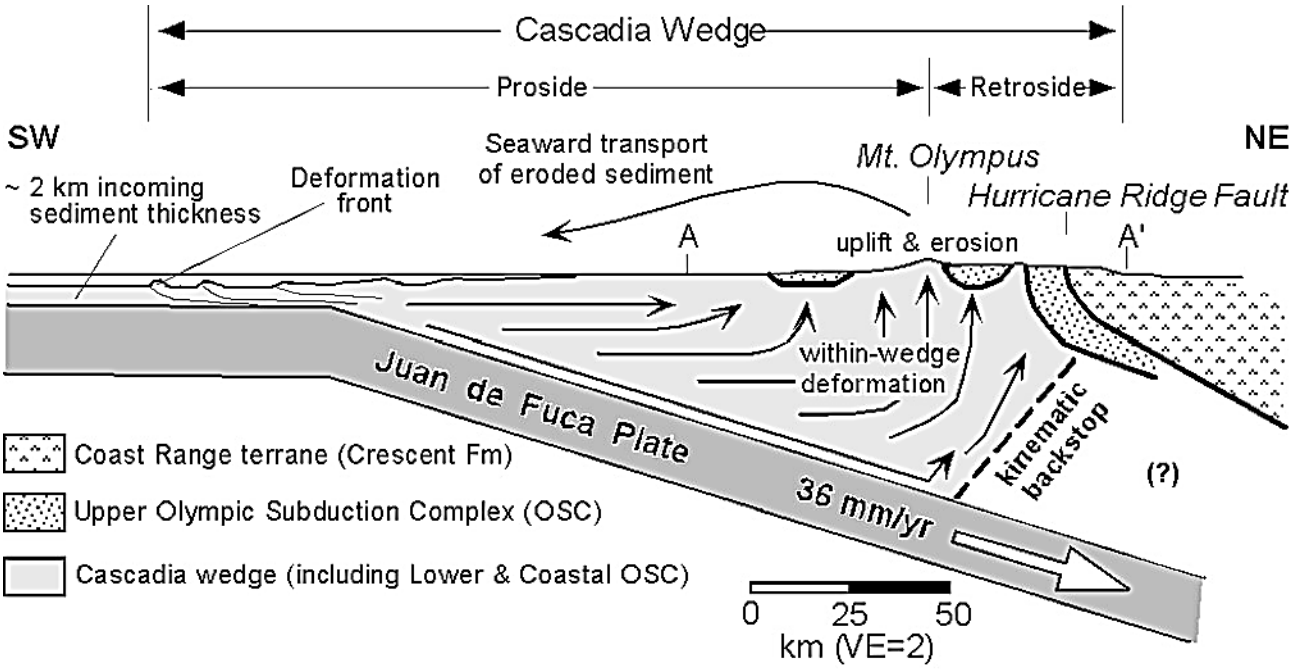

Figure 4. Schematic section (A-A' in Fig. 1) showing the regional-scale structure of the Cascadia Accretionary Wedge (after Brandon and others, 1998).

1998). Accretion occurs entirely on the proside of the wedge, resulting in decreasing material velocities toward the rear of the wedge. In the Olympics, retroside deformation is marked by folding of the Coast Range Terrane into a large eastward-vergent structure (Tabor and Cady, 1978a,b). The upper limb of that fold, which underlies the eastern flank of the Olympics (Fig. 4), is steep and locally overturned, in a fashion similar to the folding illustrated in Willett and others (1993, stage 2 in their Fig. 2). We infer from the steep topographic slope on the retroside of the wedge that folding is being driven by a flux of material from the proside of the wedge, and that the wedge has not yet begun to advance over the retroside plate (Willett and others, 1993).

Deep erosion and high topography in the Olympics are attributed to an arch in the subducting Juan de Fuca Plate (Brandon and Calderwood, 1990; Brandon and others, 1998). The subducting plate is about 10 km shallower beneath the Olympics relative to areas along strike in southwest Washington and southern Vancouver Island (Crossen and Owens, 1987; Brandon and Calderwood, 1990). Stated in another way, the shallow slab beneath the Olympics means that less accommodation space is available to hold the growing Cascadia Wedge (Brandon and others, 1998). This situation, plus higher convergence rates and thicker trench fill along the northern Cascadia Trench, has caused the Olympics to become the first part of the Cascadia Forearc High to rise above sea level. The early development of subaerial topography, plus continued accretion and uplift, account for the deep erosion observed in the Olympics. The corollary to this interpretation is that adjacent parts of the forearc high will evolve in the same way, although more slowly because of lower accretionary fluxes and a larger accommodation space for the growing wedge.

DAY 1. COASTAL EXPOSURES NEAR KALALOCH, OLYMPIC NATIONAL PARK, MOSES PRAIRIE PALEO SEA CLIFF—MODEL TERRACE IN THE CLEARWATER DRAINAGE

Miles

0.0 **Start. Kalaloch Lodge** (Fig. 5). Walk to the beach overlook for a brief overview. Kalaloch and the entire field-trip route lie in the west central part of the Olympic Peninsula, between two large drainages, the Hoh and Queets rivers that drain the northwest,

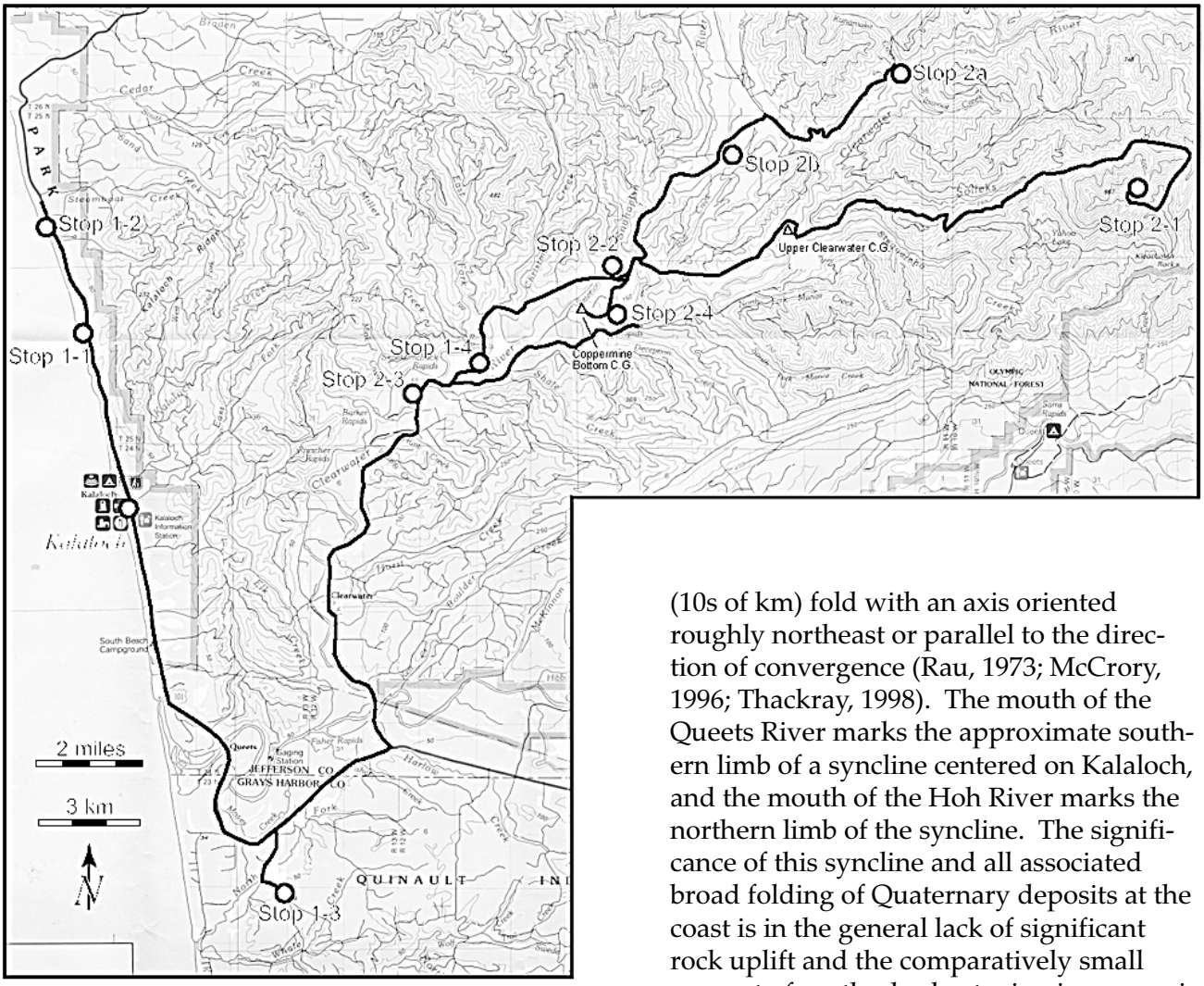

Figure 5. Field trip route and stops.

west, and southwest flank of Mt. Olympus (Fig. 1b, 3a). The Clearwater River is tucked away between these two master drainages, and we use the fluvial and glacial deposits of the Hoh and Queets rivers to constrain the ages of terraces in the Clearwater drainage (Fig. 6). The Olympic coast here is a constructional feature underlain by glaciofluvial deposits. It lacks the distinct, uplifted marine terraces characteristic of Cascadia in Oregon and northern California, although the effects of glacio-eustasy and coastal tectonics cause a major unconformity in the coastal stratigraphy. Both stratigraphy and correlation of the widespread unconformity indicate active tectonic deformation in the form of a broad (10s of km) fold with an axis oriented roughly northeast or parallel to the direction of convergence (Rau, 1973; McCrory, 1996; Thackray, 1998). The mouth of the Queets River marks the approximate southern limb of a syncline centered on Kalaloch, and the mouth of the Hoh River marks the northern limb of the syncline. The significance of this syncline and all associated broad folding of Quaternary deposits at the coast is in the general lack of significant rock uplift and the comparatively small amount of northerly shortening in comparison to the large amount of shortening and uplift in the direction of plate convergence. The relative tectonic stability of the coast is also supported by preservation of early Pleistocene glaciofluvial deposits, as well as Miocene–Pliocene neritic shelf-basin deposits like the Quinault and Montesano Formations that crop out at or near sea level. However the precise paleoelevation history of such ancient deposits, like the Quinault and Montesano formations, must be viewed in the context of the large but unknown degree of horizontal translation they have experienced because of wedge shortening.

The tectonic story that we begin weaving here has the following three major themes:

(1) Deformation that is linked to the real-time measurable effects of elastic-strain

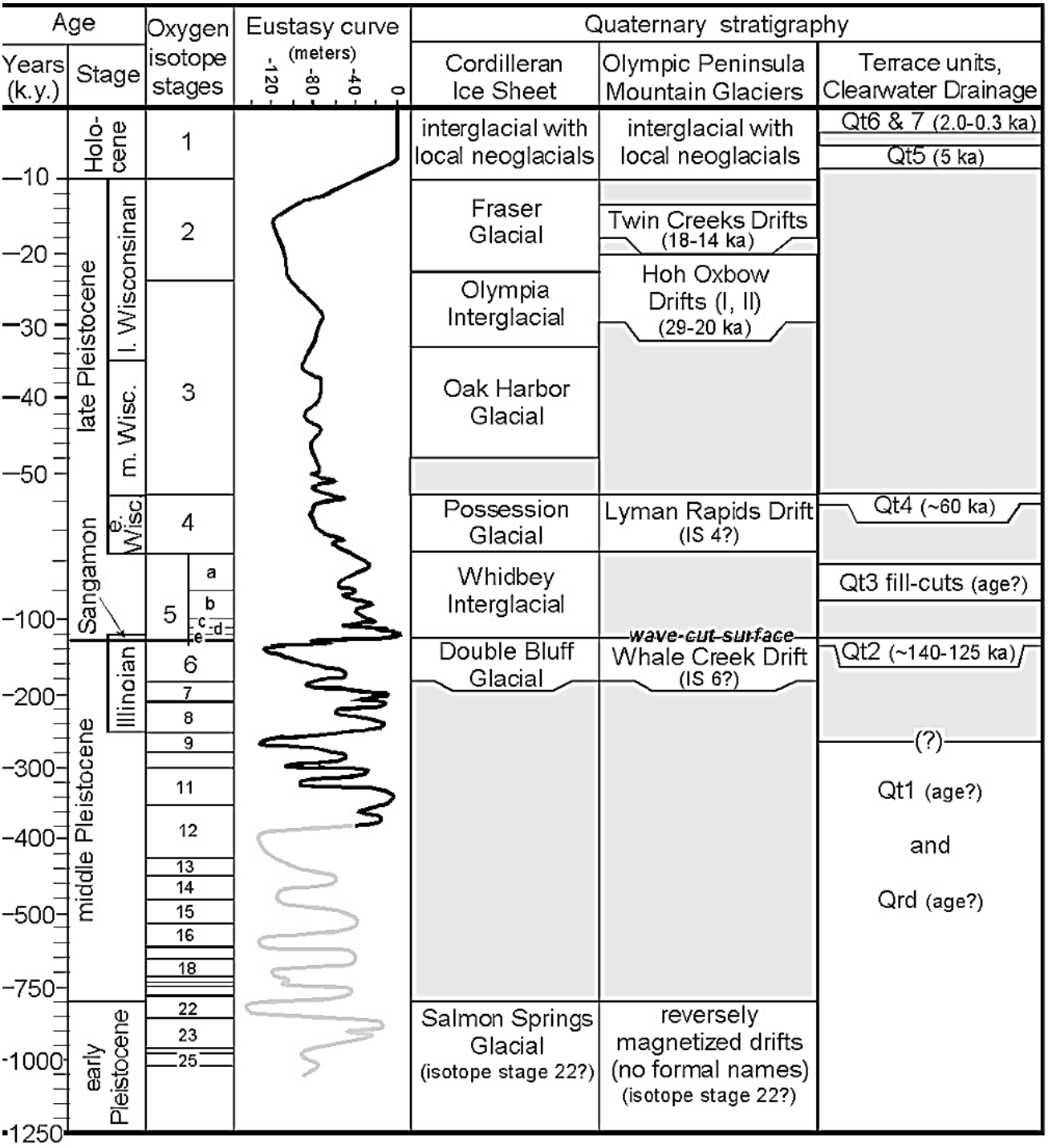

Figure 6. Regional stratigraphic correlations for glacial and fluvial deposits in the western Olympic Peninsula and surrounding regions. Note the variable scaling in the time axis. Eustasy curve is from Chappell and others (1996) for 0 to 140 ka, and Pillans and others (1998) for 140 to 300 ka. The next column shows deposits associated with advances and retreats of the Cordilleran Ice Sheet in Puget Sound, as synthesized by Easterbrook (1986). The next column shows the stratigraphic record of alpine glaciation in the western Olympics, based on the work of Thackray (1996, 2001) We have excluded his drift unit, called Oxbox Ø and estimated to be 39-37 ka, because it is based solely on an isolated sequence of lake sediment. The final column shows terrace stratigraphy in the Clearwater Valley as determined by work presented here.

accumulation and release during the subduction-earthquake cycle (Fig. 2a)

(2) Deformation linked to the long-term pattern of rock exhumation revealed by thermochronology (Fig. 2a), and

(3) Deformation linked to suggested northward translation of the Coast Range Terrane (Fig. 2b).

Our data are well suited to evaluating the geomorphic expression of points (1) and (2), and we will try to illustrate how these are likely to predominate over point (3) in orogenesis in the Olympic Mountains.

0.5 National Park Service Kalaloch Campground to your left. Highway 101 hugs the coast, traveling on a tread about 20 m in elevation. This tread is underlain by late Pleistocene alluvial and eolian deposits as well as Holocene marsh deposits.

2.5 Pass Browns Point (Beach Trail 3) and rise onto a 30-m terrace tread. This 30-m terrace is well preserved along the coast and will figure. significantly into the stratigraphic story.

3.3 **Stop 1-1. Beach Trail 4.** The purpose of this stop will be to see the rocks of the Cascadia Wedge and begin developing the stratigraphic framework of the Quaternary deposits by observing the 122 ka wave-cut unconformity. A key point is that rocks exposed at the coast may have moved northeastward into the coast, with little to no uplift. Park in the NPS parking lot and descend the trail leaving from the southeast corner of the lot and go to beach level.

The bedrock exposed here consists of turbidites of the Miocene Hoh Formation (Fig. 7a). These rocks were deposited on the continental slope in at least 2 km of water and have been uplifted here to sea level. More importantly, the Hoh Formation was laid down 50 to 100 km west of its current position and has since followed a largely horizontal trajectory to the present Olympic coastline (Fig. 4). The nearly vertically bedded bedrock is planed off at approximately 2.7 m above mean sea level by a wave-cut unconformity. A thin boulder lag locally lies atop the unconformity, and it is superceded by gray pebbly beach sand texturally and structurally identical to the modern exposed shoreface. Exposures along the trail leading to the beach clearly show the unconformity continuing west under the 30 m coastal terrace (Fig. 8). Cylindrical borings in the Hoh beneath the unconformity are interpreted as being shaped in part by pholad clams. The stratified sand, gravel, and peat overlying the beach deposits are part of the Browns Point Formation (Huesser, 1972; Fig. 7b). Gravel clasts in this deposit tend to be weathered, and their provenance is consistent with a local source, most likely Kalaloch Ridge directly to the west, rather than the Hoh or Queets Rivers, whose deposits tend to be less weathered. The Browns Point Formation seems to represent a long period of fluvial, glacio-fluvial, and marsh-type sedimentation. The base of the unit directly above the beach sands is radiocarbon dead, but stratigraphically higher deposit have a progressively younging sequence of radiocarbon ages (Huesser, 1972; Thackray, 1996). The youngest age comes from about 6 m below the terrace tread and is 16,700±160 radiocarbon years before present.

The wave-cut unconformity here (Fig. 7a) is a key stratigraphic horizon that can be traced for 80 km along the coast. It does not remain at the elevation viewed here. At Kalaloch, the unconformity is below sea level and not exposed. And it rises to a maximum of 52 m above sea level south of the mouth of the Queets River. The average elevation between the mouth of the Hoh and Queets rivers is 11 meters. Deposits both above and below the unconformity are radiocarbon dead. We propose at this stop, and then will develop the evidence at subsequent stops, that the unconformity represents a wave-cut surface, produced during eastward migration of a shoreface during the last major interglacial eustatic highstand, at 122 ka (isotope stage 5e).

5.3 Cross Steamboat Creek and slow for a left turn.

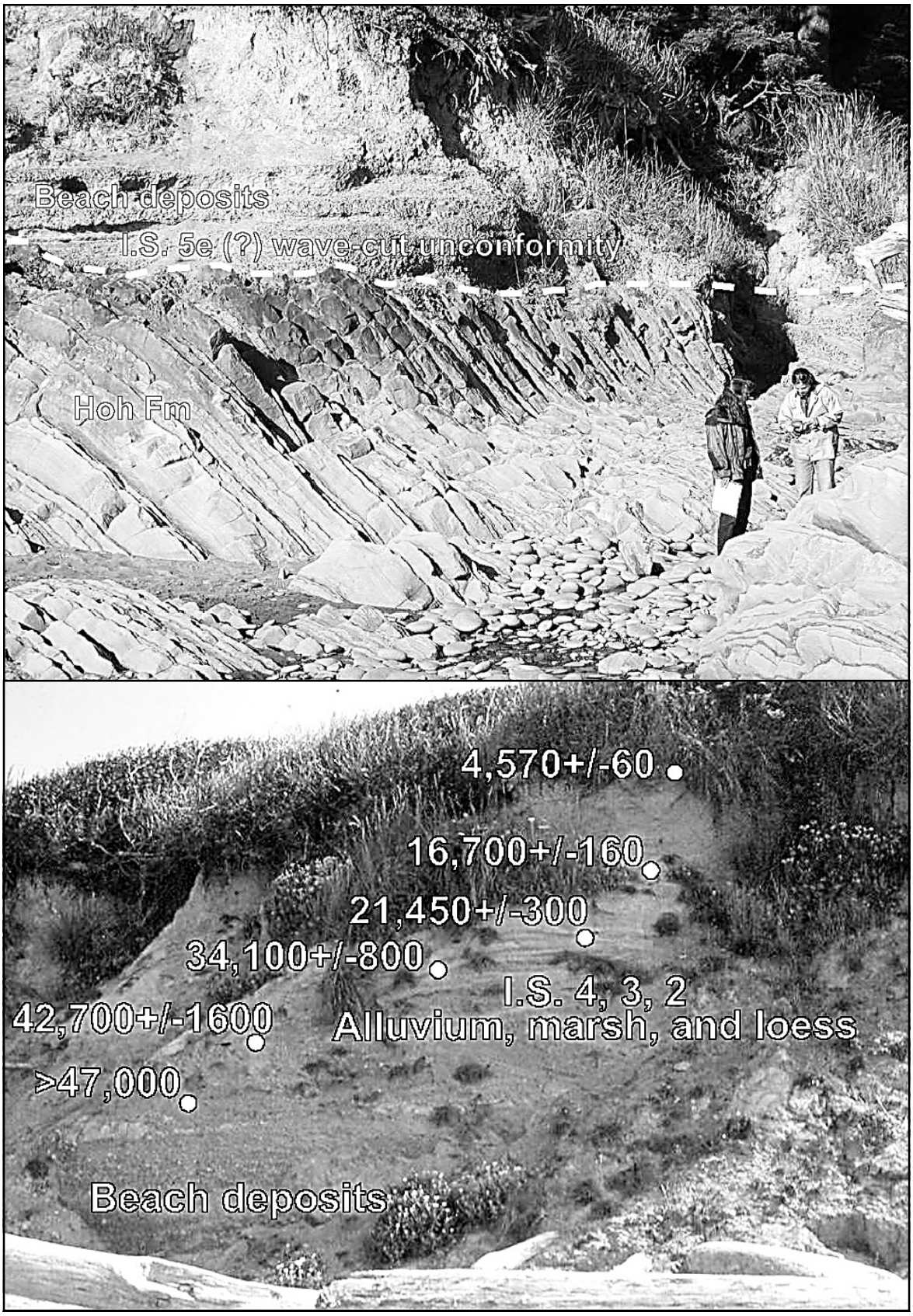

Figure 7. (Above) Photograph of the bedrock and wave-cut unconformity exposed at Beach Trail 4. (Below) Annotated photograph of the Quaternary stratigraphy and numeric ages typical of the Browns Point Formation in the vicinity of Beach Trail 4 (from Thackray, 1996).

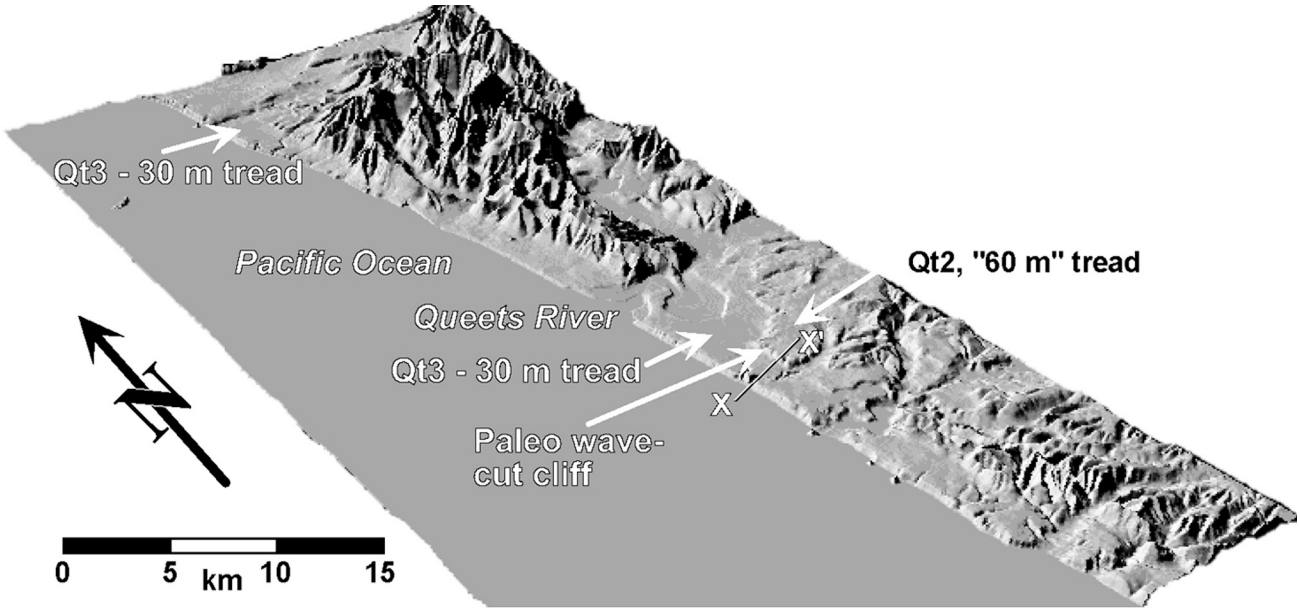

Figure 8. Digital shaded relief model showing the buried Sangamon sea cliff. The cliff appears as a subdued scarp that parallels the coast at a distance of 1500 m inland. The feature is visible in the image from about 15 km south to about 5 km north of the Queets River. Section X–X' is in Figure 10.

5.4 Turn left. **Stop 1-2. Beach Trail 6.** The purpose of this stop will be to observe the Quaternary deposits above and below the wave-cut unconformity, as well as key points for numeric ages of the deposits. We follow the field observation of these units with a map-based correlation to glacial deposits in the Hoh and Queets river valleys. Park in the National Park Service lot and access the trail that heads into the woods on the northwest corner of the lot. The exposures at Beach Trail 6 have changed significantly in recent years because of landsliding and coastal erosion. The trail is difficult to follow in places, and we urge care in descending the sea cliff. The deposits underlying the 30-m terrace are well exposed in the landslide headscarp. In particular, a 1–2 m cap of loess, with a yellowish-brown soil developed in it, can be seen conformably overlying stratified sand and gravel.

The wave-cut unconformity is higher here, at about 12 m above sea level, and is marked by a boulder lag (Fig. 9). The deposit below the unconformity was first named and described by Florer (1972) as the Steamboat Creek Formation. It is a complexly interbedded sequence of till, lacustrine deposits, glaciofluvial outwash, and sand dunes, which has yielded only infinite radiocarbon ages (below the detection limit for radiocarbon). Samples collected from lacustrine beds within this unit by Pazzaglia and Thackray, and analyzed by H. Rowe and J. Geissman at the University of New Mexico, show both normal and reversed polarities (Thackray, 1996). At this site in particular, the polarity of the sample is reversed indicating an age greater than 780 ka, the most recent reversal. Beach deposits overlie the unconformity and are succeeded by predominantly glaciofluvial outwash sourced from the Hoh drainage. The outwash within 15 m of the unconformity is interbedded locally with peaty beds that have returned radiocarbon-dead ages of >33.7 and >48 ka (Florer, 1972). Closer to the terrace tread, typically within 5 m of the surface, finite radiocarbon ages of 36,760±840, 28,352±504, and 24,422 radiocarbon years before present have been dated on woody material by Thackray (1996). The interpretation of these ages suggested by Thackray (1996, 2001) is that the outwash directly above the wave-cut unconformity is correlative to a marine isotope stage 4 (or possibly 5d,b) alpine glaciation and that the

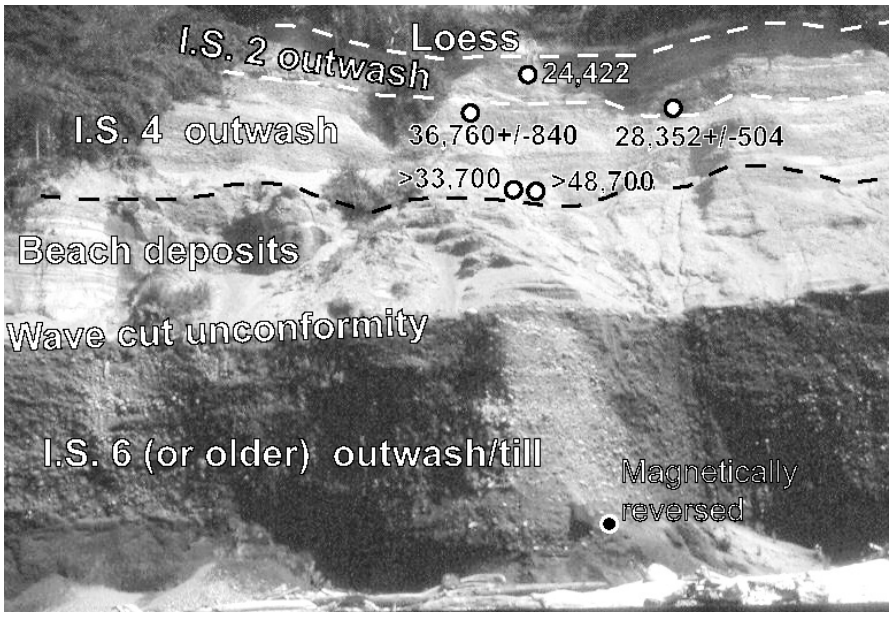

Figure 9. Annotated photograph of the Quaternary stratigraphy exposed in the vicinity of Beach Trail 6 (from Thackray, 1996).

finite radiocarbon ages near the top of the section is sourced from outwash draining isotope stage 2 or 3 alpine glaciers. A difficult to discern gravel-on-gravel unconformity between isotope stage 4 and isotope stage 2 or 3 deposits is implied by this interpretation.

The new landslides here at Beach Trail 6 expose mud diapirs that are both onlapped by and pierce the Steamboat Creek Formation (Rau and Grocock, 1974; Rau, 1975; Orange, 1990).

Return to the parking lot and assemble at the overlook of the coast and Destruction Island. The broad topographic and structural low between the mouth of the Hoh and Queets rivers filled with sediment from those two point sources, as well as from small streams draining Kalaloch Ridge (Fig. 8). The center of the low near Kalaloch has more fine-grained sediment than the regions proximal to the big river mouths. The general model is that the Queets and Hoh Rivers have periodically been point sources that built broad fans in front of the river mouths, spilling laterally into the Kalaloch low. The fans formerly extended far west of the current coast. The top of Destruction Island 5 km offshore (20 m elevation) is correlative to the 30-m tread here at the coast, and the flanged base of Destruction Island that sits only 1 m above mean tide level is the westward continuation of the wave-cut unconformity. The level of the fan tread, represented by the 30-m terrace we have been traveling on all morning, must reflect a significant amount of vertical aggradation rather than tectonic uplift. The preservation of the isotope stage 5e unconformity and approximately 800 ka Pleistocene deposits attest to the relative tectonic stability of the coast.

The most likely time for major periods of fan aggradation on a generally tectonically stable coastal setting is during a cycle of alpine deglaciation, as the river valleys are liberating a high sediment flux at the same time sea level is rising. It is difficult to imagine how the observed degree of aggradation could have occurred during relative sea level low on a coast not undergoing rapid vertical uplift. Furthermore, map relationships show how the coastal terrace treads can be traced more or less continuously up the Hoh and Queets valleys to heads of outwash (moraines). The general

glacial stratigraphy of the Hoh and Queets valleys (Thackray, 1996; 2001; Fig. 6) records a major isotope stage 4 alpine glaciation (60 ka, Lyman Rapids drift) that was responsible for the large body of outwash above the wave-cut unconformity and the construction of the 30-m terrace at the coast. Older alpine glacial periods, such as isotope 6 (150 ka, Whale Creek drift), are represented by the deposits below the wave-cut unconformity. However, there are clearly deposits older than isotope stage 6 below the unconformity, and these have a landward equivalent in various upland gravels locally called the Wolf Creek drift. Deposits of isotope stage 3 and 2 alpine glacial periods are underrepresented at the coast because of the relative small size of the glaciations.

Our next stop will further develop the correlation between the glacial and fluvial record in the river drainages to the stratigraphy at the coast by focusing on the remnants of the sea cliff present during the cutting of the isotope stage 5e wave-cut unconformity.

Return to vehicles, exit parking lot, and turn right (south) onto US 101.

10.3 Turn Right into the Kalaloch Campground. This is the **Lunch Stop**. Return to US 101 south following lunch.

10.8 Pass Kalaloch Lodge.

13.5 South Beach Campground is to the right. The 20-m tread here has been dated as 4570±60 radiocarbon years before present. The dated material unconformably overlies late Pleistocene alluvium.

15.7 Cross the Queets River. US 101 is following a big meander loop of the Queets River. To your left are several late Pleistocene to Holocene terraces and sloughs. To the right are treads of the 30-m terrace. Engineering borings for the bridge show that the alluvium is thin (6 m); there is no deep, filled thalweg beneath the river channel. In other words, the river is essentially flowing over a low-relief bedrock strath.

18.4 Turn right and stay straight on the dirt road. You are now on Quinault Nation land, and you need access permission from the tribal government in Tahola. Moses Prairie is to your left, following the valley of the North Fork Whale Creek.

19.2 Stay left on the main dirt road, cross the North Fork Whale Creek and begin to ascend the 60-m terrace.

19.9 Proceed to the fork in the road and turn around. This is **Stop 1-3. Moses Prairie**. The objective is to observe the paleo sea cliff, relate the 30-m and 60-m coastal treads to glaciations in the Hoh and Queets River valleys, and discuss how the paleo sea cliff tracks the horizontal motion of rocks and shortening of the wedge. The road from this stop crosses Moses Prairie, a site of active marsh deposition along North Fork Whale Creek, slightly inset into the 30-m tread. Pazzaglia, Thackray, and W. Gerstel extracted a hand-augered core from this bog in 1994. The core extended down 5 m until refusal in pebbly sandy silt. The point of refusal is taken to be the contact between the Moses Prairie North Fork Whale Creek marsh alluvial deposits and the isotope stage 4 glaciofluvial deposits of the 30-m terrace. Two radiocarbon determinations from the base of the core returned ages of 33,182±756 and 36,256±807 radiocarbon years before present (Thackray, 1996; 2001). These ages are consistent with the idea that the glaciofluvial outwash underlying the bulk of the 30-m terrace is radiocarbon dead but younger than the wave-cut unconformity, leading to its isotope stage 4 (60 ka) age assignment.

Our stop here is on a terrace tread 60 meters in elevation, which looks out over the 30-m tread that we have been traveling on all morning (Fig. 9). Like the 30-m terrace, the 60-m terrace tread is also underlain by alluvial and eolian deposits; however, they tend to be much more deeply weathered, to exhibit reddish soil colors, and to locally contain saprolitized gravel clasts. The terrace riser between the 30-m and 60-m terrace parallels the modern sea

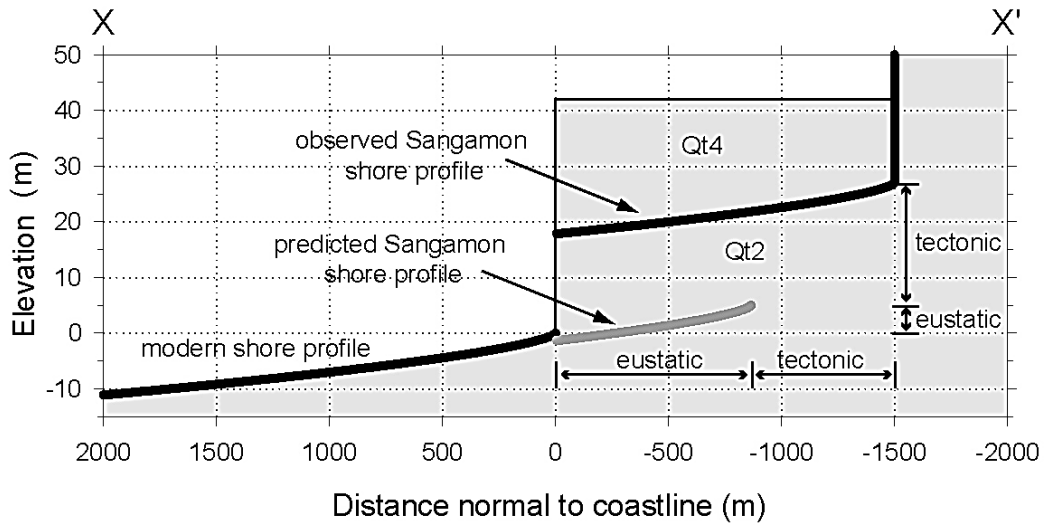

Figure 10. A schematic cross section of the modern shoreface and sea cliff and the buried Sangamon sea cliff at the mouth of the Queets River. The section follows the X–X' marked on Figure 8; it has an azimuth of 54°, parallel to the plate-convergence direction.

cliff and Queets River valley margin. We propose that the 60-m terrace represents an older, constructional top of a major aggradational fan to alluvial plain that headed in the Queets valley well before deposition of the isotope stage 4 deposits underlying the 30-m terrace. This older aggradational alluvial plain would have once extended far west of its current location. But in the same way that relatively high Holocene sea level is driving an eastward retreat of the coastal sea cliff into the 30-m terrace, the high relative sea level of the last major integlaciation, during isotope stage 5e, drove eastward retreat of a former seacliff into the older deposits underlying the 60-m terrace. Continuing with this logic, the eastward retreat of this paleo sea cliff would be synonymous with the cutting of the wave-cut unconformity. So the idea suggested at Stop 1-2, that the glaciofluvial deposits beneath the wave-cut unconformity is attributed to a isotope stage 6 (or older) alpine glacial outwash event, is strongly supported by finding remnants of the older alluvial deposits truncated by the paleoseacliff. Coastal aggradation during the isotope stage 4 alpine glacial event buried the isotope stage 5e beach deposits and subsequently filled-in the area in front of the paleo seacliff. We envision, and locally observe, a distinct buttress unconformity between the 30 m terrace tread of Moses Prairie and the terrace riser of the 60-m terrace.

The location of the paleo sea cliff with respect to the modern sea cliff contains information about how rocks are surfing horizontally through the Olympic wedge. In general, rocks at the Earth's surface move in both vertical and horizontal directions (Willett and others, 2001). Based on the apparent rapid retreat of the modern coastline during the Holocene (as discussed at the last stop), it would seem that a retreating sea cliff is able to rapidly adjust to rising sea level. Thus, we assume that the horizontal distance between the paleo sea cliff and the modern sea cliff is due solely to eustasy and tectonic displacement (Fig. 10).

We used Bruun's rule (Dean, 1991) to estimate how much the modern sea cliff would be translated landward if modern sea level were to rise to the height of the 122 ka Sangamon highstand. According to this relationship, a rise in sea level S would cause a landward shift (Δx) in the shoreline of

$$\Delta x = S\, w_w /(h_w + h_b) \qquad (1)$$

where w_w and h_w are the width and maximum depth of the breaker zone, and h_b is the berm height on the beach. A 17 year-

record for a deep-water (2780 m) buoy offshore of the Queets River indicates that waves coming into that coastline have maximum heights of 13.6 m and maximum periods of 18 seconds in the open ocean (Buoy 46005, National Data Buoy Center, 2000). Using relationships in Trenhaile (1997, see his p. 22), those waves indicate a maximum breaker depth h_w = 14.0 ± 1.0 m (uncertainties are ± 1 standard error). The nearshore profile indicates that this depth lies offshore at w_w = 2850 ± 220 m. The berm height h_b is about 1 m. Bruun's rule indicates that if modern sea level were to rise to the Sangamon highstand (S = +5 ± 0.7 m), the Sangamon sea cliff should have formed 945 ± 145 m inland with respect to the modern sea cliff. The sea cliff presently lies 505 ± 150 m farther inland, a difference that we attribute to tectonic displacement (Fig. 10).

Tectonic displacement of the sea cliff is assumed to have occurred parallel to the convergence direction, which is 26 degrees counterclockwise from perpendicular to the coast line. The cross section in Fig. 10 was constructed along the convergence direction at the mouth of the Queets River, and it shows both the horizontal and vertical components of the displacement, along with the predicted eustatic and tectonic components of those displacements. The predicted horizontal tectonic displacement is 450 ± 135 m, accomplished over 122 ± 2 ka, which gives a long-term horizontal tectonic velocity of 3.7 ± 1.1 m/k.y. relative to the adjusted highstand shoreline.

Our interpretation of this result relies on the assumption that the Olympics are in a long-term steady state, meaning that the range is not changing in size with time. This steady-state configuration implies that the shoreline is also in steady state. More specifically, we are assuming that the shoreline returns to the same location at each highstand. Of course, in practice, one would have to correct for small differences in the height of successive highstands (as we have done above). The overall implication is that when the shoreline is at steady state, erosion in the breaker zone is balanced by uplift at the coast. In this case, the calculated tectonic displacement of the paleo sea cliff would represent the horizontal velocity of rocks at the coast relative to the long-term steady-state position of the shoreline. An alternative interpretation is that the Olympics are not in steady state, and the shoreline is moving westward as the mountain range increases in size and width. The coastal geomorphology does not provide any information to distinguish between these two end-member interpretations. However, Pazzaglia and Brandon (2001) do show that frontal accretion into a steady-state Olympics wedge will produce horizontal surface velocities at the coast of 3 m/k.y. Thus, the sea cliff observations are consistent with a steady-state wedge interpretation.

Return to vehicles, and retrace the route back out to US 101.

21.4 Turn right on US 101 and continue on the 30-m tread.

24.0 Turn left on the Clearwater–Snahapish Road.

24.6 Cross the Queets River. The confluence of the Queets and Clearwater is ahead and to the left. Continue along the Clearwater River. As at the US 101 bridge, the engineering borings here demonstrate how the alluvium is thin and stream is essentially on bedrock. The road is on a Holocene (Qt6) terrace. Older Holocene (Qt5) treads are exposed in clearcuts to the right and the treads of the two big Pleistocene fill terraces (Qt2 and Qt3) underlie the hills directly ahead.

27.9 Begin ascent of the Qt3 terrace.

28.4 To your left and down the bank is a 30-m high landslide headwall exposure of Qt3 gravels unconformably overlying lacustrine beds. The lacustrine beds have been dated at > 47,000 radiocarbon years before present and are likely correlative to Qt2. The overlying Qt3 alluvium has been dated at 48,300±3,300 radiocarbon years before present.

29.9 Rise onto a degraded tread of Qt2 ~20 m above the Qt3 tread.

31.5 Cross Elkhorn Creek incised into the alluvium of Qt3. Stay straight on the paved, main road.

32.4 Cross Shale Creek. Note the Qt3 alluvium exposed in the creek banks to your right. Such windows into the terrace alluvium, in a direction normal to the main valley, help with reconstructing the 3-D shape of the terrace deposits.

32.5 Stay left on the paved main road.

33.4 Slow and pull off the road to your left in the parking area just before the bridge. The outcrop is a short walk down the dirt road leading to the river. **Stop 1-4. Holocene Strath at the Grouse Bridge**. The purpose of this stop is to introduce the concept of a strath, the terrace deposit, and some of the relative and numeric criteria in establishing strath age. Terraces are well preserved in the Clearwater drainage. There are two major flights of terraces: a higher, outer, older sequence that is underlain by thick alluvial-fill deposits, and a lower, inner, younger sequence underlain by thin alluvial deposits (Fig. 11). The terrace exposed here at the Grouse Bridge is a fine example of the lower, inner, younger sequence, and it contains all of the stratigraphic characteristics important to distinguishing and using terraces in tectonic interpretations (Fig. 12). The lower terraces like the one exposed here are composed of a basal, coarse grained, 1 to 3 m thick axial channel sandy gravel facies, and overlying fine grained 1-3 m thick sandy silt overbank facies. The sandy gravel facies locally preserves sedimentary structures consistent with lateral accretion processes, as might be expected for point and transverse bars, which we can see in the adjacent modern channel. So by analogy, we take the coarse-grained facies of the terrace deposit to represent the bedload being transported when the terrace strath was cut. In contrast, the fine grained facies represents vertical accretion atop the floodplain, presumably related to deposition during floods.

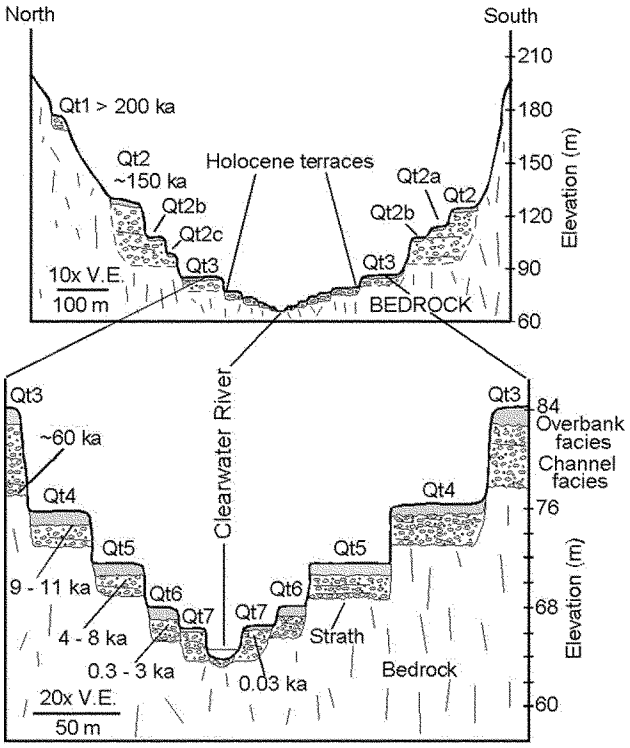

Figure 11. Composite cross section representing the terrace stratigraphy and general age ranges in the Clearwater Drainage. We adopt the convention of naming terraces in order of increasing age where "1" is the oldest (highest) terrace in the landscape and assigning numbers to straths only. In this manner, terrace Qt2 may have more than one tread, which we designate with lower case alpha numeric subscripts (as Qt2a, Qt2b).

In an active tectonic setting, the evolution of fluvial processes is both a direct consequence of and an interaction with rock uplift (Bull and Knuepfer, 1987; Wells et al, 1988; Merritts and others, 1994; Personius 1995; Gardner and others, 1992; Burbank and others, 1996; Maddy, 1997; Pazzaglia and others, 1998; Hancock and others, 1999). A important issue during the more than three decades of intense study of fluvial systems in tectonically active settings is how tectonic processes can be isolated from the myriad of geomorphic processes that also influence the genesis and subsequent preservation of fluvial stratigraphy (Schumm, 1969; Schumm and others, 1987;

Figure 12. Annotated photograph of the Qt5 strath and strath terrace exposed at the Grouse Bridge.

Bull, 1990; Bull, 1991; Sugai, 1993; Tucker and Slingerland, 1997). For example, rapid rates of rock uplift and changes in base level are expected in association with both coseismic and interseismic deformation. These factors introduce the potential for rivers to incise and abandon their valley bottoms as they seek a new base level of erosion (Bull, 1991). But the precise manner in which the rivers accomplish that incision and the nature of the terrace record left behind seems to be dominated by how the drainage responds to changes in climate, most notably, glacial-interglacial-scale climate change (Bull, 1991). Because the dramatic changes in climate tend to occur more frequently than secular changes in the rate of rock uplift, actively incising rivers have the potential to leave a relatively high-resolution record of their incision. The rate of fluvial incision is commonly interpreted in terms of the rate of rock uplift with the built-in assumption that terrace formation is a short-term disequilibria phenomena, oscillating about a long-term equilibrium profile more or less represented by the physical characteristics of the modern profile (Knox, 1975; Burbank and others, 1996; Pazzaglia and Brandon, 2001).

River terraces are the geomorphologic and sedimentologic expression of form and process adjustments in a fluvial system (Schumm and others, 1987). Terraces are unconsolidated, allostratigraphic units with a basal unconformity, typically cut across bedrock called a strath, and a constructional bench-like top, called a tread. The terrace deposit between the strath and tread varies in texture, stratification, and thickness. When it is thin (less than 3 m), it represents essentially all of the sediment in transport by a bedrock or mixed bedrock-alluvial channel during bankfull or flood discharges (Wolman and Miller, 1960). In contrast, thicker terrace deposits represent alluvial valley fills, which lift the channel off the strath for some period of time (Bull, 1991). Geologically speaking, the cutting of a strath and deposition of an overlying strath terrace gravel occur at the same time because the moving bedload is what abrades the strath. On the other hand, a fill terrace deposit may take some 100 yr to 10 k.y. to accumulate (Weldon, 1986). Thus, the fill

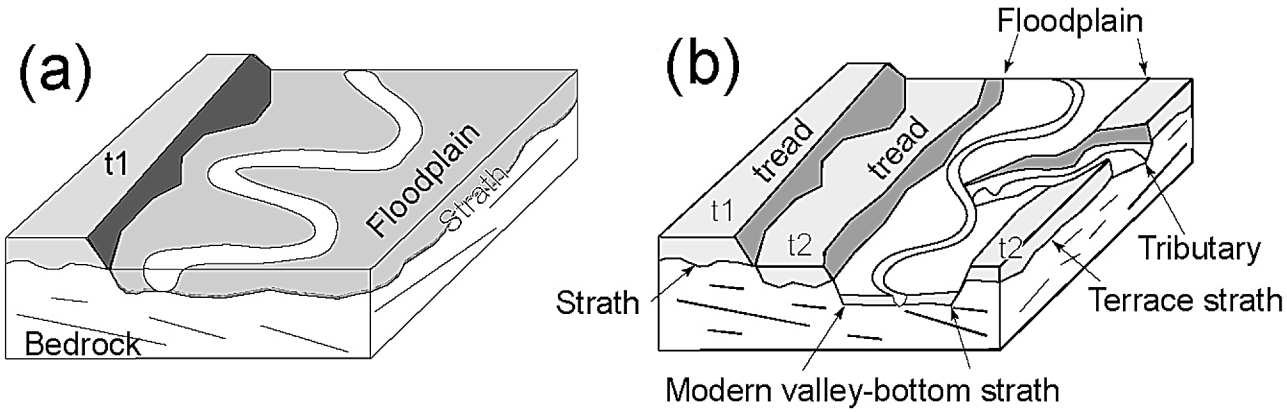

Figure 13. (a) Schematic illustrating the relationship between terraces (t1, t2), straths, the floodplain, and a valley bottom. (b) The correspondence between the width of the floodplain and the width of the valley bottom strath is corroborated by exposure of the valley bottom strath in a tributary channel, shown entering from the right side of the diagram.

provides only a minimum age for burial of the underlying strath surface.

The process of carving a strath, although not well understood, can be readily observed for many bedrock and mixed bedrock-alluvial channels (Fig. 13). In these settings, the width of the valley bottom roughly corresponds to the limits of lateral channel corrasion. Alluvium underlying the floodplain typically is not thicker than 3 m, and during low-flow conditions, bedrock exposed in the channel bottom can be observed to project laterally at the base of the floodplain. Tributary streams that have incised through the floodplain provide additional evidence that the bedrock exposed in the active channel continues laterally as an unconformity at the base of the valley fill. In this respect, the strath beneath a terrace deposit represents the bedrock base of a paleovalley floor and the terrace tread is the constructional top of a paleofloodplain.

Strath terraces are common and typically unpaired in tectonically active areas (Bull, 1991), but they may extend for many kilometers along the length of a valley. It has become clear from diverse tectonically active settings that even though terraces may lie at variable distances above the modern valley bottom, their ages tend to cluster around dates temporally coincident with known climatic changes (Bull and Knuepfer, 1987; Merritts and others, 1994; Burbank and others, 1996; Pazzaglia and others, 1998). Geomorphologists have long recognized this temporal correspondence between terrace age and documented climatic changes and commonly take this as evidence that climate was forcing the change that resulted in strath formation, terrace deposition, and the ultimate preservation of straths and fills (Schumm, 1969; Bull and Knuepfer, 1987; Bull, 1991; Pazzaglia and Gardner, 1993; Meyer and others, 1995; Pazzaglia and Brandon, 2001; Fig. 13).

In the Clearwater drainage, we have carefully mapped strath terraces at a 1:12,000 scale (Wegmann, 1999; Pazzaglia and Brandon, 2001). The mapping was carried out both on foot and by traversing the river numerous times in a canoe. Field mapping by canoe was particularly valuable in identifying terrace exposures and finding datable material. The separation between the terrace strath and valley bottom strath was measured directly in the field with a tape measure, accurate to ±0.01 m for terrace straths less than 10 m above the channel or with an altimeter, accurate to ± 1 m for terrace straths greater than 10 m above the channel. The minimum ages of the straths are estimated by 38 radiocarbon dates (35 AMS and 3 standard beta decay ages) of organic material preserved in the

overlying terrace alluvium. On one hand, the similarities between the thin alluvial mantle (< 3 m) above the strath of the modern valley bottom and atop the terrace straths leads us to believe that the cutting of the strath and deposition of the alluvial mantle are essentially contemporaneous processes for strath terraces (Merritts and others, 1994). On the other hand, woody material collected from bars in the active channel have been shown to return radiocarbon ages ranging from modern to over 1000 years (Abbe and Montgomery, 1996a,b). Multiple ages from a single terrace deposit, both at a given locality as well as along the lateral extent of a mapped terrace, helps us access the uncertainty in the age of the fill sequence. We also use these data below to argue for the likelihood of contemporaneous strath cutting and alluvium deposition.

Return to vehicles and retrace the route out to US 101 and then up to Kalaloch.

DAY 2. CLEARWATER DRAINAGE, TERRACE STRATIGRAPHY, AGE OF PLEISTOCENE TERRACES—A MODEL FOR HOLOCENE TERRACE GENESIS

0.0 **Start—Grouse Bridge in Clearwater Drainage** (Fig. 7)**.**

0.7 Cross the Clearwater River and ascend the Qt3 tread. As the road continues to climb, bedrock is exposed in the valley wall.

1.6 Cross Christmas Creek. Like the Snahapish River, alluvium from the Hoh River spilled into the Clearwater drainage through this valley.

2.0 Climb out of the Christmas Creek valley and ascend onto the Qt2 tread.

2.8 Continue along a long, flat portion of the Qt2 tread.

3.6 Begin descending the Qt2 tread, stay left on the paved road. The Coppermine Bottom Campground can be accessed via the dirt road to your right.

4.1 Cross the Snahapish River and stay to the right on the paved road (toward Upper Clearwater Campground).

5.0 Here, and at several other places, you will pass exposed gravels of the Qt2 terrace.

6.1 Crossing a Qt2 tread.

7.5 Cross the Clearwater River at the Upper Clearwater Campground. Qt5 terraces, like the one we observed at the Grouse Bridge, are exposed both upstream and downstream of the bridge on the bank in front of you.

8.1 Stay right on the C3100 road. Begin traversing the interfluve between the Solleks River and Stequaleho Creek, both two major tributaries to the Clearwater River.

9.8 Turn left onto the C3140 road. Note that this road is gated by the Washington Department of Natural Resources just past the junction with the C3100 road. Vehicle traffic past this gate is allowed by permission of the Department. To obtain permission and a key to the gate, contact the Olympic Region Office in Forks (360-374-6131). Foot and bike access is allowed without permission.

11.3 Stay on the main road.

13.6 Drop into the Solleks Valley bottom.

15.2 Cross the Solleks River.

15.7 To the south across the old gravel pit is an unobstructed view into the Grouse Creek drainage and the 1997 landslide.

16.6 Turn right onto the C3185 road. Cross the Solleks again and begin ascending the ridge on the south side of the river.

17.6 Negotiate switchbacks.

18.7 Stay to the right, turning onto the C3100 road.

19.1 Stay to the right (straight on C3100 road).

19.3 Park vehicles near the short access roads connected to the main dirt road. **Stop 2-1. Grouse Creek Landslide**. The objective here is to illustrate the magnitude of mass wastage and sediment delivery to the channel occurring during the Holocene. Note: Due to road deconstruction, one has to walk approximately 1 km to the headscarp of the landslide on the unmaintained road. On March 19th, 1997, 506,000 m^3 of rock and regolith moved off this hillslope and into the Solleks River (Serdar, 1999; Gerstel, 1999). The landslide occurred during the waning phases of a major rain-on-snow flood event that started two days prior on March 17th (the St. Patrick's Day Flood). Approximately 200,000 m^3 of material was deposited on the upper slopes of the Grouse Creek channel, with the remainder moving as a debris flow that traveled down Grouse Creek, picking up additional material from side slopes, which were scoured up to 54 m high. When the debris flow reached the Solleks River, it deposited approximately 78,000 m^3 of material. Landsliding here may have been exacerbated by both a road and associated logging activity; earlier slide scars and additional landslides cut adjacent hillslopes.

The debris delivered to the Solleks channel temporarily dammed the river and pushed the channel to the north. A plume of coarse sediment worked its way down the Solleks into the Clearwater channel by the summer of 1997. The net effect of such instantaneous, point introductions of sediment was to force the channel to enhance its lateral corrasion as the sediment was temporarily stored in floodplains and in channel bars. Downed trees recruited from floodplains trap the sediment and locally made alluvial fills behind dams of woody debris. The abundance of woody debris dams increased in frequency on the Clearwater River in the reach directly downstream of the Solleks confluence.

The exact role that logging and related anthropogenic activities have played in adjusting the hydraulic geometry of the Clearwater channel remains highly debated. The Grouse Creek slide, and other smaller slides have increased the amount of sediment delivered to the channel. That sediment seems to be mostly sequestered in a low terrace (Qt7) colonized by a stand of alder trees, about 30 years old. If changes in the liberation of sediment from hillslopes helps drive the terrace formation process, we must conclude that natural processes during the Holocene have been of greater magnitude than the effects attributed to anthropogenic processes.

The Grouse Creek slide illustrates the dominant process for eroding the steep landscape of tectonically active landscapes. Current thought is that tectonic uplift and river incision will build topography and relief until the hillslopes all have reached a critical slope of failure (Carson, 1970, 1971; Burbank and others, 1996; Montgomery, 2001). Over long periods of time, the liberation of sediment can be viewed as steady, as long as the rates of uplift and incision are steady. But over shorter time spans, the landsliding process is unsteady and is likely modulated by other driving factors, including hillslope moisture and seismically-induced ground accelerations. If the time scale of landsliding unsteadiness is commensurate with the time scale of the process of terrace genesis, we might be able to discern a climatic or possibly an earthquake-cycle tectonic signal from the resulting terrace stratigraphy.

Return to vehicles and retrace the route all the way back to the Upper Clearwater Campground and then on the paved road back to the Snahapish River bridge.

31.1 Turn right directly before the Snahapish River bridge (on the Clearwater-Snahapish Road) and begin driving up the Snahapish valley.

35.1 Turn right at the major triangle intersection onto the C2000 road.

37.9 Loop around steep tributaries. The Qt2 tread is visible in the clearcuts on the right.

39.2 Slow and turn right into dirt road marked W-5 or C2017. Pull forward and park to the left in the opening.

39.3 Walk south on the overgrown dirt road leading out to an old clearcut. **Optional Stop 2-A. Terraces at Kunamakst Creek.** This is an overview stop to illustrate the presence of terraces, straths, and their considerable separation from the modern channel in the upper Clearwater drainage.

Return to vehicles and retrace route out to the triangle intersection with the Clearwater-Snahapish Road.

47.5 Turn left onto the Clearwater-Snahapish Road.

48.4 Turn left into a well-marked gravel pit. **Optional Stop 2-B. The Qt2 Head of Outwash in the Snahapish River Valley.** The purpose is to examine the coarse-grained, proximal portion of the Qt2 outwash in a gravel pit adjacent to the Qt2 head of outwash. (Fig. 3).

Return to vehicles and continue south (down) along the Clearwater–Snahapish Road.

51.6 Turn right and cross the Snahapish River. Ascend the Qt2 tread and slow for the next stop.

52.1 Turn right into the Copper Pit. **Stop 2-2. Qt2 Terrace at the Copper Pit and Cosmogenic Surface Dating Profile.** The purpose of this stop is to show the sedimentology, stratigraphy, and weathering characteristics of the Qt2 terrace and develop the arguments that the underlying strath is 150 ka, whereas the terrace deposit and tread are correlative to the 60-m coastal terrace. Qt2 is the thickest and most widespread fill terrace in the Clearwater valley. Qt2 terrace deposits are made up of 5 to 40 m of coarse stratified sand and gravel that sit on straths 0 to 20 m above the level of the modern valley bottom (Fig. 11, 14). Locally, the fill has buried not only the paleo valley bottom (equivalent to the strath) but also the side slopes of the river valley itself, thus forming a buttress unconformity. Sedimentary structures within the terrace deposits include broad, shallow channel forms

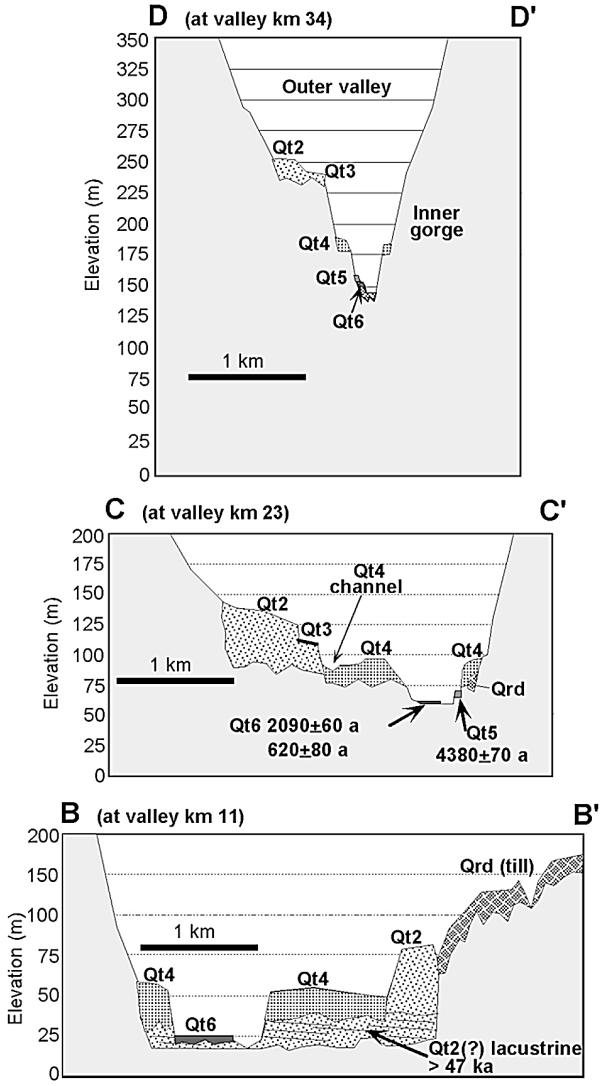

Figure 14. Cross-valley profiles of the lower (B-B'), middle (C-C'), and upper (D-D') parts of the Clearwater Valley showing the relationship of the terrace units to the local valley geometry. Locations are shown in Figure 3a.

exhibiting 0.5 to 2 m high tabular crossbeds, and smaller-scale trough crossbeds of silty sand. These sedimentary structures are generally consistent with a braided channel form and mimic the features exhibited by glaciofluvial deposits that can be physically traced to heads of outwash in adjacent, glaciated drainages. The terrace alluvium is capped by about 1 to 2 m of thin-bedded sand, locally laminated silt, and massive silt, which are interpreted as both overbank and loess deposits.

Soil profile development and clast weathering rinds (Fig. 15) in the terrace

treads allow distinctions between deposits of different age and correlation between upstream and downstream remnants of the terraces. Soil descriptions and terminology follow the U.S. Department of Agriculture Soil Taxonomy (Soil Survey Staff, 1975). For the rind-thickness methods, we follow procedures outlined in Chinn (1981), Knuepfer (1988), McSaveney (1992), and Ricker and others (1993). Rinds were measured to the nearest 1 mm on clasts of greywacke sandstone that were about 4 to 10 cm in diameter and had well-defined concentric rinds and unweathered cores. Most weathering rind studies sample clasts from the surface of the terrace, but this is not possible in the wet and heavily vegetated Clearwater drainage. Good exposures of terrace treads are only available in gravel-pit highwalls and a few road cuts. Otherwise, the treads are either densely forested with no clasts exposed at the surface, or they are significantly disturbed by logging. We avoided this problem by sampling buried clasts collected from a defined position with the terrace soil profile (Colman and Pierce, 1981, 1986). We expect that clasts buried in the soil profile should weather in the same fashion as those at the surface. The soil profile lies within the upper 3 m of the terrace, and thus is relatively thin compared to the thickness of the overall deposit, which might reach some 30 m or more. Furthermore, clasts at the surface and in the soil profile are subjected to similar wet-dry cycles, associated with infiltration of precipitation and fluctuations of the water table.

Sampling was done in high-wall gravel pits, which provide large cross sections, tens of meters in length, of the terrace treads. These exposures show that the soil profiles have been intensely bioturbated down to a depth of at least a meter, and in some cases more, including most of the B horizon of the soil profile. Clasts were collected from the base of the B horizon, where they generally preserve their original depositional fabric, indicating minimal bioturbation. The terrace tread commonly has a fine-grained cap composed of fluvial or eolian sediment. Field and airphoto observations show that

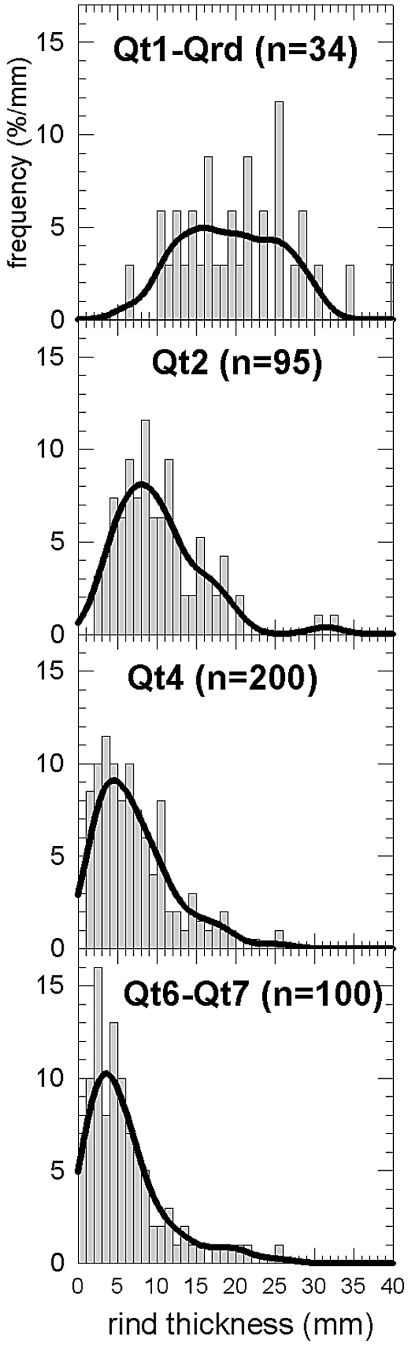

Figure 15. Thickness distributions for clast weathering rinds for terrace deposits of different stratigraphic ages. The probability density curves were calculated using the Gaussian kernel method (Brandon, 1996), with the kernel size set to 2 mm. Qt1–Qrd is from an interfluve at about 180 m elevation on the north divide of Shale Creek. Qt2 is from the Peterson Creek terrace at about 130 m elevation. Qt3 is from the Quinault quarry pit at about 30 m elevation. Qt6 is from an exposed gravel bar adjacent to the Clearwater River, near the Clearwater Picnic Area, about 2 km south of the town of Clearwater.

soil drainage is poor in areas where this fine-grained cap is thick. In our sampling, we selected areas that were well drained (i.e. minimal fine-grained cap), in order to avoid the influence of variable soil drainage on the degree of clast weathering.

Qt2 deposits have well-developed brownish-red polygenetic soils. Rind-thickness modes are between 9 and 12 mm (Fig. 15), and the oxidation depth is about 10 m in coarse sand and gravel. There are 4 distinct treads associated with the Qt2 fill, especially in the region surrounding the Snahapish-Clearwater confluence. The treads are named Qt2a through Qt2d, in order of decreasing elevation and age of the tread. All of these treads show significant postdepositional modification, caused by root bioturbation and colluviation, as well as multiple episodes of loess deposition. Morphology and soil stratigraphy vary on the treads, with well-developed soils on well-drained colluviated slopes and poorly developed loess-rich soils on eroded interfluves. In the stable low-relief parts of the tread, the soil consists of a 10 cm-thick A horizon, a local 1 to 10 cm-thick albic horizon, and a 50 to 100 cm-thick B horizon composed of brown (7.5YR) and strong brown (7.5YR) clay loam with moderately thick clay films.

Along the lower Clearwater, the Qt2 strath sits at 15 to 40 m above the modern channel, and its oldest tread, Qt2a, sits at ~60 m above the channel. In the upper Clearwater, the Qt2 strath take on a steeper gradient, rising to a maximum of 110 m above the modern channel in the uppermost part of the drainage.

The primary tread, Qt2a, marks the constructional top of the original fill unit. The next three treads, Qt2b,c,d, mark a series of unpaired fill-cut terraces that are inset into the primary deposit. These minor inset units are thought to have formed during a series of local events within the river ("complex-response" terraces of Schumm, 1973; Bull, 1991, p. 24–25) In contrast, the continuity and paired geometry of the other terrace treads, most notably Qt2a, indicates that they were formed by events that affected the entire drainage.

The Qt2 terrace alluvium represents a time of major Clearwater valley aggradation, when the middle and lower portion of the drainage were hydrologically connected to the Hoh drainage (Fig. 3). The Snahapish River, a small underfit stream, marks the former course of outwash fed from moraines in front of alpine glaciers in the Hoh valley. During the penultimate glacial epoch, the head of outwash was at the current location of the divide between the Hoh and Clearwater drainages (Fig. 3). The outwash delivered from this moraine created the Qt3 fill, which we will see at the next stop, inset below Qt2.

There is another older head of outwash straddling the middle part of the Clearwater valley (OPTIONAL STOP 2-B) that we think is directly correlative to the Qt2 alluvium and tread here at this stop. Downstream, the Qt2 tread can be traced nearly unbroken to the 60-m coastal terrace, which we have already argued is likely deposited during isotope stage 6 or about 150 ka. So here, we have the upstream projection of that isotope stage 6 fill to its head of outwash in the Snahapish valley. The timing of aggradation must be limited upstream by when the ice margin was stalled in the Snahapish valley pumping out sediment and discharge, and downstream by when sea level was rising to produce the accommodation space leading to the high elevation of the Qt2 tread. This restricts the filling to between 150 to 125 ka. So the strath at the base of Qt2 is taken as 150 ka, and the tread is considered to be younger (Fig. 6).

Return to the vehicles, exit the Copper Pit, and continue straight and to the left down to the dirt road that leads to the Coppermine Bottom campground.

52.5 Proceed straight down to the campground. Descend Qt2, cross Crooks Creek slough, and a fill unit inset into the Qt3 tread.

53.0 Traverse the Qt3 tread, and turn right.

53.5 **Lunch, Coppermine Bottom.** After lunch, loop through the campground and retrace

route out to the Clearwater-Snahapish Road.

55.1 Turn left onto the Clearwater–Snahapish Road.

59.6 Cross the Grouse Bridge and proceed on the main paved road. After crossing Shale Creek, slow and prepare to turn right.

60.6 Turn right into the entrance of an overgrown gravel pit. **Stop 2-3. Qt3 at the Elkhorn Pit.** The purpose of this stop is to show the sedimentology, stratigraphy, and weathering characteristics of the Qt3 terrace and to develop arguments that the underlying strath was buried at 60 ka, and the Qt3 terrace deposit and tread are correlative to the 30-m coastal terrace. The Qt3 terrace alluvium is sedimentologically similar to Qt2. It is everywhere inset into Qt2, buries a strath that is distinctly lower than the strath buried by Qt2, and tends to be, on average, thinner than the Qt2 alluvium (Fig.s 11 and 14). It has a moderately developed yellow soil profile, rind-thickness modes between 3 and 4 mm (Fig. 15), and an oxidation depth of 4 to 5 m, but locally 10 m in coarse alluvium. Postdepositional modification is minimal on the terrace treads, which retain a constructional morphology with well-preserved sandy overbank and silty loess deposits. The loess is more than 1 m near the Snahapish River and near the coast. Soil profiles consist of a 50 to 80 cm thick B horizon composed of yellowish brown (10YR) to brown (10YR-7.5YR) silt loam with numerous thin clay films preserved on soil ped faces. Soil profiles in fine-grained material have strong brown colors (7.5YR) and well-developed soil structure. Qt3 is best preserved below about km 24, where it locally has two treads, designated as Qt3a and Qt3b, with the Qt3b tread sitting about 4 m below the Qt3a tread. In this part of the valley, Qt3 straths maintain a gentle gradient, lying 6 to 10 m above the channel, and treads are 35 m above the channel. Above km 24, Qt3 has only one tread, and the straths take on a steeper gradient, climbing to a maximum height of 70 m above the channel (Fig. 14). This gravel-pit outcrop of Qt3 exposes a highwall cut into the Qt3b tread.

The Qt3 tread can be traced upstream through the Snahapish valley to the Lymans Rapids (isotope stage 4, ~ 60 ka) head of outwash in the Hoh Valley (Fig. 3). Like the Qt2 fill, the time of aggradation of the Qt3 fill was limited upstream to the time when the ice margin was producing discharge and sediment, and downstream to when sea level was rising at the coast. For this reason, we estimate the age of the strath buried by the Qt3 alluvium to be ~ 60 ka and the alluvial itself to be, on the average, several thousands of years younger. There are some data to suggest that the Qt3 fill and Qt3a tread is 48 to 54 ka. A few radiocarbon ages from Lyman Rapids (isotope stage 4) outwash in the Queets and Hoh valleys have finite radiocarbon ages between 47,500±3000 and 54,200+2500–1900 radiocarbon years before present (Thackray, 1996; 2001) A landslide exposure north of the town of Clearwater exposes Qt3 alluvium unconformably overlying organic-rich lacustrine beds. The lacustrine beds are radiocarbon dead (> 47,000 radiocarbon years before present), but a log in the Qt3 alluvium returned a finite age of 48,300±3,300 radiocarbon years before present (Wegmann, 1999). These ages are at the limit for radiocarbon, but they are stratigraphically consistent with our mapping which places the lower lacustrine beds correlative with the Qt2 fill, and the upper Qt3 alluvium genetically related to stage 4 alpine glaciation.

Return to vehicles and return to the Clearwater–Snahapish Road. Turn left.

61.6 Cross Shale Creek. Stay to the right and proceed onto the C1000 road. This road will ascend the Qt3 tread, here about 30 m above the valley bottom.

62.9 Ascend the degraded remnants of a Qt2 tread.

63.4 Stay right on the major C1000 road. The

dirt road leading off to the left is the old approach to the former Goodyear Bridge, an old suspension bridge no longer suitable for vehicle traffic. C1000 continues to follow a Qt3 tread.

65.2 Cross Deception Creek and then begin ascending the bedrock ridge north of the Deception Creek drainage.

65.6 Find a safe place to park. You may have to take advantage of the C1200–C1000 road intersection 0.5 mile farther up the road. This is where we need to descend the bank down to the Clearwater River. At the river, find a gravel bar and follow it onto the big north-facing meander loop. **Stop 2-4. Crooks Creek Terraces.** The objective here is to use the view to illustrate the magnitude of strath separation and resulting river incision rates. The maps and ages of Pleistocene and Holocene terraces will be used to develop models of terrace formation influenced by climatic and tectonic forcings. Visible from this locality, inset below the Pleistocene terraces, are several well preserved Holocene strath terraces (Qt4 through Qt7). These terraces are composed of a basal, coarse grained, 1 to 3 m thick axial-channel sandy gravel facies, which is overlain by a fine grained 1–3 m thick sandy silt overbank facies. The sandy gravel facies locally preserves sedimentary structures consistent with lateral accretion processes, as expected for point bar and transverse bar deposits.

The Holocene terraces are both paired and unpaired, and widely distributed, although some channel reaches are devoid of terraces. In any 500 m reach where the terraces are preserved, we can distinguish three major strath terraces Qt4, Qt5, and Qt6. The underlying straths for these different terraces are clearly at different heights, with differences of at least 2 m (Fig. 11). The Holocene terraces are best preserved between valley km 15 and 30, and provide critical information about the lateral extent and morphology of these terrace units (Fig. 16). Here the valley bottom has narrowed to 500 m, but the channel maintains an active meandering pattern. Qt5 tends to equal or exceed the width of the modern valley bottom evident on a 7.5-minute topographic map, whereas Qt6 is wholly confined to (and helps define) the modern valley bottom. Mapping the terraces through this reach clearly demonstrates that the straths have a broad lateral extent. We are able to physically trace a strath and its overlying terrace deposit for hundreds of meters, in some cases of nearly continuous exposure along the river bank. Uniform relative separation between the terrace strath and valley-bottom strath allows us to confidently project between exposures. The deposits in the modern channel are similar to the Holocene terrace deposits. The modern channel contains a mostly continuous mantle of uniform-thickness sandy gravel bars and fine grained overbank silt, sitting atop a broad, laterally continuous, low-relief bedrock strath.

The Crooks Creek exposures show a flight of Holocene terraces Qt4, Qt5, and Qt6 (Fig. 16). On the north (far) bank of the river, the alluvium overlying the highest straths (Qt4) has been dated as 8,880±65 and 6,985±60 radiocarbon years before present. The Qt4 strath is several meters lower at the large south-meander loop, coincident with a Qt4 channel inset into the strath dated at 6,040±65 radiocarbon years before present. This degree of strath relief and range in ages is the maximum we observe for a given mapped terrace. The Qt5 strath is exposed on the south bank, straddling the neck of the north meander loop. The alluvium atop the Qt5 strath is dated at 5,410±50 radiocarbon years before present. Qt6 underlies the point of the north meander loop and is bracketed by numerous ages (2020±60 to 373±40 radiocarbon years before present) both up- and downstream from the exposures at this stop.

The radiocarbon dates of all Holocene terraces define three broad age groups when plotted on a probability density curve (Fig. 17) constructed by the intergration of the probability density distributions for ^{14}C ages corrected to true age (using the OxCal program of Ramsay, 2000). The age groups are defined by prominent breaks at 600 and 1200 years where we have no record of

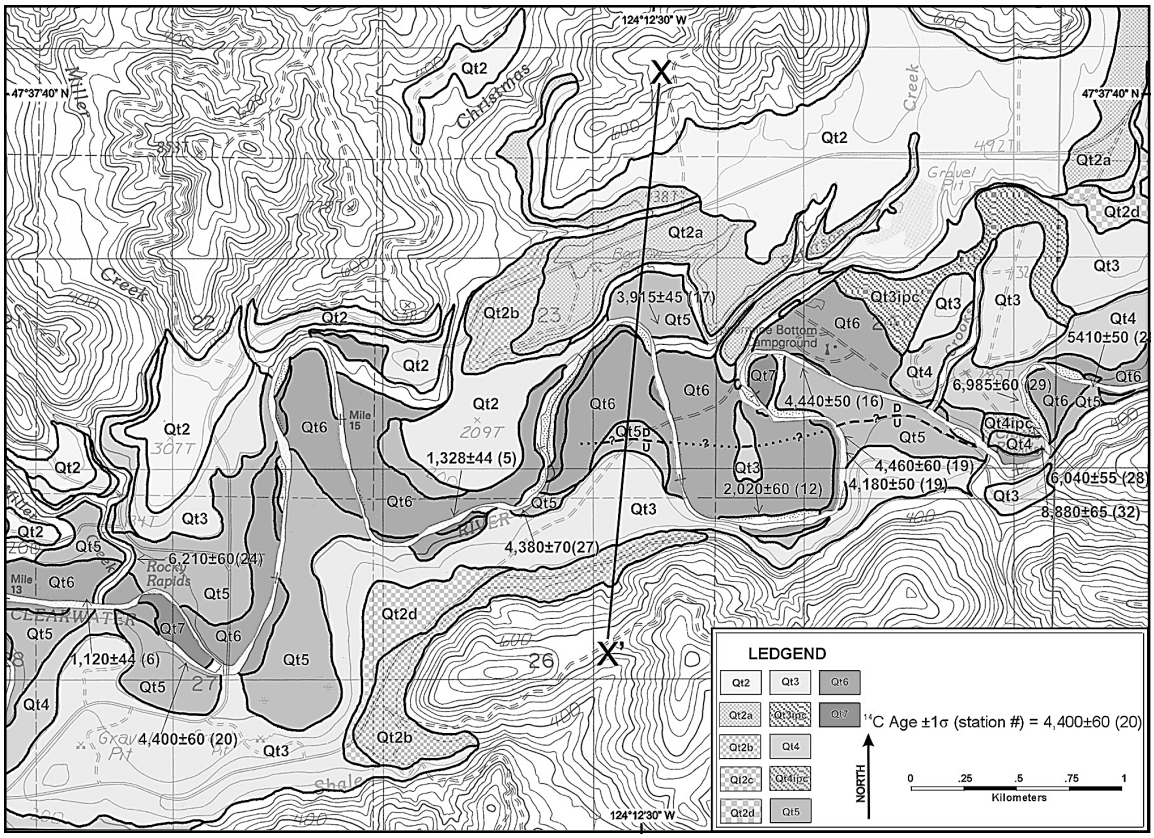

Figure 16. Map of river terraces in the medial portion of the Clearwater Valley (modified from Wegmann, 1999). Letters following terrace-name designation— a, b, c, d—indicate treads that share a common strath; ipc indicates an inset paleochannel.

terrace alluvium. From this we infer that Qt4, Qt5, and Qt6 were deposited at 9,000 to 11,000 ybp, 4,000 to 8,000 ybp, and 0 to 3,000 ybp, respectively. Our stratigraphic assignments are consistent with the age data. In other words, at no place along the river does a terrace stratigraphically seem to be Qt6, but has an age in the Qt5 range. Furthermore, stratigraphically older terraces yield the older ^{14}C ages. As a result, the elevation of the strath alone seems sufficient to judge the relative age and correlation of the terraces, even though the alluvium mantling a given strath may have a broad age range.

Bedrock incision is measured using two methods. The strath height above the channel was measured using an altimeter or measuring tape to obtain relative vertical elevation, which has a cited two standard error (2SE) precision of 1 m. Some straths greater than 20 m above the modern channel were measured by positioning the modern channel and the strath relative to the 12 m contours on U.S. Geological Survey 7.5 minute topographic maps. We used a relative standard error (RSE) of 5.5% to represent the uncertainty for all height measurements.

Estimated incision rates are affected by errors in both height and age. The approximate uncertainties (2SE) for the age of strath burial are: Qt2 = 140 ± 20 ka (±14 percent) and Qt3 = 65 ± 10 ka (±15 percent). Incision measurements and incision rates for the Qt2 and Qt3 straths are shown in Fig. 18 and 19, respectively. The error bars for the incision rates include only height errors, because the uncertainty in strath age is common to all incision rates from the same strath. The uncertainties for both height and age give a combined uncertainty of 2 relative standard error of about 18%.

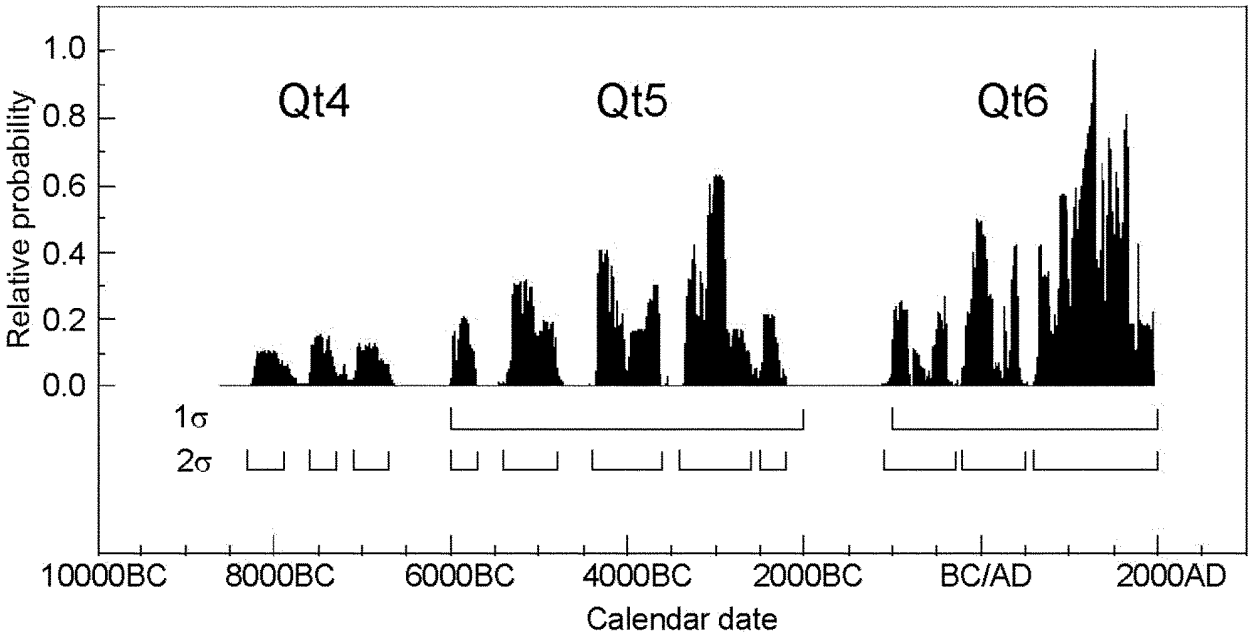

Figure 17. (a) Probability density and frequency plots for 38 radiocarbon dates of the Holocene terraces. The plot was produced by calculating calendar ages, their accompanying 1 sigma errors, and then summing the probabilities using the program OxCal (Ramsay, 2000). Note the brackets beneath the frequency histograms. At the 1σ confidence level, the group of ages between 6000–2000 BC and 1000 BC–AD 2000 statistically coincide with terraces Qt5 and Qt6 respectively.

Both Qt2 and Qt3 straths show increased incision upstream (Fig. 19). Incision rates are remarkably similar for both straths. Smooth curves fit to the data indicate incision rates ranging from 0.1 m/k.y. at the coast to 0.9 m/k.y. in the upper Clearwater valley.

Holocene incision rates are determined from the separation between dated Holocene straths and the valley-bottom strath, which is considered equivalent to the low water level during summer base-flow discharge. This is an appropriate datum from which to measure strath height separation because it helps mark the reach-length average elevation of the valley-bottom strath and avoids measurements affected by local relief in the channel. The incision rate is taken as the amount of incision that has occurred after strath burial (Pazzaglia and Brandon, 2001). Our best estimates for the timing of strath burial are the numeric ages from the overlying terrace deposit, but such ages tend to underestimate the maximum age of the alluvial fill. Thus, our estimates may be biased toward faster rates. Estimated errors include the uncertainties for the ^{14}C age, the elevation of the summer base-flow water level, and the measurement of strath height (including uncertainties with the physical measurement of the height and the natural variation in the outcrop). The relative uncertainty for incision rate is greatest for the youngest terrace (Qt6) and decreases with increasing terrace age and separation above the channel. Incision rates range from 0.05 – 1 mm/yr in the lower third of the drainage to 1 – 2 mm/yr in the medial portions, to 2 – 3 mm/yr in the upper third (Fig. 20). Although similar in pattern to the incision documented for Pleistocene terraces (Pazzaglia and Brandon, 2001), Holocene incision rates exceed Pleistocene rates by a factor of 3 to 2.

Field Trip End. Retrace route out to the paved Clearwater Road.

CONCLUDING REMARKS

Our study uses fluvial geomorphology to measure incision and rock uplift across the Olympic sector of the Cascadia Subduction Zone. A well-preserved terrace stratigraphy in an unglaciated drainage, together with reason-

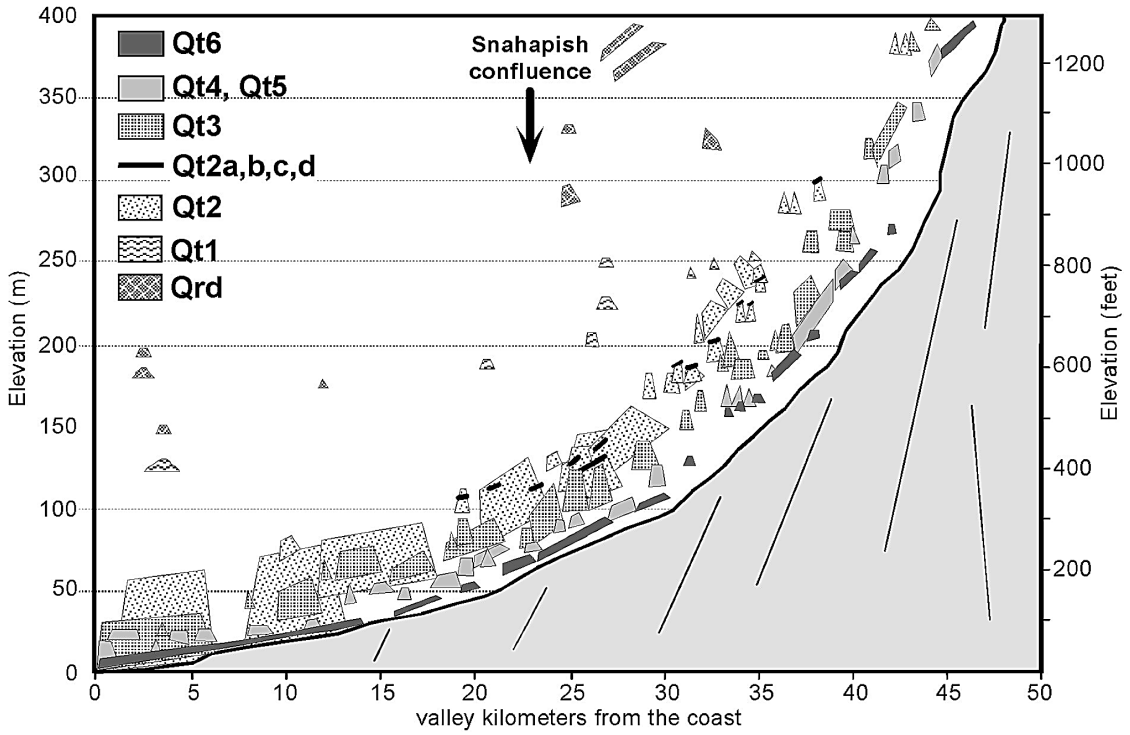

Figure 18. A long-profile section of the Clearwater Valley showing the vertical relationship of mapped terrace deposits (polygons) to the modern Clearwater River (continuous line). Terrace units were projected orthogonally into the valley profile from their mapped positions along the flanks of the Clearwater Valley (Fig. 3b). The bottom and top of each polygon corresponds to the strath and tread, respectively, for a mapped terrace deposit.

able age control for the terrace deposits, allow us to use the valley profile of the Clearwater as a crude geodetic datum. As such, we are able to quantify the effects of both the short-term earthquake cycle and permanent wedge deformation driving uplift across the interior of the Olympic Peninsula. We summarize 7 major conclusions here.

(1) Pleistocene terrace sequences in the Olympics seem to be closely tied to the glacial climate cycle through its influence on local climate, sediment supply from adjacent alpine-glaciated drainages, and eustasy. The sequence of terrace-forming events is consistent with the model of Bull (1991), but the timing of these events relative to the eustatic cycle is quite different. Bull (1991) proposed that strath formation occurred during rising and high sea level, and aggradation during falling and low sea level. In the Olympics, strath formation seems to occur during peak glaciation (when sea level is low), and aggradation during late glacial and interglacial times, when sea level is rising. We suspect that this difference is a local effect, related to the strong influence that local deglaciation has had on sediment supply, and the interaction of that enhanced sediment supply with rising sea level during interglacial times.

(2) Holocene terraces represent local-scale processes of enhanced lateral incision, valley-bottom widening, and the carving of straths accomplished with the aid of the thin alluvial deposits preserved atop the straths. The age-frequency distribution of the terrace deposits overlying a given strath is consistent with this idea, because the distributions are skewed toward the younger extreme of the age range. Valley-bottom narrowing and rapid vertical incision into bedrock is accomplished during relatively brief (1,000 yr) intervals between the carving of the major straths.

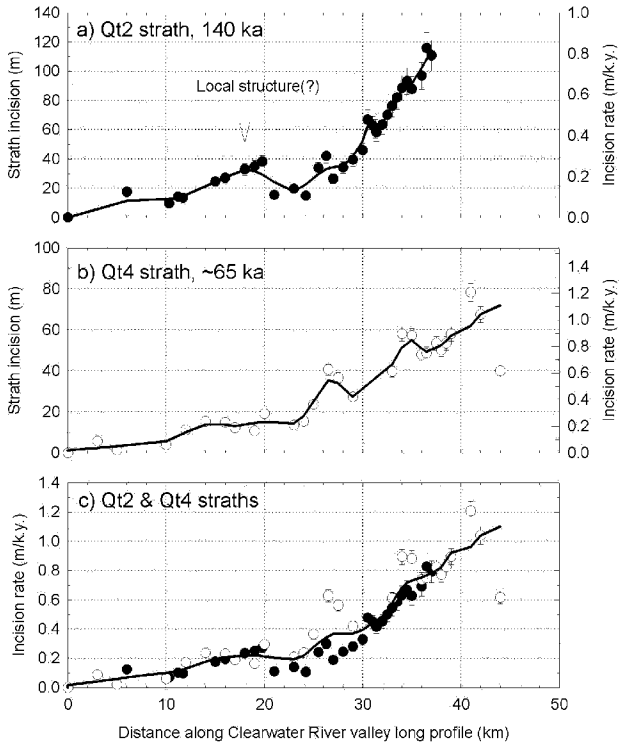

Figure 19. Incision of the (a) Qt2 and (b) Qt3 straths with respect to distance along the valley profile (see Fig. 3b). (c) Incision rates calculated from the Qt2 strath (solid circles) and Qt3 strath (open circles). Note the similarity in the estimated long-term incision rates for these two different-age straths. In general, incision and incision rates increase upstream. The small bump in the profiles at about 15 to 25 km suggests localized uplift, such as a broad fold. Error bars show ±2 standard error uncertainties due to strath height measurement errors The thick lines are smoothed from the original data using a locally weighted regression method (Lowess algorithm of Cleveland, 1979, 1981, with the interval parameter set to 0.2).

(3) We envision the Holocene Clearwater River as being at or near capacity. The alternations in rates of vertical and lateral incision may be linked to temporal variations in the liberation and delivery of hillslope sediment to the Clearwater channel that affect the "at-capacity" condition. Times of increased hillslope sediment flux favor lateral incision, especially if those times coincide with stable, steady discharges, like those envisioned for the valley-bottom-widening cycles described in Meyer and others (1995). Similarly, and following the same analogy, a reduction in the sediment yield, especially in concert with a flashier discharge, would foster valley-bottom narrowing and vertical incision. Hillslope sediment yield is probably strongly influenced by Holocene climate variation, but that climate record remains poorly understood due to a lack of local high resolution proxy records. We appeal to the possibility that seismic shaking could be a viable mechanism for liberating hillslope sediment when slope moisture conditions are favorable for slope failure, or when the slopes are primed with a sufficient thickness of regolith. We emphasize that we do not mean to link an individual earthquake to an individual terrace. For instance, large subduction zone earthquakes occur more than 5 times more frequently than major terrace fill events. We note, however, an analogous situation with frequent large fires in the intermontane west, which can occasionally destabilize a hillslope but only when the climate is relatively dry and the precipitation is seasonal (Meyer and others, 1995).

(4) The upstream divergence of straths in the Clearwater provides strong evidence that uplift is very slow at the coast and increases to a maximum in the center of the range. This conclusion runs counter to a commonly invoked assumption in fluvial geomorphology that long-term uplift rates can be taken as uniform within a single drainage.

(5) Pleistocene straths of different ages show a similar pattern of incision rates along the Clearwater, with ranges from less than 0.1 m/k.y. at the coast to a maximum of 0.9 m/k.y. in the center of the Olympics. These rates correspond closely with the pattern of long-term erosion rates indicated by apatite fission-track cooling ages. These observations indicate that, at long time scales (10 to 100 k.y.), the average form of the landscape remains close to steady state. This also implies that during each phase of strath cutting, the Clearwater Valley profile is able to return to the same steady-state form. Thus, bedrock incision rates seem to be a reasonable proxy for rock uplift rates in the Olympics.

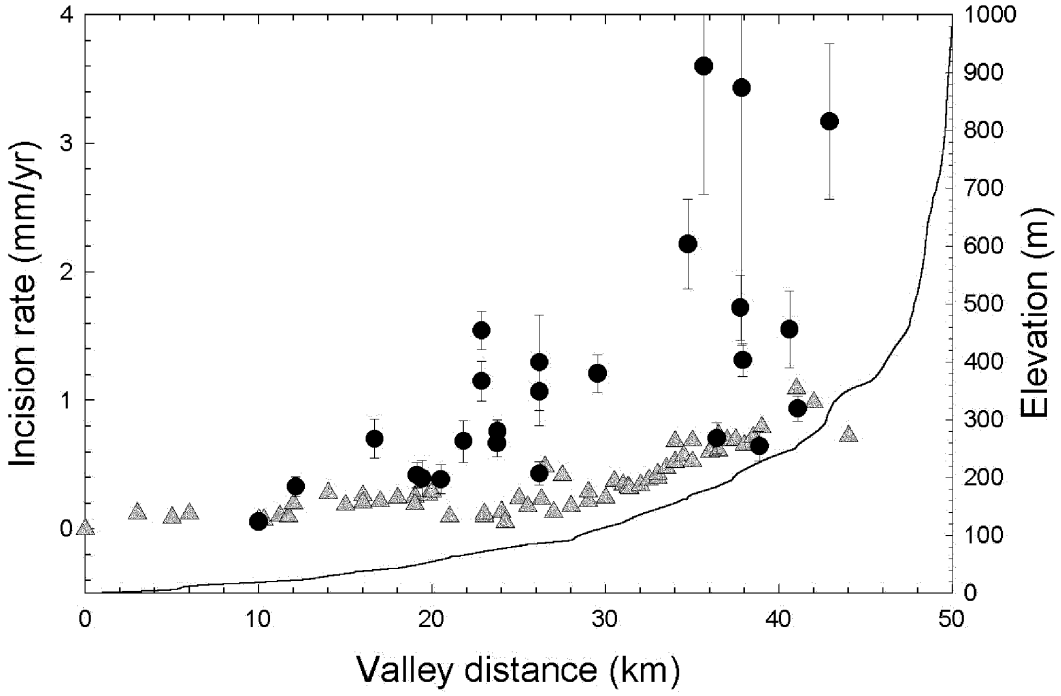

Figure 20. Incision rates (left vertical axis) determined from Holocene terraces (solid black circles) and Pleistocene terraces (gray triangles) plotted with respect to distance along the valley long profile (right vertical axis). Rates reflect calendar ages, and error bars on the Holocene data are 1 sigma standard error. Note that the incision rates for both data sets increase upstream.

(6) The profile of incision and erosion rates across the Olympics indicates a close balance between the accretionary and erosional fluxes moving in and out of the wedge. This result supports the hypothesis of Brandon and others (1998) that the Olympic sector of the Cascadia Wedge is close to a flux steady state, but note that this conclusion does not require the topography to be steady as well.

(7) A buried sea cliff, which probably formed at 122 ka, provides evidence of horizontal motion of rock relative to the modern shoreline. The rate of motion is 3.7 m/k.y. to the northeast, which is close to the 3 m/k.y. horizontal material velocity predicted for a frontally accreting steady-state wedge. If this interpretation is correct, then it implies that the shoreline has taken on a steady-state configuration with each highstand. As a result, we can view the northeast translation of the Sangamon sea cliff as recording northeast-directed shortening across the Olympic Mountains. These results are consistent with a kinematic model in which long-term horizontal velocity may account for 20 to 35 percent of the geodetically measured horizontal velocity across the Olympics (Pazzaglia and Brandon, 2001). The remaining 65 to 80% is presumably elastic deformation.

ACKNOWLEDGMENTS

We would like to acknowledge long-standing working relationships with geoscientists that have worked with us, supported us, and inspired discussion on the topics presented in this paper. These include, but are not limited to Glenn Thackray, Bill Lingley, Wendy Gerstel, Sean Willett, Joe Vance, Tony Garcia, John Garver, Mary Roden-Tice, and Brian Atwater. We thank the Quinault Nation, State of Washington, Olympic National Park, and Rayonier Inc for access to their respective lands. Research supported by NSF-EAR-9302661, 9736748, and 8707442.

REFERENCES

Abbe, T.B., and Montgomery, D.R., 1996a, Large woody debris jams, channel hydraulics and habitat formation in large rivers: Regulated Rivers: Research and Management, v. 12, p. 201-221.

Abbe, T.B. and Montgomery, D.R., 1996b, Floodplain and terrace formation in forested landscapes old wood: Geological Society of America Abstracts with Programs, v. 28, no. 5, p. 41.

Adams, J., 1984, Active deformation of the Pacific Northwest continental margin: Tectonics, v. 3, p. 449-472.

Armentrout, J.M., 1981, Correlation and ages of Cenozoic chronostratigraphic units in Oregon and Washington, *in* Armentrout, J.M., editor, Pacific Northwest Cenozoic biostratigraphy: Geological Society of America Special Paper 184, p. 137-148.

Atwater, B.F., 1987, Evidence for great Holocene earthquakes along the outer coast of Washington State: Science, v. 236, p. 942-944.

Atwater, B.F., 1996, Coastal evidence for great earthquakes in western Washington, *in* Rogers, A.M., Walsh, T.J., Kockelman, W.J., and Priest, G.R., ed., Assessing earthquake hazards and reducing risk in the Pacific Northwest: U. S. Geological Survey Professional Paper 1560, v. 1, p. 77-90.

Atwater, B.F., Stuiver, M., and Yamaguchi, D.K., 1991, Radiocarbon test of earthquake magnitude at the Cascadia Subduction Zone: Nature, v. 353, p. 156-158.

Beaumont, C., Ellis, S., and Pfiffner, A., 1999, Dynamics of subduction-accretion at convergent margins: Short-term modes, long-term deformation, and tectonic implications: Journal of Geophysical Research, v. 104, p. 17,573-17,602.

Bigelow, P.K., 1987, The petrology, stratigraphy and drainage history of the Montesano Formation, southwestern Washington and Southern Olympic Peninsula: Western Washington University MS Thesis, 263 p.

Bockheim, J.G., Kelsey, H.M., and Marshall, J.G., III., 1992, Soil development, relative dating, and correlation of late Quaternary marine terraces in southwestern Oregon: Quaternary Research, v. 37, p. 60-74.

Brandon, M.T., 1996, Probability density plots for fission-track grain age distributions: Radiation Measurements, v. 26, p. 663-676.

Brandon, M.T., and Calderwood, A.R., 1990, High-pressure metamorphism and uplift of the Olympic Subduction Complex: Geology, v. 18, p. 1252-1255.

Brandon, M.T., and Vance, J.A., 1992, Tectonic evolution of the Cenozoic Olympic Subduction Complex, Washington State, as deduced from fission track ages for detrital zircons: American Journal of Science, v. 292, p. 565-636.

Brandon, M.T., Roden-Tice, M.K., and Garver, J.I., 1998, Late Cenozoic exhumation of the Cascadia Accretionary Wedge in the Olympic Mountains, northwest Washington State: Geological Society of America Bulletin, v. 110, p. 985-1009.

Bull, W.B., 1990, Stream-terrace genesis; implications for soil development: Geomorphology, v. 3, p. 351-367.

Bull, W.B., 1991, Geomorphic response to climatic change: New York, Oxford University Press, 326 p.

Bull, W.B. and Knuepfer, P.L.K., 1987, Adjustments by the Charwell River, New Zealand, to uplift and climate changes: Geomorphology, v. 1, p. 15-32.

Burbank, D.W., Leland, J., Fielding, E., Anderson, R.S., Brozovic, N., Reid, M.R., and Duncan, C., 1996, Bedrock incision, rock uplift, and threshold hillslopes in the northwestern Himalayas: Nature, v. 379, p. 505-510.

Campbell, K.A., and Nesbitt, E.A., 2000, High resolution architecture and paleoecology of an active margin, storm-flood influenced estuary, Quinault Formation (Pliocene), Washington: Palaios, v. 15, p. 553-579.

Chappell, J., Omura, A., Esat, T., McCulloch, M., Pandolfi, J., Ota, Y., and Pillans, B., 1996, Reconciliation of late Quaternary sea levels derived from coral terraces at Huon Peninsula with deep sea oxygen isotope records: Earth and Planetary Science Letters, v. 141, p. 227-236.

Carson, M.A., 1970, The existence of threshold hillslopes in the denudation of the landscape: Institute of British Geographers Transactions, v. 49, p. 71-95.

Carson, M.A., 1971, An application of the concept of threshold slopes to the Laramie Mountains, Wyoming: Institute of British Geographers Special Publication no. 3.

Chinn, T., 1981, Use of rock weathering-rind thickness for Holocene absolute age-dating in New Zealand: Arctic and Alpine Research, v. 13, p. 33-45.

Cleveland, W.S., 1979, Robust locally weighted regression and smoothing scatterplots: Journal of the American Statistics Association, v. 74, p. 829-836.

Cleveland, W.S., 1981, LOWESS: A program for smoothing scatterplots by robust locally weighted regression: American Statistician, v. 35, p. 54.

Clowes, R.M., Brandon, M.T., Green, A.C., Yorath, C.J., Sutherland Brown, A., Kanasewich, E.R., and Spencer, C., 1987, LITHOPROBE—southern Vancouver Island: Cenozoic subduction complex imaged by deep seismic reflections: Canadian Journal of Earth Sciences, v. 24, p. 31-51.

Colman, S.M. and Pierce, K., 1981, Weathering rinds on andesitic and basaltic stones as a Quaternary age indicator, western United States: U.S. Geological Survey Professional Paper 1210, 56 p.

Colman, S.M. and Pierce, K., 1986, Glacial sequence near McCall, Idaho; weathering rinds, soil development, morphology, and other relative-age criteria: Quaternary Research, v. 25, p. 25-42.

Crosson, R.S., and Owens, T.J., 1987, Slab geometry of the Cascadia Subduction Zone beneath Washington from earthquake hypocenters and teleseismic converted waves: Geophysical Research Letters, v. 14, p. 824-827.

Dean, R., 1991, Equilibrium beach profiles: Characteristics and applications: Journal of Coastal Research, v. 7, p. 53-84.

DeMets, C., and Dixon, T., 1999, New kinematic models for Pacific–North America motion from 3 Ma to present: I, Evidence for steady motion and biases in the NUVEL-1A model: Geophysical Research Letters, v. 26, p. 1921-1924.

DeMets, C., Gordon, R.G., Argus, D.F., and Stein, S., 1990, Current plate motions: Geophysical Journal International, v. 101, p. 425-478.

Dragert, H., 1987, The fall (and rise) of central Vancouver Island: 1930-1985: Geological Survey of Canada Contribution 10586, p. 689-697.

Dragert, H., Hyndman, R.D., Rogers, G.C., and Wang, K., 1994, Current deformation and the width of the seismogenic zone of the northern Cascadia Subduction Thrust: Journal of Geophysical Research , v. 99, p. 653-668.

Easterbrook, D.J., 1986, Stratigraphy and chronology of Quaternary deposits of the Puget Lowland and

Olympic Mountains of Washington and the Cascade Mountains of Washington and Oregon, *in* Sibrava, V., Bowen, D.Q., and Richmond, G.M., editors, Quaternary glaciations in the northern hemisphere: Quaternary Science Reviews, v. 5, p. 145-159.

Florer, L.E., 1972, Quaternary paleoecology and stratigraphy of the sea cliffs, western Olympic Peninsula, Washington: Quaternary Research, v. 2, p. 202-216.

Fuller, I.C., Macklin, M.G., Lewin, J., Passmore, D.G., and Wintle, A.G., 1998, River response to high-frequency climate oscillations in southern Europe over the past 200 k.y.: Geology, v. 26, p. 275-278.

Gardner, T.W., Verdonck, D., Pinter, N.M., Slingerland, R., Furlong, K.P., Bullard, T.F., and Wells, S.G., 1992, Quaternary uplift astride the aseismic Cocos Ridge, Pacific coast of Costa Rica, Geological Society of America Bulletin 104, 219-232.

Gerstel, W.J., 1999, Deep-seated landslide inventory of the west-central Olympic Peninsula: Washington Division of Geology and Earth Resources Open File Report 99-2, 36 p.

Hancock, G.S., Anderson, R.S., Chadwick, O.A., and Finkle, R.C., 1999, Dating fluvial terraces with ^{10}Be and ^{26}Al profiles: Application to the Wind River, Wyoming: Geomorphology, v. 27, p. 41-60.

Holdahl, S.R., Faucher, F., and Dragert, H., 1989, Contemporary vertical crustal motion in the Pacific northwest, *in* Cohen, S.C. and Vanicek, P., editors, Slow deformation and transmission of stress in the Earth: American Geophysical Union Geophysical Monograph 40, International Union of Geodesy and Geophysics Volume 4, p. 17-29.

Holdahl, S.R., Martin, D.M., and Stoney, W.M. 1987, Methods for combination of water level and leveling measurements to determine vertical crustal motions, *in* Proceedings of Symposium on Height Determination and Recent Crustal Movement in Western Europe: Bonn, Dumler Verlag, p. 373-388.

Hyndman, R.D., and Wang, K., 1993, Thermal constraints on the zone of major thrust earthquake failure: The Cascadia Subduction Zone: Journal of Geophysical Research, v. 98, p. 2039-2060.

Johnson, S.Y., Potter, C.J., and Armentrout, J.M., 1994, Origin and evolution of the Seattle Fault and Seattle Basin, Washington: Geology, v. 22, p. 71-74.

Kelsey, H.M. and Bockheim, J.G., 1994, Coastal landscape evolution as a function of eustasy and surface uplift rate, Cascadia margin, southern Oregon: Geological Society of America Bulletin, v. 106, p. 840-854.

Kelsey, H.M., 1990, Late Quaternary deformation of marine terraces on the Cascadia Subduction Zone near Cape Blanco, Oregon: Tectonics, v. 9, p. 983-1014.

Knuepfer, P.L.K., 1988, Estimating ages of late Quaternary stream terraces from analysis of weathering rinds and soils: Geological Society of America Bulletin, v. 100, p. 1224-1236.

Maddy, D., 1997, Uplift-driven valley incision and river terrace formation in southern England: Journal of Quaternary Science, v. 12, p. 539-545.

McCrory, P.A., 1996, Tectonic model explaining divergent contraction directions along the Cascadia Subduction Margin, Washington: Geology, v. 24, p. 929-932.

McCrory, P.A., 1997, Evidence for Quaternary tectonism along the Washington Coast: Washington Geology, v. 25, p. 14-19.

McNeill, L.C., Goldfinger, C., Kulm, L.D., Yeats, R.S., 2000, Tectonics of the Neogene Cascadia forearc drainage; investigations of a deformed late Miocene unconformity: Geological Society of America Bulletin, v. 112, p. 1209-1224.

McNeill, L., Piper, K., Goldfinger, C., Kulm, L., and Yeats, R., 1997, Listric normal faulting on the Cascadia continental margin: Journal of Geophysical Research , v. 102, p. 12,123-12,138.

McSaveney, M., 1992, A manual of weathering-rind dating for sandstone clasts of the Torlesse Supergroup: Geological Society of New Zealand Miscellaneous Publication 63A, 106 p.

Merritts, D., Vincent, K., and Wohl, E.T., 1994, Long river profiles, tectonism, and eustasy: A guide to interpreting fluvial terraces: Journal of Geophysical Research, v. 99, p. 14,031-14,050.

Meyer, G.A., Wells, S.G., and Jull, A.J.T., 1995, Fire and alluvial chronology in Yellowstone National Park: Climate and intrinsic controls on Holocene geomorphic processes: Geological Society of America Bulletin, v. 107, p. 1211-1230.

Mitchell, C.E., Vincent, P., Weldon R.J., and Richards, M., 1994, Present-day vertical deformation of the Cascadia Margin, Pacific Northwest, U.S.A.: Journal of Geophysical Research , v. 99, p. 12,257-12,277.

Montgomery, D.R., 2001, Slope distributions, threshold hillslopes, and steady-state topography: American Journal of Science, v. 301, p. 432-454.

National Data Buoy Center, 2000, Station Information, U.S. Northwest Region. http://seaboard.ndbc.noaa.gov/stuff/northwest/nwstmap.shtml

Orange, D.L., 1990, Criteria helpful in recognizing shear-zone and diapiric melanges: Examples from the Hoh Accretionary Complex, Olympic Peninsula, Washington: Geological Society of America Bulletin, v. 102, p. 935-951.

Ouchi, S., 1985, Response of alluvial rivers to slow active tectonic movements: Geological Society of America Bulletin, v. 96, p. 504-515.

Pazzaglia, F.J. and Brandon, M.T., 2001 A fluvial record of rock uplift and shortening across the Cascadia forearc high: American Journal of Science, v. 301, p. 385-431.

Pazzaglia, F.J. and Gardner, T.W., 1993, Fluvial terraces of the lower Susquehanna River, Geomorphology, v. 8, p. 83-113.

Pazzaglia, F.J., Gardner, T.W., and Merritts, D., 1998, Bedrock fluvial incision and longitudinal profile development over geologic time scales determined by fluvial terraces, *in* Wohl E. and Tinkler, K., ed., Rivers over rock: Fluvial processes in bedrock channels: American Geophysical Union Geophysical Monograph Series, v. 107, p. 207-236.

Personius, S.F., 1995, Late Quaternary stream incision and uplift in the forearc of the Cascadia Subduction Zone, western Oregon: Journal of Geophysical Research, v. 100, p. 20,193-20,210.

Pillans, B., Chappell, J., and Naish, T.R., 1998, A review of the Milankovitch climatic beat: Template for Plio-Pleistocene sea-level changes and sequence stratigraphy: Sedimentary Geology, v. 122, p. 5-21.

Ramsay, B., 2000, OxCal v. 3.5: *available from* http://www.rlaha.ox.ac.uk/orau/index.htm.

Rau, W.W., 1970, Foraminifera, stratigraphy, and paleoecology of the Quinault Formation, Point Grenville–Raft River coastal area, Washington: Washington

Department of Natural Resources Bulletin, v. 62, 34 p.
Rau, W.W., and Grocock, G., 1974, Piercement structure outcrops along the Washington coast: Washington Division of Mines and Geology Information Circular, v. 51, 7 p.
Rau, W., 1973, Geology of the Washington coast between Point Grenville and the Hoh River: Washington Geology and Earth Resources Division Bulletin 66, 58 p.
Rau, W., 1979, Geologic map in the vicinity of the lower Bogachiel and Hoh River Valleys and the Washington coast: Washington Geology and Earth Resources Division Map GM-24, scale 1:62,500.
Rau, W., 1975, Geologic map of the Destruction Island and Taholah Quadrangles, Washington: Washington Geology and Earth Resources Division Map GM-13, scale 1:62,500.
Reilinger, R. and Adams, J., 1982, Geodetic evidence for active landward tilting of the Oregon and Washington Coastal Ranges: Geophysical Research Letters, v. 9, p. 401-403.
Ricker, K., Chinn, T., and McSaveney, M., 1993, A late Quaternary moraine sequence dated by rock weathering rinds, Craigieburn Range, New Zealand: Canadian Journal of Earth Sciences, v. 30, p. 1861-1869.
Rogers, G.C., 1988, An assessment of megathrust earthquake potential of the Cascadia Subduction Zone: Canadian Journal of Earth Science, v. 25, p. 844-852.
Savage, J.C., Lisowski, M., and Prescott, W.H., 1981, Geodetic strain measurements in Washington: Journal of Geophysical Research , v. 86, p. 4929-4940.
Savage, J.C., Lisowski, M., and Prescott, W.H., 1991, Strain accumulation in western Washington: Journal of Geophysical Research , v. 96, p. 14,493-14,507.
Schumm, S.A., 1969, River metamorphosis: Journal of the Hydraulics Division, Proceedings of the American Society of Civil Engineers, v. 95, p. 255-273.
iSchumm, S.A., 1973, Geomorphic thresholds and complex response of drainage systems, *in* Morisawa, M., ed., Fluvial geomorphology: Proceedings of the 4th Geomorphology Symposium, Publications in Geomorphology: Binghamton, State University of New York, p. 299-310.
Schumm, S.A., Dumont, J.F., and Holbrook, J.M., 2000, Active tectonics and alluvial rivers: Cambridge University Press, 276 p.
Schumm, S.A., Mosley, M.P., and Weaver, W.E., 1987, Experimental fluvial geomorphology: New York, Wiley Interscience, 413 p.
Serdar, C.F., 1999, Description, analysis, and impacts of the Grouse Creek Landslide, Jefferson County, Washington, 1997-98: Evergreen State College Master of Environmental Studies Thesis, 171 p.
Sugai, T., 1993, River terrace development by concurrent fluvial processes and climate change: Geomorphology, v. 6, p. 243-252.
Tabor, R. W., and Cady, W. M., 1978a, Geologic Map of the Olympic Peninsula: U.S. Geological Survey Map I-994, 2 sheets, scale 1:125,000.
Tabor, R.W. and Cady, W.M., 1978b, The structure of the Olympic Mountains, Washington— Analysis of a subduction zone: U. S. Geological Survey Professional Paper 1033, 38 p.
Thackray, G.D. and Pazzaglia, F.J., 1994, Quaternary stratigraphy, tectonic geomorphology, and fluvial evolution of the western Olympic Peninsula, Washington, *in* Swanson, D.A., and Haugerud, R.A., ed., Geologic field trips in the Pacific Northwest, 1994 Geological Society of America Annual Meeting, Seattle, Washington, p. 2A-1–2A-30.
Thackray, G.D., 1996, Glaciation and neotectonic deformation on the western Olympic Peninsula, Washington: University of Washington PhD Dissertation, 139 p.
Thackray, G.D., 1998, Convergent-margin deformation of Pleistocene strata on the Olympic coast of Washington, USA, *in* Stewart, I. S. and Vita-Finzi, C., ed. , Coastal tectonics: London, Geological Society Special Publication 146, p. 199-211.
Thackray, G.D., 2001, Extensive early and middle Wisconsin glaciation on the western Olympic Peninsula, Washington, and the variability of Pacific moisture delivery to the northwestern United States: Quaternary Research, v. 55, p. 257-270.
Thatcher, W., and Rundel, J. B., 1984, A viscoelastic coupling model for the cyclic deformation due to periodically repeated earthquakes at subduction zones: Journal of Geophysical Research, v. 89, p. 7631-7640.
Trenhaile, A., 1997, Coastal dynamics and landforms: Oxford, Clarendon Press, 366 p.
Tucker, G.E., and Slingerland, R.L., 1997, Drainage basin response to climate change: Water Resources Research, v. 33, p. 2031-2047.
Wang, K., 1996, Simplified analysis of horizontal stresses in a buttressed forearc sliver at an oblique subduction zone: Geophysical Research Letters, v. 23, p. 2021-2024.
Wegmann, K.W., 1999, Late Quaternary fluvial and tectonic evolution of the Clearwater River Basin, western Olympic Mountains, Washington State: University of New Mexico MS Thesis, 217 p., 4 plates.
Weldon, R.J., 1986, Late Cenozoic geology of Cajon Pass; implications for tectonics and sedimentation along the San Andreas Fault: California Institute of Technology PhD Dissertation, 400 p.
Wells, R., Weaver, C., and Blakely, R., 1998, Fore-arc migration in Cascadia and its neotectonic significance: Geology, v. 26, p. 759-762.
Wells, S.G., Bullard, T.F., Menges, C.M., Drake, P.G., Karas, P.A., Kelson, K.I., Ritter, J.B., and Wesling, J.R., 1988, Regional variations in tectonic geomorphology along a segmented convergent plate boundary, Pacific coast of Costa Rica: Geomorphology, v. 1, p. 239-265.
West, D.O. and McCrumb, D.R., 1988, Coastline uplift in Oregon and Washington and the nature of Cascadia Subduction Zone tectonics: Geology, v. 16, p. 169-172.
Willett, S.D., Slingerland, R., and Hovius, N., 2001, Uplift, shortening, and steady state topography in active mountain belts: American Journal of Science, v. 301, p. 455-485.
Wolman, M.G. and Miller, J.P., 1960, Magnitude and frequency of forces in geomorphic processes: Journal of Geology, v. 68, p. 54-74.

Landslides at Kelso,Washington, and Portland, Oregon

Scott F. Burns, Department of Geology, Portland State University, Portland, Oregon 97207; burnss@pdx.edu

H. Tom Kuper, Kuper Consulting LLC, 22680 SW 76th Avenue, Tualatin, Oregon 97062; dkuper@cybcon.com

John L. Lawes, Out Standing in the Field Co., 5812 N Amherst Street, Portland, Oregon 97203

ABSTRACT

The field trip will first start in Corvallis at 7:30 a.m. and will pick up other participants in Portland at Portland State University at 9:00 am. Vans will drop participants off in either Portland or Corvallis at the end of the trip. In the morning we will visit Kelso, Washington, site of the Aldercrest–Banyon Landslide (the second largest landslide disaster involving homes in United States history), the recently reactivated Haussler Road–Apple Lane Landslide, and the Carrolsbluff Landslide. In the early afternoon we will visit the Royse, Tumalt Creek, and Exit 35 Debris Flows in the Columbia Gorge. In the late afternoon we will spend time in the West Hills of Portland visiting the Zoo, Washington Park, and Canterbury Castle Landslides. Participants will visit large reactivated earthflows, debris flows, and small earthflows in loess. We will discuss mechanisms of failure, politics of landslides, land-use planning, and mitigation of the landslides.

INTRODUCTION

Landslides are a major geologic hazard in the Pacific Northwest. Steep slopes combined with weak soils are abundant and provide sites ready for failure. When sufficient precipitation is delivered, landslides occur. All types of slope failures are found in the Pacific Northwest. Today, we will visit two main types: earthflows and debris flows. First, we will see small earthflows that have occurred in loess on oversteepened slopes during periods of extensive rainfall. Second, we will visit large earthflows that first started moving over 10,000 years ago but have been reactivated during periods of high rainfall in recent years. Last, we will see steep drainages along the Columbia River, where large rainfall events have scoured valley bottoms and formed devastating debris flows. All in all, we will visit some "textbook" examples today.

Field Guide to Geologic Processes in Cascadia: Oregon Department of Geology and Mineral Industries Special Paper 36, 2002.

KELSO, WASHINGTON: ALDERCREST–BANYON LANDSLIDE

We will be visiting the second largest landslide disaster in U.S. history involving homes. The reactivation of an ancient landslide in 1998 destroyed 60 homes and endangered another 77 on the surrounding slopes (Fig. 1). The housing development was built in the early 1970s on a hill to the southeast of downtown Kelso. Movement was first reported in February 1998, and on October 16, 1999, the Federal Emergency Management Agency (FEMA) declared the Aldercrest–Banyon Subdivision its first "major landslide disaster area" making it open for federal funding relief.

The landslide occurred in the Troutdale Formation (a Miocene–Pliocene fluvial deposit of the ancestral Columbia River), and it moved over a paleosol on the Eocene-aged Cowlitz Formation (Geoengineers, 1998; Wegman and Walsh, 2001). The original landslide probably occurred during the Missoula Floods (15,300–12,700 years ago). Its width is approximately 1000 meters and length about 500 meters. The scarp is about 35 meters high, and the depth to the surface of failure ranges from 3 meters to about 12 meters. The maximum slide movement in 1998 was about 15–30 cm/day. Damage to private property is estimated to be about $25.7 million, and damage to infrastructure about $6.2 million (Geoengineers, 1998). The motion is mainly translational, but some inves-

Figure 1: Destroyed house on the Aldercrest–Banyon Landslide in Kelso, Washington. Note the thrust of soil under the house.

tigators have also classified it as a large earthflow.

Extraordinary precipitation for the previous three winters contributed to the reactivation of the landslide (Geoengineers, 1998). For the previous 50 years, the average annual precipitation was 1125 mm (45 inches), but the water years of 1995-1996, 1996-1997, and 1997-1998 were 1650, 1900, and 1350 mm. Also, an excavation in February 1998 to put a road across the lower part of the slide may have been a trigger to cause the initial reactivated movement, which then caused storm drains to break and storm water to be fed back into the slide. Logging opperations at the toe of the landslide may also have contributed to the reactivation.

The costs of repairing damage from this landslide were prohibitive. Home owners lost everything, because there is essentially no home insurance for landslides. The people living above the scarp wondered if their houses might also go. FEMA did help all homeowners above and below the scarp by giving $0.35 on the dollar value for their homes and property. The federal government has come in and removed all the purchased homes. Eleven homeowners still remain in their homes and are taking their chances of the upper area never reactivating.

This disaster has raised public awareness of landslides in the Pacific Northwest. If we are heading into a 20 year wet cycle, more of these ancient landslides may reactivate (Taylor and Hannan, 1999). Communities do not want to have another "Kelso Landslide" happen in their area.

STOPS ON THE FIELD TRIP

Stop 1. Aldercrest–Banyon Landslide: South End

At this site we can see the scarp of the slide and the area where the first movement was recorded. The homes above the scarp were removed in the summer of 2001.

Stop 2. Aldercrest–Banyon Landslide: Home of John Coleman

We will stop at the home of John Coleman, one of the eleven homeowners who decided to remain in their homes and not to sell to the government for a fractional price. It will give us an excellent view of the slide, and we will hear from a local person how he made the tough decision to stay, when most of his neighbors sold out and left.

Stop 3. Aldercrest–Banyon Landslide: North End

We will get a chance to see where the landslide moved the fastest. One home moved over 500 m during the landslide reactivation.

Stop 4. Haussler Road-Apple Lane Landslide: Development of a Simple Test to Quantify Reactivation

This is the site of another ancient landslide that has also started to reactivate on the southwest side of the mountain. The geology is the same as the Aldercrest-Banyon Landslide. There are 88 homes below the scarp and 42 above it. If this landslide reactivated to the magnitude of the slide on the other side of the mountain, it could lead to a disaster larger than the Aldercrest–Banyon Landslide.

Students from Portland State University developed a mechanism for assessing the homes to tell if the slide was beginning to creep and to describe where the greatest movement and destruction was occurring (Burns and others, 2001). People are building on ancient landslides more often as buildable land is becoming rarer. If one of these landslides reactivates, it can destroy many of the homes on it. Reactivation of ancient landslides is usually related to the buildup of pore-water pressure in the slide mass. Commonly this will occur very slowly in the beginning stages, especially if the climate has been wet. The initial stages of movement on open ground are difficult to recognize unless one has an inclinometer in the ground. Houses, however, because they are rigid structures, show stress in the early stages of reactivated creep of an ancient landslide, and they can be used as indicators that a landslide has begun to move. But these effects are often misinterpreted as subsidence (settling) features.

For this project, 130 homes in the Haussler Road area of Kelso, Washington, were studied. We developed a list of 18 characteristics to be monitored that may indicate landslide reactivation through stress on a house or lot. In the houses they are the following: recent propagation of cracks in the walls, nails popping out of the walls, bulging walls, separation of internal and external chimneys from walls, creaking and popping noises, light switches coming out of the walls, doors and windows that are hard to shut, twisted ceiling and floor beams, cracks in concrete floors, floors that are not level, and water seeping into the basement. On the lot outside of a house, there are changes in surface water drainage, bulges in retaining walls, scarps developing in the soil, pistol butt trees, and broken water and sewer lines.

A stable site is defined as having none of the above characteristics. Slight movement (class 1) is defined as having 1 to 5 of the above characteristics, moderate movement (class 2) from 6 to 10, and considerable movement (class 3) more than 11.

In the Kelso area, we recommended that parts of the slide showing moderate to considerable movement (more than 6 characteristics) be mitigated by dewatering of the slide mass. For areas of slight movement, we recommended that the area be monitored frequently and an inclinometer installed. We propose that communities with ancient landslides instruct homeowners about these characteristics and alert everyone to the possibility of their landslide beginning to move. If geologists know early enough that movement has started, proper mitigation measures such as dewatering and buttressing can be instituted that might stop the movement and save the homes.

At the Haussler Road–Apple Lane Landslide, we used the initial results to show the Kelso City Council that the slide was reactivating. Above the landslide scarp, 45% of the houses surveyed are displaying movement, with 27% showing significant movement (classes 2 and 3). Below the scarp, 89% of the houses indicate movement, with 65% showing significant movement (classes 2 and 3). Based on our presentation, the city council in April of 1999 decided that there was a problem and hired Geoengineers to describe the movement and make recommendations. Nine inclinometers were installed, and most of them showed

movement. The recommendation was to put in a cutoff trench to dewater the upper part of the slide. This was installed in the late spring of 1999.

At this site we will visit the small street, Ron's Court, where some reactivation was noted. We will also see the cutoff trench. We will drive around Apple Lane and see where one house was torn down and two others have been condemned. We will also see sites of retaining walls destroyed by the reactivation.

Stop 5. Carrollsbluff Landslide: Proposed Residential Subdivision on an Ancient Landslide

We will visit the Carrollsbluff Landslide at two places. We will drive to the bottom of the hill and talk about the situation. This will be Stop 5. We will then drive to the top of the hill at Stop 6 to view the slope from a rock quarry.

In February 1996, a private developer approached Tom Kuper and John Lawes, then employed at David Newton Associates, Inc (DNA), to request a geotechnical investigation for a proposed 500-lot subdivision. This development was proposed for an approximately 80 hectare site in the low foothills of the Cascade Range (altitude range 50 to 200 m), about 2 kilometers southeast of the Kelso, Washington, urban area. Tom Kuper visited the site with the client in early March and observed recent tension cracks and scarps. Concerned about these signs of possible landsliding, Tom Kuper recommended a phased approach to the investigation of the property due to the landslide features observed and to the density of the proposed development. The proposed phases would be initiated with a site reconnaissance level mapping and proceed once the mapping was completed with a more detailed subsurface investigation.

This reconnaissance, performed by John Lawes in March 1996, indicated that the site geology was dominated by deep residual soil formed on interbedded basaltic andesite flows and pyroclastic rocks of the upper Eocene to lower Oligocene Goble Volcanics. The reconnaissance also revealed at least 7 to 10 areas of active or recent landsliding. Over half of these were small rotational slump failures likely linked to streambank erosion along the first-order streams that dissect the site. However, two extremely large, actively creeping earthflows were observed, which cover at least 1.8 square kilometers of the southern part of the site (Fig. 2). Slow-moving earthflow features, including head and lateral scarps, extensive linked and en echelon tension cracks, sag ponds, disrupted vegetation, ground buckling, and toe bulging could be traced for as much as 400 m. The smaller northern earthflow seemed to be the more active. This slide had displaced an interstate natural-gas pipeline, which crossed the headscarp area, by as much as 30 cm laterally and 25 cm vertically. Following the David Newton Associates preliminary reconnaissance findings and the recommendations of the pipeline's geotechnical engineer, repairs to it were made in April 1996.

Based on these observations, we recommended a program of exploratory trenching and drilling as well as installation of monitoring instruments, particularly inclinometers and piezometers. The client declined to authorize drilling; instead, a budget-limited subsurface investigation was performed using a tracked excavator. Forty-one trenches were dug across the site. Trench T-25, dug along the axis of the northern earthflow, reached a depth of 32 feet below the ground surface without penetrating through the landslide debris. The trenching did not satisfactorily establish the depth or activity of the sliding.

By June 1996, disagreement over continuing subsurface exploration ended the relationship between David Newton Associates and the client without a final geotechnical report. The client was still attempting to develop the property as late as the fall of 1999 and had retained another consultant, who apparently interpreted the geologic conditions to have few landslide features. One source of considerable contention during the hearing process was the belated "discovery" of the David Newton Associates investigation by the City of Kelso. Our 1996 work entered the public domain only because the pipeline company presented it to the city during hearings for a final development-plan approval. We understand that the final approval of the proposed development now may be indefinitely delayed.

The following lessons can be learned from this case history. First, as development in the Pacific Northwest increasingly moves into

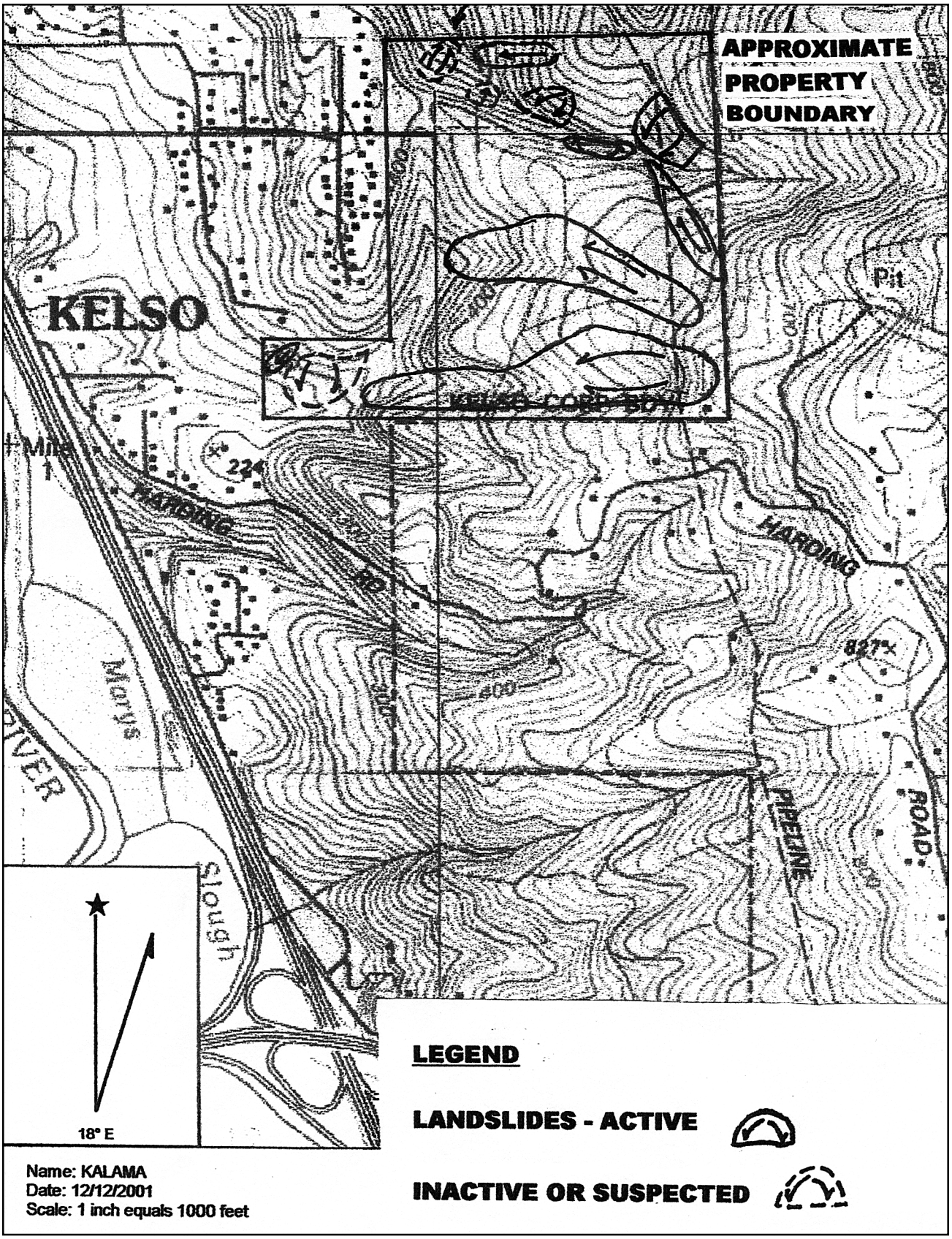

Figure 2: Map of the Carrollsbluff Landslide southeast of the Aldercrest–Banyon Landslide in Kelso, Washington.

upland parts of urban areas, uniformity of the standard of professional practice for hillside-development investigation will need to be raised. In the above example, despite our concerns regarding the subject property, a second consultant was found to provide a more optimistic assessment that allowed development to proceed until the discovery of our initial investigation.

Second, both regulatory bodies and clients in the Pacific Northwest should be educated regarding the benefits to both parties and to the public from a thorough, detailed geotechnical investigation prior to hillside development. Client education is a priority in this case, because many private developers are highly expense-sensitive and will require careful explanation of the potentially devastating liability associated with a slope failure. The relative inexperience of many Pacific Northwest planning agencies with hillside development increases the likelihood that sites in both Oregon and Washington will be approved for construction with little or no investigation. The Division of Geology of the Washington Department of Natural Resources is currently preparing updated geologic and geologic-hazard maps for the greater Kelso area. We fully support Washington in this project and recommend that these maps be incorporated into the local planning process.

Third, in complex terrain such as this, we recommend a phased investigative approach initiated with a geologic reconnaissance. This phased approach should involve the client and consultants *planning* the development in potential slope-hazard areas. We as engineering geologist professionals should be responsible for getting this message out to the development community. The above case is a good example. For a minimal fee, a prepurchase geologic reconnaissance could have helped this client to avoid purchasing this property and the risks and costs of trying to mitigate the landsliding.

Stop 6. Carrollsbluff Landslide: View from the Top

Stop 7. Dodson–Warrendale Debris Flow Alluvial Fan

This alluvial fan on the Oregon side of the Columbia River has been accumulating for the past 12,700 years. Most likely, the great Missoula Floods that were funneled through the Columbia River Gorge from 15,300 to 12,700 years ago removed a good portion of the sediment previously occupying the area. This modern and impressive alluvial fan has been forming from repeated debris flow activity from the steep bedrock canyons to the south of the river. The majority of the bedrock is in the Columbia River Basalt Group, but Troutdale Formation fluvial deposits and the Boring Lava are found toward the top of the cliffs. Sediment of the fan is made up of deposits from these three formations. This fan became famous starting in February of 1996 when six drainages to the south (Fig. 3) produced debris flows that deposited sediment across the fan (Powell and others, 1996; Johnson and Johnson, 1997). The two most famous ones are the Royse Debris Flow, which engulfed a house, and the Tumalt Creek Debris Flow, which caused extensive damage with its great velocity and power when it hit a train and trucks in the transportation corridor. Smaller debris flows occurred on the fan later in 1996 and 1997, but the most impressive one since then happened in early December of 2001 at the Exit 35 interchange with Interstate 84.

Stop 7a. Exit 35 Debris Flow

This debris flow cone started forming on December 1, 2001, and it closed the onramp and offramp from I-84 on December 2nd. The previous week was marked by heavy rains that caused extensive landslide activity in the upper drainage of the creek to the west of St. Peters Dome, a basalt promontory above Dodson. A small debris flow had occurred from that drainage in 1996. This time, the whole west and south sides of the canyon failed depositing thousands of cubic meters of sediment into the stream valley bottom. Nonstop rains mobilized the sediment into the debris flow that went right through the forest, knocking down many trees. It terminated in a cone at the onramp to I-84 (Fig. 4).

The cone continued to grow each day, with a growth of 2 meters in height occurring on December 5th. At the time of this writing, the debris cone is still in place. The highway department is waiting for it to dewater so the debris fan can be removed.

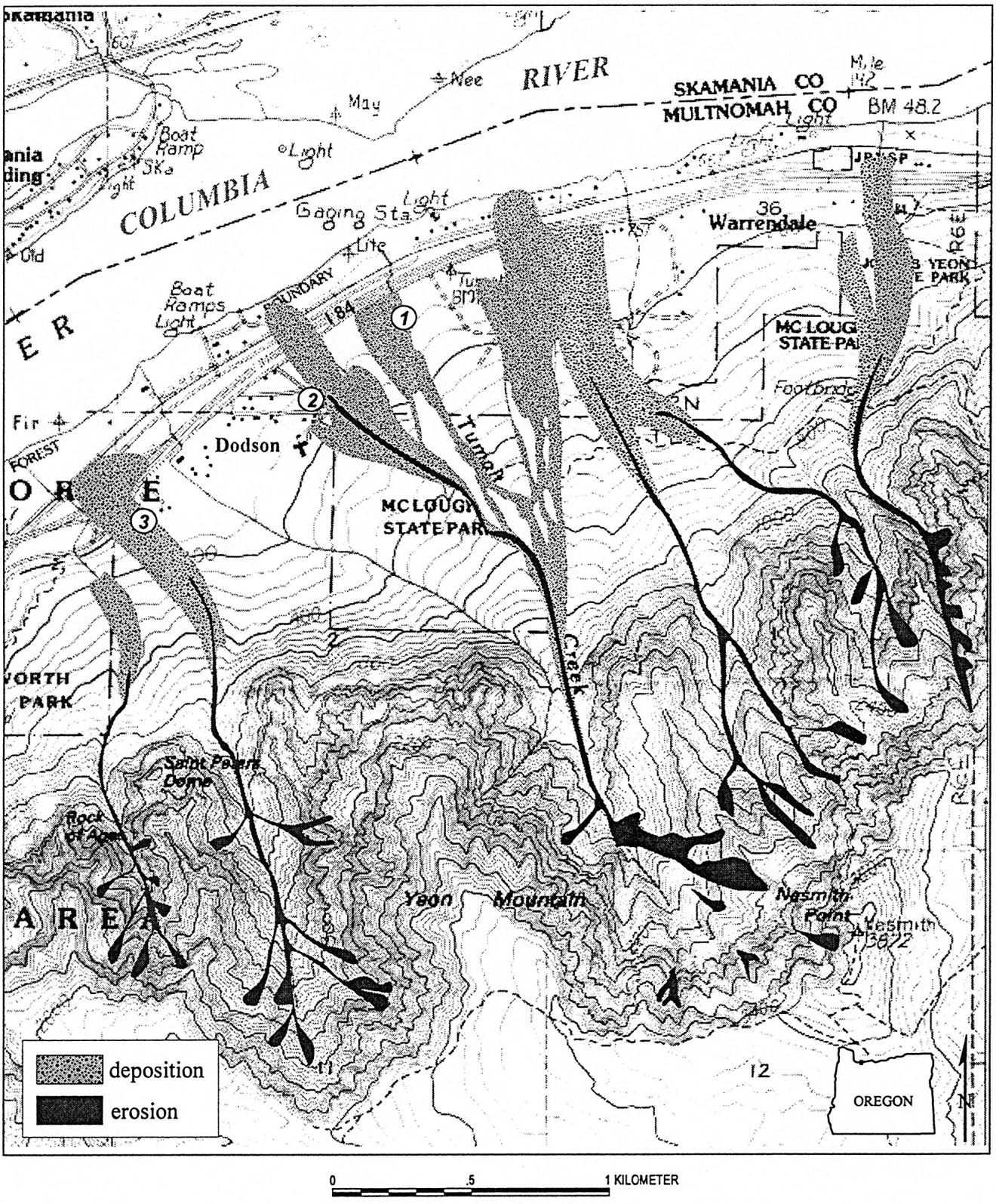

Figure 3. Areas of erosion to the east of St. Peters Dome near the canyon that produced the Royse Debris Flow in 1996 (Powell and others, 1996). A previous event in 1918 took place in the same canyon. In 2001, the canyon between the Rock of Ages and St. Peters Dome produced the Exit 35 Debris Flow. A 1987 event was in the canyon just east of Warrendale (map from Johnson and Johnson, 1997).

Figure 4. Photo of the Exit 35 Debris Flow taken in early December 2001 looking east.

Stop 7b. Royse Debris Flow

This debris flow occurred on February 7, 1996, and started about 12 noon. Mrs. Carol Royse was in her home fixing lunch when she looked out the back window of her home to the pasture and saw a wall of boulders coming toward the house from the south. She and her husband rushed from the house to safety about 200 meters away. The debris flow filled up half of the first floor of the house and most of their property to a maximum depth of about 5 meters (Fig. 5) . It continued down toward the river and stopped traffic on I-84 and on the railroad. Over the next 4 days additional flows added to the debris flow deposit. Debris came from many landslides in the drainage to the east of St. Peters Dome.

Mrs. Royse tells of her cousin's home being hit by a debris flow in about 1918. That house was to the west of the Royse's home. The Royse family has tried unsuccessfully to rebuild their home on the site, but the Federal Emergency Management Agency will only give them money to rebuild if they move off the site. They still live on the property today in a smaller house to the east of the flow. Their damaged home, which still stands today, has had its picture show up in many textbooks and publications about landslides. This is a classic example of a slow-moving debris flow that is estimated to have had a maximum velocity of 8–10 km/hr. The cobbles and boulders of the debris flow are primarily Boring Lava and not Columbia River Basalt.

Stop 7c. Tumalt Creek Debris Flow

Tumalt Creek is about 0.5 km to the east of the 12 noon, February 7, 1996, Royse Debris Flow that stopped both Interstate 84 highway traffic and the railroad. Tumalt Creek was the site of the largest of the debris flows in February of 1996.

Local inhabitants tell us that in the midafternoon of February 7th, the creek "stopped flowing". We believe that a major landslide in the headwaters of Tumalt Creek

Figure 5. The home of Carol and Hersh Royse that was destroyed by a debris flow in February 1996.

had dammed the drainage, stopping the creek. Late in that day, this landslide dam breached, and it sent all that water plus the sediment from the landslide dam rushing down the valley as a very fast moving debris flow. Traffic and the train were waiting there because of the Royse Debris Flow. People helping with rescue operations on the highway said that they could hear the Tumalt Creek Debris Flow coming 15 minutes in advance. Officials estimate that the flow hit the parked trucks on I-84 and the stopped train on the tracks at over 50 km/hr. The impact swept the boxcars in the train and the trucks on the highway into the Columbia River (Fig. 6). This is a classic example of a fast moving debris flow, the most dangerous variety.

This debris flow came very close to the elementary school for the community, which was to the south of the frontage road. It has since been closed, and the children now go to school in Cascade Locks, because authorities feared that the danger was just too great to have a school so close to the debris flow source.

Again, the main cobbles and boulders transported in the Tumalt Creek Debris Flow are from the Boring Lava. The thickness of the debris flow cone is over 6 meters at this site. Debris flows continued to come down this drainage over the next 2 years, and the culverts had to be replaced at least once. It is very lucky that no one was killed from any of the debris flows that spilled onto the fan during February 6-10, 1996.

Stop 8. Zoo Landslide

This is one of the two most famous landslides in Portland. The Zoo Landslide occupies the eastern part of an ancient landslide named the Ancient Highlands Landslide (Hammond and Vessely, 1998). The Zoo Landslide gets its name from one of the two famous cultural centers built on its toe, the Oregon Zoo and the former site of the Oregon Museum of Science and Industry (OMSI), which now houses the Portland Children's Museum. The Zoo Landslide has been the landslide that has shown reactivation. The western part of the Ancient Highlands Landslide, called the Highland Road Landslide, has not shown much activity in modern times.

The Zoo Landslide covers about 55 hectares, is about 800 meters from scarp to toe, is about 400 meters across in the upper area, and is 1100 meters across at the base (Fig. 7). The depth to the failure plane ranges from 20–30 meters. This landslide is considered a translational slide or an earthflow. The slide debris is developed in colluvium that originated from broken up pieces of Wanapum Basalt of the Columbia River Basalt Group (15 Ma) mixed with loess of the Portland Hills Silt (Beeson and others, 1991). Lying under the slide is the Grand Ronde Basalt of the Columbia River Basalt Group. The top of the Grand Ronde has weathered to form the Vantage Horizon, and this paleosol is the surface upon which the slide is moving. The angle of internal friction for the failure plane is about 7 degrees (Hammond and Vessely, 1998).

Various construction activities since the 1950s have reactivated parts of theZoo Landslide. In 1957, US 26 was widened, and the toe of the slide was cut off. That started the slide to

Figure 6. The Tumalt Creek Debris Flow looking east. Note the destruction on Interstate 84 and the Union Pacific Railroad (courtesy of The Oregonian).

move again. A drainage gallery and a rock buttress were installed. But the same thing again happened in 1969 to a lesser extent. In 1995, the headhouse for the Washington Park Station of the Westside Light Rail Tunnel was installed through the slide, and it again began to move. A drainage gallery of 14 horizontal drains and 19 shear piles were installed to stop the slide. Horizontal drains ranged from 100 to 300 m in length and produced initial flows of 300–500 liters/minute. Today, the slide is marginally stable. Seismic displacement analysis indicates, however, that 2–4 cm of movement could occur during a large earthquake.

Stop 9. Washington Park Landslide: The Phenomenal Landslide

The central 15 hectares of Portland's most beautiful city park, Washington Park, is a landslide that has been stabilized in one of the most interesting and successful stories of hazard mitigation in Portland's history. In 1893 and 1894, the city of Portland constructed two reservoirs in the ravine occupied by Tanner Creek about 4 kilometers west of downtown. Little did the workers know that the construction was cutting off the toe of an ancient landslide and causing it to begin to move. The prehistoric age of when this landslide first moved is unknown, but it probably first moved during the ancient Missoula Floods, 15,300 to 12,700 years ago. The small modern slope movements were first noted in 1894.

Under the leadership of D.D. Clarke in 1895, workers discovered that the slide is a large feature that averages 25 meters in depth. The length is 600 meters and the width ranges from 125 m at the west end to 350 m at the east

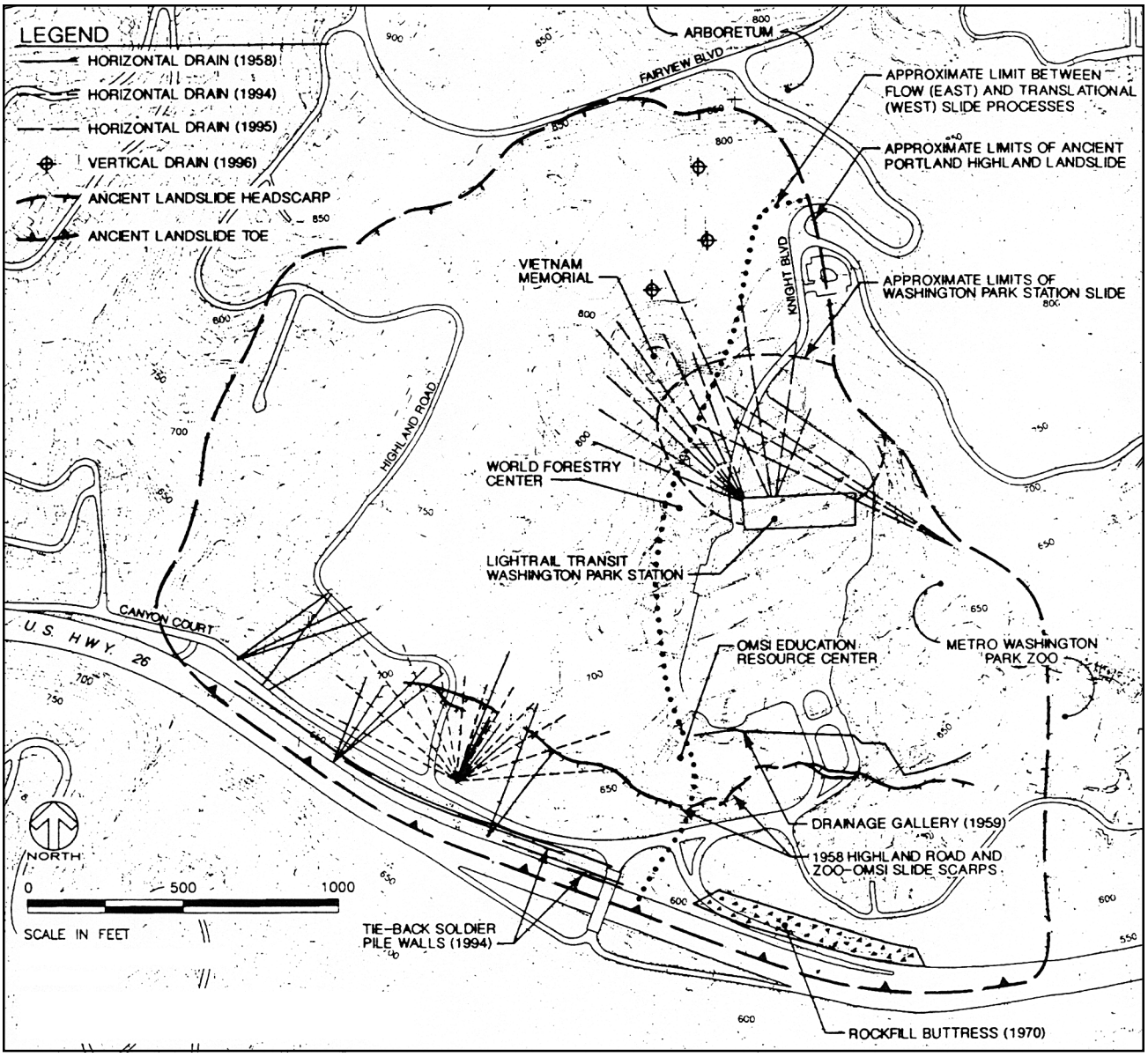

Figure 7. Map of the Zoo Landslide in Portland (after Hammond and Vessely, 1998).

end (Fig. 8). The slide mass is moving on a clay layer, possibly a paleosol in the Columbia River Basalt Group that forms the bedrock of Portland's West Hills. From 1897 to 1901, Clarke installed 22 hand-dug shafts from the ground surface to the clay layer (8-35 m deep) and connected them with 800 meters of tunnels reinforced with wood to drain the water from the slide. The first shaft had a significant effect on dewatering the slide, as 16 million liters of water were pumped from it. Slide movement rates fell from 7 cm/month in 1895 to 0.04 cm/month in 1904. City workers had essentially halted the movement of the landslide to the insignificant rate at which your fingernails grow. It is still moving at about that rate today, and signs of the movement can be seen on the tennis courts at the edge of the slide.

D.D. Clarke and his fellow workers used the scientific method to study this "phenomenal landslide", as Clarke (1904) called it. Their findings about the landslide helped defend the city against large lawsuits in 1898 and helped to mitigate the slide. They used techniques that were years ahead of their time to stabilize the

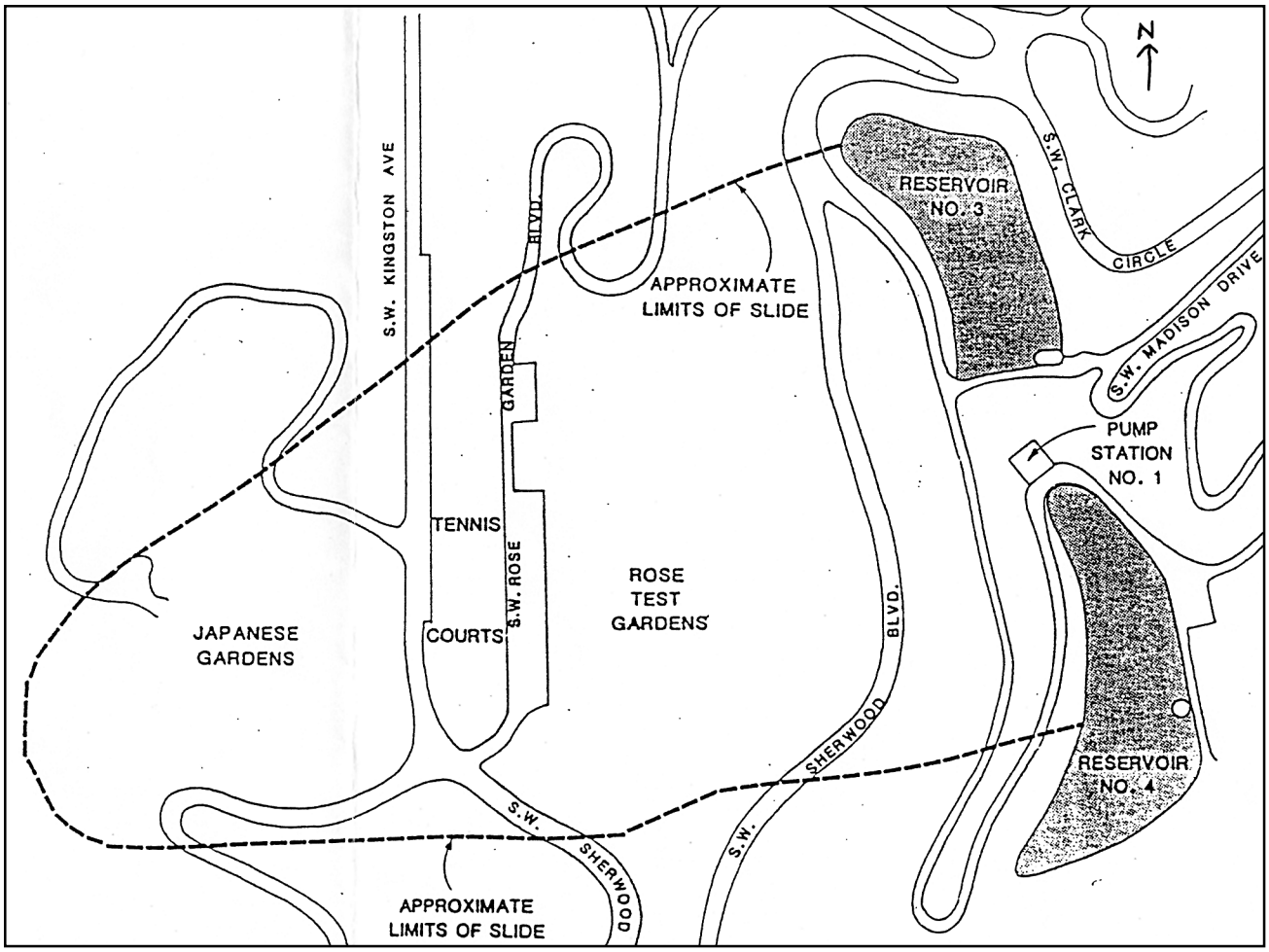

Figure 8. Map of the Washington Park Landslide.

slide and rebuild the reservoirs. The city purchased all the land of the landslide and turned it into the city park; this was an excellent example of early land-use planning in Portland. Today, sinkholes sometimes develop on its slope from the collapse of drainage tunnels beneath as the wooden timbers finally rot. But over 100 years after the discovery of this reactivated ancient landslide, the reservoir and the slope still stand intact, a tribute to the success of a brilliant Water Bureau scientist who stabilized one of the most beautiful spots in Portland.

Stop 10. Canterbury Castle Landslide

The Canterbury Castle Landslide is an earthflow that first occurred on a vacant lot next to the famous "Canterbury Castle" of Portland's West Hills (Fig. 9). It is at the intersection of Fairview and Bennington Roads and just below Canterbury Lane. The first slide happened on February 8, 1996, after 15 cm of rain had fallen in Portland (Burns, 1998). The failure occurred in loess. The earthflow left a 10 meter high head scarp, and the slide was about 30 m long and 20 m wide. The volume was approximately 6000 cubic meters on a slope of 35 degrees. Scarps of 2 to 3 meters on the sides concerned the owners of the neighboring lots, especially the owner of the national historic registered Canterbury Castle, who also owned the vacant lot. The cause of the slide was increased water that was concentrated on the vacant lot soil from storm-water runoff from Canterbury Lane, which is at the top of the scarp.

The first mitigation effort was to build a soldier pile wall during the summer across the 10 m high scarp which was 20 m wide (Fig. 10). This cost approximately $70,000. The next November, just before Thanksgiving, the hydro-

Figure 9. The Canterbury Castle Landslide the week after it occurred in February 1996.

static pressure built up in back of the wall, the wall blew out, and another slide sent mud across the street to hit a house on the other side of Fairview Avenue. No one had designed a water collection system to remove the storm water from Canterbury Lane, because no one would pay for it. Canterbury Lane is a secondary street, so the city would not pay for storm-water upgrades, and the local landowners could not come up with the money to pay for it either.

The following summer, the slope at the base of the Canterbury Castle was stabilized by freezing it by installing pipes throughout the soil and pumping freon through the system. This stabilization system was used until rockfill was brought in to fill the depression where the two slides had occurred. In 2001, a house was built on the lot adjoining the Canterbury Castle, and it occupied the whole space. In most cases we do not recommend that people build on the sites of old landslides, but in this case it is a good idea. The house stabilizes the hole in the slope with its foundation and through a new aggressive water-collection system.

ROAD LOG FOR THE FIELD TRIP

Miles

0.0 **Start at parking lot at corner of Broadway and Mill Street on the Portland State University campus.** Proceed south to Interstate 405 and go east until you intersect I-5 and follow it north.

9.4 Pass the Columbia River on I-5 from Oregon into Washington.

30.4 Pass through Woodland, Washington. This was the site of extensive flooding and landslide activity in February of 1996.

Figure 10. The soldier pile wall built at the top of the Canterbury Castle Landslide in the summer of 1996. It failed the following winter.

33.5 On the right side is the site of a major landslide that reactivated in February 1996 and covered all eight lanes of I-5.

49.2 Exit I-5 at the North Kelso Exit 39 and proceed east. Turn right onto Allen Street and go 1 block to the east. Turn right onto Kelso Drive and go south.

49.4 Turn left onto Russell Street, go 1 block, turn right, and proceed uphill. The road becomes Alma.

50.1 Turn left onto Grimm Road (appropriately named!) and travel uphill until the road ends in a T intersection.

50.8 Turn right (the road still keeps the name Grimm Road).

50.9 Turn left onto Aldercrest Road. Park vehicles and get out. **Stop 1. Aldercrest–Banyon Landslide: Southern End of the Scarp.**

50.9 Go back to north and the intersection with Grimm Road and Banyon. Proceed through the intersection onto Banyon and go 0.2 miles.

51.2 **Stop 2. Aldercrest–Banyon Landslide: Home of John Coleman.** Visit homeowner Mr. Coleman, who will tell us about living close to the slide, and view it from the north. His address is 306 Banyon.

51.2 **Stop 3. Aldercrest–Banyon Landslide: Northern End of the Slide.** Go to the bottom of the hill and park at the gate.

51.6 Turn around and go back up the hill to the intersection of Grimm and Banyon. Go through the intersection to the south and the road becomes Highland Drive.

52.6 Drive to the bottom of Highland Drive. Cross Haussler Drive and park on Ron's Court. **Stop 4. Reactivation of the Haussler Road–Apple Lane Slide.**

52.6 Get back in the vans and drive to see Apple Lane, West Vista, and then return down Haussler to the bottom of the hill.

53.7 Turn left on Kelso Drive

54.2 Turn left on Carroll Road. Go one block and turn left on Cedar Falls Road and go to the end of the road. Park.

54.5 **Stop 5. Carrollsbluff Landslide: Building a Housing Development on an Old Landslide.**

54.5 Turn around and go back to Carroll Road and turn left onto Carroll Canyon Road.

57.2 Proceed up the hill and turn left into the rock quarry. **Stop 6. View of Carrollsbluff Landslide from the Top.**

57.2 Go back downhill on Carroll Canyon Road until it ends.

58.8 Turn left on Kelso Drive and head south.

59.8 Turn left onto the Frontage Road which feeds into I-5.

60.7 You are on I-5 heading south.

90.0 Leave I-5 and get onto I-205 going south.

102.0 You are going over Government Island, which is in the middle of the Columbia River.

104.8 Get onto I-84 going east.

113.6 You are on I-84 heading east and crossing over the Sandy River.

127.3 Multnomah Falls State Park—Possible lunch stop at Exit 31.

131.4 Exit I-84 at Exit 35. **Stop 7a. Exit 35 Debris Flow of 2001.**

131.6 **Stop 7b. Royse Debris Flow.** Continue along Frontage Road and stop at buried house.

132.0 Continue along Frontage Road until you come to Tumalt Creek. **Stop 7c. Tumalt Creek Debris Flow.**

132.0 Retrace route along Frontage Road and get back onto I-84 heading west at the exit entrance.

149.6 Heading west on I-84, you are recrossing the Sandy River.

164.6 Leave I-84 as it ends and get onto I-5 heading south.

166.1 Leave I-5 and get onto I-405 heading toward Beaverton (west).

167.1 Leave I-405 and take US 26 heading west.

168.8 Take Exit 72 from US 26 at the Oregon Zoo.

169.4 Park in the parking lot of the Oregon Zoo. **Stop 8. Zoo Landslide.**

169.4 Leave the parking lot to the north.

169.5 Turn right onto Kingston Road and head east to the Rose Garden.

171.1 Washington Park and the Rose Garden. Park here. **Stop 9. Washington Park Landslide: The Phenomenal Landslide.**

171.1 Head north from the parking lot.

171.2 Turn left on Fairview Blvd.

171.8 Stop at the intersection of Fairview and Bennington. **Stop 10. Canterbury Castle Landslide.**

171.8 Return to Portland State University via the Rose Garden, taking Fairview, Kingston, Park Place, Salmon, and Broadway.

174.9 **End of field trip at Portland State University.** The vans will return to Corvallis for the convention welcoming party.

REFERENCES

Beeson, M.H., Tolan, T.L., and Madin, I.P. , 1991, Geologic map of the Portland Quadrangle, Multnomah and Washington Counties, Oregon, and Clark County, Washington: Oregon Department of Geology and Mineral Industries, Geologic Map Series 75, scale 1:24,000.

Burns, S.F., 1998, Landslides in the Portland area resulting from the storm of February, 1996, *in* Burns, S.F., ed., Environmental, groundwater, and engineering geology: Applications from Oregon: Belmont, Calif., Star Publishing, p. 353-365.

Burns, S.F., Beckstrand, D., Lunney, M., Taylor, J., Robinson, C., and Schick, J., 2001, AEG News: Association of Engineering Geologists Annual Meeting, St. Louis, Program with Abstracts, v. 44, no. 4, p. 56.

Clarke, D.D., 1904, A phenomenal landslide: American Society of Civil Engineers Transactions, v. 53, paper 984, p. 322-411.

Geoengineers, 1998, Slope failure evaluation, Aldercrest–Banyon Landslide, Kelso, Washington: Geotechnical

engineering report to the City of Kelso, 44 p.
Hammond, C.M., and Vessely, D.A., 1998, Engineering geology of the Ancient Highlands Landslide, Portland, Oregon, *in* Burns, S.F., ed., Environmental, groundwater, and engineering geology: Applications from Oregon: Belmont, Calif., Star Publishing, p. 343-352
Johnson, S.E., and Johnson, A.M., 1997, Self guided tour of Tumalt Creek debris-flow deposits, Dodson, Columbia River Gorge, Oregon: Purdue University Department of Geology, 21 p.
Powell, W.O., Robertson, C.A., and Watanabe, R.F., 1996, Geotechnical report, Dodson-Warrendale Debris Flows, Columbia River Highway, M.P. 34.5 to 37.5, Multnomah County: Oregon Department of Transportation, 11 p.
Taylor, G.H., and Hannan, C., 1999, The climate of Oregon: A state of extremes: Corvallis, Oregon State University Press, 242 p.
Wegman, K.W., and Walsh, T.J., 2001, Landslide hazard mapping in Cowlitz County—A progress report, Washington Geology, v. 29, p. 30-33.

Columbia River Gorge Landslides

Yumei Wang, Oregon Department of Geology and Mineral Industries, **800 NE Oregon Street, Portland, OR 97232; yumei.wang@dogami.state.or.us**

R. Jon Hofmeister, Oregon Department of Geology and Mineral Industries, 800 NE Oregon Street, Portland, OR 97232; jon.hofmeister@dogami.state.or.us

Vicki S. McConnell, Oregon Department of Geology and Mineral Industries, 1510 Campbell Street, Baker City, 97814; vicki.mcconnell@dogami.state.or.us

Scott F. Burns, Geology Department, Portland State University, Portland, OR 97207; burnss@pdx.edu

Patrick T. Pringle, Washington Division of Geology and Earth Resources, 1111 Washington Street, Olympia, Washington 97501; pat.pringle@wadnr.gov

Gary L. Peterson, Squier Associates, 4260 Galewood Street, Lake Oswego, Oregon 97035; garyp@squier.com

INTRODUCTION

The field trip region is characterized by breathtaking scenery, dynamic geology, and abundant active and dormant landslides. The participants will receive a broad view of diverse and large-scale historic landsliding and current landslide hazards in the western Columbia River Gorge. The varied, steep terrain in this scenic area poses risks to life, property, and the regional economy.

The Gorge, which dissects the Cascade Range, is well known for its scenic beauty. Mount Hood, rising to 3,427 m (11,240 ft), other snow-capped volcanoes, steep cliffs, lush forests, and tall waterfalls form its surroundings. Along the Columbia River shores, unstable, nearly vertical cliffs alternate with landslide areas. Destructive landslides occur frequently in this region, especially during heavy winter storms.

In 1986, the Columbia River Gorge was designated a National Scenic Area. This designation requires the regional government agencies to apply rigorous land-use planning that maintains and restricts development. Consequently, landslide-hazard-mitigation options, even in areas of known hazard, are limited except in certain incorporated areas.

For most of the trip, we will travel along Interstate Highway I-84 and portions of the original Gorge Highway that opened in 1916 and is now a scenic route (see Fig. 1). The trip route out of Portland first follows old scour channels across flood gravel until it reaches the Columbia River. We will drive about 40 miles in the western Columbia River Gorge and visit five stops: the Multnomah Falls Rockfall and Historic Columbia River Highway; the Dodson Debris Flow; the Cascade Landslide Complex; Skamania Lodge (where lunch will be served) on the Cascade Landslide Complex with a view of landslides in Cascade Locks; and the Mount Hood lahars on the Sandy River.

TRANSPORTATION CORRIDOR AND ECONOMIC RISK

The community at large is concerned about the geohazards of the Columbia River Gorge area, since it is the dominant east-trending transportation corridor for the Portland region. The Oregon Department of Geology and Mineral Industries (DOGAMI) is currently conducting a pilot study to better understand the complex relations among multimodal transportation, geohazards, and effects on communities. At Multnomah Falls, which is Stop 1, we will discuss the importance of this

Field Guide to Geologic Processes in Cascadia: Oregon Department of Geology and Mineral Industries Special Paper 36, 2002.

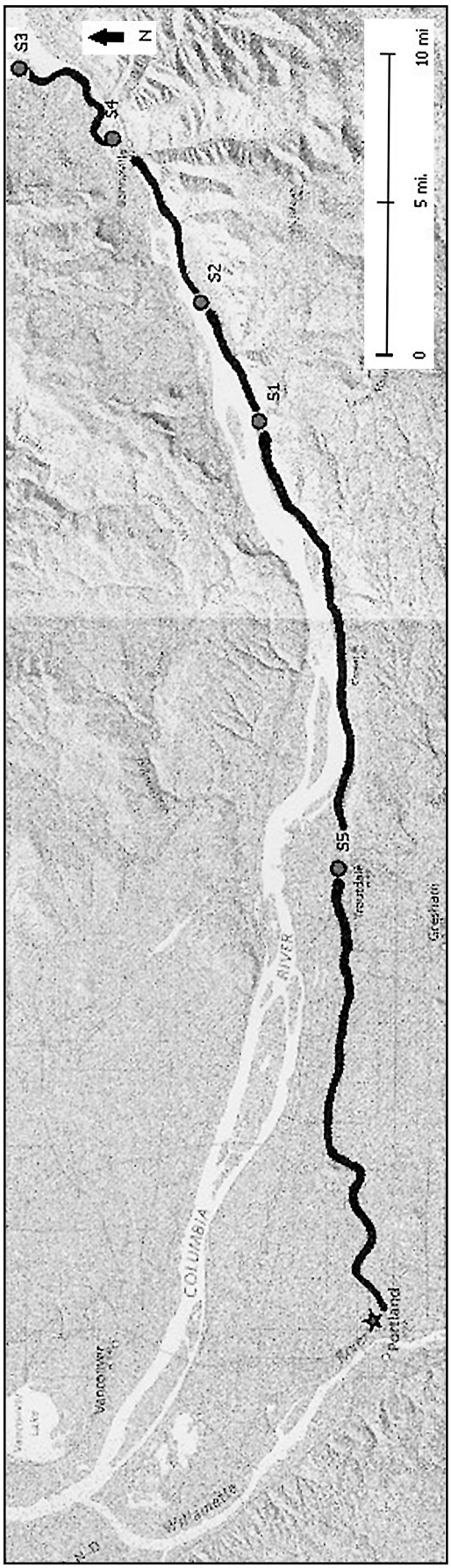

Figure 1. Columbia River Gorge Landslide Field Trip. Star, Oregon Department of Geology and Mineral Industries; S1, Multnomah Falls Rockfall; S2, Dodson and Warrendale Debris Flows; S3, Skamania Lodge—Lunch on the Cascade Landslide Complex; S4, Bonneville Dam on the Cascade Landslide Complex; S5, Mount Hood Lahar Deposit (base from Loy, 2001).

transportation corridor. At Multnomah Falls, the view to the north (Fig. 2) shows several transportation routes, including two highways, a railroad line, and the Columbia River—all within this transportation corridor. Figure 3 illustrates the landslide hazard just east of Multnomah Falls along a section of the historic Columbia River Highway. In the above-mentioned pilot study, DOGAMI will evaluate engineered systems (bridges, roads, dams, and railroad), geohazards (landslides, earthquakes), and limited economic data to determine the overall vulnerability and interdependencies of the region. More information on this study can be found below, following the discussion of the stops.

GEOLOGY OF THE COLUMBIA RIVER GORGE

The formation of the Columbia River Gorge can be associated with two violent processes that are often labeled with the terms, fire and ice. All of the geologic history exposed by the Columbia River in the Gorge and the adjacent area is limited to the Tertiary and Quaternary (Fig. 4). The spectacular stratigraphy that is exposed within the Gorge is mostly volcanic. The geomorphology of the Gorge has been modified by flooding associated with the catastrophic emptying of Pleistocene glacial Lake Missoula.

During Eocene and Oligocene time, subduction of the Farallon Plate beneath the North American Plate produced a broad belt of volcanism that formed the ancestral Western Cascade Range. Rhyolite to basalt lava flows, lahars, tuffs, and volcaniclastic rocks formed a volcanic highland trending roughly north (Tolan and Beeson, 1984). Up to 6,000 m of volcanic rocks and volcaniclastic and marine sediment define the Ohanapecosh Formation (Figure 4). Volcanic activity was intermittent with times of erosion and intense weathering of the deposits.

The Ohanapecosh Formation is the oldest rock unit exposed in the Gorge. The rocks are basalt to rhyolite lava flows and volcaniclastic rocks (including tuff and lahars), heavily weathered and intercalated with marine sediment (Tolan and Beeson, 1984) (Fig. 4). The most striking feature is their uniform and widespread zeolitic and argillic alteration. Due

Figure 2. Multimodal transportation corridor showing (from top to bottom) the Columbia River used for barge transportation, I-84 westbound, I-84 eastbound, railroad, and the historic Columbia River Gorge Highway. View from Multnomah Falls looking north.

to this alteration, the primary joints, vesicles, and other cavities are commonly filled, which results in very low permeability (Waters, 1973). Numerous large slides move on the upper surface of the unit where water collects.

In late Oligocene and early Miocene time, rotation of the subducting plate boundary or the steepening of the angle of the subducting plate resulted in renewed volcanism and a retreat of the ocean shoreline to the west. Primarily andesitic lava and lahars with interstratified laharic breccia and fluvial conglomerate make up the nearly 1,500-m-thick Eagle Creek Formation and correlative formations above the Ohanapecosh Formation (Tolan and Beeson, 1984). The top of the Eagle Creek Formation is marked by an erosional unconformity most likely associated with temporary cessation of volcanic activity and subsequent weathering and soil development (Suchanek, 1974).

The Eagle Creek Formation unconformably overlies the Ohanapecosh with a pervasive saprolitic layer, in places, up to 30 m (100 ft) thick. The Eagle Creek Formation is characterized by fluvial conglomerate and andesitic lahars, andesitic lava and breccia, and rhyolite to dacite ash-flow tuff and other volcaniclastic rocks (Fig. 4). Much of it was deposited from mudflows and slurry floods washed from nearby volcanoes. Consequently, the thickness is highly variable. In the headscarp scar of the Cascade Landslide Complex near Red Bluffs, over 300 m (1,000 ft) of bedded volcanic conglomerate and tuffaceous sandstone are exposed (Stops 3 and 4). On the Oregon shore of the Columbia River Gorge, the thickest deposit observed is 250 ft in McCord Creek about 5 mi west of Cascade Locks (Waters, 1973).

Volcanic activity originating in what is now northeastern Oregon was to dramatically change the processes at work. There, voluminous and low-viscosity flows of basalt and basaltic andesite lava of the Columbia River Basalt Group began flowing westward from fissures at approximately 17 Ma, blanketing the

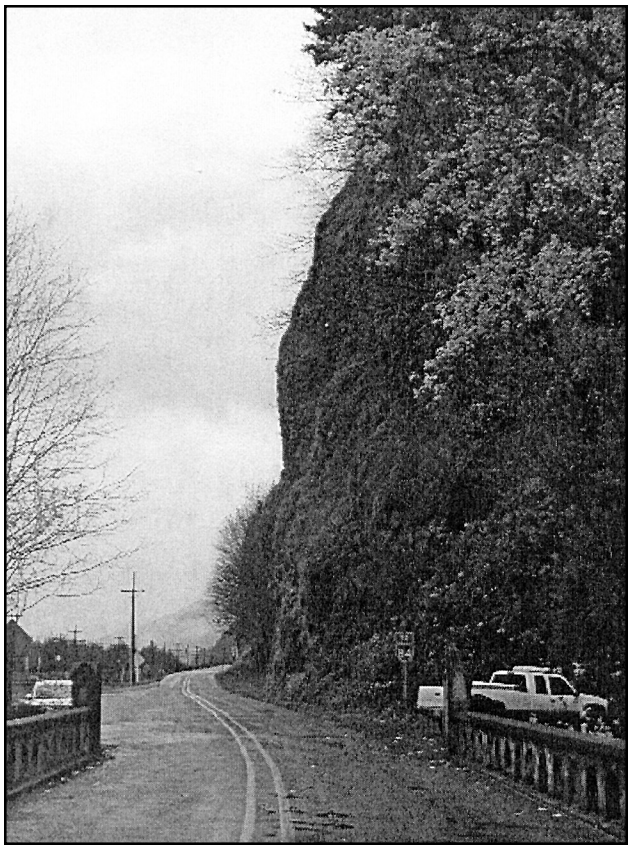

Figure 3. Landslide hazard along a portion of the historic highway. Taken from Multnomah Falls looking east.

landscape and forming a level plateau (Fig. 5). By 15 Ma, these flood basalts had advanced down the ancient river channels to reach the sea more than 750 km away (Tolan and others, 1989). It is estimated that the total volume of Columbia River Basalt Group flows approaches 175,000 km^3 (Tolan and others, 1989).

Although not all the Columbia River Basalt flows made it as far west as the Gorge, enough of them did to form a flow-on-flow landscape that is now marked by thick-layered, columnar-jointed walls of the present-day Gorge. These lava flows uncomformably overlie the weathered Ohanapecosh and Eagle Creek Formations. Several flows of the Frenchman Springs Member (approximately 15 Ma) have been identified as intracanyon flows that delineate channels of the ancestral Columbia River through the Cascade Range (Tolan and Beeson, 1984). The youngest intracanyon flow, the Pomona Member (approximately 12 Ma), is exposed in the Gorge overlying the fluvial sand and gravel deposits of the ancestral Bridal Veil Channel of the Columbia River in the Troutdale Formation (Anderson, 1980) (Fig. 4).

Both the Ohanapecosh and Eagle Creek Formations, shown stratigraphically in Figure 4, are prone to slope instability. Consequently, the overlying strata, commonly basalt flows of the Columbia River Basalt Group are subject to sliding as well, especially along the tilted upper surface of the weathered Ohanapecosh Formation.

High Cascade volcanism began in the early Pliocene (Orr and Orr, 1999). An initial period of explosive volcanism that was centered in the ancestral Mount Hood area resulted in the deposition of andesitic to dacitic lahars, tuffs, and agglomerates of the Rhododendron Formation (Fig. 4). Regional tectonic activity also began to form a series of northeast-trending folds warping the relatively flat-lying lava flows of the Columbia River Basalt Group. In

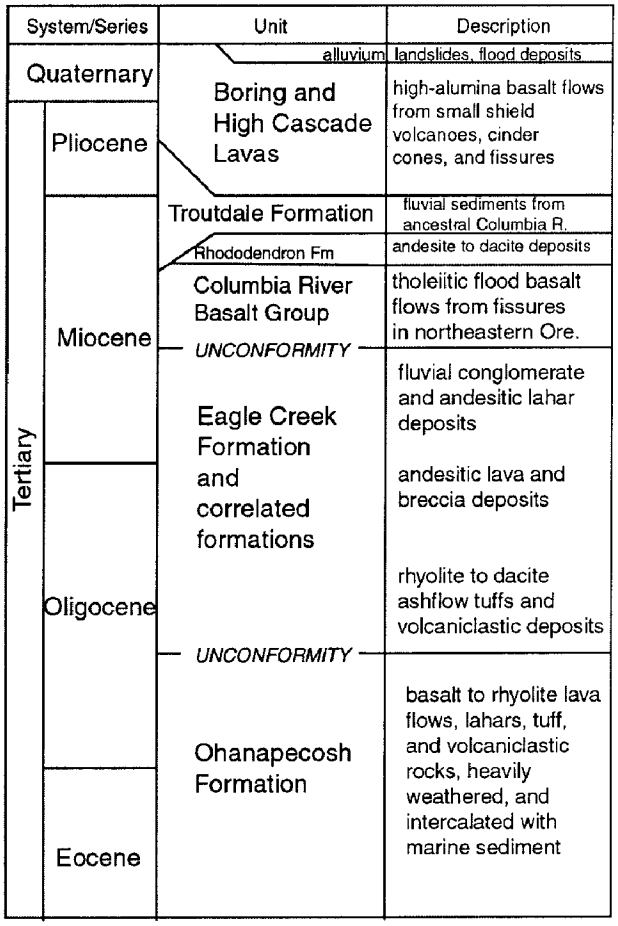

Figure 4. Generalized stratigraphy of the Columbia River Gorge (modified from Tolan and Beeson, 1984).

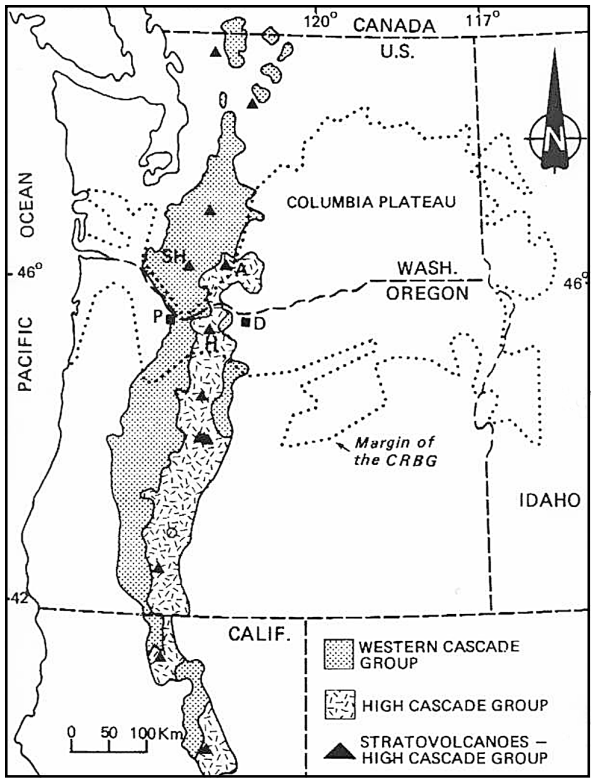

Figure 5. Generalized map showing the distribution of the Western Cascades, High Cascades, and Columbia River Basalt Group. P=Portland, D=The Dalles, H=Mount Hood, SH=Mount St. Helens, A=Mount Adams, CRBG=Columbia River Basalt Group (Tolan and Beeson, 1984).

the area of the Columbia River Gorge, the dip slope is now between 2 and 8º south.

By 5 Ma, local volcanism of the high-alumina basalt flows of the High Cascades and the Boring volcanic field farther to the west were choking the ancestral Columbia River channel with hyaloclastic debris (Tolan and Beeson, 1984) (Fig. 4). The continued filling of the channel by local basaltic lava and volcaniclastic debris forced the Columbia River to migrate northward. The river eventually established the modern-day channel where the more resistant Columbia River Basalt flows made contact with the southward-dipping, more easily eroded, underlying sedimentary and volcanic deposits (Tolan and Beeson, 1984; Orr and Orr, 1999).

Although volcanic activity during the Quaternary seems quite dramatic, with stratovolcanos such as Mount Hood and Mount St. Helens visible from the Gorge, it has actually decreased steadily since the middle Miocene (Orr and Orr, 1999). The present-day High Cascades consist of relatively small volcanic centers positioned upon the lava plateau of the earlier Western Cascade volcanism (Fig. 5).

All this continental arc volcanism had been the result of the subduction of the Juan de Fuca Plate beneath the North American Plate. During the Pleistocene, the Columbia River Gorge was widened by jökulhlaups (glacial outburst floods) from glacial Lake Missoula in Montana. Although the flooding had no impact on the course of the Columbia River, it did leave lasting impressions on the landscape, from the channeled scablands to the northeast, to the kilometers-long, ripple-marked sand-and-gravel deposits on the Columbia Plateau, the gravel deposits underlying Portland, and the fertile silt deposits of the Willamette Valley. In addition, these Missoula floods oversteepened the Gorge walls, which exacerbates slope instability.

LANDSLIDES AND LANDSLIDE HAZARDS

The Gorge, with its steep slopes and high rainfall, commonly experiences slope failures. Active landslides of diverse types can be found, each producing their own specific hazards. For example, fast-moving landslides such as rockfalls, rock avalanches, and debris flows pose significant risks to life and property. Slow-moving landslides that bulge near the toe pose maintenance concerns for highways, railroads, and other lifelines.

Geologic conditions play a major role in local landslides. As discussed in the preceding section, both the Ohanapecosh and Eagle Creek Formations are prone to slope instability. The hydrogeologic conditions of the stratigraphic units also promote sliding. Precipitation readily penetrates the columnar and hackly joints of the upper basalt flows and volcaniclastic deposits. This water tends to collect when it intercepts the less conductive Eagle Creek Formation. This condition is repeated where the Eagle Creek Formation, which has a much higher hydraulic conductivity and porosity, is in contact with the Ohanapecosh Formation, which has a very low hydraulic conductivity. Both geologic contacts provide weak, slide-prone surfaces for the thick, dense overlying basaltic lava flows (Waters, 1973).

Although the rocks typically dip only gently toward the south in the western part of the Gorge, the nature of the landslides is largely controlled by this dip. Washington State landslides tend to be of a large scale and produce low slope angles after coming to rest. On the Oregon side of the Gorge, although the same rocks are less susceptible to large-scale landsliding because they dip into the Gorge valley walls, large-scale landsliding problems do persist. For example, according to the Oregon Department of Transportation, the Fountain Landslide, 3 mi east of Cascade Locks, has remained active for more than 35 years and regularly causes distress to I-84 (Shuster and Chleborad, 1989) (see Stop 3).

The Gorge walls have been oversteepened from river erosion over time, particularly by the Pleistocene Missoula Floods. Bank undercutting occurs in some areas at the present time and contributes to slope hazards. Earthquake shaking in 2001 from the magnitude 6.8 intraplate earthquake at Nisqually, Washington, triggered rockfalls in the Gorge (David Keefer, U.S. Geological Survey, oral communication, 2001). Past earthquakes are suspected to have triggered large-scale landsliding (see Stop 4). Not surprisingly, future earthquakes also are expected to trigger landslides in this region.

The regional economic risks from potential impacts on the transportation systems are high. Episodic debris-flow activity near Multnomah Falls, Warrendale, and Dodson has forced roads and rail lines to close. In 1996, for example, debris flows at Dodson and Tumalt Creek in Warrendale closed I-84 and the railroad for 5 and 3 days, respectively. And just this winter, a series of debris flows starting on December 2, 2001, buried the I-84 Exit 35 on-ramp in Dodson, and the ramp was closed for over 12 days. This debris flow was very fluid, and mud lines were observed as high as 23 m (75 ft) up tree trunks in the transport zone.

FIVE FIELD TRIP STOPS

We will visit diverse landslides ranging from rockfalls, vast-scale landslide complexes, devastating debris flows, and lahars. Pertinent geologic characteristics that control the slope hazards will be discussed. Also, the importance of geohazards to the community and possible roles of geoscience professionals will be addressed.

Stop 1. Multnomah Falls Rockfalls

Multnomah Falls is the second-highest "year-round" waterfall in the nation. It consists of upper and lower falls with basalt cliffs (Fig. 6 and 7). At least four lava flows of the Columbia River Basalt Group can be identified. The rock at the base of the upper falls is much harder and more resistant to water erosion than the other layers, thus, creating the two falls (Suchanek, 1974). Figure 7 shows a basalt block that fell into the upper pool in the early 1990s during the night.

In 1991, a fire burned the slopes to the west of the falls and destabilized the slopes above the footpath leading up to the bridge. Immediately following the fire, the loose entablature basalt slopes started to unravel down the hill due to the loss of stabilizing vegetation. Shortly afterward, the U.S. Forest Service constructed a rock wall. Due to continued slope hazards, a 1.8 m (6 ft) chain-link fence was installed to protect the pedestrians on the footpath. In 1997, a tourist was hit and almost

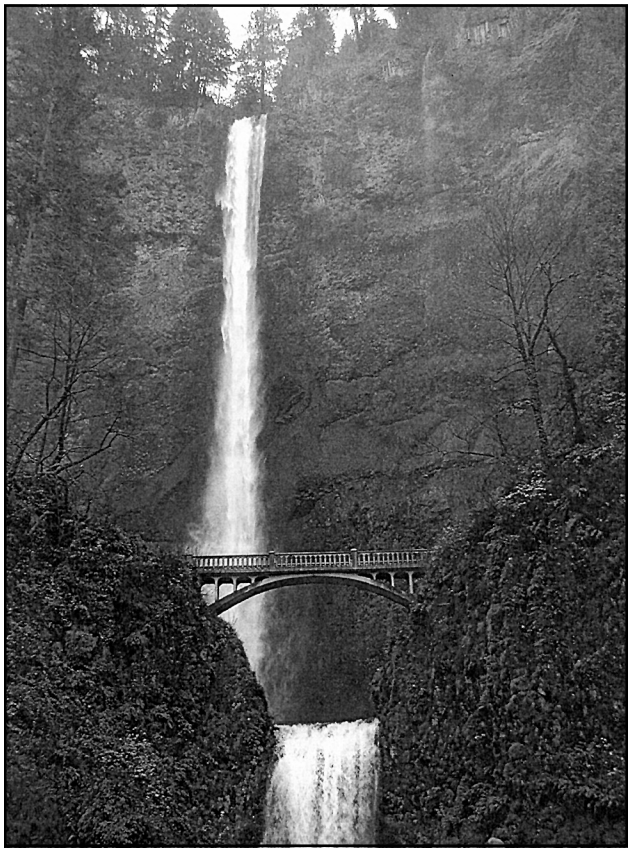

Figure 6. Multnomah Falls showing steep jointed basalt slopes. In 1995, a rockfall injured 20 people on the bridge.

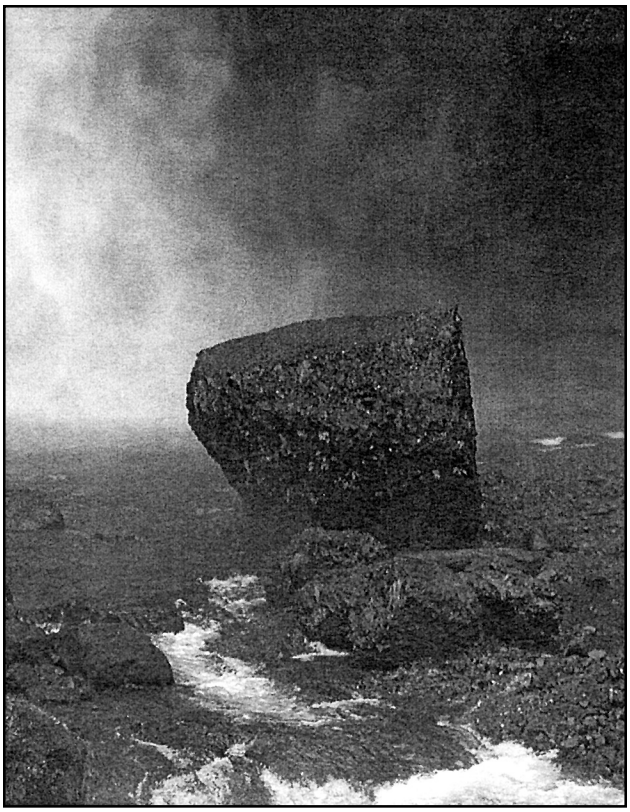

Figure 7. Multnomah Falls rockfall debris at the base of the upper falls.

killed by a 0.23-m (9-in.) rock that skipped over the fence. Other incidences with minor injuries have also occurred. To address public-safety concerns, the Forest Service replaced the chain-link fence with an impressive Brugg Cable net (Fig. 8) (Stan Hinatsu, U.S. Forest Service, oral communication, 2001). This rockfall net protects the pedestrians on the footpath leading to the bridge. The net, which has shallow concrete-block foundations (about 1 m^3 each), was designed to intercept falling rocks up to 0.46-m (18 in.) in diameter (Tim Pfeiffer, Foundation Engineering, oral communication, 2001).

On September 4, 1995, at approximately 5:30 p.m., rocks from the face of Upper Multnomah Falls broke loose and smashed down into the upper plunge pool. The upper falls are 165 m (541 ft) high. According to the Forest Service, the dislodged rock had approximate dimensions of 12 by 6 by 2 m (40 by 20 by 6 ft) and fell a distance of 69 m (225 ft). The jointed basalt block did not remain intact but, for the most part, shattered. Twenty people who were standing on the 21-m (70-ft)-high bridge received minor injuries from being hit by flying pebble-size debris. Thirteen were transported to hospitals for treatment and release. One person was held overnight for a knee injury. The upper plunge pool is now permanently closed for public-safety reasons. In addition, landslide awareness signs have been erected in response to this event (Fig. 9).

The debris from the 1995 rockfall increased the bedload in Multnomah Creek. This bedload exacerbated flooding in 1996, when the footpath was inundated by 1 m (3 ft) of water and the nearby tunnel flooded. Highly controversial dredging and other mitigative actions were undertaken (Stan Hinatsu, U.S. Forest Service, oral communication, 2001).

Portions of the historic Columbia River Highway to the east and west of Multnomah Falls have been damaged by landslides. Figure 3 shows a section of the historic highway that abuts intact, rocky slopes just east of Multnomah Falls. In February 1946, a series of

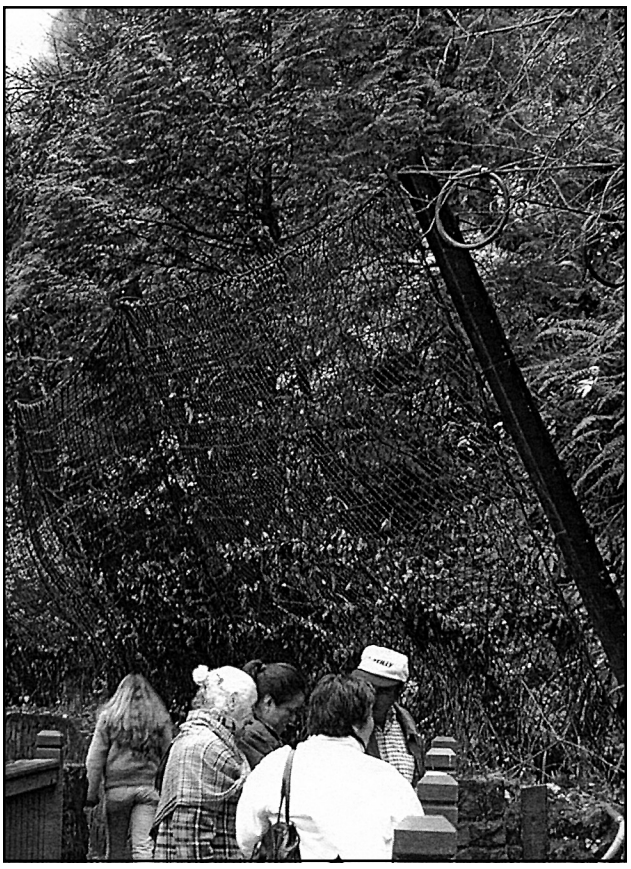

Figure 8. Multnomah Falls rock catchment net on the footpath to the bridge. This was installed by the U.S. Forest Service as a a result of a tourist injury.

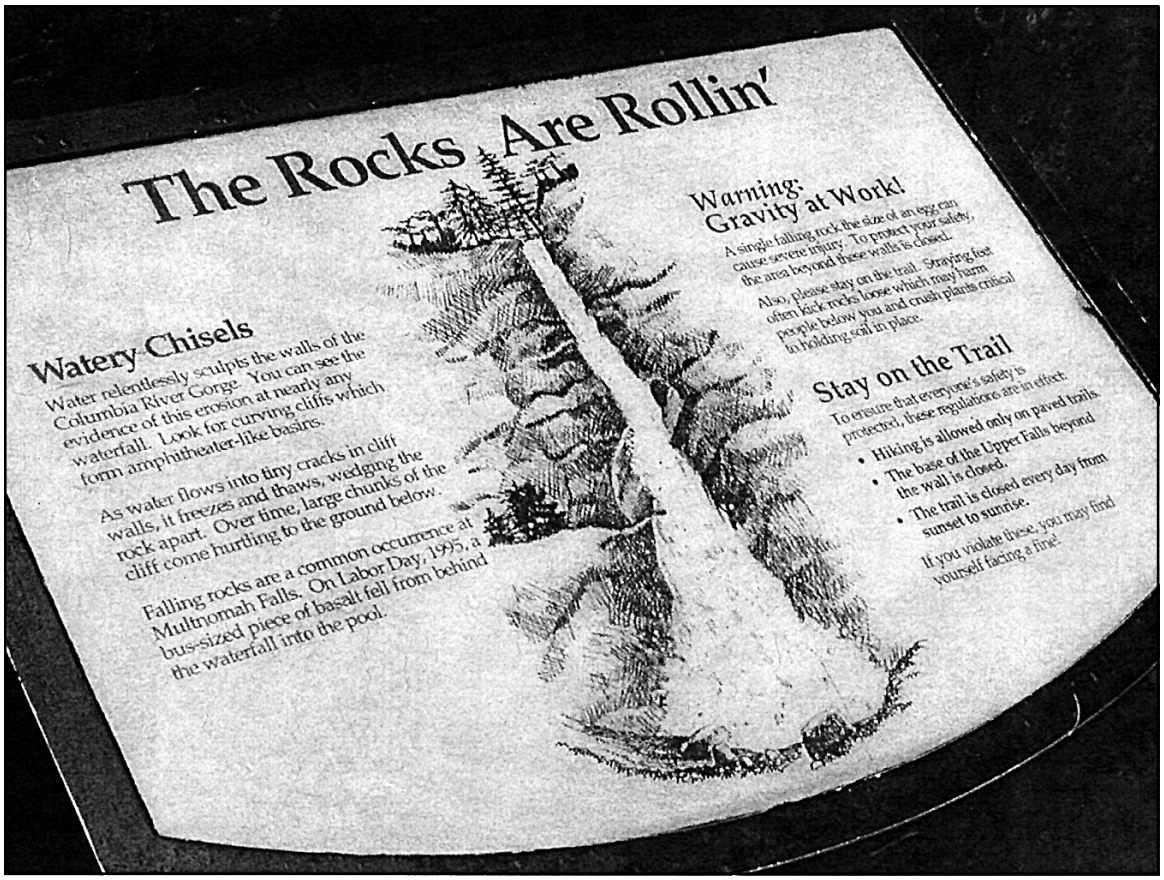

Figure 9. Multnomah Falls landslide awareness sign for the public. This was installed by the U.S. Forest Service in response to 1995 injuries.

landslides occurred and blocked the highway and the Union Pacific main line about 0.5 mi east of Multnomah Falls. The Oregon Department of Transportation reported that a landslide removed a 23-m (70-ft) section of the highway, to an average depth of 5 m (15 ft). This slide closed the road for 10 days. Union Pacific, which estimated about 1,000,000 tons of landslide debris on its tracks, reopened the track after 5 days. Western Union communication wires were severed. A telephone-line repair crew narrowly escaped death or injury when additional sliding took place. The linemen lost their equipment and tent, and repair work on a major underground cable was destroyed. In addition, the slide translated a river-navigation tower down gradient by tens of feet (Baldwin, 1946).

Stop 2. Dodson and Warrendale Debris Flows

The communities of Dodson and Warrendale are built on top of a debris-flow fan on the Oregon side of the Columbia River. This fan has been accumulating for the past 12,700 years. Most likely, the great Missoula Floods that were funneled through the Columbia River Gorge from 15,300 to 12,700 years ago cleared out a good portion of the sediment in the area. The impressive debris fan currently at the site, thus, has likely formed since then from repeated debris-flow activity down the steep bedrock canyons south of the river. Most of the steep source-area bedrock to the south is Columbia River Basalt, with Troutdale Formation fluvial deposits and Boring lavas toward the tops of the cliffs (Fig. 4). Sediment of the fan is composed of deposits from each of these three formations.

This fan became infamous in February 1996 when seven drainages to the south produced debris flows that were deposited across the fan (Squier, 1999; Fig. 10). These include the Royse Debris Flow that engulfed a house (Fig. 11) and the high-velocity Tumalt Creek Debris Flow that caused extensive damage by hitting a train and trucks in the transportation corridor.

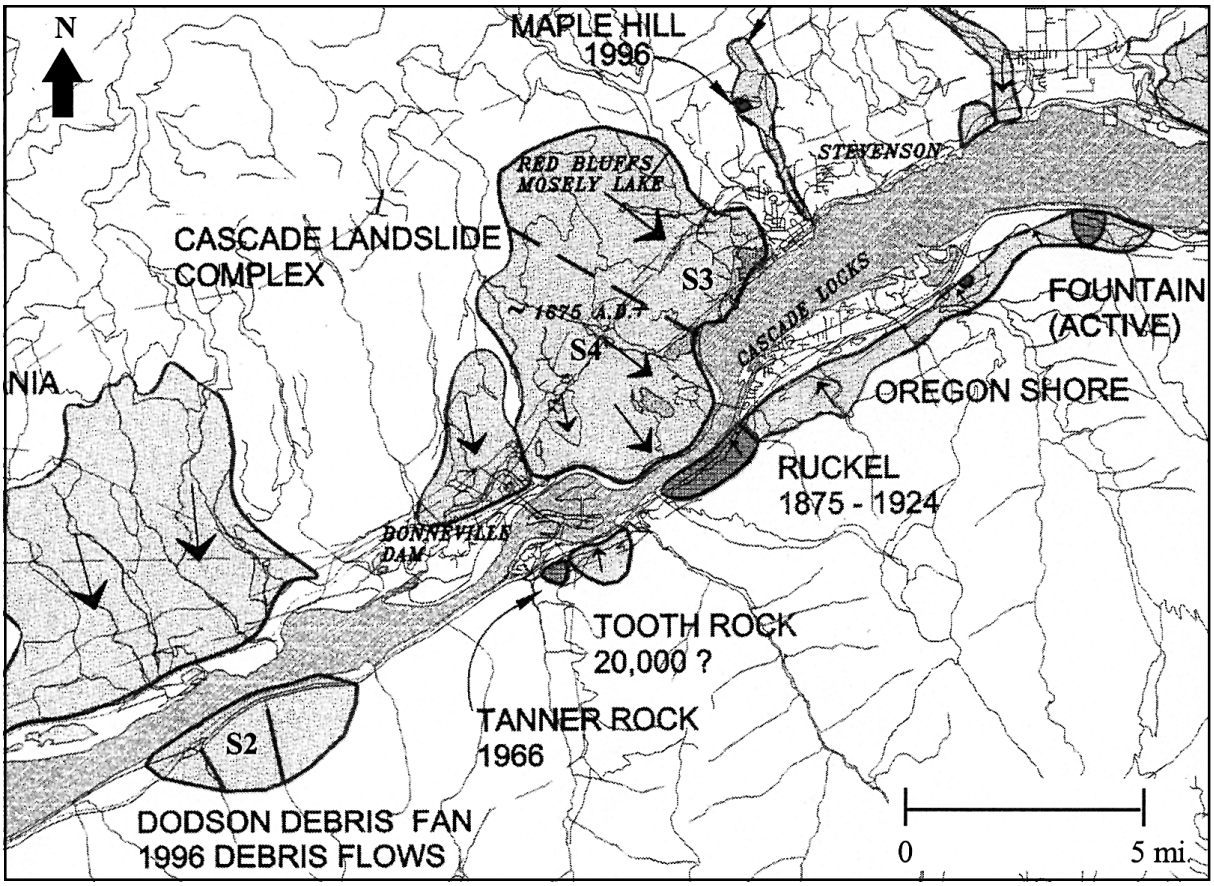

Figure 10. Location map of landslides and Stops S2, S3, and S4 (modified from Squier, 1999).

Smaller debris flows occurred on the fan later in 1996 and in 1997. The most notable recent flow (as of the time of this writing) occurred in early December 2001 at the Exit 35 interchange of the historic highway with I-84.

Stop 2a. Exit 35 Debris Flow

This debris-flow deposit, which started forming at 5 p.m. on December 2, 2001, forced the closure of the I-84 on-ramp and off-ramp. The previous week had been marked by heavy rain, which caused extensive landslide activity in the upper drainage of the creek to the west of Saint Peters Dome, a basalt promontory above Dodson. A small debris flow had occurred from that drainage in 1996. This time, the entire west and south sides of the canyon failed, depositing thousands of cubic meters of sediment into the stream valley bottom. Persistent rains moved the sediment in the debris-flow channel, and it traveled through the forest knocking down many trees. It terminated in a cone-shaped deposit covering the I-84 on-ramp.

The cone-shaped deposit continued to build to a height of approximately 2 m by December 5, 2001. By December 14, this deposit still had not been cleared due to difficulties associated with removing the highly fluid debris.

Stop 2b. Royse Debris Flow

This debris flow occurred about noon on February 7, 1996 and notably affected the Royse residence. Mrs. Royse was in her home fixing lunch when she looked out the back window to the pasture and saw a wall of boulders coming toward the house from the south. She and her husband rushed from the house to safety about 200 m away. The debris flow filled up half of the first floor of the house and covered most of their property up to about 5 m in depth (Fig. 11). It continued downhill toward the river, stopping traffic on I-84 and the railroad. Figure 12 shows the travel path of the debris flow, which was removed before the photograph was taken. Over the next 4 days, additional flows

Figure 11. Dodson Debris Flow showing a damaged 2-story residence on the debris flow runout fan. The house remains fairly intact on its foundation, but it is filled with debris.

accumulated on this deposit. Debris was transported from many landslides in the drainage to the east of Saint Peters Dome.

Even though Mrs. Royse recounts how her cousin's nearby home was hit by a debris flow around 1918, the Royse family wanted to rebuild their home on this same site. However, the Federal Emergency Management Agency (FEMA) will provide funds for rebuilding only if they relocate to a safer location. To date, they still live on the property, but in a smaller house to the east of the flow. Their debris-filled home, which still remains standing, has been documented in many articles about landslides. This is a textbook example of a slow- to moderately fast-moving debris flow, and was estimated to have had a maximum velocity of 8 to 10 km/hr. The cobbles and boulders of the debris flow are primarily from the Boring Lava (and not the Columbia River Basalt Group).

Stop 2c. Tumalt Creek Debris Flow

The Tumalt Creek Debris Flow is about 0.5 km east of the Royse Debris Flow. It was the largest debris flow in the February 1996 events. Local inhabitants tell us that the creek "stopped flowing" in midafternoon on February 7, 1996. The interpretation has been that a major landslide at the headwaters of Tumalt Creek had dammed the drainage and stopped the creek. Late in the day, this landslide dam was breached. The ponded water and debris from the landslide dam rushed down the valley as a very fast moving debris flow. People assisting with rescue operations on the highway reported hearing the debris flow advancing 15 minutes before its arrival. Traffic and the train had been stopped since noon because of the Royse Debris Flow. It is estimated that the debris flow hit the parked trucks on I-84 and the train on the tracks at over 50 km/hr. The boxcars in the train and the trucks were pushed into the Columbia River from the impact. This event illustrates the hazards associated with fast-moving landslides.

This debris flow nearly struck a school south of the frontage road. Due to the continued hazard, the school has been closed, and the children now attend school in the nearby community of Cascade Locks.

Again, the main cobbles and boulders transported by the debris flow were of Boring Lava origin. The debris-flow cone is over 6 m

thick at this site, and it is fortunate that no casualties were suffered from the February 6-10, 1996, debris flows. Throughout the last several years, debris flows have continued to recur in this drainage, and the culverts have needed to be replaced periodically.

Stop 3. Skamania Lodge: Lunch on Cascade Landslide Complex and View of Landslides in Cascade Locks, Oregon

Skamania Lodge was constructed on the eastern edge of the large Cascade Landslide Complex, which is generally considered to be stable ground. The lodge provides an excellent view of landslides across the river at Cascade Locks, Oregon.

The **Oregon Shore Landslide,** shown in Figure 10, is generally stable. However, portions of it, and adjacent slides, have shown recent activity and are discussed below.

The **Fountain Landslide** is 3 mi east of Cascade Locks within the eastern portion of the Oregon Shore Landslide. According to the Oregon Department of Transportation (ODOT), it is an ancient slide that was reactivated during highway construction activity in 1952. The slide mass includes Columbia River Basalt and other rocks overlying older volcaniclastics. The landslide covers 0.5 km^2, and its volume is 19,000,000 m^3. In 1966, the highway was widened into I-84, which accelerated the slide movement. ODOT removed 264,000 m^3 on the west side to slow the movement. Currently, it causes distress to I-84 during heavy-rainfall years (Scofield and others, 1997).

The **Ruckel Landslide** is on the western edge of the Oregon Shore Landslide (Fig. 10). This landslide, which consists of Columbia River Basalt flows over the Eagle Creek Formation, is actively creeping. During the construction of the first railroad portage in the late 1860s, this 1-km^2 slide was described as a "glacier." By 1913, tens of meters of displacement prompted mitigation in the form of drainage adits. By 1924, the displacements were slowed to a tolerable rate (Scofield and others, 1997).

Several additional landslides can be viewed from the lodge, including the **Wind Mountain Slide** about 10 mi upstream along the Washington shore.

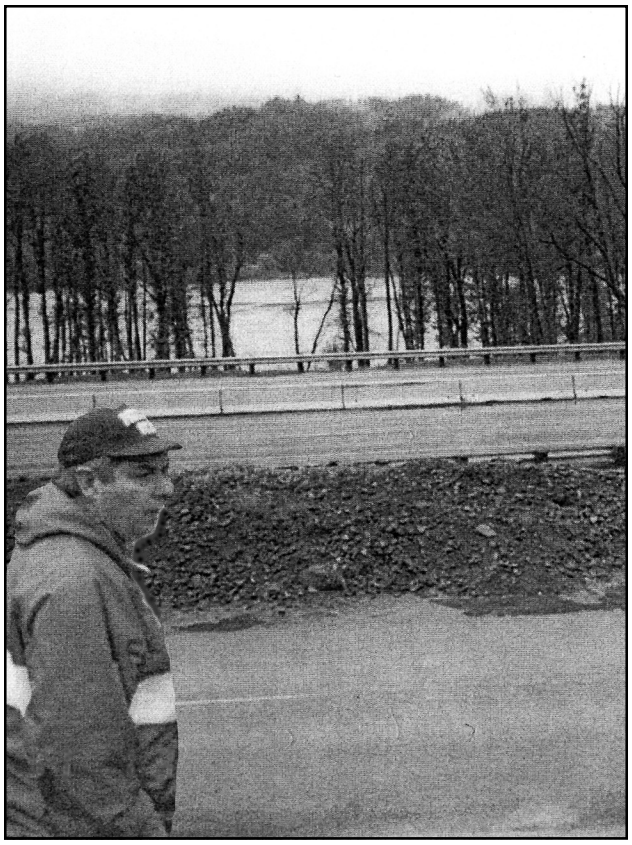

Figure 12. Sighting down the 1996 Dodson Debris Flow travel path, which terminated in the Columbia River. The debris covered I-84, the railroad, and knocked down trees before entering the river.

Stop 4. Cascade Landslide Complex and Bonneville Landslide

The Cascade Landslide Complex, as shown on Figures 10, 13, 14, and 15, is an impressive example of a landslide. The date of the movement is not tightly constrained (as discussed below); the source area included portions of Table Mountain and the Red Bluffs in Washington. Debris from the landslide was translated 3 miles laterally, and the pre-slide Columbia River channel was buried about 1 mile north of its present location (Newcomb and others, 1978). The total landslide area covers 30-36 km^2 (12-14 mi^2) with individual slide deposits of about 5-13 km^2 (2-5 mi^2). The **Bonneville Landslide** (a lobe of the Cascade Landslide Complex) has an area of about 14 km^2 (5.5 mi^2). It extends into the river and has substantially diverted the river channel toward the Oregon shoreline (Palmer, 1977).

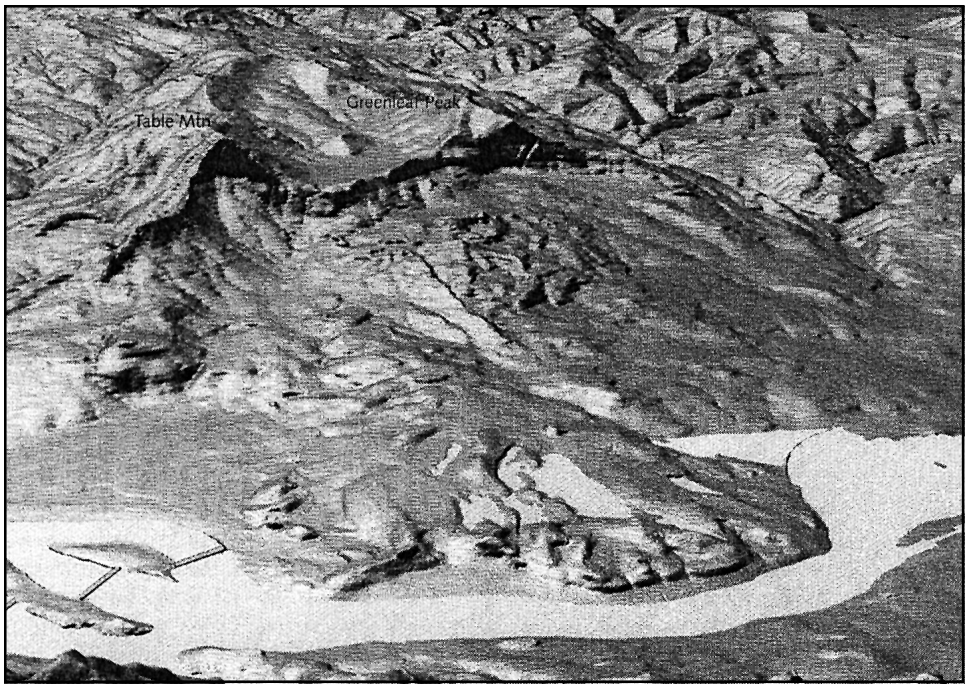

Figure 13. Cascade Landslide Complex showing the main slide area and the Bonneville Dam. The youthful Bonneville Landslide lobe is in the central foreground. View looking north-northwest. From the headscarp at Table Mtn to the right abutment of the dam is 3 1/2 miles (Loy, 2001).

An excellent viewpoint for the Cascade Landslide Complex is from the U.S. Army Corps of Engineers Visitors' Center at Bonneville Dam. During the preparation of this field trip guidebook, the visitors' center was closed for security purposes prompted by the September 11 terrorist attacks. At the time of the field trip, Stop 4 will either be at the Visitors' Center or at the best possible alternate location.

The Cascade Landslide Complex was created by multiple events. In the late 1970s, the Corps studied the landslide for the purpose of additional construction. The study found that "the mechanics of failure involved a planar movement in the rock mass and a subsequent lateral spreading at the toe of the slide. Sand liquefaction was the failure mechanism for this lateral spreading. Remnant slide blocks are found surrounded by a matrix of fine mica sand" (Shannon and Wilson, 1978). It has been proposed that the high-energy deposition resulted in liquefaction and injection of sandy dikes of the debris-covered alluvium up into the landslide deposit (Scofield and others, 1997).

Large, intact slide blocks reveal the original stratigraphy of the source zone. The youngest, uppermost unit is the Columbia River Basalt Group. It overlies the Eagle Creek Formation, which overlies a unit that the Corps informally refers to as the Weigle Formation, which is found at the toe (Sager, 1989). According to the Corps, the Weigle exists stratigraphically between the Ohanapecosh and Eagle Creek Formations and is composed of weakly indurated conglomerate, sandstone, and siltstone (Scofield and others, 1997). According to Waters (1973), the same rocks are part of the Ohanapecosh Formation.

Studies show that the river water impounded by the landslide dam rose tens of meters before the landslide dam was breached (Scofield and others, 1997). Evidence for the landslide dam includes submerged tree stumps observed upstream (Lawrence, 1937; Lawrence and Lawrence, 1958). Evidence for catastrophic flooding from the breach has been observed downstream near the mouth of the Sandy River and at other locations (O'Connor and others, 1996; Lunney and Taylor, 2000). The Cascade Rapids, which developed from

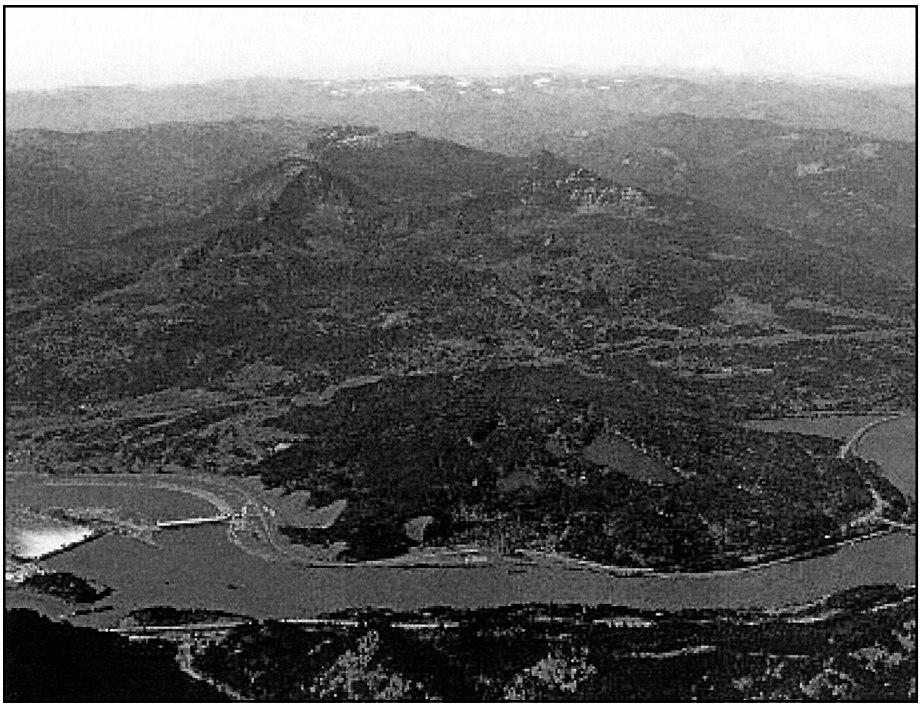

Figure 14. Air photo of the Cascade Landslide Complex taken in 1985 looking north-northwest. The toe of the Bonneville Landslide (part of the complex) is in the central foreground (courtesy of Derek Cornforth, Landslide Technology).

the breaching of the landslide dam, and the submerged forests were later inundated by the reservoir from the 1938 Bonneville Dam (Schuster and Pringle, in preparation). The great Cascade Range took its name from these landslide-generated cascades.

Although the slide complex has been extensively studied, the exact age of the slide remains a controversy. An 1830s account of an early Native American legend describes the Cascade Rapids as follows: "The Indians say those falls are not ancient, and that their fathers voyaged without obstruction in their canoes as far as The Dalles. They also assert that the river was dammed up at this place, which caused the waters to rise to a great height far above and that after cutting a passage through the impeding mass down to its present bed, those rapids first made their appearance" (Lawrence, 1937). Another version tells of the sons of Old Coyote, Wy'east (Mount Hood) and Pahto (Mount Adams) as powerful braves both in love with a maiden (Mount St. Helens). Because they crossed the "Bridge of the Gods" to fight over their love for her, Old Coyote collapsed the land bridge to keep his sons from fighting.

This "Bridge of the Gods" landslide dam was formed by the Bonneville Landslide, which is the youngest and largest of four portions of the Cascade Landslide Complex. Recent radiocarbon studies indicate a calendric age of AD 1500-1760 for this landslide (Pringle and Schuster, 1998). This age range is supported and refined by recent lichen-growth studies (Reynolds, in press), which suggest the occurrence between AD 1670-1760. Schuster and Pringle (in preparation) hypothesize that the Bonneville Landslide may have been triggered by a major earthquake and that the more recent estimates of its age put it within the time frame of the great January 27, 1700, subduction-zone earthquake.

Earlier studies support the recent radiocarbon ages or suggest earlier landslide activity. In support of the more recent dates, Edwin Hodge suggested that the slide could not be more than 500 years old (Palmer, 1977). This is based on his observations of the "undissected topography" (which we interpret to mean intact landslide blocks) and the 250-yr age limit of trees. Carbon-14 measurements on wood found within the slide have displayed a wide range of

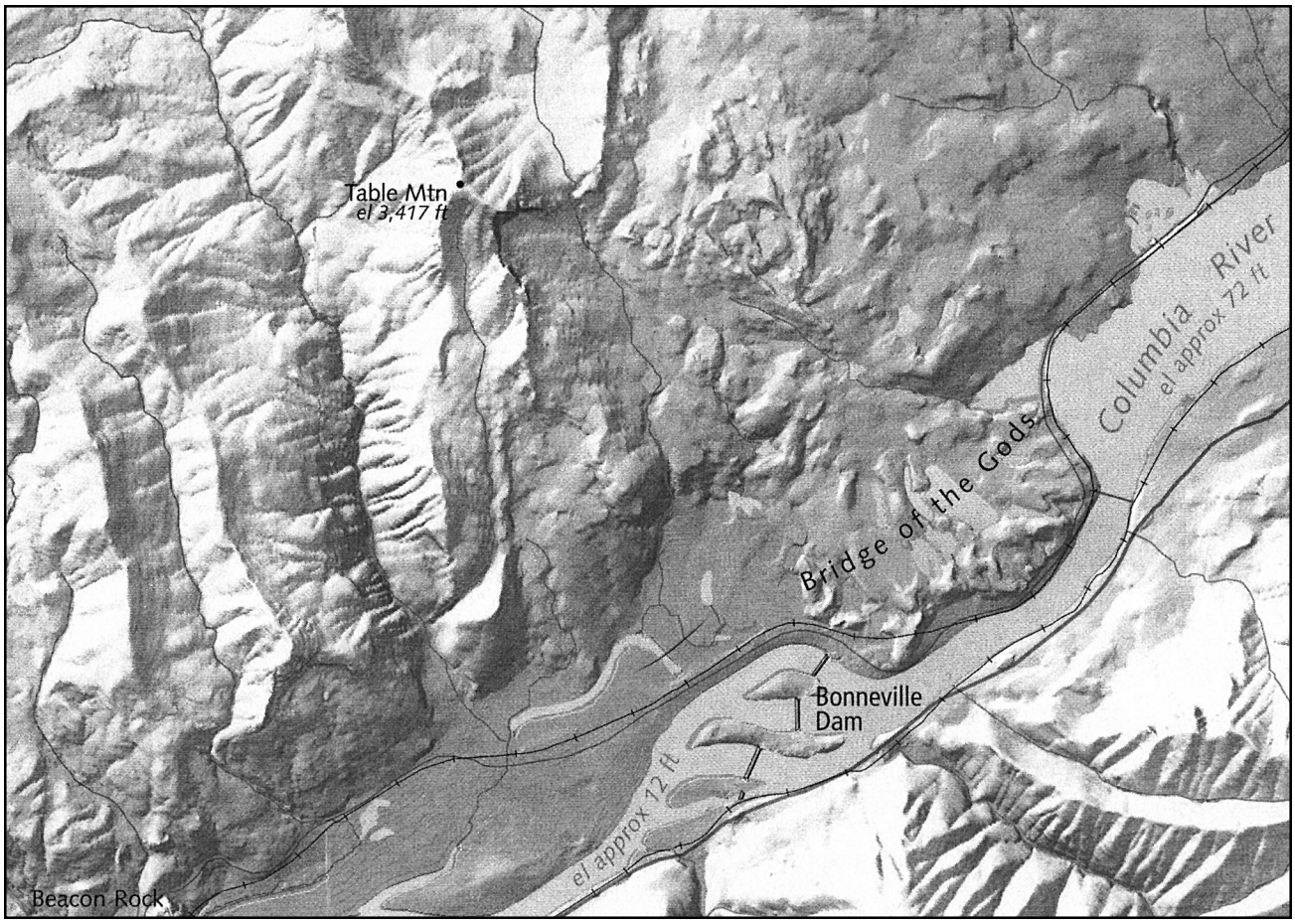

Figure 15. Smaller scale image of the Cascade Landslide Complex showing the regional topography and the Bridge of the Gods (Loy, 2001).

possible ages. For example, according to Lawrence and Lawrence (1958) and Minor (1984), radiocarbon ages of 700 ± 200 yr B.P. and 670 ± 300 yr B.P. indicate that the landslide occurred about AD 1250. However, Schuster and Pringle (in preparation) noted that Minor chose to ignore a younger age of 400 ± 70 yr B.P. They further note that the half-life of radiocarbon has been recalculated since the publication of the Lawrence data and that Lawrence and Lawrence may have taken representative samples that do not reflect the outer wood of the trees. Thus, they suggest that the ages published by Lawrence and Lawrence may be too old.

The 1938 Bonneville Dam is the last major dam in a series of dams on the Columbia–Snake River hydroelectric system. Although we focus on the Cascade Landslide Complex and the Bonneville Landslide, the dam facilities also encompass the **Tanner Creek and Tooth Rock Landslides** originating from the south shore.

Stop 5. Mount Hood Lahars in the Sandy River Drainage

Mount Hood is the nearest active High Cascade volcano to the Columbia River Gorge, sitting only a few kilometers south of the Gorge between Troutdale and Hood River (Fig. 16). Because of its location near the Portland population center and the Columbia River transportation corridor, the potential for hazardous impact from volcanic activity is high. Workers who have studied the volcanic history of Mount Hood list the expected volcanic activity as andesitic lava flows, lava-dome extrusion, and primary and lava-dome-collapse pyroclastic flows (Scott and others, 1997). Current volcanic hazards associated with the eruptive activity include lava flows, tephra falls, pyroclastic flows, debris avalanches, and lahars.

Debris avalanches and lahars pose the greatest danger to population centers over the longest period. Lahars result when water from precipitation or melted snow and ice mixes

with pyroclastic flow deposits, remobilizing the poorly sorted volcaniclastic material into a fast-moving slurry (up to 80 km/hr). This process can be repeated for many years until most of the sediment has been moved downstream. All the major drainages of Mount Hood contain lahar and debris-avalanche deposits associated with three post glacial eruptive periods (Cameron and Pringle, 1986; Figure 16).

The Sandy River Valley and its higher tributaries have been inundated by numerous lahars over the past 1,800 years. These have resulted from runoff of dome-collapse pyroclastic flows from around Crater Rock, the youngest lava dome on Mount Hood, and later remobilization of the pyroclastic deposits during periods of high precipitation. Lahars attained depths of 9-12 m above the modern valley floor in the Sandy River, and the deposits reached the Columbia River, a distance of over 90 km (Scott and others, 1997). For example, during the last eruptive episode in the 1780s, the silicic neck spine of Crater Rock collapsed, inundating Old Maid Flat. The lahar continued moving 90 km down the Sandy River into the Columbia River. Lewis and Clark in 1805 named it the Quicksand River in recognition of the 4-mi wide saturated bar of remobilized lahar at the mouth of the river. The lahar forced the Columbia River channel to the north at the mouth of the Sandy River, a situation that most likely will be repeated during future volcanic-eruption-induced sedimentation.

It is estimated that the 30-year probability of lahars in the Sandy River drainage is the same as that for renewed dome growth near Crater Rock, about 1 in 15 to 30 (Scott and others, 1997).

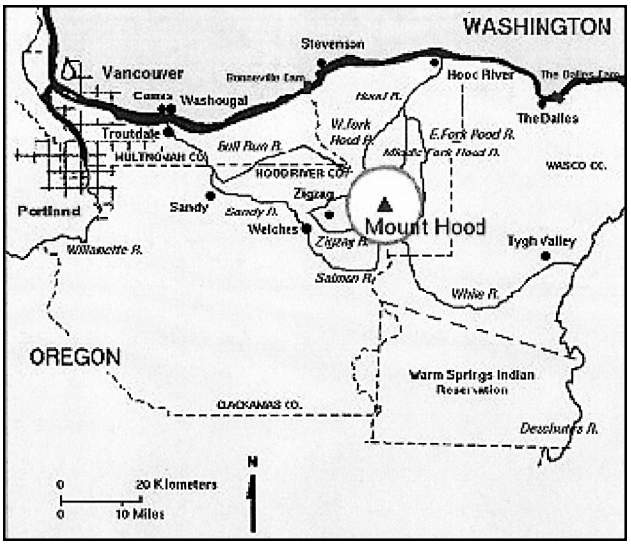

Figure 16. Mount Hood and its major river drainages, all of which contain lahar and debris avalanche deposits. The Sandy River and its tributaries have been inundated several times by lahars during the past 1,800 years, an interval that covers the most recent volcanic activity.

TRANSPORTATION CORRIDOR STUDY

The Oregon Department of Geology and Mineral Industries is currently evaluating the vulnerability of the U.S. Interstate Highway 84 transportation corridor. The study is funded by the U.S. Department of Transportation, and the study region extends from the Port of Portland on the west to the Port of Hermiston on the east.

The DOGAMI evaluation will be multimodal and address multiple natural hazards. The primary transportation systems include Interstate Highway I-84, barge traffic on the Columbia River, and rail lines. The hazards to be addressed include rockfalls, debris flows, volcanic and other landslides, earthquake ground shaking, floods, and dam-stability hazards.

In the study, information on engineered systems (bridges and roads) will be geographically evaluated with regard to existing geohazards and available economic data to highlight interdependencies. The findings of this study will be disseminated to the public and can be applied toward evaluating potential public-policy options and other mitigation alternatives to minimize risks.

ACKNOWLEDGMENTS

We owe thanks to the many people who contributed to this manuscript. Tim Pfeiffer of Foundation Engineering and Stan Hinatsu of the U.S. Forest Service provided helpful details on the Multnomah Falls mitigation. We thank the Oregon Department of Geology and Mineral Industries staff, including Neva Beck for graphics and John Beaulieu, Dennis Olmstead, and Klaus Neuendorf for their reviews of the manuscript. George Moore of Oregon State University provided the opportunity for this field trip as well as additional review.

We thank the U.S. National Academies for their professional encouragement of this field trip. We also thank the U.S. Department of Transportation for its involvement with the transportation corridor project.

REFERENCES

Anderson, J.L., 1980, Pomona Member of the Columbia River Basalt Group and intracanyon flow in the Columbia River Gorge, Oregon: Oregon Geology, v. 42, p. 195-199.

Baldwin, E.M., 1946, Report on the slide that occurred in the Columbia River Gorge beginning February 5, 1946: Report to Oregon Department of Geology and Mineral Industries, unpublished, 5 p.

Cameron, K.A., and Pringle, P.T., 1986, Post-glacial lahars of the Sandy River Basin, Mount Hood, Oregon: Northwest Science, v. 60, p. 225-237.

Lawrence, D.B., 1937, Drowned forests of the Columbia River Gorge: Geological Society of the Oregon County Geological News Letter, v. 3, p 76-83.

Lawrence, D.B., and Lawrence, E.G., 1958, Bridge of the Gods legend, its origin, history and dating. *Mazama*, v. 40, no. 13, p. 33-41.

Loy, W.G., ed., 2001, Atlas of Oregon: University of Oregon Press, ed. 2, 301 p.

Lunney, M., and Taylor, J.M., 2000, Analysis of probable Bridge of the Gods landslide dam outburst sediments in the Lower Columbia River Basin: Geological Society of America Abstracts with Programs, v. 32, no. 6, p. A-26.

Minor, R., 1984, Dating the Bonneville Landslide in the Columbia River Gorge: Report to Portland District U.S. Army Corps of Engineers under Contract No. DACW57-83-C-0033, Portland, Oregon, Heritage Research Association Report 31 p. 19.

Newcomb, R.C., Pope, R.J., and Wright, W.L., 1978, Columbia River Gorge slide studies, Oregon and Washington: Shannon and Wilson Inc. Report to Portland General Electric Company , no. O-1203, 23 p.

O'Connor, J.E., Pierson, T.C., Turner, D., Atwater, B.F., and Pringle, P.T., 1996, An exceptionally large Columbia River flood between 500 and 600 years ago—breaching of the Bridge-of-the-Gods Landslide?: Geological Society of America Abstracts with Programs, v. 28 p. 97.

Orr, E.L., and Orr, W.N., 1999, Geology of Oregon: Dubuque, Kendall/Hunt Publishing Company, 254 p.

Palmer, L, 1977, Large landslides of the Columbia River Gorge, Oregon and Washington, *in* Landslides, Reviews in Engineering Geology: Geological Society of America, p 69-83.

Pringle, P.T., Logan, R.L. and Schuster, R.L., 2000, Rock slide–debris avalanches as records of prehistoric earthquakes in western Washington State, *in* Clague, J., and others, eds., Great Cascadia earthquake tricentennial: Oregon Department of Geology and Mineral Industries Special Paper 33, p. 100-101.

Pringle, P. T., and Schuster, R. L., 1998, A new radiocarbon date for the Bonneville Landslide, Columbia River Gorge, Washington: American Association of Engineering Geologists Program with Abstracts, p. 116.

Reynolds, N., in press, Dating the Bonneville Landslide with lichenometry: A preliminary study: Washington Geology, v. 29.

Sager, J.W., 1989, Bonneville Dam, *in* Galster, R.W., ed., Engineering geology in Washington, Vol. 1: Washington Division of Geology and Earth Resources Bulletin 78, p. 337-346.

Schuster, R.L., and Chleborad, A.F., 1989, Landslides in Washington and Oregon—An overview, *in*Hays, W.W., and Huey, L, eds., Earthquake hazards in the Puget Sound, Portland Area—Proceedings of Conference 48. U.S. Geological Survey Open-File Report, p. 86-105.

Schuster, R.L., and Pringle, P.T., in preparation, Engineering history and impacts of the Bonneville Landslide, Columbia River Gorge, Washington-Oregon, USA, *in* 1st European Conference on Landslides (Prague, June 24-26, 2002) Proceedings.

Scofield, D., Harvey, A., Burns, S., and Phillips, J., 1997, Engineering geology of the Columbia River Gorge: Association of Engineering Geologists, 27 p.

Scott, W. E., Pierson, T. C., Schilling, S. P., Costa, J. E., Gardner, C. A., Vallance, J. W., and Major, J. J., 1997, Volcano Hazards in the Mount Hood Region, Oregon: U.S. Geological Survey Open-File Report 97-89.

Shannon and Wilson Inc., 1996, Causes and potential hazard analyses, Dodson debris flows, February 7 and 8, 1996, Dodson, Oregon: Report to Oregon Department of Transportation and others, March 29, 1996, unpublished, 5 p.

Squier Associates, 1999, Geotechnical Report on Maple Hill Landslide, Skamania County, Washington, Feb 25, 1999: Report to Skamania County Public Works, unpublished.

Suchanek, R., 1974, The Columbia River Gorge and the story of the river and the rocks: Ore Bin, v. 36, p. 197-213.

Tolan, T.L., and Beeson, M.H., 1984, Exploring the Neogene history of the Columbia River: Discussion and geologic field trip guide to the Columbia River Gorge, Part 1. Discussion, Oregon Geology, v. 46, p. 87-95.

Tolan, T.L., Reidel, S.P., Beeson, M.H., Anderson, J.L., Fecht, K.R., and Swanson, D.A., 1989, Revisions to the estimates of the areal extent and volume of the Columbia River Basalt Group, *in* Reidel, S.P., and Hooper, P.R., eds., Volcanism and tectonism in the Columbia River flood-basalt province, Geological Society of America Special Paper 239, p. 1-20.

Waters, A.C., 1973, The Columbia River Gorge: Basalt stratigraphy, ancient lava dams, and landslide dams, *in* Beaulieu, J.D., ed., Geologic field trips in northern Oregon and southern Washington: Oregon Department of Geology and Mineral Industries Bulletin 77, p.133-162.

Geomorphology and Hydrology of the H.J. Andrews Experimental Forest, Blue River, Oregon

Frederick J. Swanson, Pacific Northwest Research Station, U.S. Forest Service, Corvallis, Oregon 97331; fred.swanson@orst.edu

Julia A. Jones, Department of Geosciences, Oregon State University, Corvallis, Oregon 97331; jonesj@geo.orst.edu

INTRODUCTION

We served as compilers of material from a working group, and the authors of the major sections appear at their headings. The contributors may be reached through the Andrews Forest personnel directory at http://www.fsl.orst.edu/lter.

The H.J. Andrews Experimental Forest is the Lookout Creek Watershed (6400 ha) draining westward from the Western Cascade Range about 80 km east of Eugene, Oregon (Fig. 1). Since its establishment in 1948 the Andrews Forest has been a center for applied forestry and basic ecosystem research as well as numerous hydrology and geomorphology studies. Since 1980 the Andrews Forest has been one of now 25 Long-Term Ecological Research (LTER) sites funded by the National Science Foundation.

A large component of the hydrology and geomorphology research at Andrews Forest is centered on three sets of experimental watersheds (Table 1, Fig. 1). This work is complemented by studies of channel and hillslope processes elsewhere in the area, including the watersheds of Lookout Creek and upper Blue River, which have gauge records beginning in 1949.

Hydrology research has examined most elements of the hydrologic cycle, long-term trends of peak flows in response to road construction and forest cutting and regrowth (Jones and Grant, 1996; Jones 2000), road hydrology (Wemple and others, 1996), and the hyporheic zone (Wondzell and Swanson, 1996a, b, 1999). Geomorphology studies have concerned sediment yield and budgets for experimental watersheds (Fredriksen, 1970; Swanson and others 1982a, b; Grant and Wolff, 1991), mass movement processes (Dyrness, 1967; Swanson and Dyrness, 1975; Wong 1991), woody debris in streams (Harmon and others, 1986), channel form-process relations over a hierarchy of scales of channel and valley floor landforms (Grant and others, 1990, Grant and Swanson, 1995; Grant, 1997), watershed response to a major flood (Wondzell and Swanson, 1999; Swanson, 1998; Johnson and others, 2000; Nakamur, 2000, Faustini, 2000; Wemple and others, 2001).

The Lookout Creek watershed, equivalent to the Andrews Forest, ranges in altitude from 420 to 1615 m. Bedrock below about 850 m is composed of hydrothermally altered volcaniclastic rocks of late Oligocene to early Miocene age, and andesite lava flows underlie upper parts of the Andrews Forest (Swanson and James, 1975). Soils have loamy surface horizons, have aggregate structure bound by organic matter, and have porosity of 60-70% with extensive development of macropores (Ranken, 1974). This accounts for the predominance of subsurface flow to streams (Harr, 1977), because infiltration capacity greatly exceeds precipitation intensity.

The Lookout Creek Watershed has been sculpted over perhaps 3 million years by glacial, mass movement, fluvial, geochemical, and other processes. Glacial landforms (cirques and U-shaped valleys) dominate the southeastern quadrant of the area. The western part of the watershed is dominated by steep (approximately 30–35°), straight slopes and narrow ridge crests and valley floors produced by stream erosion and shallow, rapid debris slides and flows. Several areas exhibit irregular terrain of moderate slope (5–10°) resulting from deep-seated (>5m thickness) slow-moving (generally <1 m/yr) landslides, locally referred to as earthflows (Swanson and Swanston, 1977; Pyles and others, 1987). Stream environments

Field Guide to Geologic Processes in Cascadia: Oregon Department of Geology and Mineral Industries Special Paper 36, 2002.

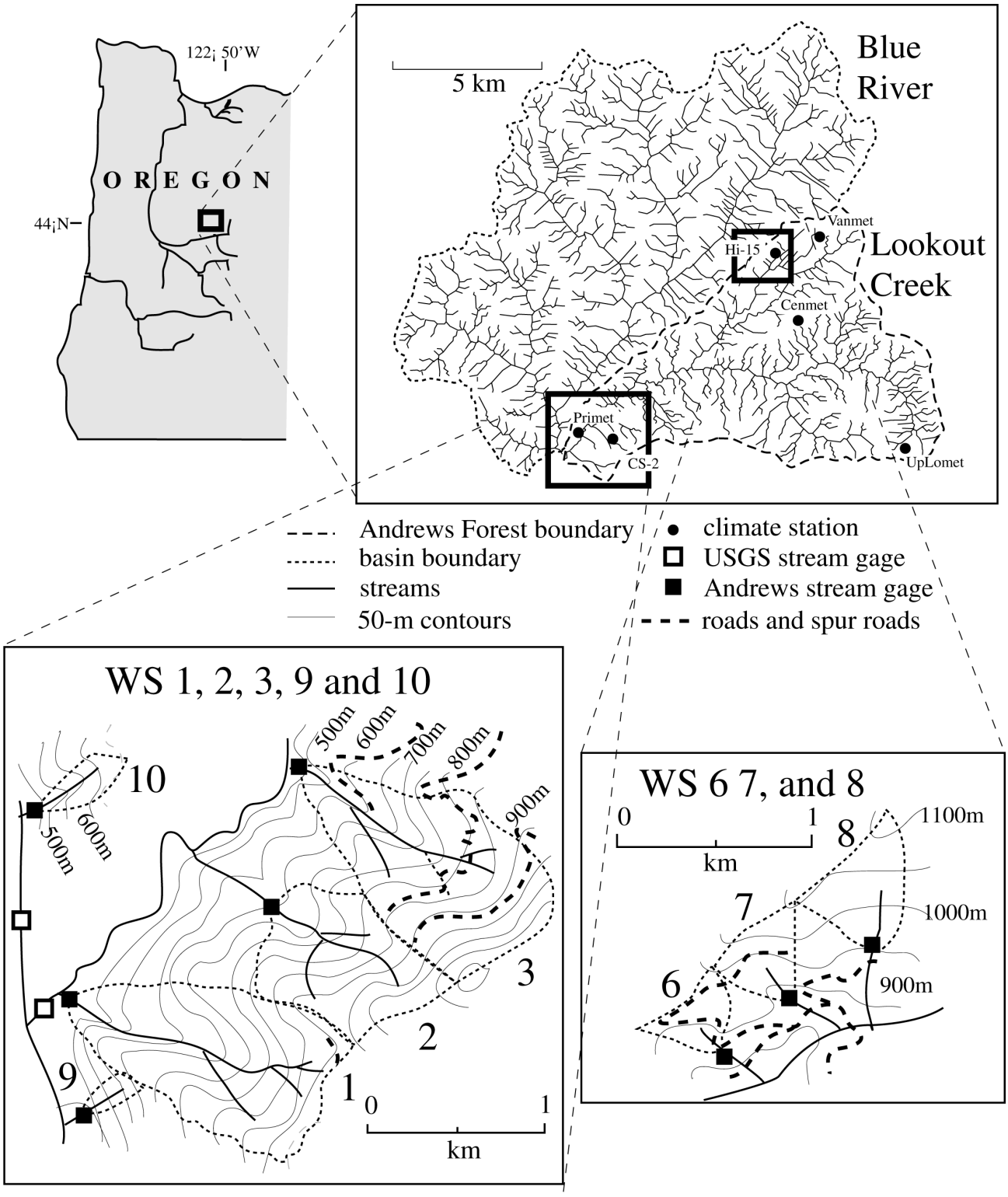

Figure 1. Andrews Forest and upper Blue River Watershed stream network and experimental watersheds (WS). Primet, Vanmet, Cenmet, and UpLomet are meteorological stations.

Table 1. Experimental watersheds in the H.J. Andrews Experimental Forest. Prior to treatments, forests were 400 to 500 yr old Douglas fir/western hemlock stands in Watersheds 1, 2, 3, 9, and 10, and 130 yr old Douglas fir stands in Watersheds 6, 7, and 8.

Basin no.	Area (ha)	Elev (m) Min	Elev (m) Max	Management history	Water, stream chemistry, and sediment records, start date[1] W[2]	C[3]	S	B
1	96	460	990	100% clearcut, 1962-66; prescribed burned 1967	1953	--	1957	1957
2	60	530	1070	control	1953	1981	1957	1957
3	101	490	1070	1.5 km (6%) roads, 1959; 25% clearcut in 3 patches, 1963	1953	--	1957	1957
6	13	880	1010	100% clearcut, 1974	1964	1972	1972	--
7	15	910	1020	50% selective canopy removal, 1974; remaining canopy removed 1984	1964	1972	1972	--
8	21	960	1130	control	1964	1972	1972	--
9	9	425	700	control	1967	1969	1969	1973
10	10	425	700	100% clearcut, 1975	1967	1969	1969	1973

[1] W = continuous stream discharge; C and S = composited 3-weekly samples of streamwater collected with proportional sampler and analyzed for chemistry (C): N, P, Ca, Mg, K, Na, alkalinity, conductivity, pH, particulate N, and particulate P; and suspended sediment (S); B = bedload sampling in ponding basin.

[2] Streamflow records are continuous up to the present, except for Watersheds 6 and 7, where streamflow was not measured from 1987 to 1994. Records are based on water year, October 1 to September 30.

[3] Long-term records with 3-weekly sampling interval began on this date.

range from steep, narrow, bedrock chutes along small streams recently scoured by debris flows to wide alluvial reaches, which have accumulated behind constrictions of the valley floor (Grant and Swanson 1995). Much of the stream network is a boulder-dominated stepped sequence of pools and steep channel units (Grant and others, 1990).

The area receives approximately 2300 mm of precipitation at low elevations, mainly as rain, and a greater amount at upper elevations, mainly as snow. Approximately 80% of the precipitation falls between October and April during long-duration low-intensity frontal storms. Snow packs are common at low elevations, but rarely persist longer than 2 weeks. A seasonal snow pack develops at altitudes of about 1000-1200 m. Major floods typically result from rain augmented by snowmelt (Harr, 1981).

HYDROCLIMATOLOGY (Julia A. Jones)

Climate

The climate of the Andrews Forest is marine temperate, with winter precipitation and high summer temperature (Fig. 2). The highest precipitation occurs in late November, and minimum precipitation occurs in late July; very little precipitation occurs between June 1 and September 30. The annual hydrograph peaks in January, and minimum streamflow occurs in July and August (Fig. 3).

Long-Term Trends in Precipitation and Streamflow

Mean annual precipitation from 1958-1996 was 2259 mm, but ranged from 1309 mm in 1977 to 3074 mm in 1972 (Fig. 4). Mean annual streamflow at Watershed 2 from 1952-1996 was

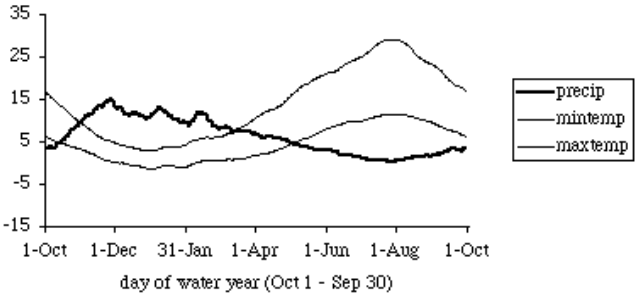

Figure 2. 15-day running mean of mean daily precipitation (mm) (1958-1996) and temperature (degrees C) (1952-1995) at Watershed 2.

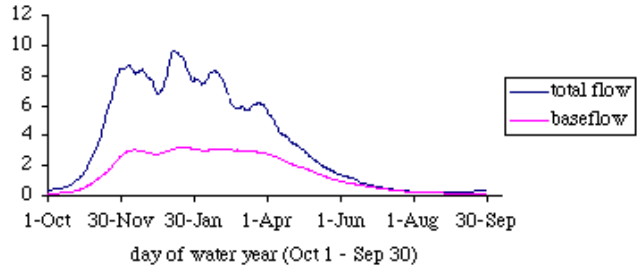

Figure 3. 15-day smoothing of unit area discharge (mm), Watershed 2, 1953-96.

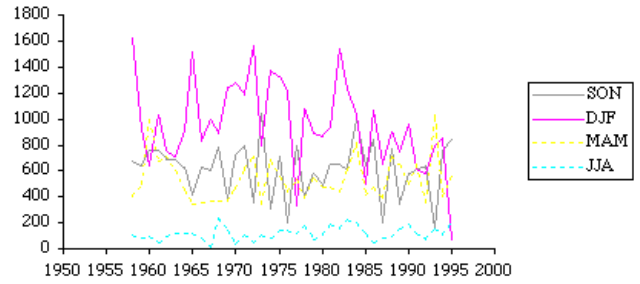

Figure 4. Annual precipitation (mm) at Watershed 2, 1958-96.

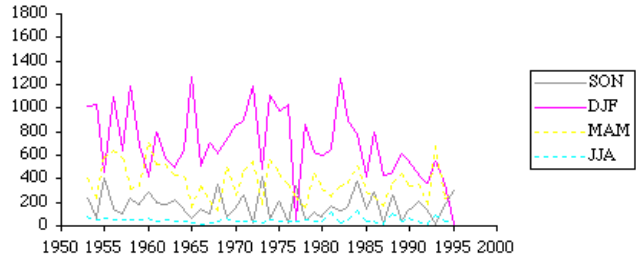

Figure 5. Annual discharge (mm) at Watershed 2, 1952-96.

1332 mm, but ranged from 370 mm in 1977 to 2187 mm in 1956. Streamflow is 56% of precipitation, but ranged from 40% in dry years to 70% in wet years. Thus, actual annual evapotranspiration is estimated to be 927 mm, or 44% of precipitation.

There has been a long-term decline in winter precipitation and winter streamflow (Fig. 4 and 5). However, the trends do not obviously follow any simple model of climate shifts, such as the proposed 1976 "climate step" of Pacific Decadal Oscillation or of El Niño/Southern Oscillation (Greenland and others, 2001).

Estimates of Evapotranspiration and Water Use

Recent research has attempted to better characterize evapotranspiration by modeling, retrospective empirical analysis, and isolating its components by direct measurements. Model estimates at Andrews Forest indicate that evapotranspiration may be as high as 6 mm/day. Retrospective estimates from long-term records at Watershed 2 (that is, the difference between average precipitation and streamflow, or 927 mm) indicate that the average daily evapotranspiration may be 2.5 mm/day, but evapotranspiration may be much higher or lower than this during key periods of the year. The probable periods of maximum evapotranspiration are fall and spring, when temperatures and moisture are moderate. Sapflow measurements during the summer indicate that water use by old-growth trees may be only 0.5 mm/day, whereas water use by 30-yr-old alder and Douglas fir may be 1.5 mm/day (B.J. Bond, unpublished data).

SMALL WATERSHEDS—STREAMFLOW RESPONSE TO FOREST REMOVAL AND ROADS (Julia A. Jones)

Responses of Peak Flows to Forest Harvest and Roads

The magnitude, seasonality, and duration of peak discharge responses to forest removal and regrowth and roads in five pairs of experimental basins in the Andrews Forest are consistent with fundamental water balance and routing concepts in hydrology. Effects of forestry treatments on evapotranspiration, snow-

pack dynamics, and subsurface flow interception vary predictably by season, geographic setting, amount of forest canopy removal, stage of canopy regrowth, and arrangement of roads in the basin. Post-treatment responses of selected subpopulations of matched peak discharge events were examined over 21-34 yr post-treatment periods in treated and control basin pairs in a range of geographic settings. Changes in evapotranspiration associated with forest canopy removal and regrowth apparently accounted for significant increases in peak discharges during the first post-harvest decade (Fig. 6). Changes in snowpack dynamics apparently accounted for significant increases (25-31%) in winter rain-on-snow events, but other types of winter events did not change in four of five basins at the Andrews Experimental Forest (Fig. 7).

Changes in subsurface flow interception by road cuts apparently accounted for significant increases (16-26%) in large (>1 yr return period) events in four of five basins, of which three had roads. Increases in small peak discharge events decreased rapidly after the first post-treatment decade, but increases in large events persisted into the second and third post-treatment decades (Jones, 2000).

Streamflow Yield Responses—Annual Yield, Summer Yield

Immediately after forest canopy removal, annual streamflow increased by 400-500 mm (40%) at all three 100% harvested basins at the Andrews Forest (Fig. 8). Twenty-five to thirty years after forest canopy removal, basins at the conifer forest site had persistent annual increases of 200-450 mm at upper elevations (Watersheds 6/8), 200-350 mm at middle elevations (Watersheds 1/2), and 100-250 mm at lower elevations (Watersheds 10/2) (Fig. 8, from Jones and Post, in review).

The apparent more rapid recovery of streamflow at the lowest elevation site (Watershed 10) is especially marked in the behavior of summer flows (Fig. 9; J.A. Jones, unpub. data). Summer streamflow recovered slightly at the high elevation basins (Watersheds 6, 8), recovered completely at the mid-elevation basins (Watersheds 1, 2), and declined to well below pre-treatment levels at the lowest elevation basins (Watersheds 10, 9).

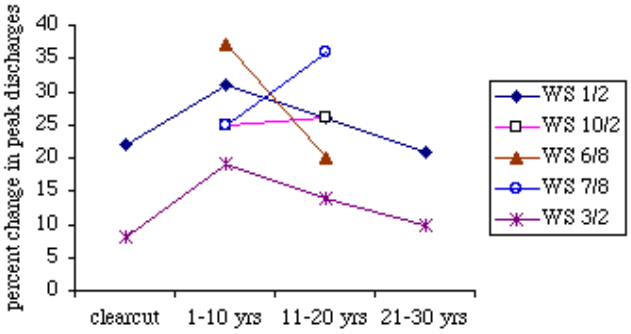

Figure 6. Statistically significant increases (%) in peak discharges of all event sizes by decade in different watersheds (WS) after forest harvest and road construction (from Jones, 2000).

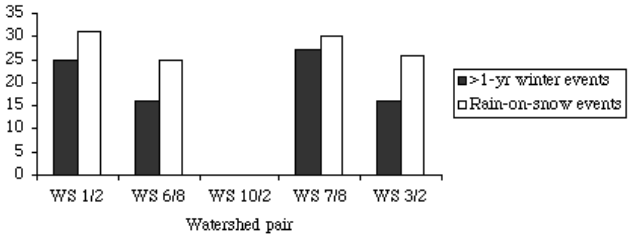

Figure 7. Statistically significant increases (%) in peak discharges of large and rain-on-snow events after forest harvest and road construction for all post-treatment years (from Jones, 2000).

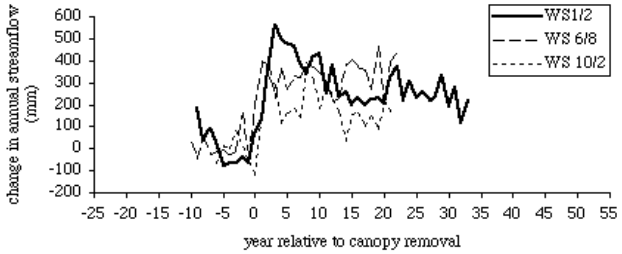

Figure 8. Absolute change in annual streamflow (mm at streamflow per unit area) over time after 100% canopy removal by watershed (WS) pairs.

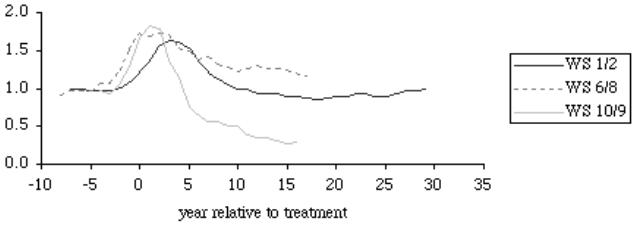

Figure 9. 5-yr smoothing of summer streamflow (June-September) responses to 100% forest harvest removal at the Andrews Forest, a fraction of pretreatment flows by year relative to treatment Pretreatment index = 1.

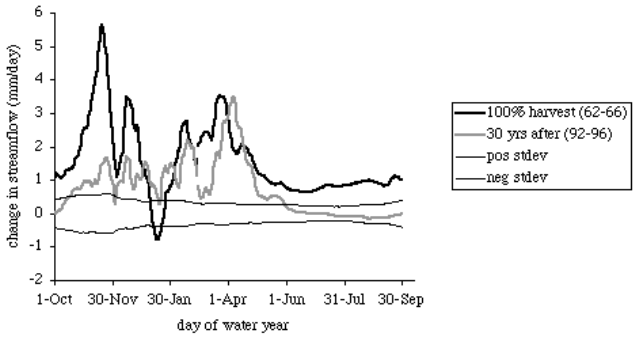

Figure 10. 15-day smoothing of absolute change (mm) in mean daily streamflow, Watershed 1 (100% harvest) v. Watershed 2 (control), for 5-yr periods after treatment. Standard deviation at control basin for period of record is shown for reference.

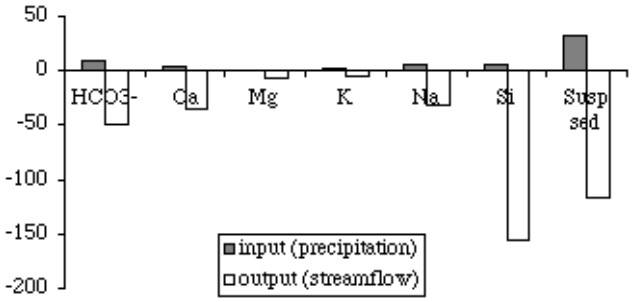

Figure 11. Budgets for inorganic constituents (kg/ha/hr) of Watershed 8 (high-elevation control) (from Martin and Harr, 1989).

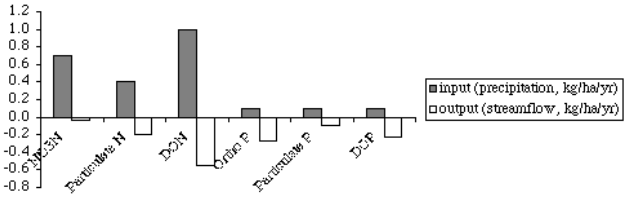

Figure 12. Budgets for organic constituents (kg/ha/hr) of Watershed 8 (high-elevation control) (from Martin and Harr, 1989).

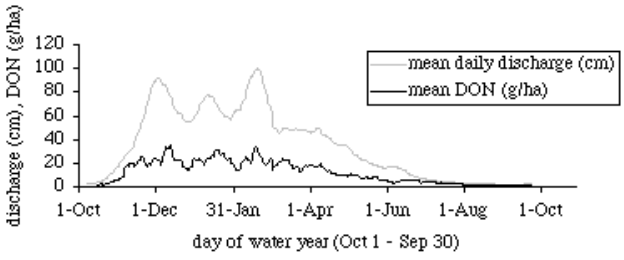

Figure 13. 15-day running means of daily streamflow and dissolved organic N in streamflow from Watershed 2, 1981-1997.

Hydrologic Responses to Forest Harvest and Regrowth by Day of Year

Forest harvest produced the biggest absolute increases in streamflow during the fall and spring at the Andrews Forest, based on the example of Watersheds 1/2 (Fig. 10). Streamflow increases were greatest in the fall, then the spring, and modest during the summer. Midwinter streamflow did not respond to 100% forest canopy removal in Watershed 1. Several alternative hypotheses have been proposed for the lack of response at this time of the year. First, interception, snow, and soil reservoirs may be full, hence transmitting all inputs, so removal of the canopy reservoir has no effect on streamflow. Second, losses of interception storage may be balanced by losses of cloudwater interception. Third, increased water delivered to the forest floor may be stored in a cooler more persistent snowpack, contributing to streamflow increases in the spring. Increases in summer streamflow disappeared within 5 yr after forest cutting, and increases of fall streamflow had mostly disappeared by 35 yr after it (Fig. 10). This recovery is probably due to increased summer and fall water use by regenerating vegetation. However, streamflow increases during the spring persisted with little decline for 35 yr after forest canopy removal.

SMALL WATERSHEDS—NUTRIENT CYCLING (Julia A. Jones)

Stream chemistry at the Andrews reveals many of the complex interconnections between the geophysical and ecological systems. Stream chemistry, and hence export of dissolved materials from small watersheds, has been studied in detail since the 1960s at the Andrews forest. Fluxes of materials in stream water have been measured since 1969 at the low elevation paired basins (Watersheds 9 and 10); since 1972 at the upper elevation paired basins (Watersheds 6, 7, and 8); and since 1981 at the mid-elevation control basin (Watershed 2) (see Introduction, Table 1, Fig. 1).

Nutrient Budgets

Cations, N, P, conductivity, alkalinity, and pH have been measured, and N and P measurements have been made both for dissolved and particulate forms. In general, the fluxes of

cations are very high and seem to be coupled to physical processes (precipitation, runoff, and mass movement). Streams export up to 10x more cations and Si than is input in precipitation. Moreover, fluxes of cations and Si are two to three orders of magnitude higher than fluxes of N and P (Fig. 11 and 12, adapted from Martin and Harr, 1989).

The fluxes of biologically relevant nutrients, especially N and P, show more complex patterns. Both occur in very low concentrations and seem to be quite tightly held in the forest and stream ecosystem. Exports of N are lower than inputs from precipitation, but exports of P are about equal to inputs from precipitation (Fig. 12, adapted from Martin and Harr, 1989).

N and P in Control Basins With Old-Growth Forest

Export of N and P in streamflow from old-growth forests is very low. Over the period 1981-87, total N in Watershed 2 ranged from 0-0.154 kg/ha, NH3N (NH_3 nitrogen) ranged from 0-0.13 kg/ha, and DON (dissolved organic nitrogen) ranged from 0-0.1 kg/ha. Particulate N ranged from 0-0.26 kg/ha, except in the flood of record on 7 Feb 96, when it reached 4.1 kg/ha. Over the period 1969-97, total N in Watershed 9 ranged from 0-0.21 kg/ha, NO3N (NO_3 nitrogen) ranged from 0-0.07 kg/ha, and DON ranged from 0-0.2 kg/ha. Particulate N ranged from 0-0.26 kg/ha, except in the flood of record on 7 Feb 96, when it reached 2.3 kg/ha.

Over the course of the year, all N and P forms closely follow streamflow. DON fluxes follow streamflow in general, but they deviate from streamflow in some suggestive ways (Fig. 13) (Vanderbilt, 2000; Vanderbilt and others, in press). In particular, DON rises rapidly during the early part of the wet season (October–November) and then remains somewhat constant during the period from December to February. Thus, there is both a dilution effect (nutrient output is proportional to streamflow) and a secondary effect (nutrient output reaches a maximum earlier in the water year than streamflow). A number of possible explanations for the secondary effect are being explored. These include atmospheric dry deposition of dust from the Willamette Valley, flushes of DON from soils, DON release from litterfall on soils or into streams, or DON release from early fall mortality of stream organisms.

Stream N and P Over Time

Long-term trends in N and P are dominated by seasonal variability. DON is the predominant or only N form in streamflow most of the time, but other N forms (NO3, NH4) are important during the fall (just after October in Fig. 14). In dry years (mid-1980s, early 1990s), DON remains the dominant component of N fluxes throughout the year (DON never falls below 50% of total N). However, in other years (early 1980s, late 1980s, 1990-91), DON is overwhelmed by short-duration fluxes of NO3 and NH4 (Fig. 14, J.A. Jones, unpub. data).

Changes in Stream N and P Before/After Forest Removal

Stream N increased after 100% forest harvest in Watershed 6 in 1974 and Watershed 10 in 1975. Stream P did not appear to be affected by forest harvest. Stream N recovered to pre-treatment levels and in some cases declined to below pre-treatment levels by 15-20 yr after 100% forest canopy removal. This finding implies that early successional vegetation was using as much or more N and P than old-growth forest. Stream chemistry recovery at Watershed 10 and Watershed 6 does not match the recovery trajectory of annual streamflow or summer streamflow, which remained elevated above pre-treatment levels through the second post-harvest decade. Absolute changes in stream N after 100% forest removal were very small. Recovery of DON and NO3N in streamflow to pre-treatment levels was faster at the low-elevation basin with shallow soils (Watershed 10) than at the high elevation basin (Watershed 6).

Relative to the pretreatment period (1969-74), all N forms at Watershed 10 increased relative to Watershed 9 in the first 5-8 yr after 100% forest canopy removal (see, for example,

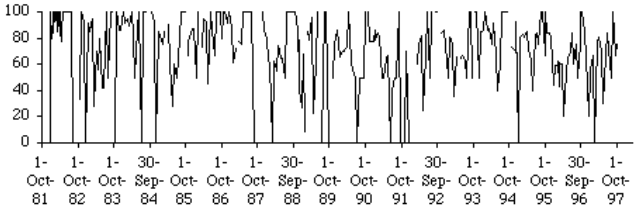

Figure 14. Dissolved organic N as percent of total N, Watershed 2.

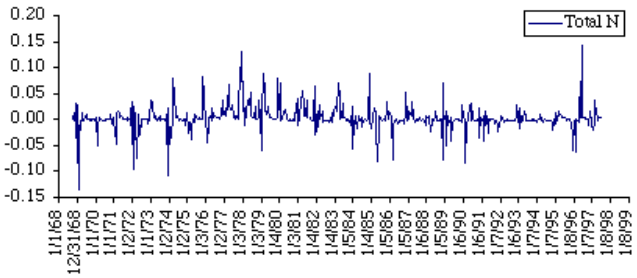

Figure 15. Absolute change in total N (kg/ha), Watershed 10 v. 9.

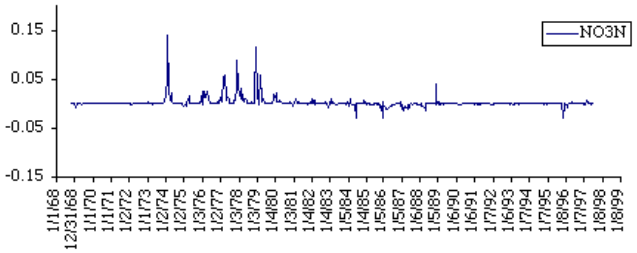

Figure 16. Absolute change in NO3N (kg/ha), Watershed 10 v. 9.

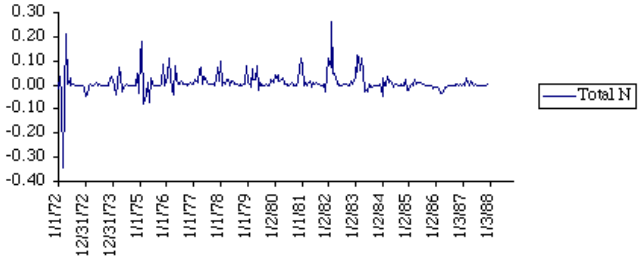

Figure 17. Absolute change in total N (kg/ha), Watershed 6 v. 8.

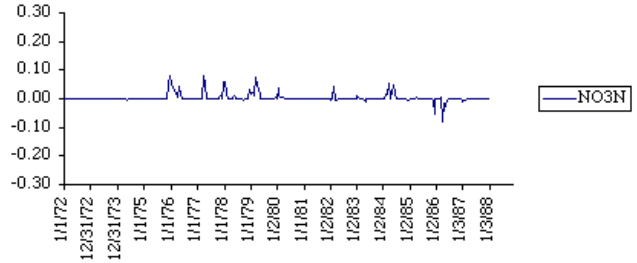

Figure 18. Absolute change in NO3N (kg/ha), Watershed 6 v. 8.

total N and NO3N (Fig. 15 and 16). By the early 1980s these increases had diminished, and by 1990, 15 yr after forest canopy removal, they had disappeared. Similar trends are apparent after treatment in 1974 at Watersheds 6 and 8, although the pre- and posttreatment records are shorter (Fig. 17 and 18).

SEDIMENT YIELD OF SMALL WATERSHEDS (Gordon E. Grant and Shannon K. Hayes)

A persistent and often contentious debate surrounds evaluating effects of forest harvest activities on streamflow and sediment yield. Despite abundant discussion of peak flow changes following timber harvest in paired-watershed studies in the Andrews Forest and other basins in western Oregon (Jones and Grant, 1996, 2001a, 2001b; Thomas and Megahan, 1998, 2001; Beschta and others , 2000; Jones, 2000), no studies have evaluated the geomorphic response to observed peak flow changes—a question of great interest in interpreting potential downstream consequences of forest management on channels and ecosystems.

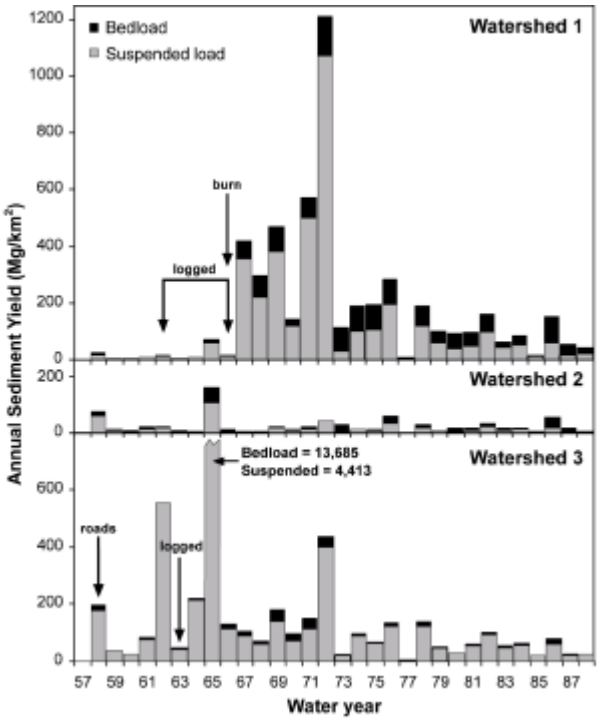

Figure 19. Annual sediment yields for Watersheds 1 (100% clear-cut), 2 (control), and 3 (25% clear-cut + roads) for water years 1958-1988 (from Grant and Wolff, 1991).

Decades of paired-watershed studies at the Andrews Forest have enhanced our understanding about the impacts of forest harvest on sediment transport through small mountain watersheds (Fig. 19). Early studies focused on the impacts of forest harvest on suspended sediment and bedload yields from experimental Watersheds 1, 2, and 3 (for example, Fredriksen, 1970; Grant and Wolff, 1991), and hillslope and channel sediment budgets from Watersheds 9 and 10 (Swanson and others , 1982a). Current research is aimed at disentangling the combined effects of hydrologic changes and increased sediment supply have on fluvial sediment transport following clearcutting (Grant and Hayes, 2000).

These studies document significant increases in sediment yields from harvested basins following treatment (Fig. 20). Although fluvial transport of sediment increased by at least an order of magnitude following treatment, episodic mass movements dominate long-term sediment output from some small watersheds. In Watershed 3, debris flows during the December 1964 storm transported 88% of the total post-treatment sediment yield through 1988; subsequent debris flows during the February 1996 storm moved comparable large volumes. Debris flows scoured the Watershed 3 channel of available sediment, so transport in intervening years was quite low. In the absence of large mass movements, sediment yields show a roughly exponential decline following treatment, although bedload and suspended sediment transport recover at different rates. Suspended sediment output from Watershed 1, which did not have debris flows, declined to pre-treatment levels within two decades following treatment, but bedload yields exceeded pre-treatment levels as recently as 1999.

The sediment yield histories from this paired-basin study suggest that the timing of land use changes with respect to large storms exerts significant control on magnitude and timing of sediment yield. Watershed 3 was prepared to exhibit a land-use-effects response to the December 1964 and January 1965 floods, but Watershed 1 was not because logging was only partially completed and fallen timber may have stabilized some hillslopes and channels.

Since the relation between sediment transport and discharge typically follows a power law, small increases in discharge can translate into large increases in sediment transport. But timber harvest typically influences both the hydrologic regime and sediment supply of a watershed, making it difficult to isolate the peak flow effect alone. We addressed this problem by using paired-watershed data from Watersheds 1 and 2 to predict streamflow response in the absence of cutting. We combined the predicted hydrology with observed relations between discharge and sediment transport to disentangle the relative effects of changes in hydrology and sediment supply. While peak flow increases alone can account for modest increases in both suspended and

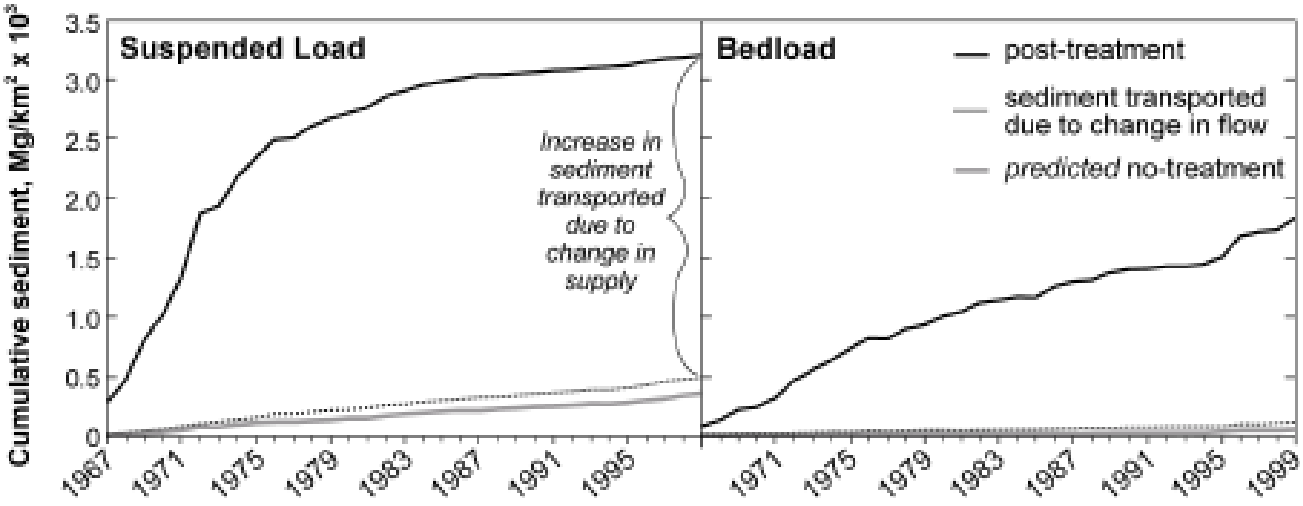

Figure 20. Watershed 1 sediment yield after clearcut and prescribed fire for water years 1967-1999.

bedload transport in Watershed 1, the peak flow effect is dwarfed by the increased supply of sediment following treatment.

SEDIMENT BUDGETS OF SMALL WATERSHEDS (Frederick J. Swanson)

Sediment budgets have been used to characterize the fluxes and storages of soil and sediment within and through watersheds or subsystems within watersheds. A sediment budget was compiled for the forested condition of 10-ha Watershed 10 which was covered with old-growth and some mature forest before clearcut logging (with only a ridge road and prescribed burning in a small area near the ridge) in 1975 as part of experimental watershed studies during the International Biological Program (Table 2). This sediment budget study revealed that the most episodic transport process, debris flow, accounted for about half of the long-term export, although only one debris flow is estimated to occur in about 600 years under forest cover, based on the extensive debris flow inventory data for the Andrews Forest (Swanson and others , 1982a). The pervasive and persistent process of dissolved export accounted for about 30% of annual average export.

In the first 12 years after logging (1975-1986) surface erosion increased from 80–200 kg/ha/yr, dissolve load from 332–354 kg/ha/yr, suspended load from 70–320 kg/ha/yr, and bedload from 90–305 kg/ha/yr. In general the rates of surface erosion and these export processes experienced increases for several years and then declined. On February 22, 1986, rainfall on melting snow triggered a 300 m^3 slide from a bedrock hollow at the head of the south fork. This mass moved down the channel as a debris flow, ultimately destroying the gauging station and depositing 700 m^3 of inorganic and organic debris (approximately 50:50) in the sediment basin and on the head of the alluvial fan at the mouth of the watershed. This single event accounted for about 85% of post-logging export, and the export for the

Table 2. Process characterists and transfer rates of organic and inorganic material to a channel by hillslope processes (T/yr) and export from the channel by channel processes (T/yr) for Watershed 10.

Process	Frequency	Area influenced (% of watershed)	Material transfer	
			Inorganic	Organic
Hillslope processes				
Solution transfer	Continuous	99	3	0.3
Litterfall	Continuous, seasonal	100	0	0.3
Surface erosion	Continuous	99	0.5	0.3
Creep	Seasonal	99	1.1	0.04
Root throw	1/yr	0.1**	0.1	0.1
Debris avalanche	1/370 yr	1-2**	6	0.4
Slump/earthflow	Seasonal*	5-8%	0	0
TOTAL			10.7	1.4
Channel processes				
Solution transfer	Continuous	1	3.0	0.3
Suspended sediment	Continuous, storm	1	0.7	0.1
Bedload	Storm	1	4.6	0.3
Debris torrent	1/580 yr	1	4.6	0.3
TOTAL			8.9	1.0

*Inactive in past century in Watershed 10.
**Area influenced by one event.

period was about 7 times estimated background, based on sediment yield from multiple experimental basins and slide inventories for a more extensive area. In the flood of February 6, 1996, another debris flow (about 200 m^3) began as a streamside slide on the north fork, hit the gauging station, inflicting only minor damage, and accumulated in the sediment basin and on the adjacent road. Channel scouring by the 1996 event was less severe than the 1986 event because of smaller size and amount of large wood, and bank protection by wet snow.

Less complete sediment budgets have been compiled for other watersheds, but comparisons reveal some interesting similarities and differences (Fredriksen, 1970; Swanson and Fredriksen, 1982). Watersheds 3 and 10, for example, have been quite susceptible to debris flows, which can flush sediment from channel storage, including material that had entered channels before logging. Thus the sediment export histories of these two basins have been dominated by debris flows. Poor roads in bad locations, such as through toes of large landslide deposits, have been a major source of sediment and debris flows in Watershed 3. Watershed 1 (clearcut and burned) has not been susceptible to debris flows, possibly because of relatively wide valley floor, moderate channel gradient, and more limited number of initiation sites in its headwaters. The hot prescribed burning of the steep slopes in Watershed 1, on the other hand, appears to have contributed a large amount of surface erosion to the channel (Swanson and Fredriksen, 1982). Thus, both intrinsic watershed properties and specific aspects of management practices affect sediment routing through watersheds and its representation in sediment budgets, such as expressed in the relative significance of episodic and more continuous processes.

Sediment budgets for small watersheds do not necessarily represent larger watersheds in which they are embedded. We have not developed sediment budgets for the Lookout Creek watershed, for example, but the larger basin includes geomorphic processes and depositional features not represented in small watersheds, such as earthflow terrain and alluvial valley floor areas upstream of passive (bedrock notches) or active (landslide) constrictions.

FLOOD HISTORY AND 1996 FLOOD CHANNEL CHANGE (Julia A. Jones, John M. Faustini, and Frederick J. Swanson)

Major storms and floods in Dec 1964 and Jan 1965 strongly influenced the Andrews Forest landscape and had a strong imprint on scientists' and land managers' perceptions of landscape change. Many stream reaches and riparian zones experienced disturbance by debris flows, floodwaters, and floated wood. Debris slides from recent cutting units and roads contributed to the extent of disturbance, although about a quarter of inventoried mass movement events initiated in forested areas (Dyrness, 1967). The flood of February 1996 gave contemporary researchers the chance to observe such events first hand and to assess flood effects with abundant data and knowledge of preflood conditions. Gordon Grant shot video during the flood in the lower Lookout Creek and Blue River Reservoir area (see Torrents of Change video produced by Association of Forest Service Employees for Environmental Ethics, Eugene, Oregon).

Flood History and Meteorology

Many large floods have occurred over the 50-yr record at the Andrews (Table 3). The largest of these floods occurred in Dec 64/Jan 65, Feb 96, Nov 77, Jan 72, and Feb 86. All major floods have occurred between late November and the end of February, the periods of highest precipitation, but large floods differ in their character. Some large floods were forest-wide and occurred on the same day; the three largest floods at Lookout Creek (7 Feb 96, 22 Dec 64, and 21 Jan 72) ranked within the top 6 floods at all basins that had gages. Other floods were forest-wide, but peaked at different times over a 2-3 day period; the floods of 22-23 Feb 86 and 27-28 Jan 65 produced multiple peaks within 2 days, ranking in the top 15 at one or two basins. Still other floods affected only part of the forest: the fifth-largest event at Lookout Creek (25 Nov 77) produced a peak ranking in the top 15 only at the highest elevation basin.

Large floods at the Andrews Forest typically occur during "rain-on-snow" conditions, when a warm, subtropical front delivers precipitation and warm winds to a landscape blanketed with a snowpack (Harr, 1981, 1986). Rain-on-snow floods may be exacerbated by the

Table 3. Date and unit area peak discharge ($m^3/s/km^2$) of the largest 15 floods at Lookout Creek and three unharvested control basins over periods of record (see column headings) at the Andrews Forest.

Rank	Lookout 62 km2, all elevations (1949-96)		WS9 9 ha, low elevation (1968-96)		WS2 60 ha, mid elevation (1952-96)		WS8 21 ha, high elevation (1963-96)	
	Date	$m^3/s/km^2$	date	$m^3/s/km^2$	date	$m^3/s/km^2$	date	$m^3/s/km^2$
1	7-Feb-96	4.93	7-Feb-96	1.47	7-Feb-96	2.17	22-Dec-64	1.93
2	22-Dec-64	3.03	1-Jan-76	1.35	22-Dec-64	1.65	13-Dec-77	1.50
3	21-Jan-72	1.90	9-Dec-71	1.26	27-Jan-65	1.35	21-Jan-72	1.45
4	18-Jan-53	1.65	2-Mar-72	1.14	20-Dec-57	1.29	7-Feb-96	1.31
5	25-Nov-77	1.39	11-Jan-72	1.12	18-Jan-53	1.27	25-Nov-77	1.30
6	13-Dec-77	1.36	23-Feb-86	1.11	21-Jan-72	1.27	23-Feb-86	1.12
7	20-Dec-57	1.31	9-Jan-89	1.07	8-Jan-76	1.19	4-Dec-75	1.08
8	23-Feb-86	1.23	21-Jan-72	1.06	23-Feb-86	1.19	25-Dec-80	1.07
9	11-Dec-56	1.16	16-Jan-71	0.97	28-Jan-65	1.16	14-Dec-77	0.90
10	22-Nov-53	1.13	30-Nov-75	0.95	11-Dec-56	1.15	24-Dec-64	0.88
11	21-Dec-55	1.10	13-Jan-95	0.94	22-Feb-86	1.11	27-Dec-73	0.87
12	10-Feb-61	1.07	13-Feb-84	0.93	9-Jan-89	1.03	6-Dec-81	0.81
13	18-Jan-71	1.07	5-Dec-71	0.93	10-Feb-61	1.03	13-Feb-84	0.80
14	25-Dec-80	1.01	23-Jan-82	0.92	13-Feb-84	1.01	28-Jan-65	0.78
15	4-Dec-68	0.98	6-Dec-81	0.92	19-Dec-61	0.99	18-Jan-71	0.78

creation of gaps in the forest, including by clearcutting, because snowpacks accumulate to greater depths during snow precipitation, and melt more rapidly during rain events, than under forest cover (Harr, 1986; Marks and others, 1998). The geomorphic work performed by large floods has profound ecological implications, including changes in riparian structure and function (Swanson and others , 1998; Johnson and others, 2000) and associated changes in aquatic ecology (Hunter, 1998).

Rain-on-snow conditions are a key ingredient of the recipe for the largest floods at the Andrews (Fig. 21). Three factors contribute to this behavior. First, the highest amounts of precipitation occur when snow is on the ground. Second, some subbasins during the period of record had been harvested, and changes in snowpacks augmented their flood peaks by up to 10 or 20% (Jones, 2000). Third, controlling for precipitation amount, some aspect of flood production in subbasins and routing to the Lookout Creek gage augments rain-on-snow peaks beyond those recorded in the control basins (Jones and Perkins, in prep.)

In addition, not all subbasins in the Andrews Forest have an equal capacity to produce large floods. The (log-transformed) distributions of peak discharges from these basins (Fig. 22) shows that Lookout Creek has a much greater capacity to produce large flood peaks than any of the instrumented first and second-order subbasins. This suggests that channel routing and synchrony of flood peaks are critical ingredients in producing the largest floods at Andrews Forest (Perkins and Jones, in prep.; Jones and Perkins, in prep.)

Flood of 1996

The flood of 1996, as does any flood, triggered a great variety of physical processes operating in isolation and in combination. We attempted to capture some of this notion by adopting a disturbance propagation perspective to describe how a suite of processes transforms from one to another down through the stream network (Nakamura and others , 2000). One aspect of this perspective is to place some focus on transitions from one process to the next and the roles of landforms, including roads, in those transformations.

Land use effects are revealed in part by comparisons of effects of floods of 1964-1965 with 1996 (Johnson and others , 1997; Swanson

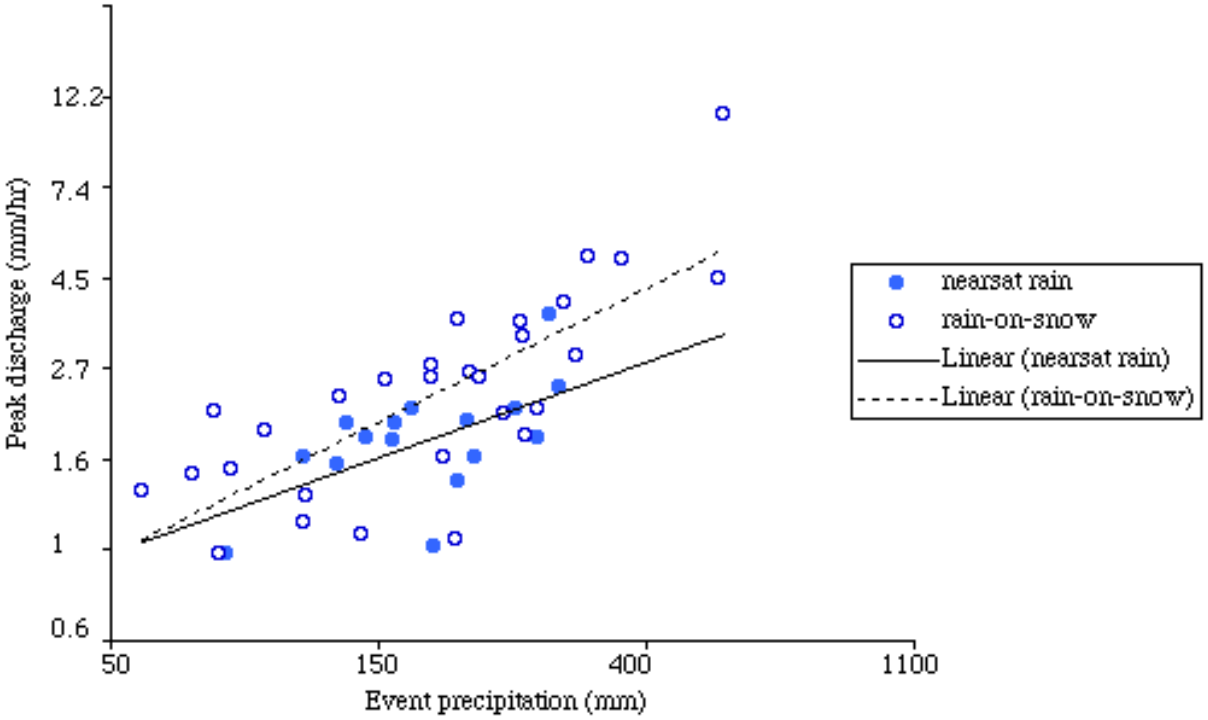

Figure 21. Lookout Creek >0.4 yr peak discharges coded by event type at Watersheds 2, 8; dotted line indicates 1-yr peak discharge; solid line = near saturated rain events; dashed line = near-saturated rain-on-snow events (from Jones and Perkins, in review).

and others, 1998). In the Lookout Creek watershed in 1964, clearcuts less than 15 yr old covered nearly 20% of the landscape accompanied by a road system that included practices of the 1950s. Numerous debris slides and flows occurred in both forest areas and associated with roads and clearcuts. These events delivered batches of large wood to the mainstem channel, where the moving wood appears to have aggravated disturbance of valley floor and riparian forests (Johnson and others , 2000). Paucity of cutting and road construction in the Andrews Forest after 1970 resulted in the 1996 storm sensing a landscape with clearcuts with forest stands mainly over 20 yr in age, a network of older roads where the most unstable sites had failed in earlier storms, and many of the channels most prone to debris flows had been previously flushed of large wood and not had a chance to restock. Therefore, the watershed seems to have had a more muted response to the 1996 flood.

Ecological responses to the 1996 flood ranged greatly by physical capability and life history traits of individual species and by location within the watershed (Swanson and others, 1998). The more mobile stream and riparian species generally showed little population response to the flood, and some species exhibited positive responses over the next few years, such as cutthroat trout that may have benefited by more extensive, cleaner spawning gravel. Where wood moved though mainstem channels in congested masses, such as below the confluence of a channel that debouched a debris flow, stands of young red alder (*Alnus rubra*) riparian vegetation were commonly removed (Johnson and others , 2000). Where wood moved in uncongested fashion (individual pieces) toppling of riparian alder was

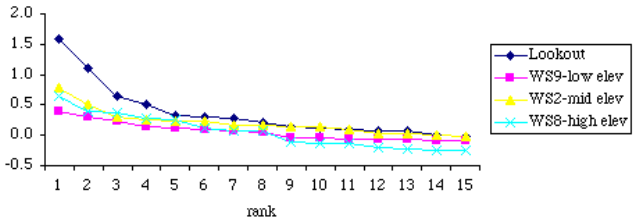

Figure 22. Frequency distribution of 15 largest peak discharges in small subbasins (Watersheds [WS] 2, 8, 9, each ~1% of Lookout) of Lookout Creek. Units are 1n(peak discharge, $m^3/s/km^2$).

more common. Simple inundation of streamside alder trees by water and sediment caused little mortality. Much of this riparian disturbance occurred in sites previously disturbed by the 1964-1965 floods. Some sites have geomorphic conditions favoring disturbance, such as proximity to sources of mobile wood and locations in flow paths.

Floods and Stream Channel Changes

Stream channels experienced varied amounts of change in response to floods (Faustini, 2000). Stream cross sections have been instrumented at five locations in Andrews Forest since 1978, with approximately annual repeat surveys (Fig. 23).

The presence of large wood in stream channels increases channel resistance to change during small (5-7 yr return period) floods in the Mack Creek cross-section sites (see Fig. 23) (Faustini and Jones, in review). The longitudinal profile of a site without large wood at the Mack Creek clearcut reach (MCC) is more variable than the reach with large wood (MAC in old-growth forest) at the finest scale (~1 m) due a greater frequency of boulder steps, but the reach with large wood is more variable at the channel unit scale. The reach with abundant large wood was less responsive to moderate streamflow events (return period < 5-7 yr), but it responded similarly to peak flows with a return period of about 10-25 yr. Although the average magnitude of cross-section changes was the same during the largest flood in the record (25 yr return period), the reach without large wood experienced scour and coarsening of the bed surface, whereas the reach with large wood experienced aggradation upstream of large wood structures. Mack Creek may be representative of many steep mountain streams in which channel structure is controlled by nonfluvial processes: a legacy of large boulders from glacial or mass-movement processes and a legacy of dead wood from ecological processes (Faustini and Jones, in review).

At the Lower Lookout Site (LOL), the stream channel experienced a cycle of changing roles of wood interacting with the stream channel (Fig. 24). After the major floods of 1964, 1965, and 1972, the stream channel lacked large

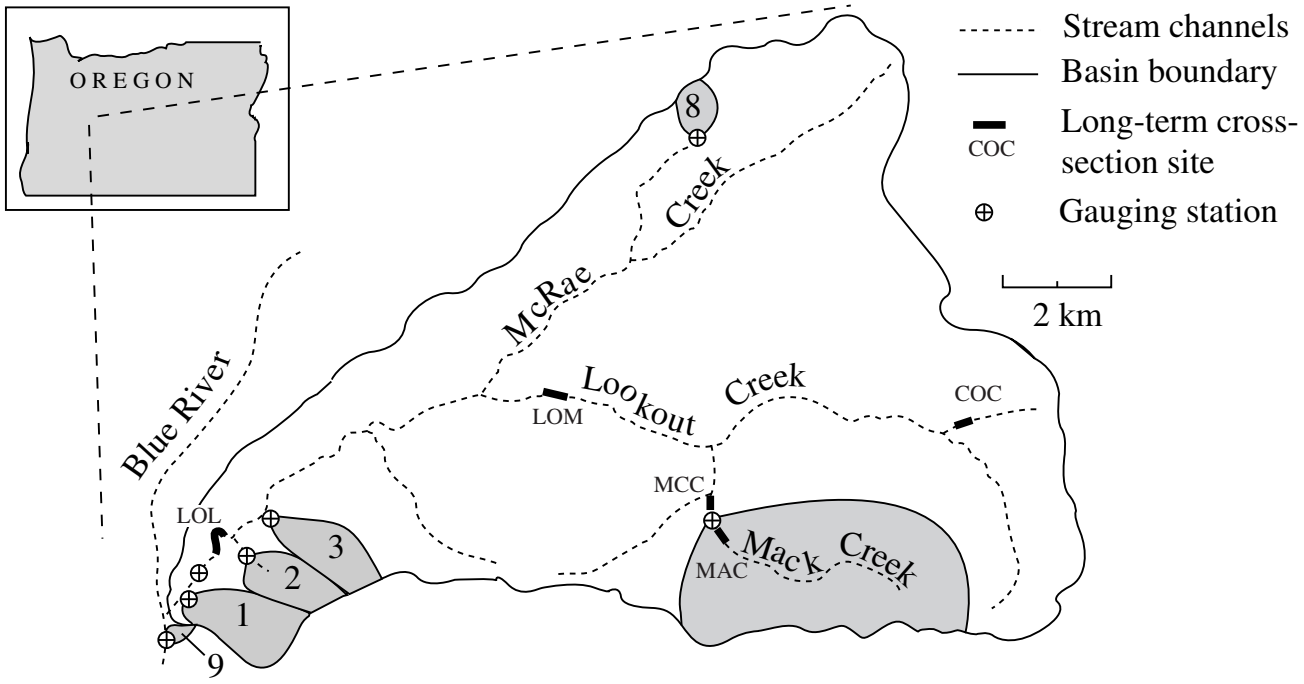

Figure 23. Location of long term cross-section monitoring sites, small experimental watersheds, and gauging stations in the Lookout Creek Watershed.

wood (Fig. 24a). By 1984, several large wood pieces had fallen into the channel and some pieces had floated in from upstream (Fig. 24b). By 1990, small floods had brought in small wood pieces that accumulated to create wood jams (Fig. 24c). In the 1996 flood, all of this wood was removed (Fig. 24d). Today this section has accumulated more pieces of large wood, beginning to resemble the 1984 diagram.

Both minor and major changes in stream channel cross-sectional geometry were documented over the period 1978-1997. Cross sections 5-8 at the lower Lookout Creek site, for example, experienced major changes in the stream channel during the 1996 flood, but only minor changes from 1996-1998 (Fig. 25).

At the watershed scale, results of long-term cross-section monitoring support the idea that the spatial scale and frequency of channel adjustment should increase in the downstream direction. The magnitude of channel response was log-linearly related to flood-return period, but channel responsiveness (the slope of this relationship) varied among sites (Faustini, 2000). The high-gradient first-order stream, Cold Creek, which has large boulders and large wood, had only minor change in response to any flow during the monitored period. Some intriguing differences were apparent in the responses of the third-order streams with and without large wood, and the fourth- and fifth-order streams. This pattern is the expected result of a downstream increase in sediment supply relative to transport capacity, which results in more transportable sediment in the channel and hence increased bed mobility. Consistent with this hypothesis, cross sections from the fourth- and fifth-order sites exhibit larger, more frequent and, in years with large flood events, more spatially continuous, changes than cross sections at second- and third-order sites (Fig. 26). At finer scales, this pattern is modified by variations in the degree of channel confinement by bedrock and landforms, the abundance of large roughness elements, such as individual large logs and log jams, and local stochastic processes, such as debris flow inputs from tributaries (Faustini, 2000).

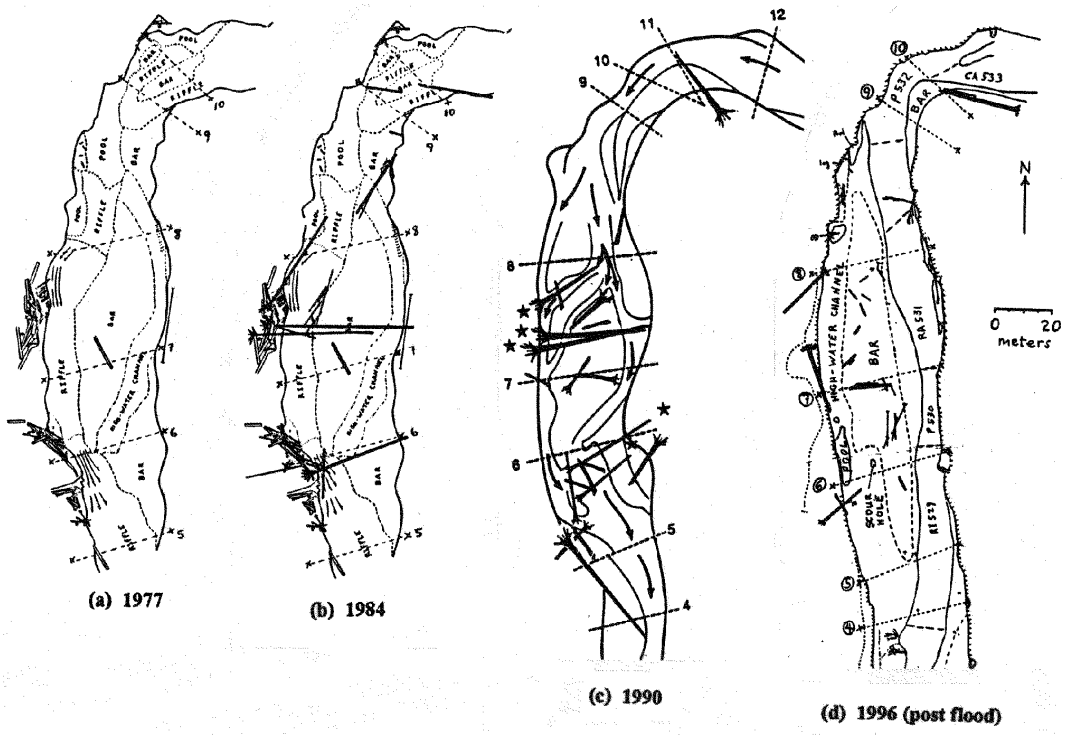

Figure 24. Schematic diagrams of the lower Lookout cross-section site in (a) 1977, (b) 1984, (c) 1990, and (d) 1996 after the flood (from Nakamura and Swanson, 1993; Faustini, 2000).

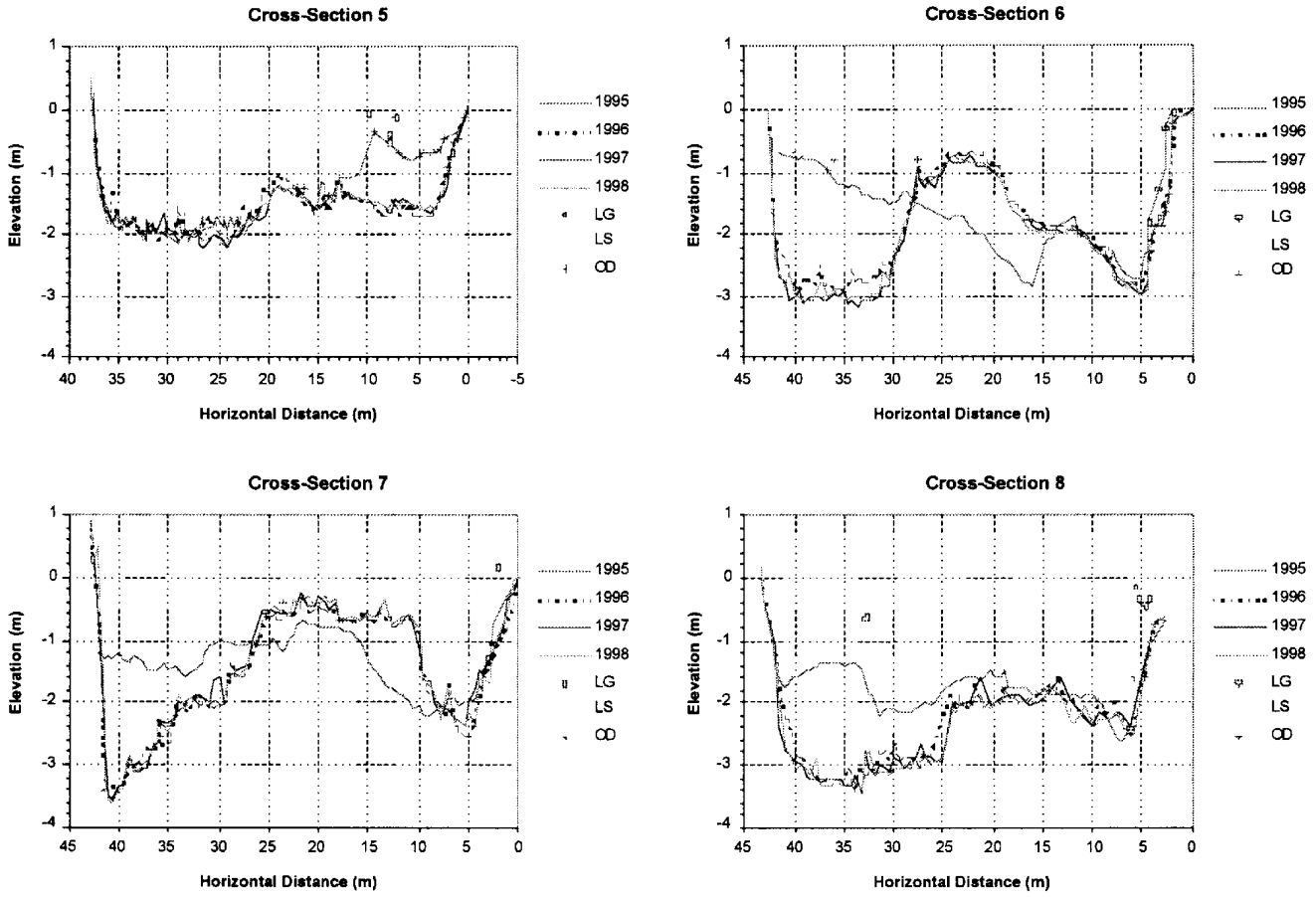

Figure 25. Selected cross-section profile plots for the Lower Lookout Creek (LOL) Site, 1995-98. Cross-section locations are shown in Figure 23 (from Faustini, 2000).

WOOD IN STREAMS (Frederick J. Swanson)

Wood in streams has been an important theme of Andrews Forest research since the early 1970s, beginning with inventory of wood as part of stream-ecology studies (Froehlich, 1973) and then mapping of wood to assess structure and dynamics (Swanson and others , 1976; Lienkaemper and Swanson, 1987). Initial emphasis was on ecologic and geomorphic functions of static wood pieces and accumulations in streams. Studies in part of the River Continuum project (Vannote and others, 1980), which occurred in the Andrews Forest and four other sites across the country, placed emphasis on variation in wood conditions and processes down through a stream network (Keller and Swanson, 1979). Later modeling studies (Braudrick and others , 1997; Braudrick and Grant, 2000) and the experience of the 1996 flood (Swanson and others, 1998; Johnson and others, 2000) led to interest in the ecologic functions of mobile wood. Static wood can protect patches of riparian vegetation from flood disturbance, but once the wood begins to move can it serve as tools for riparian disturbance.

Amount, arrangement, dynamics, and functions of wood vary with stream size. Small (first- and second-order) streams flowing through old-growth Douglas fir forest contain large amounts of wood (500 to >1000 m^3/ha, Harmon and others , 1986) generally randomly located where it fell from the adjacent stand. In channels subject to periodic debris flows this material and associated sediment deposits may undergo cycles of gradual filling and abrupt evacuation. The third-order Mack Creek flowing through old growth contains about 600 m^3/ha of wood that is somewhat clumped around large "key" pieces which anchor jams. Long-

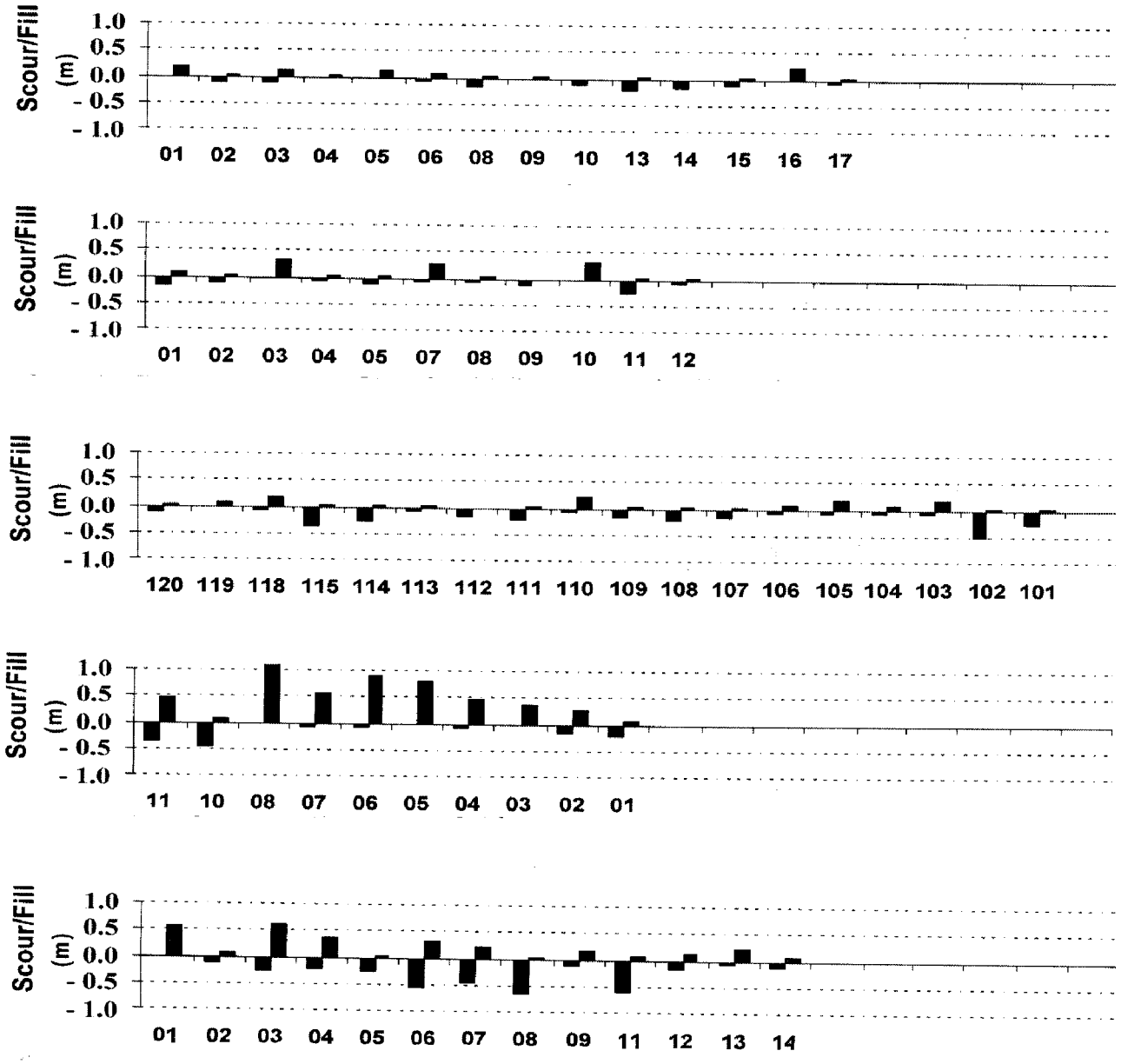

Figure 26. Changes in scour and fill at Andrews Forest cross sections during the February 1996 flood at sites from the top shown on Figure 23: COC, MAC, MCC, LOM, LOL (Faustini, 2000).

term observations indicate that wood pieces longer than channel width tend to remain in place, but smaller pieces can be moved during high flows (Lienkameper and Swanson, 1987). Lower Lookout Creek (fifth order) contained about 200 m^3/ha in the late 1970s, but the amount and arrangement varied rather dramatically with gradual accumulation over the 1964-1996 interflood period and then substantial flushing in the 1996 flood. In progressively larger channels the relative importance of wood-delivery processes shifts, and a higher proportion of pieces is mobile. This results in attendant shifts in patterns of structures (more aggregation) and functions (reduced sediment-storage function) (Keller and Swanson, 1979).

Forest-stand conditions, such as size distribution of trees, species, stocking levels, and disturbance history affect past, present, and future conditions of wood in streams. More massive and productive forests with wood of slow decay rates and tendency to topple as fresh wood (vs. dying and decaying while standing) are conditions that favor accumulation of high levels of wood in streams (Harmon and others, 1986).

Wood pieces have been placed in streams throughout the Pacific Northwest with the intent of improving fish habitat. However, few experiments have been conducted to assess effects of these practices. Two studies are underway in the Andrews Forest and vicinity: the Quartz Creek (South) Study with wood structures placed in a single reach and the Pool Complexity Study with installations of three levels of wood complexity in pools with treatments replicated at three study reaches. Three of four sets of structures survived the 1996 flood well. In the fourth case, sediment deposition in pools and lateral channel change rendered many structures ineffective. Fish response to the structures has been nil to slightly positive—more wood equals more fish. The Quartz Creek Study demonstrated that placement of the largest part of the size distribution of wood found in an old-growth reach (Mack Creek used as reference) resulted in recruitment of the full old-growth size distribution of wood pieces in about 5 yr, as a result of input from upstream and the adjacent riparian stand (Fig. 27 and 28).

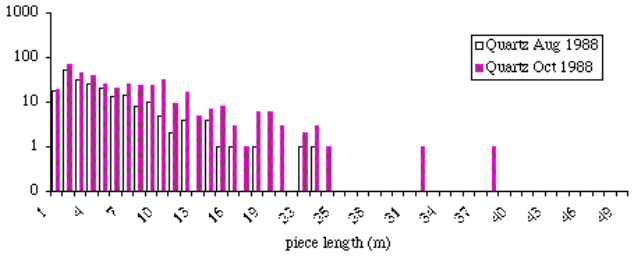

Figure 27. Quartz Creek (South) wood piece size distributions in stream before and after placement of large pieces in 1988 (from Randy Wildman, Oregon State University).

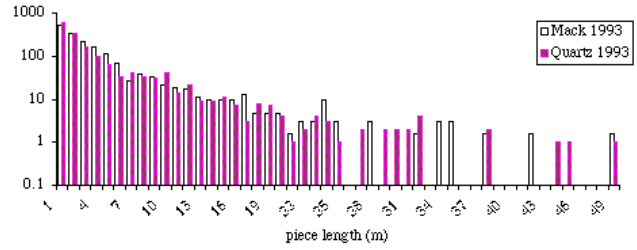

Figure 28. Quartz Creek (South) wood piece size distribution at year 5 after wood input (1993), relative to wood distribution in old-growth stream at Mack Creek in 1993 (from Randy Wildman, Oregon State University).

ROAD HYDROLOGY AND GEOMORPHOLOGY (Frederick J. Swanson, Julia A. Jones, and Beverley C. Wemple)

Effects of roads on routing of water, sediment, wood, and other materials, such as propagules of exotic plants, through landscapes have been the subjects of many studies in the Andrews Forest. These studies have taken a variety of perspectives, such as focus on processes of peak-flow generation and routing of sediment and disturbances through stream networks. From a landscape-ecology perspective we are interested in how road networks interact with stream networks in part because concepts of network properties are not well developed in this field, which has been dominated by terrestrial ecology studies in landscapes composed of vegetation patchworks. On a fundamental level, roads can be viewed as corridors facilitating movement along them, barriers to movement, sources of materials, such as landslides, or sinks for organisms or materials, such as roadkill reducing a population of organisms (Fig. 29). We therefore examine how road segments function in relation to their location in the landscape, such as proximity to ridges and patterns of intersection with stream networks. Beverley Wemple's work gives examples of many of these issues (Wemple and others, 1996, 2001; Wemple, 1998).

To test the hypothesis that roads may increase peak flows in Watershed 3 in the Andrews Forest (Jones and Grant, 1996), Wemple surveyed apparent extent of road ditches that carry channelized flow, similar to the stream network. Upper Blue River and Lookout Creek have drainage densities of about 3.0 km km^{-2} and road densities of 1.9. Wemple and others (1996) found that about 60% of the road network seemed to route surface runoff and subsurface water caught in cutslopes down ditches and into the natural drainage network. Work to measure water routing associated with roads in upper Watershed 3 seems to confirm that such processes can contribute to increased peak flows from this 100 ha watershed (Wemple, 1998; Wemple and Jones, in review).

The February 1996 flood triggered varied types of erosion and deposition events (Fig. 30) associated with roads in the upper Blue River and Lookout Creek area.

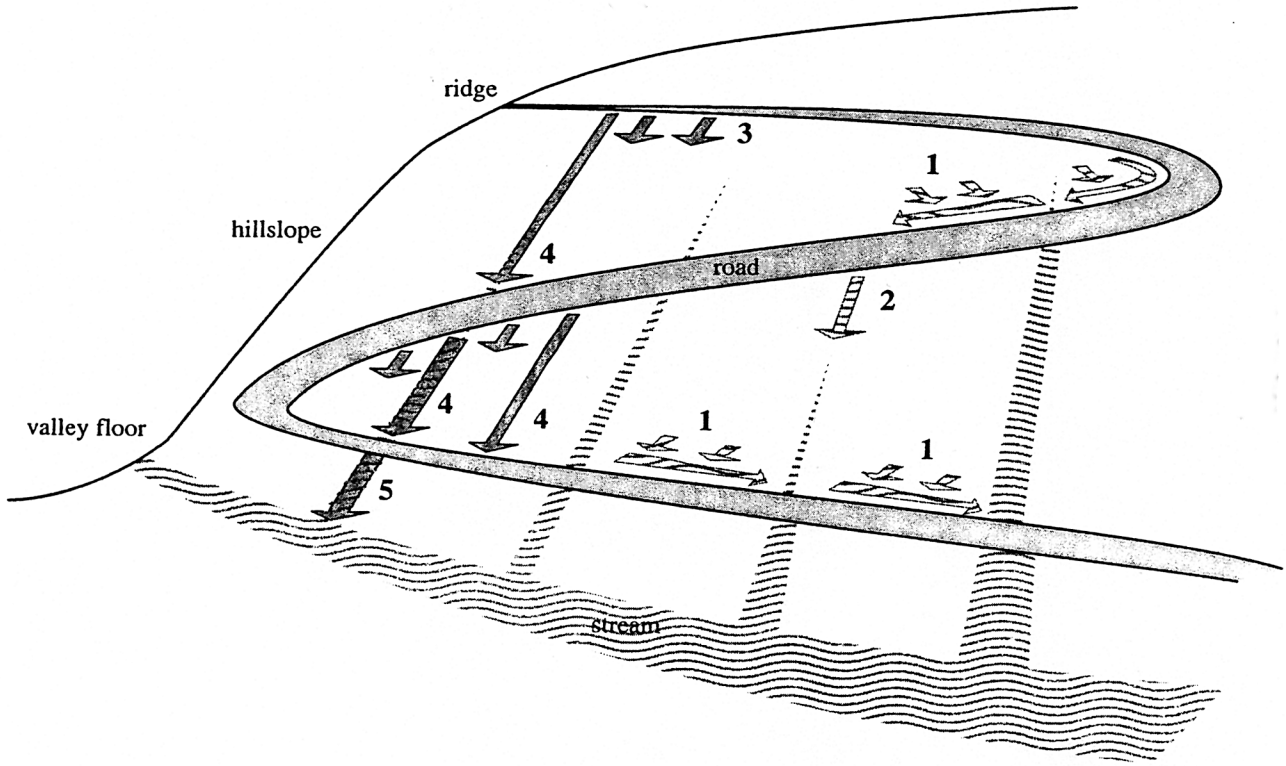

Figure 29. Interactions between road and stream networks. The road network consists of a valley floor road segment parallel to a large stream, hillslope road segments perpendicular to streams, and near-ridge roads without streams. Roads (1) intercept water in surface and subsurface flowpaths, (2) alter water flowpaths and extend the channel network, (3) initiate mass movements of sediment in unstable roadfills, (4) deposit sediment moved by mass movements on roads and (5) on valley floors. Overall, roads function to divert water and sediment from paths followed in roadless landscapes, and they initiate multiple new cascading flowpaths.

Wemple and others (2001) inventoried these events and stratified their occurrence on the upper slope (within 100 m of ridge), midslope (below the upper slope zone), and valley floor (floodplain, terrace, alluvial fan landforms). Frequency of these features increased downslope (Table 4). Roads caused cascades of events involving transformations from one type of sediment-transport process to another. For example, excess bedload plugged culverts, diverting flow down a ditch, which was gullied, until water flowed over the road, saturating a fill, leading to a fillslope slide (Fig. 31). Upper-slope roads were net sources of sediment (0 m^3 reached the road from upslope and 5450 m^3 moved downslope from roads). Midslope roads were net sources of sediment to downslope areas (12,500 m^3 reached roads, 27,100 m^3 moved downslope). Valley floor roads were net sinks for sediment (13,200 m^3 reached roads, 6,100 m^3 moved downslope).

DEBRIS SLIDES AND DEBRIS FLOWS

(Frederick J. Swanson and Kai U. Snyder)

Shallow (failure planes 1-3 m deep), rapid (up to approximately 10 m s^{-1}) mass movements of soil, sediment, and organic matter are common in the Andrews Forest, as they are elsewhere in western Oregon and similar steep wet landscapes. Terminology for these processes has changed somewhat over the years; we use *debris slide* to refer to processes operating on hillslopes and *debris flow* to refer to processes in stream channels. Commonly debris slides continue their movement down channels. We make the slope-channel distinction because of the different implications for the ecosystem, sediment routing, and land management.

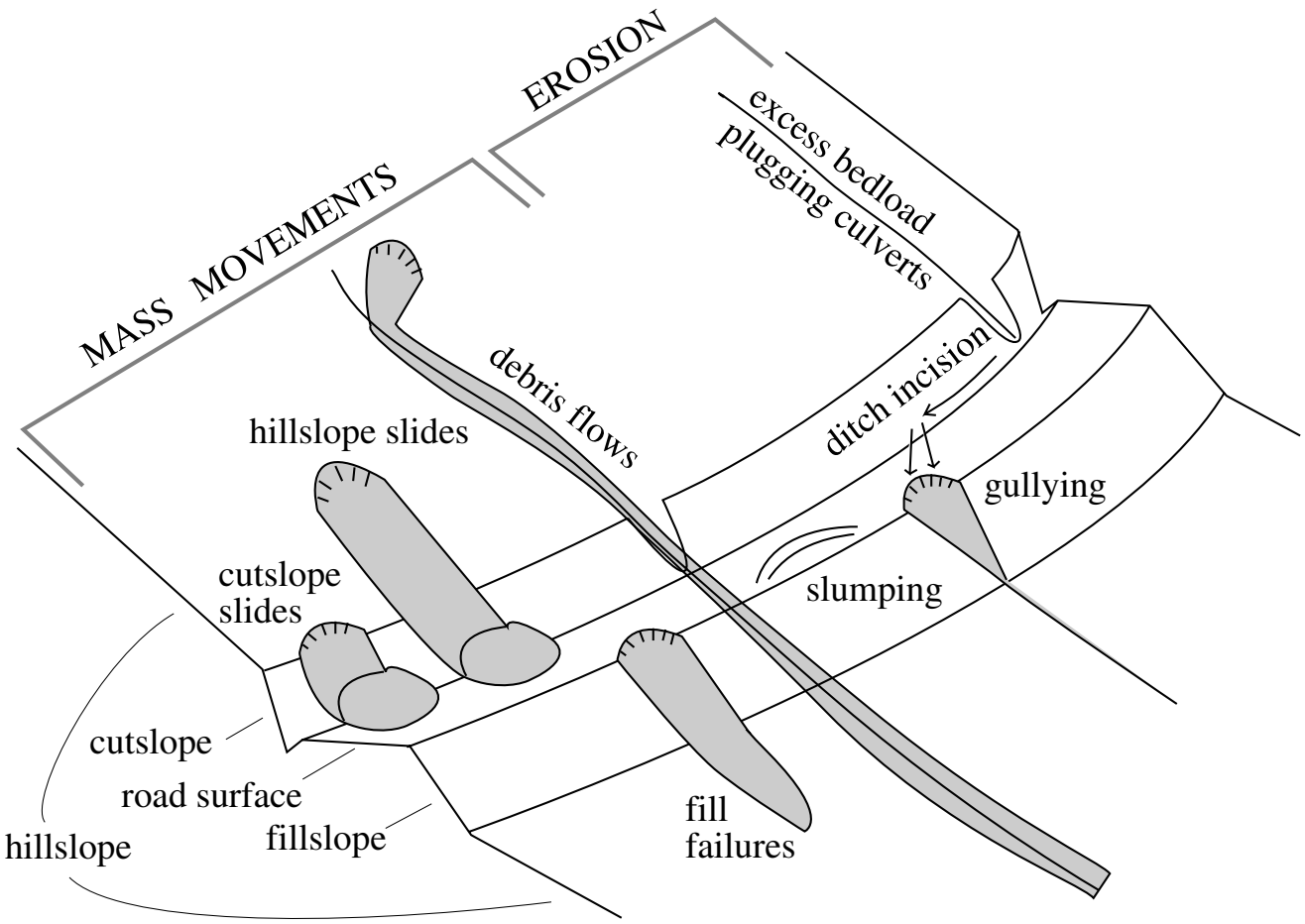

Figure 30. Eight types of road failures inventoried in the Lookout Creek and Blue River watershed (from Wemple and others, 2001).

Effects of land management on these processes and the role of mass movements of different types in natural systems on sediment production, routing, and ecosystem disturbance have been important research themes at Andrews Forest since early efforts to document these processes mainly in the context of small-watershed studies (Fredriksen, 1970). Inventory of debris slides and flows for the 1950-1975 period revealed that (1) these are natural processes under forest cover, (2) the landscape can be broadly zoned into areas with different susceptibility to sliding, (3) recently (<20 yr) clearcut areas had soil erosion rates by slides that exceeded uncut forest rates by several fold, and (4) road rights-of-way had soil erosion rates about 30 times forest rates (Dyrness, 1967; Swanson and Dyrness, 1975). These findings parallel results of similar inventories elsewhere in slide-prone landscapes.

The occurrence of numerous debris slides and debris flows in the February 1996 flood prompted updating of these inventory records. The extent of slides and flows in forested parts of the watershed were similar in 1996 and 1964-1965, which, along with similarities of discharge from the low-elevation experimental watersheds, suggests that these events had similar effects on soil moisture conditions. The near absence of logging and road construction in the watershed since 1970 made it possible to examine effects of about 25 yr of passive watershed restoration from past forestry land use and glimpse into future effects of establishment of Late Successional Reserves as part of the Northwest Forest Plan. The rate of sliding from clearcut areas was much lower in the 1996 storm, possibly because the greater age of cutting units permitted recovery of root strength and site hydrologic processes and

Table 4. Distribution and frequency (numbers per kilometer of road length) of mass movement and fluvial features associated with roads, according to hillslope position and function of the road in intercepting or producing sediment (from Wemple and others, 2001).

Slope position / function	Road length (km)	Number		Frequency (no./km)	
		Mass movement	Fluvial feature	Mass movement	Fluvial feature
Upper slope					
Intercepted by roads		0	0	0	0
Produced on roads		5	0	0.05	0
Total	102	5	0	0.05	0
Midslope					
Intercepted by roads		11	9	0.05	0.04
Produced on roads		41	5	0.20	0.02
Total	205	52	14	0.25	0.07
Valley floor					
Intercepted by roads		10	4	0.24	0.10
Produced on roads		10	8	0.24	0.20
Total	41	20	12	0.49	0.29

perhaps because unstable sites had failed in earlier storms. The 91 inventoried debris flows occurring in the 1946-1996 period took place in only 12 yr and 75% occurred in 1964-1965 and 1996 (Snyder, 2000). Inventoried debris slides occurred mainly in the lower elevation parts of the landscape (Fig. 32) where slopes are steep, soils contain expansive clays, early land-use practices were most extensive, and snowmelt during warm rain events has the greatest potential to create extreme soil-water conditions.

From an ecologic perspective we have been interested in how debris flows create disturbance patches and leave refuges in stream networks (Fig. 32). Note that the stream networks of some tributary watersheds have been thoroughly scoured by debris flows. However, most tributary watersheds contain first-order and in some cases larger channels that were not scoured, thus providing relatively intact stream and riparian ecosystems to serve as refuges through the 1996 flood and sources of organisms for recolonization of severely disturbed stream reaches.

WATER USE BY MAJOR TREE SPECIES

(Barbara J. Bond, Julia A. Jones, Georgianne Moore, Jeff McDonnell, and Nathan Phillips)

Vegetation water use by evapotranspiration accounts for an estimated 500 mm annually in old-growth forests at the Andrews, based both on water budgets and on measured increases in annual water yield after forest canopy removal (see stream response module). Recovering forest, aged 30 to 35 yrs, may use up to 150 or 200 mm of water per year. Vegetation may influence water budgets through a variety of processes, including interception (both of precipitation and of cloudwater), evaporation, and transpiration.

Since 1999, new research at the Andrews Forest has focused on measuring vegetation water use, particularly in Watersheds 1 (clearcut in 1962-66) and 2 (control) (see Table 1 of introduction). In the summers of 1999 and 2000, sap flow was measured at 20-minute intervals in trees of varying ages and species. In 1999, sap flow was measured from July 1–September 8 in seven Douglas fir and seven red alder, selected to represent the typical range in

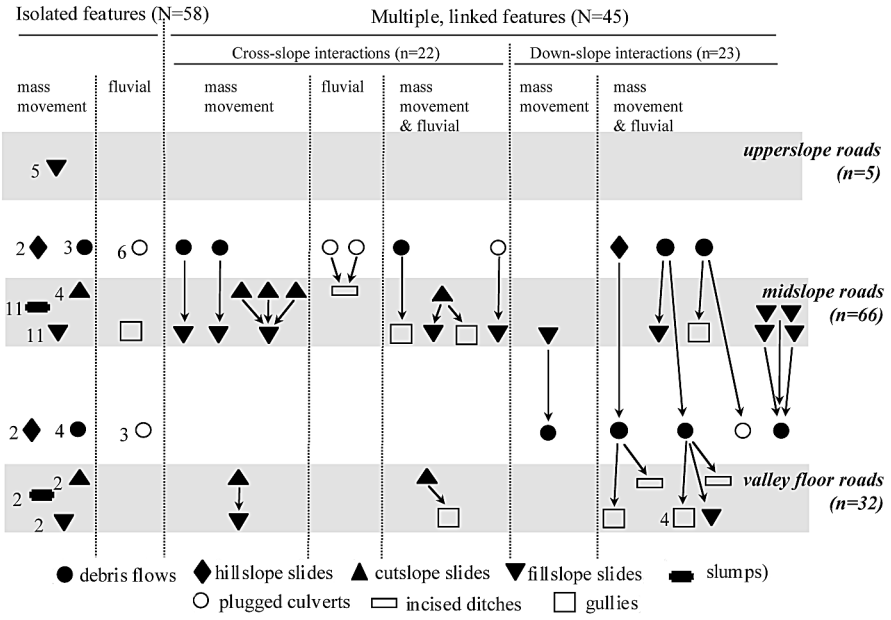

Figure 31. Mass movements and fluvial features associated with roads from the flood of February 7, 1996, as a function of hillslope position (Wemple and others, 2001). Arrows indicate features that triggered an associated feature, and numbers beside symbols indicate number of inventoried features of that type.

size for this site, along a ~60-m transect running upslope perpendicular to the stream in Watershed 1. In 2000, sap flow was measured in seven 30-yr-old Douglas fir in Watershed 1 and five 450-yr-old Douglas fir and western hemlock on the alluvial fan donwstream from the gage at Watershed 2 (Bond and others, submitted; Moore and others, in preparation). Tree-level measurements were converted to a ground-area basis using estimates of the sapwood basal area of all woody vegetation from vegetation surveys. In 1999, species and sapwood basal area of trees > 1 cm diameter at breast height were measured in 100 m^2 plots

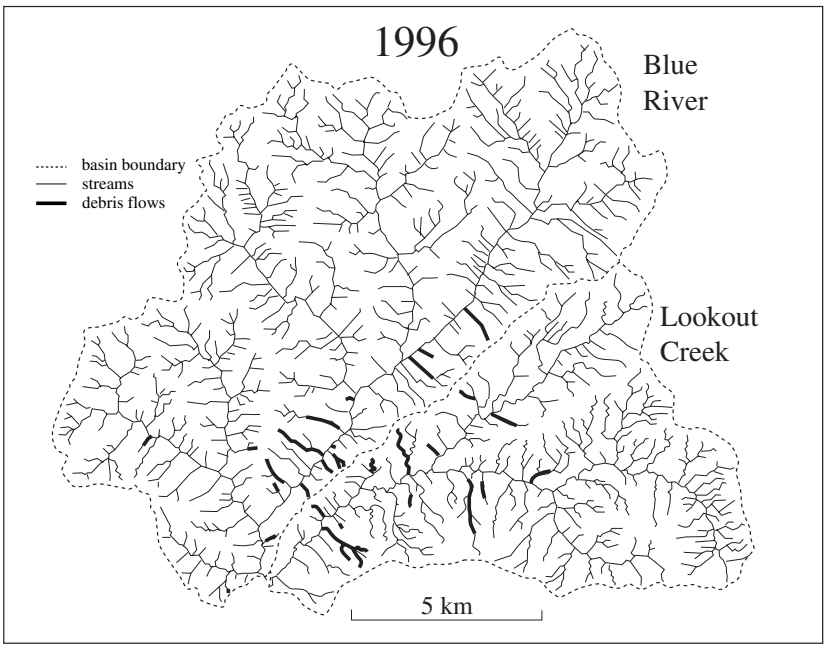

Figure 32. Debris flow paths of Lookout Creek and part of the upper Blue River for 1946-1996 (Snyder, 2000).

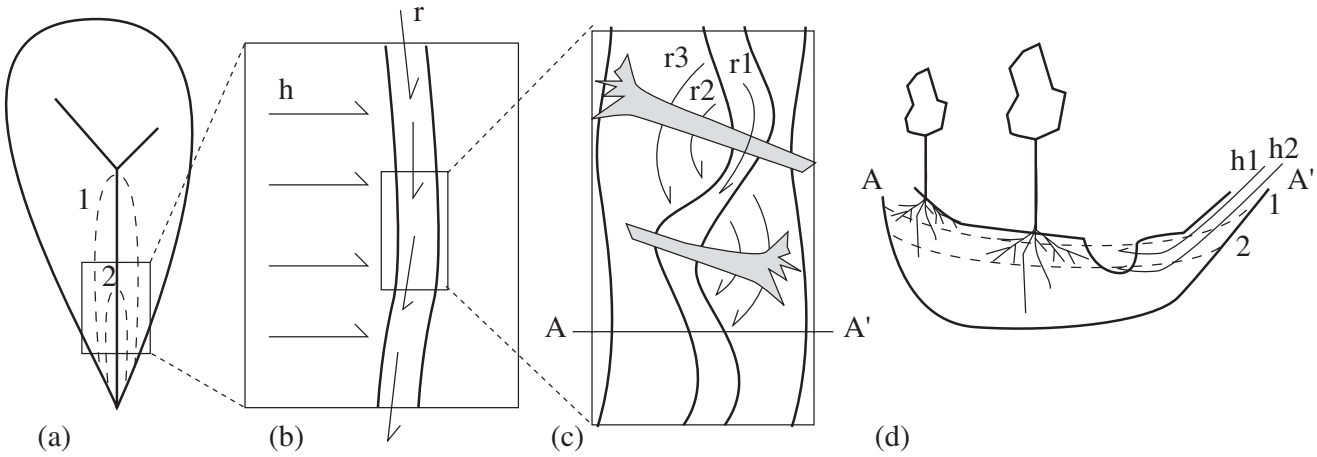

Figure 33. Conceptual model of vegetation-hydrology coupling at diel time scales over the summer baseflow recession period in a headwater basin (Watershed 1) in the Andrews Forest. (a) The basin consists of hillslopes and the valley floor (including the stream channel and floodplain/terraces), the groundwater system, and the riparain zone. (b) Hyrologic flowpaths operate on hillslopes (h) and in the riparian zone (r). (c) Riparian zone flowpaths include in-stream flow (r1), near-stream, fast, hypotheic exchange flowpaths (r2), and far-from-stream, slow, hyporheic exchange flowpaths (r3), created by sediment and large wood stored on the valley floor. (d) A cross section of the valley floor shows shallow flowpaths (h1) and deep flowpaths on hillslopes contributing lateral flow to the valley floor and stream, and the changing positions of a water table or near-saturated zone in early summer (time 1) and late summer (time 2). The vegetation zone of influence on diel cycles in streamflow can be envisioned as an area of lower hillslopes and the riparian zone (a) with a water table at a given height (1 or 2 in part d of figure).

arranged systematically along seven 50 m transects perpendicular to the stream— each transect included five contiguous plots. Douglas fir, *Pseudotsuga menziesii* (Mirb) Franco, accounts for about 66% of the total sapwood basal area and nearly 100% of coniferous basal area within the riparian corridor (arbitrarily defined as a 100-m-wide swath centered on the streambed). Most of the remaining 34% of the sapwood basal area is hardwoods, with big leaf maple, *Acer macrophyllum* , and red alder, *Alnus rubra* Bong, dominating (Bond and others, submitted).

Diel patterns of streamflow and sapflow

A strong diel (day-night) variation was apparent in the stream flow of Watershed 1 during some of the summers from 1952 to the mid-1990s, stimulating the installation of a V-notch weir starting in 1999 to more accurately capture small variations in stream flow. The diel signal in 1999 to 2001 appeared in late June and disappeared by mid-September. Thus, the diel cycle must be due to vegetation water use, rather than to snowmelt or temperature effects on water viscosity. In the early to mid summer, the combination of high evaporative demand, relatively high soil moisture content and very heavy vegetation cover result in very high rates of transpiration. In the spring and early summer, the diel signal was often obscured by precipitation-induced fluctuations in stream flow and cloud cover-induced reductions in transpiration. Both measured transpiration rates and "missing stream flow" (the area between successive daily maximum stream-flows on days without precipitation) were greatest in late June and early July. By mid-July, missing stream flow accounted for between 5 and 6 percent of total daily stream flow (Bond and others , in press).

In early summer (June 24-30), maximum sap flow explained 80% of the variation in minimum stream flow 4 hours later ($r^2 = 0.76$). By August 5-11, maximum sap flow accounted for only 50% of the variation in minimum stream flow, and the lag had increased to 8 hours.

According to our conceptual model (Fig. 33) the strongest coupling and the shortest lag between maximum water use by vegetation

and minimum stream flow each day should occur during the early summer, when vegetation is using water in short hyporheic exchange flowpaths. As the summer progresses, diel stream flow fluctuations become less sensitive to transpiration rates, as vegetation increasingly taps water in long hyporheic exchange flowpaths.. During the early part of the summer (from about June 24 to July 14), transpiration increased, and so did missing stream flow as a percent of total stream flow. The estimated effective zone of influence of vegetation on daily stream flow was only about 0.3 ha (0.3% of the total basin) in the early summer. However, during the latter part of the summer (from about July 15 to August 11), transpiration decreased only slightly, but missing stream flow as a percent of total stream flow declined significantly. The estimated zone of influence contracted in the late summer compared with early summer. We infer that from July 15 onward, vegetation water use was increasingly decoupled from the short hyporheic exchange flowpaths and increasingly coupled to long hyporheic exchange flowpaths (Bond and others, in press).

REFERENCES

Beschta, R.L., Pyles, M.R., Skaugset, A.E., and Surfleet, C.G., 2000, Peakflow responses to forest practices in the western cascades of Oregon, USA: Journal of Hydrology, v. 233, p. 102-120.

Bond, B.J., Jones, J.A., Moore, G., Phillips, N., Post, D.A., and McDonnell, J.J., in press, The zone of vegetation influence on baseflow revealed by diel patterns of streamflow and vegetation water use in a headwater basin: Hydrological Processes.

Braudrick, C.A., and Grant, G.E., 2000, When do logs move in rivers?: Water Resources Research, v. 36, p. 571-583.

Braudrick, C.A., Grant, G.E., Ishikawa, Y., and Ikeda, H., 1997, Dynamics of wood transport in streams: A flume experiment: Earth Surface Processes and Landforms, v. 22, p. 669-683.

Dyrness, C.T., 1967, Mass soil movements in the H.J. Andrews Experimental Forest: U.S. Forest Service Pacific Northwest Forest and Range Experiment Station Research Paper PNW-42, 13 p.

Dyrness, C.T., 1969, Hydrologic properties of soils on three small watersheds in the western Cascades of Oregon: U.S. Forest Service Pacific Northwest Forest and Range Experiment Station Research Note PNW-111, 17 p.

Dyrness, C.T., 1973, Early stages of plant succession following logging and burning in the western Cascades of Oregon: Ecology, v. 54, p. 57-69.

Faustini, J.M., 2000, Stream channel response to peak flows in a fifth-order mountain watershed: Oregon State University PhD Dissertation, 339 p.

Faustini, J.M., and Jones, J.A., submitted, Influence of large woody debris on channel morphology and dynamics in steep, boulder-rich mountain streams, western Cascades, Oregon: Geomorphology.

Fredriksen, R.L., 1970, Erosion and sedimentation following road construction and timber harvest on unstable soils in three small western Oregon watersheds: U.S. Forest Service Pacific Northwest Forest and Range Experiment Station Research Paper PNW-104, 15 p.

Fredriksen, R.L., 1971, Comparative chemical water quality in natural and disturbed streams following logging and slash burning, *in* Proceedings of a Symposium on Forest Land Uses and Stream Environment, Corvallis, Oregon, October 1970: Oregon State University Continuing Education Publications, p. 125-137.

Fredriksen, R.L., 1972, Impact of forest management on stream water quality in western Oregon, *in* Mater, M.H., ed., Pollution abatement and control in the forest products industry, 1971-1972: Forest Products Research Society Proceedings, 26th Annual Meeting, June 1972, Dallas, Tex., p. 37-50.

Froehlich, H.A., 1973, Natural and man-caused slash in headwater streams: 33rd Pacific Logging Congress, Portland, Ore., Loggers Handbook.

Grant, G.E., 1997, Critical flow constrains flow hydraulics in mobile-bed streams: A new hypothesis: Water Resources Research, v. 33, p. 349-358.

Grant, G.E., and Hayes, S.K., 2000, Geomorphic response to peak flow increases due to forest harvest activities, western Cascades, Oregon : Eos, v. 81, p. S220.

Grant, G.E., and Swanson, F.J., 1995, Morphology and processes of valley floors in mountain streams, western Cascades, Oregon, *in* Costa, J.E., Miller, A.J., Potter, K.W., and Wilcock, P., eds., Natural and anthropogenic influences in fluvial geomorphology: The Wolman volume: American Geophysical Union Geophysical Monograph 89, p. 83-101.

Grant, G.E., Swanson, F.J., and Wolman, M.G., 1990, Pattern and origin of stepped-bed morphology in high-gradient streams, Western Cascades: Oregon: Bulletin of the Geological Society of America, v. 102, p. 340-352.

Grant, G.E., and Wolff, A.L., 1991, Long-term patterns of sediment transport after timber harvest, western Cascade Mountains, Oregon, USA, *in* Peters, N.E., and Walling, D.E., eds., Sediment and stream water quality in a changing environment: Trends and explanation: Proceedings of the Vienna IAHS Symposium, Vienna, Austria, August 1991, International Association of Hydrological Sciences Publication 203, p. 31-40.

Greenland, D., Bierlmaier, F., Jones, J., McKee, A., Means, J., Swanson, F., and Whitlock, C., in preparation, Climate variability and ecosystem response at the H.J. Andrews Long-Term Ecological Research Site, *in* Greenland, D., ed., Climate variability and ecosystem response: New York, Oxford University Press.

Halpern, C.B., 1989, Early successional patterns of forest species: Interactions of life history traits and disturbance: Ecology, v. 70, p. 704-720.

Halpern, C.B., and Spies, T.A., 1995, Plant species diversity in natural and managed forests of the Pacific Northwest: Ecological Applications, v. 5, p. 913-934.

Harmon, M.E., Franklin, J.F., Swanson, F.J., Sollins, P., Gregory, S.V., Lattin, J.D., Anderson, N.H., Cline, S.P., Aumen, N.G., Sedell, J.R., Lienkaemper, G.W., Cromack, K., Jr., and Cummins, K.W., 1986, Ecology of coarse woody debris in temperate ecosystems, *in* MacFadyen, A., and Ford, E.D., eds., Advances in ecological research: Orlando, Academic Press, p. 133-302.

Harr, R.D., 1977, Water flux in soil and subsoil on a steep forested slope: Journal of Hydrology, v. 33, p. 37-58.

Harr, R.D., 1981, Some characteristics and consequences of snowmelt during rainfall in western Oregon: Journal of Hydrology, v. 53, p. 277-304.

Harr, R.D., 1986, Effects of clearcutting on rain-on-snow runoff in western Oregon: A new look at old studies: Water Resources Research, v. 22, p. 1095-1100.

Hunter, M.G., 1998, Watershed-level patterns among stream amphibians in the Blue River Watershed, west-central Cascades of Oregon: Oregon State University MS Thesis, 97 p.

Johnson, S.L., Grant, G.E., Swanson, F.J., and Wemple, B.C., 1997, Lessons from a flood: An integrated view of the February 1996 flood in the McKenzie River Basin, *in* Laenen, A., ed., The Pacific Northwest Floods of February 6-11, 1996: Proceedings of the Pacific Northwest Water Issues Conference, Portland, Ore., October 1997, American Institute of Hydrology, p. 159-167.

Johnson, S.L., and Jones, J.A., 2000, Stream temperature responses to forest harvest and debris flows in western Cascades, Oregon: Canadian Journal of Fisheries and Aquatic Sciences, v. 57 (Suppl. 2), p. 30-39.

Johnson, S.L., Swanson, F.J., Grant, G.E., and Wondzell, S.M., 2000, Riparian forest disturbances by a mountain flood—The influence of floated wood: Hydrological Processes, v. 14, p. 3031-3050.

Jones, J.A., 2000, Hydrologic processes and peak discharge response to forest removal, regrowth, and roads in 10 small experimental basins, western Cascades, Oregon: Water Resources Research, v. 36, p. 2621-2642.

Jones, J.A., and Grant, G.E., 1996, Peak flow responses to clear-cutting and roads in small and large basins, western Cascades, Oregon: Water Resources Research, v. 32, p. 959-974.

Jones, J.A., and Grant, G.E., 2001a., Comment on "Peak flow responses to clear-cutting and roads in small and large basins, western Cascades, Oregon: A second opinion" by R.B. Thomas and W.F. Megahan: Water Resources Research, v. 37, p. 175-178.

Jones, J.A., and Grant, G.E., 2001b, Comment on "Peak flow responses to clear-cutting and roads in small and large basins, western Cascades, Oregon" by J.A. Jones and G.E. Grant: Water Resources Research, v. 37, p. 179-180.

Jones, J.A., and Perkins, R.M., in preparation, Rain-on-snow floods, forest canopy removal, and flood routing in forested basins, western Cascades, Oregon.

Jones, J.A., and Post, D.A., in preparation, Contrasting streamflow responses to harvest at four diverse forested sites.

Jones, J.A., Swanson, F.J., Wemple, B.C., and Snyder, K.U., 2000, Effects of roads on hydrology, geomorphology, and disturbance patches in stream networks: Conservation Biology, v. 14, p. 76-85.

Keller, E.A., and Swanson, F.J., 1979, Effects of large organic material on channel form and fluvial processes: Earth Surface Processes, v. 4, p. 361-380.

Levno, A., and Rothacher, J., 1969, Increases in maximum stream temperatures after slash burning in a small experimental watershed: U.S. Forest Service Pacific Northwest Forest and Range Experiment Station Research Note PNW-110, 7 p.

Lienkaemper, G.W., and Swanson, F.J., 1987, Dynamics of large woody debris in streams in old-growth Douglas-fir forests: Canadian Journal of Forest Research, v. 17, p. 150-156.

Luoma, J.R., 1999, The hidden forest: The biography of an ecosystem: New York, Henry Holt and Company, 228 p.

Marks, D., Kimball, J., Tingey, D., and Link, T., 1998, The sensitivity of snowmelt processes to climate conditions and forest cover during rain-on-snow: A case study of the 1996 Pacific Northwest flood: Hydrological Processes, v. 12, p. 1569-1587.

Marshall, J.D., and Waring, R.H., 1986, Comparison of methods of estimating leaf-area index in old-growth Douglas-fir: Ecology, v. 67, p. 975-979.

Martin, C.W., and Harr, R.D., 1988, Precipitation and streamwater chemistry from undisturbed watersheds in the Cascade Mountains of Oregon: Water, Air, and Soil Pollution, v. 42, p. 203-219.

Martin, C.W., and Harr, R.D., 1989, Logging of mature Douglas-fir in western Oregon has little effect on nutrient output budgets: Canadian Journal of Forest Research, v. 19, p. 35-43.

Nakamura, F., and Swanson, F.J., 1993, Effects of coarse woody debris on morphology and sediment storage of a mountain stream system in western Oregon: Earth Surface Processes and Landforms, v. 18, p. 43-61.

Nakamura, F., Swanson, F.J., and Wondzell, S.M., 2000, Disturbance regimes of stream and riparian systems—A disturbance-cascade perspective: Hydrological Processes, v. 14, p. 2849-2860.

Perkins, R.M., and Jones, J.A., in preparation, Climatic and physiographic controls on peak discharges in small forested basins, western Cascades, Oregon.

Pyles, M.R., Mills, K., and Saunders, G., 1987, Mechanics and stability of the Lookout Creek Earth Flow: Bulletin of the Association of Engineering Geologists, v. 24, p. 267-280.

Ranken, D.W., 1974, Hydrologic properties of soil and subsoil on a steep, forested slope: Oregon State University MS Thesis, 117 p.

Rothacher, J., 1963, Net precipitation under a Douglas-fir forest: Forest Science, v. 9, p. 423-429.

Rothacher, J., 1970, Increases in water yield following clear-cut logging in the Pacific Northwest: Water Resources Research, v. 6, p. 653-658.

Snyder, K.U., 2000, Debris flows and flood disturbance in small, mountain watersheds: Oregon State University MS Thesis, 53 p.

Sollins, P., Grier, C.C., McCorison, F.M., Cromack, K., Jr., Fogel, R., and Fredriksen, R.L., 1980, The internal

element cycles of an old-growth Douglas-fir ecosystem in western Oregon: Ecological Monographs, v. 50, p. 261-285.

Swanson, F.J., and Dyrness, C.T., 1975, Impact of clear-cutting and road construction on soil erosion by landslides in the western Cascade Range, Oregon: Geology, v. 3, p. 393-396.

Swanson, F.J., and Fredriksen, R.L., 1982, Sediment routing and budgets: Implications for judging impacts of forestry practices, *in* Swanson, F.J., Janda, R.J., Dunne, T., and Swanston, D.N., eds, Sediment budgets and routing in forested drainage basins, : Portland, Oregon, U.S. Forest Service, Pacific Northwest Forest and Range Experiment Station General Technical Report PNW-141, p. 129-137.

Swanson, F.J., Fredriksen, R.L., and McCorison, F.M., 1982a, Material transfer in a western Oregon forested watershed, *in* Edmonds, R.L., ed., Analysis of coniferous forest ecosystems in the western United States, US/IBP Synthesis Series 14: Stroudsburg, Penna., Hutchinson Ross Publishing Company, p. 233-266.

Swanson, F.J., Grant, G.E., and Lienkaemper, G.W., 1987, Field trip guide to the H.J. Andrews Experimental Forest: Corvallis, Oregon, U.S. Forest Service Pacific Northwest Research Station, 46 p.

Swanson, F.J., Harr, R.D., and Fredriksen, R.L., 1980, Field trip guide: Geomorphology and hydrology in the H.J. Andrews Experimental Forest, western Cascades, *in* Geologic field trips in western Oregon and southwestern Washington, Geological Society of America Cordilleran Section, 76th Annual Meeting, Corvallis, Ore., March 1980: Oregon Department of Geology and Mineral Industries Bulletin 101 p. 217-232.

Swanson, F.J., and James, M.E., 1975, Geology and geomorphology of the H.J. Andrews Experimental Forest, western Cascades, Oregon: U.S. Forest Service Pacific Northwest Forest and Range Experiment Station Research Paper PNW-188, 14 p.

Swanson, F.J., Janda, R.J., Dunne, T., and Swanston, D.N., eds., 1982b, Workshop on sediment budgets and routing in forested drainage basins: U.S. Forest Service Pacific Northwest Forest and Range Experiment Station General Technical Report PNW-141, 165 p.

Swanson, F.J., Johnson, S.L., Gregory, S.V., and Acker, S.A., 1998, Flood disturbance in a forested mountain landscape: BioScience, v. 48, p. 681-689.

Swanson, F.J., Jones, J.A., and Grant, G.E., 1997, The physical environment as a basis for managing ecosystems, *in* Kohm, K.A., and Franklin, J.F., eds., Creating a forestry for the 21st Century: The Science of Ecosystem Management: Washington, Island Press, p. 229-238.

Swanson, F.J., Lienkaemper, G.W., and Sedell, J.R., 1976, History, physical effects, and management implications of large organic debris in western Oregon streams: U.S. Forest Service Pacific Northwest Forest and Range Experiment Station General Technical Report PNW-56, 15 p.

Swanson, F.J., and Swanston, D.N., 1977, Complex mass-movement terrains in the western Cascade Range, Oregon: Reviews in Engineering Geology, v. 3, p. 113-124.

Thomas, R.B., and Megahan, W.F., 1998, Peak flow responses to clear-cutting and roads in small and large basins, western Cascades, Oregon: A second opinion: Water Resources Research, v. 34, p. 3393-3403.

Thomas, R.B., and Megahan, W.F., 2001, Reply to "Comment on 'Peak flow responses to clear-cutting and roads in small and large basins, western Cascades, Oregon: A second opinion' by R.B. Thomas and W.F. Megahan" by J.A. Jones and G.E. Grant: Water Resources Research, v. 37, p. 181-183.

Triska, F.J., Sedell, J.R., and Cromack, K., Jr., 1984, Nitrogen budget for a small coniferous forest stream: Ecological Monographs, v. 54, p. 119-140.

Vanderbilt, K.L., 2000, Patterns of nitrogen fluxes in watersheds of the H.J. Andrews Experimental Forest, Oregon: Oregon State University MS Thesis, 110 p.

Vanderbilt, K.L., Lajtha, K., and Swanson, F.J., in press, Biogeochemistry of unpolluted forested watershed in the Oregon Cascades: Temporal patterns of precipitaation and stream nitrogen fluxes: Biogeochemistry.

Vannote, R.L., Minshall, G.W., Cummins, K.W., Sedell, J.R., and Cushing, C.E., 1980, The river continuum concept: Canadian Journal of Fisheries and Aquatic Sciences, v. 37, p. 130-137.

Waring, R.H., and Franklin, J.F., 1979, Evergreen coniferous forests of the Pacific Northwest: Science, v. 204, p. 1380-1386.

Waring, R.H., Gholz, H.L., Grier, C.C., and Plummer, M.L., 1977, Evaluating stem conducting tissue as an estimator of leaf area in four woody angiosperms: Canadian Journal of Botany, v. 55, p. 1474-1477.

Waring, R.H., and Running, S.W., 1976, Water uptake, storage, and transpiration by conifers: A physiological model, *in* Lange, O.L., Kappen, L., and Schulze, E.-D., eds., Water and Plant Life. Ecological Studies: Analysis and Synthesis, Volume 19: Heidelburg, , Springer-Verlag, p. 189-210.

Wemple, B.C., 1998, Investigations of runoff production and sedimentation on forest roads: Oregon State University PhD Dissertation, 168 p.

Wemple, B.C., and Jones, J.A., in preparation, Runoff production on forest roads in a steep mountain watershed.

Wemple, B.C., Jones, J.A., and Grant, G.E., 1996, Channel network extension by logging roads in two basins, western Cascades, Oregon: Water Resources Bulletin, v. 32, p. 1195-1207.

Wemple, B.C., Swanson, F.J., and Jones, J.A., 2001., Forest roads and geomorphic process interactions, Cascade Range, Oregon: Earth Surface Processes and Landforms, v. 26, p. 191-204.

Wondzell, S.M., and Swanson, F.J., 1996a, Seasonal and storm dynamics of the hyporheic zone of a 4th-order mountain stream. I: Hydrologic processes: Journal of the North American Benthological Society, v. 15, p. 3-19.

Wondzell, S.M., and Swanson, F.J., 1996b, Seasonal and storm dynamics of the hyporheic zone of a 4th-order mountain stream. II: Nitrogen cycling: Journal of the North American Benthological Society, v. 15, p. 20-34.

Wondzell, S.M., and Swanson, F.J., 1999, Floods, channel change, and the hyporheic zone: Water Resources Research, v. 35, p. 555-567.

Wong, B.B.-L., 1991, Controls on movement of selected landslides in the Coast Range and western Cascades, Oregon:Oregon State University MS Thesis, 193 p.

Geology of Vineyards in the Willamette Valley, Oregon

George W. Moore, Department of Geosciences, Oregon State University, Corvallis, Oregon 97331; mooreg@geo.orst.edu

INTRODUCTION

Corvallis lies near the center of the Willamette Valley, one of the world's premier grape growing and winemaking regions. The word Willamette (pronounced wil-LAM-et) means spilled water in the Calapooya Indian language, and it originally referred to the Willamette Falls at Oregon City. The Willamette Valley Appellation is the largest of Oregon's six wine-growing regions. The others are the Umpqua, Rogue, and Applegate Valleys, all wholly within Oregon, and the Columbia Valley and Walla Walla, shared with the state of Washington.

The first grapevines in Oregon were planted in the 1850s, soon after the Oregon Trail was opened. The modern winemaking industry, however, dates from a much later time—from the period after World War II. By then, two factors led to the industry's rapid and efficient expansion. First, 2 centuries of grape growing in France had shown by trial and error which grape varieties in which microclimates make the best wine. And second, during the 1940s, Maynard Amerine of the University of California at Davis developed a climatic formula by which a potential wine-growing area could be compared with a matching area in France, so that its grape varieties could be adopted.

A free booklet *Vintage Oregon* has been published by the Oregon Wine Advisorary Board. It includes thumbnail road maps to the state's winerys and is available at chambers of commerce and information centers. The AAA county maps also spot the wineries and are excellent for wine-country touring.

CLIMATE AND GRAPES

The grape *Vitis* is a cool-climate genus that grows between latitudes 30 and 50°. In Europe, a single species is native, *Vitis vinifera* Linné, but it has more than 700 varieties (4000, including crosses and clones). These constitute the world's wine grapes. *Vitis vinifera* generally cannot tolerate temperatures below -15°C (5°F).

The genus *Vitis* also has about 15 additional species in Asia and 20 in America, including the Concord grape, *Vitis labrusca* Linné. These other species make wine that is generally considered to taste too grapey, but American grapes provide the grafted rootstocks for most commercial winegrapes worldwide.

Vitis vinifera is believed to have originated in what is now the Republic of Georgia. Extensive cultivation of it occurred throughout the Roman Empire, including in France. But societal breakdown during the Middle (Dark) Ages partially disrupted the previously well-organized wine industry. It finally became established in its present form in France about 1720. During the intervening period, the grapes had continued living in the wild, where natural selection based on the various local environments across Europe produced the varieties that we know today.

During the period when the wild varieties of European grapes were evolving, birds were a principal agent of grape natural selection. Grapes are adapted to be sour and unpalatable while their seeds are not yet mature. During a brief period in the fall, just before the first local frost, the seeds mature, and the grapes abruptly turn sweet. The birds gorged on them and dispersed the seeds, producing the tight coupling between grape varieties and climatic zones. In the Willamette Valley today, propane cannons, synthetic bird distress calls, and nets repel the robins during their fall migration.

Genetic studies of the DNA of the grape varieties produced a surprise when researchers discovered that Cabernet Sauvignon, the premier variety in Bordeaux and Napa Valley, is a wild cross between Cabernet Franc and Sauvignon Blanc. Pinot Noir and the other members of its heterozygous series, Pinot Gris and Pinot Blanc, is older than most other varietals. It originated in the Burgundy-Rhine

Field Guide to Geologic Processes in Cascadia: Oregon Department of Geology and Mineral Industries Special Paper 36, 2002.

region, probably before the Roman period. Wild crosses between it and Gouais Blanc, which the Romans brought in from Croatia in AD 280, produced Chardonnay, Gamay Noir, and several other varietals (Bowers and others, 1999).

The European grape varieties were planted around the world in suitable climatic zones during the 1800s, where at first they flourished. In 1858 and1862, however, American *Vitis* species were sent as botanical specimens to France. They carried the yellow aphid-like root louse *Phylloxera vastatrix*. Soon the French grapevines were dying, and after that all French varietals around the world began to succumb. The American *Vitis* species are resistant to *Phylloxera*. But like the European diseases that came the other way across the Atlantic to decimate the Native Americans, *Phylloxera* was devastating to the nonresistant *Vitis vinifera.*

Thomas Munson from Denison, Texas, an expert on American grapes, suggested a solution: Graft European vines onto American roots (Munson, 1909). That soon was done, although some grape varieties had been so thoroughly annihilated in France that restocking had to come from surviving scions in the United States. Today, several American species are used as rootstocks in France to provide both *Phylloxera* resistance and adaptability to France's generally limy soils. In the Willamette Valley, with basalt and tuffaceous sandstone soils, about 20 percent of the rootstocks come from the American species *Vitis riparia*, native to the northeastern United States, and about 70 percent consist of several clones of hybrids between *V. riparia* and *V. rupestris*, native to creek beds in Arkansas, Missouri, and Tennessee.

About 60 percent of vineyards in Oregon still grow *V. vinifera* varietals on their own roots, and they must scrupulously prevent contaminated material from coming in. Current plantings are generally of grafted stock. Once an infestation begins, about 4 years are available to bring grafted stock into production, at first commonly side-by-side with the old plants.

Maynard Amerine's climatic formula consists of a unit called degree days (Amerine and Winkler, 1944). Degree days are the number of hours annually between May 15 and October 15 when the temperature exceeds 10°C (50°F). Typical values average about 4,000 for Fresno, California, and 3,000 for both Bordeaux, France, and Napa Valley, California. Burgundy, France, and the Willamette Valley, Oregon, have a degree days average of 2,000, which explains why Willamette Valley winemakers mainly produce the principal grapes of Burgundy: Pinot Noir, Chardonnay, and Pinot Gris.

The 45th Parallel passes through both France and Oregon. The winds in the North Atlantic and North Pacific, the Westerlies, drive oceanic currents toward France and Oregon. The narrowness of the North Atlantic, however, causes its current to produce warmer coastal temperatures in France than the wide North Pacific does in Oregon. Hence the degree days in coastal Bordeaux at latitude 45° match those farther south in Napa Valley at latitude 38° (Howell and Swinchatt, 2000). The Westerlies continue toward the east across both Europe and North America, where they gain continental influence that eventually produces winter temperatures too cold for the tender *Vitus vinifera*.

An intermediate level of rainfall is an additional factor in grapevine growth. The intervening Coast Range limits rainfall in the Willamette Valley, which lies 50 km (30 miles) from the Pacific Ocean. The Massif Central controls the rainfall in Burgundy, 500 km (300 miles) from the Atlantic Ocean. Burgundy's greater distance inland adds a continental influence that compensates for the warmer starting temperature at the Atlantic Coast.

The Willamette Valley and Burgundy differ in that Burgundy has more rainfall during the summer. Both places are subject to the annual climatic variations that can lead to either great or not-so-great vintages. In the Willamette Valley, a cool summer can slow the ripening, and early rains can do the same, as well as diluting the fruit flavor and sometimes producing *Botrytis* bunch rot. These year-to-year climatic variations contribute to the diversity of the resulting wines.

GEOLOGY

The Earth's crust in western Oregon and the Willamette Valley is unusual. A borehole drilled there would pass directly from rocks of the Cenozoic Era (the age of mammals) into the Earth's mantle below the crust. It would not intersect any rocks of the Mesozoic Era (the age of reptiles) or the Paleozoic Era (the age of invertebrates). Western Oregon was created as

"new ground" on the surface of the Earth soon after the dinosaurs had died out.

The area of the Willamette Valley was originally underlain by old rocks similar to those in the Klamath Mountains of southern Oregon. About 58 million years ago, however, northward drag from an offshore tectonic plate tore western Oregon and Washington away from the Klamath Mountains and transported them to southern Alaska (Moore, 1984).

The moving fragment resembled today's Baja California Peninsula. As it moved northward, it left behind new seafloor analogous to the floor of the present Gulf of California. The basaltic seafloor melted out of the underlying Earth's mantle as the seafloor stretched. That basalt, the Siletz River Volcanics, since then has been slowly covered by the various rock layers that are important to Oregon's vineyards (Yeats and others, 1996).

The hole in the ocean floor off Oregon initially had a depth of 2,500 meters (8,000 feet), the same depth as at actively forming (hot) seafloor-spreading axes. Marine sandstone and shale that eroded from the remaining land began to fill the hole rapidly. The first deposits at the Willamette Valley, which belong to the Eocene Epoch (55 to 38 million years ago), started with the Tyee Formation and ended with the Spencer Formation. These were followed by sedimentary rocks of the Oligocene Epoch (38 to 24 million years ago), such as the Eugene Formation, and then of the Miocene Epoch (24 to 5 million years ago), such as the Scotts Mills Formation. These marine formations in places contain shells of fossil clams and snails.

By Oligocene and Miocene time, the hole left by the northward rifting of the original western Oregon had been largely filled. Some of the marine sandstone and shale then interfingered with lava from the Cascade volcanoes on the east side of the Willamette Valley and with volcanic ash that made tuff which contains fossil leaves.

About 15 million years ago, during the Miocene Epoch, a new wave of basaltic lava began erupting from vents in far eastern Washington and Oregon. This highly fluid lava flowed as sheets across Washington and Oregon toward the sea, including across the northern half of the Willamette Valley. Solidified crusts on its surface retained the heat until the lava reached the sea. It flowed between the spaced-out Cascade volcanoes and down the valley of the ancestral Columbia River. The Coast Range had not yet been raised as a barrier to the flow of the lava, so it moved all the way to the shoreline and beyond. It left behind the Columbia River Basalt Group, the bedrock of the red hills that now bear vineyards in the northern Willamette Valley.

A great thickness of sedimentary and volcanic rocks by then overlay the basement of the Siletz River Volcanics. All the while, the floor of the Pacific Ocean was sliding toward the east down under western Oregon at the Cascadia Subduction Zone. The decending slab fed water to the roots of the Cascade volcanoes, which fluxed and melted the hot mantle material there. Some of the erupting melt fed back as volcanic ash to the sedimentary rocks of the valley.

But this well-oiled system had a stoppage about 5 million years ago, during the Pliocene Epoch. While the tectonic plate from the Pacific was moving down into the lower mantle underneath the Cascade volcanoes, North America had been moving toward it at the slow but unyielding rate of 20 km (12 miles) per million years. In the 50 million years since the Siletz River basement had been emplaced, North America had overridden the West Coast subduction zone by about 1000 km (600 miles).

Abrupt changes then occurred. The plate boundary moved inland at California to the San Andreas Fault, Baja California began to pull away from mainland Mexico, and the Cascade volcanoes jumped 50 km (30 miles) eastward from the old Western Cascades to the presently active High Cascades. The ultimate cause of the changes in western Oregon was that the subducting slab abandoned its old alignment and reinserted itself in a more stable position farther west.

The slab has a thickness of 100 km (60 miles). As its butt end reentered the Earth's mantle, it disrupted the edge of the continental crust. The formerly smooth sedimentary basin that extended seaward from the volcanic arc was pushed upward to create Oregon's Coast Range. Erosion of this new mountain range over the 5 million years since then has cut it down to where even the Siletz River Volcanics now appear at the surface in the hills.

A final geologic event, and an unusual one, was next to affect Oregon's future wine industry. Although the Ice Age glaciers never reached the floor of the Willamette Valley, a distant glacier had a profound effect on it. A lobe of the Canadian Ice Sheet dammed a river in Idaho and created the large ancient Lake Missoula. After about 60 years, Lake Missoula filled to a level where it floated its ice dam. The dam broke, and a huge flood swept across the Channeled Scablands of eastern Washington and brim-full down the Columbia River Gorge. The water then swirled into and filled the Willamette Valley to a depth of 100 meters (330 feet) (O'Connor and others, 2001).

The water drained out of the valley over about 1 week, and it left behind a layer of silt 7 centimeters (4 inches) thick. Meanwhile, the glacier readvanced and created a new ice dam and a new Lake Missoula. Again, after 60 years, the dam rebroke, the Willamette Valley was refilled with water, and another layer of silt was deposited. The cycle repeated itself about 60 times from 15,000 to 13,000 years ago. Today the Willamette Silt is 4 meters (13 feet) thick. It covers the lower slopes of many vineyards to an altitude of 100 meters (330 feet) and creates the rich farmland of the valley floor.

SOILS

The soil name for the Willamette Silt is the Woodburn Series, named after a town in the valley. It is rich in nutrients, hence grows wine grapes very well. Their flavor, however, is less complex than that of grapes grown on the soils of the bedrock slopes. Vineyards blessed with both types of soil can often achieve the best of both worlds by blending their wines. Typical wineries whose estate vineyards incorporate some grapes grown on the Woodburn Series are Duckpond Cellars, Houer of the Dauen, and Tyee Vineyards.

The unique origin of the Willamette Silt produced an almost instant soil. But the 13,000 years since the silt was deposited has made a true soil. Its A horizons at the top, where some clay has been leached downward, are 40 cm (17 inches) thick. The B horizons, enriched in clay, extend from 40 to 140 cm (17 to 54 inches). Below that, the C horizon consists of the parent silt. These soils of the Woodburn Series are very dark brown (wet), brown (dry), and have a moderately acidic surface pH of 5.9.

Soils are defined first by climate, second by slope angle, third by soil thickness, and forth by parent material. All the Willamette Valley soils have the same climate, which consists of about 1000 millimeters (40 inches) of precipitation, an average annual air temperature of 12°C (53°F), and a frost-free season of about 180 days. Altitude of most vineyards ranges from 90 to 200 meters (300 to 700 feet), because a thermal inversion warms the air within that altitude range. The Woodburn Series has a slope of 0 to 1°, and during some years its lower reaches below the thermal inversion can be subject to vine-killing temperatures from the topographic drainage of cold air.

Most vineyards on hard bedrock slope from 1 to 7°, values that result in good drainage but are gentle enough to provide resistance to soil erosion. For reasons partly of proximity to the state's population center at Portland, many vineyards lie on soils of the Columbia River Basalt Group, because it makes nearby hills of the requisite slopes. Their soils belong to the Jory Series, named after a basaltic prominence in the Salem Hills. Soils of the Jory Series are dark reddish brown (wet), reddish brown (dry), 150 cm (60 inches) to bedrock, well drained, and have a surface pH of 5.6. Their thickness indicates that they are at least $^1/_2$ million years old.

Oregon's analog of Burgundy's Cote d'Or (Slope of Gold) is the southeast-facing slope of the Dundee Hills. Several vineyards that produce Pinot Noir and other varietals on the southeast front of the hills are Archery Summit, Cameron Winery, and Sokol Blosser Winery.

Uplift of the Coast Range 5 million years ago folded the rocks of the Columbia River Basalt Group. In the Dundee Hills, three individual lava flows dip toward the southeast. Erosion has etched the outcropping edges of these flows into ridges somewhat like those on weathered wood. The erosion produced excellent higher level vineyard sites back from the front of the hills, such as the Prince Hill Vineyard of Erath Vineyards.

Vineyard soils on tuffaceous sandstone and shale in the Willamette Valley commonly consist of the Willakenzie Series. Its name

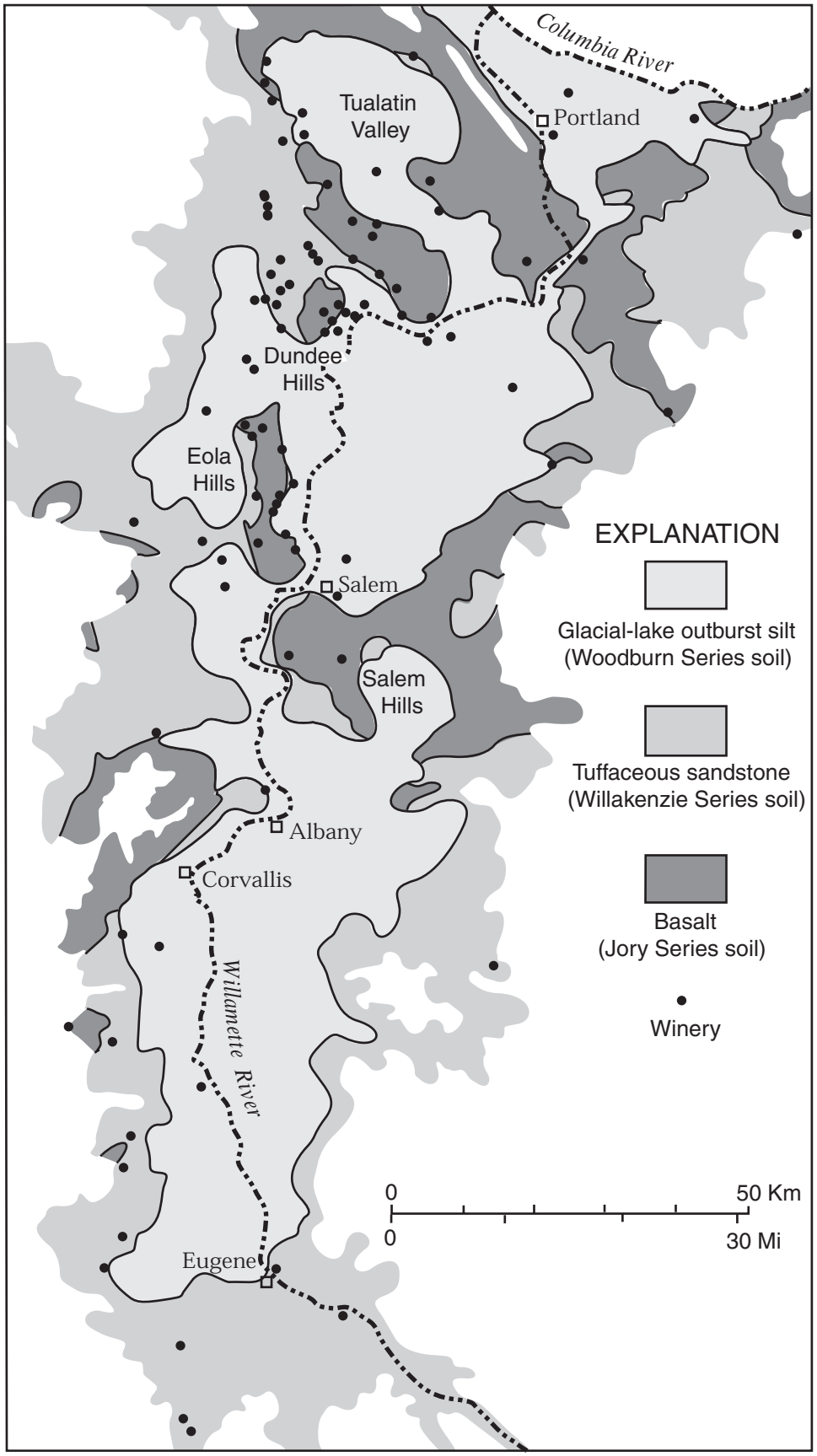

Figure 1. Distribution of wineries in Oregon's Willamette Valley showing the major soils and their parent materials.

comes from the confluence of the Willamette and McKenzie Rivers north of Eugene, and typical parent materials consist of the Eugene and Spencer Formations. Soils of the Willakenzie Series are dark brown (wet), brown (dry), 80 cm (30 inches) to bedrock, well drained, and have a surface pH of 5.9. Typical wineries with vineyards on the soils of the Willakenzie Series are Airlie Winery, Elk Cove Vineyards, and Willakenzie Estate.

The Nestucca Formation of Eocene age consists of tuffaceous sandstone containing beds of basalt formed before the Western Cascades took their final alignment. Coleman Vineyards, on the Nestucca Formation near McMinnvile, has soils that range from those of sandstone to basalt, and a bed of pillow lava crops out on the road leading to the winery.

Several other soil series grade into the principal soils that support vineyards on bedrock slopes in the Willamette Valley. On basalt, the Yamhill Series is thinner to bedrock (100 cm; 38 inches) than the Jory, and its B horizons contain less clay introduced from above. The Nekia Series is still thinner (75 cm; 30 inches) and contains more fragments of basaltic colluvium. On tuffaceous sandstone, the Bellpine Series overlaps with the Willakenzie Series at higher altitudes and extends up to 1000 meters (3000 feet). Slopes carrying it range up to 35°, the depth to bedrock averages 60 cm (33 inches), and sandstone colluvium fragments make up a higher percentage of the soil than with the silty Willakenzie. The Amity Series represents poorly drained parts of the Woodburn Series (on the Willamette Silt). It has a conspicuous light-colored leached layer (an E horizon) between the A and B horizons.

An additional parent material that resembles the Willamette Silt, but which is older and has a more mature soil, is wind-blown silt in the northern part of the valley. This loess, older than the young loess of the Portland Hills Silt, was produced from dust blown onto the hills from glacial outwash during the early part of the Pleistocene Epoch (Scott F. Burns, personal communication, 2002). It contains 1-centimeter ($^1/_2$-inch) pisolites (spherical cemented bodies), which attest to the oldness of the unit. Tualatin Estate Vineyards contain about $^1/_4$ meter (2 feet) of this material over an old Jory soil, and Shafer Vineyard Cellars has several meters of it over the Pittsburg Bluff Formation (Willakenzie Series). The vines likely tap the bedrock, but the nutrient level is slightly elevated in the old loess, and the plants require some leaf pulling and grape-cluster pruning.

Tuffaceous siltstone of the Spencer Formation underlies Bellfountain Cellars, southwest of Corvallis. The vineyard soil, mapped as the Bellpine (Willakenzie) Series, in places is redder than usual. Basaltic intrusions crop out near the vineyard, and thin sills of basalt cut the Spencer Formation there. Because this vineyard is planted in a south-facing basin, it can ripen Cabernet Sauvignon as well as the Burgundian varieties.

Reed Glasmann of Oregon State University has analyzed the clay minerals from several Willamette Valley vineyards. For the present study, he analyzed Jory soil from Prince Hill Vineyard (Erath Vinyards) and Willakenzie soil from Willakenzie Estates. The main difference between soils on basalt and on tuffaceous sandstone is that the clay-sized fraction over the sandstone contains quartz and that over the basalt does not. On both rock types, the clay minerals consist of halloysite, $Al_2Si_2O_5(OH)_4 2H_2O$, and gibbsite, $Al(OH)_3$, and the red to yellow iron oxide coloring agents consist of hematite, Fe_2O_3, and goethite, FeO(OH).

Native vegetation on both the basalt and tuffaceous sandstone of the Willamette Valley consists of Douglas fir, Oregon white oak, wild rose, poison oak, snowberry, and bracken fern. Native vegetation on the Willamette Silt consists of grass and widely spaced Oregon white oak.

Two alternative methods are used in the Willamette vineyards to prevent erosion and to retain moisture and soil air between the rows of grapes. In the first method, the previous winter's cover crop is lightly tilled in the spring to produce a water-retaining mulch, then red clover and oats are replanted near grape harvest time to prevent erosion from the winter rains. In the second method, mixed natural vegetation consisting of up to 11 species is allowed to grow continuously between the vines, where it is mowed and resembles a wildflower-studded lawn.

WINES

During grapevine pruning in most vineyards, two strong canes produced during the preceding year are tied to supports and cut back to about ten buds on each. The other annual growth is removed. The buds begin to leaf out by early April, and tiny flowers, which are self-pollenating, appear in June. Leaves are pulled during the growing season, chiefly to provide mildew-preventing air circulation but also to let the sun strike the grapes. This mild "suntanning" can inhance their flavor, while the main leaf canopy cools them.

The Scott Henry trellis system, developed in Oregon, is now increasingly used around the world (Henry, 1992). Two levels of two canes each provide two lines of grape clusters, one above the other. A gap between the lines gives excellent air circulation and protection from powdery mildew.

Vineyards commonly grow several clones of each grape variety. Also, different fermentation yeasts may be used to vary the effects from the different grape clones, from the various soils within the vineyard, and from the different ripening conditions in diffferent years. The resulting wines are barrelled separately, and they then are blended before bottling in proportions that give the best flavor.

White grapes are generally crushed as whole clusters, and the juice is removed from the skins before fermenting to reduce tannins, maintain higher acidity, and retain delicate aromas. Skins remain on red grapes during fermentation. The skin pomace floats to the top of the usually stainless-steel fermentation tanks. This cap is pushed down regularly by the winemakers to maintain contact with the developing wine.

Some wines are stopped after the yeast fermentation is complete, whereas others are taken through a subsequent bacterial fermentation. This malolactic fermentation utilizes the already present or introduced bacteria *Leuconostoc oenos* to convert the grapes' malic acid into the milder lactic acid. The process increases the wine's pH from about 3.4 to 3.9, and depending on the strain used, it can impart a buttery flavor.

Three types of oak are used for barrel aging: French *Quercus robur*, (eastern) American *Quercus alba*, and Oregon *Quercus garryana*.The mild French oak is generally favored for the Willamette Valley's Pinot Noir, whereas the stronger American oak can be used for the more robustly flavored Cabernet Sauvignon. Oregon white oak is intermediate between the other two.

The oak has two functions: to impart its own flavor to the wine, and to provide an active surface for the winemaking process. For delicately flavored wines, batches from new oak barrels are usually blended with batches from old barrels that don't provide flavor but do supply the reaction surface. The old barrels last indefinitely.

The wood of most barrels, as in the case of Oregon oak barrels, is split rather than sawn into boards, so that the grain is parallel with the surface. Then they are planed to the proper thickness and shape for the staves and heads. Finally, the staves are heated to bend them, they are drawn together by an encircling steel cable, and the steel hoops are put in place.

The barrels are gently toasted to caramelize the sugars remaining in the oak pores. This process differs from the charring that is used for whiskey barrels, which is intended to impart a smoky flavor. Wine barrels are toasted before the heads are installed. The open-ended barrels are placed over small fires burning the same wood as the barrels. Production is maintained by moving them along a series of fires. Then the staves are tightened down on the heads.

To illustrate the importance of blending to winemaking, Scott Shull of Raptor Ridge Winery, Scholls, Oregon, published the tests that went into blending his 1995 reserve Pinot Noir (Shull, 1996). The test used six colleagues and himself and three Pinot Noirs of several clones grown on two bedrock types. The initial wines and then the three tested blends were presented to the panel from numbered beakers.

Sample 1 was mostly a Pommard clone grown in Willakenzie soil on tuffaceous sandstone, colored pale ruby, with tones of violet, almond, plum, and a woodsy nose. Sample 2 was mostly a Dijon clone grown in Willakenzie soil, colored medium garnet, with tones of black cherry, flowers, earthy wood, and coffee. Sample 3 was a Wadenswil clone grown in Jory soil on basalt, colored almost black as ink, with

tones of chocolate, menthol, vanilla oak, blackberry, dust, and heather.

An equal 33 percent blend of the three wines, as initially had been planned by the winemaker, had good color, but its taste was flat. Next came a blend of 45 percent Pommard-Willakenzie, 45 percent Dijon-Willakenzie, and 10 percent Wadenswil-Jory. This was good. The cherry fruit flavor came through well, but the desired earthiness was masked. The final blend was 50 percent Pommard-Willakenzie, 40 percent Dijon-Willakenzie, and 10 percent Wadenswil-Jory. The small percent of Wadenswil gave good color to the blend. The cherry tone came through well, and hints of oak, blackberry, and heather remained. This was released as the Winemaker's Reserve, and another release consisted mostly of the Wadenswil.

Medical demographers have known since the 1970s that populations which drink red wine regularly, such as in France, are less subject than others to cholesterol clogging of their arteries. Laboratory studies have recently offered an explanation. The cell product endothelin is known to cause arterosclerosis. Polyphenols in red wine (but not in white wine or in unfermented red grape juce) inhibit endothelin production and hence seem to be the cause of this beneficial effect (Corder and others, 2001).

Winemakers blend their wines to increase the complexity, an especially useful practice within a single estate, or amongst neighbors. Shipping grapes for long distances to blend them may produce commercial wines for national distribution, but it suppresses the wines' terroirs—their unique vine-bedrock-soil-microclimate linkage (Wilson, 1998). King Estate in Lorrane, Oregon, for example, which has a large acreage of vinyards at the winery on tuffaceous sandstone of the Spencer Formation, imports and blends from the whole state, even from different appellations. The winemaker does make the wines separately, but the blending is cosmopolitan from across the state. A different practice is that used by other wineries, including St. Innocent Winery, Salem, where the vineyard names are printed on the labels, even though they may lie some distance away from the winery.

As Oregon's wine industry continues to develop, the individual terroirs may gain further name recognition, so that preserving and specifying them can become even more marketable.

ROAD LOG FROM OREGON STATE UNIVERSITY TO BELLFOUNTAIN CELLARS, CORVALLIS

(The winery's regular hours are weekends, noon to 5 p.m. Distances in miles.)

0.0 North entrance to Oregon State University's CH2M Hill Alumni Center, 26th Street near Western (Fig. 2). Proceed left (south) on 26th Street.

0.1 Cross Western Avenue.

0.3 Turn right (west) on US Highway 20 (Philomath Blvd).

2.0 Enter lane for left turn and turn left (south) at 53rd Street (stoplight).

2.9 Turn right (west) on Plymouth Drive.

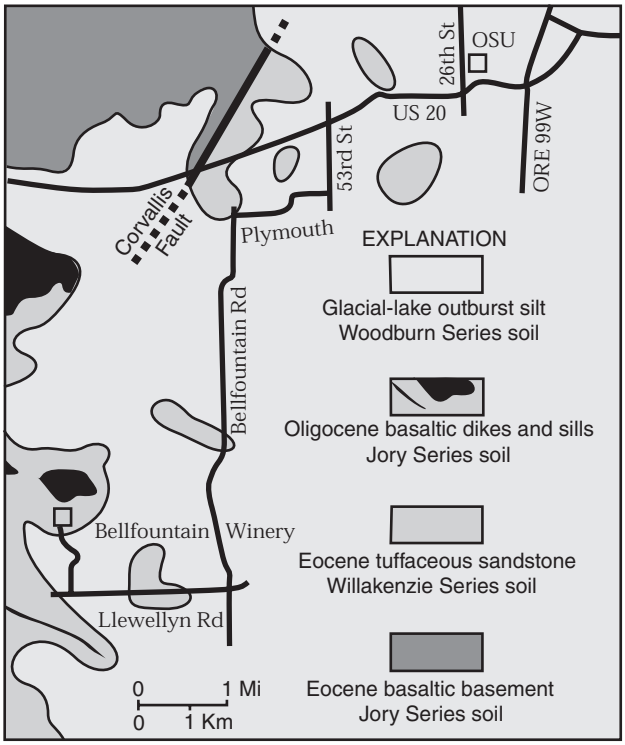

Figure 2. Geologic map of the Corvallis area showing the route to Bellfountain Cellars.

3.4 The white Victorian house on the right has an 1889 date on its gable. Where the road swings back to the west, Neubeach Hill lies ahead on the right. It is made of steeply dipping tuffaceous sandstone of the late Eocene Spencer Formation. The northeast-trending Corvallis Fault lies on the northwest side of Neubeach Hill. The fault has about 5000 meters of vertical displacement, and it bounds the Spencer and basalt of the early Eocene Siletz River Volcanics, the basement rock of western Oregon. Most movement on the Corvallis Fault occurred during the late Eocene, and the fault is believed to be inactive now.

4.1 Turn left (south) on Bellfountain Road.

4.7 Cross the Marys River. The river is monitored by a telemetered gauging station. For about the next mile, we cross an arm of the Willamette Valley used for growing grass seed for lawns. Marys Peak, highest point in the Coast Range (1,249 m, 4,098 ft) forms the skyline to the west. It is held up by an erosion-resistant basaltic sill of Oligocene age. On extremely clear days the Three Sisters Volcanoes and Mt Jefferson can be seen to the east from this place. The flat floor of the Willamette Valley is covered by the Willamette Silt, about 4 meters thick, which was deposited by repeated floods from glacier-dammed lakes in Montana. The floods ended about 13,000 years ago, and the Woodburn Series soil has formed on the surface since then.

6.8 Crest of a hill underlain by the Spencer Formation. We won't stop, but the road cuts at Deerhaven Drive to the right (west) expose the yellowish brown Spencer Formation. Above it are about 2 meters of brown soil typical of the Willakenzie Series.

6.9 Cross Airport Road (flashing yellow light).

7.5 Poplar trees to the west, used for paper and particle board.

8.6 Turn right (west) on Llewellyn Road (flashing yellow light).

9.5 A Christmas tree farm. Trees are shipped to all parts of the country and the world from the Corvallis area.

10.0 Intersection of Fern Road from the north.

10.4 Turn right (north) into the driveway of Bellfountain Cellars. The winery is visible among the trees near the skyline.

11.0 Bull Run. The pond is an active beaver pond.

11.1 View of the winery at the top of the hill. The lower border of the vineyard below is covered by the Willamette Silt (Woodburn Series soil). The vineyard has hybrid soils, generally the Willakenzie Series on the Spencer Formation, but with red streaks trending toward the Jory Series on 1/2 meter basaltic sills that cut the Spencer. Basalt is more unstable than tuffaceous siltstone in the modern weathering environment, so the sills do not extend through the soil to the surface, whereas yellow siltstone chips from the Spencer do.

11.6 Bellfountain Cellars. Wine tasting is up the steps. A reddish hybrid soil lies behind the winery (gravel road to right), and a Spencer Formation outcrop lies behind the small barn. Our hosts are Rob and Jeanne Mommsen.

REFERENCES

Amerine, M.A., and Winkler, A.J., 1944, Composition and quality of must and wines of California grapes: Hilgardia, v. 15, p. 493-675.

Bowers, J., Boursiquot, J.M, This, P., Chu, K., Johansson, H., and Meredith, C., 1999, Historical genetics: The parentage of Chardonnay, Gamay, and other wine grapes of northern France: Science, v. 285, p. 1562-1565.

Corder, R., and others, 2001, Endothelin-1 synthesis reduced by red wine: Nature, v. 414, p. 863-864.

Henry, S., 1992, Scott Henry trellis system, *in* Casteel, T., ed., Oregon winegrape grower's guide: Portland, Oregon Winegrowers' Association, ed. 4, p. 119-123.

Howell, D.G., and Swinchatt, J.P., 2000, A discussion of geology, soils, wines, and history of the Napa Valley region: California Geology, v. 53, no. 3, p. 4-12.

Moore, G.W., 1984, Tertiary dismemberment of western North America: 3rd Circum-Pacific Energy and Mineral Resources Conference Transactions, p. 607-612.

Munson, T.V., 1909, Foundations of American grape culture: New York, Orange Judd Company, 252 p.

O'Connor, J.E., Sarna-Wojcicki, A., Wozniak, K.C., Polette, D.J., and Fleck, R.J., 2001, Origin, extent, and thickness of Quaternary geologic units in the Willamette Valley, Oregon: U.S. Geological Survey Professional Paper 1620, 52 p.

Shull, S., 1996, There's no accounting for taste: Oregon Wine Magazine, September 1996.

Wilson, J.E., 1998, Terroir—The role of geology, climate, and culture in the making of French wines: Berkeley, University of California Press, 336 p.

Yeats, R.S., Graven, E.P., Werner, K.S., Goldfinger, C., and Popowski, T.A., 1996, Tectonics of the Willamette Valley, Oregon: U.S. Geological Survey Professional Paper 1560, p. 183-222.

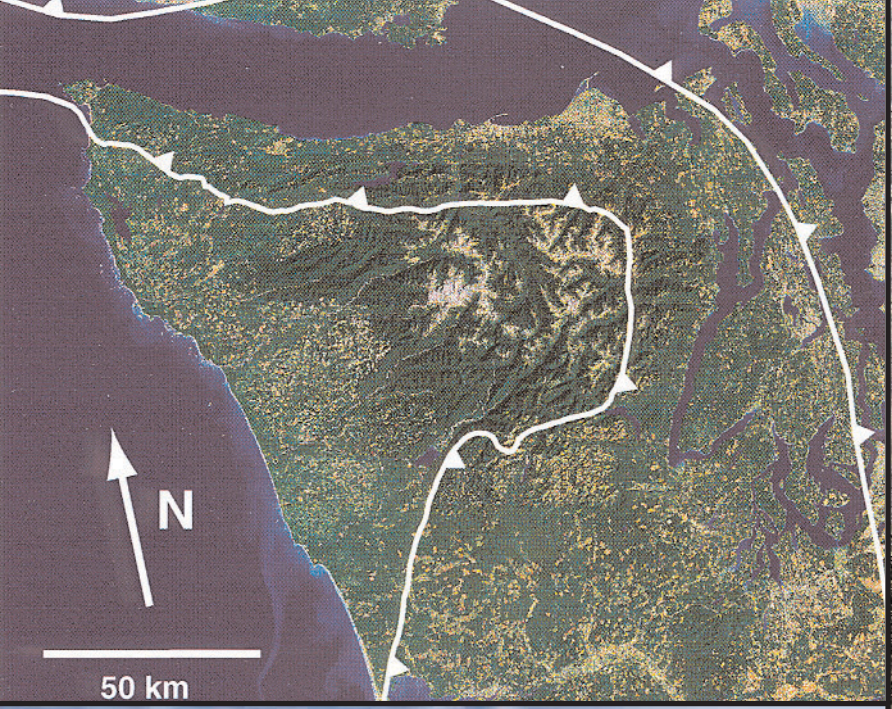
N
50 km